Investigating *HK2* as a potential therapeutic target in glioblastoma

Daniel Blakeway, MSc

A thesis submitted in fulfilment of the requirements of the University of Wolverhampton for the degree of

Doctor of Philosophy

Brain Tumour Research Centre Research Institute in Healthcare Sciences Faculty of Science and Engineering University of Wolverhampton

September 2019

Authors Declaration

This work or any part thereof has not previously been presented in any form to the University or to any other body whether for the purposes of assessment, publication or for any other purpose (unless otherwise indicated). Save for any express acknowledgments, references and/or bibliographies cited in the work, I confirm that the intellectual content of the work is the result of my own efforts and of no other person.

The right of Daniel Blakeway to be identified as author of this work is asserted in accordance with ss.77 and 78 of the Copyright, Designs and Patents Act 1988. At this date copyright is owned by the author.

Daniel Blakeway

Signature ……..

Date ……27/02/2020…….

ACKNOWLEDGEMENTS

I would like to express my deepest gratitude to my supervisor, Prof. Tracy Warr for providing me with the privilege and opportunity to pursue my PhD. Her tremendous support and guidance throughout this project have been a major factor in its successful completion and has helped shape the scientist I am today.

I am very grateful to my co-supervisor's Dr Katherine Karakoula and Dr Mark Morris, for their valuable support, suggestions and constant encouragement that have always been inspiring. I also have great appreciation to Prof. John Darling, Dr Farzana Rowther and Dr Angel Armesilla for all their valuable support. I would like to thank my colleagues at the university, of which there are too many to thank, but I do want to note my key appreciation of Dr Lawrence Eagles and Dr Maggie Trela for their help, encouragement and support over the last few years, it has been a pleasure to work alongside them. I am grateful to the technical staff at the University of Wolverhampton for all the support over my time here. I especially want to thank the efforts of Dr Angie Williams, Henrik Townsend and Clare Murcott for the technical support. I would like to thank the University for its philosophy, without which I would not have been able to undertake this PhD project.

I am grateful to the Colin Oliphant Charitable Trust for funding this project and for the Sydney Driscoll Trust for their support. I also extend my thanks to the collaborators in this project, brain tumour north west and Mr Andrew Beggs from the University of Birmingham, for providing support. I am grateful to all my friends outside the University, for their love and encouragement.

On a personal note, I would love to thank my parents, family and partner Jessica, for their constant source of encouragement, love and support, and for always being there pushing me onward and upward to greater things.

Lastly, I would like to thank my brother Chris, who's influence, and nurture has impacted my life beyond measure and shaped the person I am today and will continue to aspire to emulate.

This PhD would not have been possible without all your help. Thank you!

DEDICATION

To my parents and brother

Abstract

Glioblastoma is the most common high-grade primary brain tumour in adults. Current treatments have limited success with average survival comprehensively low. Effective drug treatments are hindered predominantly by the complex genetic background of glioblastoma heterogeneity, as such there is a compelling need for the development of effective therapeutics. An approach is to target abnormal metabolic pathways that are universally dysregulated in glioblastoma. The identification of potential targets and the development of therapeutic agents is crucial for the advancement of treatment. *Hexokinase 2 (HK2)* has a prominent role in glycolysis, acting as the rate-limiting step in the pathway. *HK2* is highly expressed in many cancers and its role as the rate-limiting step of glycolysis may potentially contribute to tumour growth. Overexpression of *HK2* has also been associated with drug resistant phenotypes, in parallel, its inhibition has improved the effectiveness of anticancer agents, suggesting *HK2* as a potential therapeutic target. The role of methylation and its association with expression levels of *HK2* was determined in glioblastoma fresh frozen biopsies and patient-derived cultures, through pyrosequencing and quantitative PCR. CRISPR knockout was utilised to investigate the effect of inhibiting *HK2* on proliferation and to determine the role of *HK2* in chemoresistance. The anti-proliferative effects of *HK2* inhibitors 3-bromopyruvic-acid (3-BPA) and metformin were investigated via cytotoxic assays and FACS analysis was used to determine their mechanism of action. Additionally, downstream expression changes were investigated via expression profiler arrays, across 84 key genes involved in the regulation and enzymatic pathways of glucose metabolism. Hypomethylation was demonstrated in all biopsies (n=100) and cultures (n=15) compared to normal brain tissue; with average methylation of 4.6% compared to 26% respectively ($p<0.0001$) determined across 15-CpGs. A significant increase ($p<0.0001$) in *HK2* expression was discovered, ranging between 6 to >1000- fold change in all biopsies and cultures compared to normal brain tissue and a strong correlation between hypomethylation and increased level of expression ($p<0.0001$) was established. Furthermore, elevated levels of *HK2* revealed notably poorer survival outcomes. Sensitivity to 3-BPA in glioblastoma cultures was associated with

elevated expression of *HK2*. Significantly different levels of apoptosis were observed with average levels 38% greater in high *HK2* expressing cultures ($p=0.0014$). A significant growth rate reduction ($p<0.007$) was demonstrated in *HK2*-KO cultures compared to parent cultures. Importantly sensitivity to both metformin and TMZ was also significantly increased ($p<0.0001$) in response to *HK2*-KO, with substantial reduction in both ID_{50} values and cell survival. Notably, *HK2*-KO cultures yielded greater synergistic effects with metformin and TMZ combination treatment. Array data revealed significant downstream gene expression alterations ($p<0.005$) with *HK2*-KO and with the supplementation of both 3-BPA and metformin, where >50% genes demonstrated reduced levels of expression compared to the corresponding parent/non-treated cultures. This study demonstrates the predominant role of *HK2* within the glycolytic pathway, with overexpression potentially key in driving the genetic alterations downstream. This study also verifies a strong correlation between increased expression of *HK2* and hypomethylation, additionally highlighting the impact *HK2* has on inferior patient prognosis. *HK2*-KO revealed considerable ubiquitous reductions in downstream gene expression compared to glioblastoma biopsy tissue and parent cultures. Additionally, an increase in drug sensitivity was depicted with the loss of *HK2* signifying the potential of targeting *HK*2 as a novel therapy in a significant subset of glioblastoma.

TABLE OF CONTENTS

LIST OF TABLES

LIST OF FIGURES

Abbreviations

µM	Micro Molar
1p/19Q	Deletion of the short arm of chromosome 1 and the long arm chromosome 19
3-BPA	3-Bromopyruvic acid
3-HB	3-hydroxybuterate
5mC	5-methylcytosine
AIC	4-Amino-5-imidazole-carboxamide
AKT	Protein kinase B
AMPK	AMP-activated protein Kinase (AMPK)
APOBEC1	Apolipoprotein B mrna-editing enzyme 1
ATRX	A-thalassemia/mental retardation syndrome protein
BBB	Blood/brain barrier
BBTB	Blood brain tumour barrier
CDK	Cyclin dependent kinase
cDNA	Complementary DNA
CGI	Cpg islands
CNS	Central nervous system

CpG	Cytosine-guanosinedinucleotides
CRISPR	Clustered Regularly Interspaced Short Palindromic Repeats (CRISPR-cas9)
CRUK	Cancer research UK
DDx	Differential diagnosis
DMEM	Dulbecco's modified Eagle medium
DMSO	Dimethyl sulfoxide
DNA	Deoxyribonucleic acid
DNMT	DNA methyltransferases
EGFR	Epidermal growth factor receptor
ERK	Extracellular signal regulating kinase
FBS	Foetal bovine serum
FCS	Foetal calf serum
FITC	Fluorescein isothiocyante
GBM	Glioblastoma multiforme
G-CIMP	Glioma-CpG island methylator phenotype
HBSS	Hanks buffered salt solution
HCC	Hepatocellular carcinoma
HEPES	4-(2-hydroxyethyl)-1-piperazineethanesulfonic acid)
HIF	Induces hypoxia-inducible factor
Hk1	Hexokinase 1
HK2	Hexokinase 2
ICGC	International cancer genome consortium
IDH1	Isocitrate dehydrogenase 1
IDH2	Isocitrate dehydrogenase 2
KEGG	Kyoto encyclopaedia of genes and genomes
LDH	Lactate dehydrogenase
LINE	Long interspersed nuclear element
LND	Lonidamine
MDR	Multiple Drug resistance
MGMT	O6-methylguanine-DNA-methyltransferase
MiRNA	Microrna

mM	Milli Molar
Mrna	Messenger ribonucleic acid
MSPCR	Methylation specific PCR
MTIC	Methytriazine
mTOR	Mammalian target of rapamycin
NADPH	Nicotinamide adenine dinucleotide phosphate
NHA	Normal human astrocytes
OD	Optical density
OS	Overall survival
PBS	Phosphate buffered saline
PCR	Polymerase chain reaction
PET	Positron emission tomography
PFS	Progression free survival
PHGDH	Phosphoglycerate dehydrogenase
PI3K	Phosphoinositide 3-kinase
PIP3	Phosphatidylinositol-3,4,5 -triphosphate
PRC2	Polycomb repressive complex 2
PTEN	Phosphatase and tensin homolog
Q-PCR	Quantitative reverse transcription PCR
REDD1	Regulated in development and DNA damage response 1
RISC	RNA-induced silencing complex
RLU	Relative light units
RNA	Ribonucleic acid
RT	Radiotherapy
RT-PCR	Reverse transcription PCR
siRNA	Small interfering RNA
SMI	Small-molecule inhibitors
SRB	Sulforhodamine
TCA	Trichloro-acetic acid
TCGA	The cancer genome atlas
TF	Transcription factor

TMZ	Temozolomide
TP53	Tumour protein 53
TSS	Transcription start site
TTFields	Tumour treating fields
VEGF	Vascular endothelial growth factor
VHL	Von Hippel-Lindau tumour suppressor
WHO	World health organisation
ΔΨ	Mitochondrial membrane potential

CHAPTER 1

Introduction

1.1 Cancer

Cancer is a disease that affects all ages and populations and is one of the leading causes of morbidity and mortality in the world (Siegel *et al.*, 2016). Data published in 2018 by the World Health Organisation (WHO) International Agency for Research on Cancer (IARC) estimated the global cancer burden to have reached 18.1 million new cases and 9.6 million deaths in 2018 (IARC, 2018). The total number of people worldwide who are alive within 5 years of diagnosis of cancer is estimated to be 43.8 million (McGuire, 2016). The increasing rates of cancer are due to several factors which includes population growth and ageing and the additional changes in prevalence in certain cancers linked to social and economic development. The increased cancer incidence can also be partly attributed to the advancements of cancer detection methods (Christopher *et al.*, 2014; Torre *et al.*, 2015; Philips *et al.*, 2018).

1.2 Brain tumours

Tumours comprising of the brain and the central nervous system (CNS) are some of the rarest cancer types. It is estimated that in 2015 these tumour types represented 1.4% of newly diagnosed cancer cases and were responsible for approximately 2.6% of related mortalities in that year (Howlader *et al.*, 2016). A recent review stated that there is a continuing substantial increase in the prevalence of glioblastoma across a diverse age range, which cannot be accredited to a particular risk factor, suggestive of comprehensive environmental and lifestyle aspects (Philips *et al.*, 2018). Data obtained in 2016 concludes that glioblastoma exceeded leukaemia as the leading cause of cancer death in the adult population in the United States (Ladomersky *et al.*, 2019). Glioma form a heterogeneous group of tumours of the CNS that develop from glial cell origins. They are traditionally classified based on histologic type and malignancy grade, where most (diffuse) gliomas show extensive infiltration in the CNS parenchyma. Gliomas can be further grouped as astrocytic or oligodendroglia (Perry and Wesseling, 2016). Oligodendrogliomas are a rare type of brain tumour that develop from glial cells called oligodendrocytes, which function normally to provide insulation (myelin) to neurons. Oligodendrogliomas are more

prevalent in adults than in children. Astrocytoma develop from glial cells called astrocytes, which function normally to transport nutrients and hold neurons in place (van den Bent, *et al.*, 2017). Gliomas are characterised based on the severity from grade I to IV. Tumours that are categorised in grade I – II are collectively known as low grade gliomas, which are distinguished with slower growth rates. High grade tumours, grade III- IV, are typified with increased aggressive physiognomies and malignancy. Astrocytomas can be any grade, where Grade I are pilocytic astrocytomas, the most common grade 2 is a diffuse astrocytoma. Anaplastic astrocytoma's are classified as a grade III, and glioblastoma as grade IV (Eckel-Passow *et al.*, 2015).

1.2.1 Glioblastoma

Although glioblastoma is rare tumour with global incidence of less than 10 per 100,000 people, its poor prognosis with survival rate of 14-15 months after diagnosis makes it a crucial public health issue (Hanif *et al.*, 2017). It accounts for 50% of all gliomas in all age groups (Rock *et al.*, 2014). It can occur at any age, but the peak incidence is between 55 to 60 years (Ohgaki and Kleihues, 2007). The ratio of GBM incidence is higher in men as compares to women (Ohgaki and Kleihues, 2007; Thakkar *et al.*, 2014). The western world has higher incidence of gliomas then less developed countries (Thakkar *et al.*, 2014), which could be due to under reporting of gliomas cases, limited access to health care and differences in diagnostic practices (Fisher *et al.*, 2007). Glioblastoma is the most common type of brain tumour with over 65% of confirmed cases, though compared to other cancer types it is rare, with global incidence of less than 10 per 100,000 people (Hanif *et al.*, 2017). Patient outcome has an extremely poor prognosis with median survival at approximately 15 months, with survival greater than 2 years drastically reduced in less than 35% of patients (Brodbelt *et al.*, 2015).

1.2.2 Glioblastoma classification

Glioblastoma develops universally with tumour cells exhibiting high morphology and have significant genetic heterogeneity, encompassing a broad range of mutations, deletions and other genomic and epigenetic aberrations. (Howlader *et al.*, 2016). Glioblastoma cell morphology can drastically vary, furthermore the nuclei have membrane irregularities with typically oval or elongated shapes and hyperchromatic chromatin (Schultz *et al.*, 2005). A key distinguishing feature of glioblastoma cells from low grade tumours are large areas of necrosis often focused centrally in the tumour area, known as necrotic foci, which is habitually surrounded by pseudopalisading cellular areas, noted as a garland like arrangement of hypercellular tumour nuclei (Noch *et al.*, 2009). Since 1925, the classification of glial and CNS tumours has relied heavily of histological appearance of biopsy material. Modern classification of tumours stringently follows WHO guidelines which were updated in 2016 to include molecular subtyping to characterise different tumour sub-groups (Arevalo *et al.*, 2017). Pre-2016 glioblastoma was classified into 2 subgroups dependant on primary or secondary tumours. Primary glioblastoma accounted for greater than 90% of cases in adults and were defined as having a source of origination without any prior tumours, classed as de novo (Ohgaki and Kleihues, 2007). Secondary glioblastoma occurrence was classified by the development from a lower grade astrocytoma. Currently, classification of glioblastoma is based upon isocitrate dehydrogenase (*IDH*) mutation status (Arevalo *et al.*, 2017), determined by molecular analysis as shown in Figure 1.1. IDH is an enzyme that catalyses the oxidative decarboxylation of isocitrate, producing α-ketoglutarate and CO_2. There are 3 isoforms of IDH, which catalyse the third step of the citric acid cycle, IDH1 and IDH2 convert $NADP^+$ to NADH in the mitochondria whilst IDH3 uses NAD^+ as a cofactor instead. This step in the citric acid cycle is irreversible due to the large negative free energy change and is regulated to avoid depletion of isocitrate and the accumulation of the ketone alpha-ketoglutarate. Substrate availability (isocitrate, NAD^+ or $NADP^+$), product inhibition (NADH or NADPH) and competitive feedback inhibition (ATP) balance the reaction (Maeting et a., 2000).

Isocitrate dehydrogenase (IDH) mutation is a critical genomic alteration occurring in lower grade and secondary glioblastoma patients. *IDH* mutations primarily are seen in secondary glioblastoma subtypes and are rarely found in primary tumour tissue (Yan *et al*., 2009). More than 90% of IDH mutation is located at codon R132 of IDH1 gene and is responsible for the increased production of 2—hydroxyglutarate. This "oncometabolite" induces epigenetic alterations resulting in DNA global methylation and histone methylation (Yan *et al*., 2009; Korshunov *et al*., 2017). IDH mutation has been recognised as an early genomic event which is frequently retained during tumour progression from lower grades to high and has become a therapeutic target. However, clinical statistics have shown that overall survival in patients with IDH-mutations to be 31 months, compared to 15 months with those with IDH-wildtype (Kaminska *et al*., 2019). It has been suggested that the R132H mutation in IDH1 mutation reduces the malignant progression of glioma by causing a less aggressive phenotype of glioblastoma stem-like cells (GSCs) which are involved in the Wnt/β-catenin signalling, thus reducing proliferation, cell survival and invasion (Cui *et al*., 2016). IDH1 is responsible for the principle source of NADPH in the brain protecting it from oxidative stress via the catalysed production of α-ketoglutarate (KG) from the substrate isocitrate through oxidative decarboxylation (Bleeker *et al*., 2010). Additionally, IDH1 modulates insulin secretion therefore determining the cellular response to glucose concentrations (Guay *et al*., 2013). Mutations in IDH1 in secondary glioblastoma was initially identified in the TCGA project in 2008, which revealed the frequent occurrence of aberrant IDH1, as well as indicating the presence of wild type IDH1 in the primary glioblastoma cohort. The role of IDH1 as an early event in tumorigenesis in adult glioma has further been support in studies conducted since the TCGA project glioma (Horbinski *et al*., 2013). Recent data suggests IDH1 mutation is a less aggressive phenotype resulting in a reduced malignant progression of glioma (Yao *et al*., 2018).

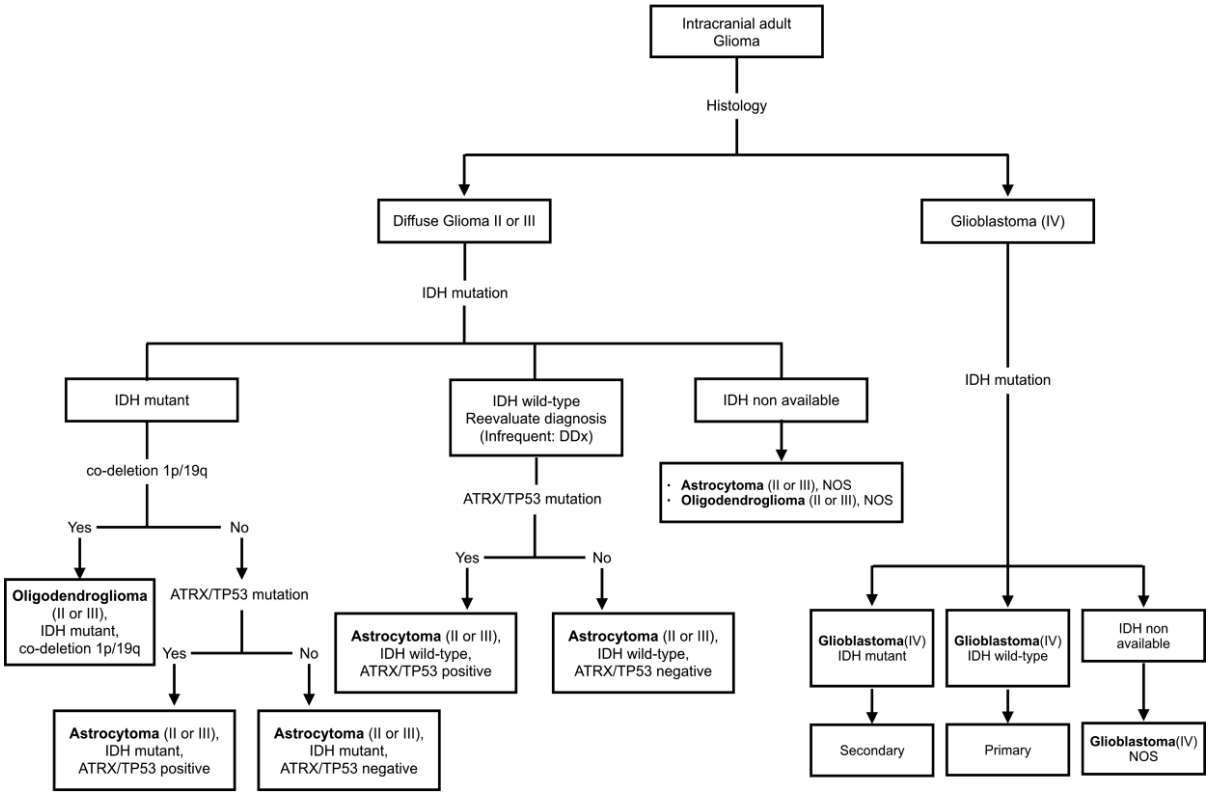

Figure 1.1 WHO classification of adult gliomas Primary stratification based on histological separation followed by IDH mutation status for the segregation of glioblastoma. Diffuse glioma are segregated based off co-deletion present on chromosome 1p/19q or the mutation of ATRX/TP53. GBMs are divided into two categories: IDH-wild-type (wt) GBM and IDH-mutant GBM. IDH-mutant GBM progresses from low-grade diffuse astrocytoma or oligodendroglioma. Oligoastrocytomas were omitted due to rarity. DDx, Differential diagnosis; IDH, Isocitrate dehydrogenase; ATRX, TP dependent helicase ATRX; T P53 Tumour protein p53; NOS, not otherwise specified (Arevalo *et al.*, 2017).

1.3 Treatment of GBM

The current treatment for glioblastoma is a multimodal approach which involves surgical resection of the tumour tissue, fractional radiotherapy treatment at 60Gy followed by concomitant chemotherapy with temozolomide (Stupp *et al.*, 2015). The foremost therapeutic agent used in the treatment of glioblastoma is the alkylating agent temozolomide (TMZ) since a study by Stupp *et al.* (2005) reported an increase in 2 year-survival 10.4% to 26.5% when patients were treated with TMZ in combination with radiotherapy. The effectiveness of TMZ treatment in glioblastoma is strongly determined by *MGMT* methylation status.

The current treatments have limited success with median survival only 14 months. Furthermore, considerable side effects (including nausea, fatigue, headaches and loss of appetite) are regularly associated, impacting on patient wellbeing (Goldberg *et al.*, 2004; Jordan *et al.*, 2005; Hesketh, 2008). Effective drug treatments are hindered predominantly by the complex genetic background of glioblastoma, with significant intra- and inter- tumour heterogeneity drastically limiting monotherapies (Backes *et al.*, 2015). The blood brain barrier (BBB) is an additional limitation for both the development and success of chemotherapeutic agents to be delivered to target the tumour, with its principle role to restrict the movement of potentially hazardous agents from reaching the brain tumour (Oberoi *et al.*, 2015). The BBB consists of several layers, the core of which is made up of specialised capillary endothelial cells, which form complex structures built up of transmembrane and membrane associated proteins (Feustel *et al.*, 2012). Tight junction structures are formed in-between adjacent cells and closely regulate the transport and signalling from the capillary (Luissint *et al.*, 2012). Additionally, astrocytes and pericytes accompany the endothelial cell complexes, where the astrocytes sheath the BBB, contributing and maintaining the endothelial cells and tight junctions (Hong *et al.*, 2015). Pericytes offer supplementary regulation of endothelial cell expression and the polarisation of astrocytes to the BBB (Armulik *et al.*, 2010). The BBB can facilitate several transport mechanisms to move required molecules into the brain tissue. Studies have shown, however, that glioma tumours can have an antagonistic effect upon both the structure and integrity of the BBB (Wong *et al.*, 2013). Glioma cells invade the perivascular area around the capillary, which leads to the displacement of astrocytic cells, resulting in the degradation of the BBB integrity. Consequently, reduction in pericytes ensues impeding regulatory processes and increasing permeability of the BBB to molecules by endothelial transcytosis (Watkins *et al.*, 2014; Armulik *et al.*, 2010). At the site of the blood brain tumour barrier (BBTB), the affected capillaries have an increased permeability in turn allowing for potentially easier vascular access to the tumour site (Deeken, 2007). Although damage to the BBB essentially increases the effectiveness of chemotherapeutic agents, the aggressive nature of glioblastoma cells results in migration and invasion

of areas away from the damaged BBTB site, into areas of functional sections of BBB, offering protection from drugs (Van Tellingen, 2015).

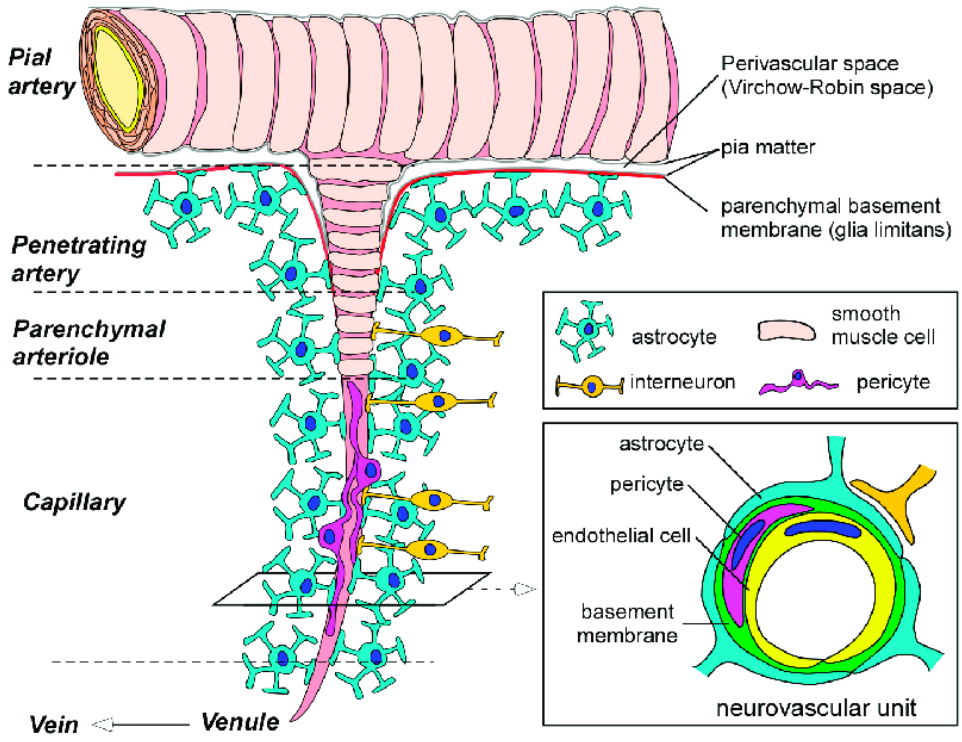

Figure 1.2 Composition and structure of the BBB The BBB is a multi-layered barrier regulating signalling and transport of molecules into brain tissue. Material exchange occurs at the endothelial cells in capillaries that are protected by tight junctions. Interspersed among the endothelial cells are pericytes that help regulate expression levels of near-by endothelial and astrocytic cells. Astrocyte cells wrap the BBB, and both regulate and maintain the BBB (from Yamazaki *et al.*, 2017).

It is well documented that cancer cells rely increasingly on the glycolytic pathway as the predominant mechanism for energy production, favouring it over the more efficient mechanism of oxidative phosphorylation, even with sufficient oxygen availability (Marie *et al.*, 2011). The metabolic reprogramming in tumour cells is known as the Warburg effect (Poteet *et al.*, 2013) and results in a high demand for glucose and large amounts of energy to maintain functional metabolism; however, the ability of tumour cells to use aerobic glycolysis confers a significant growth advantage (Zhao *et al.*, 2011). The increased dependence on glucose consequently leads to over production of lactate (Goodwin *et al.*, 2015), leading to an increase in lactic acid concentration and a lower pH in the tumour microenvironment. A higher

acidity in the tumour microenvironment subsequently suppress infiltrated immune cells by inhibiting T-cell secretion, resulting in a reduction in T-cell response, proliferation and cytokine production, contributing to tumour immune evasion (Wang, 2017).

One of the ways in which to modulate therapeutic strategies is through immunotherapy models with the aim of reprogramming the patients innate immune system to detect and mount an immune response against tumour cells. The technique requires patient samples, to which differentiated dendritic cells are presented to tumour biopsy cells, the primed dendritic cells are then transplanted back into the patient where they induce an aggressive T-cell response (Prins *et al.*, 2011). The method of priming a patient's immune cells for the detection of tumour cells allows for the potential targeting of numerous cellular targets. Additionally, vaccination with specific and non-specific antigens and the immunomodulation via pathway inhibition are potential treatments (Reardon *et al.*, 2014). An alternative to priming a patient's immune response is the use of monoclonal antibodies with the aim of interrupting receptor signalling through the competitive binding of cell surface receptors, resulting in a loss of downstream activation and the downregulation of the deregulated signalling pathway (Melstrom and sentovich, 2017). Bevacizumab is an example of a monoclonal antibody that is currently being utilized in a range of cancers, with the aim to reduce elevated levels of angiogenesis within tumours via the targeting and downregulation of the VEGF pathway. Recent data however has stated that the addition of Bevacizumab/monoclonal antibody treatment reaps no benefits when compared to standard treatment methods (Gilbert *et al.*, 2014), with the drawback that VEGF downregulation may induce tumour survival genes with the risk of increasing both the chemo-resistance and aggressive invasive behaviour of the cells (de Groot *et al.*, 2010).

The inhibition of dysregulated pathways in tumour cells is a key factor in the treatment for many cancer types. Advancements in nanotechnology has led to the development of small-molecule inhibitors (SMI) designed to block specific pathways and/or regulate epigenetic alterations occurring within the tumour. Previous studies revealed SMIs that were developed to induce both caspase activity and apoptosis

within tumour cells, however due to the relative complexity of development and construction cost many SMIs have not been put forward for the clinical trial process (Kitambi *et al.*, 2014). Amplification of EGFR and its active mutant EGFRvIII occur frequently in glioblastoma, currently 3 generations of tyrosine tyrosine kinase inhibitors (TKI) have been developed. Of the first generation, including Gefitinib, Erlotinib and Lapatinib it was concluded that they were not very effective in clinical trials in glioblastoma. Dacomitinib is a second-generation inhibitor which is demonstrating promising results in pre-clinical trial models (Reardon *et al.*, 2013; Zahonero *et al.*, 2015; An *et al.*, 2018). The advancement of technologies will inevitably lead to the creation of more effective inhibitory treatments (Arkin *et al.*, 2014).

An alternative therapeutic idea is the treatment of glioblastoma through the utilization of electromagnetic energy fields. The proposed idea is a wearable device which generates anti-mitotic electrical fields known as tumour treating fields (TTFields); studies have shown the TTFields to have contributed to a reduction in glioblastoma cell proliferation (Chaudhry *et al.*, 2015). The development of novel therapeutics in the treatment of glioblastoma offer optimism for a potential breakthrough from the stark prognosis of current care for afflicted patients.

1.4 Molecular biology of glioblastoma

In glioblastoma, genetic aberrations offer functional advantages to the tumour including increased chemoresistance, proliferation and survival and invasive traits. The identification of key mutations and genetic changes in tumour promoting and tumour suppressing genes is crucial to develop multifaceted approach to treatments.
It has long been understood that cancer is a disease of the genome, with genetic aberrations including mutations, deletions, copy number changes, and rearrangements (Hanahan and Weinberg, 2011). Multiple sequencing cohorts including the International Cancer Genome Consortium (ICGC) have identified a multitude of mutations occurring in key genes across more than 50 types of cancer (International network of cancer genome projects, 2010). The deregulation of several key pathways has been identified including p53, RTK/RAS/PI3K and the retinoblastoma protein (RB) (Tomczak *et al.*, 2015).

There is also a frequent occurrence of DNA-repair defects in cancer cells, leading to an increased mutation rate (Puente *et al*., 2011). More recently, research has highlighted the significance of mechanisms that contribute to gene silencing without alterations to the primary DNA sequence (Grasso *et al*., 2012). These epigenetic changes include DNA methylation and post translational histone modifications, which are stable and can be inherited and have been shown to contribute to oncogenic progression (Baylin and Jones, 2011). The combined effect of genetic and epigenetic disruptions results in stable phenotypic changes (You *et al*., 2012; Timp *et al*., 2013) and mutations in epigenetic regulators have been characterised in a range of cancer types including renal cell carcinoma (Varela *et al*., 2011) , bladder cancer (Gui *et al*., 2011), hepatocellular carcinoma (Fujimoto *et al*., 2012) and adult brain tumours (Sturm *et al*., 2012). Additionally, epigenetic inactivation of DNA repair genes such as *MGMT* and *BRCA1* has also been confirmed, resulting in elevated mutation incidences and genomic instability (Esteller *et al*, 2000; Hedenfalk *et al*., 2001). The understanding of the relationship between genetic and epigenetic changes is of increasing importance in the progression of cancer research.

Glioblastoma have been shown to possess multiple genetic aberrations, including nucleotide substitutions, chromosol abnormalities and divergent epigenetic alterations (Cancer Genome Atlas Research Network, 2008). The advancement in high-throughput molecular biology techniques over the last few years along with the establishment of large scale, multi-dimensional research projects with the aim of detailing the genetic variations present within tumour tissue has resulted in some improvement in our knowledge of these tumours. The Cancer Genome Atlas (TCGA) resource collates and catalogues genetic data across multiple human tumours (Kim *et al*., 2018). The TCGA data for glioblastoma was initially analysed in 2015, determining key genetic features (Tomczak *et al*., 2015). Studies have established the deregulation of multiple pathways in glioblastoma including p53 and retinoblastoma protein (RB), RTK/RAS/PI3K, the epidermal growth factor receptor (EGFR) and isocitrate dehydrogenase (IDH) (Verhaak *et al*., 2010). Furthermore, the multidrug resistance protein-1 (MDR-1), which is part of the ATP-binding cassette transporter superfamily has been shown to be upregulated and over-expressed in

glioblastoma, allowing the removal of chemotherapeutic agents from the cancer cells (Munoz *et al*., 2014; Alifieris and Trafalis, 2015). Recent advances in genetic high throughput screening of glioblastoma tumours have identified distinct subtypes, Proneural, Neural, Classical and Mesenchymal. The subtypes present different genetic abnormalities, survival length, patient age and treatment response (Meyer *et al*.,2015).

1.4.1 PI3K/Akt pathway alterations

The tumour suppressor protein phosphatase and tensin homolog (PTEN) regulates the P13K/AKT pathway, ultimately controlling cell growth, survival and the progression of the cell cycle. Mutations, amplifications and deletions affecting the PI3K complex have been shown to occur in glioblastoma (Benitez *et al*., 2017; Chen *et al*., 2018), with *PTEN* mutations leading to increased tumorigenicity via macrophage recruitment and chemoresistance by histone regulation. The loss of *PTEN* i*n vitro* has been shown to promote cell survival, tumorigenesis and chemosresitance in glioblastoma cells (Parsa *et al*., 2007; Zheng *et al*., 2008). PTEN functions as a feedback regulation mediating the PI3K pathway through the dephosphorylation of PIP3 and the consequent inhibition of Akt activation. *PTEN* mutations are present in approximately 25-40% in adult glioblastoma, and loss of heterozygosity in 60% to 80% of all cases (Zarghooni *et al*., 2010; Barrow *et al*., 2010; Brennan *et al*., 2013; Shin *et al*., 2019). Studies have shown AKT to stimulate the expression of glucose transporters which enhances glucose uptake, and directly phosphorylates enzymes such as Hexokinases, committing glucose to the glycolytic pathway and driving the Warburg effect (Elstrom *et al*. 2004; Robey and Hay 2009). Figure 1.3 details the Akt pathway.

1.4.2 EGFR alterations

Epidermal growth factor receptor (EGFR) is a transmembrane receptor tyrosine kinase (RTK) with an extracellular domain which is activated by extracellular ligands including growth factors, cytokines and hormones to initiate the activation of intrinsic tyrosine kinase activity (Krause and van Etten, 2005). The binding of the ligand leads to phosphorylation which consequently activates Ras further inducing the

MEK/ERK1/2 and MAP3K pathways as well as the activation of PI3K complex resulting in the upregulation of Akt and mTOR (Cancer Genome Atlas Research Network, 2008). The signalling cascades ultimately regulate cellular division, differentiation and migration (Delgado-Lopez and Corrales-Garcia, 2016). Deregulated RTK signalling has been shown (Rusten *et al.*, 2007; Abella *et al.*, 2009) to be a fundamental mechanism utilized by tumour cells to avoid regulatory growth controls with mutation or overexpression of key genes often contributing to the development of various cancers. Gene amplification and/or mutations in EGFR are found in approximately 60-85% of glioblastoma (Brennan *et al.*, 2013) and overexpressed levels demonstrated in 40% of glioblastoma, responsible for increased proliferation levels and resistance to radiotherapy (Monga *et al.*, 2017; Xu *et al.*, 2017) The active mutant EGFR variant EGFRvIII occurs frequently in glioblastoma, which is usually present in gene amplification, generated by the deletions of exons 2-7. The resulting amplification leads to a truncated protein which is constitutively phosphorylated playing a critical role in pathogenesis inducing increased cell differentiation and proliferation (Pollack *et al.*, 2006; Zadeh *et al.*, 2013). Current treatments, EGFR-tyrosine kinase inhibitors (TKIs) have shown limited efficacy in patients (An *et al.*, 2018). A review of 6 phase III clinical trials incorporating 2697 patients was conducted, which concluded that the effect of TKIs on patient outcome depended on EGFR status. It was suggested that chemotherapy benefited patients with wild type EGFR, and TKIs benefited patients with EGFR mutations, concluding that TKIs might be unsuitable for unselected patients (Vale *et al.*, 2015). Furthermore, most clinical trials of EGFR TKIs have been restricted to patients with tumours demonstrating harbouring common EGFR mutations, excluding those with uncommon EGFR mutations (Park *et al.*, 2019).

1.4.3 p53 pathway alterations

p53 has a key role regulating and suppressing tumour development through its wide range of functions which include the detection of DNA damage as well as regulating cell division and is the most common mutation to be found in all human cancers (Kandoth *et al.*, 2013). The p53 and RB pathways interconnect to regulate cell division, predominately in the G1/S phase of the cell cycle arrest (Sherr and

McCormick, 2002). p53 is upregulated under cell stress, such as DNA damage by the alternative reading frame (ARF) protein, which leads to the inhibition in the cell cycle progression and the promotion of apoptosis (Basu and Murphy, 2016). Mutations in *p53* are more common in IDH^{mut} glioblastoma tumours in approximately 60-70% of cases compared to IDH^{wt} glioblastoma tumours where the rate is approximately 25-30% (England *et al.*, 2013). *p53* mutations result in the reduction of mRNA and protein expression or its modification leading to deregulated DNA binding. A study found that PGC-1α, a known positive regulator of metastasis is bound by mutant forms of p53 and was associated with increased metastasis and poor prognosis in breast cancer (Basu *et al.*, 2018). Dysfunctional p53 allows for the tumour cells to exploit molecular pathways, in the absence of transient or permanent growth arrest, increasing the potential invasive and proliferative capabilities as well as increased migration, drug resistance, angiogenesis and overall progression of cell cycle survival (Nguyen *et al.*, 2014).

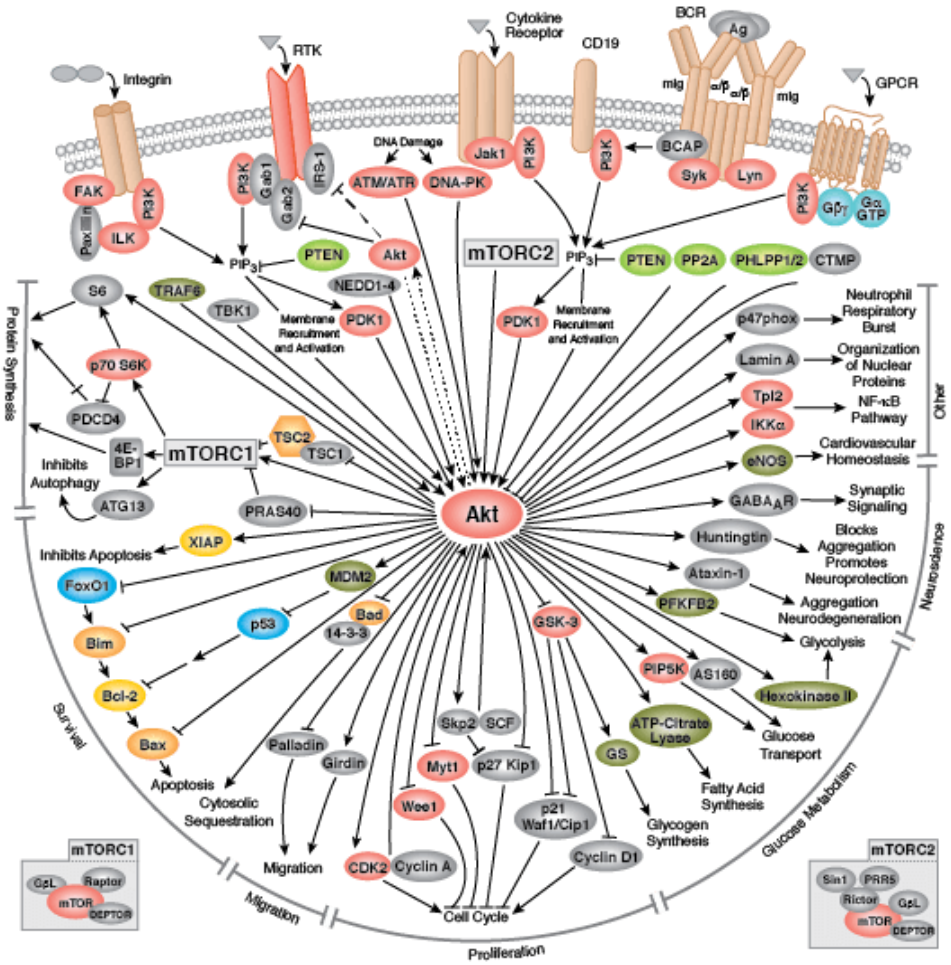

Figure 1.3. **The AKT signalling pathway** AKT is activated by PI3K, which itself is activated by several upstream signalling pathways such as insulin receptors, RTKs and cytokine receptors, including EGFR. AKT targets several downstream molecules changing their activity by phosphorylation or complex formation. AKT is involved in cell proliferation, glucose metabolism, cell survival, cell cycle, protein synthesis, and in neuronal morphology and plasticity by regulation of several downstream molecules shown in this figure. AKT regulates glucose metabolism through regulation of GSK-3, and HK2. It also interaction with mTOR signalling affect protein synthesis (Cellsignal, 2019).

1.5 The role of epigenetics in cancer

The concept of epigenetics emerged in the 1940s, with initial studies focused on the interactions between genes leading to specific phenotypes (Goldberg *et al*, 2007). The significant increase in the understanding of epigenetics has revealed their important role in the modification of mechanisms in both healthy and disease states (Stephens *et al*., 2013). Epigenetics broadly refers to the stable and heritable phenotypic changes within a cell, whilst the primary DNA sequence is left unchanged. DNA methylation, histone modification and non-coding RNAs are the primary mediators of epigenetic modifications (Bernstein *et al*., 2007). Studies have shown that the interactions between the epigenetic mechanisms are synchronised and regulated, and are essential for the propagation of precise gene expression profile patterns for healthy developmental processes (Stephens *et al*., 2013); Furthermore, disruptions in these regulatory mechanisms have been shown to lead to aberrant gene expression and signalling pathways as commonly exhibited in cancer cells (Sharma *et al*., 2010).

1.5.1 DNA methylation

DNA methylation involves the covalent transfer of a methyl group (-CH3) from S-adenosylmethionine (SAM) to the 5‵carbon on the cytosine (C) moieties within the cytosine-guanosinedinucleotides (CpGs) resulting in the formation of 5-methylcytosine (5mC) (Bernstein *et al*., 2007). CpG sites are located across the entire genome, with some distributed in distinct clustered regions known as CpG islands (CGIs). These regions are defined with approximately the GC content at 55% across a 500bp area with an expected CpG ratio of 0.65 (Takai and Jones, 2002). The CpG islands frequently span the vicinity surrounding gene promotor regions covering approximately 60% of human gene promoters. The CpG island are also associated with transcription start sites (TSSs) and cover the area of first exons

(Sharma *et al.*, 2010). Studies have shown CpG islands to be regularly present often in an unmethylated state in both housekeeping and tissue-specific genes (Hackenberg *et al.*, 2010). The methylation of DNA is crucial for maintaining chromosomal stability through the prevention of potentially harmful regions of the genome being transcribed, including areas containing repeat elements and viral inserts (Herman and Baylin, 2003). DNA methylation is highly regulated by DNA methyltransferases (DNMTs) which add methyl groups or DNA demethylases which conversely remove methyl groups (Stephens *et al.*, 2013). The DNA methyltransferase family comprises a range of enzymes including DNMT1, DNMT3 (DNMT3A, DNMT3B) and DNMT3L, where both DNMT3A and DNMT3B can initiate methylation of CpG sites independently from replication, on unmethylated and hemimethylated DNA (Herman and Baylin, 2003) and have been shown to have a significant role in maintaining methylation activity at repeat elements (Liang *et al.*, 2002; Chen *et al.*, 2003). The maintenance methyltransferase, DNMT1 functions during replication and commonly initiates methylation on hemimethylated DNA (Bashtrykov *et al.*, 2012). DNMT3L is absent of catalytic ability and its primary function is to enhance the methyltransferase activities of the other members of the methyltransferase family (Jurkowska *et al.*, 2010; Neri *et al.*, 2013). DNA demethylases also influence the activity and function of DNA methylation, consisting of activation-induced cytidinedeaminase (AID), apolipoprotein B mRNA-editing enzyme 1 (APOBEC1) and ten-eleven translocation (TET) (De Carvalho *et al.*, 2010, Ito *et al.*, 2010). The primary function of the DNA demethylases is the oxidation of 5-methylcytosine to 5-hydroxymethylcytosine, a reaction primarily catalysed by the TET family and further augmented by AID and APOBEC1 proteins leading to the demination forming cytosine (Pastor *et al.*, 2013).

Although the mechanism of DNA methylation mediated gene silencing is not fully understood, there are two proposed methods. The first determines that the addition of the methyl group physically inhibits the direct binding of transcription factors (TFs), such as c-Myc/Myn and NFκB, which have recognition sites containing CpG sites and have been shown to be inhibited by methylation (Hervouet *et al.*, 2009). The other proposed model involves the binding of methyl-CpG-binding proteins (MBPs) to CpG sites, competitively blocking the binding of TFs. There are currently

three identified families of MBPs, which are responsible for the contribution of transcription repression (first group), and the detection of methylated DNA via specialised zinc finger domains (second group) (Unoki *et al*, 2004).

1.5.1.2 DNA methylation in cancer

Perturbed methylation patterns in tumour cells are a regular occurrence in a range of cancer types, frequently manifesting as global hypomethylation, or region-specific hypermethylation, dependant on the normal basal methylation level within a specific tissue-type (Zhang*et al*., 2013). DNA methylation patterns in glioblastoma were analysed in the TCGA cohort, which revealed a subgroup of gliomas with a specific DNA methylation status. The subset of glioblastomas demonstrate concerted hypermethylation across a large number of loci, classified as the glioma-CpG island methylator phenotype (G-CIMP) (Nagarajan *et al*., 2014).

A study determined that the G-CIMP phenotype to be associated with an IDH-mutant origin, of which two additional clinically relevant subsets of G-CIMP tumours exist, G-CIMP-high and G-CIMP-low, dependant on the degree of DNA methylation, thus enabling further refinement of glioma classification and improving the prediction of patient outcome independent of grade and histology; with the potential enhancement of effective therapeutic strategies tailored to each patient. (Malta *et al*., 2018).

Patient prognosis is inferior with initial diagnosis of G-CIMP-high subtype in primary glioma tumours, however in recurrent tumours G-CIMP-low has been shown to have a poorer clinical outcome (Ferreira de Souza *et al*., 2018), and is defined as mimicking IDH-wild-type and stem cell-like primary glioblastoma. The occurrence of genome-wide DNA hypomethylation in cancer cells as long been established as a recurrent epigenetic alteration. The changes in DNA methylation in normal and tumour cells is illustrated in Figure 1.4.

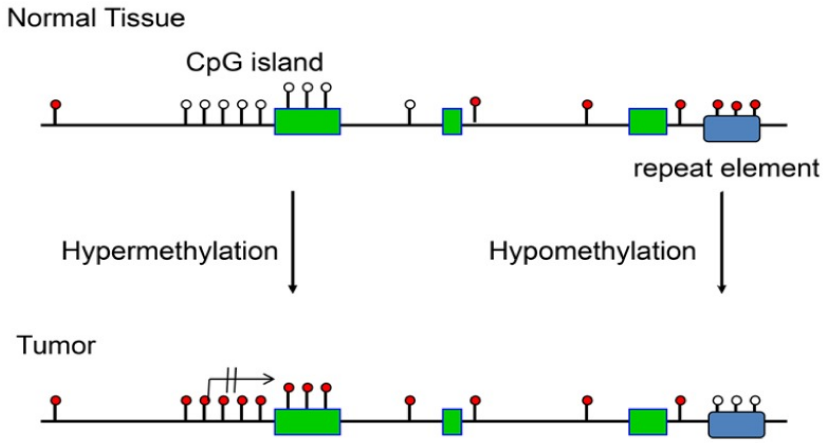

Figure 1.4. Changes in DNA methylation of tumour suppressor genes in normal and tumour cells Outline of the most relevant DNA methylation changes observed in human cancers. Includes CpG-island-specific DNA hypermethylation occurring at gene promoters, locking the affected gene into an inactive state. Loss of DNA methylation (hypomethylation) occurs genome-wide and is often observed at repetitive regions of the genome, leading to overexpression. White circles indicate unmethylated CpG sites and red circles show methylated CpG sites. The crossed-out arrow indicates the transcription start site and the permanent lack of transcription after DNA methylation. Green boxes show exons and the blue rectangle marks the position of a repetitive element (from Pfeifer, 2018).

Studies have shown that the loss in global methylation can lead to adverse effects, supporting tumorigenic conditions associated with malignant development in a range of cancer types including adult glioblastoma (Cadieux *et al*., 2006). An example of a hypomethylated gene associated with tumour progression is the protease urokinase *(PLAU/uPA),* which has been shown to be both hypomethylated and overexpressed in breast cancers (grades 1, 2 and 3) and prostate cancers (Ehrlich, 2009). A recent study identified novel hypomethylated genes, cytoplasmic polyadenylation element binding protein (*CPEB1)*, PR-domain zinc finger protein 16 (*PRDM16*) and LIM domain only 3 (*LMO3*) in glioblastoma, all of which showed increased levels of expression; however, a cause-and-effect relationship of their molecular mechanisms was not established (Li P and Wu M, 2017). Global hypomethylation has been associated with the activation of transcriptional proto-oncogenes, such as *HRAS* in melanoma. Hypomethylation has been shown to lead to genomic instability and

mitotic recombination, resulting in translocations, deletions, viral oncogenes, and growth-related imprinted genes like *IGF* (Ehrlich, 2009). Additionally, hypomethylation has also been associated with the reactivation of various transposable elements including long interspersed nuclear elements (LINEs) responsible for reverse transcriptase, where hypomethylation of LINE-1 located in the *MET* onco- gene is associated with bladder cancer tumorigenesis (Wolff *et al*., 2010). Studies have shown the effects of increased methylation across promotor specific DNA has been linked with the inactivation of tumour suppressor genes as a prevalent event in tumour development (Jones *et al*., 2002). Hypermethylation is also linked with cancer development through the inactivation of regulatory genes involved in a variety of cellular processes including apoptosis, metastasis, cell cycle, angiogenesis and metabolism (Herman and Baylin, 2003). Examples of hypomethylation include the deregulation of *RB* in renal cell cancers (Herman *et al*, 1994) and the disruption of DNA repair genes such as *BRCA1* resulting in a decreased capacity for cells to repair genomic errors, contributing to the susceptibility of tumour formation (Esteller, 2002). Recent research has focused on the identification and classification of hypermethylated genes as a tool for stratification of response to therapeutic agents, for example the O6-methylguanine–DNA methyltransferase (*MGMT*) status in predicting the response with the use of TMZ in the treatment of glioblastoma (Weller *et al*., 2009).

1.5.1.3 MGMT methylation status

O6-methylguanine–DNA methyltransferase (*MGMT*) is a DNA management and repair gene The *MGMT* enzyme removes guanine at the 06 position, impacting the effectiveness of alkylating agents such as the commonly used therapeutic agent TMZ in glioblastoma (Esteller *et al*., 2002; Bell *et al*., 2018). In approximately 45% of glioblastoma tumours, the promotor region of *MGMT* is hypermethylated and these patients have a significantly better outcome due to increased effectiveness of alkylating agents in the absence of the DNA repair mechanism (Hegi *et al*., 2005; Oliver *et al*., 2014). A recent study analysed *MGMT* correlation with survival in a well-characterized cohort of 111 IDH wildtype glioblastoma patients, it was concluded that *MGMT* correlated with significantly improved progression-free survival

(PFS) and overall survival (OS). Median PFS was 7.2 months in the unmethylated group compared to 19.83 months in the highly methylated group and median OS was 13.4 months in the unmethylated group compared to 29.93 months in the highly methylated group (Radke *et al.*, 2019). *MGMT* methylation status has become a clinical marker determining the effectiveness of the standard glioblastoma treatment (Molenaar *et al.*, 2014).

1.5.2 Non-coding RNAs/ Micro RNAs

Non-coding RNAs are fundamental in the regulation of gene expression (Ling *et al.*, 2015). Micro RNAs (miRNAs) which are short non-coding regions of RNA up to approximately 30 base pairs. miRNA have a significantly important function in post-transcriptional regulation and the silencing of other RNAs (Santa-Maria *et al.*, 2015). Their regulation can modify and influence a range of cellular processes such as proliferation, survival, differentiation and motility (Christopher *et al.*, 2016). miRNAs are predominantly located intra-cellularly although their regulatory effects can be detected extracellularly, recent research has focused on the detection of circulating miRNAs in blood plasma as a clinical biomarker for a range of diseases including cancer (Pirola *et al.*, 2015). Studies have shown the occurrence of variations in the expression profile of miRNA associated with cancer cells (Butkytė *et al.*, 2016). miRNA strands are incorporated into a miRNA-induced silencing complex (miRISC) (Fabian and Sonenburg, 2012), which has the facility to bind to mRNA sequences within the cytoplasm, resulting in the silencing of the mRNA as a consequence of the loss of ability for ribosome translation template (Sheu-Gruttadauria *et al.*, 2018). miRNA binding to mRNA acts as a post transcriptional method of silencing subsequently leading to the degradation of the bound mRNA (Michlewski and Cáceres, 2019).

1.5.2.2 miRNA in cancer

Dysregulation in both mRNA and miRNA is a recurrent event in tumour cells (Lin *et al.*, 2015; Hata and Lieberman, 2015). The role of miRNA in tumorigenesis often varies dependant on the individual miRNA, which can contribute towards an oncogenic or tumour suppressive affect. For example, overexpression of miR-21 is

present in most cancer types including glioblastoma (Yang *et al.*, 2013). Its primarily targets the *FBX011* tumour suppressor gene, resulting in a loss of expression. Additionally, in glioblastoma, miR-21 has been strongly associated with impacting the p53 and mitochondrial apoptosis pathways (Papagiannakopoulos *et al.*, 2008). The significantly increased expression of miR-21 is associated with chemo and radio-resistance in glioblastoma (Maachani *et al.*, 2016). TCGA data obtained from the glioma cohort revealed the impact of miR-148a and miR-31 in the development of glioblastoma, the miRNAs were shown to influence hypoxia-inducible factor 1-alpha promoting both tumour growth and increasing angiogenesis. The identification and stratification of individual miRNAs role in cancer is challenging, studies have shown that specific miRNA can have alternative roles in different cancer types. An example is miR-222 where (Fuse *et al.*, 2012) demonstrated it to be detrimental in prostate cancer acting as a tumour suppressor, however (Zhang *et al.*, 2010) revealed miR-222 to positively impact prognosis in glioblastoma via regulation of cellular apoptosis.

1.6 Cancer as a metabolic disease

1.6.1 The glucose pathway

The high mutation rate in cancer cells leads to aberrant cellular metabolism and alterations of these metabolic pathways significantly contribute in the development and growth of many tumours (Cantor and Sabatini, 2012; DeBerardinis and Tompson, 2012). It is well documented that cancer cells require increased amounts of energy in order to maintain the augmented rates of proliferation and survival (vander Heiden *et al.*, 2009; Kami *et al*, 2013). Normal cells predominately produce energy via oxidative phosphorylation (OXPHOS). In contrast, cancer cells undergo a metabolic transformation relying increasingly on the glycolytic pathway as the predominant mechanism for energy production, favouring it over the more efficient OXPHOS even when sufficient oxygen is available (Marie *et al.*, 2011). The switch from OXPHOS to glycolysis, along with the associated accumulation of lactate by-products in the tumour microenvironment, characterises the best known alteration in

cancer cell metabolism, the phenomenon known as aerobic glycolysis or the "Warburg effect" (Gatenby and Gillies, 2004; Vander Heiden *et al*. 2009; Goodwin *et al*., 2015). This metabolic switch results in increased acidity from by-products in the tumour microenvironment which promotes cancer cell adaptation and aids in the development of the tumour niche (Gatenby and Gillies 2004). The prevailing view as to the function of the metabolic switch is the production of cellular energy in the form of ATP, where glycolysis has been shown to drive ATP production at an increased (albeit less efficient) rate in comparison to ATP production via mitochondrial OXPHOS, and this is essential to support the increased energy demands in cancer cells (Cairns *et al*., 2011). Aerobic glycolysis also benefits tumour cells allowing the cells to adapt to intermittently hypoxic conditions, a common occurrence in poorly vascularised tumours.

Although different cancers develop through abnormalities in different pathways, the metabolic requirements for the tumour cells are very similar, involving the pathways to support core functions like anabolism, catabolism, and redox balance. Normal cells activate PI3K and the downstream pathways AKT and mTOR, promoting an anabolic agenda involving increased glycolytic flux and fatty acid synthesis (Yuan and Cantley, 2008).Comparatively tumour cells must produce energy in the form of ATP in order to produce precursors for macromolecule biosynthesis for the support of cell growth development, whilst managing the oxidizing effects as a result from their increased metabolism through the reduction of ROS damage (Cairns *et al*., 2011). The tumour cells frequently contain mutations associated with the PI3K-AKT-mTOR pathway resulting in an increased level of signalling activity, whilst often bypassing extrinsic stimulation by growth factors (Fruman *et al*., 2017). Many oncogenes and tumour suppressors are involved in the PI3K-AKT-mTOR network, and aberrant activation of this pathway is common in a diverse set of cancers (DeBerardinis and Tompson, 2012). There is evidence that cancer cells undergo continuous metabolic reprogramming to ensure they are utilizing the most effective method of producing cellular energy (Phan *et al*., 2014). Cancers are often auxotrophic for specific non-essential amino acids, resulting in abnormalities in amino acid biosynthetic pathways. This is advantageous as metabolic reactions

involved in the synthesis of non-essential amino-acids are high energy-consuming (Zhang and Yang, 2013). An example is serine metabolism which is frequently dysregulated in cancers, most commonly melanoma and breast cancers (Locasale *et al*., 2011, Possemato *et al*., 2011) and in gliomas (Liu *et al*., 2013). In many cases, extracellular serine is sufficient to support cancer cell proliferation, however an increase in serine synthesis from glucose even in the presence of abundant extracellular serine is present in some cancer cells. A recent study suggested that increased serine synthesis may be a resultant requirement to facilitate amino acid transport, folate metabolism and nucleotide synthesis (Mattaini *et al*., 2016). Recent therapeutic approaches have been designed to inhibit tumour cell glycolysis, including the inhibition of critical steps in the pathway, such as those catalysed by lactate dehydrogenase (LDH) and hexokinase 2 (HK2) (Le *et al*. 2010; Wolf *et al*. 2011).

1.6.2 Hexokinase

An overview of the glycolytic pathway is shown in Figure 1.5. *Hexokinase* (HK) has a crucial role catalysing the initial step of the pathway, the ATP-dependent phosphorylation of glucose to yield glucose-6-phosphate (G6P). The phosphorylation of glucose to G6P promotes a concentration gradient enabling glucose entry into cells thus facilitating the major glycolytic pathways. *Hexokinases,* therefore, influence the magnitude and direction of glucose flux within cells (Patra *et al*., 2013). There are four major *HK* isoforms expressed in mammalian tissues, encoded by separate genes, Cairns *et al*, (2011) comprising *HK1, HK2, HK3*, and *HK4* (also known as glucokinase), they share common biochemical properties, but their fundamental enzymatic activity and tissue distribution vary (Robey and Hay, 2006). HK1, HK2, and HK3 are high-affinity isoforms, whereby HK1 and 2 are inhibited by excess of G6P and HK3 by physiological concentrations of glucose (Wilson, 2003). HK4 has a low affinity and is predominantly expressed in liver hepatocytes and pancreatic β-cells. HK1 and HK2 are associated with mitochondria and are implicated in cell survival and proliferation (Gottlob *et al*., 2001, Majewski *et al*., 2004). Unlike HK1, which is expressed in most mammalian adult tissues, HK2 is only expressed in

a select number of adult tissues including adipose, skeletal, and cardiac muscles, however it is highly expressed in embryonic tissues (Wilson, 2003). The *HK2* gene is located on chromosome 2p12 and consists of 60,705 bases, containing 19 exons and 17 introns, and a promoter region of approximately 4 kb. Studies have shown HK2 to be abundantly and selectively overexpressed in a range of cancer types arising in tissues that normally express only HK1, including lung and breast (Mathupala *et al*., 2001; Wang *et al*., 2014; Anderson *et al*., 2016. There is evidence that *HK2* overexpression in cancer cells promotes tumour invasion as well as enhanced resistance to chemotherapy (Wolf *et al*., 2011). HK2 binds to the outer mitochondrial membrane via a mitochondrial binding motif at the N-terminal. HK2 bind to the outer mitochondrial membrane protein voltage-dependent anion channel 1 (VDAC1), forming a contact site between the outer and inner membranes of the mitochondria initiating opening of the channel (Palmieri *et al*., 2009). The mitochondrially bound HK2 enables preferential access of ATP generated by mitochondria, whereby the ADP generated by mitochondrial HK2 catalytic activity is transferred back into the mitochondria to be re-phosphorylated to further fuel the glycolytic metabolic advantage (Roberts *et al*., 2015). Additionally, the binding to mitochondria undergoes feedback inhibition by G-6P. The association of HK2 overexpression mediating cell survival may partly be due to the activation of Akt, which stimulates expression of both glucose transporters and maintains the HK2-VDAC complex, which has been shown to prevent the release of cytochrome C (Cyt C) consequently inhibiting apoptotic mechanisms (Okatsu *et al*., 2012). It has been proposed that HK2 competitively competes with pro-apoptotic proteins, suppressing the activation of BAX and BAK which are important mediators of mitochondrial membrane permeability. This has been shown in glioblastoma and in HeLa cells, where the binding of HK2 to mitochondria inhibited the mitochondrial translocation of Bax and the release of cytochrome c (Wolf *et al*, 2010; McCommis *et al*., 2012). The study also showed HK2 ability to interact with the mitochondrial permeability transition pore (PTP) in response to Akt pathway activation, thus impacting the regulation of the intrinsic apoptotic pathway (McCommis *et al*., 2012). The association between HK2 and mitochondria in inhibiting cell apoptosis is also recognized as a key factor in survival of glioma cells (Neary *et al*, 2013; Zhuo *et al*., 2015; Vartanian *et al*., 2016).

HK2 also protects against molecular changes such as oxidative stress, whereby its kinase activity bound to the mitochondrial membrane contributes to the inhibition of mitochondrial death pathways (Roberts *et al.*, 2015). A plausible explanation for the selective overexpression of the HK2 isoform in cancer cells may be due to HK2 possessing two active catalytic domains in its amino- and carboxy- termini, in comparison HK1 only possess a single active catalytic domain in its carboxy-terminus. The two catalytic domains have different kinetic properties more suited for the metabolic nature of cancer cells with the advantage of HK2 retaining activity under conditions that are inhibitory for the single catalytic domain (Wilson, 2003). Recently, selective inhibitors have been developed to target HK2 in order to reduce tumour growth and aggression with minimal adverse effects (Lin *et al.*, 2016). Currently, there are no effective treatments targeting HK2. Notably the one of the most common positron emission tomography (PET) radiolabelled tracer molecules used is 18F-fluorodeoxyglucose (18F-FDG), which is a radiolabelled glucose molecule which can be utilised to determine sites of abnormal glucose metabolism and to characterise and locate many tumours, including gliomas, oesophageal and breast (Hui *et al.*, 2018). Overexpression of HK2 in glioblastoma is not fully understood, however its selective overexpression in cancer cells and relatively restricted distribution in normal adult tissues proposes an attractive potential selective target for cancer therapy with nominal side effects to healthy cells.

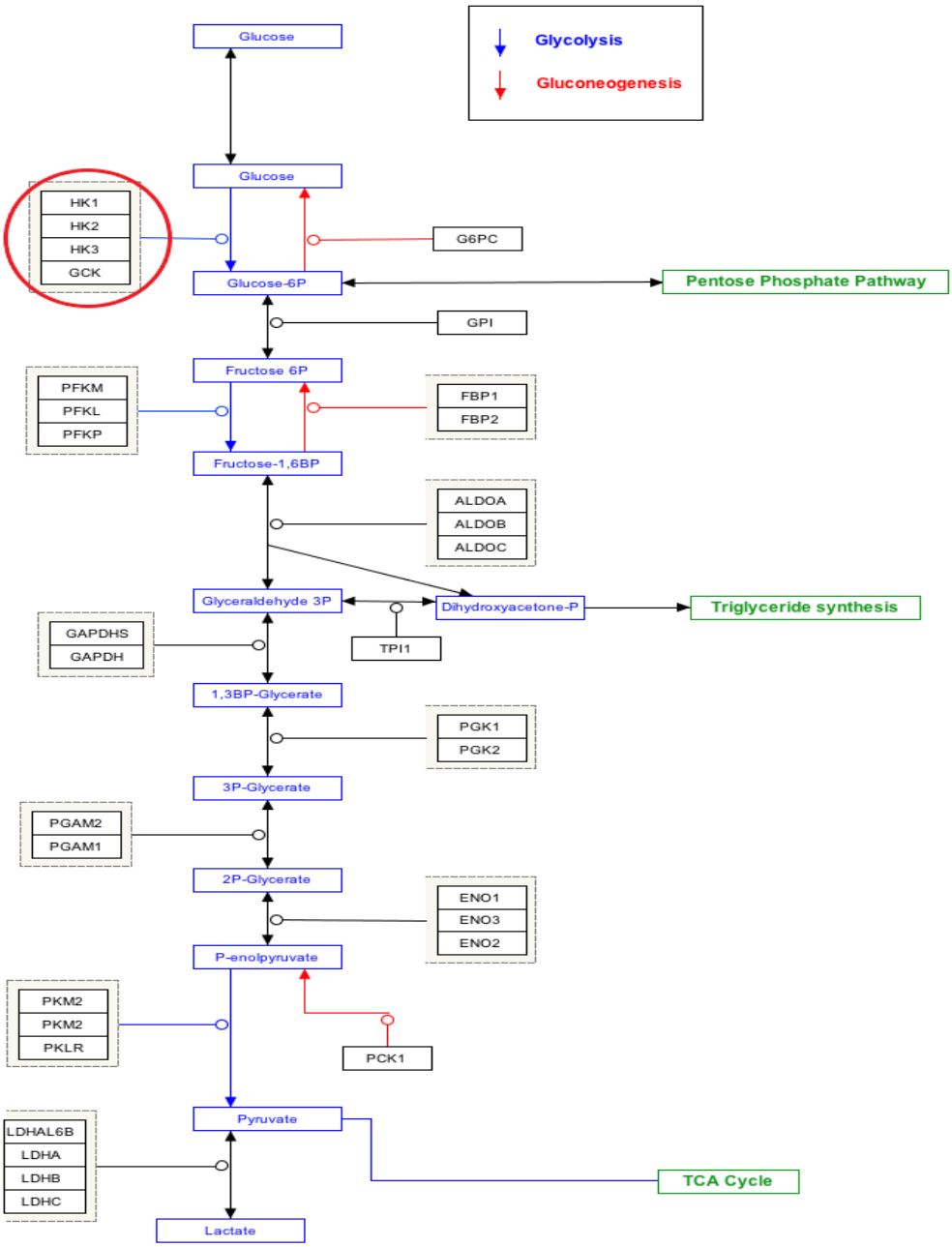

Figure 1.5. The glucose pathway in cancer cell metabolismHK is highlighted, its crucial role catalysing the initial step of the glycolytic pathway, the ATP-dependent phosphorylation of glucose to yield glucose-6-phosphate (G6P). HK2 overexpression has been established in a range of cancers (from Bricker *et al.*, 2012).

1.6.3 The Pentose Phosphate Pathway

Sufficient levels of NADPH are crucial for rapid cell growth and proliferation and to ensure an adequate level is maintained, cells can use an alternative route of glucose metabolism called the pentose phosphate pathway (PPP). The PPP is predominantly

anabolic and is responsible for producing ribose sugars which in turn are utilized in nucleotide biosynthesis and NADPH production (Cairns *et al*., 2011). Glucose-6-phosphate (G6P) lies at the start of two pathways, glycolysis and the pentose phosphate pathway. It may be isomerized to fructose 6-phosphate by phosphoglucose isomerase (PGI) when cellular needs are for energy or carbon skeletons for synthesis. Alternatively, for increased NADPH production, G6P is oxidized by G6P dehydrogenase (G6PDH) in an irreversible reaction as the initial step of the pentose phosphate pathway (Patra *et al*., 2013). The PPP also facilitates the generation of nucleotide precursors of DNA for growth and synthesis via G6P being dehydrogenated initialising biosynthetic pathways that support anabolic growth (Cairns *et al*., 2011).

1.6.4 *Pyruvate Kinase M2*

The production of biosynthetic precursors via the tricarboxylic acid cycle (TCA) is regulated by pyruvate kinase in a rate limiting step in the glycolytic pathway. In healthy cells, phosphoenolpyruvate (PEP) to pyruvate is catalysed by pyruvate kinase M1 (PKM1) with the associated phosphorylation of ADP to ATP for energy production. Conversely, the embryonic isoform of pyruvate kinase, PKM2 is expressed in tumour cells (Christofk *et al*., 2008; Vander Heiden *et al*., 2010). PKM2 is a fundamental driver of aerobic glycolysis and has been associated with increased cell proliferation through the promotion of Mammalian target of rapamycin (mTOR) pathway (Ye *et al*., 2012). PKM2 promotes anabolic growth via the interaction with hypoxia-inducible factor 1 (HIF1) which promotes the activation of HIF-responsive genes (Brocato *et al*., 2014). PKM2 exists in the catalytically distinct tetrameric and dimeric states, its tetrameric form exhibits high catalytic activity and has been linked to catabolic metabolism and ATP synthesis. Comparatively PKM2 in its dimeric state has a low catalytic activity and a less active state, it has been associated with nucleotide synthesis and facilitating the production of glycolytic intermediates to enter the glycolysis pathway including the PPP, producing NADPH; which in turn suppress ROS production (Dong *et al*., 2016). Furthermore, in its dimer state PKM2 has been shown to regulate gene transcription in the nucleus of cancer cells and is the major isoform that triggers glycolysis, facilitating and important role in tumour cell energy supply, invasion and cell proliferation (Zhang *et al*., 2019). Due to its low

activity, potential effectors can be utilised to promote the formation of tetrameric PKM2 could potentially switch glycolysis to mitochondria and inhibit PKM2 entry into the nucleus; thus, impairing metabolic demand and growth-supporting signalling in tumour cells (Hsu *et al.*, 2018).

The high rate of expression of PKM2 in cancer cells and its considerable effect on the rate of glycolysis and cell growth emphasises its potential as a metabolic biomarker in the treatment of cancer (Cairns *et al.*, 2011).

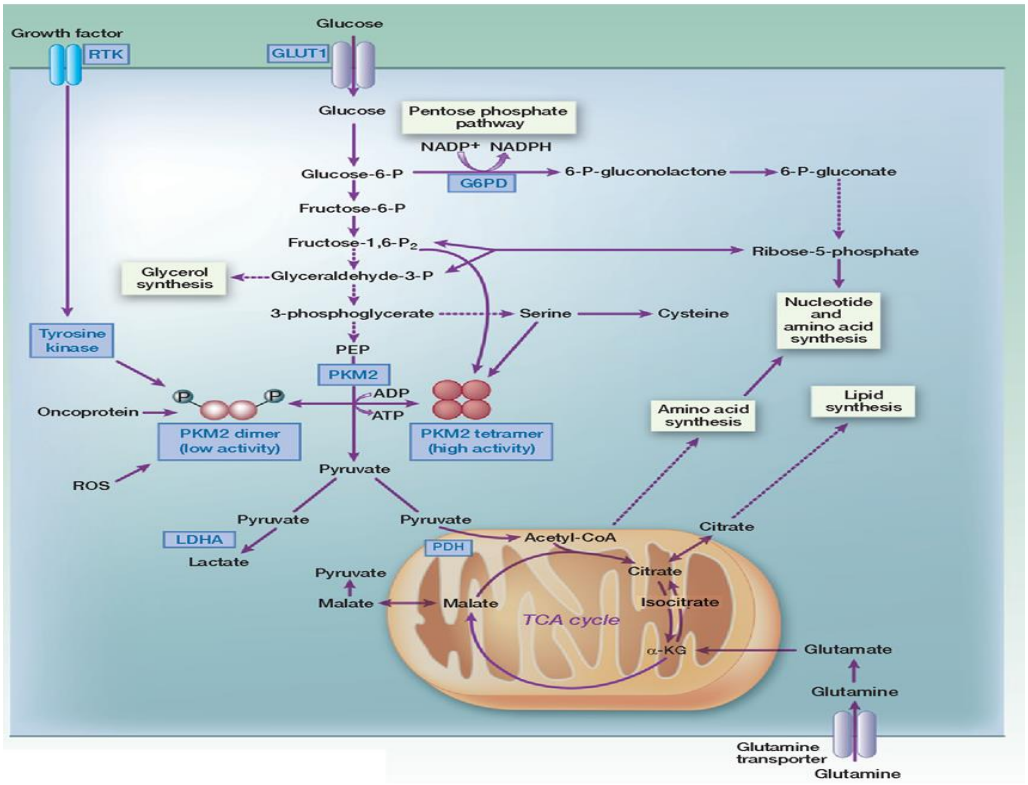

Figure 1.6. Metabolic pathways utilised by cancer cells, showing both the glycolytic and PPP pathways Embryonic pyruvate kinase M2 is over expressed in cancer cells driving the Warburg effect. PKM2 promotes the conversion of pyruvate to acetyl-CoA and is associated with increased cell proliferation through the promotion of mTOR pathway. PKM2 also promotes anabolic growth via the interaction with HIF1. Isocitrate (IDH1) enables tumour cells to generate lipids from citrate and promotes glioma aggression (from Mayumi *et al.*, 2012). Other metabolic mechanisms: The overexpression of phosphoglycerate dehydrogenase (PHGDH) has been associated with glioma cell proliferation and invasion (Liu *et al.*, 2013). Overexpression of PHGDH results in the inhibition of pyruvate, redirecting metabolites away from the TCA cycle instead to produce serine for the biosynthesis of proteins (Locasale *et al.*, 2011). IDH1 wild type has been linked with increased aggressive glioblastoma, it allows tumour cells to generate lipids from citrate supporting anabolic growth (Sun & Denko, 2014; Miroshnikova *et al.*, 2016).

1.6.5 Hypoxia-Induced Transcription Factors

Hypoxia-induced transcription factors characterise secondary mechanisms of adaptation in cancer cells which are upregulated by the PI3K/Akt1/mTOR pathway (Koizume *et al.*, 2015). Cancer cells induce significant transcriptional effectors, predominantly hypoxia-inducible factor 1 and 2 (HIF1 and HIF2) in response to hypoxic microenvironmental stress. The reduction in oxygen results in the stabilisation of HIF subunits which consequentially initiates hypoxic transcriptional response that increases glycolysis and shunts OXPHOS (Sun *et al.*, 2016). HIF-1 can be activated via Akt under normoxic conditions (Inoki *et al.*, 2005; Lu *et al.*, 2008), or by fumarate hydratase (FH) (Greer *et al.*, 2012). FH cells accumulate fumarate which induces HIF1 (Frezza *et al.*, 2011). HIF1 enhances cellular glycolytic potential by increasing the transcription of glucose transporters and glycolytic enzymes, and is a crucial component facilitating the PI3K pathway to drive the Warburg effect (Marbaniang *et al.*, 2018). HIF1 also induces upregulation of phosphoinositide-dependent kinase-1 (PDK1), a key mediator for the activation of AKT. Up-regulated PDK1 restricts the entry of pyruvate into the mitochondrial TCA cycle thus reducing oxidative phosphorylation and ROS, further enhancing the up-regulation of glycolysis mediated by HIF1 (Kim *et al.*, 2009; Lu *et al.*, 2008). HIF1 upregulation has also been shown to have inhibitory effects on a range of factors involved in apoptosis and stress responses (Chen *et al.*, 2009; Yang *et al.*, 2012).

1.7 Development of new treatments

1.7.1 Clinical trials and drug development

TMZ has been a frontline chemotherapeutic agent since it was first licensed for the treatment of glioblastoma in 1999, and since 2005 it has become the primary drug utilized in a multi-faceted approach, involving surgical resection of the tumour tissue and whole brain radiation treatment (Stupp *et al.*, 2005; Hesketh, 2008; Sansom, 2009). A significant barrier in the development of novel drugs is the time taken to conduct rigorous clinical trials to determine safety and efficacy (Piantadosi, 2017). The development of a new therapeutic agent from the initial research to the clinical trials often takes many years, with the risk that the drug may either not prove effective or will not gain approval (Ozdemir-Kaynak *et al.*, 2018). The high-risk

investment, often resulting in a low return for a successful marketable drug has led to considerable reduction in funding (Pammolli, *et al.*, 2011). The consequential outcome is the reduction in the research and development productivity in drug discovery, which further compounds the problem of generating novel therapeutic agents in the pursuit of enhanced cancer treatments (Schuhmacher *et al.*, 2016). In recent years, the development of novel therapeutic agents for the treatment of glioblastoma has had many setbacks in a range of drugs, where levels of success have fallen short and proven to be less effective than TMZ, examples include Mibefradil (Holdhoff *et al.*, 2017), Gliadel (Alphandéry, 2018) and the EGFR inhibitor Afatinib (Reardon *et al.*, 2014). Recent advances in genetics via accessible high throughput next generation sequencing have identified distinctive glioblastoma subtypes with unique genetic abnormalities, which has begun to alter the approach of treatment. Acknowledging the importance of identifying glioblastoma as heterogeneous entities, with genetic abnormalities and relevant biomarkers expressed by specific subtypes has become crucial for both the prediction of survival length and response, and for the stratification of personalised treatments that target unique genetic changes (Verhaak *et al.*, 2010; Meyer *et al.*, 2015; Tefferi *et al.*, 2015). An alternative approach is to target abnormal metabolic pathways that are universally dysregulated in glioblastoma cells and there is growing interest in the development of inhibitors to relevant targets of the glycolytic pathway. Treatments which modulate metabolism are likely to be effective in a higher percentage of patients, whilst sparing normal cells and reducing negative side effects (Wolf *et al.*, 2010). Studies have also shown an increased efficacy of conventional chemotherapeutic drugs in multiple tumour types that have had their metabolism altered (Zaal *et al.*, 2018), although the synergistic connection is yet to be fully understood. As previously discussed in 1.6.3. HK2 has a crucial role in the deregulated glycolytic pathway in cancer cells including glioblastoma (Wolf *et al.*, 2011). The development of HK inhibitors has gained interest in recent years, including 3- bromopyruvic acid (3-BPA), a synthetic derivative of pyruvic acid which has an inhibitory effect on HK2 in a range of tumour cells including liver and breast cancers (Gandham *et al.*, 2015). 3-BPA will be further discussed in 1.8.1. Another HK2 inhibitor, lonidamine (LND) inhibits aerobic glycolysis in cancer cells by targeting

condensed mitochondrion and inhibiting mitochondrially bound hexokinases, leading to a decrease in glycolysis and cellular ATP (Akins *et al*., 2018). Another study has suggested that LND induces metabolic changes through inhibition of lactate transport and its accumulation which leads to intracellular acidification (Nancolas *et al*.,2016).

1.8 *HK2* inhibitors

1.8.1 3- Bromopyruvic acid

3-BPA is a halogenated analog of pyruvate which demonstrates strong alkylating properties toward biomacromolecules (enzymes and proteins). 3-BPA has been shown to be an efficient energy blocker through its inhibitory ability targeting several key glycolytic enzymes or related metabolic enzymes post glycolysis, including HK2, LDH and pyruvate dehydrogenase complex (PDH), making it a potential candidate as an antitumor drug (Cardaci *et al*., 2012; Azevedo-Silva *et al*., 2016; Lis *et al*., 2016, Fan *et al*., 2019). 3-BPA has also been shown to inhibit the expression of HK2 through direct inhibition of the mitochondrial bound HK2 via covalent modification of its cysteine residues, resulting in its dissociation from the mitochondrial membrane (Ko *et al*., 2001; Chen *et al*., 2009). Consequently, 3-BPA induces cell apoptosis, from HK2 dissociation which induces the release of mitochondrial apoptosis-inducing factor (AIF), to the cytosol resulting in cell death. The release of Cyt-C alongside elevated expression of proapoptotic caspase-3 and a decrease of antiapoptotic Bcl-2 and Mcl-1 has been shown post 3-BPA treatment (Xu *et al*., 2005; Yadav *et al*., 2017).

3-BPA was first studied as an antitumor molecule in 2001, with cytotoxic effects in hepatocellular carcinoma (HCC) cells (Ko *et al*., 2001). Follow up studies have also showed selective inhibition with normal tissue remaining unaffected by 3-BPA treatment (Geschwind *et al*, 2002; Ko *et al*., 2004). An *in vivo* mouse model study illustrated the significant reduction in both tumour volume and growth rates in 3-BPA-treated mice when compared to the control mice, and that 3-BPA induced apoptosis via HK2 inhibition leading to the activation of apoptotic signals (Kim *et al*., 2007). 3-BPA has also been shown to recruit BAX to mitochondria in cancer cells,

resulting in the activation of caspase-3 and the inhibition of antiapoptotic Bcl-2, and Mcl-1 (Xu *et al*., 2005; Icard *et al*., 2012; Zhang *et al*., 2012; Xiao *et al*., 2013; Lee *et al*., 2017). 3-BPA administered at high doses causes necrosis in HL60 human myeloid leukaemia cells due to complete depletion of ATP (Calvino *et al*., 2014). 3-BPA also has an inhibitory effect on anabolic processes and production through the downregulation of the PPP pathway; the inhibition of HK2 may potentially result in the reduction of G6P activity and diminished G6PDH, the first substrate/step of the PPP pathway, resulting in increased cytotoxic oxidative conditions (Cardaci *et al*., 2012; Chiasserini *et al*., 2017).

1.8.1.1 Tumour specificity

Cancer cells overexpress monocarboxylate transporters (MCTs), which export excess lactate excreted to avoid intracellular acidification resulting in cell death (Lee *et al*., 2016). This leads to an acidic extracellular microenvironment, and cell invasion and metastasis. Additionally, this lactate can be taken-up by tumour cells via MCTs to resupply cell growth (Halestrap *et al*., 2012). It is hypothesised that the lactate MCTs and 3-BPA are structurally similar, thus allowing 3-BPA to enter the cancer cells via this up-take process (Fan *et al*., 2019). 3-BPA has been shown to be more stable in acidic conditions, which may contribute to the reduced toxicity in normal tissues, and for its high specific toxicity against tumour tissues because of the increased acidity in the extracellular microenvironment (Glick *et al*., 2014).

1.8.1.2 Clinical trials, combination treatments and novel chemotherapeutic strategies of 3-BPA

The combination of 3-BPA with chemotherapeutic drugs has potential to reduce tumour resistance thereby allowing for lower dosages of chemotherapeutic drugs administered to lessen adverse effects. 3-BPA inhibitory effects on both glycolysis and mitochondria resulting in the deprivation of ATP in turn may decrease chemoresistance due to the inhibition of macromolecule synthesis and DNA repair (Ihrlund *et al*., 2008).

Studies have shown multidrug resistance (MDR) leukaemia cells (HL60) to doxorubicin (DOX) and vincristine remained sensitive to 3-BPA, and when treated in

combination the HL60 cells showed increased sensitivity (Xu *et al.*, 2018). 3-BPA also increased the sensitivity of pancreatic cancer cells to the heat-shock protein 90 (HSP90) inhibitor geldanamycin (Cao *et al.*, 2008) in mice xenograft models, with significant tumour growth reduction and increased survival rates. Similar results have been seen in colorectal cancer cells (Ihrlund *et al.*, 2008). Currently there is no data from clinical trials for approved 3-BPA. However, there are reported cases of the administration of 3-BrPA to voluntary patients with advanced tumours including advanced fibrolamellar hepatocellular carcinoma (Ko *et al*, 2012), and in a patient with stage IV metastatic melanoma, who received the treatment of 3-BPA via intravenous infusion (El Sayed *et al*, 2014).

The development of a better drug delivery system to administer 3-BPA will significantly increase its practical application in a range of cancers whilst simultaneously reducing any adverse effects. Studies have shown the use of a biodegradable polymer substantially increased survival in animal high-grade glioma models whilst showing no neurological or systemic toxicity (Wicks *et al.*, 2015). The application of nanotechnology has also been highlighted, where several studies utilised stable liposomal nanoparticles for selectively delivery of 3-BPA to tumours sites, with the advantage of increased BBB permeability for glioma tumours (Gandham *et al.*, 2015; Zhang *et al.*, 2018; Fan *et al.*, 2019).

1.8.2 Lonidamine

Lonidamine (LND), a derivative of indazole-3-carboxilic acid is an anti-tumour drug effective at selectively sensitising tumours to chemotherapy. It inhibits aerobic glycolysis and mitochondrial respiration reducing levels of ATP via targeting condensed mitochondrion and the interference with membrane bound HK2 (Floridi *et al.*, 1981). Subsequent studies have also hypothesised that LND blocks the transport of lactic acid across the plasma membrane through the inhibition of monocarboxylate transporter (MCT), leading to accumulation and intracellular acidification (Nancolas *et al.*,2016; Akins *et al.*, 2018). Furthermore, it has also been suggested that LND is an inhibitor of the mitochondrial pyruvate carrier (MPC) (Nath

et al., 2015). A recent study demonstrated the ability of LND to inhibit the MPC, and as a result enhances the inhibition of MCT activity by preventing oxidation of the accumulated L-lactate through its conversion to pyruvate, consequently, blocking entry into the mitochondria and the citric acid cycle (Nancolas *et al*., 2016). The resulting effect would render the cancer cell unable to compensate for the loss in glycolytic ATP. LND induces apoptosis in cancer cells and whilst it has limited antineoplastic activity as a single therapeutic agent, it offers impressive synergistic effects modulating the activities of conventional chemotherapeutic agents such as temozolomide (Prabhakara *et al*., 2008). LND since first being introduced in 1979 as an antispermadocidic agent has shown low levels of toxicity to normal tissues when administered intravenously, suggesting a high affinity for cancer cells, through the selective inhibition of HK2 and other glycolytic components that are overexpressed in tumours (Price *et al*., 1996).

1.9 Ketone bodies: 3-hydroxybuterate

Another therapeutic approach is targeting the metabolic dysregulation occurring in tumour cells via the reduction of the availability of glucose, either pharmacologically or through the use of a high-fat, low-carbohydrate ketogenic diet (KD). The KD provides increased blood ketones to support the energy needs of normal tissues as an alternative substrate to glucose during prolonged starvation, whilst simultaneously diminishing the glucose energy source that cancer cells increasingly rely upon (Woolf *et al*., 2016). Their ability to cross the blood–brain barrier reduces the reliance of the brain on glucose (Rodrigues *et al*., 2017).

Studies have shown that the incorporation of a KD leads to the reduction in tumour growth, along with the reduction in angiogenesis, inflammation, migration and invasion. Additionally, the KD has also shown to enhance the activity of radiation and chemotherapy in glioma mouse models (Marsh *et al*., 2008; Shelton *et al*., 2010). Strict compliance to the KD is essential to obtain positive results, and this can be difficult with the use of prescribed medication such as steroids which often increase hunger and raise blood glucose levels, alongside issues of quality of life (Woolf *et al*.,

2016). The use of ketone bodies such as 3-hydroxybuterate (3-HB), which is synthesised in the liver from acetyl-CoA and secreted into the blood, offer a potential therapeutic benefit from which many tissues can up take ketone bodies and oxidatively metabolise. 3-HB has a higher calorific value compared to glucose and offers an efficient provision of energy per molecule of oxygen compared to glucose, however cells need functioning mitochondria as well as sufficient oxygen in order to generate energy (Veech *et al*., 2004). 3-HB is transported into cells via MCTs and is degraded via ketolysis into acetyl-CoA, which functions to deliver the acetyl group to the TCA to be oxidized for energy production (Newman *et al*., 2014; Vidali *et al*., 2015). *In vitro* studies have demonstrated 3-HB to elicit ketosis in gliomas, therefore possessing antitumor effects (Skinner *et al*., 2009; Rossi *et al*., 2015), furthermore the supplementation of ketone bodies has shown to augment the effectiveness of the KD (Shukla *et al*., 2014). Studies have shown the effectiveness of 3-HB in reducing the proliferation of tumour cells in a range of cancers, including human glioblastoma cell lines, even in the presence of high glucose (Woolf *et al*., 2016). 3-HB treatment has also demonstrated the ability to increase the sensitivity of cancer cells to ionizing radiation, the increased effectiveness allows for the potentiation of lower doses (Rossi *et al*., 2015; Silva-Nichols *et al*., 2015). Furthermore, 3-HB has shown to increase the effectiveness of chemotherapeutic agents when used in combination in glioblastoma cells (Scheck *et al*., 2012), suggesting ketone supplementation provides an effective therapeutic approach in addition or without the stringent KD approach. Paradoxically a group of studies have shown 3-HB to promote growth in cancer cells (Bonuccelli *et al*, 2010; Martinez-Outschoorn *et al*., 2012). It was hypothesised (Rodrigues *et al*., 2017), that the effect of ketone bodies upon the cancer growth was dependant on the energetic phenotype of the tumour, for the predominantly glycolytic "Warburg-like phenotype" tumour cells would lack the ability to metabolize 3-HB resulting in the inhibition of growth and tumorigenesis. Ketone bodies have also demonstrated regulatory roles in epigenetic states transcription of gene expression via chromatin modification (Schimazu *et al*., 2013). 3-HB is a known inhibitor of histone deacetylases (HDAC), responsible for the removal of acetyl epigenetic marks from histones. Deregulation of histone acetylation has been shown to result in abnormal expression profiles of genes

involved in cell proliferation and differentiation and is associated with malignancy (Rodrigues *et al.*, 2017).

1.10 Metformin

The development of a new drug through the process of clinical trials often takes many years with total costings potentially reaching as high as $2 billion dollars. Fastened with the lack of guarantee for clinical approval, investment and generation of new therapeutic agents has lessened in recent years (Massey and Robertson, 2018). An alternative is the repurposing of existing licenced medication which is advantageous in many aspects. Existing drugs are already regarded as safe for human use, thus reducing the costs and time of the clinical trial process. The repurposing of existing licenced drugs for the treatment of glioblastoma offers a potential alternative crucial for faster implementation of new therapeutic treatments (Abbruzzese *et al.*, 2017). Recent studies have highlighted several potential candidates that could be repurposed for the treatment of glioblastoma, these include metformin and disulfiram (Brenneman *et al.*, 2016; Chae *et al.*, 2016). Population studies discovered that type II diabetes patients treated with the anti-diabetic drug metformin had a reduced incidence of malignant cancers (Evans *et al.*, 2005).

Metformin (1,1-dimethylbiguanide hydrochloride) is a biguanide drug used to treat type 2 diabetes. It is an oral drug that prevents the production of glucose in the liver, leading to an improvement in the sensitivity towards insulin, resulting in the reduction of sugar absorbed by the intestine (Maruthur *et al.*, 2016). Metformin was first synthesised in 1929 and has been comprehensively utilized in the treatment of diabetes in the United Kingdom from the 1950s (Hadden, 2005). Studies conducted in 2005 revealed metformin to potential moderate the risk of cancer, in patients being treated with type 2 diabetes (Evans *et al.*, 2005). More recently, clinical trials

have assessed metformin and its anti- cancer potential in a range of tumours (Chae *et al.*, 2016; Heckman-Stoddard *et al.*, 2017). The repurposing of metformin as a potential cancer therapeutic agent is a low risk factor, as stated metformin offers the advantage of being orally administered with inconsequential primary side effects which can be amended via dose control (Matsuzaki, 2017). Moreover, metformin crucially has demonstrated the ability to cross the BBB which is often a major obstacle for the formulation of new or existing anti-cancer drugs. Additionally, metformin has exhibited a potential to upregulate the functions of the BBB including an overall reduction in the permeability via the activation of AMP-activated protein Kinase (AMPK) tissue (Łabuzek *et al.*, 2010; Takata *et al.*, 2013). Metformin offers the additional advantage with its worldwide availability including less developed countries, due to its classification as an essential medication (World Health Organization, 2017).

1.10.2 Metformin clinical trials

Ongoing clinical trials have assessed metformin and its anti- cancer potential in a range of tumours with the resulting success variant. Examples of metformin having a positive impact include the phase II trial of ovarian, fallopian tube and primary peritoneal cancer (stage II/III/IV), where metformin was utilized in conjunction with both adjuvant chemotherapy drugs and surgery (Buckanovich *et al.*, 2017). The promising additive effect of metformin in this trial led to the use of metformin in phase-III trials. A recent clinical trial for early stage breast cancer (Dowling *et al.*, 2018) stated the comprehensive constructive effect of the addition of metformin, with the significant reduction of cancer biomarkers (Dowling *et al.*, 2018). Other clinical trials state the inhibitory effects of metformin on altered gene expression in cancer patients (Lord *et al.*, 2016), however numerous clinical trials report metformin to have no synergistic impact including a high-risk breast cancer trial (Yee *et al.*, 2017) and a phase II late stage pancreatic cancer clinical trial where no significant impact was determined (Kordes *et al.*, 2015). The clinical trial data does offer an insight into the anti-cancer potential of metformin, particularly in early stage cancer whereby it was shown to have the greatest impact as a combination treatment (Chae *et al.*, 2016). The mechanism of the anti-tumour activity of

metformin is currently not fully understood, studies (Pollak, 2012; He and Wondisford, 2015) however state that metformin inhibits respiratory complex I of the electron transport chain in mitochondria leading to the activation of AMPK and the inhibition of the mTOR pathway.

1.11 Drug synergy and combination treatments

The identification of synergistic partners for both new and repurposed inhibitors would increase their scope for usage in the treatment of glioblastoma, as part of a multi model treatment regime, most notably with the mainstay chemotherapeutic agent TMZ. TMZ is the frontline therapeutic agent in glioblastoma treatment (Messaoudi *et al.*, 2015), forming part of the STUPP protocol. TMZ is an alkylating agent that causes DNA damage resulting in cell death, as with metformin it is orally administered and absorbed in gastrointestinal tract (Lee *et al.*, 2018). TMZ is pH responsive, in environments greater than pH7 it hydrolyses into methytriazine (MTIC) (Di Martino, *et al* 2017). In vitro studies have shown that TMZ has a 30-minute half- life before hydrolysing into MTIC, which has an approximate half- life of 25 minutes before degrading into the inactive form 4-Amino-5-imidazole-carboxamide (5-AIC) (Aldea *et al.*, 2014), as shown in Figure 1.7. The effectiveness of inhibitors, for example the *HK2* inhibitors discussed and metformin, in a combination treatment would potentially increase their inhibitory capability (Aldea *et al.*, 2014), and the prospective capacity of TMZ.

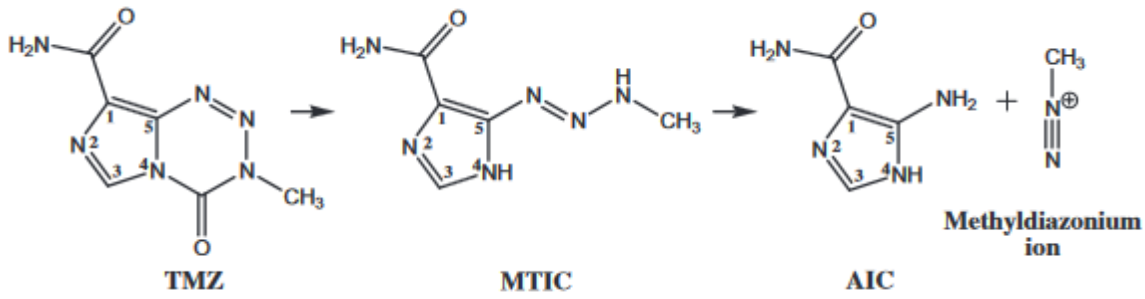

Figure 1.7. TMZ structure TMZ must become hydrolysed into its reactive component form of a methydiazonium ion and an inactive AIC. The activation of hydrolysis is regulated by a pH greater than 7. (Lopes, *et al* 2013).

1.12 Mechanisms of cell death induced by inhibitors

1.12.1 Apoptosis

Programmed cell death via apoptosis is a crucial cellular mechanism for the maintenance of a healthy equilibrium, with the destruction and removal of cells in a controlled manner. Apoptosis uses intracellular mechanisms to perform a range of functions which include structural development, immune response, chemical-induced cell death and hormone dependant atrophy (Elmore, 2007). Apoptosis involves multiple cellular pathways leading to the irreversible activation resulting in the breakdown of the cell and cellular function. The extrinsic and intrinsic pathways are both are operated and regulated through specific caspase proteins (Budihardjo *et al.*, 1999), as shown in Figure 1.8. The two pathways are instigated via different stimuli; the intrinsic pathway is synchronised to the various functions of the mitochondria, including the activation of the caspase pathway and the Apoptotic Peptidase Activating Factor 1 (APAF1), which encodes a cytoplasmic protein initiating apoptosis by cleaving caspase 9 pre-proprotein (Fulda and Debtain, 2006). Conversely, the extrinsic pathway is facilitated by cell surface receptors, which are stimulated by death ligands presented by immune-effector cells resulting in the formation of the death-inducing signalling complex (DISC). DISC is comprised of the death receptor, and caspase 8, which activates the downstream signal cascade of caspase pathways resulting in apoptosis (Kischkel *et al.*, 1995). The intrinsic pathway is tightly regulated by the mitochondria which control the pathway through downstream caspase effectors via the release of cytochrome C (Cyt C), which in turn activates the cysteine protease caspase 9 resulting in the activation of caspase 3 and 7, which are responsible for destroying the cell from within (Hunt, 2002; Boehning *et al.*, 2003). The mitochondrial membrane potential ($\Delta\psi$) is a fundamental factor in mitochondrial activity, which drives the tricarboxylic acid cycle (TCA) (Martínez-Reyes *et al.*, 2016). The combination of apoptogenic factors released by the mitochondria with the addition of the depolarisation of the transmembrane potential and the loss in oxidative phosphorylation are key factors in eliciting the intrinsic apoptotic pathway (Martínez-Reyes *et al.*, 2016). Apoptosis in cancer is frequently disrupted, with tumour cells acquiring adaptations in order to prevent and block apoptotic pathways. A common occurrence in cancer are the mutations of key pro-

apoptotic genes leading to the deregulation of apoptosis, including mutation of the cell surface receptors CD95 and TNF-related apoptosis-inducing ligand (TRAIL) which are responsible for the induction of caspase dependant apoptosis (Fulda and Debatin 2006; Song *et al*., 2008). These key mutations have been revealed as a frequent occurrence in head and neck osteosarcoma (Dechant *et al*., 2004). Additionally, the activation of extrinsic pathways can be blocked by an increased concentration of anti-apoptotic molecules, which inhibit phosphorylation and ubiquitylation of caspase activation and activity, resulting in the loss of receptor activation, as often demonstrated in tumours.

Therapeutic treatments that can restore apoptotic functionality are being investigated. However, the activation of the extrinsic pathway through extracellular receptors is relatively non-specific and there has been limited progress in the development of extrinsic caspase pathway therapies. On-going clinical trials targeting TRIAL and CD95 using receptor agonists, such as tumour necrosis factor alpha (TNF-α) have so far proved ineffective. However, the development of novel agents to reinstate apoptosis potentially offer effective treatment methodologies in a range of cancers (Merchant *et al*., 2012, von Pawel *et al*., 2014; Ashkenazi, 2015; von Karstedt *et al*., 2017).

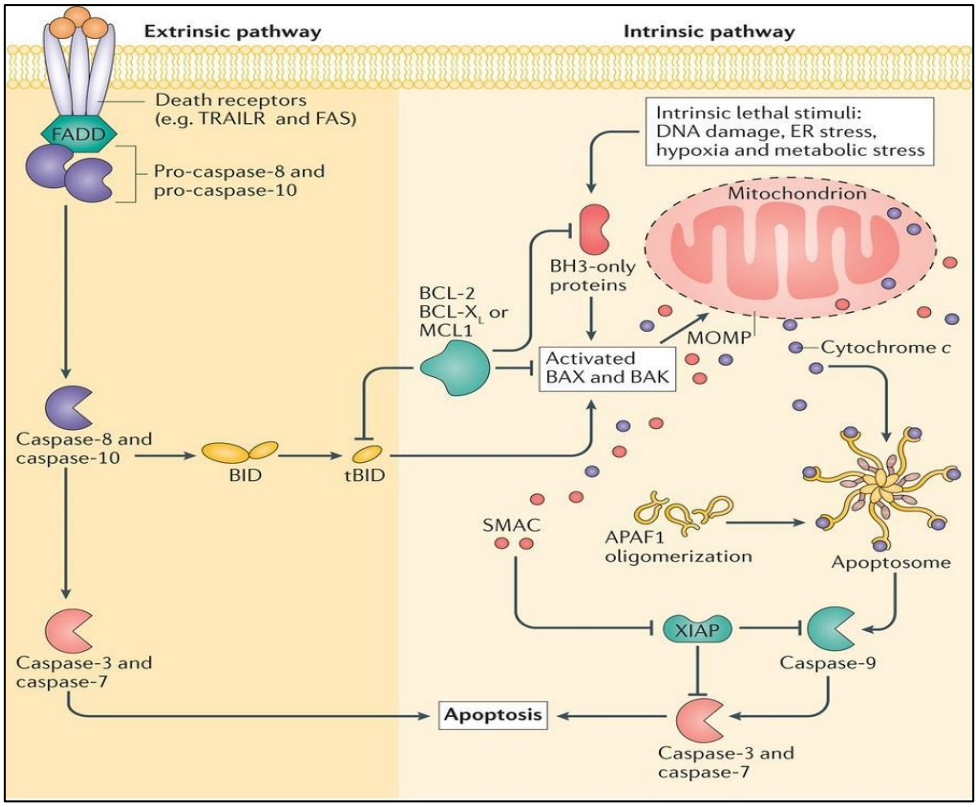

Figure 1.8 Extrinsic and intrinsic apoptotic pathways Apoptosis uses a range of signalling pathways and comprises of two versions based on the initial signalling trigger. Intrinsic apoptosis has multiple triggers relating to metabolism, DNA damage and cellular stress. Extrinsic apoptosis is initiated by extra cellular signals, resulting in the generation of DISC (Schleich *et al.*, 2013).

1.12.2 Cell cycle

Cell cycle is a crucial mechanism in the maintenance of healthy cell populations and the regulation in the generation of new cells. The progression through the various stages of the cycle are tightly regulated and controlled with multiple checkpoints in order to ensure that faulty cellular processes are constrained and unauthorized to progress further in the cycle (Vermeulen *et al.*, 2003). The checkpoints regulate fundamental stages of cell division, crucial for the prevention of DNA damage and aberrant cell behaviour, in healthy cells the cycle arrests and cellular division is prevented with the occurrence of a checkpoint pre- requisite failure (Bertoli *et al.*, 2014).

The deregulation of the mechanisms maintaining control is a frequent occurrence in tumour development (Evan and Vousden, 2001). The regulatory mechanism maintained in cell cycle is controlled predominantly by two main groups of molecules, which are cyclins and cyclin-dependent kinases (CDK) (Spoerri *et al.*,

2015). The role of CDK is the binding of cyclins resulting in the formation of active kinase protein complexes, in the absence of cyclin CDK has little kinase activity. Cyclin-CDK complexes phosphorylate substrates appropriate for the specific cell cycle phase (Spoerri *et al.*, 2015). Mammalian cells contain at least nine CDKs, four of which are associated directly with cell cycle regulation, including CDK1, 2, 3, and 4 (Crosby, 2007). CDK1 with its partners cyclin A2 and B1 can alone drive cell cycle. Cyclin-CDK complexes from earlier phases in the cell cycle instigate later phase cyclin-CDK complex activation. Figure 1.9. shows the list of cell cycle checkpoints associated with cyclin CDK complexes and the summery of cell cycle developmental.

3-BPA has been shown to induce cell cycle arrest in cancer cells through a range of mechanisms. In breast cancer cells after the treatment of 3-BPA, the G0 and G1 phases were dramatically decreased. Additionally, expression levels of Bcl-2, c-Myc and mutant p53 were significantly reduced all of which are associated with the programmed cell death signal transduction pathway (Liu *et al*, 2009). 3-BPA has also shown effective inhibition of cell cycle in colorectal cancer cells, eliciting the downregulation of cyclin-dependent kinase CDK4 and CDK2 resulting in a G1 phase arrest (Chong *et al.*, 2017). Metformin has also been shown to cause cell cycle arrest in a range of cancer cell types via various mechanisms. Metformin was shown to induce G1 cell cycle arrest in lung cancer cells through the inhibition of the atypical repressor E2F8; overexpression of this transcription factor is associated with poor patient prognosis (Jin *et al.*, 2017). In recent studies, metformin was shown to induce G2/M cell cycle arrest in glioblastoma cells when treated in combination with TMZ (Adeberg *et al.*, 2017), and in breast cancer cells cyclin G2 was upregulated as a response to treatment with metformin, which is a key regulator for the G2/M checkpoint inhibiting CycB1-Cdc2 complex formation Cdc2 (Zimmermann *et al.*, 2012, Zimmermann *et al.*, 2016). The crucial regulatory role of CDKs have emphasised their potential as a target for anti-cancer treatment, with the development of specific inhibitors to target CDK action, interrupting the cell cycle regulation.

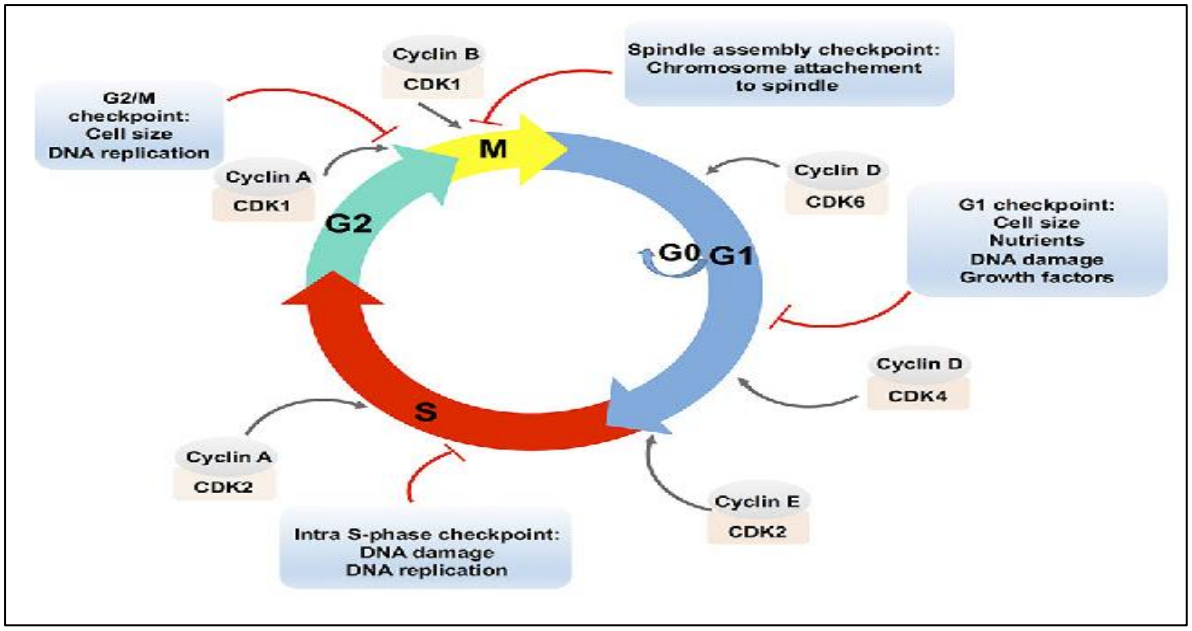

Figure 1.9 Cell cycle developmental progression checkpoints The four main stages to cell cycle progression: G1, S, G2 and M phase. Controlling the cells movement through the phases are four check points, G1 to S phase transition, S phase checkpoint, G2 phase checkpoint and the spindle assembly checkpoint, ensuring that the cell has not suffered damage and that correct prerequisite stages have been completed. G1/S, S phase and G2 phase check for DNA damage in order to stop any mutations and errors post division. The checkpoints also ensure that the previous step was correctly completed, G1/S asses that previous mitosis, S phase checks for duplicated genetic material and G2 assess the cell mitotic preparation. The spindle check point assesses establishment of mitotic spindle for correct allocation of chromosomes. Each stage is controlled by the creation of a specific cyclin Cdk protein complex (Filho *et al.*, 2017).

1.12.3 AMPK and mTOR

Mammalian target of rapamycin (mTOR), a serine/threonine protein kinase, integrates responses from a wide variety of signals including nutrients, hormones, growth factors, and cellular stresses in order to regulate several downstream processes including protein and lipid synthesis, cell survival, cell motility, autophagy and transcription (Hay *et al.*, 2004). mTOR forms two distinct protein signalling complexes, mTORC1 and mTORC2 which maintain control of downstream pathways (Lipton *et al.*, 2014; Saxton *et al.*, 2017). The rapamycin-sensitive mTORC1 complex regulates a range of cellular mechanisms including protein synthesis, cell cycle progression, cell growth, and proliferation. Less is known of the functions of the mTORC2 complex, however AKT activation has been associated, which is a key

influence in cell migration and survival through the inhibition of apoptosis and autophagy (Pópulo *et al*., 2012; Kim *et al*., 2015). The activation of AMPK has shown to inhibit mTOR acting as a tumour suppressor, however it has also been associated as an oncogene through its facilitating role in cell division and metabolic reprogramming (Jeon *et al*., 2012; Liu *et al*., 2013). In glioblastoma cells AMPK has been shown to be actively upregulated (Liu *et al*., 2013). Figure 1.10 shows the mTOR signalling network and pathways. The effectiveness of 3-BPA at inhibiting mTOR is still not fully understood, it has been reported in both lung and liver cancer cells that 3-BPA did not add a synergistic effect in combination with rapamycin, instead the addition of rapamycin alone blocked the mTOR signalling pathway. However, the combination of rapamycin and 3-BPA demonstrated enhanced antitumor efficacy with respect to the reduction of glycolytic activity, indicating that the dual inhibition of both mTOR signalling and glycolysis offers a potential effective therapeutic strategy for cancer treatment (Zhang *et al*., 2015). It has been suggested that metformin has the capability to inhibit the mTOR pathway via several pathways, and in pancreatic cancer its mechanism of action has been shown to act through the downregulation of transcription factors which result in the downstream inhibition of mTOR signalling (Nair *et al*., 2014).

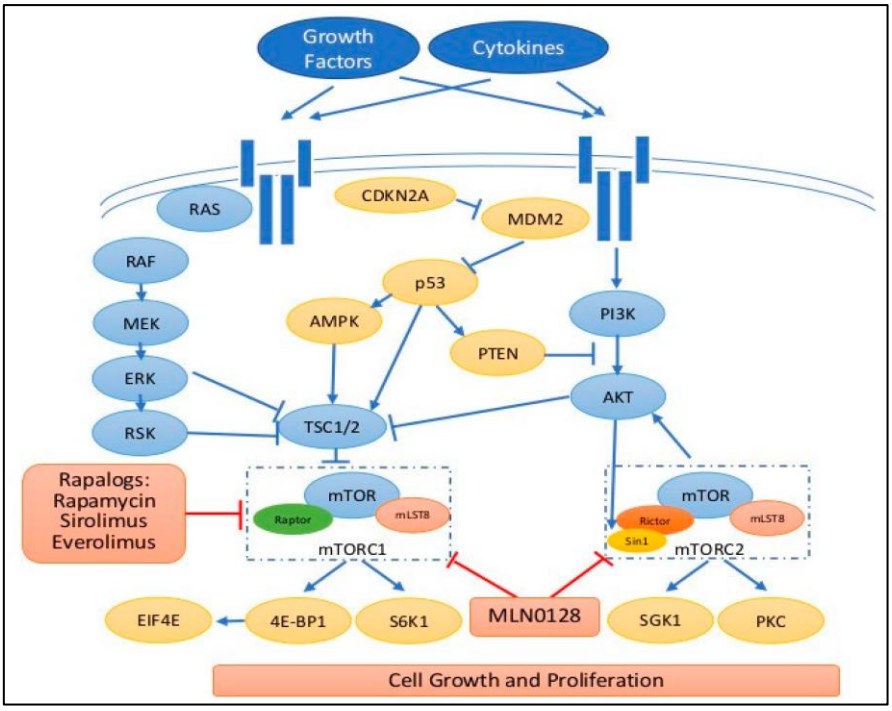

Figure 1.10 Figure showing the mTOR pathwaymTOR forms two separate complexes mTORC1 and mTORC2 to regulate multiple downstream effectors. mTORC1 affects anabolic and catabolic pathways. mTORC2 affects cellular proliferation pathways including cell survival, metabolism and cytoskeletal organisation. mTORC1 is primarily inhibited by AMPK phosphorylation of RAPTOR and the AKT substrate PRAS40 (Kim *et al*. al., 2015).

1.12.4 Autophagy

Autophagy is an alternative method of cell destruction compared to the apoptotic programmed cell death. Autophagosomes which comprise of double membrane cytosolic vesicles transverse across the cell up taking and absorbing macromolecules and organelles, eventually combining with the lysosomes thus becoming autolysosomes. The function of the autolysosome complex is to break down the absorbed macromolecule content leading to cellular degradation and the recycling of molecules (Ramirez *et al*.,2013; Nakamura *et al*., 2017). Primary regulation of autophagy is through the controlled signalling of Phosphoinositide 3-kinase (P13K) and AKT (Heras-Sandoval *et al*., 2014) as well as the regulation of the mTOR pathway, as shown in Figure 1.10. The activation of autophagy in glioblastoma offers a therapeutic target (Yan *et al*. 2016). Autophagy can also be utilized in a controlled cellular process, whereby lysosomes deconstruct internal cellular structures, in order to maintain balance, including the removal for the of damaged

organelles and the regulation of metabolism (Parzych *et al.*, 2014; Kobayashi, 2015). The autophagy regulation pathway is shown in Figure 1.11. Additional to inducing apoptosis, 3-BPA has also been shown to instigate autophagy under apoptosis-deficient conditions via the formation of a complex with receptor-interacting serine/threonine-protein kinase 3 (*RIP3*) (Moriwaki *et al.*, 2013). RIP3 is a component of the tumour necrosis factor (*TNF*) receptor-I signalling complex, which mediates necroptosis via the activation of autophagy (Yuan and Kroemer, 2010). In colorectal cancer cells 3-BPA has been shown to induce cell death by multiple mechanisms including autophagy at the same time via the depletion of cellular energy stores (Sun *et al.*, 2015). Metformin has also been shown to instigate autophagy via the induction of cellular stress and ATP reduction (Lindqvist *et al.*, 2018), in colorectal cancer cells studies have shown autophagy was induced via p53 after metformin treatment (Buzzai *et al.*, 2007). Autophagy activation by metformin has also been shown in thyroid and endometrial cancer cells (Song *et al.*, 2017; Gu *et al.*, 2017). Studies have also found metformin to induce autophagy in glioblastoma cells via the activation of *AMPK* and *REDD1*, downregulating the mTOR pathway (Sesen *et al.*, 2015).

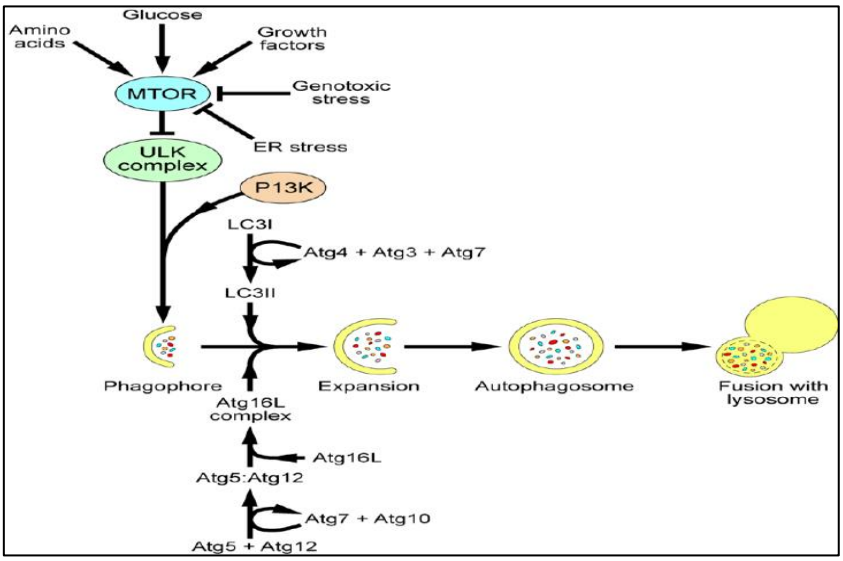

Figure 1.11. Autophagy regulation pathway The primary mechanism controlling autophagy is mTOR. mTOR downregulation can occur from a range of cellular signalling including cellular stress, growth factors and glucose levels. The downregulation results in substrates produced by *P13K* complexes and the ULK complex to move to the phagophore. Further protein complexes are then recruited to create the complete autophagosome (Maier and Britton, 2012).

1.13 Cell culture models

Cell culture is an important *in vitro* tool for the generation of data that cannot be attained via *in vivo* techniques, such as the impact of inhibitory molecules upon cellular mechanisms, including proliferation, cell cycle, apoptosis and autophagy. The replication of a suitable microenvironment in which to grow cells is essential for such work to commence, however tissue culture can result in genetic and phenotypic changes (Bara *et al*., 2014, Nestor *et al*., 2015). Studies have shown that glioblastoma cells in culture significantly loose the amplified levels of expression of EGRF present within the tumour tissue (William *et al*., 2017).

Additional complications with cell culture models are the heavily relied upon immortalized human cancer cell lines, which are abundantly available worldwide, advantageous when compared to primary cell material which are extracted from small finite biopsy tissue samples. Commonly used glioblastoma cell lines include U251MG, U87MG and U373MG (Ponten *et al*., 1968, Westermark *et al*., 1973; Ponten *et al*., 1978). In recent years with the advancement of techniques the reliability of immortalised cell lines has been scrutinized, studies have shown that the cell line U251MG exhibits altered genotypic and phenotypical features compared to the progenitor sample. It was shown over time that higher passage U251MG loses its original glioblastoma signature with the acquirement of additional genetic deletions (Torsvik *et al*., 2014). A more accurate alternative model is the use of patient-derived cultures, which utilizes extracted cells in the same manner. The cell line however is set for use only as a short-term low passage culture reducing the probability of both genetic and phenotypic deviations from the original sample whilst providing a functional cellular system (Roberts *et al*., 2017).

1.14 Aim and objectives

Glioblastoma are genetically and phenotypically heterogeneous; current treatment options are limited with unpromising outcomes. The development of novel therapies targeting aberrant metabolism in glioblastoma could generate potential therapeutic advantages.

This study hypothesises that glycolytic inhibitors can be effective anti-glioblastoma agents *in vitro*. Furthermore, that the combining of therapies to target energy

metabolism through several different mechanisms simultaneously will minimise development of resistance. The aim of this study was to investigate the efficacy of disrupting glucose metabolism in killing glioblastoma cells. The objectives of this study were:

- To determine whether hexokinases *HK1* and *HK2* are differentially expressed in glioblastoma compared to normal brain. *HK2* has been shown to be highly expressed in a range of cancers, a distinguishing factor compared to normal tissue.

- To ascertain whether promoter CpG methylation status is involved in the regulation of *HK1* and *HK2* expression in glioblastoma as there is evidence that expression of some metabolic enzymes is regulated by epigenetic mechanisms.

- To establish the efficacy of HK2 inhibitors in suppressing growth of glioblastoma cells in characterised patient-derived cell cultures and to determine whether the degree of growth inhibition correlates with levels of HK2 expression.

- To investigate whether combining HK2 inhibitors with either metformin or temozolomide is more effective than using these drugs in isolation.

- To understand the molecular pathways through which glycolytic inhibitors act, including identification of the mechanism of action utilised in induction of cell death in glioblastoma cultures via flow cytometric assays.

- To determine the effects of physiological conditions on tumour cell response to inhibition of HK2, including oxygen and glucose availability utilising characterised patient-derived cell cultures.

CHAPTER 2
Materials and Methods

This study was conducted under ethical approval granted by the Life Science Ethics Committee, University of Wolverhampton, LSEC/22/0909

2.1 Cell culture

This study was conducted under ethical approval granted by the Life Science Ethics Committee, University of Wolverhampton, Cell biology and genetic investigations of primary and metastatic brain tumours (renewal), LSEC/2016/17/TW/11.

2.1.1 Glioblastoma biopsies

Fresh, frozen glioblastoma biopsy samples were obtained from the REC-approved Brain Tumour North West and Walton Research Tissue Banks (Ethics Committee approval reference numbers 09/H0304/8 and WRTB 13_02). Written informed consent has obtained from all patients prior to their donation of surplus tumour and normal brain tissue for research at the primary treatment centre for surgical treatment. All tissue samples were fully anonymised prior to their release from the tissue banks. Histological sections of the tumour tissues were examined by neuropathologists and were diagnosed according to the WHO classification system (Louis *et al.*, 2016).

2.1.2 Glioblastoma cell cultures

Patient-derived short-term cell cultures were derived from fresh tumour biopsy material as described by Lewandowicz *et al.* (2000) and stored in liquid nitrogen until further use. Nineteen glioblastoma patient-derived cell cultures were used in this study, which were recovered from liquid nitrogen at low passage (<10) and utilized up to passage 20. The established cell lines U251MG and U87MG were supplied by Dr Darrell Bigner, Duke University, USA (Bigner *et al.*, 1981) between passages 78-86. HEPES-buffered Ham's F-10 media (Life Technologies Ltd., UK) supplemented with 10% foetal calf serum (PAN biotech, UK) were used to culture all cells used in this study. Details of the samples used in this study are shown in Table 2.1.

2.1.3 Control Cells

Normal human foetal astrocytes (NHA) were used as a non-cancerous control in this study as a comparison for the astrocytic origin of the short-term cultures. The NHA (Lonza, UK) were utilized to passage 10. Additionally, normal brain tissue was also used as a non-cancerous control

2.1.3 Maintenance and cell culture methods

Cell culture work was completed within a Biomat 2 sterile class II Laminar flow hood using Sarstedt tissue culture consumables; sterilised with 70% ethanol (Sigma-Aldrich, UK) and 1% Trigene (Sigma-Aldrich, UK) solution. Cultured cells in cryovials were removed from liquid nitrogen and thawed immediately in a water bath at 37ºC. The cells were transferred from the cryovial to a fresh sterile 25ml universal tube, 3ml of pre-warmed (37ºC) media was then added via dropwise. The tube was then centrifuged for 5 minutes at 1000 rpm. The supernatant was aspirated, and the cell pellet was gently resuspended in 10 ml of fresh media. The contents were then transferred to a T25 (25 cm^2) growth flask and placed in a non- carbon dioxide incubator (Panasonic MCO-170AIC-PE IncuSafe, Panasonic UK) at 37ºC. Media was replaced to growing cultures every 24-48 hours.

Table 2.1 Details and characterisations for all Institute of Neurology (IN) patient derived cell cultures

Culture	Sex	Age at diagnosis	Location	TP53 deletion	*MGMT* status	EGFR over representation
IN859	F	72	R frontal	Yes	Methylated	chr 7p
IN1265	F	70	R occipital	WT	Unmethylated	chr 7p
IN1461	F	44	L Parietal	WT	Unmethylated	chr 7p
IN1472	F	46	Unknown	Yes	Unmethylated	-
IN1528	M	61	R temporo-parietal	Yes	Methylated	chr 7p
IN1612	M	53	R post-temporal	Yes	Unmethylated	chr 7p
IN1682	F	48	R parietal	WT	-	chr 7p
IN1760	F	56	L temporal	WT	Partial methylation	chr 7p
IN1951	M	30	R parietal	WT	Unmethylated	-
IN1979	M	46	L temporo-parietal	Yes	Unmethylated	-
IN2045	M	25	L frontal	WT	Partial methylation	-
IN2093	M	55	R frontal	WT	Unmethylated	-
IN2132	M	57	-	WT	-	-
U251MG	-	-	-	WT	Partial methylation	chr 7p
U87MG				WT		
NHA	N/A	N/A	N/A	WT	Unmethylated	
UWLV22	M	65	-	-	-	-
UWLV48	M	43	-	-	-	-
UWLV53	F	48	-			
UWLV152	M	37	-	-	-	-
UWLV156	F	52	-	-	-	-
UWLV212	M	69	-	-	-	

Details and characterisations for all Institute of Neurology (IN) patient derived cell cultures. M = Male, F = Female; Age listed in years at diagnosis; L = Left, R = Right; The mutation status of the tumour protein gene p-53 characterised through sequencing (Potter *et al.*, 2018); *MGMT* status identified by methylation specific PCR (Licchesi *et al*, 2009).

2.1.5 Growth Media

All glioblastoma short-term cultures and established cell lines were grown in HAMs F-10 supplemented with 10% FCS from Pan Biotech FBS GOOD EU range (Pan Biotech), without antibiotics or anti-microbial agents. Cultures were grown in non - vented flasks in a standard incubator under normoxic conditions at 37ºC. The cultures were grown in non-CO_2 conditions as the F-10 media contains HEPES buffer to maintain optimal pH levels. For certain experiments where cells were grown under various glucose levels, glucose-free HAMS F-10 (Pan Biotech) was utilized, which was supplemented with 10% FCS and 10% HEPES as standard along with glucose (Sigma, UK) at the desired concentrations.

Appendix I includes the F-10 media formulations used for all experiments. Normal human foetal astrocytes were grown in ABM Basal Medium and were supplemented with AGM SingleQuot Kit and Growth Factors (Lonza, UK). The manufacturer standardised cell growth medium contains 4.80% gentamicin sulphate to inhibit microbial growth. Cultures were grown in vented flasks with 5% CO2 and incubated at 37ºC. Cell cultures were routinely monitored for changes in the growth media and cell density, and were regularly fed between 36-48 hours, or when needed due to a change in pH of the growth medium.

Cells were passaged when confluent in order to expand their population and to provide enough nutrients and space to divide and grow. Media was aspirated from the culture flask and cells were washed with 1x HBSS (Life Technologies) (1ml for T25 flasks and 5ml for T75 flasks). Treatment of 1xTrypsin (Sigma-Aldrich, UK) was added to the flask (1ml for T25 flasks and 3ml for T75 flasks) and spread evenly in order to cover the entire surface. The cells were incubated for 5 minutes at 37ºC to detach the adhered cells, and verified using a microscope, ensuring cells were detached before inactivating the trypsin via the addition of fresh culture media (3ml for T25 flasks and 10ml for T75 flasks). The contents of the flask were then transferred to a sterile 25ml universal tube and centrifuged for 1000 rpm for 5 minutes. After removing the supernatant, the cell pellet was then resuspended in fresh media and passaged at a ratio of 1:3 into T75 flasks containing fresh media.

Cell pellets were also frozen for long-term storage in liquid nitrogen, $1x10^6$ cells were re-suspended in a 1ml volume containing 10% DMSO (Sigma Aldrich, MERCK, UK) and 90% FCS. The cell suspension was transferred to labelled cryovials (Nalgene Cryoware™ Labware, Roskilde, Denmark) and left for 24 hours at 80ºC in a NALGENE® Mr. Frosty (Thermo Scientific, UK). The cryovials were then transferred to liquid nitrogen tank (-196ºC) for indefinite storage. All short-term cultures were routinely tested for mycoplasma contamination, where approximately 100,000 cells were counted and attached to a glass slide using a cytospin centrifuge, fixed in ice-cold methanol (Sigma-Aldrich, UK) and stained with Hoescht dye (Sigma-Aldrich, UK) for visualisation under a fluorescent microscope for the presence of extranuclear dots.

2.1.6 Growth proliferation curves

Growth proliferation curves were conducted to determine the exponential growth phase. Cells were seeded in 7 x T25 flasks and measured over a 10-day time period. Cells were initially seeded at $1x10^5$ and readings were taken at day 1, 2, 3, 5, 7, 9, 10 days. At each time point cells were trypsinised, centrifuged and collected before being resuspended in growth media and counted on a Countess Cell Counter (Thermo Fisher). This method utilizes the staining of live cells with trypan blue, using a 1:1 ratio with growth media. Two separate readings were taken for each cell count where an average was calculated. Growth curves were repeated three times.

2.2 Growth Inhibition Assays

2.2.1 Drugs

3-bromopyruvic acid, metformin, 3-hydroxybuterate, lonidamine, camptothecin and temozolomide were purchased from Sigma Aldrich.

2.2.2 Sulforhodamine B (SRB) cell proliferation assay

The inhibitory effect of the experimental drugs upon cell proliferation was determined via SRB colorimetric assay. Cells were seeded in 96 well plates in triplicates at 4000 cells per well in 200µl growth media and incubated at 37ºC until the determined exponential growth phase was reached. The growth media was then

aspirated and fresh media (200µl/well) containing an appropriate concentration of drug was added. The plate was then incubated for 72 hours. Drug concentrations were prepared to required concentrations and serially diluted in growth media in a separate 96 well plate before being transferred to the cells. Daily re-treatments of fresh drugs were dependant on the half-life of the drug. Control cells were grown in media without the presence of the drug. Following the incubation, the media was aspirated, and the cells were fixed to the plate using 150µl of 10% (wt/vol) ice-cold trichloroacetic acid (TCA) and placed at 40C for 1 hour. The plate was then washed three times to remove excess TCA and air dried before being stained with 100 µL of 0.4% SRB (Sigma-Aldrich, UK) (dissolved in 2% (vol/vol) acetic acid) (Sigma, Merck) and incubated for 30-60 minutes at room temperature. SRB colorimetric assay was used to assess the viability of the cells, via protein-binding (Vichai *et al.*, 2006). After incubation the plate was washed three times to remove excess unbound SRB before being dried. 100 µL of 10mM Tris base solution (Sigma Aldrich, Merck) was added to the wells and mixed gently for 5 minutes until the SRB dye has been solubilised. The optical density absorbance was read at 560 nm wavelength on a GloMax® Multi Microplate Reader (Promega). Results were analysed using MS excel and GraphPad Prism. Each plate had triplicate repeats of 8 concentrations of drug and 2 negative controls.

2.2.4 Calculation of ID_{50} values

SRB and MTT data were analysed using MS excel GraphPad PRISM software. ID_{50} values were determined using a log (inhibitor) vs. Response or a four-parameter logistic curve (4PL) algorithm. This method utilised all O.D absorbance data points generated against log molar dosages. The method assumes a non-standard, variable slope. This is outlined in Fig 2.1 ID_{50} values for each drug are calculated from this method for each culture tested. Groupings of data were analysed for significant difference via the use of an un-paired students t-test.

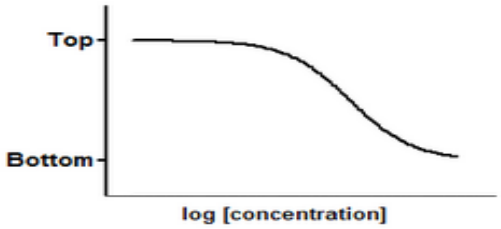

Figure 2.1 Mathematical model used for all analysis on graph pad prism The method allows for variable analysis of the drug response yielding more accurate ID_{50} than seen on a standard curve model.

2.2.5 Experiments utilizing ID_{50} values

Experiments that utilised the ID_{50} values were set-up in the same manner, these include all experiments involving flow cytometry. Cells were seeded at the same concentration (4000/well) as tested on the 96 well plates. T25 flasks were seeded with 5ml at 12,000 cells per ml and T75 flasks were seeded with 15 ml of cells at 80,000 cells per ml.

2.2.6 Drug Synergy Assays

Drug synergy assays were conducted to determine the inhibitory effects of paired drug combinations. Cultures were treated with either an individual drug or a paired combination and the ID_{50} values were calculated as previously outlined. The concentration of the drugs used in combination were ensured to be equimolar, as equivalent to the cells treated with a singular drug. The Chou-Talay method of determining the combination index (CI) was utilized to calculate the synergy between drugs in the combination treatments (Chou *et al.*, 2010); the equation is shown in full in Figure 2.2. CI values represent how synergistic (values <1) or antagonistic (values >1) the combination treatments are; additionally, values of 1 are defined as of having an additive effect when used in combination. The greater the CI value from 1 is representational of having a stronger effect. Combination treatments were run in duplicates per plate, which was repeated three times.

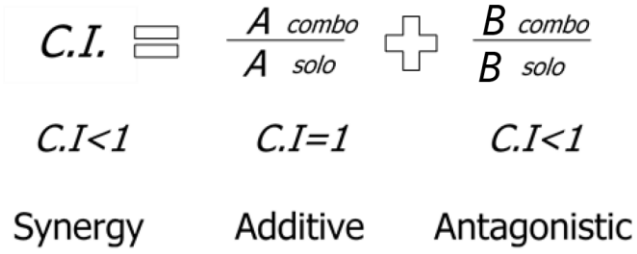

Figure 2.2 – Chou Talay synergy equation The equation for working out the CI of each drug assessed with the Chou Talay synergy assay (Chou, 2010). Drug A and B solo ID_{50} values represent the sensitivity of the cell to that individual drug. Drug A and B combo represent the ID_{50} of the drugs when used together in an equimolar combination. The equation divides the combination ID_{50} value by its individual treatment counterpart. The CI index is then generated from the values for each drugs response. An average contribution to the total CI index of less than 0.5 is determined as achieving a synergistic response. A resulting CI index of less than 1 implies the combination of the drug produces a response greater than sum of the individual treatments.

2.3 Extraction and assessment of nucleic acids

2.3.1 Genomic DNA extraction

Genomic DNA was extracted from both patient- derived short-term glioblastoma cultures and frozen biopsy material using DNeasy blood and tissue extraction kit (Qiagen, Manchester, UK). Extraction was conducted by the manufacturer's instructions. DNA extraction from fresh-frozen biopsy tissue required approximately 25 mg of tissue to be finely sliced, a 180 µl of Buffer ATL was then added and the sample was homogenised with the use of a syringe and needle for effective lysis. 50 µl proteinase K was then added to the homogenised sample, vortexed and left to incubate at 56ºC, occasionally vortexed until the tissue was completely lysed. DNA extraction from cells required a cell suspension containing 2 to 3 $x10^6$ cells, which was centrifuged at 1000 rpm for 5 minutes. The supernatant was removed, and the pellet was resuspended in 200 µl of PBS and 20 µl of proteinase K. The sample was vortexed and left to incubate at 56ºC until completely lysed. Proteinase K was added to aid with degradation of proteins. Once the tissue/ cell sample had been fully lysed, 4 µl of RNase A (100mg/ml) was added. The lysate was vortexed and incubated for 5 minutes at room temperature. After the incubation, RNA-free genomic DNA was obtained, to which 200 µl of Buffer AL and incubated for 10 minutes at 56ºC. 200 µl of 100% ethanol was then added to the isolated DNA

sample, mixed and transferred to a DNeasy mini spin column, which was centrifuged at 8000 rpm for 1 minute. The DNA bound to the filter membrane inside the spin column, was then washed with 500 µl Buffer AW1 and centrifuged for 1 minute at 10000 rpm. This step was repeated with a second wash with Buffer AW2 and centrifuged at 1000 rpm for 3 minutes in order to dry the filter and prevent ethanol carry over with the DNA elution step. 20 µl of nuclease-free water (Life Technologies, UK) was added to the filter at the centre of the column and incubated at room temperature for 1 minute. The columns were then spun at 1000 rpm to collect the eluted DNA. The collection tube was stored at -20 ºC until required.

2.3.2 RNA extraction

mRNA was extracted from both patient-derived glioblastoma cultures and frozen biopsy material using either RNeasy mini kit (Qiagen, Manchester, UK) or miRVANA RNA extraction kit (Invitrogen™).

RNA extraction using the RNeasy mini kit was conducted by the manufacturer's instructions. RNA extraction from fresh-frozen biopsy tissue required approximately 20-25 mg pf tissue, to be finely sliced. The tissue was then homogenised with the addition of 600 µl of Buffer RLT, which contained β-mercaptoethanol (10 µl per 1 ml Buffer RLT) and with the use of a syringe and needle and kept on ice. The homogenised lysate was then centrifuged at 14000 rpm for 3 minutes and the supernatant was transferred to a new nuclease -free microcentrifuge tube. RNA extraction from cells required a cell suspension containing 1 to 2 $x10^6$ cells, which was centrifuged at 1000 rpm for 5 minutes. The supernatant was removed, and the pellet was resuspended in 350 µl of Buffer RLT. Once the tissue/ cell sample had been fully lysed it was mixed with 1 volume of 70% ethanol (600 µl for tissue samples and 350 µl for cell samples). Ethanol was added to provide optimal binding conditions for the RNA. A maximum of 700 µl of sample was then transferred to an RNeasy mini spin column which was placed in a 2 ml collection tube and centrifuged at 10000 rpm for 15 seconds. The RNA bound to the filter membrane inside the spin column was then washed with 700 µl of Buffer RW1 and centrifuged for 10000 rpm

for 15 seconds. The washed step was repeated twice with 500 µl of Buffer RPE, before an additional centrifugation step for 2 minutes at 10000 rpm to dry the filter and prevent ethanol carry over with the RNA elution step. 20 µl of nuclease-free water was added to the filter at the centre of the column and centrifuged at 10000 rpm for 1 minute. The collection tube was stored at -80ºC until required.

RNA extraction using the miRVANA RNA extraction kit was in accordance with the manufacturer's instructions. RNA extraction from cells required a cell suspension containing 1 to 2 $x10^6$ cells, which was centrifuged at 1000 rpm for 5 minutes. The supernatant was removed, and the pellet was resuspended in 450 µl of Lysis/binding buffer, which was vortexed until the cells were lysed. 45 µl of Homogenate Additive was then added to the lysate mixture, which was incubated on ice for 10 minutes. After incubation 450 µl of acid-phenol: chloroform was added to the sample and vortexed for 60 seconds to mix. The mixture was immediately centrifuged for 5 minutes at 13000 rpm. After centrifugation the upper phase aqueous layer was transferred to a fresh tube without disrupting the lower phase. To the recovered mixture, 1.25 volume of 100 ethanol was added and vortexed before being transferred to a filter cartridge. The cartridge was centrifuged for 10000 rpm for 15 seconds, and to the RNA bound to the filter membrane inside the spin column, 700 µl of miRNA Wash solution 1 was added and centrifuged for 15 seconds at 1000 rpm. This step was repeated twice with 500 µl of Wash solution 2/3, before an additional centrifugation step for 1 minute 13000 rpm to remove any residual liquid and prevent carry over with the RNA elution step. The filter cartridge was transferred to a new nuclease -free microcentrifuge tube, and a 100 µl of pre-heated 90 ºC nuclease-free water was added to the filter at the centre of the column and centrifuged at 13000 rpm for 30 seconds. The collection tube was stored at -80 ºC until required.

2.3.3 Nucleic acid assessment

A Nanodrop 2000 (Thermo Scientific, UK) spectrophotometer was utilized to assess the quality and quantity of extracted nucleic acids. The calculated concentration of nucleic acids was outputted as ng/µl, which was equated using a modified Beer-

Lambert equation whereby c = (A*ϵ)/b. C is the concentration in ng/µl, A is the absorbance in Au (260 nm), ϵ is the wavelength dependent extinction coefficient (50 ng-cm/µL for double stranded DNA and 40 ng-cm/µL for RNA) and b is the pair length (cm). The quality of the sample is determined via the ratio of absorbance of the genetic material (260nm) and the precipitated proteins (280nm) – (260/280). A ratio of ·1.8 for DNA and ·2.0 for RNA were accepted as pure and deemed functional for experiments. The ratio of wavelengths between genetic material (260nm) and organic compounds/chaotropic salts (230nm) was also additionally used to assess quality of each sample. If the 260/230 ratios were greater than the respective 260/280 ratios the samples were deemed to be extremely pure. Nanodrop quantification ensured that all DNA/RNA samples were equalised to the same concentration for the respective experiments.

2.4 DNA amplification: Polymerase chain reaction (PCR)

2.4.1 Bisulfite modification of genomic DNA

Extracted genomic DNA from both fresh frozen glioblastoma biopsies and short-term cultures were bisulfite treated for methylation assays, using EZ DNA Methylation Gold kit (Zymo Research, USA) in accordance with the manufacturer instructions. Sample concentrations of DNA were equalised to contain 1 µg in 20 µl (diluted where needed with nuclease-free water); 130 µl of CT conversion reagent was then added to the 20 µl of DNA sample. The sample was vortexed and incubated for 10 minutes at 98ºC followed by 2.5 hours at 64ºC, after incubation the samples were transferred to ice. 600 µl of M-Binding buffer was then added to each sample, mixed and transferred to a Zymo-spin IC column and centrifuged at 14000 rpm for 30 seconds. The spin column which contained the bisulfite treated DNA (bound to the filter membrane) was washed with 100 µl of M-Wash buffer and centrifuged at 13000 rpm for 30 seconds. 200 µl of M-Desulphonation buffer was added to the spim columns and left to incubate for 15-20 minutes, after which the column was centrifuged at 13000 rpm for 30 seconds before being washed twice with 200 µL of M-Wash Buffer. The DNA sample was then eluted with 30 µL of M-Elution buffer and stored -20ºC until required.

2.4.2 Complementary DNA (cDNA) synthesis

cDNA was synthesised from extracted total RNA from both fresh frozen glioblastoma biopsies and short-term cultures, using Quantitect Reverse Transcription Kit (Qiagen, UK). Sample concentrations of RNA were equalised to 500 ng/µl in a total of 12 µl (diluted where needed with nuclease-free water). 2 µL of gDNA Wipeout buffer was added to the solution and incubated at 42ºC for 2 minutes to eliminate genomic DNA. The samples were immediately placed on ice, and 6 µL of reverse-transcription master mix containing 1 µL Quantiscript reverse transcriptase, 1 µL RT Primer mix and 4 µL 5x Quantiscript RT buffer was added to each sample. The samples were incubated at 42ºC for 30 minutes, followed by a 95ºC step at 3 minutes to cause inactivation of the Quantiscript reverse transcriptase. The reactions were placed on ice for immediate use or stored -20 ºC until required.

2.4.3 Methylation-Specific PCR (MS-PCR)

Methylation-Specific (MS-PCR) primers were designed using MethPrimer software: (http://www.urogene.org/methprimer/) using specified settings in order to maximise amplification efficiency. The candidate gene CpG islands and sequence were obtained using Ensembl gene browser (https://www.ensembl.org/index.html) or UCSC Genome browser (http://genome.ucsc.edu/cgi-bin). Primers were designed to not contain recognition sequences (CGCG) and were designed to ensure they spanned and amplified 200-300 bp, across at least one CpG island (an area of multiple CpG sites), encompassing a minimum of at least 4CpG sites. The oligo primers were ordered via Sigma (Sigma, UK), which were designed with a melting temperature (Tm) set between 55-60 ºC and were received at a concentration of a 100 µM. (The list of primer sequences is provided in Appendix). MS-PCR protocol as follows: 2 µl of bisulfite modified DNA (1 µg) was amplified using gene specific primers, in a total reaction of 20 µl. The reaction master mix contained 2 µL 10xPCR Buffer, 0.4 µL forward primer, 0.4 µL reverse primer, 0.4 µL 2mM dNTPs, 0.8 µL 2.5 mM MgCl2, 0.2 1UµL HotStarTaq DNA polymerase and 13.8 µL PCR grade water per sample. For each DNA sample two separate PCR reactions were performed, each reaction contained a pair of either methylated sequence primers or unmethylated

sequence primers. Universally methylated and unmethylated samples were used as a positive control, these were purchased from Zymo; additionally, a non-template control was utilized as a negative control to ensure PCR regents were contamination free. Once the PCR master mix was complete, the sample was transferred to a thermal cycler, the cycling conditions were: an initial heat activation at 94ºC for 15 minutes, followed by 30 cycles of 94ºC for 1 minute, Tm (dependent on individual primer sets 55-60 ºC) for 1 minute and 72ºC for 1 minute, a final extension of 72ºC for 10 minutes completed the program. The products were then run immediately on a 2% agarose gel via electrophoresis or stored at 4 ºC overnight.

Table 2.2 MS-PCR *HK2* primers

Primer	Sequence
HK2 methylated	AGGTTTTATTGTTCGAGTGGAGTC
HK2 unmethylated	ATCTCCGAAAACGTAATTTTAAC

2.4.4 Semi-quantitative RT- PCR

RT-PCR primers were designed using Primer 3 software software: (http://primer3.ut.ee). Exon sequences of the desired genes were obtained using Ensembl gene browser (https://www.ensembl.org/index.html) or UCSC Genome browser (http://genome.ucsc.edu/cgi-bin). Primers were designed to not contain recognition sequences (CGCG) of the restriction enzyme, and were designed to ensure they spanned no greater than 200 bp. The oligo primers were ordered via Sigma (Sigma, UK), which were designed with a melting temperature (Tm) set between 55-60 ºC and were received at a concentration of a 100 µM. (The list of primer sequences is provided in Appendix). The design of the primers at the 3‘complementarity was set to 0 to avoid primer-dimers, the primer pairs were also selected ensuring at least one would encompass an intron-exon junction in order to certify that the amplified product was from the sample cDNA and not from any other DNA contaminant. RT-PCR protocol as follows: 2 µl of sample cDNA (500 ng/µl) was amplified using gene specific primers, in a total reaction of 20 µl. The reaction master mix contained 2 µL 10xPCR Buffer, 0.4 µL forward primer, 0.4 µL reverse primer, 0.4 µL 2mM dNTPs, 0.8 µL 2.5 mM MgCl2, 0.2 1UµL HotStarTaq DNA

polymerase and 13.8 µL PCR grade water per sample. Once the PCR master mix was complete, the sample was transferred to a thermal cycler, the cycling conditions were: an initial heat activation at 94ºC for 15 minutes, followed by 30 cycles of 94ºC for 1 minute, Tm (dependent on individual primer sets 55-60 ºC) for 1 minute and 72ºC for 1 minute, a final extension of 72ºC for 10 minutes completed the program. The house keeping gene, βactin was used as positive control. The products were then run immediately on a 2% agarose gel via electrophoresis or stored at 4 ºC overnight.

Table 2.3 RT-PCR *HK2* primers

Primer	Sequence
Forward Primer	AACAAATTTCCGGGTCCTGC
Reverse Primer	GCCCATGTACTCGAGGAAGT

2.4.5 Gel Electrophoresis

The amplified PCR products were electrophoresed on a 2% agarose gel (Themo fisher), in 1 x TBE buffer (Geneflow). Ethidium bromide (SIGMA, MERCK) staining was utilized for visualisation via scanning using a Gel DocTM EZ imager, which was analysed with Syngene Gel software. A 50 bp DNA ladder (ThermoScientific, UK) was used as a comparison to confirm amplification of the product.

2.4.6 Quantitative Real-time PCR (qPCR)

Gene expression levels of selected candidate genes were determined using qPCR. Levels were quantified with the use of TaqMan assays (Fisher Life Technologies UK) with FAM dye reporter (Ogrean *et al.*, 2010) via an Applied Biosystems 7500 Fast Real-Time PCR system. The TaqMan assay included a pre-designed primer pair and a probe that was unique for each specific gene target being investigated. cDNA that had previously been transcribed as defined in 2.4.2 was utilised with the qPCR protocol as follows: 2 µl of sample cDNA was added to the qPCR reaction mix of total volume 20 µl, which consisted of 10 µl of 2x TaqMan qPCR master mix, 1 µl of TaqMan gene expression Primer/Probe set and 7 µl of nuclease free PCR grade

water. GAPDH was used as endogenous reference control as well as a no-template control (NTC), which was included to assess reagent contamination. Additionally, all reactions were performed in triplicate in a 96 well plate which was sealed with sterile optical clear seal. The PCR cycling conditions were: Initial enzyme activation at 95ºC for 15 minutes, denaturation step at 95ºC for 1 minute followed by an annealing step at 60ºC for 1 minute for 40 cycles. The final extension was at 72ºC 10 minutes. The threshold cycle (Ct) baseline was manually defined using the log view of the amplification plots. A value above the background signal, but within the lower 1/3 of the linear phase of amplification was selected. Data was analysed through MS Excel and the relative level of gene expression fold change were calculated via comparative Ct (2 -ΔΔCt) method, whereby target gene expression is normalised to GAPDH and compared to the control sample.

2.5 Flow Cytometry

Flow cytometry was carried for multiple assays using a BD Accuri C6 Plus cell analyser (BD Biosciences UK). As defined by the manufacturer's guidelines, all protocols were set to record 20,000 cell counts from the specific required gating. To ensure an accurate cell count, samples were run at a slow flow rate speed, at 14 µl/ minute (the lowest setting, keeping core stream size to a minimum), thus reducing the spread of coincidental events. Gating for each assay was initially set through the preliminary use of U251MG in order to extrapolate the most efficient settings, this was conducted with and without treatment of the control campthothecin. Campthothecin was utilized as a positive apoptotic control, cells were treated at the concentration of 100 µM over a 72-hour period to induce apoptosis.

2.5.1 Detection of apoptosis

The detection of apoptosis via flow cytometry was employed in order to assess the anti-proliferative effects of specific inhibitors upon the growth of glioblastomas cells, furthermore, to determine if the mechanism of action in which the inhibitors acted was via the apoptotic pathway. Early apoptosis was investigated using the BD

Pharmingen Annexin V FITC Apoptosis Detection Kit 1. Prior to flow cytometry, cells were seeded at 5 x 10^3 in T25 flasks and incubated at 37ºC until the determined exponential growth phase was reached, as determined by growth rate analysis. After which Cells were then treated at the relevant ID_{50} values as detailed in 2.2.5 and left for 72 hours. To ensure a total cell population was analysed, all media was collected from the T25 flask, including both floating and adherent cells, which were detached using trypsin. The harvested cell pellet was then washed twice in cold PBS, centrifuged at 1200 rpm for 5 minutes before being resuspended in 1X binding buffer at a concentration of $1x10^6$ cells/ml, as set out in the manufacturer's kit protocol. $1x10^5$ cells (100 µl) was then transferred to a sterile 25 ml universal where 5µl of PI and 5µl of FITC Annexin V dye was added to the cell solution, the tube was then vortexed and incubated in the dark for 30 minutes at room temperature. After incubation, 400 µl of 1X binding buffer was added to the tube, the cell suspension was gently mixed and transferred to a flow cytometry tube ready to be run. The gating parameter settings used in the analysis of early apoptosis was adapted from the template provided by BD Biosciences, as stated in 2.5, optimised for glioblastoma cells using U251. The gating was aligned for the untreated control of each culture used, to ensure the reading were accurate.

2.5.2 Mitochondrial membrane potential

Mitochondrial membrane potential was analysed in order to detect any membrane potential changes in cells, this was investigated using the cationic, lipophilic JC-1 dye (part of the JC-1 Mitochondrial Membrane Potential Assay Kit) (BD MitoScreen). JC-1 in normal cells is taken up and concentrated within the mitochondrial matrix, when bound it forms red fluorescent aggregates.

JC-10 in apoptotic and necrotic cells, however, diffuses out from the dysfunctional mitochondria

And changes to a monomeric form, which stains cells with green fluorescence. The potential of the mitochondrial membrane (ΔΨ) was assessed by the shift in green emission, which was analysed in via fluorescence channel 1 (FL1), fluorescence channel 2 (FL2) detected the orange emission (Liu Z *et al*, 2014). Camptothecin was used as an apoptotic control, at 100µM over a 72-hours. Cells were seeded at 5 x 10

3 in T25 flasks and incubated at 37ºC until the determined exponential growth phase was reached. After which Cells were then treated at the relevant ID_{50} values as detailed in 2.2.5 and left for 72 hours. Cells were trypsinised and transferred to a 10ml sterile universal and centrifuged for 1200 rpm for 5 minutes. The cell pellet was washed in 5ml of PBS before being resuspended in 500 µl JC-1 working solution, which was then incubated for 15 min in a 37ºC incubator. After incubation the cells were centrifuged at 1200 rpm and washed with 1x assay buffer before being analysed in a flow cytometer. The gating parameter settings used to analyse mitochondrial membrane potential was adapted from the template provided by BD Biosciences, as stated in section 2.5, and optimised for glioblastoma cells using U251. The gating was aligned for the untreated control of each culture used, to ensure the reading were accurate.

2.6 Caspase pathway analysis

The level of caspase 3/7 proteins present within the cultures were investigated with the selected inhibitors, to determine if a caspase-dependent apoptotic pathway was the main mechanism leading to cell death in glioblastoma cells. To assess levels, the Caspase-Glo® 3/7 Assay (Promega, UK) was utilized, which is a homogeneous luminescent assay allowing for caspase 3 and 7 activities to be measured. The kit contains a luminogenic caspase-3/7 substrate, which is a reagent containing a tetrapeptide sequence-DEVD, optimised for caspase and luciferase activity. The addition of the Caspase-Glo® 3/7 Reagent causes cell lysis, which results in caspase cleavage of the substrate and in turn leads to the generation of a luminescent signal produced from a luciferase reaction. The amount of luminescence detected by the plate reader is proportional to the amount of caspase activity present within the sample.

Cells were seeded simultaneously at 4000 cells per well on two 96 well plates and incubated at 37ºC until the determined exponential growth phase was reached. After which cells were then treated at the relevant ID_{50} values as detailed in 2.2.5, in a 100 µl of media and left for 72 hours. One plate was stained and analysed using the

SRB assay, as detailed in section 2.2.2. To the other plate, 200µl of Caspase-Glo® 3/7 Reagent was added to the 200 µl of media in both treated and untreated wells, the contents were gently mixed for 10 minutes at 300 rpm on a plate shaker and incubated at room temperature for 1 hour in the dark. After incubation the plate was transferred to a 96 well white walled plate and analysed on a Promega Glomax plate reader to measure the luminesce. The Caspase-Glo measured values were then normalised against its respective sample value from the SRB plate, the normalisation ensured a better representation of caspase 3/7 activity per cell. Camptothecin was used as an apoptotic control, at 100µM over a 72-hours.

2.7 CRISPR mediated gene knockout

HK2 was knocked out using CRISPR in short-term patient-derived glioblastoma cultures and the established cell line U251MG. CRISPR vectors were purchased from OriGene All-in-one vector kit (Origene, USA). The kit contained 2 gRNA vectors and 1 donor DNA and is a complete kit to knockout any coding gene and with a knock-in selection cassette. The gRNA vectors were provided in pCas-Guide vector with a target sequence cloned, with both target sequences located at the 5' end of the ORF; gRNA vectors therefore will precisely cleave at the 5' end of the ORF of the gene loci. with HDR-based (Homology Directed Repair) donor vector construction. A puromycin resistant gene was included within the donor construct. (Figure 2.4) The vector targeted sequences are: HK2 gRNA vector 1 in pCas-Guide vector, Target Sequence: AAGGTAAGTCAGCGCGGGCG, and HK2 gRNA vector 2 in pCas-Guide vector, Target Sequence: GAAGTAGGCAAGCAGATGCG. The donor plasmid was integrated into the genome via homology-directed repair (HDR) mechanism. A scrambled control vector was used as a negative control.

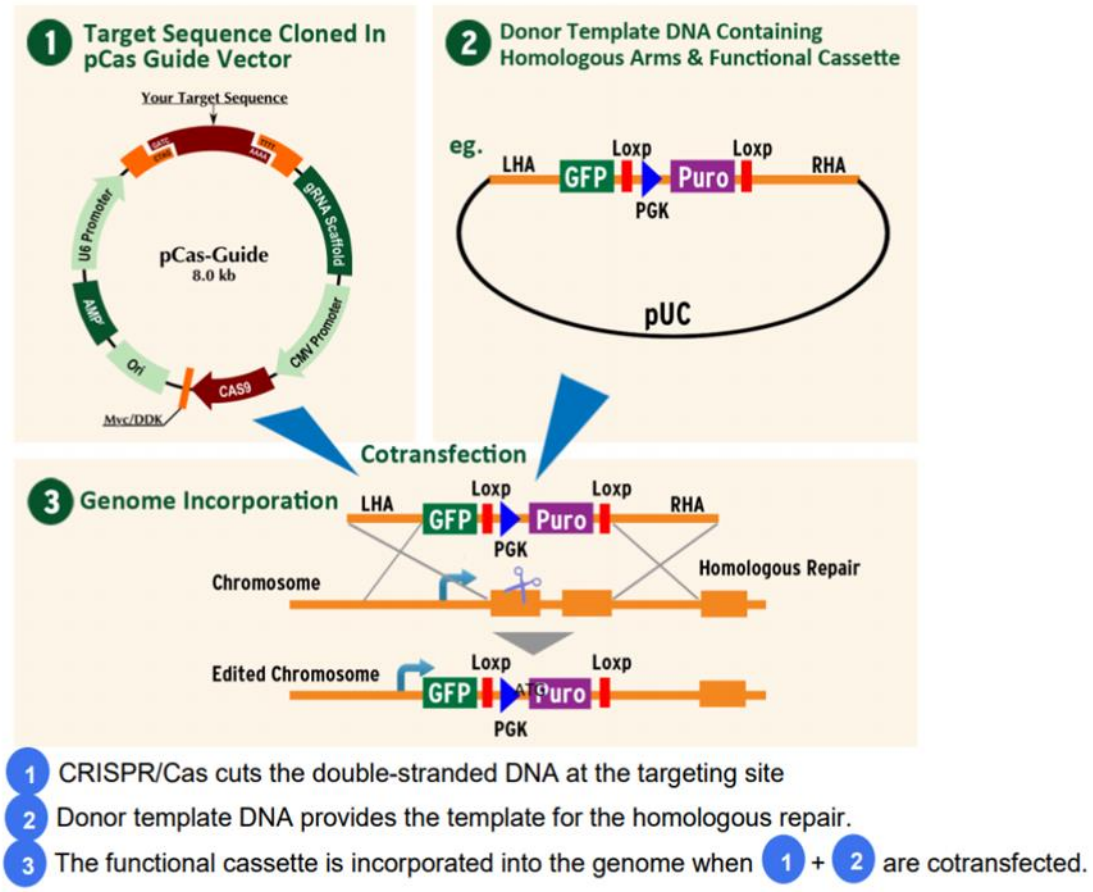

Figure 2.4 Scheme of genome-editing knockout kit Donor vector for each kit contains around 600 bp locus specific homologous sequence on each side of the donor selection cassette. LHA – left homologous arm, RHA – right homologous arm (Origene, 2019).

The CRIPSR protocol was adapted from the Origene template, where cells were seeded approximately 24 hours before transfection at $3x10^5$ cells per well in 2 ml of culture medium in T a 6-well plate, this ensured between 50-75% confluence for transfection the following day. Transfection was undertaken in complete culture medium, in three separate transfections (wells), one for each gRNA vector and the scramble control. In a sterile tube(s) the transfection reagents were added in a prescribed order, the order of which the reagents were added was important to optimise transfection success. 1 µg of each gRNA or scramble vector was diluted in 250 µl of Opti-MEM 1 (Life Technologies) transfection media, and vortexed gently to mix. To each tube 1 µg of the donor DNA was added to the 250 µl of Opti-MEM I solution. Individual vectors were diluted into separate sterile tubes in order to test the gRNA transfection efficiency. To each tube 9 µl of TransFast™ Transfection Reagent (Promega, UK) was added and gently mixed, and incubated for 15 minutes

at room temperature. The ratio of transfection Reagent to donor DNA was optimised, following the initial guidelines of Origene. After incubation the transfection reagents mixture was added dropwise to the cells plated 24 hours prior (without media change). The 6-well plate was rocked gently to ensure the transfection complex was evenly distributed, the cells were incubated for 48 hours in a 5% CO2 incubator. After incubation the cells were split 1:10 and grown for an additionally 3 days, before being split again 1:10. This was repeated for a total of 7 passages to ensure that the cells containing puromycin resistance from the plasmid donor DNA (before genomic integration) were diluted out of culture, increasing the amount of successful transfected cells to maintain puromycin resistance before applying the puromycin selection. After 7 passages cells were split 1:10 and grown in 10 cm dishes in media containing puromycin the range of puromycin used was 1µg/ml to 5µg/ml). A dose curve was utilized to determine the lowest dose that killed non-transfected cells completely 7 days post selection, which was dependant on specific cultures. The media containing the puromycin was changed ever 2-3 days. After 7 days of selection, the surviving cell colonies were isolated using a dilution method, whereby cells were seeded <10 cells per well in a 96 -well plate. After 10 days, cells containing a single cell colony were expanded first into a 6 well plate and then into T25 flasks. The puromycin resistant cells were then analysed and verified via genomic qPCR to ensure the integration of the functional cassette. qPCR was conducted as detailed in section 2.4.6.

2.8 Pyrosequencing

Pyrosequencing was utilized to analyse and quantify levels of methylation of specific gene targets across the genome in glioblastoma cell cultures and fresh frozen biopsy tissue. Pyrosequencing was conducted using Qiagen's PyroMark CpG Assays (Qiagen, UK), using pre-designed highly specific primers for pyrosequencing methylation analysis. The pre-designed primer set includes both the PCR and sequencing primers for the quantification of DNA methylation by Pyrosequencing. The PCR primers are biotinylated, generating biotinylated PCR product from the template bisulfite converted DNA. The biotinylated PCR product is then bound to streptavidin-coated sepharose beads, which are captured using a PyroMark Vacuum Workstation, where

they are washed and denatured resulting in a single-stranded DNA which is suitable for pyrosequencing. The single-stranded template DNA is transferred to a Pyrosequencing reaction plate which contains the sequencing primer provided with the PyroMark CpG Assay kit. After the sequencing primer had annealed the plate was sequenced on a PyroMark Q96 instrument using a specific sequence to analyse. The resulting data generated gave percentage of methylation across each CpG site within the sequence. The protocol was adapted and optimised from Qiagen template as follows. DNA was extraction, quantified and bisulfite treated as previously detailed. Bisulfited treated DNA was amplified using Qiagen PyroMark CpG PCR primers on a 96-well plate, the cycling conditions were: an initial heat activation at 94ºC for 15 minutes, followed by 30 cycles of 94ºC for 1 minute, Tm (dependent on individual primer sets 55-60 ºC) for 1 minute and 72ºC for 1 minute, a final extension of 72ºC for 10 minutes completed the program. After amplification 37 µl of binding buffer and 3 µl of streptavidin-coated sepharose beads was added to each sample well. The plate was sealed with sterile film and placed on a plate shaker for 5 minutes at 1300 rpm. 38.5 µl of annealing buffer and 1.5 µl of sequencing primer (10 pmol/ µl) was added to a separate sequencing plate, designed for the PyroMark Q96 instrument. After mixing the plate was taken to the PyroMark Vacuum Workstation, which consisted of a 4-step process. The probes of the hedgehog appliance were initially washed in distilled water, the hedgehog was then slowly lowered into the well of the 96-well plate in order to capture the DNA bound to the sepharose beads. Once captured the beads were washed in 100% ethanol for 5 seconds, and then washed for an additional 10 seconds in a denaturising solution, as part of a kit (Qiagen, UK). The final step was to wash off excess denaturising solution with wash buffer before lowering the hedgehog over the sequencing plate. The vacuum Workstation was switched off and the beads were released into the annealing buffer containing the sequencing primer, the sequencing plate was placed immediately on a heat block at 80 ºC for 2 minutes. After the incubation the plate was transferred to the PyroMark Q96 instrument. Additionally, a Q96 cartridge was placed into the pyrosequencer, which was loaded with the correct DNTPs for the sequence to be analysed, the enzyme, substrate and RNA-free water. The amount of each reagent was specific for the sequence to analyse.

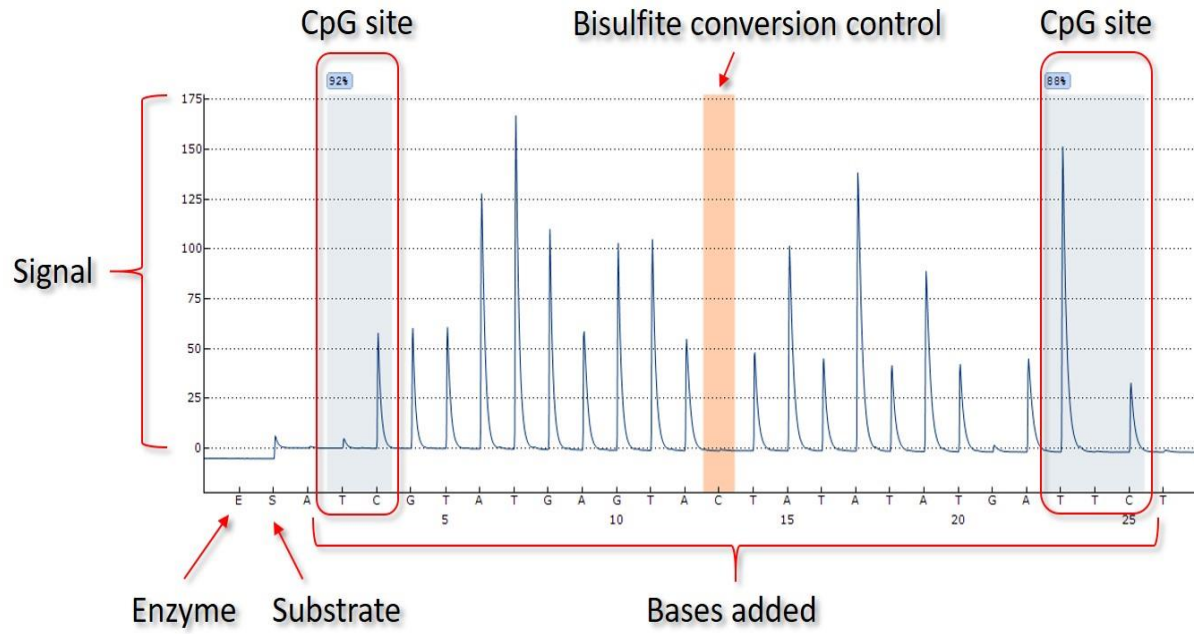

Figure 2.5. Showing pyrograms for DNA methylation analysis A hypothetical DNA sequence. The x-axis is the dispensation sequence (time), and the y-axis is the intensity of the bioluminescence. The presence of a peak indicates the injected dNTP was incorporated, whereas the absence of a peak indicates the polymerase was unable to incorporate the dispensed dNTP. Peak height is proportional to the number of deoxynucleotide triphosphates incorporated. A virtual pyrogram demonstrates that the height of the peaks is proportional to the number of nucleotides incorporated. For example, the first G peak is taller than the first T peak, indicating more deoxyguanosine triphosphates were incorporated compared to deoxythymidine triphosphate. The dispensation order was optimized by Qiagen for the known gene targets (Qiagen, 2019).

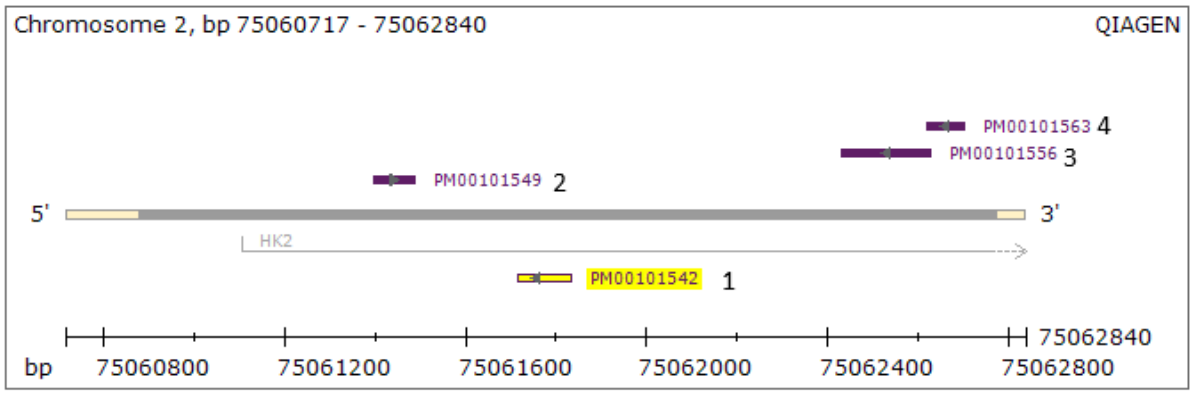

Figure 2.6 Showing the location of the Qiagen pyrosequencing *HK2* sequencing primer sets The location of the primers is labelled 1-4, incorporating multiple CpGs as listed in Table 2.2.

Table 2.4 Pyrosequencing: *HK2* sequencing primers

Primers	Sequence	
Primer set 1 CpG 1-4	Sequence to Analyse	CTGCCGCCCCGCCCGCGC

	Sequence After Bisulfite Treatment	TTGTYGTTTYGTTYGYGT
Primer set 2 CpG 5-7	Sequence to Analyse	CGGACACGTCGT
	Sequence After Bisulfite Treatment	YGGATAYGTYGT
Primer set 3 CpG 8-11	Sequence to Analyse	ACGCGGCGCGT
	Sequence After Bisulfite Treatment	AYGYGGYGYGT
Primer set 4 CpG 12-15	Sequence to Analyse	CGGCCGCGGTGAGCGC
	Sequence After Bisulfite Treatment	YGGTYGYGGTGAGYGT

Table showing the 4 Qiagen pyrosequencing *HK2* sequencing primer sets. Primer set 1 spans CpGs 1-4, set 2 spans CpGs 5-7, set 3 spans CpGs 8-11 and set 4 spans CpGs 12-15.

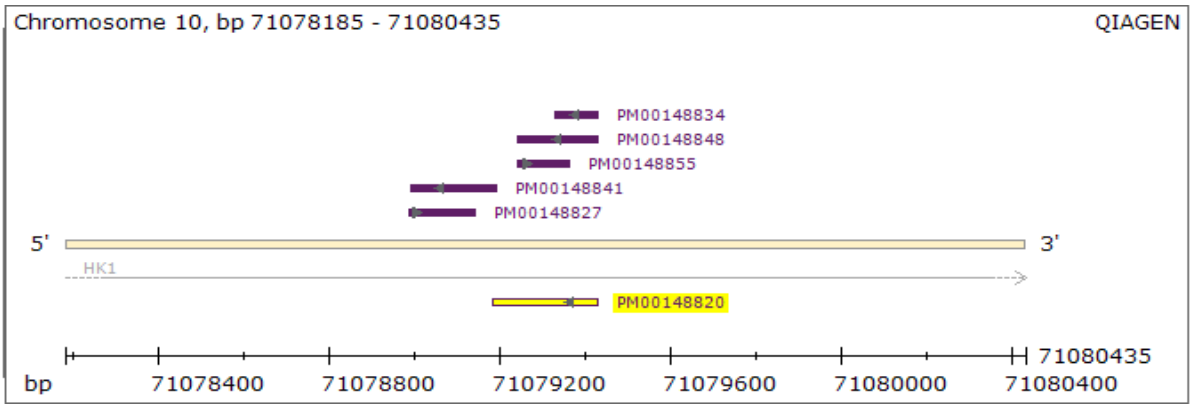

Figure 2.7 Showing the location of the Qiagen pyrosequencing *HK1* sequencing primer sets The selected primer set is highlighted in yellow, spanning multiple CpG sites.

Table 2.5 Pyrosequencing: *HK1* sequencing primers

Primer set	Sequence to Analyse	GCCCGGCGACAGCTTCTCCGGGGCACCCGA
	Sequence After Bisulfite Treatment	GTTYGGYGATAGTTTTTTYGGGGTATTYGA

Table showing the pyrosequencing *HK1* sequencing primer set. The primer set spans 4 CpGs and was selected due to maximum coverage across the *HK1* promotor region.

2.9 Expression Profiler Array

Qiagen RT expression profiler arrays (Qiagen, UK) were utilized to analyse the expression of 84 key genes involved in the regulation and enzymatic pathway of glucose metabolism in glioblastoma biopsy tissue, patient derived short-term cell cultures and U251 MG. The profiler arrays were conducted using an optimized protocol from Qiagen. Extracted RNA was initially converted to cDNA using a cDNA Synthesis RT First Strand kit (Qiagen, UK), at an optimal concentration of 500 ng/µl

in a total of 10 µl (diluted where needed with nuclease-free water). 2 µL of gDNA Wipeout buffer GE was added to the solution at incubated at 42ºC for 5 minutes to eliminate genomic DNA. The samples were immediately placed on ice, and 10 µL of reverse-transcription master mix containing 4 µL Buffer BC3, 1 µL control P2, 1 µL RE3 Reverse Transcriptase mix and 3 µL nuclease-free water was then added to each sample. The samples were gently vortexed to mix, and incubated at 42ºC for 15 minutes, followed by a 95ºC step at 5 minutes to cause inactivation of the Quantiscript reverse transcriptase. 91 µL nuclease-free water was then added to the sample to ensure the right concentration of cDNA was present (manufacturers protocol) for each well of the array plate. The array plate consisted of 84 target genes, 5 housekeeping genes and positive/negative controls, the primer/probe for each gene was pre-pelleted to each designated well. From the synthesised cDNA, 102 µL was added into a SYBR Green master mix (Qiagen, UK) with a total volume of 2700 µL, this consisted of, 1350 µL of 2X RT SYBR Green master-mix and 1248 µL nuclease-free water. The master-mix was designed for a complete 96 well plate with 300 µL excess volume for pipette carry over, and to perform any quality control analysis. 25 µL of master-mix containing the cDNA was transferred into each well of the 96- well array plate, the plate was sealed with optical adhesive seal and centrifuged at room temperature at 1000g for 1 minute. After centrifugation the plate was checked to ensure no bubbles were present in any well before being transferred to the Applied Biosystems 7500 Fast Real-Time PCR system. The PCR cycling conditions were initial Hot star DNA enzyme activation at 95ºC for 10 minutes, denaturation step at 95 ºC for 15 seconds followed by an annealing step at 60 ºC for 1 minute for 40 cycles. During the 40 cycles fluorescence data was collected. The threshold cycle (Ct) baseline was manually defined using the log view of the amplification plots. A value above the background signal, but within the lower 1/3 of the linear phase of amplification was selected. The Ct values were exported to excel and then uploaded using Qiagen PCR array data analysis web-based software.

2.10 Statistical Tests

Most experiments conducted have a minimum of three biological repeats, to ensure for accurate statistical analysis. Standard deviation and standard error were carried out were appropriate on data sets to identify any significant trends. Graphs were

created on both Microsoft Excel Open office version 1701 and GraphPad Prism 7.03, error bars on all graphs show standard error of the mean for each sample based upon the biological replicates. Graph pad prism was utilised to determine ID_{50} values for all samples and to calculated linear regression.

2.10.1 Student's t-test

The statistical significance of differences between two groups was determined using student's t-test, by comparing the mean value of each data set. Student's t-test was carried out using GraphPad Prism web tool software (http://www.graphpad.com/quickcalcs/contMenu/). Significant difference was defined as a p-value to be less than 0.05.

2.10.3 Keplan-meir curve and Mantel-Cox test

Compares two or more survival curves where some of the observations may be censored and where the overall grouping may be stratified. The methods are nonparametric in that they do not make assumptions about the distributions of survival estimates. The Mantel-Cox test statistic compares estimates of the hazard functions of the two groups at each observed event time. It is constructed by computing the observed and expected number of events in one of the groups at each observed event time and then adding these to obtain an overall summary across all-time points where there is an event. The tests were performed using GraphPad Prism 7.03.

Chapter 3

Increased expression of HK2 in glioblastoma

3.1 Introduction

The development of novel therapeutic targets for the treatment of glioblastoma has had very limited success, despite continuous efforts, in in prolonging the survival and quality of life of patients (Zhang *et al.*, 2012; Howlader *et al.*, 2016). Primary management is surgical resection, radiation and concomitant treatment with temozolomide, however average survival is only 14 months (Stupp *et al.*, 2015; Lee *et al.*, 201). Effective drug treatments are hindered predominantly by the complex genetic background of glioblastoma, with significant intra- and inter- tumour heterogeneity drastically limiting monotherapies (Backes, *et al.*, 2015). Another obstacle is the translation of validated molecular targets and inhibitors from *in vitro* studies through to *in vivo* models and into a clinical setting, largely due to

inadequate well-characterised pre-clinical models. For many years established cell lines have been principally used as experimental therapeutic models *in vitro*, and whilst these studies have contributed to the existing understanding of glioblastoma biology, these models do not accurately represent the genetic constitution seen within patient tumours, due to their tendency to acquire additional genetic alterations through increasing numbers of cell passage (Torsvik *et al.*, 2014). The genetic and epigenetic heterogeneity found both within the same tumour and between different glioblastoma is fundamentally difficult to reiterate *in vitro* (Sottoriva *et al.*, 2013; McGranahan and Swanton, 2015). However, primary cultures derived from tumour biopsies have been shown to maintain considerable genetic characteristics of the parent biopsy and studies have shown that glioblastoma derived cell cultures retain copy number changes, mutations, expression profiles and methylation status comparable to the original biopsy tissue (Potter *et al.*, 2009; Yost *et al.*, 2013). With substantial tumour heterogeneity across both the same tumour and between tumours, an alternative approach is to target abnormal metabolic pathways that are universally dysregulated in glioblastoma. Treatments which modulate metabolism are likely to be effective in a higher percentage of patients, whilst sparing normal cells and reducing negative side effects (Wolf *et al.*, 2010). Studies have also shown an increased efficacy of conventional chemotherapeutic drugs in combination, in multiple tumour types that have also had their metabolism targeted, although the synergistic mechanism is yet to be fully understood (Bayat Mokhtari *et al.*, 2018). The glycolytic enzyme hexokinase (HK), and its isoforms 1 and 2 are associated with mitochondria and are implicated in cell survival, proliferation and in aerobic glycolysis in cancer cells including glioblastoma (Patra *et al.*, 2013). There is evidence that HK2 overexpression in cancer cells increases tumour invasion and aggression as well as enhanced resistance to therapies (Wang *et al.*, 2014; Anderson *et al.*, 2016). There have been preliminary studies investigating the role of HK2 in glioblastoma, however the establishment of HK2 overexpression is currently not fully understood (Wolf *et al.*, 2011).

The aim of this study was to further determine the role of Hexokinase 1 and 2 in the development of glioblastoma and to ascertain its apparent role in patient outcome; by investigating the expression levels of HK1 and HK2 in both patient biopsies and

patient derived glioblastoma derived cell cultures. In addition, epigenetic alterations were ascertained via methylation analysis and patient survival studies were conducted. Furthermore, the effective genetic representation of patient derived glioblastoma cultures, compared to biopsy material was established. The established cell lines U251MG and U87MG were utilized alongside 19 patient derived cultures (including both IN and UWLV cultures as shown in table 2.1) throughout this study.

3.2 Quantitative assessment of *Hexokinase 2* expression

In order to determine alterations in expression of *HK2* in glioblastoma, mRNA levels were analysed by real time quantitative PCR in 103 glioblastoma biopsies as well as in 5 normal brain tissue samples. Additionally, 19 glioblastoma patient-derived cell cultures and 2 established cell lines were investigated and compared to both NHA and normal brain samples.

An increase in *HK2* mRNA expression was observed in all 103 glioblastoma biopsies compared to normal brain tissue, as shown in Figure 3.1 and Table 3.1. Overexpression of *HK2* ranged from 3.83 to 897.54-fold-change compared to normal brain tissue, normalised to 1-fold change (all normal brain samples showed little variance in fold change, with a fold change difference of 0.4), with significantly increased levels demonstrated in 101 biopsies ($p<0.0001$) (as determined via students t-test). *HK2* overexpression was also observed in all glioblastoma patient-derived cultures and the established cell lines U251MG and U87MG, as shown in Table 3.2 and Figure 3.2. Elevated levels of *HK2* ranged from 85.73-fold change to 995.12-fold change increase in glioblastoma patient-derived cultures compared to normal brain. The established cell line U87MG had an increased fold change of over 1294, and U251MG demonstrated upregulation of approximately 1502.61-fold change increase compared to normal tissue. Furthermore, the level of mRNA expression was also increased in cultured normal human astrocytes in comparison to normal tissue, with an increase in fold change of 30.42.

The data shows overexpression of *HK2* is a frequent occurrence in glioblastoma, furthermore, the elevated change in mRNA expression is also maintained *in vitro* in

patient-derived cultures. The level of HK2 expression was additionally compared to *MGMT* status for the 103 biopsy samples. The *MGMT* status for the samples was determined via MS-PCR. No significant correlation between the level of HK2 overexpression and *MGMT* status was demonstrated in the biopsies. Average HK2 expression for unmethylated *MGMT* biopsies was 204.5- fold change, comparatively the HK2 expression for methylated *MGMT* biopsies was 241.9- fold change. There was, however, a correlation with *MGMT* status and the level of HK2 expression in the culture samples, where average HK2 expression for unmethylated *MGMT* cultures was 207.7- fold change, compared to 661.1- fold for the methylated *MGMT* cultures. The data indicates that HK2 overexpression is independent of *MGMT* status in glioblastoma biopsies, and therefore is a potential additional therapeutic target for further stratification of patients. *MGMT* data is shown in the appendix.

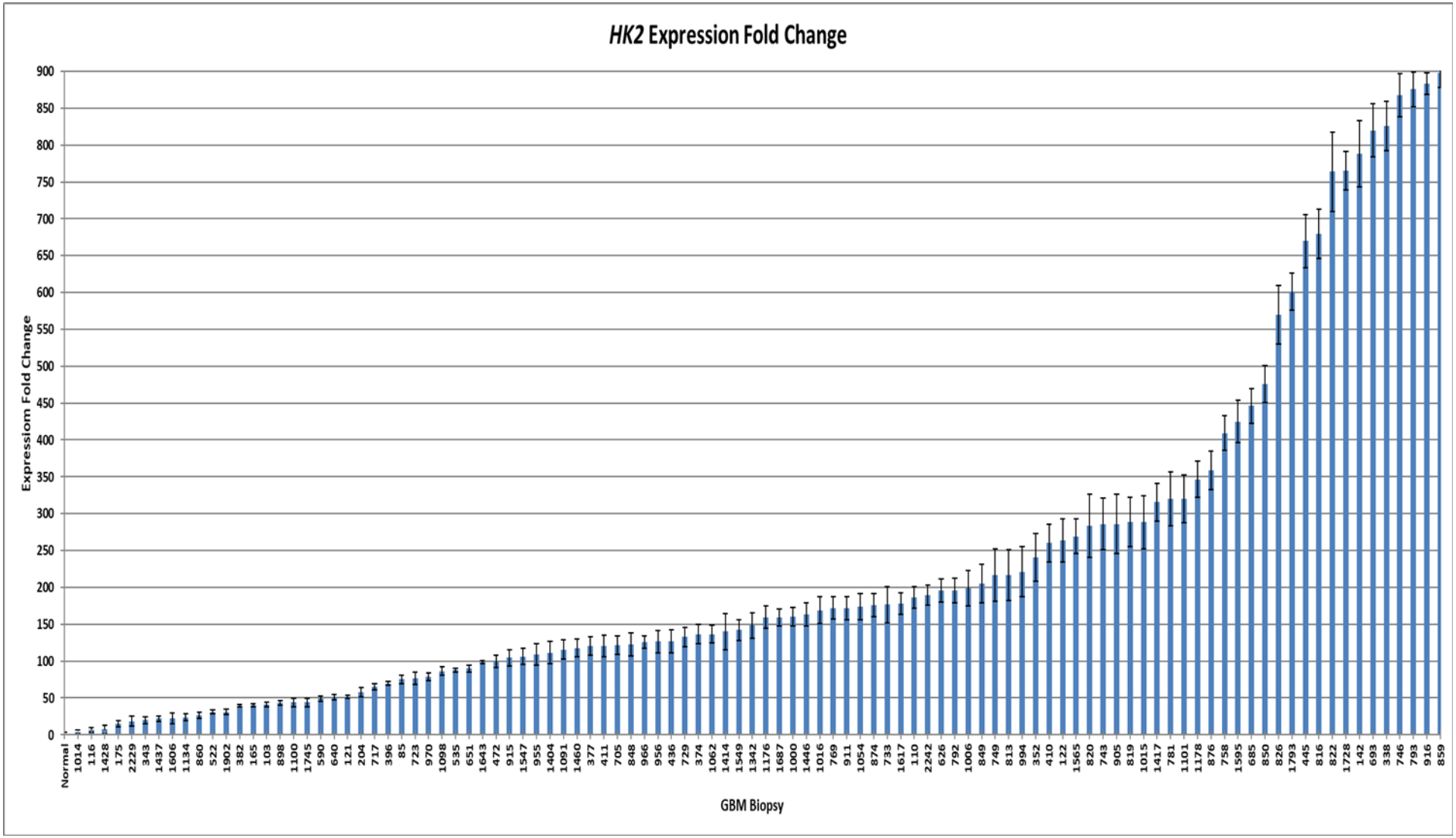

Figure 3.1. Expression fold change of *HK2* mRNA in glioblastoma biopsies relative to normal tissue. Fold change has been normalised against average expression level of normal brain tissue (n=5). *HK2* expression is elevated in all glioblastoma biopsies compared to normal tissue. Data shown is taken from an average fold change value of 3 replicates.

Table 3.1 Expression fold change of *HK2* in glioblastoma biopsies

Biopsy Sample	HK2 Fold Change (SD (±))	Biopsy Sample	HK2 Fold Change (SD (±))
Normal	1 (0.62)	1342	148.30 (2.11)
1014	3.82 (2.64) *	1176	159.44 (3.34)
116	6.69 (1.24) *	1687	159.51 (0.12)
1428	7.42 (4.45)	1000	159.83 (0.98)
175	14.90 (3.46)	1446	163.25 (2.55)
2229	18.38 (0.45)	1016	169.03 (3.17)
343	20.06 (2.43)	769	172.1 (3.78)
1437	21.91 (1.65)	911	172.11 (2.12)
1606	22.35 (0.98)	1054	173.91 (2.11)
1134	23.62 (3.56)	874	175.96 (0.87)
860	26.13 (2.91)	733	176.43 (1.68)
522	30.76 (1.66)	1617	178.38 (0.38)
1902	31.09 (3.45)	110	186.29 (3.41)
382	39.29 (0.54)	2242	189.65 (2.65)
165	40.137 (2.45)	626	195.29 (0.91)
103	41.05 (3.21)	792	195.96 (3.11)
898	43.57 (1.73)	1006	198.95 (1.95)
1100	43.7 (1.49)	849	205.23 (3.91)
1745	43.80 (1.36)	813	216.01 (2.44)
590	49.06 (2.46)	749	216.22 (0.68)
640	51.06 (0.92)	994	221.62 (0.39)
121	51.72 (3.12)	410	260.13 (3.1)
204	57.37 (2.82)	122	263.73 (1.53)
717	65.2 (4.59)	1565	269.09 (2.16)
396	69.44 (3.65)	352	276.749 (2.72)
85	75.21 (1.98)	820	283.29 (3.58)
723	77.03 (0.21)	905	285.23 (3.18)
970	78.72 (1.24)	743	285.95 (0.24)
1098	86.34 (3.54)	1015	288.18 (1.25)
535	87.79 (2.46)	819	288.41 (1.83)
651	89.84 (2.99)	1417	315.68 (0.57)
1643	98.54 (1.53)	1101	320.24 (2.65)
472	99.50 (3.12)	781	320.44 (2.91)
915	104.50 (0.47)	1178	346.43 (2.52)
1547	106.30 (3.1)	876	358.76 (3.18)
955	109.23 (2.66)	758	409.23 (0.49)
1404	111.39 (2.29)	1595	425.07 (0.83)
1091	115.78 (3.42)	850	475.89 (4.14)

1460	117.87 (1.97)	826	569.76 (3.95)
377	120.25 (1.22)	1793	600.96 (1.17)
411	120.72 (0.89)	445	669.94 (1.73)
705	121.62 (3.54)	816	679.90 (2.72)
848	122.11 (2.82)	822	763.67 (4.81)
966	125.62 (2.11)	1728	764.9 (2.33)
956	126.62 (2.43)	142	788.29 (3.3)
436	127.23 (1.53)	693	819.78 (2.01)
729	132.68 (1.6)	338	825.58 (2.78)
374	136.68 (0.9)	746	867.61 (3.14)
1062	136.68 (2.56)	793	875.78 (1.51)
1414	140.13 (1.21)	916	883.25 (4.11)
1549	142.07 (2.34)	859	897.54 (2.81)
685	446.03 (2.73)		

Fold change has been normalised against average expression level of normal brain tissue. *HK2* expression is over-expressed across all glioblastoma biopsies compared to normal tissue. Standard deviation for each average is listed after each result (±). All samples show significantly ($p<0.0001$) increased fold change compared to normal unless denoted with *.

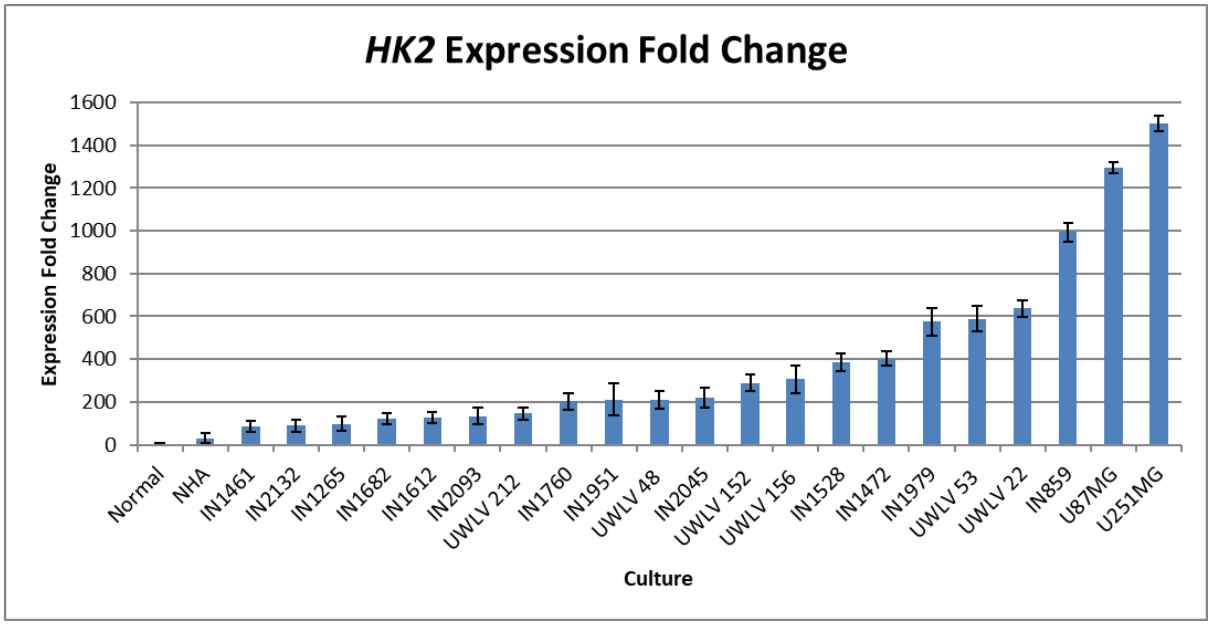

Figure 3.2. Expression fold change of *HK2* in glioblastoma cultures relative to normal tissue Real time qPCR analysis of *HK2* glioblastoma cultures and cell lines. Fold change has been normalised against average expression level of normal brain tissue. *HK2* expression is elevated in all glioblastoma cultures and established cell lines compared to normal tissue, indicative that overexpression occurring within glioblastoma is maintained in culture. *HK2* expression was also increased in NHA compared to normal brain. Data shown is taken from an average fold change value of 3 replicates.

Table 3.2 Expression fold change of *HK2* mRNA in glioblastoma cultures

Culture Sample	*HK2* Fold Change (SD (±))
Normal	1 (1.23)
NHA	30.42 (3.12)
IN1461	85.73 (2.94)
IN2132	88.35 (3.58)
IN1265	97.35 (3.41)
IN1682	120.54 (2.65)
IN1612	126.63 (0.91)
IN2093	132.75 (0.24)
UWLV 212	145.42 (1.25)
IN1760	201.96 (1.83)
IN1951	210.63 (1.95)
UWLV 48	211.43 (0.57)
IN2045	219.82 (1.22)
UWLV 152	289.65 (0.89)
UWLV 156	306.89 (3.54)
IN1528	385.95 (2.82)
IN1472	403.36 (2.11)
IN1979	574.39 (3.01)
UWLV 53	589.16 (1.92)
UWLV 22	637.35 (0.48)
IN859	995.11 (1.54)
U87MG	1294.26 (2.11)
U251MG	1502.61 (1.96)

Real time qPCR analysis of HK2 glioblastoma cultures and cell lines. Fold change has been normalised against average expression level of normal brain tissue. HK2 expression is elevated across all glioblastoma cultures and established cell lines compared to normal tissue. HK2 expression was also increased in NHA compared to normal tissue. Standard deviation for each average is listed after each result (±).

Average expression of *HK2* across the biopsies was approximately 229.4-fold change increase compared to normal tissue and median of the 103 biopsy samples was 154-fold change. The samples were separated into 2 groups for further analysis depending on the level of *HK2* expression above or below the median value thus determining the cut off between subpopulations. The statistical significance between the subgroups, of <154-fold change and >154-fold change increase, was assessed via a students unpaired T-test, whereby a significant difference ($p<0.0001$) was perceived between the 2 groups of biopsy sub-populations as shown in Figure 3.3. A significant difference of $p=0.0006$ was also apparent between normal tissue and the

subgroup >154-fold change, and a significance of p=0.0003 was observed between normal tissue and the subgroup <154-fold change with respect to the level of *HK2* expression. Utilizing similar statistical methods, qPCR data revealed 2 divergent subtype populations across the glioblastoma cultures, with respect to *HK2* expression values. Average expression of *HK2* across the glioblastoma cultures was approximately 410.5-fold change increase compared to normal tissue, with a median value of 220. The samples were separated into 2 groups for further analysis depending on the level of HK2 expression above or below the median value. A statistical significance (p=0.0004) between the subgroups was established, additionally, both glioblastoma culture subgroups demonstrated a significant difference of expression compared to both NHA (p=0.0019) and normal brain tissue (p<0.0001) as shown in Figure 3.4.

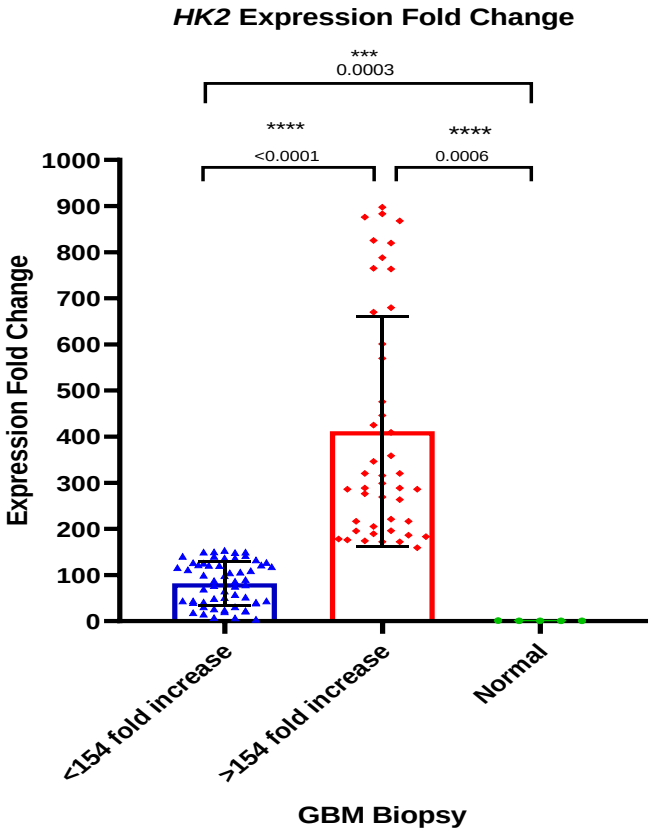

Figure 3.3 Expression fold change of *HK2* in subpopulations of glioblastoma biopsies relative to normal tissue Real time qPCR analysis of *HK2* glioblastoma biopsies. Fold change has been normalised against average expression level of normal brain tissue. Two distinct populations of glioblastoma expressing upregulated *HK2* levels, <154 -fold change increase and >154-fold change increase, p value significance is denoted with * between groups. The bars represent mean and SD deviation.

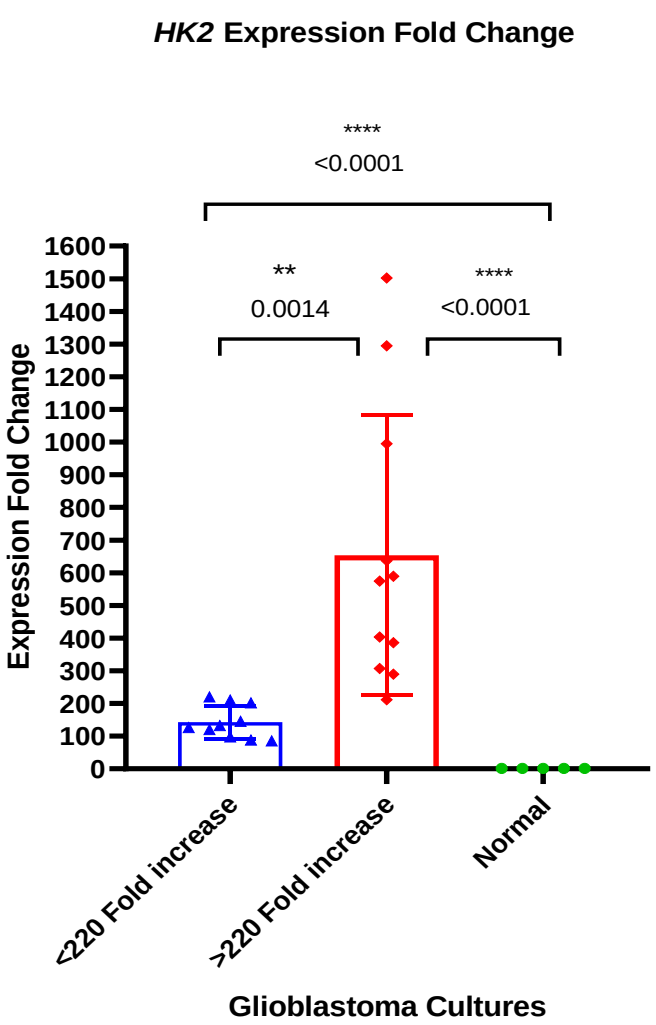

Figure 3.4 Expression fold change of *HK2* in subpopulations of glioblastoma cultures relative to normal tissue Real time qPCR analysis of *HK2* glioblastoma cultures. Fold change has been normalised against average expression level of normal brain tissue. Two distinct populations of glioblastoma expressing upregulated *HK2* levels, <220- fold change increase and >220-fold change increase. p value significance is denoted with * between groups. The bars represent mean and SD deviation.

3.3 Quantitative assessment of *Hexokinase 2* methylation

The methylation status of the promotor region of *HK2* was investigated to determine whether epigenetic alternations occur in glioblastoma compared to normal tissue using both MS-PCR and pyrosequencing. The methylation status of *HK2* was determined in 36 glioblastoma biopsies and 10 cultures by MS-PCR. More than 90% (n=33) of the biopsies showed some hypomethylation of HK2, including 5 biopsies (374, 110, 743, 705, 1617) that were completely hypomethylated. There was also

complete hypomethylation of *HK2* in 4 cultures (U251MG, IN859, IN2093, IN1528), whereas the remaining 6 cultures had only partial methylation. Additionally, there was complete hypermethylation of HK2 present in 3 biopsy samples, as seen in Figure 3.5. Full quantification of the level of methylation in glioblastoma samples was then determined by pyrosequencing. Fifteen individual CpG sites were investigated across the promotor region of *HK2* as shown in Figure 3.7. Ten glioblastoma biopsies and 2 normal brain tissue samples were initially investigated via pyrosequencing, using 4 Qiagen predesigned primer sets, as shown in 2.8, to determine which CpG sites were to be selected for further investigation for all the glioblastoma samples. A positive human methylated and unmethylated control was used, purchased from Zymo research. The data obtained is shown in Table 3.3 and Figures 3.8 and 3.9. Primer set 3, which included CpG site 8-11 was selected for further methylation analysis across the 103 biopsies, due to both its location on the promotor region and the substantial difference in levels of methylation between the glioblastoma samples (both biopsy tissue and culture) compared to normal brain tissue. Average percentage levels of methylation for normal tissue across CpG site 8-11 was 26.2%. A significant reduced level ($p<0.0001$) of methylation was observed in both glioblastoma biopsies, with methylation level of 6.2% (a range of 1.8 - 12.6%) and cell cultures of 4.1% (a range of 1.4-8.7%). The noteworthy change in hypomethylation was not as substantial across the other primer CpG regions (Average values: CpG 1-4 - normal 10.9%, biopsy 4.1%, culture 1.8%; CpG 4-7 - normal 6.3%, biopsy 12.5%, culture 6.3%; CpG 12-15 - normal 19.2%, biopsy 4.8%, culture 5%), as shown in Table 3.3 and Figures 3.8 and 3.9.

To further investigate the alterations in methylation levels across CpG sites 8, 9, 10 and 11, 103 glioblastoma biopsies were investigated, with an additional 21 glioblastoma patient-derived cell cultures and 2 established cell lines and compared to both NHA and 5 normal brain tissue samples. A positive methylation control was used as stated in 2.8. The average methylation across CpG sites 8-11 was significantly ($p<0.0001$) different between normal brain tissue and the 103 glioblastoma samples. The percentage of methylation ranged from 1.2% to 17.6% in the biopsy samples, with an average methylation of 5.5% compared to an average methylation of 25.5% in the normal tissue samples with a range between 23.67% to

26.86%, as seen in Figure 3.10 and Table 3.4. Furthermore, a significant reduction ($p<0.0001$) in the level of methylation across these CpG sites was also demonstrated throughout the glioblastoma patient-derived cultures and established cell lines, where a loss of greater than 20% was demonstrated compared to normal brain tissue. The percentage of methylation ranged from 2.6% to 9.7% with an average of 5.4%, as seen in Figure 3.11 and Table 3.5. The established cell lines exhibited a higher level of hypomethylation compared to the patient-derived cultures, with average levels of methylation of 2.8% contrasted to that of 5.6% respectively. Hypomethylation was also demonstrated in all glioblastoma cultures compared to NHA, which showed methylation levels of 16.8%. The reduction of methylation in NHA (16.8%) compared to normal brain tumour (25.5%) samples may be attributed to the NHA being foetal cells, where *HK2* has been shown to be highly expressed in embryonic tissues (Wilson, 2003). Analysis of CpG 10 revealed the largest altered levels of methylation in the glioblastoma samples, where the average level of methylation in normal tissue was 42.1% compared to 5.4% average methylation in biopsy samples ($p<0.0001$) and 3.8% average methylation in cultures ($p<0.0001$). NHA also had a significantly ($p<0.0001$) reduced level of methylation of 14.74%, as shown in Figures 3.12 and 3.13 and Table 3.6 and 3.7. In both glioblastoma biopsy and culture, an average loss of 21% ($p<0.0001$) in the level of methylation across CpGs 8, 9, 10 and 11 was established compared to normal brain tissue, indicative that hypomethylation is a common occurrence in glioblastoma tissue, which is also maintained in cell culture. Individual CpG data is shown in the appendix Table A2.

Figure 3.5. MS-PCR gels for both biopsy and culture samples Methylation status of *HK2* was determined in 36 glioblastoma biopsies and 10 cultures via MS-PCR. Partial hypomethylation was seen in 90% of the biopsy samples and 60% of the cultures. Complete hypomethylation was seen in 5 biopsies (374, 110, 743, 705, 1617) and 4 cultures (U251MG, IN859, IN2093, IN1528). Additionally, total hypermethylation of HK2 was present in only 3 biopsy samples (484, 377, 717). M= methylated, U = unmethylated. DNA ladder on gels represent 50bp, amplified band size is 210bp.

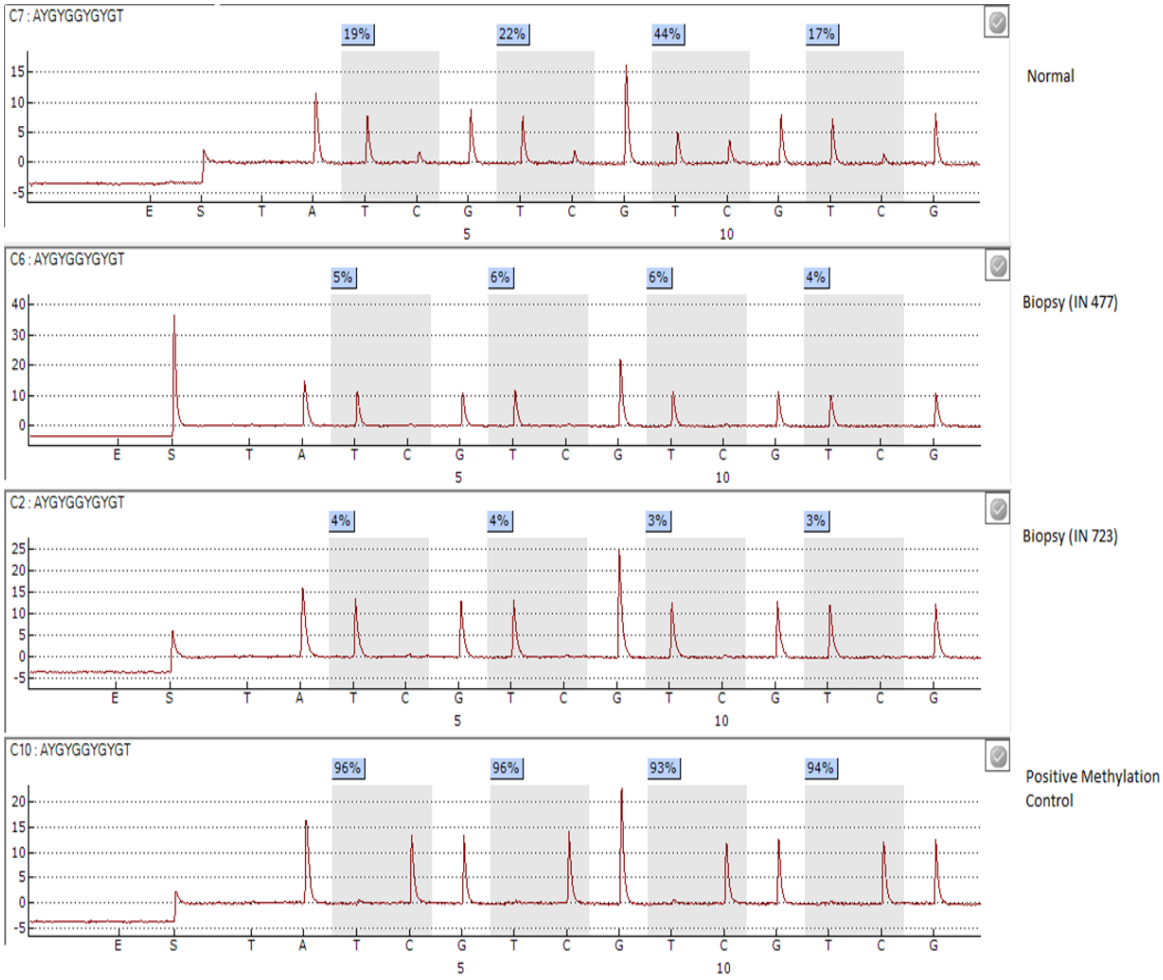

Figure 3.6 Example of a pyrogram generated via the Q96 pyrosequencer
Pyrogram showing levels of methylation (%) in 2 biopsy samples compared to normal brain tissue and a positive methylation control sample. CpG sites 8-11 are highlighted respectively in pale blue across the pre-designed Qiagen sequence. A loss of methylation is demonstrated in the glioblastoma samples compared to the control samples. Y-axis demonstrates % methylation, x-axis shows the nucleotide dispensation order.

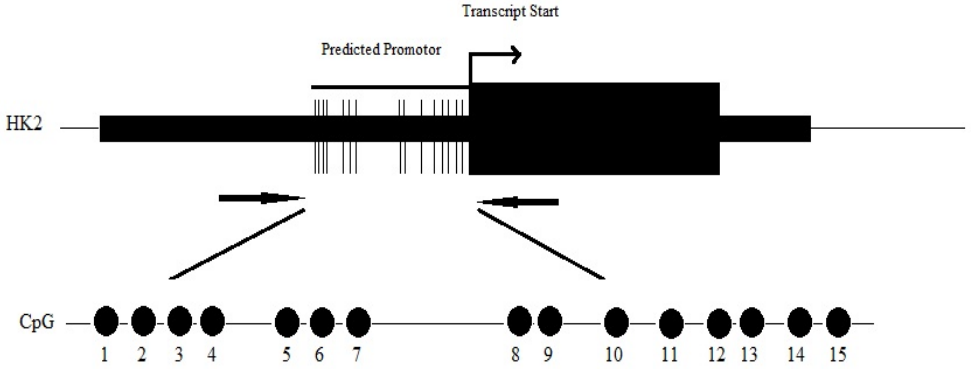

Figure 3.7 Qiagen primer sets and the location of the associated CpG CpG 1 to 15 shown with respect to *HK2* promotor region.

Table 3.3. Percentage of methylation across 15 CpG sites within the promotor region of *HK2*

1745	2229
5.3	4.1
1.2	4.7
1.3	5.3
1.5	3.9
2.3	4.5
7.3	17.4
5.2	22.8
9.3	20.6
7.3	20.2
1.8	**6.9**
8.5	**8.5**
8.5	**7.4**
12.6	**6.5**
7.8	**7.3**
7.6	4.6
4.5	4.9
2.0	4.9
6.3	4.2
5.1	4.7

Table 3.3. Percentage levels of methylation across individual CpG sites in glioblastoma. Methylation in biopsies (n=10) and normal brain tissue (n=2). Average levels of methylation are represented for each Qiagen primer set, covering multiple CpG sites. A reduction in methylation was seen across most CpG sites in glioblastoma samples compared to normal tissue. Significant ($p<0.0001$) hypomethylation was demonstrated in all glioblastoma samples across CpG's 8-11, with average levels of methylation reduced from 25.5% in normal tissue to 6.2% in glioblastoma tissue and 4.1% in culture.

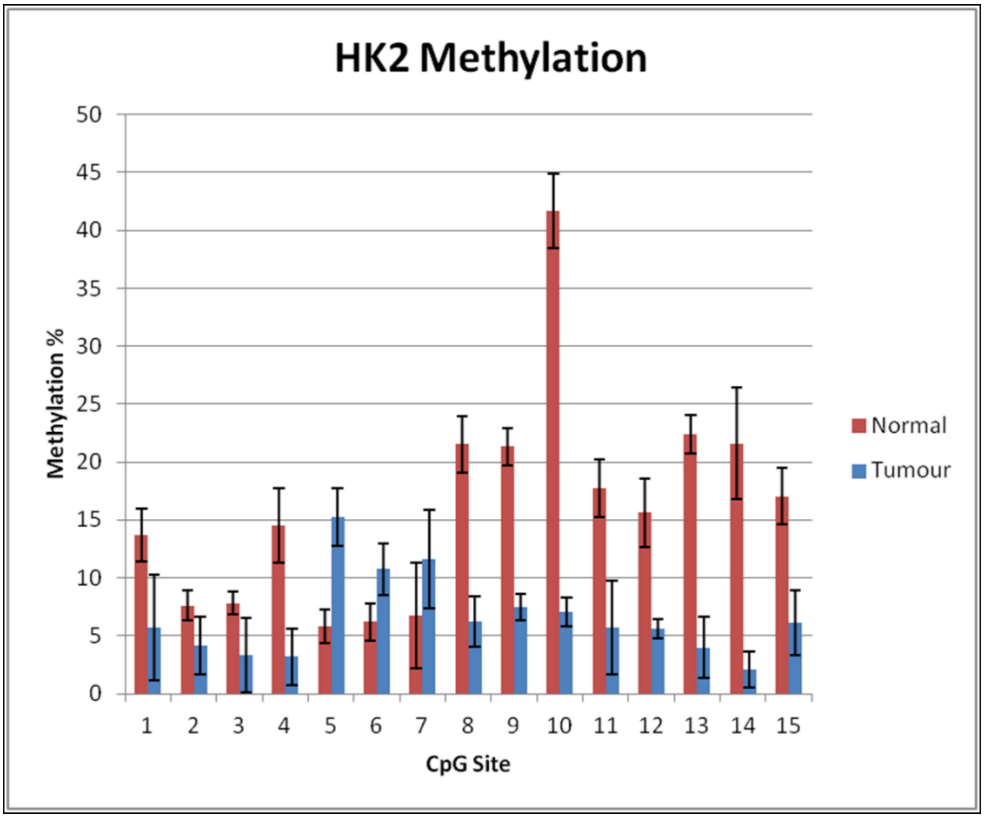

Figure 3.8 *HK2* methylation across 15 individual CpG sites within the promotor region Average methylation values are taken from 10 biopsies and 2 normal brain tissue samples. A loss of methylation is demonstrated across 12 of the CpG sites, with a significant reduction from CpG site 8-11 and 13-14. Red represents normal brain; blue represents biopsy samples.

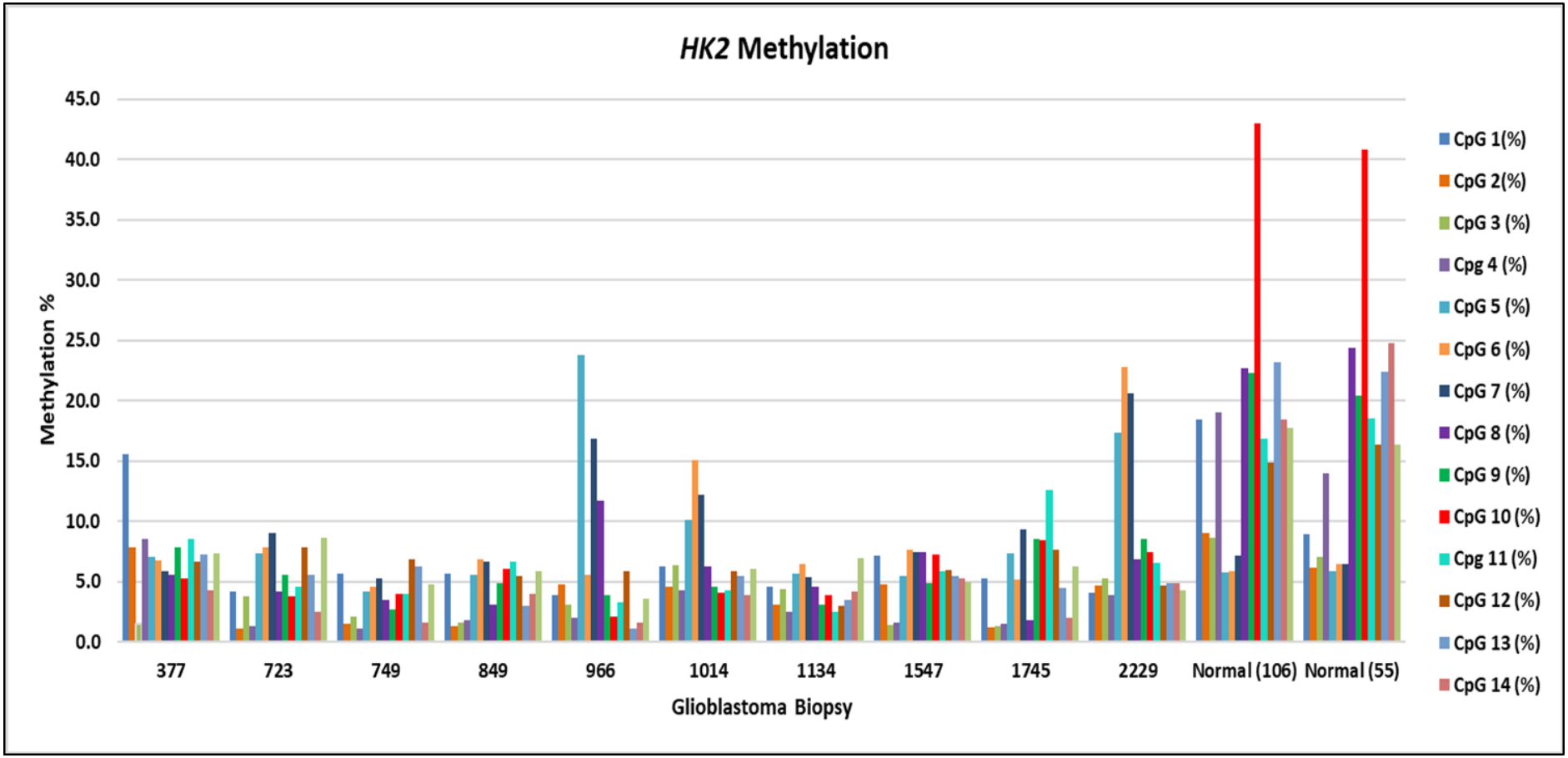

Figure 3.9. *HK2* methylation of glioblastoma biopsies across CpG sites 1 to 15
HK2 methylation percentage across 15 CpG sites within the promotor region. CpG 10 shown in red demonstrated the greatest loss ($p<0.0001$) of methylation across all 10 biopsy samples, with average levels of methylation 5.5% compared to normal tissue 25.5%.

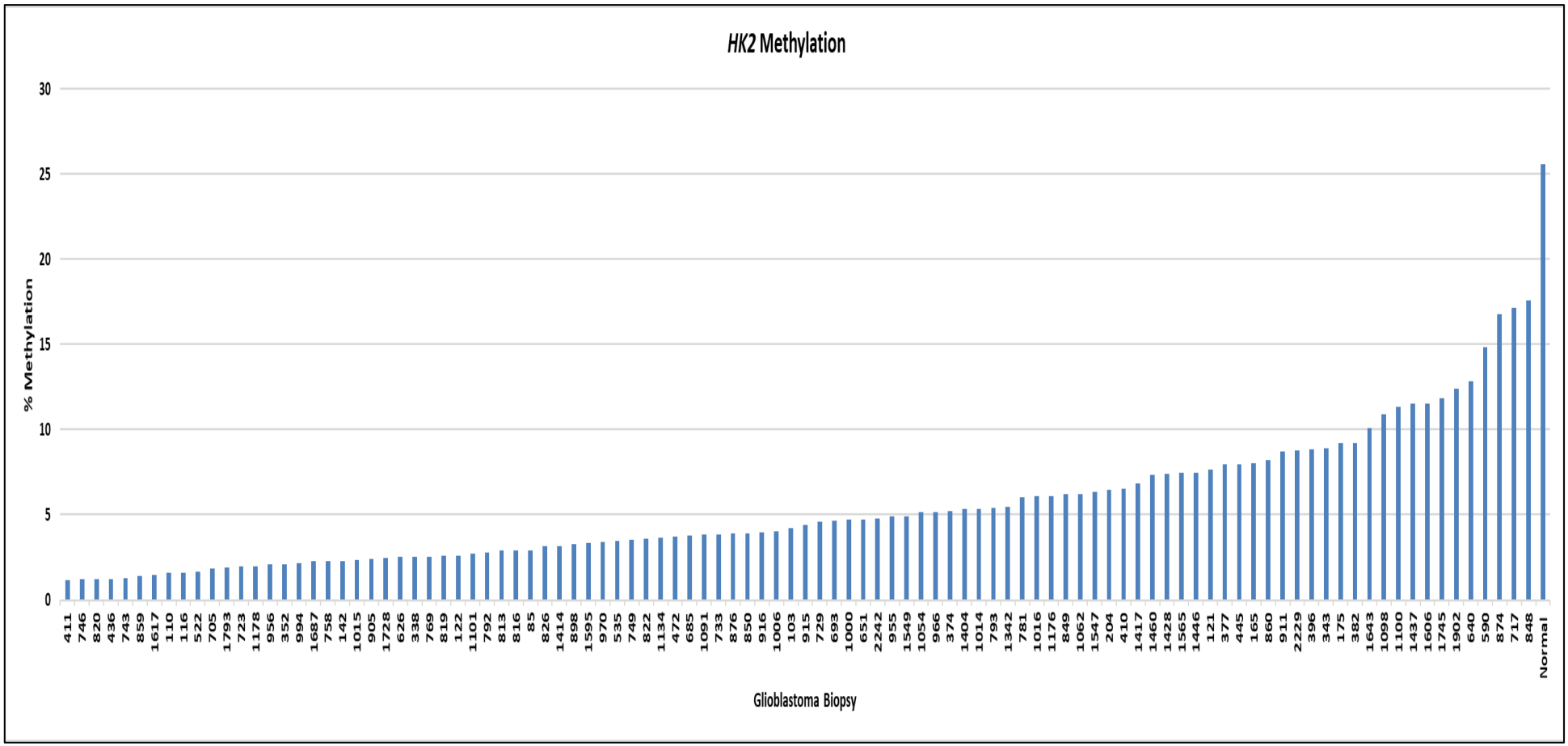

Figure 3.10. *HK2* average methylation of glioblastoma biopsies across CpG sites 8, 9, 10 and11
Average *HK2* methylation percentage across CpG sites 8-11 within the promotor region. A significant ($p<0.0001$) loss of methylation is demonstrated across all 103 biopsy samples, with average levels of methylation 5.5% compared to normal tissue 25.5%.

Table 3.4. Average level of *HK2* methylation (%) across glioblastoma biopsies, compared to expression fold change values

Biopsy	Average Methylation %	Expression Fold Change (SD (±))	Biopsy	Average Methylation %	Expression Fold Change (SD (±))
411	1.18	120.72 (0.89)	729	4.62	132.68 (1.6)
746	1.2	867.61 (3.14)	693	4.66	819.78 (2.01)
820	1.21	283.29 (3.58)	1000	4.73	149.83 (0.98)
436	1.22	127.23 (1.53)	651	4.74	89.84 (2.99)
743	1.31	285.95 (0.24)	2242	4.76	189.65 (2.65)
859	1.41	897.54 (2.81)	955	4.9	109.23 (2.66)
1617	1.46	178.38 (0.38)	1549	4.905	142.07 (2.34)
110	1.57	186.29 (3.41)	1054	5.15	173.91 (2.11)
116	1.57	6.69 (1.24)	966	5.18	125.62 (2.11)
522	1.63	30.76 (1.66)	374	5.19	136.68 (0.9)
705	1.86	121.62 (3.54)	1404	5.34	111.39 (2.29)
1793	1.9	600.96 (1.17)	1014	5.36	3.82 (2.64)
723	1.99	77.03 (0.21)	793	5.43	875.78 (1.51)
1178	2	346.43 (2.52)	1342	5.46	148.30 (2.11)
956	2.07	126.62 (2.43)	781	6.04	320.44 (2.91)
352	2.09	240.749(2.72)	1016	6.07	159.03 (3.17)
994	2.16	221.22 (0.39)	1176	6.1	149.44 (3.34)
1687	2.26	149.51 (0.12)	849	6.19	205.23 (3.91)
758	2.28	409.23 (0.49)	1062	6.21	136.68 (2.56)
142	2.29	788.29 (3.3)	1547	6.35	106.30 (3.1)
1015	2.36	288.18 (1.25)	204	6.46	57.37 (2.82)
905	2.43	285.23 (3.18)	410	6.55	260.13 (3.1)
1728	2.49	764.9 (2.33)	1417	6.82	315.68 (0.57)
626	2.51	195.29 (0.91)	1460	7.33	117.87 (1.97)
338	2.52	825.58 (2.78)	1428	7.37	7.42 (4.45)
769	2.52	172.1 (3.78)	1565	7.44	269.09 (2.16)
819	2.59	288.41 (1.83)	1446	7.45	153.25 (2.55)
122	2.6	263.73 (1.53)	121	7.63	51.72 (3.12)
1101	2.73	320.24 (2.65)	377	7.97	120.25 (1.22)
792	2.77	195.96 (3.11)	445	7.99	669.94 (1.73)
813	2.9	216.01 (2.44)	165	8.03	40.137 (2.45)
816	2.91	679.90 (2.72)	860	8.24	26.13 (2.91)
85	2.92	75.21 (1.98)	911	8.69	172.11 (2.12)
826	3.15	569.76 (3.95)	2229	8.76	18.38 (0.45)
1414	3.17	140.13 (1.21)	396	8.86	69.44 (3.65)
898	3.31	43.57 (1.73)	343	8.92	20.06 (2.43)
1595	3.33	425.07 (0.83)	175	9.21	14.90 (3.46)
970	3.43	78.72 (1.24)	382	9.21	39.29 (0.54)
535	3.44	87.79 (2.46)	1643	10.09	98.54 (1.53)
749	3.52	216.62 (0.68)	1098	10.89	86.34 (3.54)
822	3.59	763.67 (4.81)	1100	11.34	43.7 (1.49)
1134	3.65	23.62 (3.56)	1437	11.52	21.91 (1.65)
472	3.73	99.50 (3.12)	1606	11.54	22.35 (0.98)
685	3.78	446.03 (2.73)	1745	11.83	43.80 (1.36)
1091	3.83	115.78 (3.42)	1902	12.4	31.09 (3.45)
733	3.86	176.43 (1.68)	640	12.81	51.06 (0.92)
876	3.91	358.76 (3.18)	590	14.82	49.06 (2.46)
850	3.93	475.89 (4.14)	874	16.75	175.96 (0.87)
916	3.98	883.25 (4.11)	717	17.13	65.2 (4.59)
1006	4.01	198.95 (1.95)	848	17.58	122.11 (2.82)
103	4.24	41.05 (3.21)	Normal	25.54	1 (1.23)
915	4.42	104.50 (0.47)			

Table showing average percentage levels of methylation across CpG sites 8-11 in glioblastoma biopsy samples, compared to normal brain tissue. Hypomethylation is seen across all biopsies, with average levels of methylation 5.5% in glioblastoma biopsies compared to normal tissue (25.5%). *HK2* fold change is also represented for comparison respectively.

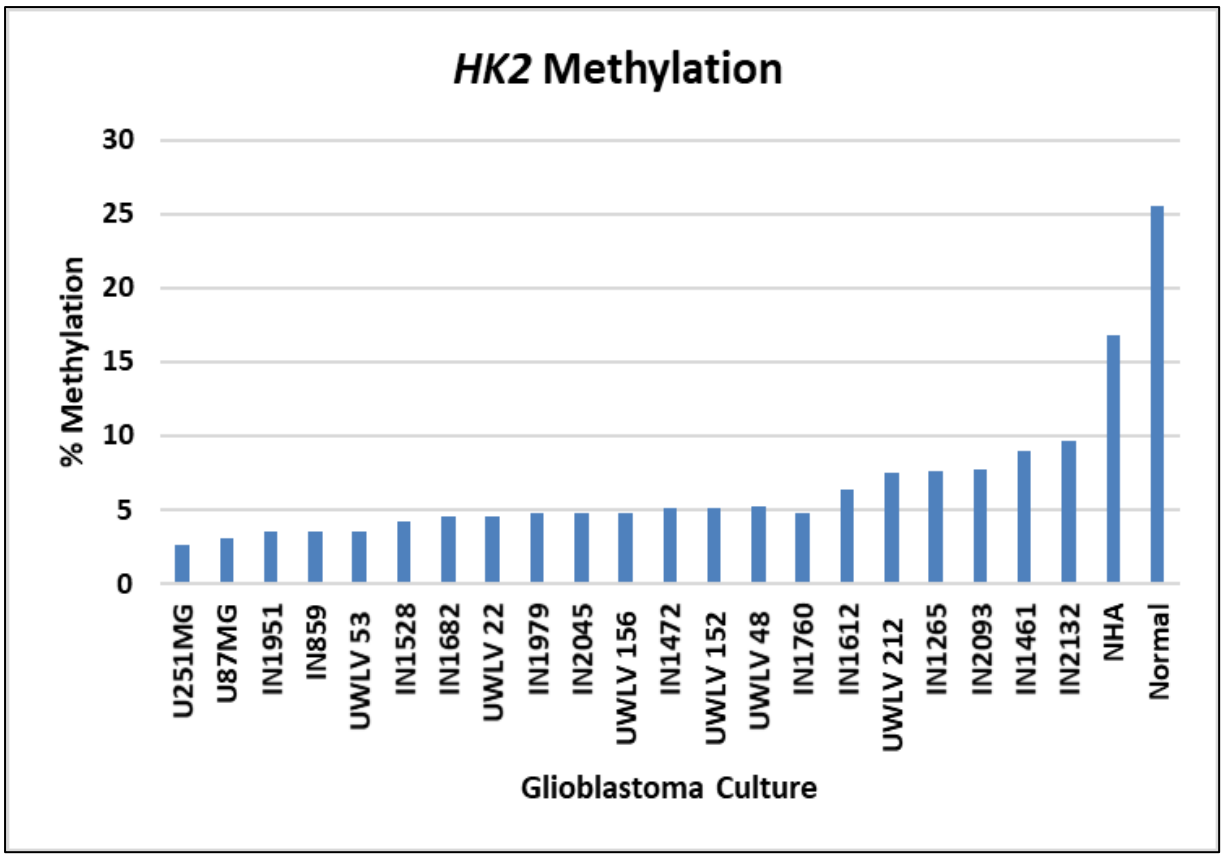

Figure 3.11. *HK2* average methylation of glioblastoma cultures across CpG sites 8-11
Average *HK2* methylation percentage across CpG sites 8-11 within the promotor region. A significant ($p<0.0001$) loss of methylation is demonstrated across all 21 patient-derived cell cultures and 2 established cell lines biopsy samples, with average levels of methylation 5.4% compared to normal tissue 25.5%. Hypomethylation is also seen in NHA, with average methylation of 16.8%.

Table 3.5. Average levels of *HK2* methylation (%) across glioblastoma cultures, compared to expression fold change values

Culture Sample	Average Methylation %	*Expression* Fold Change (SD (±))
U251MG	2.62	1502.61 (1.96)
U87MG	3.07	1294.26 (2.11)
IN1951	3.56	210.63 (1.95)
IN859	3.57	995.11 (1.54)
UWLV 53	3.58	589.16 (1.92)
IN1528	4.25	385.95 (2.82)
IN1682	4.52	120.54 (2.65)
UWLV 22	4.56	637.35 (0.48)
IN1979	4.72	574.39 (3.01)
IN2045	4.82	219.82 (1.22)
UWLV 156	4.82	306.89 (3.54)
IN1472	5.11	403.36 (2.11)
UWLV 152	5.15	289.65 (0.89)
UWLV 48	5.21	211.43 (0.57)
IN1760	4.82	201.96 (1.83)
IN1612	6.36	126.63 (0.91)
UWLV 212	7.47	145.42 (1.25)
IN1265	7.58	97.35 (3.41)
IN2093	7.73	132.75 (0.24)
IN1461	8.92	85.73 (2.94)
IN2132	9.67	88.35 (3.58)
NHA	16.83	30.42 (3.12)
Normal	25.55	1 (1.23)

Table showing average percentage levels of methylation across CpG sites 8-11 in glioblastoma culture samples, compared to both NHA and normal brain tissue. Hypomethylation is seen across all cultures, with average levels of methylation 5.4% in glioblastoma cultures compared to normal tissue (25.5%). A loss in methylation is also seen in NHA, with average methylation of 16.8%. *HK2* fold change is also represented for comparison respectively.

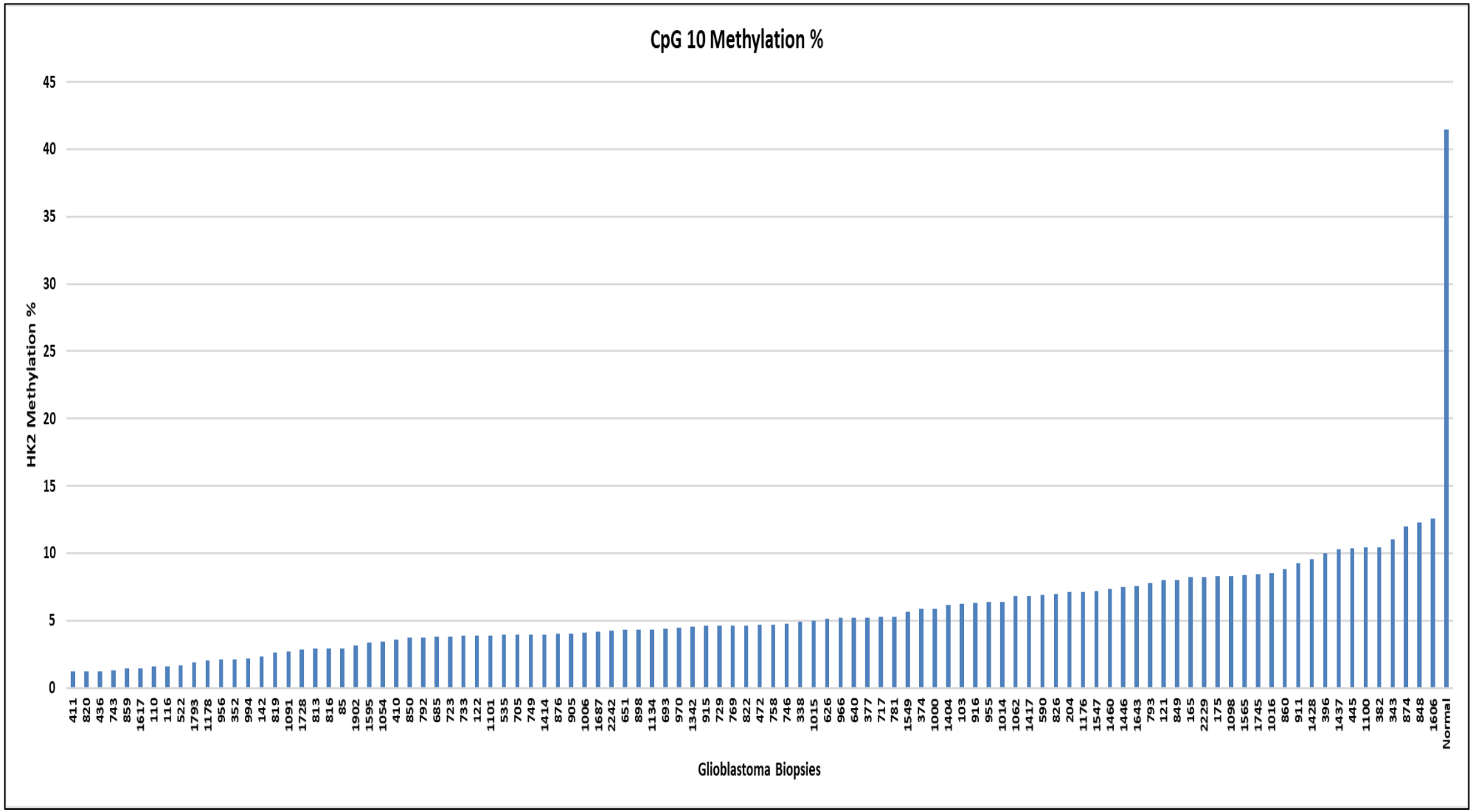

Figure 3.12. *HK2* methylation of glioblastoma biopsies in CpG 10. *HK2* methylation percentage across CpG site 10 within the promotor region. A significant ($p<0.0001$) loss of methylation is demonstrated across all 103 biopsy samples compared to normal tissue.

Table 3.6. CpG 10 methylation (%) across glioblastoma biopsies

Biopsy Sample	CpG 10 Methylation %	Biopsy Sample	CpG 10 Methylation %
411	1.2	338	4.87
820	1.21	1015	4.97
436	1.22	626	5.1
743	1.31	966	5.18
859	1.41	640	5.19
1617	1.46	377	5.22
110	1.57	717	5.28
116	1.57	781	5.28
522	1.63	1549	5.63
1793	1.9	374	5.83
1178	2	1000	5.87
956	2.07	849	6.02
352	2.09	1404	6.13
994	2.16	103	6.21
142	2.29	916	6.32
819	2.59	955	6.35
1091	2.67	1014	6.39
1728	2.86	1062	6.79
813	2.9	1417	6.82
816	2.91	590	6.92
85	2.92	826	6.94
1902	3.11	204	7.09
1595	3.33	1176	7.11
1054	3.44	1547	7.22
410	3.54	1460	7.33
850	3.74	1446	7.45
792	3.75	1643	7.56
685	3.78	793	7.79
723	3.82	121	7.98
733	3.86	165	8.25
122	3.9	2229	8.25
1101	3.9	175	8.27
535	3.91	1098	8.28
705	3.94	1565	8.35
749	3.96	1745	8.45
1414	3.96	1016	8.5
876	4	860	8.83
905	4	911	9.25
1006	4.09	1428	9.56
1687	4.15	396	9.98
2242	4.23	1437	10.32
651	4.33	445	10.35

898	4.34	1100	10.43
1134	4.35	382	10.46
693	4.42	343	10.99
970	4.46	874	11.95
1342	4.55	848	12.24
915	4.58	1606	12.57
729	4.62	Normal	42.98
769	4.64	Normal	40.85
822	4.64	Normal	41.78
472	4.69	Normal	42.22
758	4.7	Normal	42.43
746	4.78		

Table showing HK2 methylation % in biopsies and normal tissue in CpG10 via pyrosequencing. CpG 10 showed the highest level of deregulated methylation between normal tissue (average of 42.1%) and biopsies (average of 5.4%) and cultures (average of 3.8%).

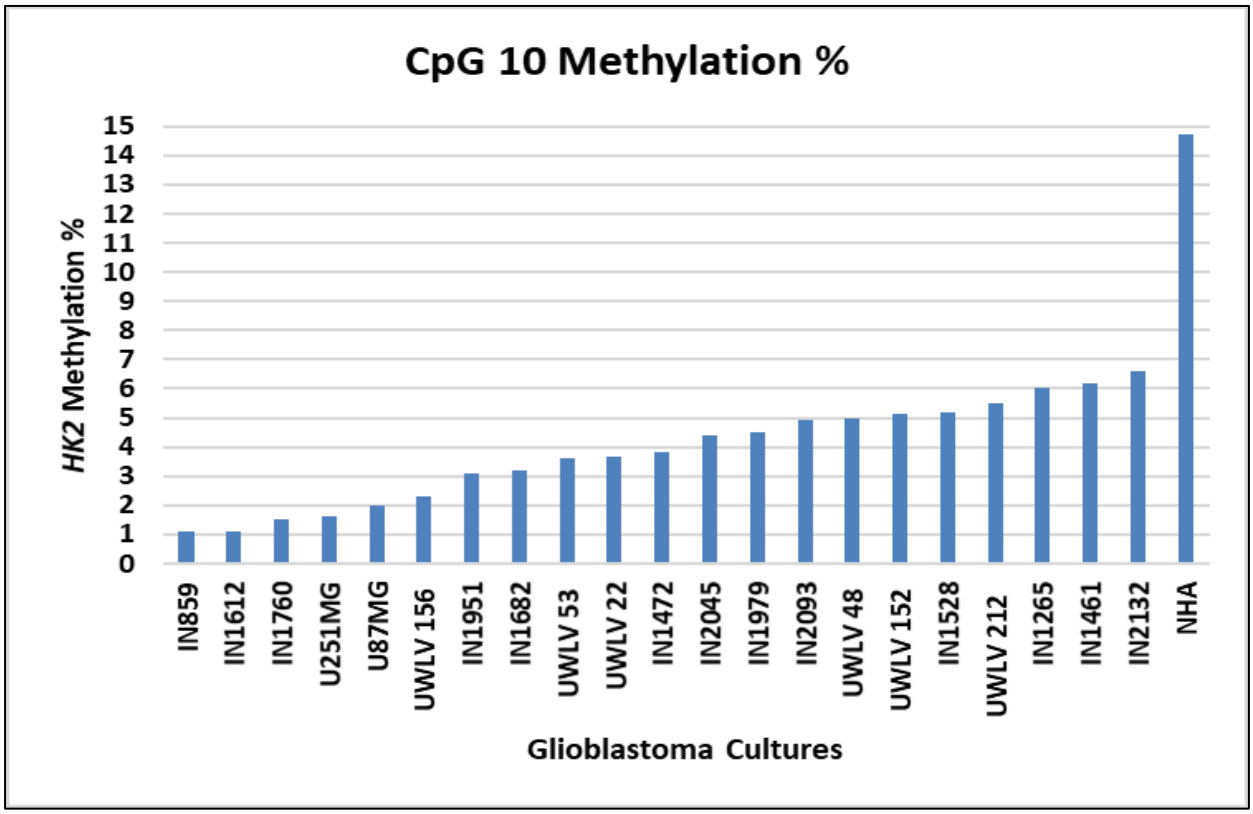

Figure 3.13 *HK2* methylation of glioblastoma cultures in CpG 10 *HK2* methylation percentage across CpG site 10 within the promotor region. A significant ($p<0.0001$) loss of methylation is demonstrated across all 21 patient-derived cell cultures and 2 established cell lines biopsy samples compared to normal tissue 25.5%. Hypomethylation is also seen in NHA, with average methylation of 16.8%.

Table 3.7. CpG 10 methylation (%) across glioblastoma cultures

Culture Sample	CpG 10 *HK2* Methylation %
IN859	1.1
IN1612	1.1
IN1760	1.5
U251MG	1.6
U87MG	2.01
UWLV 156	2.3
IN1951	3.11
IN1682	3.22
UWLV 53	3.6
UWLV 22	3.68
IN1472	3.82
IN2045	4.42
IN1979	4.51
IN2093	4.94
UWLV 48	4.98
UWLV 152	5.11
IN1528	5.21
UWLV 212	5.52
IN1265	6.03
IN1461	6.16
IN2132	6.59
NHA	14.74

Table showing HK2 methylation % in cultures and NHA in CpG10 via pyrosequencing.

3.4 Correlation of hypomethylation and levels of overexpression of *HK2*

A loss in methylation was established across all glioblastoma samples including in both tissue and culture, with significant hypomethylation frequently occurring across multiple CpG sites. The diminished levels of *HK2* methylation in glioblastoma was further investigated to determine if epigenetic alterations impacted mRNA transcription. The level of *HK2* fold change expression attained from qPCR was compared to the methylation data from pyrosequencing for individual biopsies (n=103) and cultures (n=21) and compared to both NHA and normal brain tissue. A strong correlation between the percentage of methylation and level of expression across the CpG sites 8-11 ($p < 0.0001$) was demonstrated. From this, samples were grouped dependant on the standard deviation above and below the average

methylation level. Figure 3.14 shows the differentiated groups, above and below 5.5% methylation, with the corresponding *HK2* expression. The comparative glioblastoma biopsy groups are significantly different with both methylation percentage ($p < 0.0001$) and levels of *HK2* expression fold change. Samples exhibiting hypomethylation levels of <5.5% demonstrated considerably increased levels of *HK2* expression, where fold change ranged from 3.8 to 897.5, with an average expression level of 297.3. This was significantly ($p < 0.0001$) different to the contrasting group, where levels of methylation were >5.5%, average *HK2* expression fold change was 99 with a fold change range of 7.4 to 320.2 (compared to normal tissue). Additionally, both subgroups of glioblastoma biopsy samples were significantly different to normal tissue ($p < 0.0001$), with average methylation values 25.5% across CpG's 8-11. The increased level of hypomethylation is indicative that epigenetic alternations influence mRNA transcription, contributing to elevated levels of *HK2* expression in glioblastoma biopsies. Utilizing the same approach, glioblastoma cultures were grouped dependant on their average level of methylation, as stated above. From this samples were grouped dependant on the standard deviation above and below the average. Figure 3.15 shows the differentiated subgroups, above and below 5.4% methylation, with the corresponding *HK2* fold change levels. Both glioblastoma culture subgroups were substantially different to normal brain tissue, with significantly ($p < 0.0001$) reduced levels of methylation (%) compared to normal tissue and NHA, additionally both subgroups also demonstrated significant variabilities in methylation levels ($p < 0.0001$). Samples exhibiting hypomethylation levels of <5.4% demonstrated considerably increased levels of *HK2* expression, where fold change ranged from 120.5 to 1502.6, with an average expression level of 529.5. This was statistically ($p=0.0276$) different to the contrasting group, where levels >5.4% methylation, average *HK2* expression fold change was 112.7 with a range between 85.7 to 145.4- fold expression (compared to normal tissue). *HK2* methylation levels in NHA were also significantly different to normal tissue ($p=0.0003$), and to both glioblastoma culture subgroups ($p < 0.0001$). This significant difference between the sample groups and NHA was also distinguishable with respect to expression fold change, with average levels of 27.93 ($p < 0.0001$ compared to normal brain, $p=0.0042$ for <5.4% methylation group and

p=0.0130 for >5.4% methylation group). Hypomethylation was demonstrated in both glioblastoma biopsies and culture compared to NHA and normal brain tissue, furthermore the reduction in *HK2* methylation corresponded with extensive overexpression in all glioblastoma cultures, indicating that hypomethylation is an influential factor for significantly increased levels of expression of *HK2* in glioblastoma.

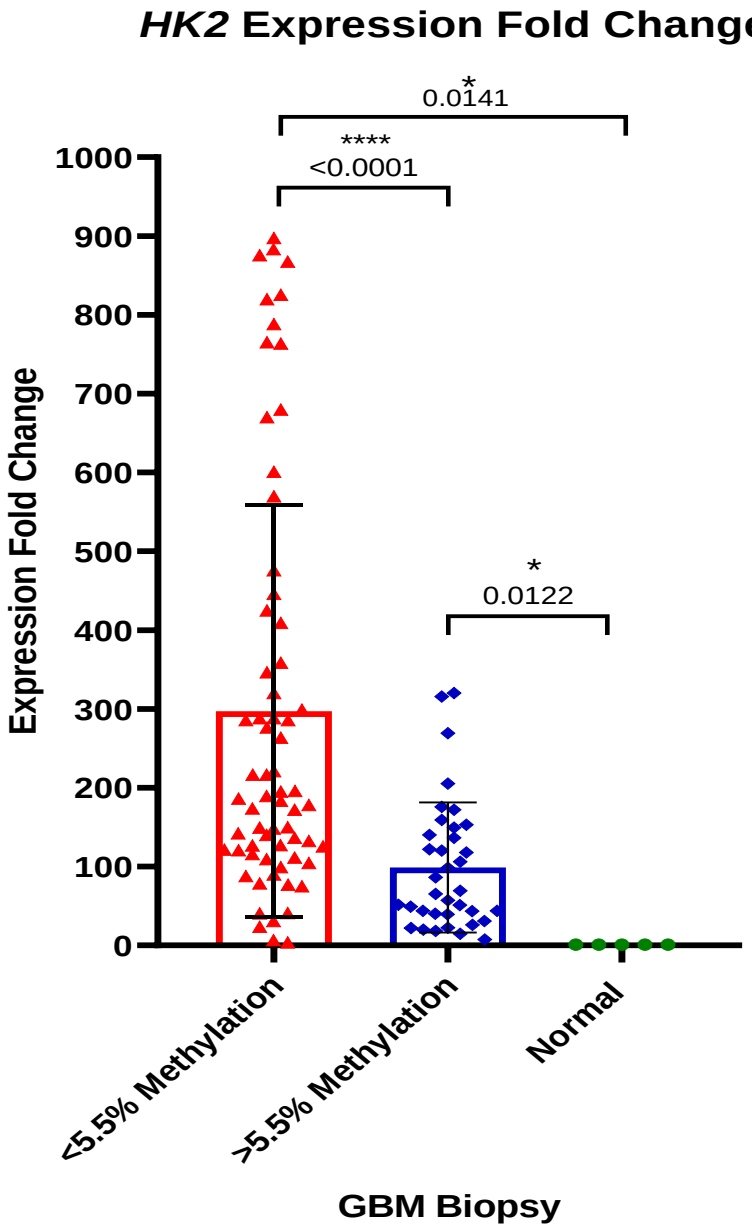

Figure 3.14 *HK2* methylation levels compared to fold change expression in glioblastoma biopsies (n=103) compared to normal brain tissue. Differentiated subgroups of glioblastoma biopsies, show significant (p< 0.0001) differences, in samples where methylation is less than 5.5% *HK2* expression is massively increased, with average levels of 297.3-fold compared to normal tissue. In comparison where methylation is greater than 5.5%, average *HK2* expression is 99-fold when

compared to normal brain tissue. Both glioblastoma subtypes are significantly different to normal tissue, with extensive hypomethylation and sizeable overexpression of *HK2*. The bars represent mean and SD deviation.

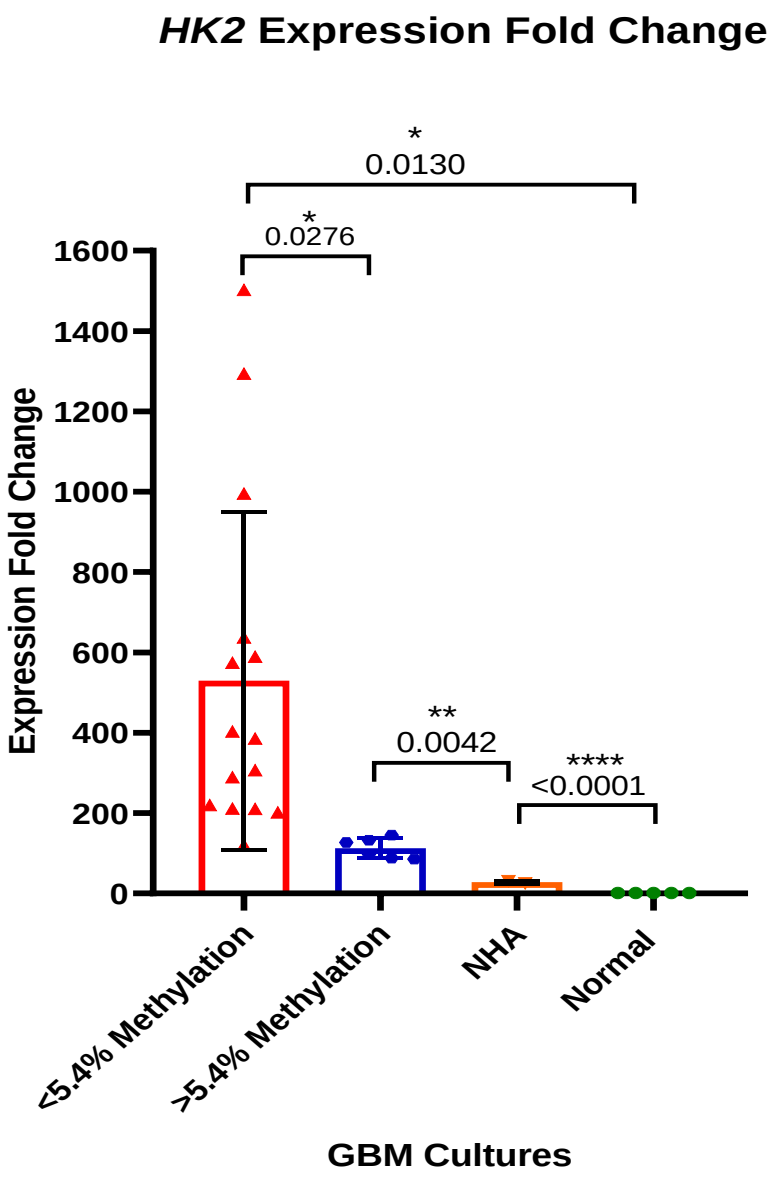

Figure 3.15 *HK2* methylation levels compared to fold change expression in glioblastoma cultures (n=21) and NHA compared to normal brain tissue. Differentiated subgroups of glioblastoma cultures show significant (methylation p< 0.0001, fold change p=0.0276) differences, in samples where methylation is less than 5.4% *HK2* expression is greatly increased, with average levels of 529.5 compared to normal tissue. In comparison where methylation is greater than 5.4%, average *HK2* expression is 112.7, when compared to normal brain tissue. Both glioblastoma subtypes are significantly (methylation p< 0.0001, fold change p=0.0130) different to normal tissue, with extensive hypomethylation and sizeable overexpression of *HK2*. NHA also demonstrated significant differences between both the glioblastoma samples (methylation p< 0.0001, fold change p=0.0042) and normal tissue (p=0.0003, fold change p< 0.0001), with reduction in methylation levels occurring and a noteworthy increase in *HK2* expression. The bars represent mean and SD deviation.

3.5 Quantitative assessment of *Hexokinase 1* expression

In order to determine alterations in expression of *HK1* in glioblastoma, mRNA levels were analysed by qPCR in 70 glioblastoma biopsies, 15 glioblastoma patient-derived cell cultures and established cell lines and compared to both NHA and 5 normal brain tissue samples.

Sixty (85.7%) biopsies exhibited *HK1* downregulation or no change in level of methylation ranging from 0.00034 to 1.12- fold change expression compared to normal brain tissue (normalised to 1-fold change), with significant loss of expression in 31 of the biopsies. Additionally, there were 10 biopsies with ranging from 1.2- to 2.2- fold change increase in *HK1* gene expression as shown in Figure 3.16. An altered level of gene expression was also determined across the glioblastoma cultures, where all 15 patient-derived and established cell lines demonstrated an increased level of *HK1* expression, ranging from 1.2 up to 7.4 – fold change increase compared to normal brain (normalised to 1-fold change). Additionally, NHA exhibited an increase of 1.67- fold change expression, as shown in Figure 3.17. Detailed figures for each biopsy and culture fold change can be seen in Table 3.8 and 3.9. *HK1* expression is downregulated in 84.2% of the biopsies, indicating a potential HK isoform switch in glioblastoma. Overexpression of *HK1* was frequent in the culture samples, suggesting that the availability of nutrients in the *in vitro* microenvironment upregulates metabolic processes including *HK1* whilst also manintaing the switch to *HK2.*

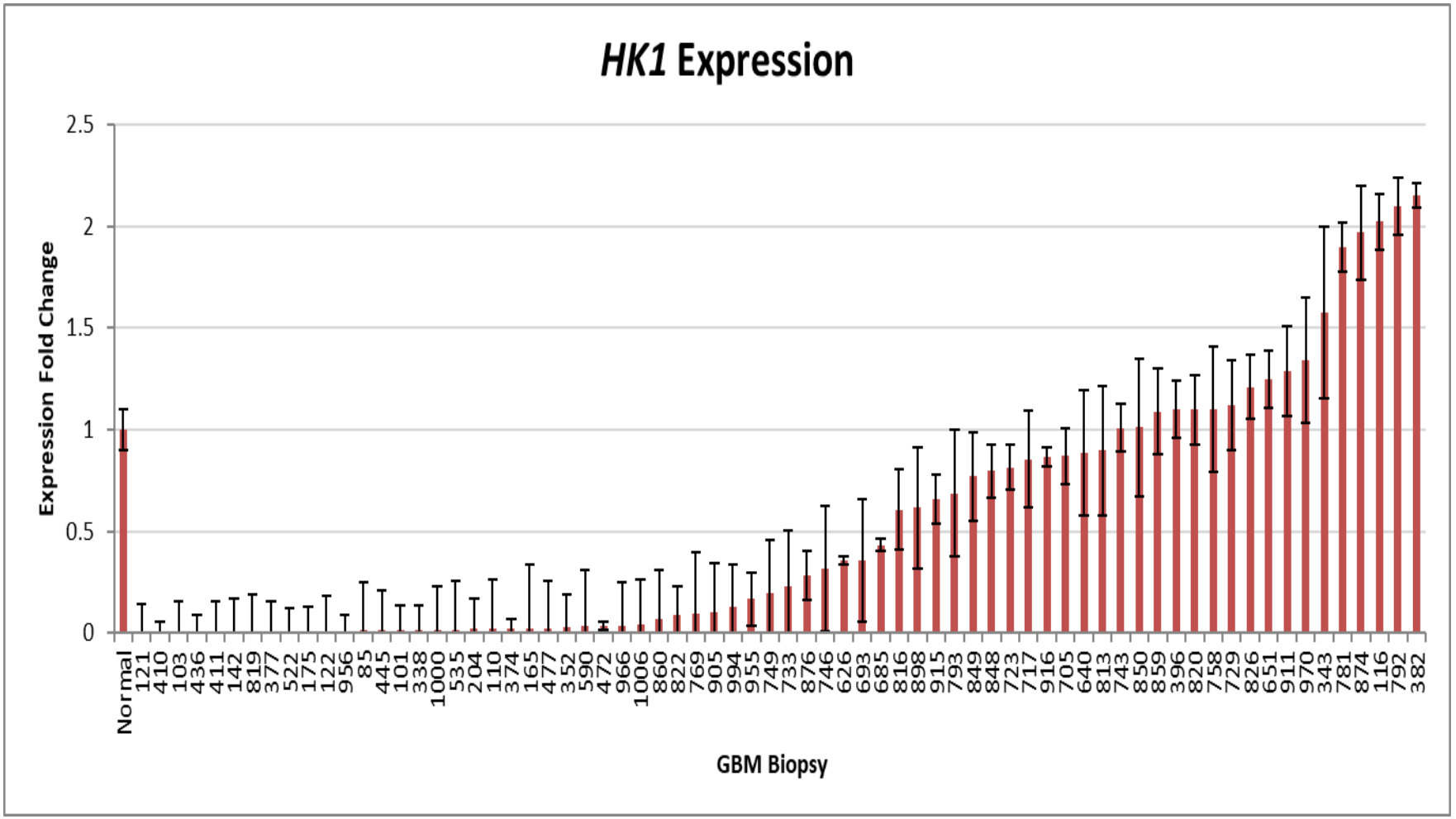

Figure 3.16 Expression fold change of HK1 in glioblastoma biopsies relative to normal tissue. Real time qPCR analysis of HK1 glioblastoma biopsies (n=80). Fold change has been normalised against average expression level of normal brain tissue (n=5). *HK1* expression is downregulated in 84.2% of the biopsies, indicating a potential HK isoform switch in glioblastoma.

Table 3.8. Expression fold change of *HK1* in glioblastoma biopsies

Biopsy Sample	HK1 Fold Change (SD (±))	Biopsy Sample	HK1 Fold Change (SD (±))
Normal	1 (0.10)	733	0.22 (0.28)
121 *	0.00034 (0.15)	876	0.28 (0.12)
410 *	0.005 (0.05)	746	0.31 (0.31)
103 *	0.0068 (0.14)	626	0.35 (0.02)
436 *	0.007 (0.08)	693	0.35 (0.3)
411 *	0.0072 (0.15)	685	0.43 (0.03)
142 *	0.0075 (0.16)	816	0.6 (0.2)
819 *	0.0077 (0.18)	898	0.61 (0.3)
377 *	0.0078 (0.15)	915	0.65 (0.12)
522 *	0.008 (0.11)	793	0.68 (0.31)
175 *	0.0083 (0.12)	849	0.7 (0.22)
122 *	0.0097 (0.17)	848	0.79 (0.13)
956 *	0.0098 (0.08)	723	0.81 (0.11)
85 *	0.011 (0.24)	717	0.85 (0.24)
445 *	0.011 (0.2)	916	0.86 (0.05)
101 *	0.012 (0.12)	705	0.86 (0.14)
338 *	0.016 (0.13)	640	0.88 (0.31)
1000 *	0.016 (0.21)	813	0.89 (0.32)
535 *	0.017 (0.24)	743	1.02 (0.12)
204 *	0.018 (0.15)	850	1.05 (0.34)
110 *	0.02 (0.24)	859	1.08 (0.21)
374 *	0.021 (0.05)	396	1.09 (0.14)
165 *	0.022 (0.31)	820	1.09 (0.17)
477 *	0.023 (0.23)	758	1.09 (0.31)
352 *	0.027 (0.16)	729	1.12 (0.22)
590 *	0.031 (0.28)	826	1.2 (0.16)
472 *	0.033 (0.23)	651	1.24 (0.14)
966 *	0.037 (0.21)	911	1.28 (0.22)
1006 *	0.042 (0.22)	970	1.34 (0.31)
860 *	0.068 (0.24)	343	1.57 (0.42)
822 *	0.086 (0.14)	781	1.89 (0.12)
769 *	0.097 (0.3)	874	1.96 (0.23)
905	0.01 (0.24)	116 *	2.02 (0.14)
994	0.12 (0.21)	792 *	2.09 (0.12)
955	0.16 (0.13)	382 *	2.15 (0.06)
749	0.19 (0.26)		

Table showing qPCR analysis of *HK1* glioblastoma biopsies. Fold change has been normalised against average expression level of normal brain tissue. *HK1* expression is downregulated in 84.2% of the biopsies compared to normal tissue. Standard deviation for each average is listed after each result (±). * denotes significant altered expression level compared to normal.

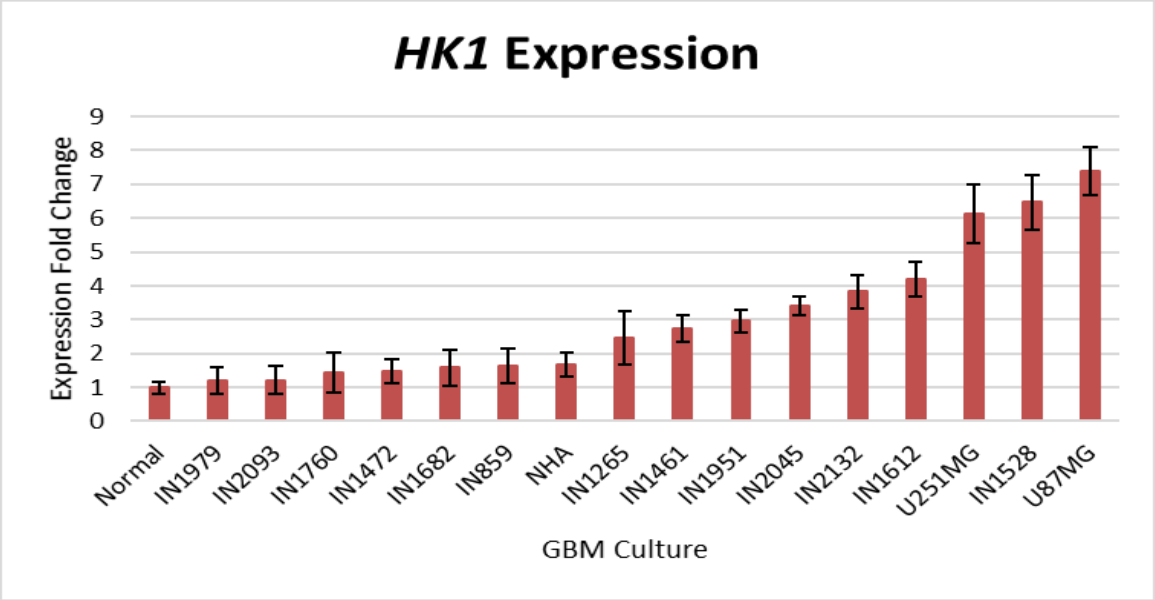

Figure 3.17 Expression fold change of *HK1* in glioblastoma cultures relative to normal tissue. Real time qPCR analysis of *HK1* glioblastoma cultures and cell lines (n=15). Fold change has been normalised against average expression level of normal brain tissue. *HK1* expression is elevated across all glioblastoma cultures and established cell lines compared to normal tissue (n=5), indicative that overexpression is occurring within a cell culture environment. *HK1* expression was also increased in NHA compared to normal tissue.

Table 3.9. Expression fold change of *HK1* mRNA in glioblastoma cultures

Culture Sample	*HK1* Fold Change (SD (±))
Normal	1 (0.18)
IN1979	1.21 (0.4)
IN2093*	1.22 (0.42)
IN1760*	1.43 (0.6)
IN1472	1.48 (0.34)
IN859	1.63 (0.53)
NHA	1.67 (0.34)
IN1682*	1.58 (0.53)
IN1265	2.46 (0.8)
IN1461*	2.74 (0.4)
IN1951*	2.97 (0.33)
IN2045	3.41 (0.27)
IN2132*	3.83 (0.5)
IN1612	4.21 (0.51)
U251MG	6.12 (0.87)
IN1528	6.47 (0.8)
U87MG	7.39 (0.72)

Real time qPCR analysis of *HK1* glioblastoma cultures and cell lines. Fold change has been normalised against average expression level of normal brain tissue. *HK1* expression is elevated across all glioblastoma cultures and established cell lines compared to normal tissue. *HK1* expression was also increased in NHA compared to normal tissue. Standard deviation for each average is listed after each result (±). * denotes significant altered expression level compared to normal.

The data obtained from qPCR revealed a variation within the glioblastoma biopsy population, with respect to *HK1* expression values. 10 biopsy samples from the 70-cohort tested exhibited increased levels of *HK1* expression, of which 3 samples had significantly ($p=0.0003$) increased expression (116, 792, 382) compared to normal brain tissue, furthermore this group was statistically different ($p<0.0001$) to the remaining 60 biopsy samples which demonstrated either a minor reduction in *HK1* expression (31 biopsies showed no HK1 expression) or no-change (n=28) compared to the control tissue. Additionally, *HK1* over-expression was exhibited across all glioblastoma cultures and NHA compared to normal tissue.

3.6 Quantitative assessment of *Hexokinase 1* methylation

HK1 methylation status was also investigated to reveal whether any epigenetic alternations occur in glioblastoma compared to normal tissue. Pyrosequencing was used to facilitate full quantification of the level of methylation in tumour samples. *HK1* primers were selected from Qiagen pre-designed sequencing primers as stated in 2.8, spanning 4 CpGs and offering maximum coverage across the *HK1* promotor region. Fifty glioblastoma biopsies and 15 glioblastoma patient-derived cell cultures and established cell lines (Table 3.11) were investigated and compared to both NHA and 5 normal brain tissue samples. The data revealed no significant differences between the average level of methylation in the biopsies (4.1%) and normal brain (6.9%), however 44 biopsies demonstrated reduced levels of methylation compared to normal brain tissue.

The degree of methylation across the 50 glioblastoma samples ranged from 1.33% to 7.46% with an average of 4.05%, in comparison normal brain tissue methylation (6.9%), with a range between 5.78 % to 8.03%, as shown in Figure 3.18 and Table 3.10. Furthermore, only 1 culture (IN1951) showed a significant ($p=0.0063$) reduction in the level of methylation compared to normal brain, no substantial alterations were demonstrated in the other cultures compared to normal brain tissue ($p= 0.1431$), or between NHA ($p= 0.5100$). The range in methylation across the 15 cultures was from 2.47% to 9.67% with an average of 5.48%, in comparison NHA had a methylation level of 4.46% with normal brain at 6.95 as shown in Figure 3.19 and Table 3.11. The data revealed no hypermethylation of *HK1* occurring in normal

tissue, with a minor loss of methylation demonstrated across 44 biopsies, of which 8% demonstrated a significant reduction compared to normal tissue. No significance alteration in the methylation state was shown across the cultures (except for IN1951). The data indicates that *HK1* is expressed in normal tissue and methylation does not control gene expression, no universal deregulation in the level of methylation present in glioblastoma.

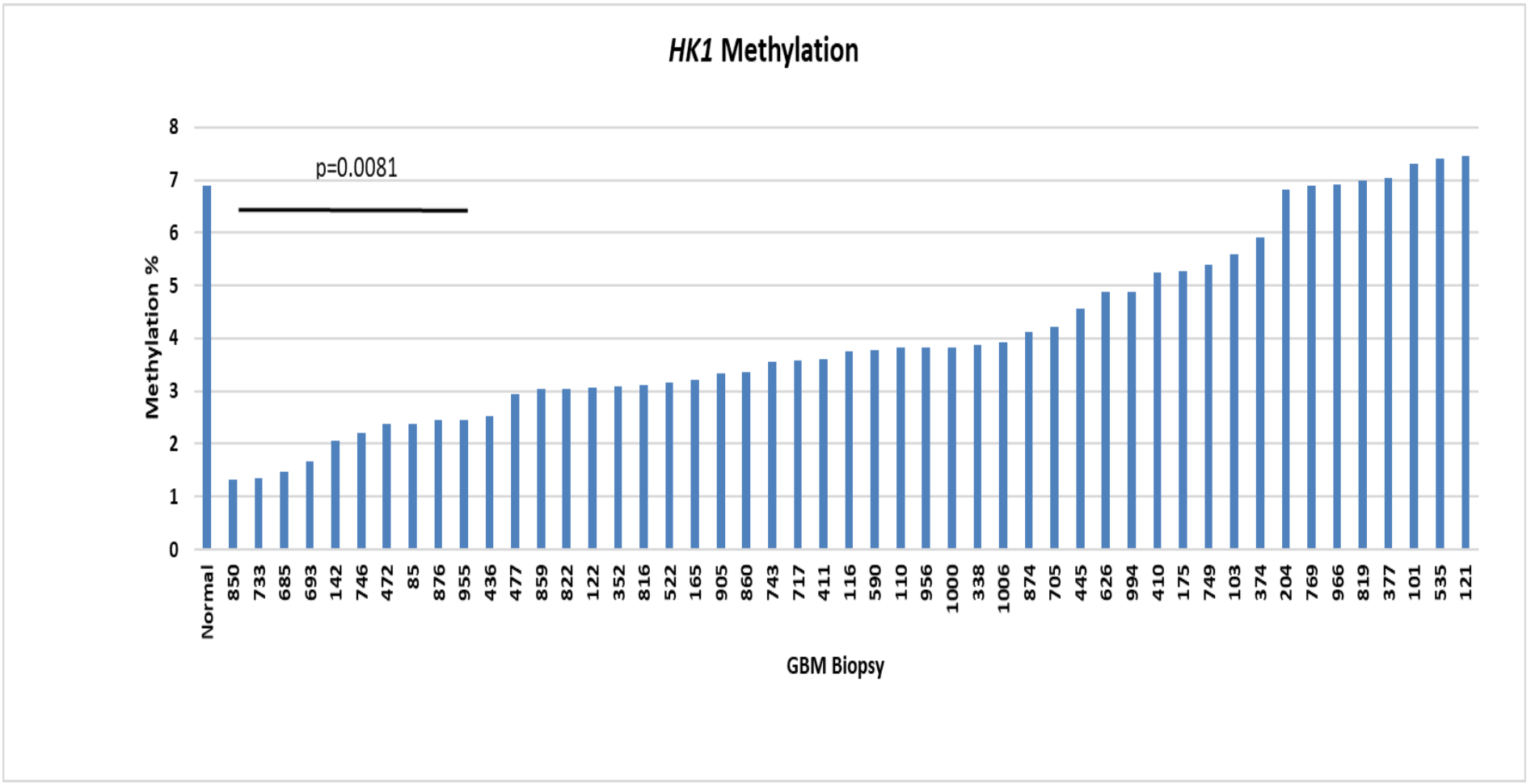

Figure 3.18 *HK1* average methylation of glioblastoma biopsies. Average *HK1* methylation percentage across CpG sites within the promotor region. An altered level of methylation is demonstrated across all 50 biopsy samples, with average levels of methylation 4.1% compared to normal tissue 6.9%.

Table 3.10. Average level of *HK1* methylation (%) across glioblastoma biopsies, compared to expression fold change values

Biopsy Sample	Methylation %	HK1 Fold Change (SD (±))	Biopsy Sample	Methylation %	HK1 Fold Change (SD (±))
Normal	6.905	1 (1.32)	116	3.75	2.02 (2.56)
850	1.33*	1.01 (1.89)	590	3.77	0.031 (0.72)
733	1.35*	0.22 (0.35)	110	3.82	0.02 (4.05)
685	1.48*	0.43 (1.38)	956	3.82	0.0098 (1.29)
693	1.68*	0.35 (1.48)	1000	3.83	0.016 (3.17)
142	2.06	0.0075 (3.67)	338	3.87	0.016 (4.22)
746	2.22	0.31 (4.86)	1006	3.93	0.042 (0.62)
472	2.37	0.033 (0.63)	874	4.13	1.96 (0.87)
85	2.39	0.011 (4.13)	705	4.22	0.86 (4.57)
876	2.45	0.28 (0.14)	445	4.56	0.011 (3.21)
955	2.45	0.16 (4.68)	626	4.89	0.35 (1.63)
436	2.53	0.007 (1.13)	994	4.89	0.12 (2.53)
477	2.95	0.023 (1.72)	410	5.24	0.005 (2.47)
859	3.03	1.08 (3.02)	175	5.28	0.0083 (4.82)
822	3.05	0.086 (2.38)	749	5.39	0.19 (2.57)
122	3.07	0.0097 (3.18)	103	5.6	0.0068 (1.64)
352	3.09	0.027 (2.89)	374	5.92	0.021 (2.74)
816	3.11	0.6 (0.73)	204	6.83	0.018 (1.59)
522	3.16	0.008 (1.82)	769	6.89	0.097 (3.63)
165	3.22	0.022 (3.16)	966	6.93	0.037 (2.34)
905	3.33	0.099 (0.46)	819	6.98	0.0077 (2.72)
860	3.37	0.068 (2.59)	377	7.03	0.0078 (3.11)
743	3.56	1.02 (1.76)	101	7.32	0.012 (2.51)
717	3.59	0.85 (1.74)	535	7.42	0.017 (2.81)
411	3.61	0.0072 (0.32)	121	7.46	0.00034 (0.46)

Table showing average percentage levels of methylation across 4 CpG sites in glioblastoma biopsy samples, compared to normal brain tissue. Hypomethylation is seen in some of the biopsies, with average levels of methylation 4.1% in biopsies compared to normal tissue (6.9%). *HK1* fold change is also represented for comparison respectively. * denotes statistical significance.

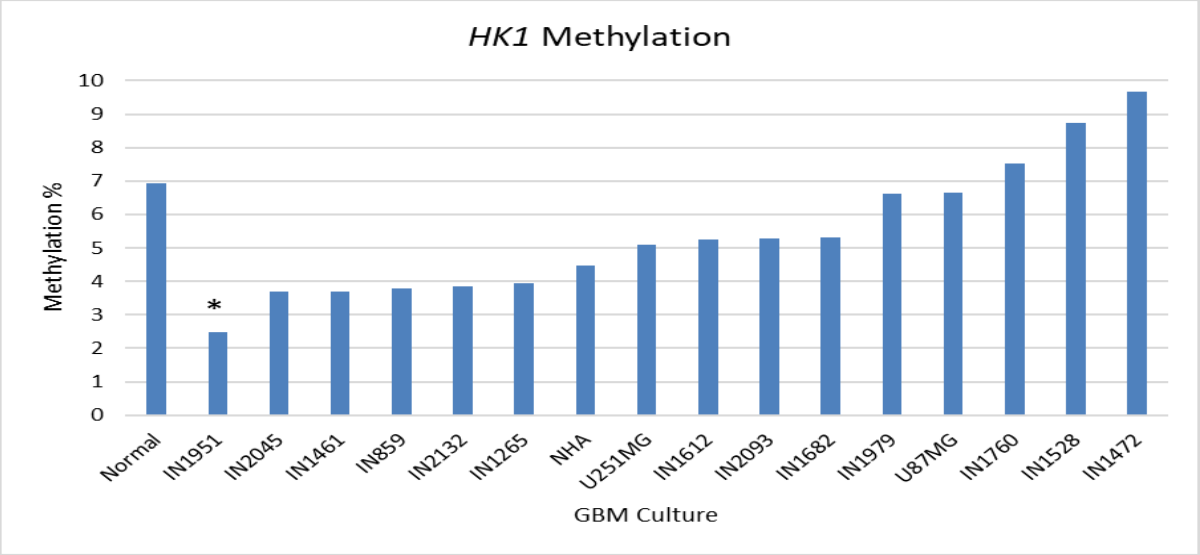

Figure 3.19 *HK1* average methylation of glioblastoma cultures
Average *HK1* methylation percentage across 4 CpG sites within the promotor region. An altered level of methylation is demonstrated across culture samples, with average levels of methylation 5.5% compared to normal tissue 6.9%. * denotes significance.

Table 3.11. Average level of *HK1* methylation (%) across glioblastoma cultures, compared to expression fold change values

Culture Sample	Methylation %	*HK1* Fold Change (SD (±))
Normal	6.94	1 (1.53)
IN1951	2.47*	2.97 (3.65)
IN2045	3.68	3.41 (0.47)
IN1461	3.71	2.74 (4.59)
IN859	3.79	1.63 (3.54)
IN2132	3.85	3.83 (3.1)
IN1265	3.95	2.46 (2.82)
NHA	4.46	1.67 (2.46)
U251MG	5.11	6.12 (1.53)
IN1612	5.25	4.21 (2.99)
IN2093	5.28	1.22 (1.98)
IN1682	5.32	1.58 (2.66)
IN1979	6.61	1.21 (3.12)
U87MG	6.64	7.39 (0.58)
IN1760	7.53	1.43 (0.21)
IN1528	8.75	6.47 (3.12)
IN1472	9.67	1.48 (1.24)

Table showing average percentage levels of methylation across 4 CpG sites in glioblastoma culture samples, compared to both NHA and normal brain tissue. Hypomethylation is seen in 80% of the cultures, with average levels of methylation 5.5% in glioblastoma cultures compared to normal tissue (6.9%). A loss in methylation is also seen in NHA, with average methylation of 4.46%. *HK1* fold change is also represented for comparison respectively.

The epigenetic deregulation of *HK1* methylation in glioblastoma was further investigated to determine if it had any impact upon mRNA transcription, resulting in a change in level of *HK1* expression. *HK1* fold change expression attained from qPCR was compared to the methylation data from pyrosequencing for individual biopsies (n=50) and cultures (n=15) and compared to both NHA and normal brain tissue. Samples were grouped dependant on the standard deviation above and below the average. The comparative biopsy sub-populations are significantly different with levels of methylation ($p < 0.0001$), however there was no statistically significant differences illustrated with corresponding levels of expression. Samples exhibiting methylation levels of <4% did not demonstrate significantly increased levels of *HK1*-expression.

Utilizing the same approach, glioblastoma cultures were grouped dependant on their level of methylation, the average methylation level across the 15 cultures was calculated (as stated above). Samples exhibiting methylation levels of <5.5% demonstrated increased ($p = 0.0112$) levels of *HK1* expression, there was no significant difference to the contrasting culture sub-population, where methylation levels >5.5%, average *HK1* expression fold change was 3.6 with a range between 1.21 and 7.39-fold change difference. The data suggests that levels of *HK1* methylation in glioblastoma biopsies does not have a critical function impacting *HK1* expression levels. Furthermore, the data concludes that the level of *HK1* methylation does not impact upon mRNA expression in culture, were no significant correlations were determined in any of the cultures; overall a minor decrease in methylation was demonstrated in the biopsy samples, which did not translate into an increase in expression. The results indicate that a separate mechanism instead of methylation regulates *HK1* expression, which may instead be driven through histone modification or miRNA interaction (Peschiarol *et al.*, 2013). A potential hexokinase isoform switch may also be plausible, *HK2* possesses two active catalytic domains with varying kinetic properties more suited for the metabolic nature of cancer cells, offering beneficial growth conditions (Wilson, 2003).

3.7 The relationship between *Hexokinase 2* overexpression and outcome

To investigate a potential association of raised levels of *HK2* with patient outcome, expression data was compared to overall survival (OS) for 86 glioblastomas as shown in Figure 3.20. Linear regression was used to determine statistical significance, whereby the P value indicates whether the relationship between an independent variable (Days elapsed since diagnosis) and the dependent variable (Expression level of *HK2*) is statistically significant. Linear regression analysis revealed a statically significant (p=0.0017) intersect on the Y-axis at 340- fold change expression, indicating the level of *HK2* expression to have a significant effect upon outcome. The biopsies were then grouped according to their *HK2* fold change levels where the samples were either greater than 340-fold change increase or less than 340-fold increase compared to normal brain tissue levels of *HK2*.

Survival data comparing the 2 biopsy groups illustrated a significant difference with regards to outcome as shown in Figure 3.21.
In biopsy samples with *HK2* levels >340-fold increase, median patient survival was 102 days, with a range from 19 to 491 days post operation. In comparison glioblastoma samples with *HK2* levels <340-fold increase, had significantly (Log-rank Mantel-Cox test, p=0.0002) longer median survival, at approximately 296 days post operation with a range from 12 to 1374 days.

The correlation between *HK2* expression and OS was also investigated when patients were grouped dependant on sex, allowing for further stratification and to determine the effectiveness of potential inhibitors. The 86 biopsies were grouped dependant on patient sex, according to their *HK2* fold change levels, either greater than 340-fold change increase or less than 340-fold increase compared to normal brain, as shown in Figure 3.22. Significantly (p=0.0002) different survival times were determined in males (n=53), when *HK2* fold change was >340, median survival time was 133 days (ranging from 12-1374) compared to 373 days (ranging from 19 to 768) post operation with *HK2* fold change <340. No significance was determined between *HK2* expression levels and survival in females (n=33) where median survival time is 205

days compared to 316 days post operation between the respective groups (Mantel-Cox test, p= 0.8532).

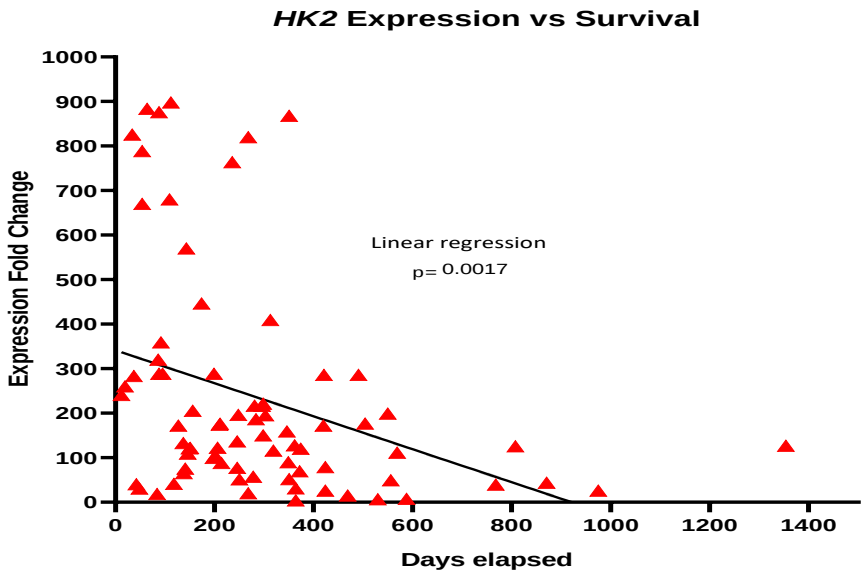

Figure 3.20 Showing patient survival vs level of *HK2* expression in glioblastoma biopsies Survival time shown in days compared to level of *HK2* expression in glioblastoma. Linear regression was used to determine the statistical significance, where the relationship between days elapsed and level of *HK2* is statistically significant. Linear regression analysis revealed a statically significant (p=0.0017) intersect on the Y-axis at 340- fold change expression, indicating the level of HK2 expression to have a significant effect upon outcome.

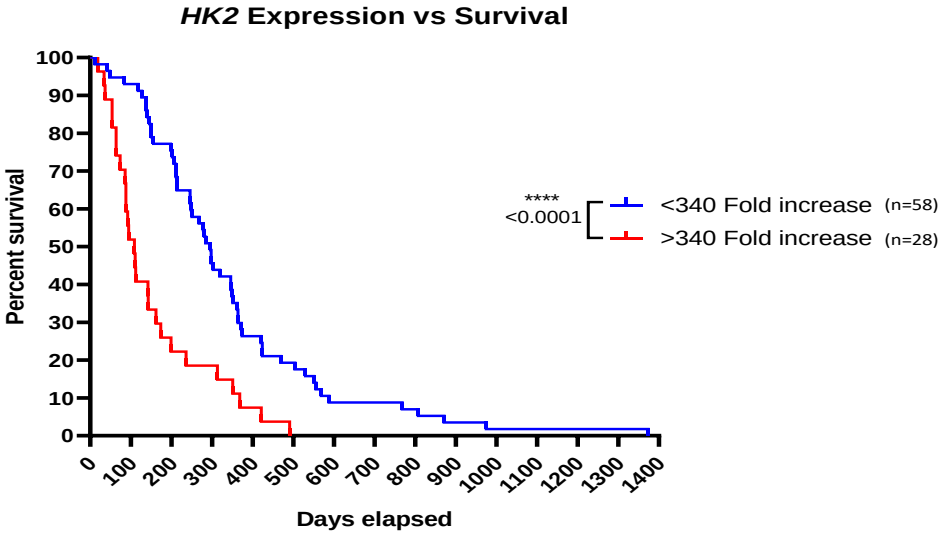

Figure 3.21 Showing patient survival in percentage vs days, comparing 2 subgroups of glioblastoma biopsies. Survival time shown between 2 subgroups of glioblastoma determined via *HK2* expression levels. Significantly (p=0.0002) different survival times were determined, when *HK2* fold change is >340, median survival time is 102 days compared to 296 days post operation with *HK2* fold change <340.

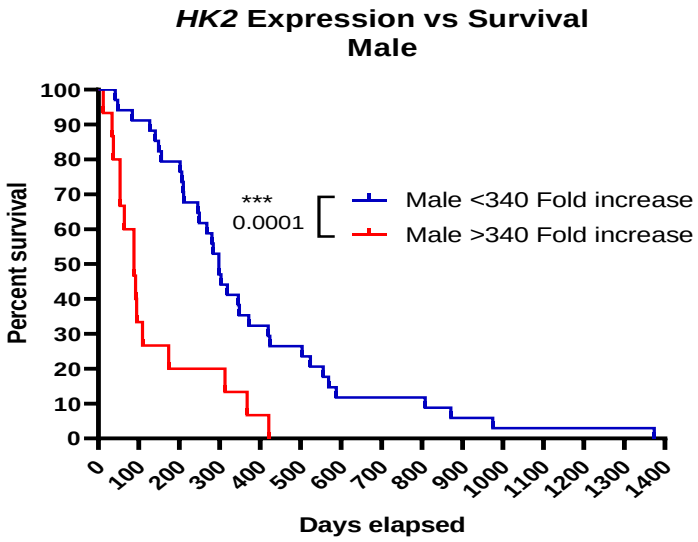

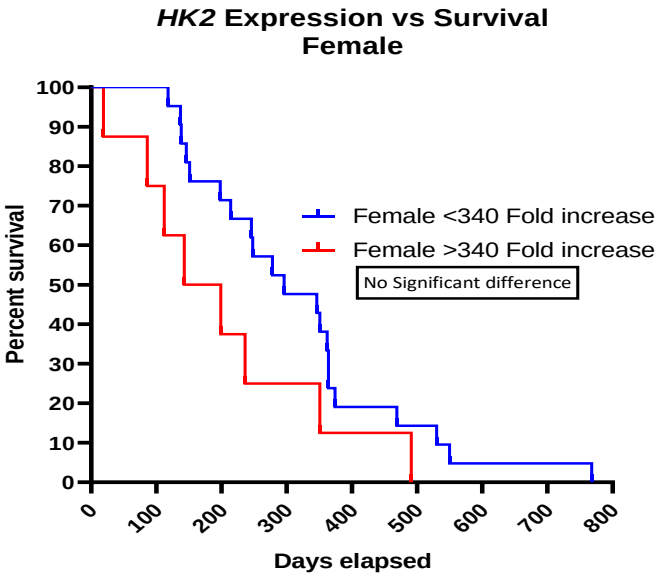

Figure 3.22 Showing patient survival in percentage vs days, comparing the sex of the patient. Survival time shown between 2 subgroups of glioblastoma determined via *HK2* expression levels in both male and female patients. Significantly (p=0.0002) different survival times were determined in males (n=53), when *HK2* fold change is >340, median survival time is 133 days compared to 373 days post operation with *HK2* fold change <340. No significance was determined between *HK2* expression levels and survival time in females (n=33) where median survival time is 205 days compared to 316 days post operation between the respective groups.

3.8 The relationship between *Hexokinase 1* overexpression and outcome

To investigate a potential association of *HK1* with patient outcome, expression data was compared to OS for 70 glioblastomas as shown in Figure 3.23. The biopsies were grouped according to their *HK1* fold change levels as shown in 3.3, the

grouping was determined by HK1 downregulation (n=32), no change of expression (n=28) or HK1 upregulation (n=10). Survival data comparing the groups illustrated no significant difference using Mantel-Cox test, with regards to patient prognosis. In samples where *HK1* was downregulated, median patient survival was 328 days, in comparison samples demonstrating overexpressed levels of *HK1,* the median patient survival was 315 days and 244 days in samples showing no fold change (compared to normal tissue). Additional patient details are in the appendix, including Sex vs *MGMT* methylation for OS (Figure A4), Sex vs *HK2* expression for OS (Figure A5) and Sex vs age for OS (Figure A6). Table A8 details patient biopsy information, *including MGMT* status, *HK2* expression, sex and OS.

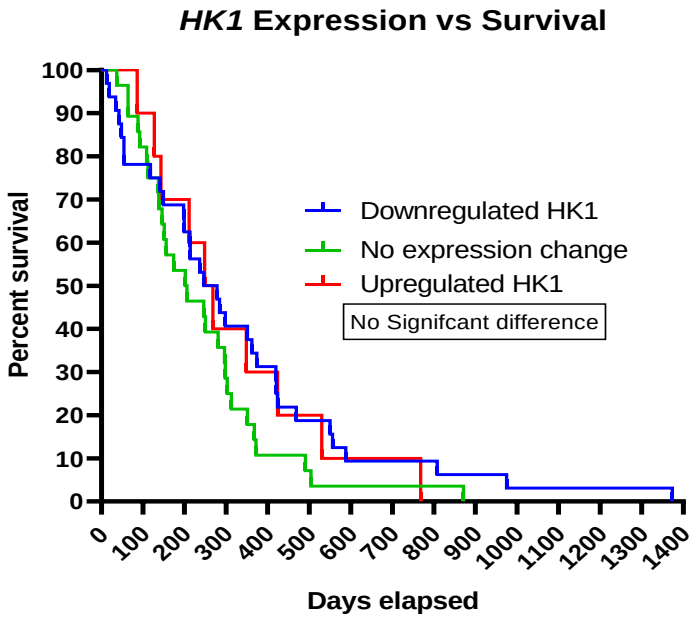

Figure 3.23 Showing patient survival in percentage vs days, comparing HK1 expression in biopsies. Survival time shown between groups of glioblastoma biopsies determined via *HK1* expression levels, dependant on either overexpression (n=10), downregulation (n=32) or no change in expression (n=28) compared to normal tissue. No significance was determined between the level *HK1* expression and survival time across elapsed days post operation.

3.9 Growth curves

All glioblastoma cultures were grown under conditions detailed in Section 2.1.4. Growth curves were completed for all cultures used. The doubling time for each of the cultures was calculated from measuring the highest gradient within the exponential growth phase. The doubling times for each culture are detailed in Figure

3.24 and Table 3.12. The times ranged from 24 hours to 70 hours with a median doubling time of 42 hours. In comparison the doubling time for NHA was 63 hours. A correlation between the rate of growth and *HK2* expression was established, where significantly higher (p=0.0021) expressing cultures were shown to have a shorter doubling time. The data is shown in the appendix. The data here suggests *HK2* involvement with an increased rate of proliferation, this will be further explored in Chapter 4.

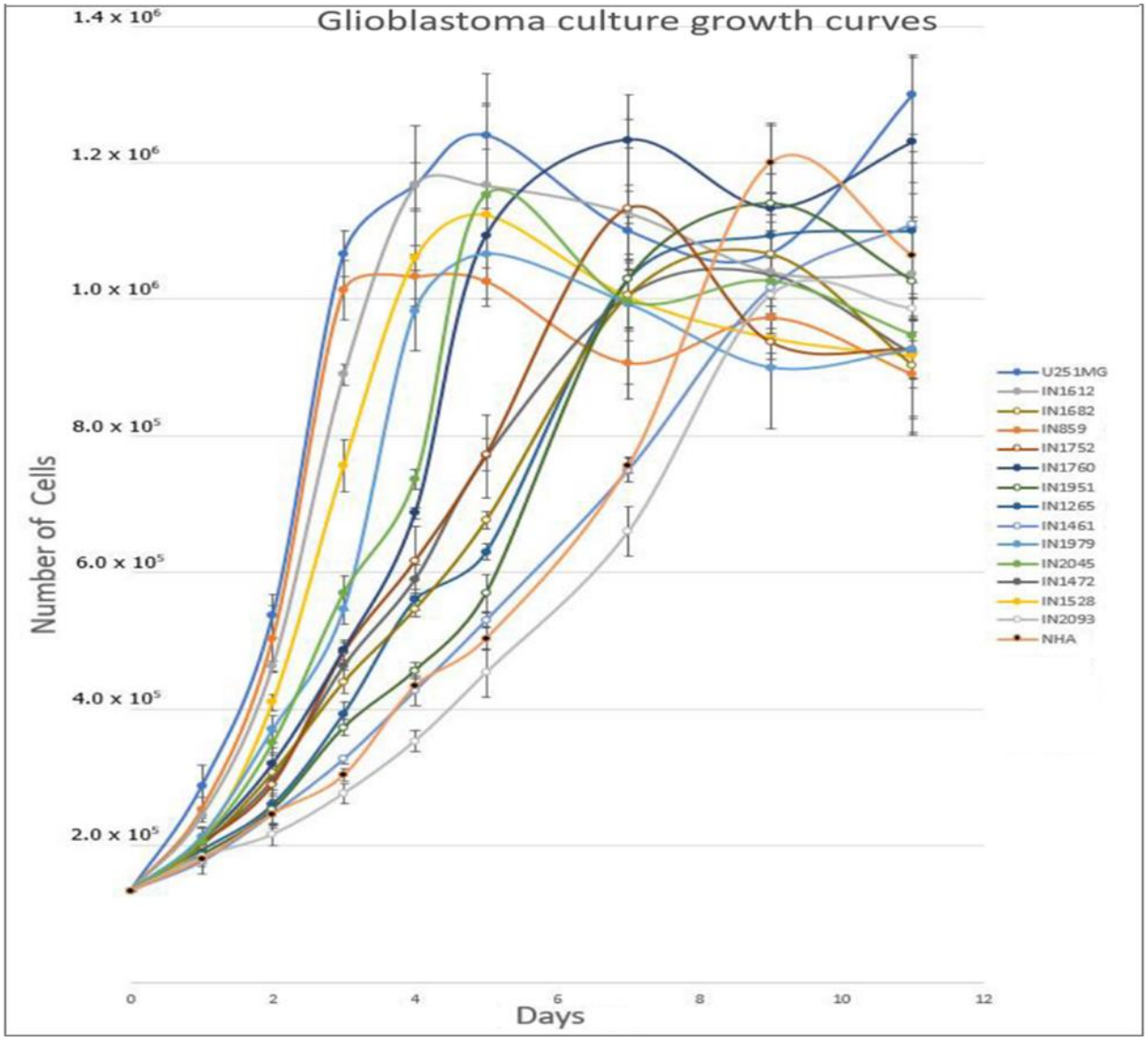

Figure 3.24 Growth curve data for all glioblastoma cultures and NHA All cultures were seeded with 2x10^5 cells at day zero. Two cell count readings were collected at 8 time points. Data shown is averaged from three replicate time courses. Doubling times were each culture was

determined from the highest gradient in its exponential growth phase. y-axis represents cells/cm2 of growth media.

Table 3.12 Doubling time of culture panel

Culture	Doubling time (Hours)	*HK2* expression	Culture	Doubling time (Hours)	*HK2* expression
U251MG	24 (±1.56)	1502.61 (1.96)	IN2132	44 (±2.56)	88.35 (3.58)
U87MG	24 (±2.01)	1294.26 (2.11)	IN1472	45 (±1.75)	403.36 (2.11)
IN859	24 (±2.22)	995.11 (1.54)	IN1682	50 (±1.42)	120.54 (2.65)
IN1612	28 (±1.5)	126.63 (0.91)	IN1265	50 (±2.8)	97.35 (3.41)
IN1528	32 (±1.26)	385.95 (2.82)	IN1951	55 (±2.08)	210.63 (1.95)
IN1979	34 (±2.51)	574.39 (3.01)	IN1461	60 (±1.82)	85.73 (2.94)
IN2045	36 (±1.64)	219.82 (1.22)	NHA	63 (±2.62)	30.42 (3.12)
IN1760	40 (±3.1)	201.96 (1.83)	IN2093	70 (±3.22)	132.75 (0.24)

All cultures were seeded with $2x10^5$ cells at day zero. Two cell count readings were collected at 8 time points. Data shown is averaged from three replicate time courses. Doubling times were each culture was determined from the highest gradient in its exponential growth phase. *HK2* expression is shown for each culture.

3.10 Discussion

This chapter has focussed on the investigation of the differential mRNA expression of hexokinase isoforms in 103 glioblastoma biopsies compared to normal brain tissue, with the aim of understanding the potential involvement of *HK2* overexpression in glioblastoma development. Patient-derived glioblastoma cell cultures were also investigated (n=21) to determine altered mRNA expression compared to NHA. Additionally, the epigenetic mechanism regulating hexokinase expression was identified through methylation studies utilizing pyrosequencing in both biopsy samples and cultures compared to both normal brain tissue and NHA. The findings of this study highlight the dysregulation of hexokinase expression in glioblastoma, and reiterate the altered metabolism associated within cancer cells (Goodwin *et al.*, 2015). Expression analysis in this study revealed distinct *HK2* expression and methylation profiles in both glioblastoma biopsies and patient -derived cell cultures compared to their normal counterparts. A variation in mRNA overexpression of *HK2* was observed amongst the biopsies which may reflect the characteristic inter-tumour heterogeneity of heterogeneity of glioblastoma.

Hexokinase 2 overexpression is prevalent in glioblastoma

In this study the gene expression profile of glioblastoma biopsies and patient-derived cell cultures investigated show altered levels of *HK2* gene expression levels. Both glioblastoma biopsies (n=103) and patient-derived cell cultures (n=21) demonstrated overexpression of *HK2* across all samples compared to normal brain tissue and NHA, with the average expression of *HK2* in the biopsy samples approximately 229-fold change increase and 411-fold change increase in the cultures compared to normal tissue. The similar expression profiles of *HK2* in both the biopsy samples and the patient-derived cultures in this study is encouraging and an important finding, the advancement of a more accurate model of glioblastoma is crucial for the development of therapeutic treatments.

Overexpression of *HK2* has been documented in range of cancers, including both lung and breast cancer (Wang *et al*., 2014; Anderson *et al*., 2016). One of the reasons for the upregulation of *HK2* in glioblastoma may be attributed to the influence of the well-known metabolic transformation in cancer cells, with the increasing reliance upon the glycolytic pathway as the predominant mechanism for energy production; as a resultant requirement of increased amounts of energy to maintain augmented proliferation and cell survival (vander Haiden *et al*., 2009; Kami *et al*, 2013). Another plausible explanation for the selective overexpression of the HK2 isoform in cancer cells maybe a result of compatibility with cancer cells intrinsic properties, where *HK2* unlike *HK1* possesses two active catalytic domains in its amino- and carboxy- termini, in comparison *HK1* only possess a single active catalytic domain in its carboxy-terminus. The two catalytic domains have different kinetic properties more suited for the metabolic nature of cancer cells with the advantage of *HK2* retaining activity under conditions that are inhibitory for the single catalytic domain, such as hypoxia (Wilson, 2003).

Overexpression of *HK2* has also been shown to offer significant growth advantages in many tumours including ovarian, medulloblastoma and breast cancers (Jiang *et al*., 2012; Gershon *et al*., 2013; Siu *et al*., 2019). Its crucial catalytic role initiating

the glycolytic pathway has been associated with driving the accelerated glucose flux as seen in the Warburg effect cells as well as increasing tumour invasion, aggression and enhanced therapeutic resistance (Patra *et al*., 2013; Wolf *et al*., 2011 Galluzi *et al*, 2013; Lindgvist *et al*., 2018). The variation in the level of *HK2* overexpression in glioblastoma tissue could be attributed to tumour heterogeneity (Verhaak *et al*., 2010), or epigenetic alternations occurring to varying extents. The data obtained signifies *HK2* overexpression as a common occurrence in glioblastoma which may well contribute to tumour growth.

Hypomethylation of *Hexokinase 2* drives overexpression

Establishing the potential factors influencing the mechanism of *HK2* overexpression occurring in glioblastoma is key for the stratification of patients, providing a further refinement in glioblastoma classification, with an increased potential at predicting patient outcome and may be translated into effective therapeutic strategies tailored to each patient. One approach to determine if *HK2* overexpression is epigenetically regulated is to investigate alterations in methylation of the promotor region of the gene. Comprehensive changes of *HK2* promotor hypermethylation in glioblastoma have not been previously investigated using pyrosequencing, however studies have shown extensive *HK2* CpG island hypomethylation in hepatocellular carcinoma (Lee *et al*., 2016). The current study established a reduction in the level of *HK2* methylation to be present in all 103 glioblastoma biopsies, with an average methylation level 20% lower across 4 CpG sites (CpG 8, 9, 10, 11) compared to normal brain tissue ($p<0.0001$). Hypomethylation was also established in all patient-derived cultures, with average levels of methylation of 5.4%, significantly ($p<0.0001$) lower than normal brain tissue. The greatest level of *HK2* promotor hypomethylation in the biopsies was observed at CpG10, with a significantly ($p<0.0001$) reduced methylation level by 36.7% compared to normal tissue. Promotor hypomethylation was also seen in the culture samples with significantly ($p<0.0001$) reduced levels of methylation of 38.3% compared to normal tissue. NHA also had a significantly ($p<0.0001$) reduced level of methylation of 14.74%, which may be accounted for by its foetal origins. *HK2* has been shown to be expressed in

embryonic tissues, involved with development but it is downregulated in healthy adult tissue except for adipose, skeletal, and cardiac muscle (Wilson, 2003).

The distinct shifts in DNA methylation patterns are well documented in cancer cells, with the common occurrence of CpG island promoter hypermethylation often associated with the silencing of tumour suppressor genes (Miranda-Gonçalves *et al.*, 2018). The most recognised of these epigenetic disruptions are of the tumour suppressors *BRCA1, CDKN2A, MLH1, and VHL*, which have been identified as drivers for lung, colorectal, breast and renal cancer progression (Jones and Baylin, 2007; Esteller, 2000). A recently amended glioma classification utilises the molecular diagnosis of *isocitrate dehydrogenase* (*IDH*) mutational status, whereby IDH-mutant glioma manifest CpG island methylator phenotype (G-CIMP) (de Souza *et al.*, 2018). The identification of clinically relevant subsets of G-CIMP tumours (G-CIMP-high and G-CIMP-low) provided an additional refinement for glioma classification, for the prediction of patient outcome (Malta *et al.*, 2018). Global hypomethylation has also been associated with the activation of transcriptional protooncogenes, such as *HRAS* in melanoma, and with genomic instability leading to translocations and deletions (Ehrlich, 2009). Studies have also established the presence of global hypomethylation as a common occurrence in primary human glioblastomas, where elevated hypomethylation was associated with copy number alterations, suggesting that hypomethylation may be one factor predisposing to specific genetic alterations commonly occurring in glioblastoma (Cadieux *et al.*, 2006).

Promoter hypomethylation of *HK2* has been associated with *HK2* upregulation in a range of cancers including hepatocellular carcinoma and glioma cells, thus the epigenetic disruption primes the cells to favour the glycolytic flux (Wolf *et al.*, 2011; Crispo *et al.*, 2019). The data obtained shows that hypomethylation of *HK2* is frequently occurring across multiple CpG sites.

HK2 hypomethylation impacts mRNA expression

The impact of *HK2* hypomethylation on gene transcription was also investigated. A strong correlation between the percentage of methylation and level of expression

across the CpG sites examined ($p < 0.0001$) was demonstrated in all glioblastoma samples. Biopsies exhibiting hypomethylation levels of <5.5% demonstrated significantly ($p < 0.0001$) increased levels of *HK2* expression, with a fold change average expression level of 297.3 compared to 99. Additionally, culture subgroups showed similarities, where hypomethylation levels <5.4%, a significantly ($p=0.0276$) increased level of *HK2* expression was established, with an average fold change of 529.5 compared to 112.7. Studies have shown the presence of hypomethylation of CpG islands within intron 1 of *HK2* in both developmental human foetal brain and glioblastoma tissue via MS-PCR, where in both cases *HK2* is abundantly expressed (Zhen and Hongjuan, 2018). Hypomethylation of *HK2* was also shown to enhance levels of *HK2* expression in hepatocellular carcinoma, in which the hypomethylation phenotype (*HK2*-CIMP) was associated with poor clinical outcome. (Lee *et al.*, 2016). DNA hypomethylation has also been directly associated with increased upregulation across a range of genes in many cancer cells including lymphocytes, colorectal, gastrointestinal and gynaecologic cancers; studies have shown multiple genes to be perturbed in these cancer cells, with prevalent overexpression in tissues that are commonly undetected in normal cells, (Ehrlich, 2009; Jeong *et al.*, 2014; Wong *et al.*, 2015). The methylation data in this study also revealed a variation in levels of methylation across the multiple individual CpGs investigated. Promoter hypomethylation varied >15% across 4 CpGs (8,9,10,11) in the 103 biopsies that were investigated, highlighting the occurrence of single base-pair DNA methylation changes involved with progressive epigenetic alterations during tumour evolution. A study employing genome-wide DNA methylation profiling established highly variable individual CpG methylation levels in a large proportion of the genome in a range of cancer samples including colorectal, breast, liver, glioma, neuroblastoma, prostate and lung, opposed to their invariant normal counterparts. It was suggested that the single base-pair DNA methylation changes showed evidence of positive selection, mutual exclusivity and tissue specificity with potential cancer-driving effects participating in neoplastic transformation (Vidal *et al.*, 2017).

Association of *HK2* overexpression and patient outcome

Increased *HK2* overexpression correlated to poorer patient outcome. A significant difference (P<0.0001) of 194 days was revealed between the median outcome in the group of biopsy samples expressing less than 340- fold change compared to samples expressing greater than 340- fold change. Furthermore, different survival times were determined in male patients (n=53), where increased *HK2* overexpression correlated to poorer patient outcome. A significant difference (p=0.0002) of 240 days was revealed between the median outcome in the group of biopsy samples expressing less than 340- fold change. No significance was determined between HK2 expression levels and survival in female patients (n=33) where median survival was 205 days compared to 316 days post operation between the respective groups. The association of outcome with *HK2* overexpression has been previously documented in other cancers. Studies have shown when stratified by tumour type, the impact of *HK2* overexpression on poor prognosis was observed in a range of digestive cancers including gastric and colorectal cancers, where elevated *HK2* expression was significantly associated with shorter OS. The negative effect of *HK2* overexpression on OS was observed in hepatocellular carcinoma, gastric and colorectal cancer but not in pancreatic cancer (Liu *et al.*, 2016; Wu *et al.*, 2017). Additionally, the correlation between *HK2* and OS was independent of MGMT status, as shown in Appendix table A2. The association between *HK2* expression and outcome offers an important insight to a potential prognostic marker for both the impact and additional stratification of glioblastoma patients. The stratification of patients separated by the prognostic expression biomarker is beneficial for the utilization of treatments that target HK2. High expression of *HK2* may not only predict poor prognosis but also be a potential promising therapeutic approach to develop strategies against this protein.

***HK1* is downregulated in a subset of glioblastoma** Sixty (85.7%) biopsies exhibited HK1 downregulation or no change in the level of methylation compared to normal brain tissue. Additionally, 44% of these biopsies demonstrated a significant

loss in expression (p=0.0006). No significant upregulation was determined however 10 biopsies did demonstrate slight increased level of expression. An altered level of gene expression was also determined across the glioblastoma cultures, where all patient-derived and established cell lines demonstrated an increased level of HK1 expression, NHA also exhibited an increase. Both *HK1* and *HK2* are associated with mitochondria and are implicated in cell survival and proliferation (Gottlob *et al.*, 2001, Majewski *et al.*, 2004). Although *HK2* is overexpressed in a range of cancers, including lung and breast, there is no significant change in expression levels of *HK1* in these cancers (Patra *et al.*, 2013). It is thought cancer cells favour the higher activity of HK2 which possesses two active catalytic domains with the potential to maintain metabolic activity in adverse environments, presenting a potential explanation for the selective isoform switch from HK1 to the overexpression of *HK2* in cancer cells (Wilson, 2003). The study also concluded that normal brain tissue preferentially expresses *HK1* and undergoes oxidative glucose metabolism. A recent study concluded that *HK2* overexpression was a key driver of metabolic regulation in glioblastoma, and that the function of *HK2* is independent of its isoform *HK1* (Sameer *et al.*, 2018). *HK1* expression was shown to be downregulated in over 84% of the glioblastoma biopsies, indicating a potential HK isoform switch in glioblastoma.

Altered expression of Hexokinase 1 is not methylation-specific

The change in methylation status was investigated to determine if the deregulated expression of *HK1* is epigenetically driven. In this study the methylation profiles of glioblastoma biopsies and patient-derived cell cultures were investigated, comprehensive changes of *HK1* methylation in glioblastoma have not previously been investigated by pyrosequencing. There were no significant differences between the average level of methylation in the biopsies (4.1%), ranging from 1.33% to 7.46% and normal brain (6.9%), however a small subset of biopsies (n=4) demonstrated significant reduced levels of methylation (p= 0.0008). Furthermore, only 1 culture (IN1951) showed a significant (p=0.0063) reduction in the level of methylation compared to normal brain, no substantial alterations were demonstrated

in the other cultures compared to normal brain tissue. This data confirms that down-regulation of *HK1* in glioblastoma is not due to hypermethylation.

Studies investigating the various hexokinase isoforms state that although *HK1* is the most highly expressed hexokinase isoform, there is little evidence to suggest it has a function in human cancer, with little significant alterations in levels of expression or methylation (Peschiaroli *et al.*, 2013; Kim *et al.*, 2019). In another study it was shown that although deregulation of methylation is not a frequent occurrence in cancer cells, there is evidence of the occurrence of histone modification, with reported *HK1* phosphorylation of histones sites H1 and H2A (Ignacak and Stachurska, 2003). Currently however little is known about these phosphorylation sites and their biological functions in cancer (Qin *et al.*, 2019). Histone posttranslational modifications represent a versatile set of epigenetic features involved in dynamic cellular processes which include transcription and DNA repair, studies have identified a range of deregulated histone modifications known to impact cellular function. The impact of miRNAs associated with metabolic reprogramming to oncogenesis is of growing interest. A range of miRNAs are responsible for driving altered gene expression. mir-143 has been shown to correlate to *HK2* expression in lung tumours and has demonstrated effective inhibition of *HK2*, disrupting glucose metabolism in colon cancer cells. (Gregersen *et al.*, 2012; Peschiarol *et al.*, 2013). Additionally, it has also been suggested that mir-143 also targets *HK1* as well as other glucose pathway components (Hatziapostolou *et al.*, 2013). The biopsies that did show significant *HK1* hypomethylation may be impacted by global methylation - associated in glioblastoma. Aberrant DNA methylation patterns are common events in the genesis and progression of tumours (Jones *et al.*, 2007). It has been shown that in general a global loss in the level of methylation (genomic hypomethylation) occurs in cancer cells increasing genomic instability. Currently the perturbed DNA methylation on a genome-wide scale is still not fully understood in glioblastoma, however a recent study utilizing next-generation sequencing identified a total of 104 hypomethylated and 524 hypermethylated regions in glioblastoma, indication the potential aberrant global methylation present in glioblastoma (Li and Wu, 2017).

Another study showed that intratumor DNA methylation heterogeneity is present within glioblastoma; in biopsies classified as *IDH* wt/mutated by methylation analysis, the intratumor DNA methylation differed in samples from the same patient (Wenger *et al.*, 2019). The data presented here suggests that the level of *HK1* methylation in glioblastoma does not have a critical function impacting *HK1* expression levels, the occurrence of *HK1* downregulation in glioblastoma may be instigated through histone modification and/or miRNA activity.

The impact of Hexokinase 1 altered expression related to outcome

To investigate the effect of altered levels of *HK1* on survival prognosis, expression data was compared to patient survival information. The biopsies were grouped according to their *HK1* fold change levels, the grouping was determined by *HK1* downregulation (n=32), no change of expression (n=28) or HK1 upregulation (n=10). Survival data comparing the groups illustrated no significant difference using Mantel-Cox test, with regards to patient prognosis. In samples where HK1 was downregulated, average OS was 328 days, in comparison samples showing no fold change OS survival was 244 days. The data here concludes that altered levels of *HK1* does not impact outcome in glioblastoma, this has also been shown in other studies which state that *HK2* not *HK1* impact tumour metabolism and cell growth resulting in an undesirable clinical outcome, specifically poor prognosis in patients (Vartanian *et al.*, 2014). *HK1* is associated with catabolism and the regulation whereas *HK2* is associated with the anabolic roles driving proliferation. A recent study focused on gastric cancer and lymphatic metastasis stated patients with *HK1* expression showed remarkable shorter survival duration, and that overexpression of *HK1* was significantly associated with lymphatic metastasis and unfavourable prognosis in gastric cancer (Gao *et al.*, 2015).

Conclusion

The study highlights the importance of *HK2* promotor hypomethylation leading to gene dysregulation and mRNA overexpression in glioblastoma, impacting negatively

on overall survival. In comparison, expression of *HK1* was decreased in over 75% of biopsy samples compared to normal tissue, demonstrating a potential shift in expression of *HK* isoforms in tumour tissue. *HK1* downregulation in glioblastoma may be instigated via histone modification and/or miRNA activity, independent of methylation.

Chapter 4

HK2 promotes tumour growth and chemoresistance in glioblastoma

4.1 Introduction

Genetic analysis of 103 biopsies (detailed in Chapter 3, Section 3.2) established that overexpression of *HK2* is prevalent in glioblastoma, with significant upregulation frequently occurring compared to normal brain tissue. A potential therapeutic *HK2* inhibitor is 3-bromopyruvic acid (3-BPA), which is a synthetic derivative of pyruvic acid. 3-BPA has been shown to have an inhibitory effect on a range of tumour cells including liver and breast cancers although, currently there is no data for its efficacy in glioblastoma (Gandham, *et al*., 2015). 3-BPA causes dissociation of *HK2* from its mitochondrial bound complex through covalent modification, resulting in *HK2* being subsequently released into the cytosol and the stimulation of apoptosis inducing factor (AIF) which consequently leads to cell death (Gandham, *et al*., 2015). Another *HK2* inhibitor, lonidamine (LND) has been shown to inhibit aerobic glycolysis in cancer cells by targeting condensed mitochondria and inhibiting mitochondrially bound hexokinases in tumour cells, leading to a decrease in glycolysis and cellular ATP (Caputo, *et al*., 1984). Studies have also shown the major metabolic changes induced by LND are inhibition of lactate transport and its accumulation which leads to intracellular acidification (Nancolas *et al*., 2016). More recently it was suggested that using LND in combination treatment with TMZ increased the effectiveness of TMZ at inhibiting tumour growth in glioblastoma cells, and importantly reduce the dose of temozolomide required for radio sensitization of brain tumours (Prabhakara *et al*., 2008). Another potential *HK2* inhibitor is the anti-diabetic drug metformin. Studies have shown its effectiveness as an anti- cancer therapeutic in a range of tumours targeting deregulated glycolytic metabolism (Saber *et al*., 2018). The reduction in glucose has been shown to significantly increase survival rates in a range of cancers, with significant reductions in proliferation due to a lack of energy source (Thi Tieu *et al*., 2015). A recent clinical trial for early stage breast cancer

noted the significant reduction of cancer biomarkers with the addition of metformin (Dowling *et al*., 2018). Population studies have also demonstrated that type II diabetes patients treated with metformin had a reduced risk of cancer (Evans *et al*., 2005). The mechanism of the anti-tumour effects is not fully understood although there is some evidence that metformin affects the activation of AMPK and the inhibition of the mTOR pathway (He *et al*., 2015). *HK2* inhibitors and metformin offer therapeutic potential in the treatment of glioblastoma. The inhibitors are in relatively stable form making them potentially ideal agents to test in both *In vitro* and *In vivo* models. The drugs dissolve in water and/or DMSO allowing for stable and successful delivery for cell culture (Sankar *et al*., 2013). The analysis of the inhibitors via cell culture is crucial for the advancement in understanding the mechanisms of action, the anti-tumour effect they elicit in glioblastoma cells; and to also ascertain their potential as effective anti-cancer agents. The microenvironment created in tissue culture is often altered in comparison to the natural cellular environment which can generate genetic alterations, for example the concentration of glucose available to the cell. A healthy adult on average has circulating glucose levels around 5-6mmol/l, in comparison the glucose concentration in average tissue culture media ranges from 10-25 mmol/l. To address this discrepancy the use of an alternative culture media that has a similar glucose concentration was used, Hams F-10, which has a 6mM concentration of glucose, comparable to the circulating blood glucose of the human body. The exaggerated abundance of glucose in the culture media can have detrimental and inaccurate effects on cellular responses to inhibitory molecules such as ketone bodies, glucose pathway inhibitors and metformin, the latter of which has been shown to have reduced efficacy in both breast and ovarian cancer in such cases (Wahdan-Alaswad, *et al*., 2013; Litchfield, *et al*., 2015).

The aim of this current study was to investigate the anti-proliferative effectiveness of selected HK2 inhibitors, assessed across a panel of 13 patient-derived glioblastoma cultures (IN lines only, UWLV cultures were not accessible at this time in the study) and 2 established cell lines (U251MG AND U87MG) as shown in Table 2.1. The mechanisms of action were investigated via flow cytometry. Additionally, the ketone body 3-hydroxybuterate (3-HB) was used to establish any comparable effects of the

downregulation of HK2 via the reduction of glucose, and to determine the impact of ketogenesis on glioblastoma cell proliferation.

4.2 CRISPR-mediated *HK2* knockout

CRISPR knockout was utilised to investigate the effect of inhibiting *HK2* on proliferation in glioblastoma cultures and to determine the role of *HK2* in chemoresistance. *HK2* is the initial rate limiting step in the glycolytic pathway (Wolf *et al*., 2011). The effectiveness of inhibitors (including 3-BPA, TMZ and metformin) were also investigated in the presence of *HK2-KO* in the glioblastoma cultures.

4.2.1 Verification of stable *HK2* downregulation

HK2 was knocked out in three patient-derived cultures (IN1979, IN859 and IN2045) and the established cell line U251MG, a using CRISPR all-in-one vectors (Origene) which contain both guide RNA, Cas9 expression, T7 vectors, gRNA and Cas9 separate vectors; with HDR-based (Homology Directed Repair) donor vector construction, as stated in 2.7. The selected glioblastoma cultures represented both high and low expressing *HK2*, Chapter 3 demonstrated that cultures with the higher levels of *HK2* expression had faster growth rates and doubling times ($p=0.0021$). After transfection, a puromycin dose curve was established to determine the lowest dose that killed non-transfected cells completely, 7 days post selection. The range of puromycin used was 1µg/ml to 5µg/ml, dependant on specific cultures. After 7 days of treatment the surviving cell colonies were isolated using a dilution method, whereby cells were seeded <10 cells per well in a 96 -well plate. After 10 days, wells containing a single cell colony were expanded first into a 6 well plate and then into T25 flasks. The puromycin resistant cells were then analysed and verified via genomic qPCR to ensure the integration of the functional cassette. The downregulation of *HK2* was shown in all CRISPR treated cultures compared to the

respective parent culture, with an average reduction in *HK2* expression of 0.94 – fold change, as shown in Figure 4.1.

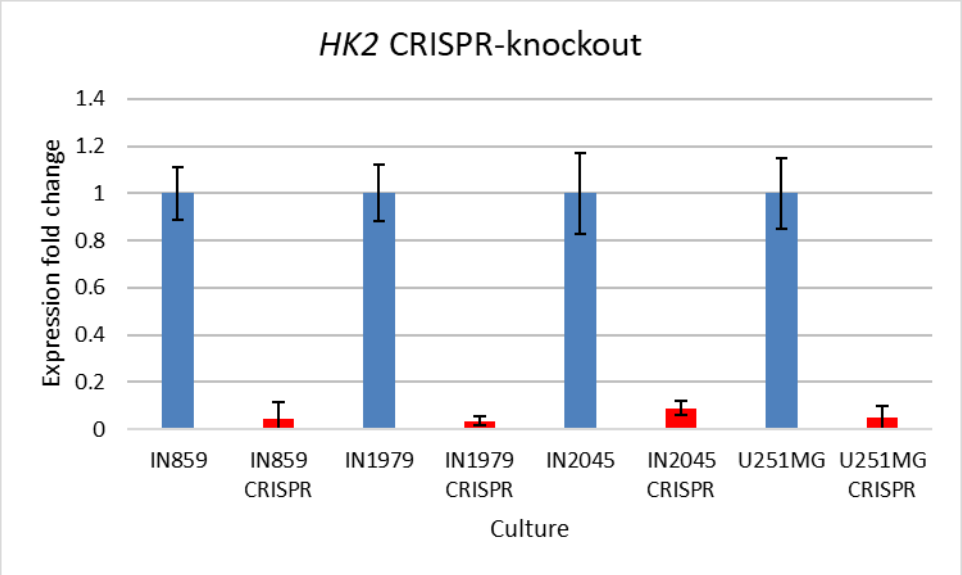

Figure 4.1 Downregulation of *HK2* in CRISPR treated cultures
qPCR data for each CRISPR treated culture compared to parent culture, showing downregulation of *HK2*. Puromycin selection was utilized to kill non-transfected cells, surviving colonies were isolated and expanded giving successful *HK2* knockout cultures. Expression reduction values for each culture compared to parent culture are: IN859 *HK2*-KO = 0.046, IN1979 *HK2*-KO= 0.034, IN2045 *HK2*-KO= 0.088, U251MG *HK2*-KO= 0.048.

4.3 The effect of *HK2* downregulation on cell proliferation

Once established, the 4 *HK2*-KO cultures (IN1979, IN859, IN2045 and U251MG) were grown under conditions detailed in Section 2.1.4. Growth curves were established on all CRISPR *HK2*- KO cultures and parent cultures, as shown in Figure 4.2.

A significant ($p<0.007$) decrease in cell growth between 38 to 44% was demonstrated in CRISPR *HK2*-KO modified cultures after 7 days compared to parent cultures, as shown in Figure 4.2. The largest reduction in cellular proliferation occurred in U251MG-*HK2*-KO and IN859-*HK2*-KO ($p<0.001$), where growth rates were reduced by >40% after 7 days. Notably, the parent cultures had previously shown the highest levels of *HK2* overexpression, 1502.6 and 995.1 expression fold change for U251MG and IN859, respectively, compared to normal tissue. In comparison, the parent IN1979 and IN2045 cultures had substantially lower levels of

overexpression, with values of 574.4 and 219.8respectively, compared to normal brain tissue. Chapter 3 demonstrated that cultures with higher levels of *HK2* expression had faster growth rates and doubling times, the data here shows the impact of *HK2* downregulation upon the rate of proliferation in glioblastoma cultures (p=0.0021), suggesting its potential role in promoting tumour growth in glioblastoma.

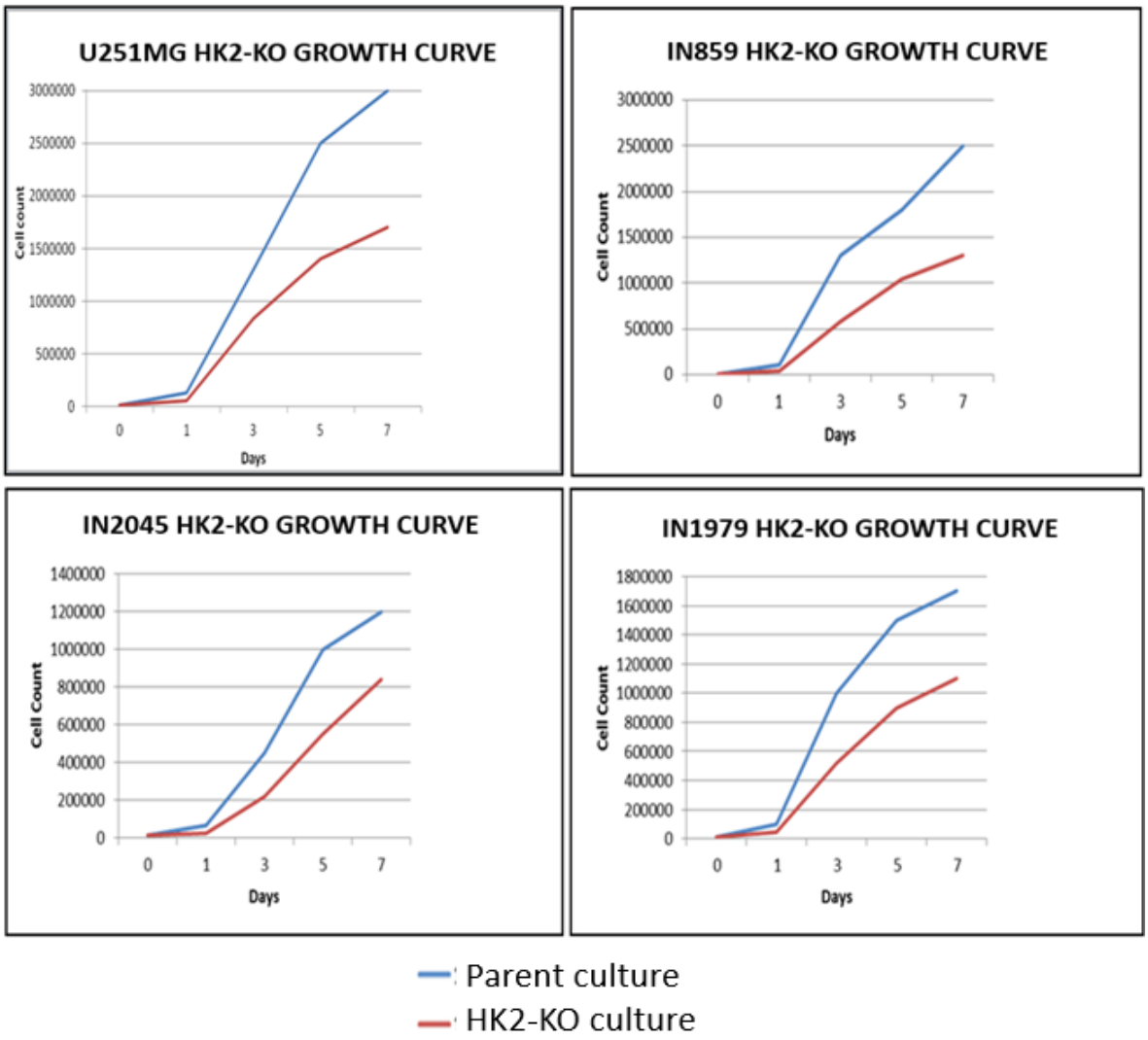

Figure 4.2 Comparing the level of proliferation between *HK2*-KO and parent respective cultures. The growth curve data for each CRISPR treated culture compared to the parent culture. A significant decrease in cell growth between 38 to 44% was demonstrated in all CRISPR *HK2*-KO modified cultures after 7 days compared to parent cultures respectively (IN2045 p=0.011, IN859 p=0.005, U251MG p=0.003, IN1979 p=0.008). y-axis represents cells/cm2 of growth media.

4.4 Growth inhibition

4.4.1 3-Bromopyruvic Acid

All glioblastoma cultures treated for 72 hours with 3-BPA demonstrated an inhibitory response and the ID_{50} values ranged from 12.9 – 61.4μM, as shown in Figures 4.3 and 4.4 and Table 4.1. U251MG (14.3 μM) and U87MG (12.9 μM) were the most sensitive cultures after 72 hour treatment and IN1979 was the short-term culture that demonstrated the highest sensitivity to 3-BPA with an ID_{50} value of 19.4 μM. NHA had a high tolerance of 3-BPA with the highest ID_{50} value (62.3 μM) compared to all the glioblastoma cultures, as expected for a non-tumour control. Glioblastoma cultures were grouped according to *HK2* expression, whereby the cultures were grouped dependent on the median value of fold change (219.8- fold change). Cultures that expressed higher levels of *HK2* were more sensitive to 3-BPA and generally had lower ID_{50} values compared to cultures that exhibited lower levels of *HK2*. A significant difference in ID_{50} values ($p= 0.0079$) was seen between cultures with >219.8- fold change expression and those with <219.8- fold change increase, where average ID_{50} values were 18.9 μM compared to 37.8 μM respectively, as shown in Figure 4.4.

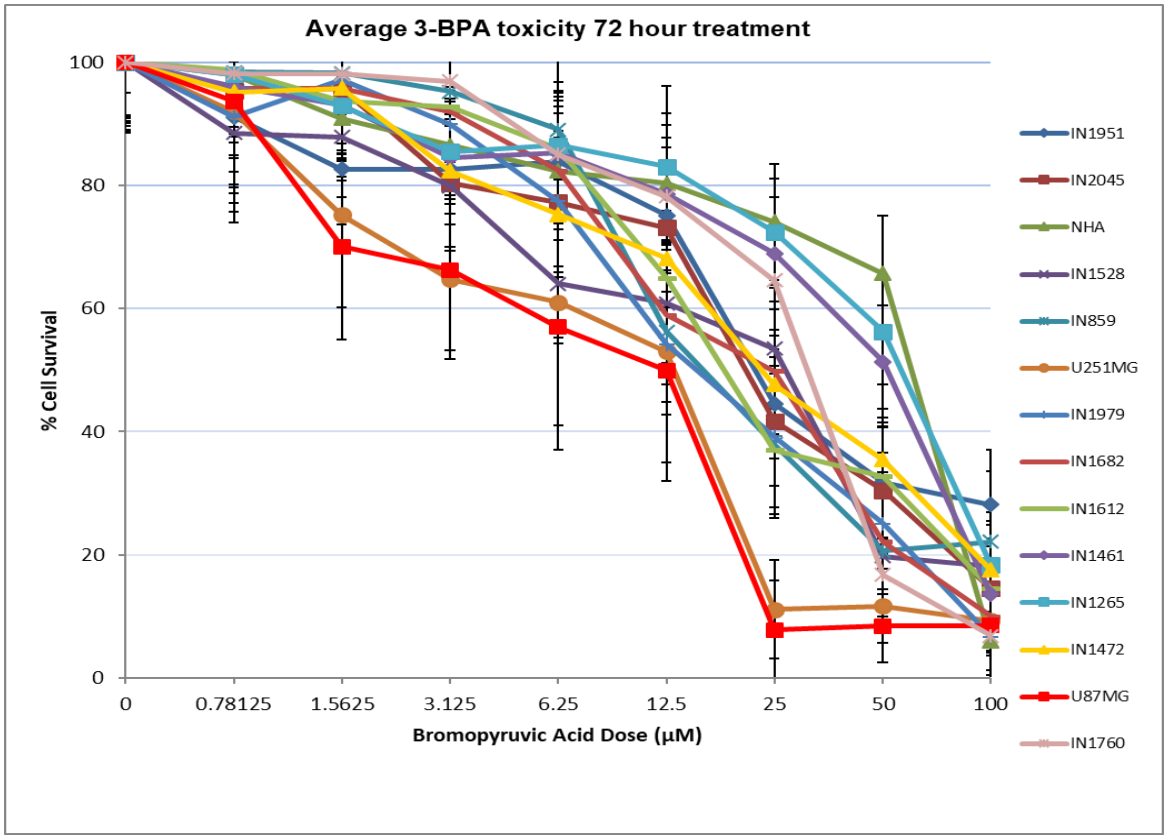

Figure 4.3 SRB cytotoxicity assay results for the glioblastoma cultures after 72 hours treatment with 3-BPA. Cell survival percentage is measured through the comparison of each optical density value to the value of the control wells (0µM 3-BPA + Tris buffer). Error bars represent standard deviation averaged from 3 replicate assays. Serial dilution of 3-BPA ranged from 100 to 0.78125 µM.

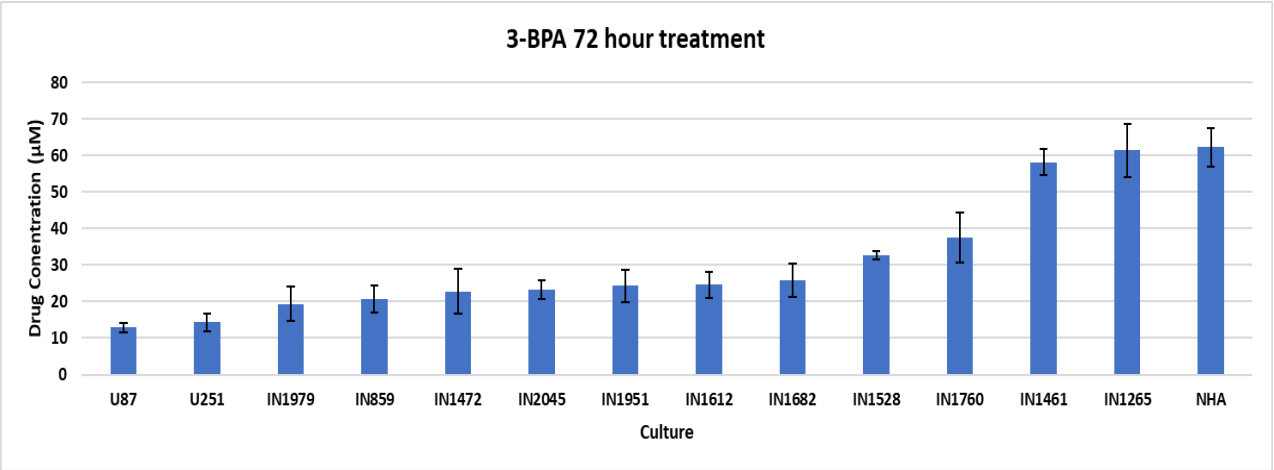

Figure 4.4 ID_{50} values for each glioblastoma culture and NHA after 72- hour treatment with 3-BPA. Cultures are ordered lowest to highest based on the ID_{50} value after 72-hours treatment with 3-BPA. Error bars represent standard deviation averaged from 3 replicate assays.

Table 4.1 ID_{50} values for all cultures treated with 3-BPA

Culture	3-BPA ID_{50} 72 hours (µM)	*HK2* Expression Fold Change
U87	12.9 (±1.21)	1294.3
U251	14.3 (±2.43)	1502.6
IN1979	19.4 (±3.74)	574.4
IN859	20.6 (±3.62)	995.1
IN1472	22.8 (±5.20)	403.36
IN2045	23.3 (±6.23)	219.8
IN1951	24.4 (±2.46)	210.6
IN1612	24.6 (±4.43)	126.6
IN1682	25.8 (±4.59)	120.6
IN1528	32.7 (±1.21)	386
IN1760	37.6 (±4.59)	202
IN1461	58.2 (±6.78)	85.7
IN1265	61.4 (±3.56)	97.4
NHA	62.3 (±7.27)	30.4

Table showing 3-BPA ID_{50} concentration for all cultures. Standard deviation for each average is listed after each result (±). Cultures are ordered lowest to highest based on the ID_{50} value after 72-hours treatment with 3-BPA ID_{50}. *HK2* expression fold change compared to normal brain is also shown for each culture. Higher expressing cultures had lower ID_{50} values.

4.4.2 Metformin

All glioblastoma cultures treated for 72 hours with metformin demonstrated an inhibitory response and the ID_{50} values ranged from 8.7 – 68.55 mM, as shown in Figures 4.5 and 4.6 and Table 4.2. U251MG (9.4 mM) and U87MG (8.7 mM) were the most sensitive cultures after 72- hour treatment and IN1472 was the patient-derived culture that demonstrated the highest sensitivity to metformin with an ID_{50} value of 9.75 mM. NHA had a high tolerance of metformin with the highest ID_{50} value (84.7 mM) compared to all the glioblastoma cultures, as expected for a non-tumour control. Glioblastoma cultures were grouped according to *HK2* expression, whereby the cultures were grouped dependent on the median value of fold change (219.8- fold change). Cultures that expressed higher levels of *HK2* did not correlate with increased sensitivity to metformin, no significant difference in ID_{50} values ($p= 0.0729$) were determined compared to cultures that exhibited lesser levels of *HK2*.

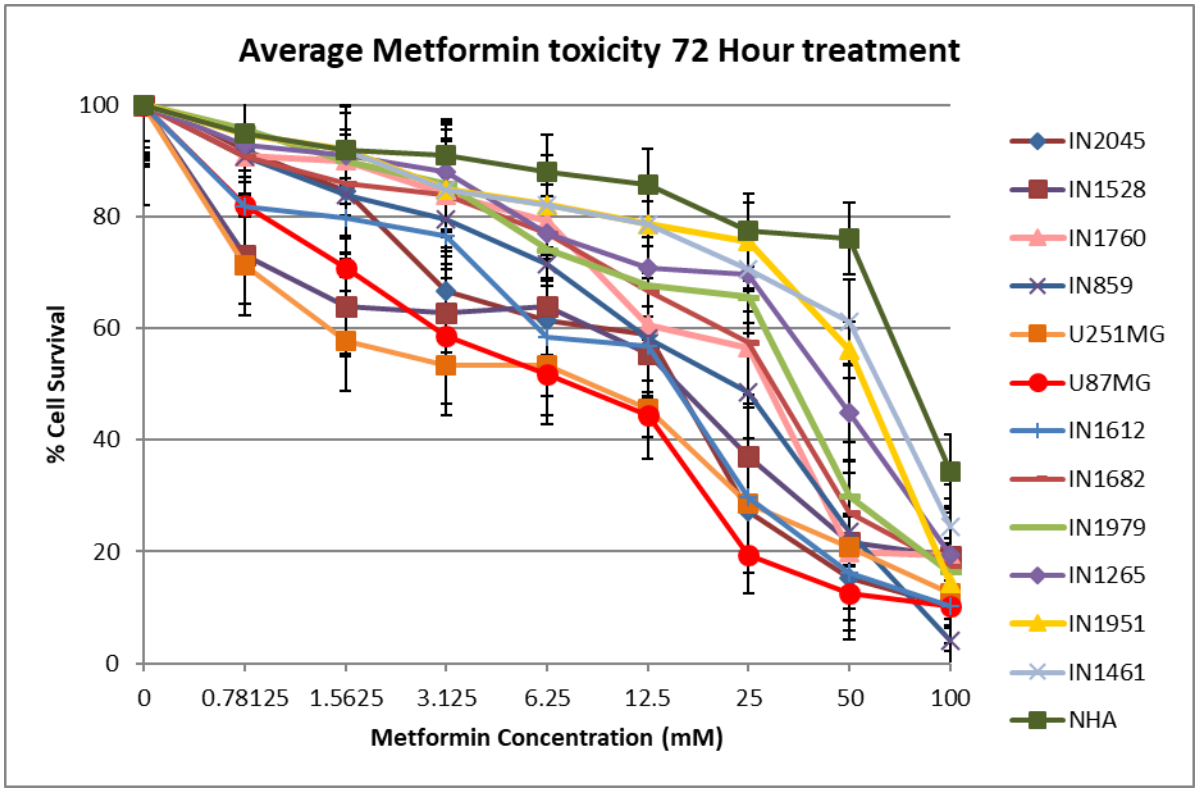

Figure 4.5 SRB cytotoxicity assay results for the glioblastoma cultures after 72 hours metformin treatment. Cell survival percentage is measured through the comparison of each optical density value to the value of the control wells (0mM metformin). Error bars represent standard deviation averaged from 3 replicate assays. Serial dilution of metformin ranged from 100 to 0.781 mM.

Table 4.2 ID_{50} values for all cultures treated with metformin

Culture	Metformin ID_{50} 72 hours (mM)	*HK2* Expression Fold Change
U87	8.7 (±1.74)	1294.3
U251	9.4 (±1.21)	1502.6
IN1472	9.7 (±3.11)	403.3
IN2045	15.6 (±2.47)	219.8
IN1612	15.7 (±2.78)	126.6
IN1528	19.2 (±1.52)	386
IN859	23.2 (±5.24)	995.1
IN1760	26.6 (±8.78)	202
IN1682	28.1 (±3.27)	120.6
IN1979	35.7 (±4.27)	574.4
IN1265	41.2 (±5.89)	97.4

IN1951	58.8 (±7.69)	210.6
IN1461	68.5 (±5.27)	85.7
NHA	84.7 (±6.43)	30.4

Table showing metformin ID_{50} values for all cultures. Standard deviation for each average is listed after each result (±). Cultures are ordered lowest to highest based on the ID_{50} value after 72-hours treatment with metformin. *HK2* expression fold change compared to normal brain is also shown for each culture.

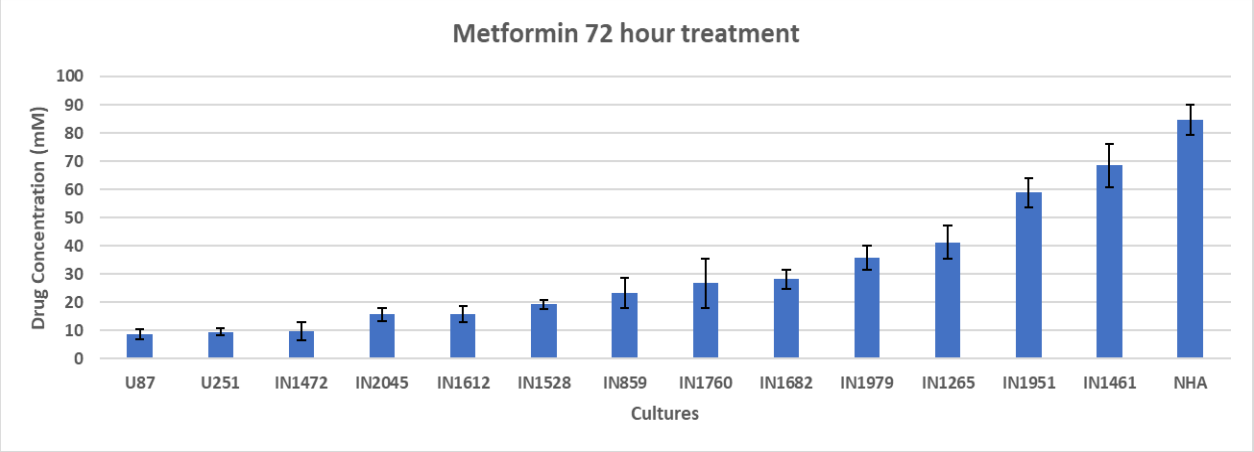

Figure 4.6 ID_{50} for each glioblastoma culture and NHA after 72- hour treatment with metformin. Cultures are ordered lowest to highest based on the ID_{50} value after 72-hours treatment with metformin. Error bars represent standard deviation averaged from 3 replicate assays.

4.4.3 Lonidamine

All glioblastoma cultures treated for 72 hours with LND demonstrated an inhibitory response and the ID_{50} values ranged from 211.4 – 763.5 µM, as shown in Figures 4.7 and 4.8 and Table 4.3. IN2045 was the most sensitive culture after the 72- hour treatment which demonstrated the highest sensitivity to LND with an ID_{50} value of 211.4 µM, followed by U251MG (235.9 µM) and U87MG (228.4 µM). NHA had a high tolerance of LND with the highest ID_{50} value (865.2 µM) compared to all the glioblastoma cultures, as expected for a non-tumour control. Glioblastoma cultures were grouped according to *HK2* expression, whereby the cultures were grouped dependent on the median value of fold change (219.8- fold change).

Cultures that expressed higher levels of *HK2* were more sensitive to LND and generally had lower ID_{50} values compared to cultures that exhibited lesser levels of *HK2*. A significant difference in ID_{50} values ($p= 0.0039$) was seen between cultures with >219.8- fold change expression and those with <219.8- fold change increase,

where average ID_{50} values were 572.9 µM compared to 312.8 µM respectively, as shown in Figure 4.8.

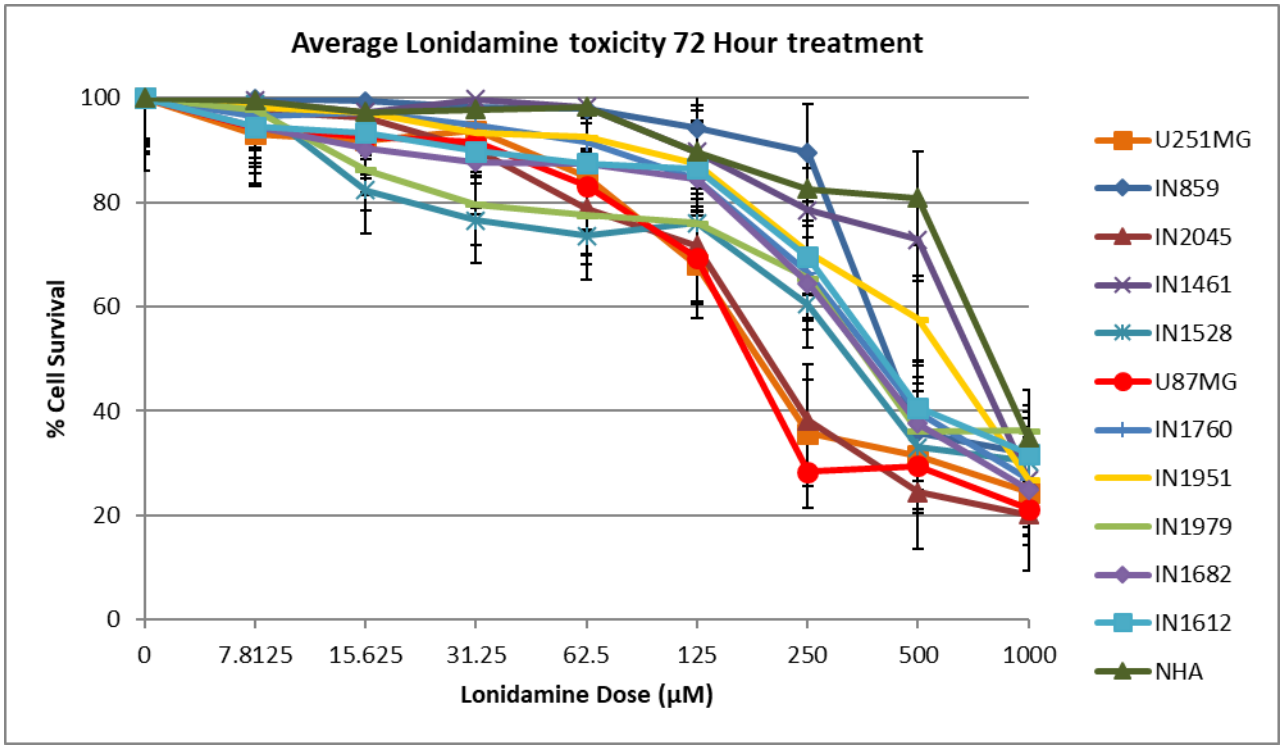

Figure 4.7 SRB cytotoxicity assay results for the glioblastoma cultures after 72 hours lonidamine treatment. Cell survival percentage is measured through the comparison of each optical density value to the value of the control wells (0µM lonidamine). Error bars represent standard deviation averaged from 3 replicate assays.

Table 4.3 ID_{50} values for all cultures treated with lonidamine

Culture reference	Lonidamine ID_{50} (µM)	*HK2* Expression Fold Change
IN2045	211.4 (±31.34)	219.8
U87MG	228.4 (±27.21)	1294.3
U251MG	235.9 (±34.2)	1502.6
IN1528	387.3 (±24.83)	386
IN1979	398.4 (±18.46)	574.4
IN859	415.6 (±29.73)	995.1
IN1682	475.8 (±23.57)	120.6
IN1760	483.4 (±27.33)	202
IN1612	494.2 (±24.43)	126.6

IN1951	647.5 (±28.27)	210.6
IN1461	763.5 (±43.99)	85.7
NHA	865.2 (±47.04)	30.4

Table showing metformin ID_{50} values for all cultures. Standard deviation for each average is listed after each result (±). Cultures are ordered lowest to highest based on the ID50 value after 72-hours treatment with lonidamine. *HK2* expression fold change compared to normal brain is also shown for each culture.

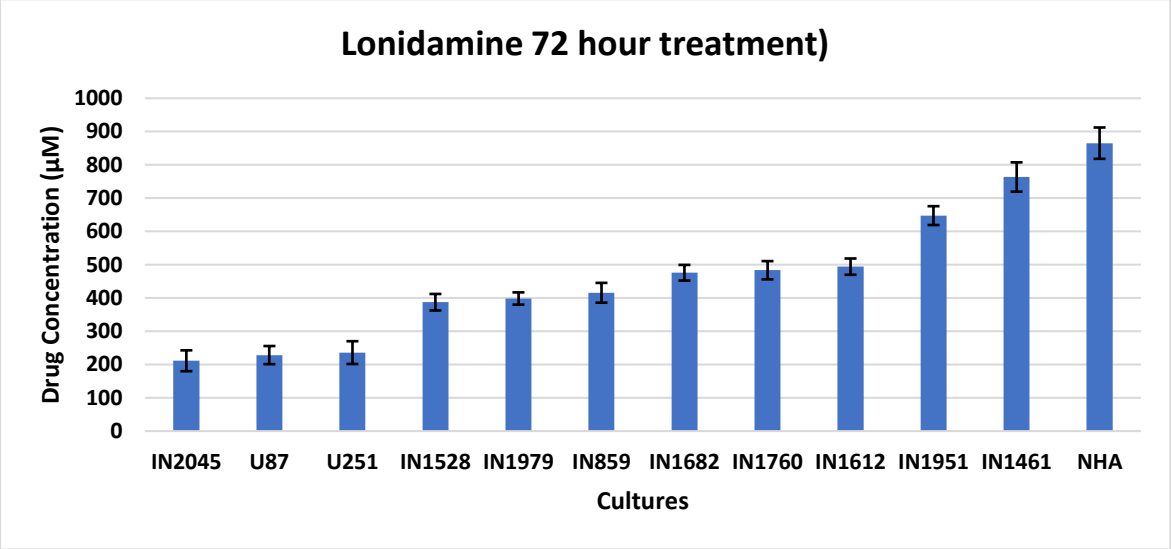

Figure 4.8 ID_{50} for each glioblastoma culture and NHA after 72- hour treatment with lonidamine. Cultures are ordered lowest to highest based on the ID_{50} value after 72-hours treatment with lonidamine. Error bars represent standard deviation averaged from 3 replicate assays.

4.5 Hypoxia

Hypoxia is common characteristic of tumour microenvironments. It is well documented that hypoxic tumours are significantly more malignant as their increased proliferation out-grows their ability to generate a blood supply, as well as being associated with chemoresistance and poorer patient prognosis (Vaupel *et al*, 2004). The effectiveness of 3-BPA and metformin under hypoxic conditions were investigated. All glioblastoma cultures treated for 72 hours with 3-BPA demonstrated an inhibitory response under hypoxic conditions, the ID_{50} values ranged from 42.23 – 76.18 µM, as shown in Figures 4.9 and 4.10 and Table 4.4. U251MG (44.9 µM) and U87MG (42.2 µM) were the most sensitive cultures after 72 hour treatment under hypoxia and IN1979 was the patient-derived culture that demonstrated the highest sensitivity to 3-BPA with an ID_{50} value of 47.41 µM. NHA had a high tolerance of 3-BPA with the highest ID_{50} value (81.3 µM) compared to all the glioblastoma cultures, as expected for a non-tumour control. A significant difference in ID_{50} values (p

<0.0001) was seen between all glioblastoma cultures treated for 72 hours with 3-BPA under hypoxic conditions compared to normoxia. Under hypoxic conditions all glioblastoma cultures acquired an increased tolerance of 3-BPA treatment, with an average increase of 56.6% in ID_{50} values. Under hypoxic conditions the ID_{50} values of the cultures ranged from 42.23 to 76.18 µM with an average ID_{50} value of 54.53 µM, in comparison the ID_{50} values in the same cultures treated in normoxia ranged from 12.9 to 37.6 µM with an average value of 23.56 µM. The greatest change in ID_{50} values were seen in cultures that expressed higher levels of *HK2*, including U87MG, U251MG, IN1979 and IN1528 which had a 57 to 69% increase in ID_{50} values. The comparatively lower *HK2* expressing cultures, IN1760, IN2045 and IN1612 had an increased ID_{50} change between 41 and 53% as seen in Table 4.4. A similar trend was also exhibited in NHA where 3-BPA ID_{50} values increased by 23.44% in hypoxia, although this wasn't significant. *HK2* expression was shown to be higher in cultures grown under hypoxic conditions (as shown in table 4.4) however, the increased tumour cell resistance to therapeutic agents linked with secondary mechanisms associated with hypoxic augments survival adaptation in cancer cells (Mathupala *et al.*, 2001).

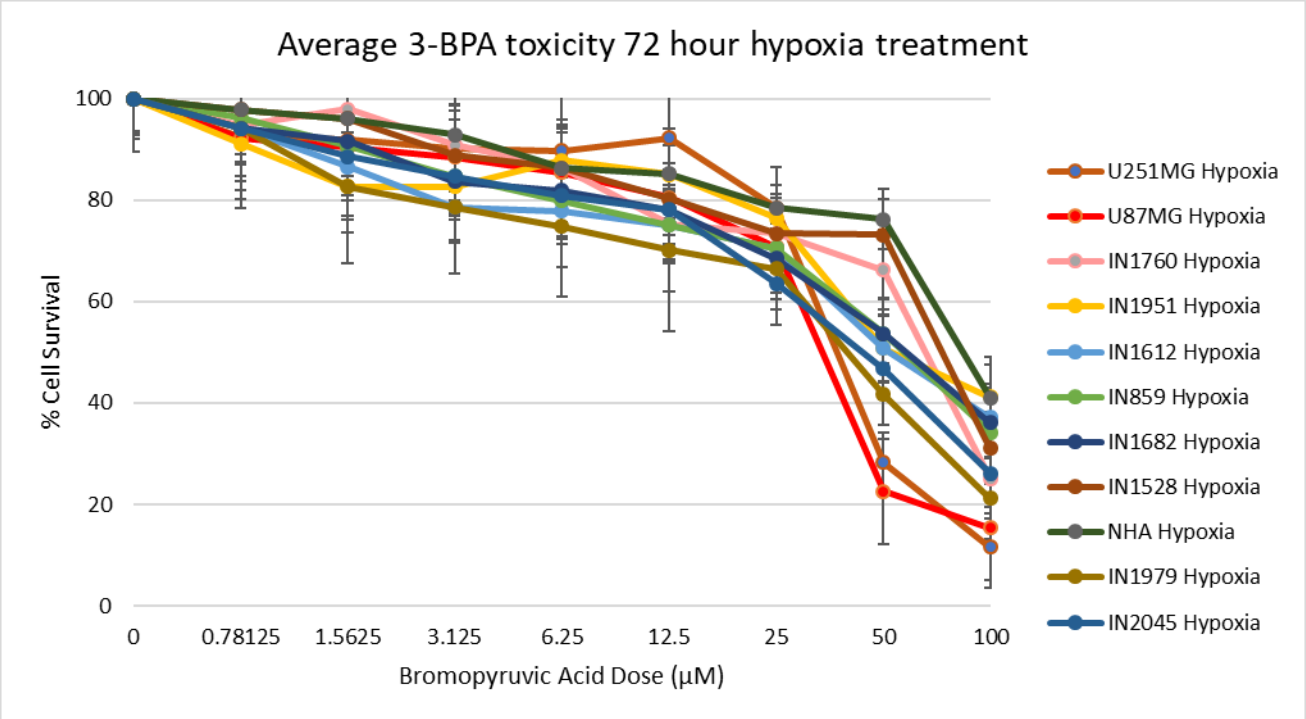

Figure 4.9 SRB cytotoxicity assay results for the glioblastoma cultures after 72 hours 3-BPA treatment under hypoxic conditions. Cell survival percentage is measured through the comparison of each optical density value to the value of the control wells (0µM 3-BPA). Error bars

represent standard deviation averaged from 3 replicate assays. Serial dilution of 3-BPA ranged from 100 to 0.78125 µM.

Table 4.4 ID_{50} values for all cultures treated with 3-BPA in both normoxia and hypoxia

Culture	3- BPA ID_{50} (µM)	3-BPA Hypoxia ID50 (µM)	% change in ID50 value	*HK2* expression normal	*HK2* expression hypoxia
U87MG *	12.9 (±1.21)	42.2 (±9.28)	69.4	1294	1350
U251MG *	14.3 (±2.43)	44.9 (±14.3)	68.2	1743	1810
IN1979 *	19.4 (±3.74)	47.4 (±2.34)	59	574	620
IN859 *	20.6 (±3.62)	55.98(±8.32)	54.2	1095	1099
IN2045 *	23.3 (±6.23)	49.2 (±12.51)	52.7	220	228
IN1951 *	24.4 (±2.46)	53.4 (±9.65)	54.3	206	224
IN1612 *	24.6 (±4.43)	52.56(±9.73)	53.2	127	131
IN1682 *	25.8 (±4.59)	59.4 (±6.46)	56.6	121	136
IN1528 *	32.7 (±1.21)	76.1 (±14.6)	57.1	386	391
IN1760 *	37.6 (±4.59)	63.8 (±3.56)	41.1	196	232
NHA	62.3 (±7.27)	81.3 (±13.3)	23.4	30	41

Table showing 3-BPA ID_{50} values for all cultures in normoxia and hypoxia. Standard deviation for each average is listed after each result (±). Cultures are ordered lowest to highest based on the on the ID50 value after 72-hours treatment with 3-BPA. * denotes significant change in ID_{50}.

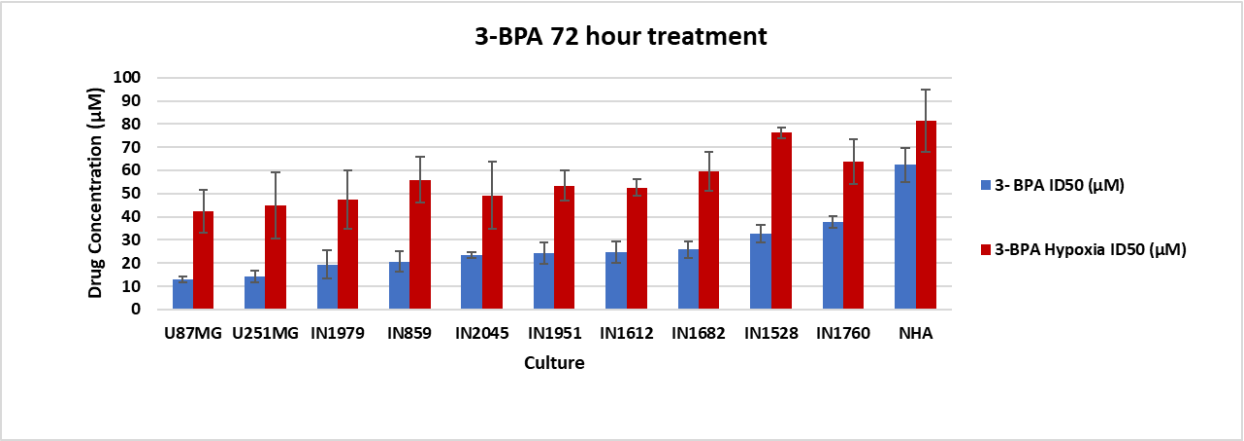

Figure 4.10 ID_{50} for each glioblastoma culture and NHA after 72- hour treatment with 3-BPA in both normoxic and hypoxic conditions. Cultures are ordered lowest to highest based on the ID_{50} value after 72-hours treatment with 3-BPA. Error bars represent standard deviation averaged from 3 replicate assays. All cultures showed a significant increase in ID_{50} value, except for NHA.

All glioblastoma cultures treated for 72 hours with metformin demonstrated an inhibitory response under hypoxic conditions, the ID_{50} values ranging from 32.85 to 71.28 mM, as shown in Figures 4.11 and 4.12 and Table 4.5. U251MG (37.2 mM) and U87MG (32.8 mM) were the most sensitive cultures after 72- hour treatment under hypoxia and IN1612 was the short-term culture that demonstrated the highest

sensitivity to metformin with an ID_{50} value of 37.25 mM. NHA had a high tolerance of metformin with the highest ID_{50} value (97.4 mM) compared to all the glioblastoma cultures, as expected for a non-tumour control. A significant difference in ID_{50} values ($p=0.0125$) was seen between cultures treated for 72 hours with metformin under hypoxic conditions compared to normoxia. Under hypoxic conditions all glioblastoma cultures acquired an increased tolerance of metformin treatment, an increase in ID_{50} values was demonstrated in all culture samples, with an average increase of 56.1%. Under hypoxic conditions the ID_{50} values of the cultures ranged from 32.85 to 71.28 mM with an average ID_{50} value of 50.61 mM. In comparison, the ID_{50} values in the same cultures treated in normoxia ranged from 8.7 to 58.85 mM with an average value of 24.12 mM. A similar trend was also exhibited in NHA where metformin ID_{50} values increased by 13.09% in hypoxia. Notably, both IN1951 and NHA had substantially lower changes in ID_{50} values in hypoxia compared to the rest of the cultures, with a 17.3% and 13.1% change respectively, >30% less than the other cultures. The differences in ID_{50} values was not dependent on the level of *HK2* expression in normoxia.

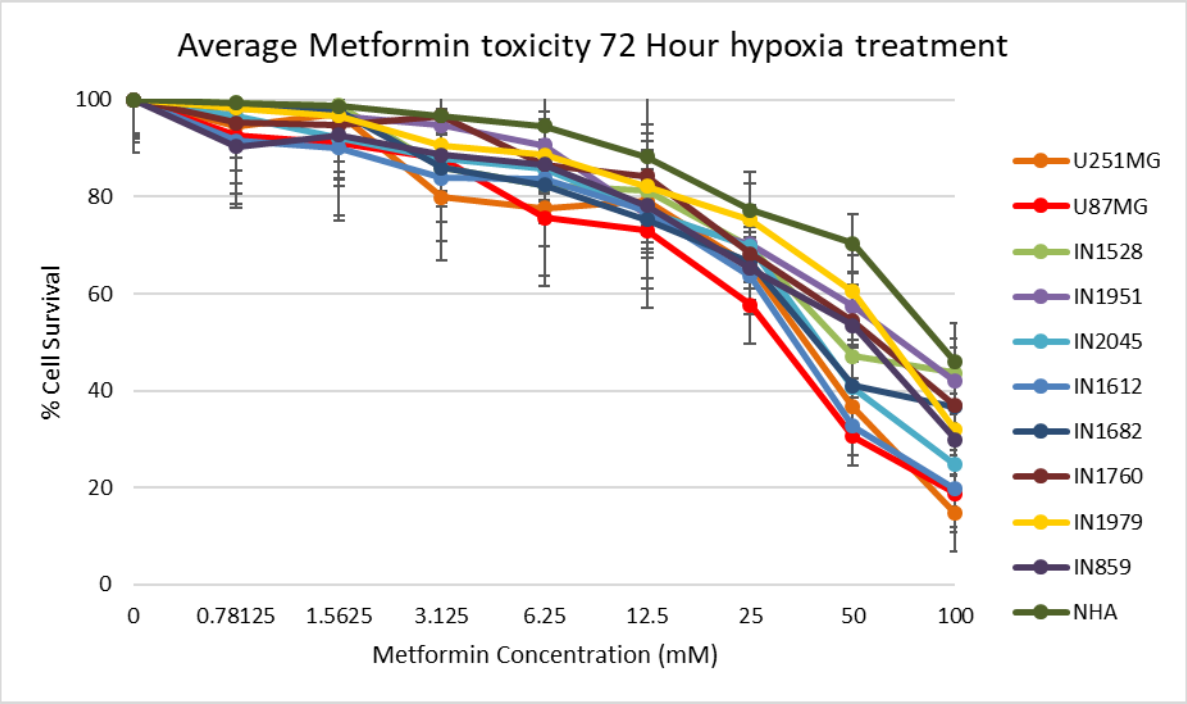

Figure 4.11 SRB cytotoxicity assay results for the glioblastoma cultures after 72- hour treatment with metformin in both normoxic and hypoxic conditions. Cell survival percentage is measured through the comparison of each optical density value to the value of the control wells (0mM metformin). Error bars represent standard deviation averaged from 3 replicate assays. Serial dilution of metformin ranged from 100 to 0.78125 mM.

Table 4.5 ID_{50} values for all cultures treated with metformin in both normoxia and hypoxia

Culture	Metformin ID_{50} (mM)	Metformin Hypoxia ID_{50} (mM)	% change in ID50 value
U87MG	8.7 (±1.74)	32.8 (±2.56)	73.5
U251MG	9.4 (±1.21)	37.2 (±4.21)	75.1
IN2045	15.6 (±2.47)	40.6 (±5.83)	61.6
IN1612	15.7 (±2.78)	37.2 (±6.74)	57.8
IN1528	19.2 (±1.52)	47.3 (±12.59)	59.4
IN859	23.27 (±5.24)	59.3 (±11.45)	60.8
IN1682	28.1 (±4.41)	42.9 (±9.89)	45.8
IN1760	26.66 (±8.78)	65.4 (±8.32)	59.3
IN1979	35.76 (±4.27)	71.2 (±8.29)	49.8
IN1951	58.85 (±7.69)	71.2 (±12.63)	17.3
NHA	84.7 (±6.43)	97.4 (±10.7)	13.1

Table showing metformin ID_{50} values for all cultures in normoxia and hypoxia. Standard deviation for each average is listed after each result (±). Cultures are ordered lowest to highest based on the ID50 value after 72-hours treatment with metformin.

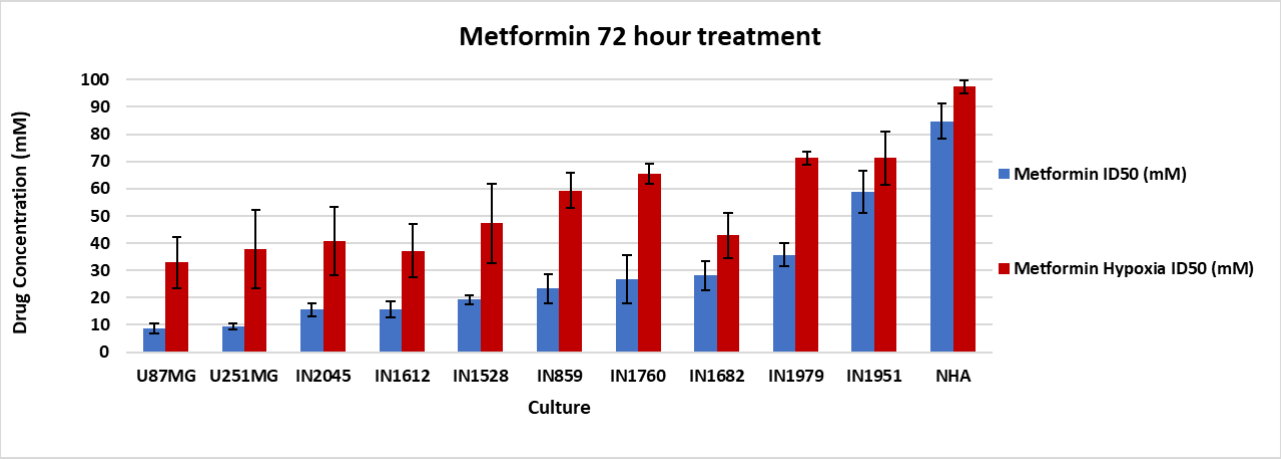

Figure 4.12 ID_{50} for each glioblastoma culture and NHA after 72- hour treatment with metformin in both normoxic and hypoxic conditions. Cultures are ordered lowest to highest based on the 72-hour metformin ID_{50}. Error bars represent standard deviation averaged from 3 replicate assays. * indicated no significant change.

4.6 Assessing drug synergy in glioblastoma cultures

4.6.1 The effect of *HK2*-KO with response to inhibitors

4.6.1.1 3-BPA

There was a considerable difference in the response of *HK2* –KO cultures to inhibitors. All *HK2* –KO cultures treated for 72 hours with 3-BPA showed significantly diminished sensitivity ($p<0.0001$) with the absence of the *HK2* target, as shown in Table 4.7. All cultures demonstrated an increased tolerance to 3-BPA, with ID_{50} values significantly increased in all KO cultures ($p<0.0001$). The effectiveness of 3-BPA was reduced through the loss of the *HK2* target, with an average ID_{50} value increase of 93% across the *HK2*-KO cultures compared respectively to the parent culture, as shown in Figure 4.13. The greatest increase was observed in IN1979-*HK2*-KO, which had an ID_{50} value of 42.6 µM, a 120% increase compared to the parent IN1979 culture, which had an ID_{50} value of 19.4 µM. IN2045-*HK2*-KO had the smallest increase, of 67% with an increase in ID_{50} value from 23.3 to 38.9 µM in the parent and *HK2*-KO cultures, respectively.

4.6.1.2 Temozolomide

Temozolomide is currently the most effective drug used to treat glioblastoma (Messaoudi *et al.*, 2015; Lee *et al.*, 2017), and hence, it was assessed as a potential synergistic partner with 3-BPA and metformin and *HK2*-KO cultures. The 6 glioblastoma cultures were treated with TMZ and a cytotoxic response was shown after 72- hours. TMZ was re-supplemented daily during the 72- hour incubation due to its short half-life, of approximately 2 hours at pH7 (Brian *et al.*, 1994; Patel *et al.*, 2003). No additional fresh media or glucose was provided to the cells during TMZ supplementation to prevent the increase in cell growth via extra nutrients. U251MG had the highest sensitivity to TMZ with an ID_{50} value of 145.29 µM, IN1760 had the highest tolerance with an ID_{50} value of 363.7 µM., as detailed in Table 4.6. Recent studies have shown TMZ to have an increased efficiency in glioblastoma samples with methylated *MGMT*, cultures presenting methylated *MGMT* would have expected increased sensitivity to TMZ (Tosoni *et al.*, 2017; Bell *et al.*, 2018). No substantial

pattern was determined from the comparison of ID_{50} values and *MGMT* status of the cultures tested, *MGMT* status for the culture panel is shown in the appendix.

Table 4.6 ID_{50} values for all cultures treated with TMZ

Culture	Temozolomide ID_{50} 72 hours (μM)	*MGMT* Status
U251MG	148.2(±2.62)	Methylated
IN1528	195.53 (±3.78)	Methylated
IN859	280.3 (±5.31)	Methylated
IN1951	328 (±2.88)	Unmethylated
IN2045	360.1 (±5.63)	Methylated
IN1760	363.7 (±4.72)	Methylated

ID_{50} values for temozolomide at 72 hours. Cultures ordered lowest ID_{50} to highest. *MGMT* methylation is a known factor in the sensitivity of tumour response to temozolomide.

All *HK2* –KO cultures treated for 72 hours with TMZ showed significantly increased ($p<0.0001$) sensitivity in the absence of the *HK2* expression with ID_{50} values significantly decreased ($p<0.0001$) in all KO cultures as shown in Table 4.8. The effectiveness of TMZ was increased, with an average ID_{50} value decrease of 42.5% across the *HK2*-KO cultures compared respectively to the parent culture, as shown in Figure 4.14. The greatest change in sensitivity was observed in IN859-*HK2*-KO which had an ID_{50} value of 126.5 μM, a 55% decrease compared to the parent IN859 culture, which had an ID_{50} value of 280.3 μM. IN2045-*HK2*-KO had the smallest decrease, with an ID_{50} value of 249.4 μM, a 67% decrease compared to the parent IN2045, which had an ID_{50} value of 360.1 μM.

4.6.1.3 Metformin

All *HK2* –KO cultures treated for 72 hours with metformin showed significantly increased ($p<0.0001$) sensitivity in the absence of the *HK2* expression, with an average ID_{50} value decrease of 46.8% across the *HK2*-KO cultures compared respectively to the parent culture, as shown in Table 4.9 and Figure 4.15. The greatest change in sensitivity was observed in U251MG-*HK2*-KO which had an ID_{50} value of 3.6 mM, a 61.1% decrease compared to the parent culture, which had an ID_{50} value of 9.4 mM. IN2045-*HK2*-KO had the smallest decrease, with an ID_{50} value of 9.8 mM, a 37% decrease compared to the parent IN2045, which had an ID_{50} value of 15.6mM μM. IN2045 is the lowest expressing *HK2* culture in the sample

cohort, cultures expressing higher levels of *HK2* showed greater alterations in response to the inhibitors.

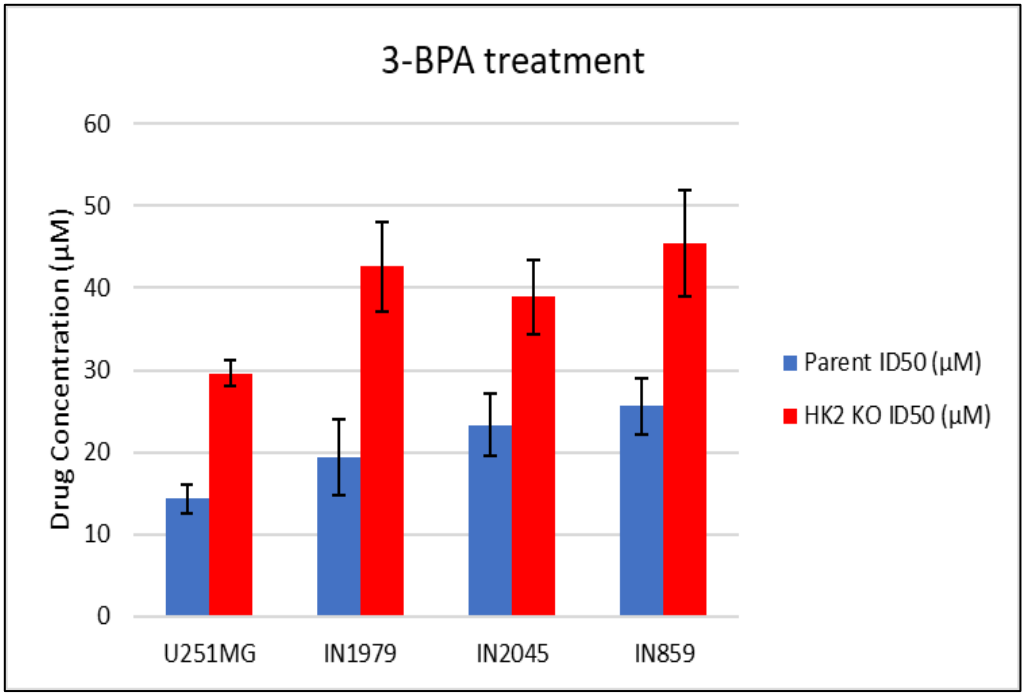

Figure 4.13 ID_{50} values for each *HK2*-KO and respective parent culture after 72- hour treatment with 3-BPA. A significant ($p<0.001$) increase in ID_{50} values was shown in *HK2*-KO cultures compared to respective parent cultures after 72- hour treatment with 3-BPA. An average increase of 50% in ID_{50} values were demonstrated across all cultures in the absence of *HK2.*

Table 4.7 ID_{50} values for after treatment with 3-BPA for 72 hours in parent and *HK2*-KO cultures

Culture	Parent ID_{50} (µM)	*HK2* KO ID_{50} (µM)	ID_{50} Change	p values
U251	14.3	29.6	107%	<0.0001
IN1979	19.4	42.6	120%	<0.0001
IN2045	23.3	38.9	67%	<0.0001
IN859	25.6	45.4	77%	<0.0001

ID_{50} values of the *HK2* inhibitor 3-BPA were compared between parent and CRISPR *HK2*-KO cell cultures. A significant increase in ID_{50} values was exhibited across all cultures with *HK2*-KO compared to the respective parent culture.

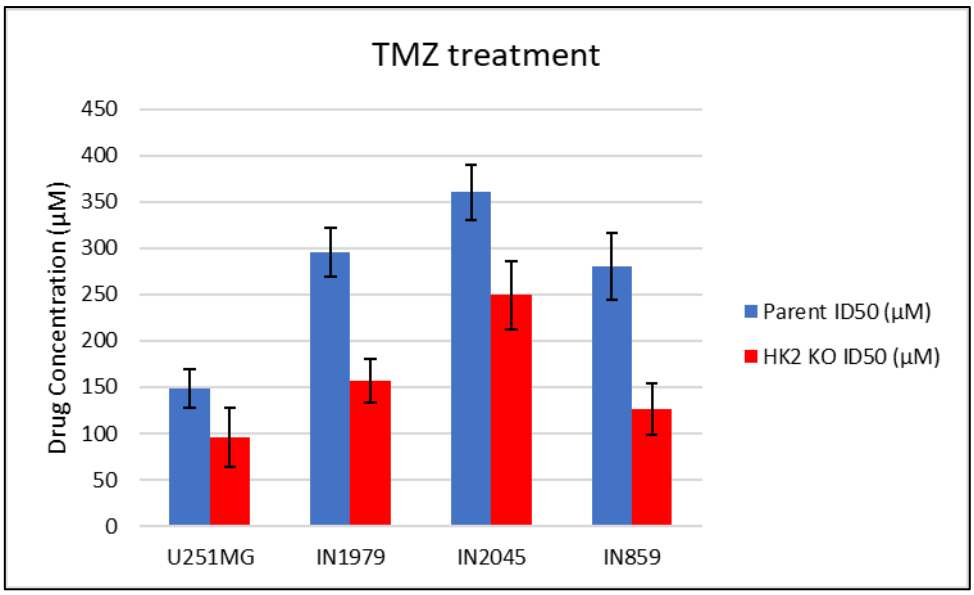

Figure 4.14 ID_{50} values for each *HK2-KO* and respective parent culture after 72- hour treatment with TMZ. A significant ($p<0.001$) decrease in ID_{50} values was shown in *HK2*-KO cultures compared to respective parent cultures after 72- hour treatment with TMZ. An average decrease of 77.5% in ID_{50} values was demonstrated across all cultures in the absence of *HK2.*

Table 4.8. ID_{50} values for after treatment with TMZ for 72 hours in parent and *HK2*-KO cultures

Culture	Parent ID_{50} (µM)	*HK2* KO ID_{50} (µM)	ID_{50} Change	p values
U251	148.2	95.3	-37%	<0.0001
IN1979	295.7	156.8	-47%	<0.0001
IN2045	360.1	249.4	-31%	<0.0001
IN859	280.3	126.5	-55%	<0.0001

ID_{50} values of TMZ were compared between parent and CRISPR *HK2*-KO cell cultures. A significant decrease in ID_{50} values was exhibited across all cultures with *HK2*-KO compared to the respective parent culture.

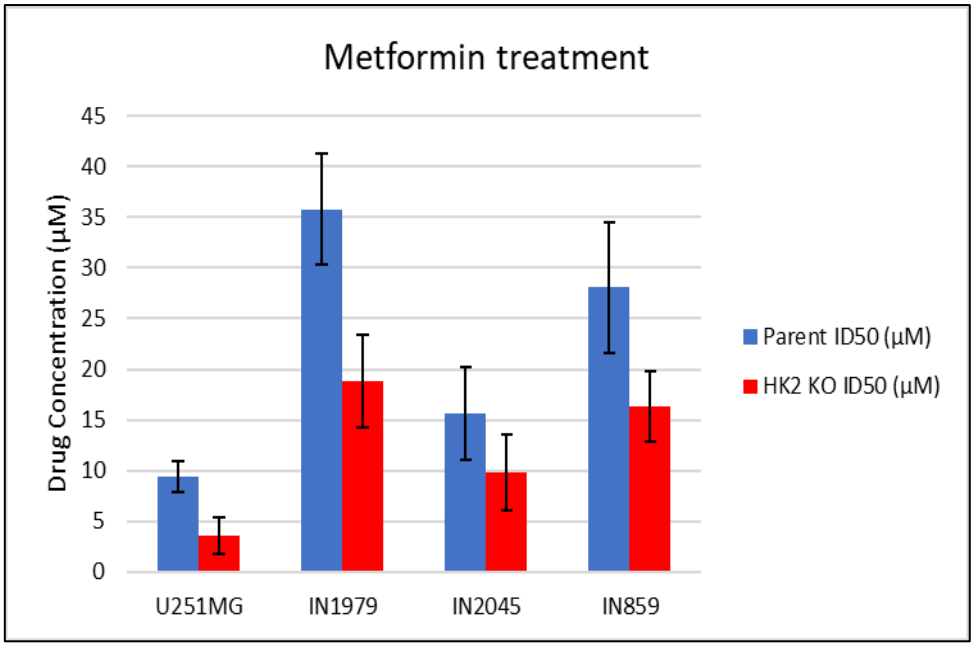

Figure 4.15 ID_{50} values for each *HK2*-KO and respective parent culture after 72- hour treatment with metformin. Average metformin ID_{50} values for CRISPR treated culture compared to parent culture. A significant ($p<0.001$) decrease in ID_{50} values was shown in *HK2*-KO cultures compared to respective parent cultures after 72- hour treatment with metformin. A decrease of 95.8% in ID_{50} values was demonstrated across all cultures in the absence of *HK2.*

Table 4.9. ID_{50} values for after treatment with metformin for 72 hours in parent and *HK2*-KO cultures

Culture	Parent ID_{50} (mM)	*HK2* KO ID_{50} (mM)	ID_{50} Change	p values
U251	9.4	3.6	-61%	<0.0001
IN1979	35.8	18.8	-47%	<0.0001
IN2045	15.6	9.8	-37%	<0.0001
IN859	28.1	16.3	-42%	<0.0001

Showing ID_{50} values of metformin comparing parent to CRISPR *HK2*-KO cell cultures. A significant decrease in ID_{50} values was exhibited across all cultures with *HK2*-KO compared to the respective parent culture.

4.6.3 The effect of *HK2*-KO on cell survival Cell survival post *HK2* knockout was also analysed over a 120-hour time course, when cultures were treated with 3-BPA, metformin and TMZ. With both metformin and TMZ treatments, the percentage of cell survival was significantly ($p<0.0001$) decreased in *HK2* -KO cultures compared to the respective parent cultures. The average reduction in cell survival seen across all *HK2*-KO cultures was 19.9% compared to the parent cultures after 120 hours of metformin treatment. The highest change in survival was in U251MG *HK2*-KO with a 25% reduction compared the parent culture. IN2045 had the lowest alteration in cell

survival after 120 hours of metformin treatment, with a 16.8% reduction in the absence of *HK2.* A similar reduction in cell survival after 120 hours of TMZ treatment (retreated daily) was demonstrated in *HK2*-KO cultures, where average reduction was 20.5% compared to parent cultures. The highest change in survival was in U251MG *HK2*-KO with a 28.6% reduction compared the parent culture. IN2045 had the lowest alteration in cell survival after 120 hours of TMZ treatment, with a 18.4% reduction in the absence of *HK2.* Treatment with 3-BPA over 120 hours reiterated the data presented in Section 4.6.1, with cell survival significantly ($p=0.0024$) increased in all *HK2*-KO cultures compared to parent cultures. IN859 had the highest change in cell survival with a 34.7% increase in the absence of *HK2.* Eliminating the HK2 target reduces the effectiveness of 3-BPA, verifying the specificity of the inhibitor. There was an improved effectiveness of metformin and TMZ in the absence of *HK2,* which has been shown to increase chemoresistance and is associated with HIF-1, which has been shown to enhance cell survival (Menendez *et al.*, 2015). Metformin's ability to activate AMPK may potentially be increased in the absence of *HK2*, resulting in the inhibition of the mTOR pathway reducing proliferation and survival (Pollak, 2012; He and Wondisford, 2015). *HK2* knockout via CRISPR revealed considerable increases in sensitivity to both metformin and TMZ in all glioblastoma cultures, signifying the potential of *HK2* inhibition as a novel therapy in a significant subset of glioblastoma.

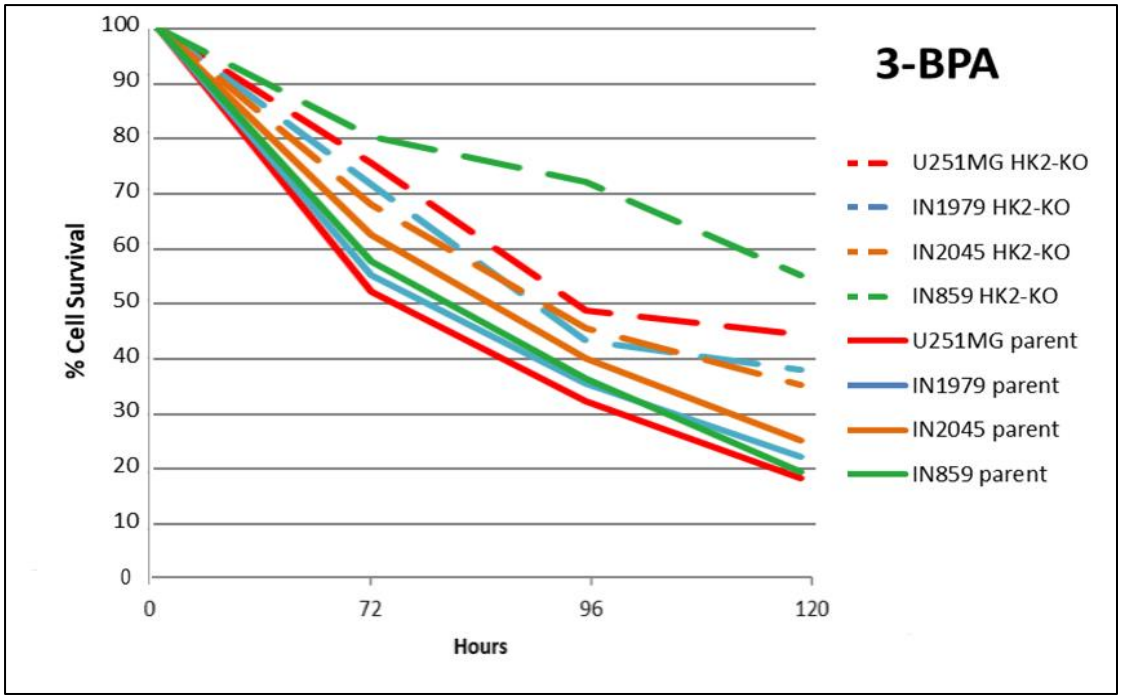

Figure 4.16 Cell survival over 120 hours in *HK2*-KO cultures treated with 3-BPA. Cell survival over 120 hours in glioblastoma cultures treated with 3-BPA compared to corresponding CRISPR *HK2*-KO cultures. An increase in cell survival across all *HK2*-KO cultures was shown compared to parent cultures.

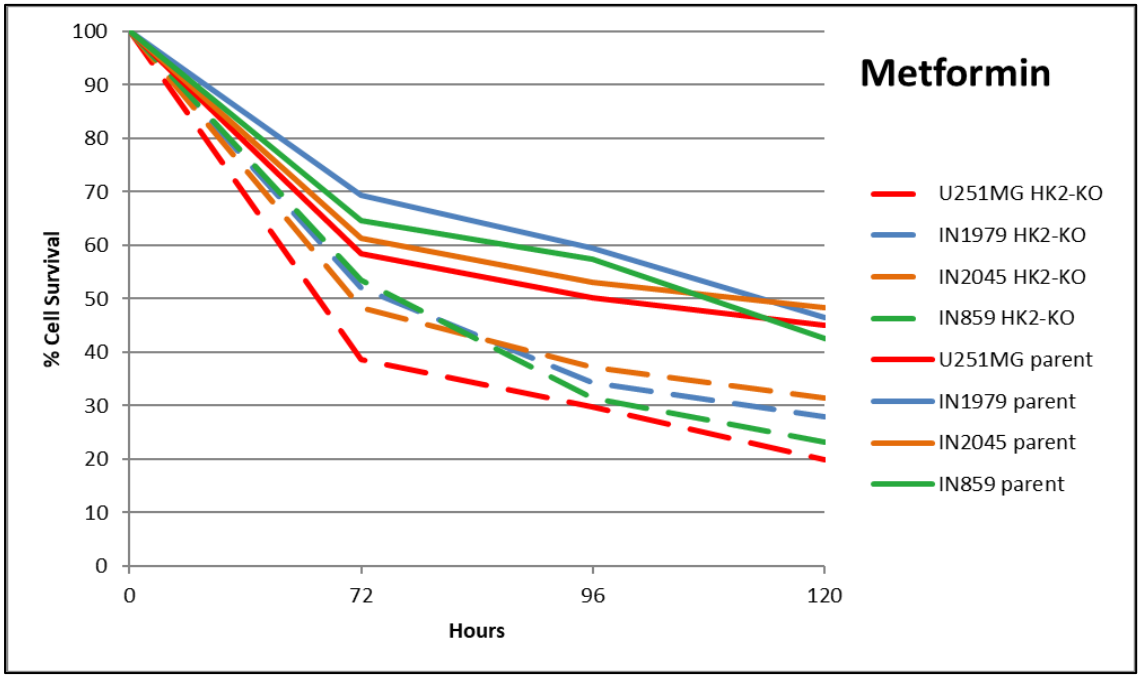

Figure 4.17 Cell survival over 120 hours in *HK2*-KO cultures when treated with metformin. Cell survival over 120 hours in glioblastoma cultures treated with metformin compared to corresponding CRISPR *HK2*-KO cultures. A decrease in cell survival across all *HK2*-KO cultures was shown compared to parent cultures.

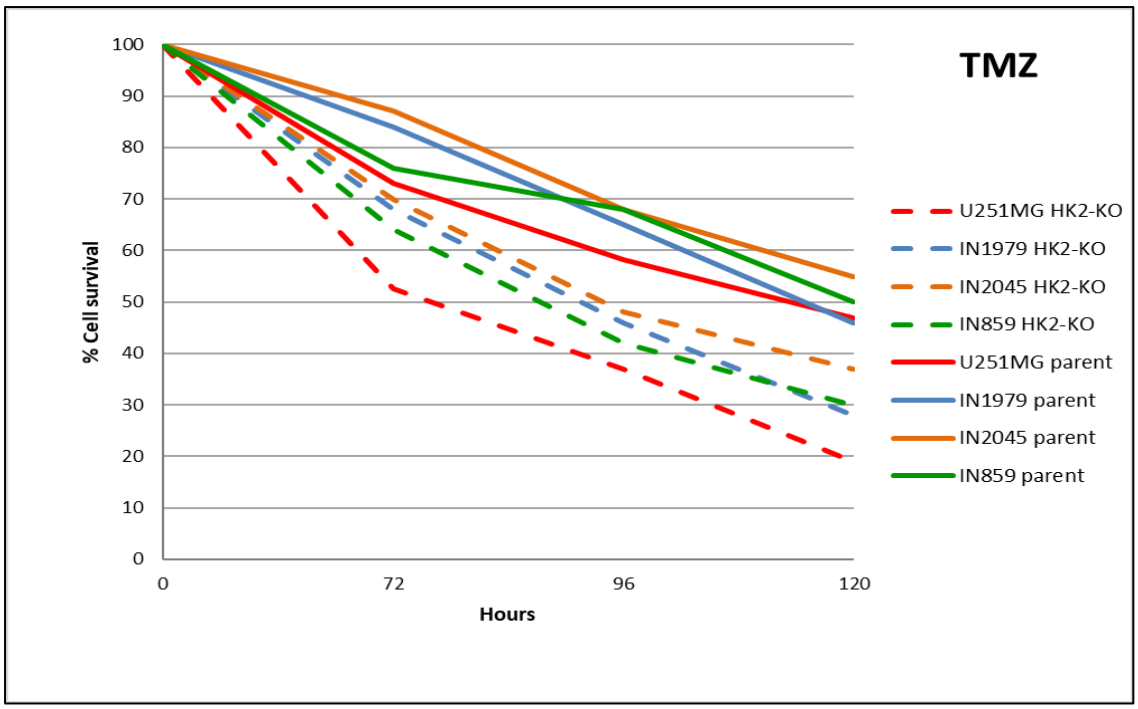

Figure 4.18 Cell survival over 120 hours in *HK2*-KO cultures when treated with TMZ. Cell survival over 120 hours in patient derived glioblastoma cultures treated with TMZ compared to corresponding CRISPR *HK2*-KO cultures. A decrease in cell survival across all *HK2*-KO cultures was shown compared to parent cultures.

4.6.2 Combination treatments

3-BPA and metformin demonstrated a growth inhibitory response after 72- hour drug treatment as monotherapies. An increased effectiveness in combination treatment, however, would offer a greater potential of use in clinical trials (Aldea *et al.*, 2014). The potential synergistic partners that were assessed were 3-BPA, metformin and temozolomide, using an SRB assay to determine the combined treatment effect. The concentrations used in the combined drug wells were equimolar to the equivalent wells of the mono-drug treatment. These 2 *HK2* inhibitors were selected based on their inhibitory efficacy, and TMZ was included due to its pre-existing importance as a therapeutic agent in glioblastoma treatment (Messaoudi *et al.*, 2015). Five patient derived cultures (IN1760, IN859, IN1528, IN2045, IN1951) and U251MG were assessed and included a range of *HK2* expression levels. Table 4.10 shows the comparative drug combinations. Synergy of combination drug treatments were analysed using the cho-talay therom (Chou., 2010), which generates a combination

index. The CI measures the effectiveness of each drug as both a monotherapy and when paired.

Table 4.10 Drug concentrations used in synergy analysis

Drug	Units	Drug Concentration								
3-BPA	μM	100	50	25	12.5	6.26	3.125	1.563	0.781	0
Metformin	μM	100000	50000	25000	12500	6250	3125	1563	781	0
Temozolomide	μM	500	250	125	62.5	31.25	15.62	7.81	3.9	0

All drugs were utilized both individually and in equimolar doses. All drugs tested for synergy analysis were dissolved in water. All experiments compared ID50 independently and combined. Control values in wells with Tris buffer only.

4.6.2.1 Combination of 3-BPA and metformin

The combination of 3-BPA and metformin was investigated, to determine whether targeting the *HK2* protein with 3-BPA in combination with metformin replicates the same effect seen in metformin treatment in *HK2*-KO cells. Cultures treated in combination did not demonstrate any altered sensitivity, with no significant alterations in ID_{50} values, compared to when treated individually with both 3-BPA and metformin, as seen in Figure 4.19. The combination treatment showed no synergistic inhibitory effects in any of the 6 cultures, with all cultures exhibiting a combination index value greater than 1, suggesting an antagonistic effect with the combination of 3-BPA and metformin (Table 4.11). The lowest CI index value was 1.02 seen in IN1528. The combination dose curves exhibit similar trends to both the 3-BPA and metformin curves.

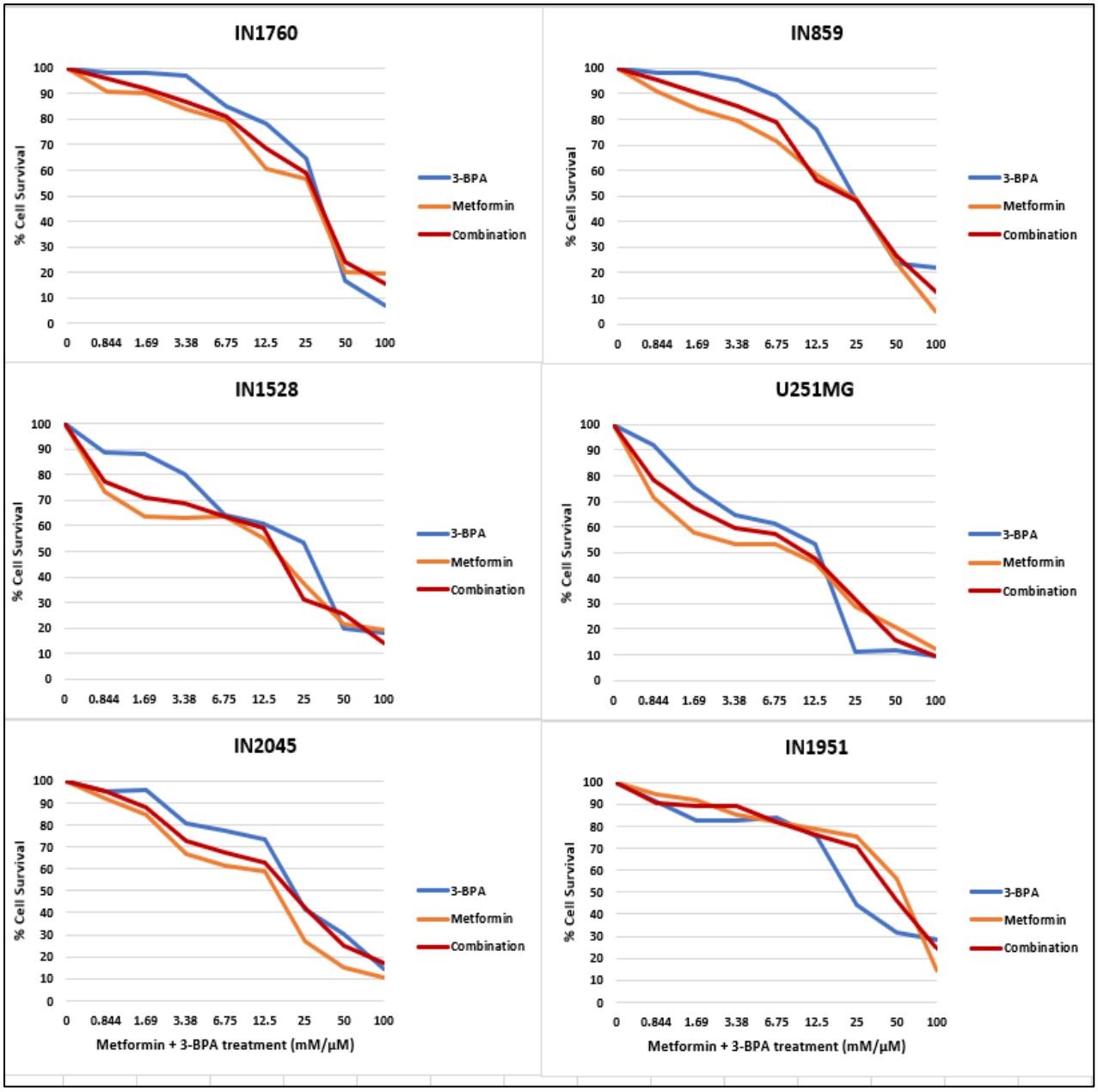

Figure 4.19 Drug combination synergy treatments of 3-BPA and metformin. All cultures tested in both mono- and combination treatment in equimolar dosages over a 72-hour period. Combination treatments show no synergistic properties.

Table 4.11 Drug synergy analysis of metformin and 3-BPA

Metformin and 3-BPA combination Test		
Culture	CI Index	Result
U251MG	1.34 (±0.192)	Antagonism
IN859	1.83 (±0.179)	Antagonism
IN1528	1.02 (±0.097)	Antagonism
IN1760	1.41 (±0.325)	Antagonism
IN2045	1.33 (±0.122)	Antagonism
IN1951	1.26 (±0.138)	Antagonism

Combination index result as a measure of synergy comparing each drug individually to an equimolar combination. Synergy analysis based on average combination index result. All cultures showed an antagonistic response. CI Index >1 – Antagonism, CI Index = 1 – Additive, CI Index <1 = Synergy.

4.6.2.2 Combination of 3-BPA and TMZ

The combination of 3-BPA and TMZ treatment demonstrated synergy in 2 of the 6 cultures as shown in Table 4.12, with CI values <1 for U251MG (CI=0.88) and IN1760 (CI= 0.97). Both cultures were *MGMT* methylated. An antagonist response was shown in the other 4 cultures with CI values all >1. The concentration range of the inhibitors is shown in Table 4.9. The glioblastoma cultures in the synergy and antagonism groups share no common factor that distinguishes them. U251MG expresses high levels of *HK2* (1502.6 increased fold change compared to normal tissue) and has demonstrated a higher sensitivity to *HK2* inhibitors (3-BPA ID_{50} =14.3 μM), however IN1760 has been shown to have significantly lower *HK2* levels (202.0 increased fold change compared to normal tissue) and has demonstrated a higher tolerance to *HK2* inhibitors (3-BPA ID_{50} = 27.6 μM).

Table 4.12 Drug synergy analysis of 3-BPA and TMZ

3-BPA and TMZ combination Test		
Culture	CI Index	Result
U251MG	0.88(±0.10)	Synergism
IN859	1.08(±0.16)	Antagonism
IN1528	1.22(±0.14)	Antagonism
IN1760	0.97(±0.7)	Synergism
IN2045	1.04(±0.12)	Antagonism
IN1951	1.16(±0.15)	Antagonism

Combination index result as a measure of synergy comparing each drug individually to an equimolar combination. Synergy analysis based on average combination index result. 2 cultures showed a synergistic response and 4 showed an antagonistic response. CI Index >1 – Antagonism, CI Index = 1 – Additive, CI Index <1 = Synergy.

4.6.2.3 Combination of metformin and TMZ

The combination of metformin and TMZ treatment demonstrated synergy in 3 of the 6 cultures as shown in Table 4.13, with CI values <1 for U251MG (CI=0.93), IN1760 (CI= 0.87) and IN2045 (CI=0.89). All three cultures were *MGMT* methylated. An antagonist response was shown in the other 3 cultures with CI values >1 and these cultures displayed an increased ID_{50} when treated in monotherapy, compared to when treated in combination. The 3 cultures exhibiting synergy had extensive variation in the level of overexpression of *HK2* (U251MG =1502.6, IN1760 =202.0 and IN2045= 219.8 increased fold change compared to normal tissue). Furthermore, these cultures also showed substantially different levels of sensitivity to metformin treatment, with ID_{50} values ranging from 9.4 mM (U251MG) to 26.7mM (IN1760).

Table 4.13 Drug synergy analysis of metformin and TMZ

Metformin and TMZ combination Test		
Culture	CI Index	Result
U251MG	0.93(±0.05)	Synergism
IN859	1.34(±0.11)	Antagonism
IN1528	1.06(±0.42)	Antagonism
IN1760	0.87(±0.11)	Synergism
IN2045	0.89(±0.9)	Synergism
IN1951	1.41(±0.18)	Antagonism

Combination index result as a measure of synergy comparing each drug individually to an equimolar combination. Synergy analysis based on average combination index result. 3 cultures showed a synergistic response and 3 showed an antagonistic response. CI Index >1 – Antagonism, CI Index = 1 – Additive, CI Index <1 = Synergy.

The combination drug treatments were analyzed using the strict separation used by the Chou-Talay method. Additive effects are hard to determine using this methodology resulting in cultures exhibiting antagonistic effects. For example, for the combination of 3-BPA and TMZ the cultures IN2045 (CI =1.04) and IN859 (CI =1.08) are classed as antagonistic, however considering the standard deviation values of the repeats the value could be interpreted as synergistic with a CI value less than 1. U251MG in both 3-BPA -TMZ, and metformin - TMZ combinations had synergistic values and this could potentially be accounted for due to it being a long-term cell culture resulting in altered genetic and metabolic characteristics (Torsvik, *et al*. 2014). Additionally, the short half-life of temozolomide and its pH dependency to remain stable could potentially factor. Although fresh TMZ was added daily during

the 72- hour treatments, the media was not changed (to ensure experimental conditions with regard to glucose availability were maintained), and the pH towards the end of the experiment may have altered. The measurement of pH changes in culture media over a time course would be an important future study.

4.7 Mechanisms of cell death induced by *HK2* inhibitors

Programmed cell death via apoptosis is a crucial cellular mechanism for the maintenance of a healthy equilibrium, of cells in the human body, with the destruction and removal of cells in a controlled manner. Apoptosis in cancer is frequently disrupted, with tumour cells acquiring adaptations in order to prevent and block apoptotic pathways. Examples include mutations in key pro-apoptotic genes such as the cell surface receptors *CD95* or *TNF-related apoptosis-inducing ligand (TRAIL)* which are responsible for the induction of caspase dependant apoptosis (Song *et al*., 2008; Fulda and Debatin 2006). Studies have shown that the 3-BPA affects mitochondria through the targeting of *HK2* bound complex which results in subsequent stimulation of apoptosis inducing factor (AIF) consequently leading to cell death (Gandham, *et al*., 2015), although this has not been shown in glioblastoma cells. The anti-tumour mechanisms of metformin are still not fully clarified (Chae *et al*., 2016). Metformin has also been shown to affect the mitochondria via multiple pathways leading to mitochondrial stress resulting in apoptosis. Its mechanisms of action has been shown to differ based on the type of cancer; the inhibition of mTOR through AMPK activation has been shown to be a dependency for tumour inhibition in several cancers and independent in others (Liu *et al*., 2014). Identifying specific mechanism and pathways through which these inhibitors act on glioblastoma is an important factor to assess their potential use as a cancer therapeutic.

4.7.1 Apoptosis

Apoptosis was assessed via flow cytometric analysis, utilizing Annexin V and 7-AAD cellular staining. The flow cytometry technique allows for the tracking of the

progression of cellular populations across three pre-defined gated quadrants, determined by the level of binding of the specific fluorophores. The quadrant in the lower left is representational for live cells, which are negative for both annexin V and 7-AAD. The second quadrant positioned on the lower right, represents apoptotic cells, indicative of positive binding of annexin V via the protein phospholipid phosphatidylserine. This protein is associated with extracellular signaling in apoptotic pathways and under normal conditions, it is positioned facing the cytosolic (inner) of the cell membrane (Segawa and Shigekazu, 2015). The proteins, however, become exposed during early apoptosis (Koopman *et al.*, 1994) and once the cell enters a later stage of cell death, an increase in the permeability of the cell membrane occurs, resulting in the diffusion of annexin V into the cystol and interacting with the internal membrane. The third quadrant (top right) is an indication of cell death, representational of positive binding by 7-AAD, which distinguishes healthy and dead. The dye binds to DNA, inserting between cytosine and guanine bases (Xiucai *et al.*, 1991; Philpott *et al.*, 1996). 7-AAD, however, lacks the ability to penetrate cellular membranes. Therefore, 7-AAD positive bound cells are characterized as having damaged cellular membranes, whereas negatively bound cells still possess a functional membrane. The top left quadrant represents cellular necrotic markers; however, the flow cytometry assay is unable to accurately distinguish the later stage methods of cell death once the cells have reached the upper left quadrant. These mechanisms of cell death include autophagy, necrosis and late-stage apoptosis. In these mechanisms, the membrane permeability has already been altered, so flow cytometry is unable to distinguish between early and late cell death. Using this flow cytometry method, early apoptosis is defined as the positive binding of annexin V, which results in an increase in the FL2 channel and thus an increase in cell population in the second quadrant. An increase in quadrant three through increased binding to 7-AAD, indicate a compromised membrane representational of late stage cell death. The quadrants outcomes from flow cytometric analysis are summarized in Figure 4.20 and the potential outcomes are summarised in Table 4.18.

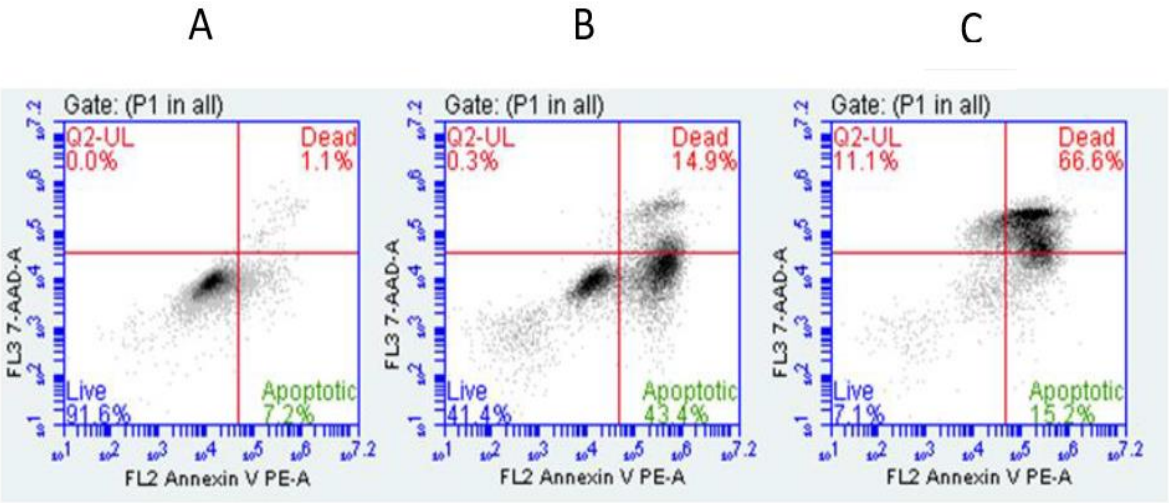

Figure 4.20 Identification of apoptosis through flow cytometry. A: Showing an untreated sample, a dense population of cell in the 1st (bottom left) quadrant. B: Showing samples treated with the control campthothecin (100 µM over a 72-hour period). A second population of cells in the second quadrant representing positive apoptotic cells through positive binding of annexin V. 7-AAD negative binding in these cells indicating a functional cell membrane. C: Showing cells treated with campthothecin for 96 hours. The cell population has shifted to the third quadrant, and are positively bound with 7-AAD, indicating a permeable membrane and cell death.

Table 4.14 Interpretation of the binding of the two fluorochromes to measure apoptosis

Quadrant	Label	Annexin V (FL2)	7-AAD (FL1)
Lower left	Live cells	Negative	Negative
Lower right	Apoptotic cells	Positive	Negative
Upper right	Dead cells	Positive	Positive
Upper left	Necrotic cells	Negative	Positive

Shows the potential outcomes from flow cytometry analysis of apoptosis.

4.7.2 Apoptosis induced by 3-BPA

Eight glioblastoma cultures (with various levels of *HK2* expression) and NHA were treated with relevant ID_{50} concentrations of 3-BPA for 72 hours as determined in Section 4.4 and compared to an untreated control of the same culture. For all cultures a 72- hour treatment with 100µM camptothecin was used as a positive control for induction of apoptosis. Figure 4.21 shows a comparative flow cytometry chart showing both an apoptotic positive result and an untreated control.

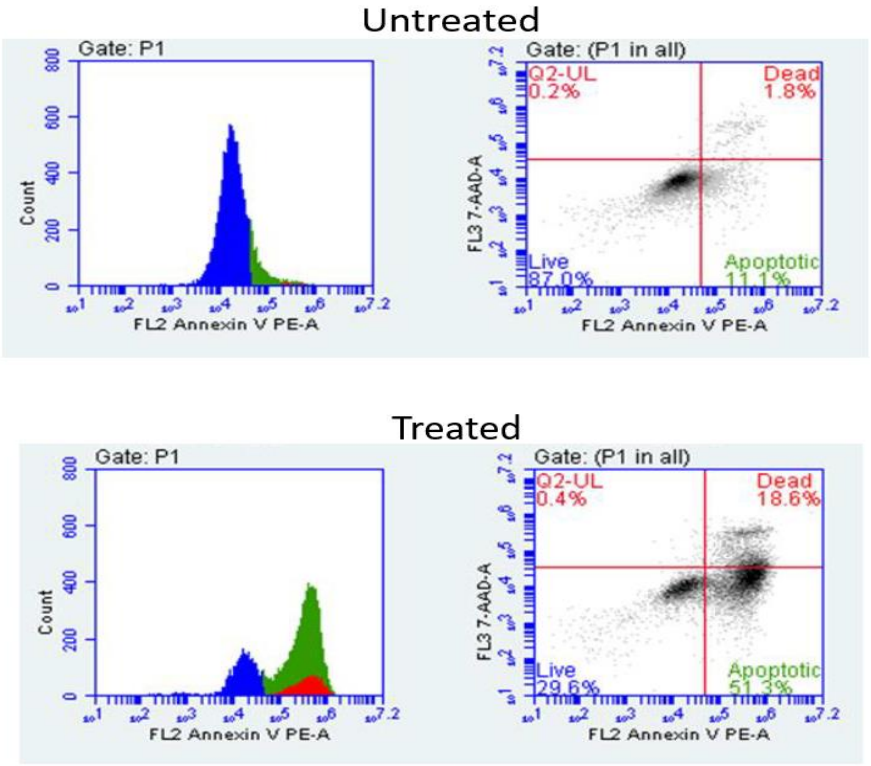

Figure 4.21 Induction of apoptosis in U251MG, treated with 100 µM campthothecin after 72- hours. Untreated U251MG cells show little positive binding to annexin V (2nd quadrant) compared to campthothecin treated U251MG cells, which show a large population of cells in the right quadrant, indicating positive binding of annexin V. Quadrants are colourised for graphical interpretation: Blue – live cells, Green- apoptotic and Red-dead cells.

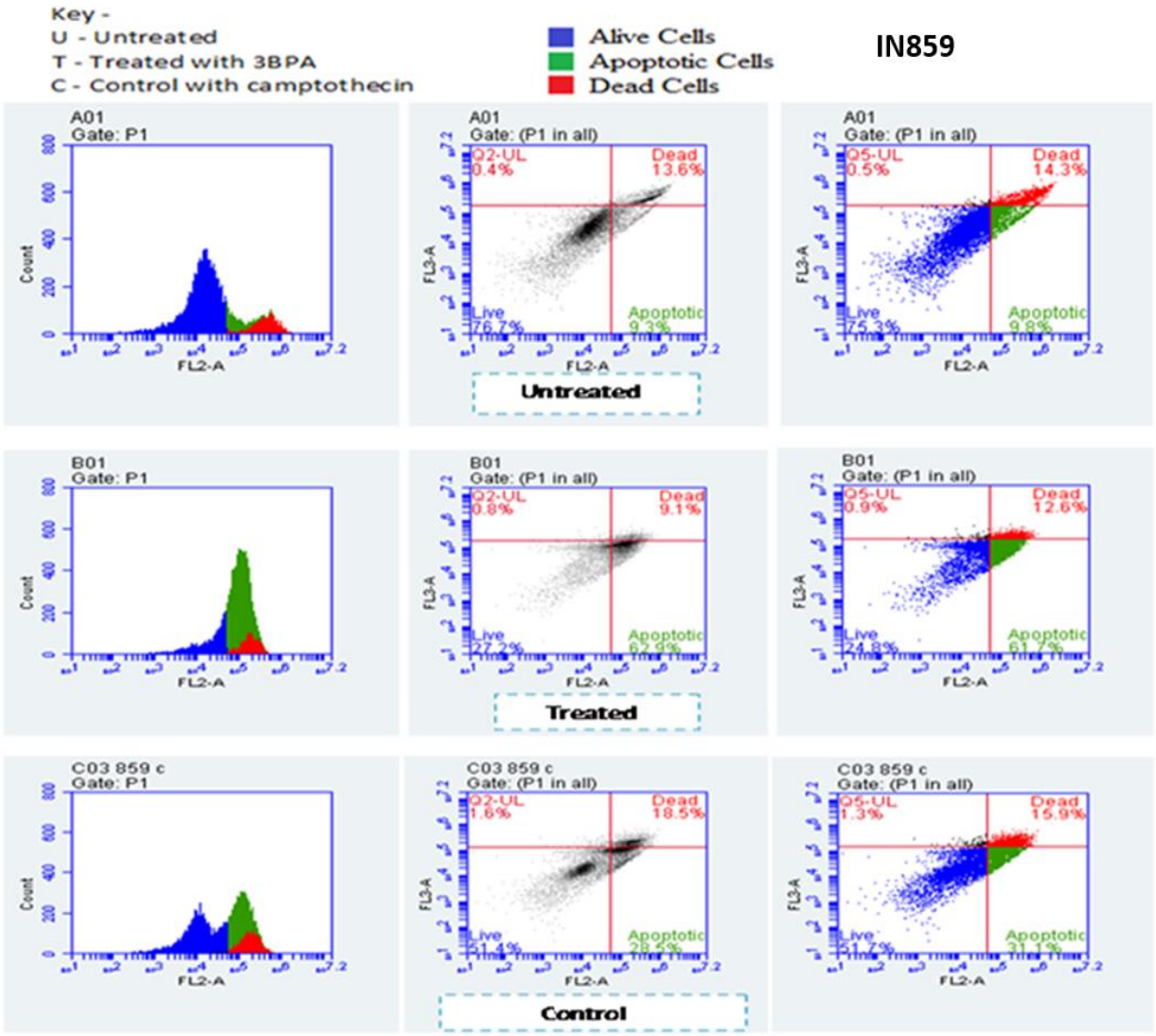

Figure 4.22 Induction of apoptosis in IN859, treated with 3-BPA or 100 µM campthothecin after 72- hours. Untreated IN859 cells show little positive binding to annexin V (2nd quadrant) compared to the 3-BPA treated IN859 culture, which show a large population of cells in the right quadrant. An increase of 51.9% in apoptosis was demonstrated after 3-BPA treatment. Campthothecin treated IN859 also showed an increase in apoptosis. Quadrants are colourised for graphical interpretation: Blue – live cells, Green- apoptotic and Red-dead cells.

An apoptotic sub-population was detected in all glioblastoma cultures after ID_{50} treatments with 3-BPA compared to the respective untreated cultures, with an increase of the sub-population in the 2nd quadrant indicating positive binding of annexin V uptake. Figure 4.22 shows an example of untreated, 3-BPA treated and campthothecin treated (control) populations in IN859. In the group of high *HK2* expressing cell cultures (>220 – fold change), a significantly increased ($p<0.0001$)

level of apoptosis was observed, with an average increase of 38% in apoptosis, ranging from 30% to 52%. The largest increase in apoptosis was observed in IN859 (52%) ($p<0.0001$) and the lowest in IN1979 (30%) ($p<0.0001$), as shown in Table 4.15. The high *HK2* expressing cultures had a greater increase in levels of apoptosis after 3-BPA treatment, in comparison to cultures that had a lower *HK2* expression. The lower expressing cultures showed, with an average increase of 9.3 % apoptosis after 3-BPA treatment, ranging from 7% to 14%. This increase was only significant in IN2045 which showed an increase of 14% ($p=0.005$), as shown in Table 4.15 Furthermore, there was a slight increase in apoptosis induced by 3-BPA in NHA, with an increase of 3.8%, as expected or a non-cancer control. As expected, the live cell population was reduced in all treated samples at the same ratio as the increase in apoptosis. 3-BPA effectiveness across glioblastoma cultures is associated with levels of *HK2* expression, with significantly higher levels ($p= 0.0007$) of early apoptosis occuring in cultures that have higher levels of *HK2* expression (>220 – fold change).

Table 4.15 Apoptosis induced by 3-BPA treatment

High Expressing *HK2* cultures	**Apoptosis (%) untreated**	**Apoptosis (%) 3-BPA treated**	**Apoptosis (%) increase**
IN859	9.8	61.7	52*
U251MG	15.9	52.6	36.7*
IN1979	10.8	40.8	30*
IN1528	11.7	45.7	34*
Mean	12.1	50.2	38.175
Low Expressing *HK2* cultures	**Apoptosis (%) untreated**	**Apoptosis (%) 3-BPA treated**	**Apoptosis (%) increase**
IN1461	8.2	19.2	11
IN1951	14.5	21.5	7
IN1682	12.9	17.9	5
IN2045	7.4	21.4	14
Mean	10.8	20	9.25
NHA	6.8	10.6	3.8

Cultures expressing higher levels of *HK2* showed increased levels of apoptosis treated with 3-BPA for 72- hours compared with cultures expressing lower levels of *HK2* mRNA overexpression (compared to normal brain tissue). * significance $p > 0.005$.

4.7.3 Apoptosis induced by metformin

In contrast, no apoptosis was seen in glioblastoma cultures (n=6) following 72-hours treatment with metformin. Average levels of apoptosis increased by 2.1% (with a range of 1.6 – 2.7%) in high *HK2* expressing cultures, and by 3.7% (with a range of 3- 4.4%) in low *HK2* expressing cultures as detailed in in Figure 4.23 and Table 4.16. NHA also showed no significant increase in the apoptotic population after metformin treatment. An increase in cells in the upper right quadrant was detected, which demonstrates the effect of metformin supplementation leading to cell death. The data indicates that metformin does not generate cell death via apoptosis in glioblastoma, but may act through another mechanism of cell death such as autophagy or necrosis.

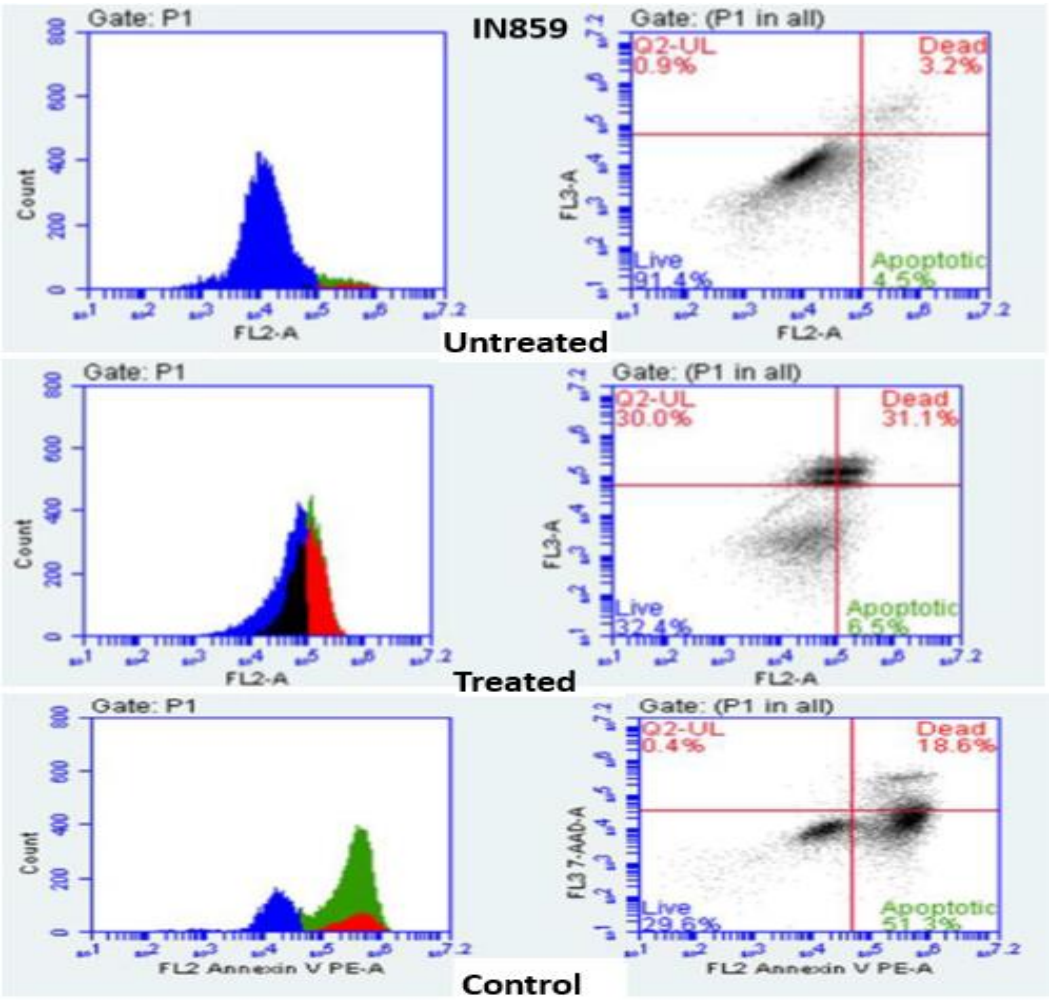

Figure 4.23 Apoptotic detection after 72- hour treatment with metformin and 100 µM campthothecin. Untreated IN859 cells show little positive binding to annexin V (2nd quadrant). No increase in apoptosis was detected after 72 hours metformin treatment at specific ID_{50}, however an

increase in cell death was detected. Quadrants are colourised for graphical interpretation: Blue – live cells, Green- apoptotic and Red-dead cells.

Table 4.16 No substantial apoptosis induced by metformin treatment

High Expressing *HK2* cultures	**Apoptosis (%) untreated**	**Apoptosis (%) metformin treated**	**Apoptosis (%) increase**
IN859	4.5	6.5	2
U251MG	5.9	8.6	2.7
IN1528	8.8	10.4	1.6
Mean	6.4	8.5	2.1
Low Expressing *HK2* cultures	**Apoptosis (%) untreated**	**Apoptosis (%) metformin treated**	**Apoptosis (%) increase**
IN1951	7.4	10.4	3.0
IN1682	5.9	9.7	3.8
IN2045	8.2	12.6	4.4
Mean	7.2	10.9	3.7
NHA	5.9	11.5	5.6

No significant apoptosis was demonstrated across any glioblastoma culture treated with metformin 72- hours.

4.7.1.2 Apoptosis of cells grown under hypoxia

The analysis of cells for apoptotic markers was also completed over a 72- hour time course under hypoxic conditions, to determine the effectiveness of 3-BPA in generating early apoptosis under depleted oxygen, as commonly exhibited in the tumour microenvironment. Cultures were treated with relevant hypoxic ID_{50} values for 3-BPA as determined in Section 4.3.4 and compared to an untreated control of the same culture. For all cultures a 72- hour treatment with 100μM campthothecin was used as a positive control for induction of apoptosis. All cultures were grown in a sealed hypoxic incubator. An apoptotic sub-population was detected in all glioblastoma cultures after ID_{50} treatments with 3-BPA compared to the respective untreated cultures, with an increase of the sub-population in the 2nd quadrant indicating positive binding of annexin V uptake. Figure 4.24 shows an example of both untreated, 3-BPA treated and campthothecin treated (control) in hypoxia and Table 4.17 shows percentage of apoptosis under hypoxic conditions for all cultures tested.

A significantly increased ($p<0.0001$) level of apoptosis was exhibited in all cultures expressing higher levels of *HK2* under hypoxic conditions, as seen similarly under normoxic conditions. In the panel of high *HK2* expressing cell cultures, there was an

average decrease of 19.5% in apoptosis ranging from 13.4% to 33.5%. The largest decrease in apoptosis was observed in IN859 (33.5%) ($p<0.0001$) and the lowest in IN1528 (13.4%) ($p<0.0001$), as shown in Table 4.17. The high *HK2* expressing cultures had a greater decrease in levels of apoptosis after 3-BPA treatment under hypoxic conditions in comparison to cultures that had a lower *HK2* expression, which showed significantly different ($p<0.0001$) levels of apoptosis. The lower expressing cultures showed a slight decreased level of apoptosis after 3-BPA treatment in hypoxia, with an average decrease of 3.7% ranging from 1.3% to 6.3%. No significant change in apoptosis was detected in these cultures, as shown in Table 4.17. Furthermore, there was no decrease in apoptosis induced by 3-BPA in NHA. Additionally, there was significant ($p= 0.0091$) differences between levels of apoptosis in high *HK2* expressing cultures treated under normoxic and hypoxic conditions. There was an 19% change in average apoptotic levels, with average levels of apoptosis across high expressing cultures in normoxia of 50.2% after 72-hour treatment with 3-BPA, compared to 19.2% under hypoxia conditions. The level of apoptosis ranged from 40.8% (IN1979) to 61.7% (IN859) in normoxia treated cultures compared to 16.5% (IN1979) to 18.5% (IN859) in hypoxia treated cultures. The highest change in apoptotic levels between normoxic and hypoxic conditions was demonstrated in IN859 with a 33.5% reduction exhibited after 3-BPA treated in deprived adequate oxygen supply. There was no significant difference between levels of apoptosis in lower *HK2* expressing cultures in normoxia or hypoxia with average levels of 9.3% and 5.6 respectively. The level of apoptosis ranged from 5% (IN1682) to 13% (IN2045) in normoxia treated cultures compared to 3.7% (IN1682) to 7.9% (IN2045) in hypoxia treated cultures as shown in Table 4.17. Levels of apoptosis across all cultures under normoxic and hypoxic conditions can be seen in Figure 4.25.

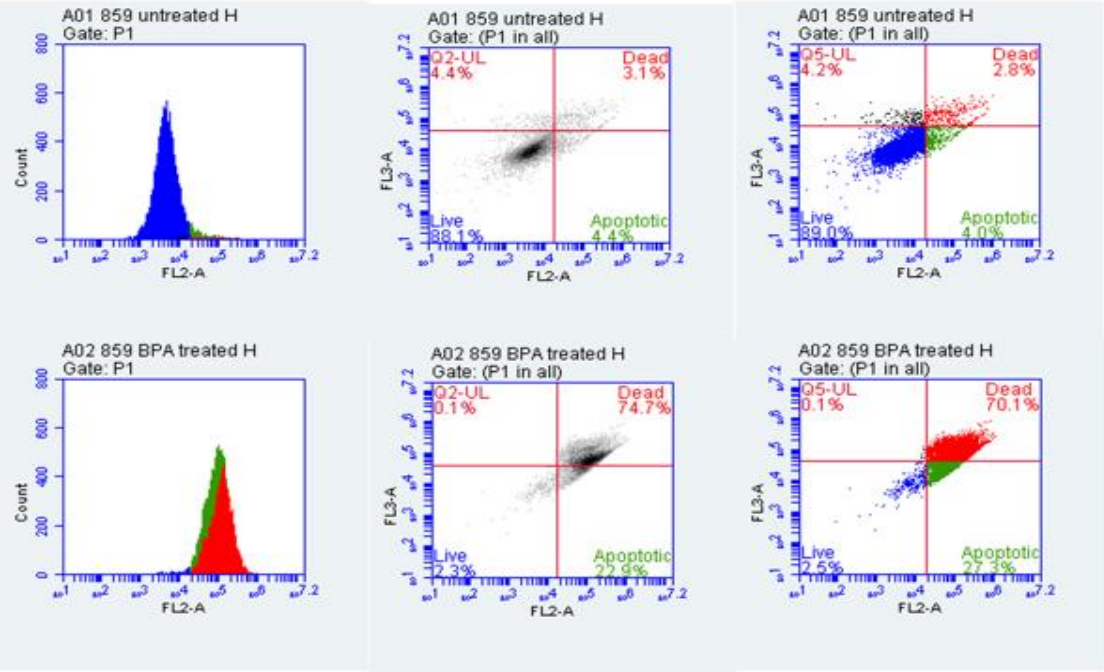

Figure 4.24 Induction of apoptosis in IN859, treated with 3-BPA after 72- hours under hypoxic conditions. Untreated IN859 cells show little positive binding to annexin V (2nd quadrant) compared to the 3-BPA treated IN859 culture, which show an increased population of cells in the right quadrant. An increase of 19.2% in apoptosis was demonstrated after 3-BPA treatment under hypoxia. A significant ($p<0.0001$) increase of 67.3% in dead cells was also observed. Quadrants are colourised for graphical interpretation: Blue – live cells, Green- apoptotic and Red-dead cells.

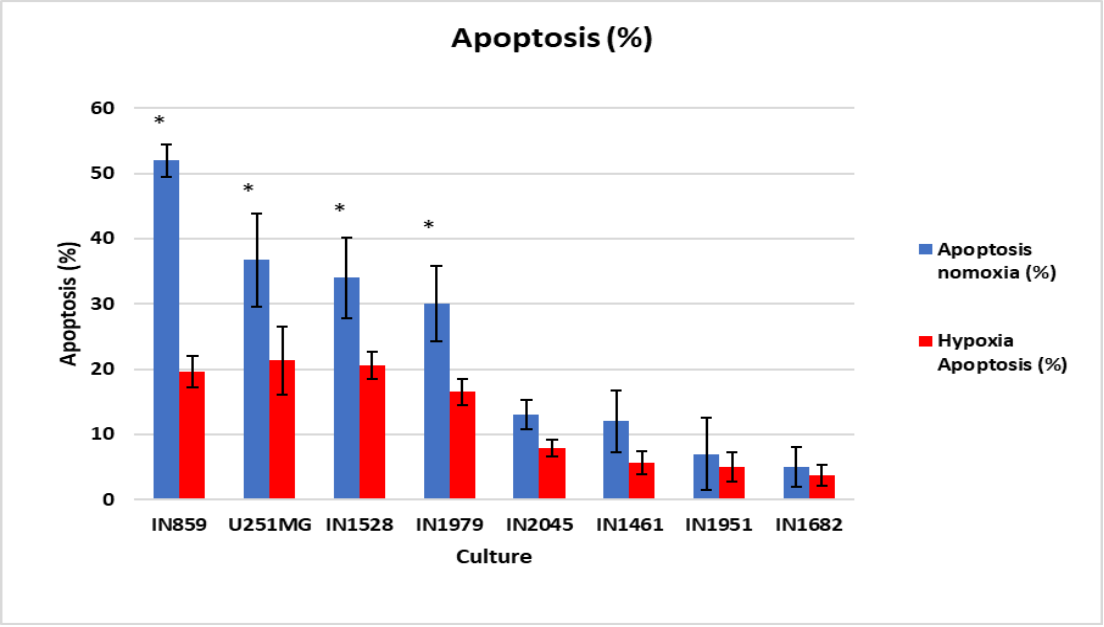

Figure 4.25 Induction of apoptosis in all glioblastoma cultures treated with 3-BPA after 72- hours in normoxic and hypoxic conditions. The percentage of apoptosis was reduced across all cultures after 3-BPA treatment under hypoxia. Cultures expressing higher levels of *HK2* showed a significantly ($p<0.0001$) decreased levels of apoptosis after 3-BPA treatment under hypoxic conditions; compared with cultures expressing lower levels of *HK2* mRNA overexpression (compared to normal brain tissue). * indicates high expressing cultures.

Table 4.17 Reduced levels of apoptosis induced by 3-BPA treatment under hypoxic conditions

High Expressing *HK2* cultures	**Apoptosis (%)**	**Hypoxia Apoptosis (%)**	**% Change in Apoptosis**
IN859	52	18.5	33.5*
U251MG	36.7	21.3	15.4*
IN1528	34	20.6	13.4*
IN1979	30	16.5	13.5*
Mean	38.2	19.2	19*
Low Expressing *HK2* cultures	**Apoptosis (%)**	**Hypoxia Apoptosis (%)**	**% Change in Apoptosis**
IN2045	13	7.9	5.1
IN1461	12	5.7	6.3
IN1951	7	5	2
IN1682	5	3.7	1.3
Mean	9.25	5.6	3.675

Table showing percentage of apoptosis in both hypoxia and normoxia across all cultures after 72-hour treatment with 3-BPA. The level of apoptosis percent was reduced across all cultures under hypoxia after 3-BPA treatment. Cultures expressing higher levels of *HK2* showed a significantly ($p<0.0001$) decreased levels of apoptosis after 3-BPA treatment under hypoxic conditions; compared with cultures expressing lower levels of *HK2* mRNA overexpression (compared to normal brain tissue). * denotes significance.

4.7.1.3 Apoptosis induced by HK2 inhibitors in HK2-KO cultures

The analysis of cells for apoptotic markers was also completed over a 72- hour time course in four CRISPR induced *HK2*- KO cultures, to demonstrate the mechanism of 3-BPA in generating early apoptosis is fundamentally specific to the *HK2* target. Cultures were treated with the relevant *HK2*- KO ID_{50} values for 3-BPA as determined in 4.5, with normal growth media (F10) and compared to an untreated control of the same culture. For all cultures a 72- hour treatment with 100 µM camptothecin was used as a positive control for induction of apoptosis. As expected no substantial levels of apoptosis were detected across any of the *HK2*-KO glioblastoma cultures after the 72- hour treatment with 3-BPA, the average percentage of apoptosis across all cultures after 3-BPA treatment was 0.68% compared to the untreated *HK2*-KO cultures, as shown in Table 4.18 and Figure 4.26. Additionally, there was significant ($p<0.0001$) reduction in the percentage of apoptotic sub-population detected across all *HK2*-KO cultures compared to the respective parent cultures after 3-BPA treatment. Average percentage of apoptosis in 3-BPA cultures were 38.2%,

compared to the respective *HK2*-KO cultures where there was a substantial loss of apoptosis, with a value of 0.58%. Campthothecin positive apoptotic control illustrated apoptosis in all cultures after 72- hour treatment, validating results generated after 3-BPA treatment. Notably, levels of apoptosis in the untreated *HK2*-KO cells were lower in comparison to the parent cultures (IN2045 3.9% reduction, IN1979 9.4% reduction, IN859 7.4% reduction and U251MG 11.3% reduction). The loss of the *HK2* target in the CRISPR transfected cultures demonstrates the specificity of 3-BPA, in the absence of the *HK2* protein, the inhibitor has minimal cytotoxic effect upon the cells, leading to no initiation of the early apoptotic pathway.

Table 4.18 Reduced levels of apoptosis induced by 3-BPA treatment in *HK2*-KO cultures

Cultures	Apoptosis (%) untreated	Apoptosis (%) 3-BPA treated	% Change in Apoptosis
IN2045- *HK2*-KO	3.5	5.1	1.6
IN1979- *HK2*-KO	1.4	1.5	0.1
IN859- *HK2*-KO	2.4	2.8	0.4
U251MG- *HK2*-KO	4.6	5.2	0.6

Table showing percentage of apoptosis in *HK2*-KO cultures after 72- hour treatment with 3-BPA. No significant levels of apoptosis were demonstrated in any of the *HK2*-KO cultures after 72- hour treatment with 3-BPA compared to untreated cultures.

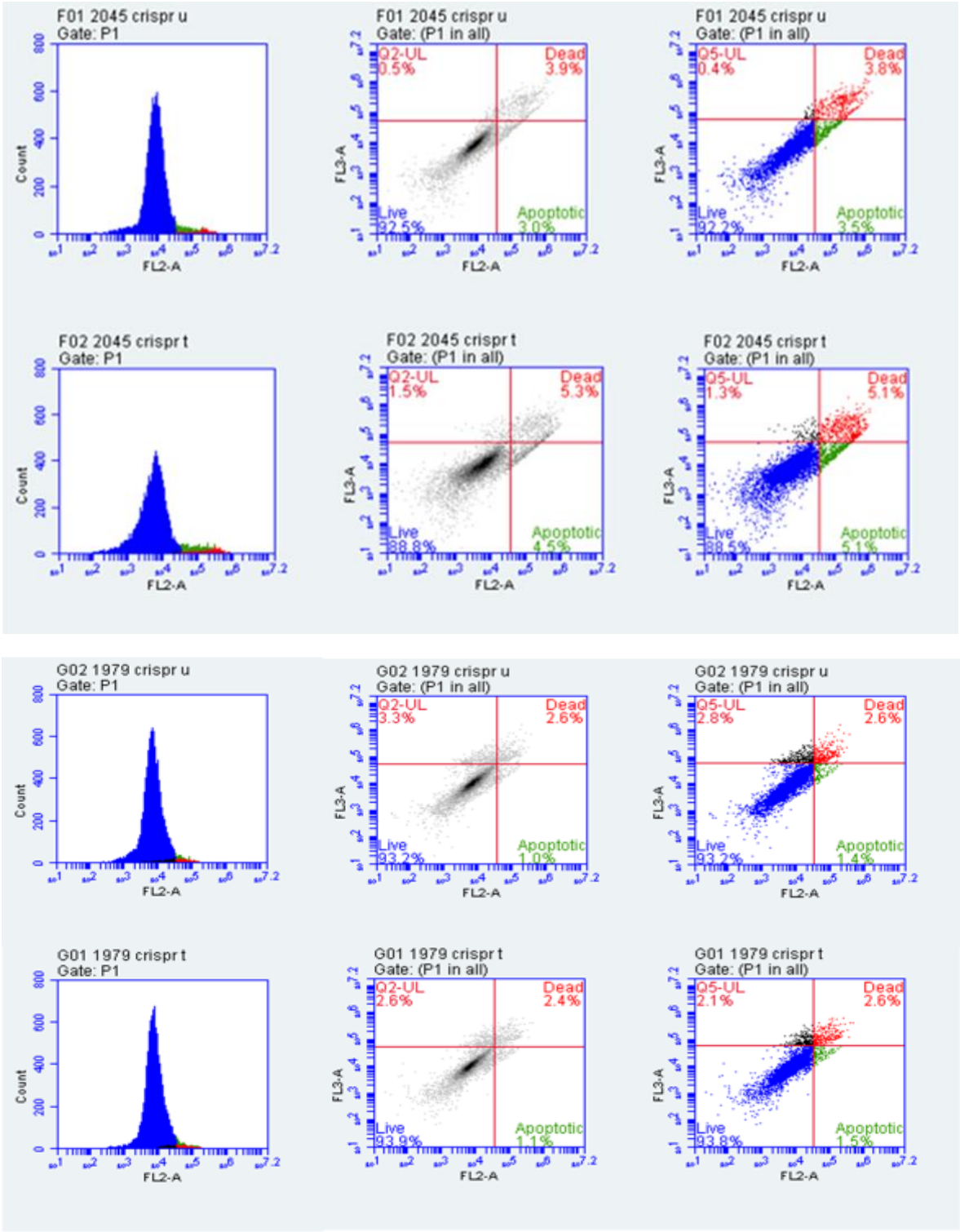

Figure 4.26 Level of apoptosis in IN2045 and IN1979 *HK2*-KO cultures, treated with 3-BPA after 72- hours. Both untreated and treated cultures show little positive binding to annexin V (2nd quadrant). No significant increase in the percentage of apoptosis was demonstrated after 3-BPA treatment in the *HK2*-KO cultures. Quadrants are colourised for graphical interpretation: Blue – live cells, Green- apoptotic and Red-dead cells.

4.7.2 Mitochondria potential

The analysis of mitochondrial membranes was investigated using flow cytometry, to further investigate the mechanism of action of 3-BPA. 3-BPA has been shown to interact with the mitochondrial membrane, causing the dissociation of *HK2* from its mitochondrial complex via covalent modification, resulting in the release of apoptosis inducing factor (AIF) into cytosol leading to cell death. JC-1 is a membrane-permeable lipophilic cationic fluorochrome that penetrates both the cellular and mitochondrial membrane (Darzynkiewicz *et al.*, 2001, Cossarizza *et al.*, 1993). An emission spectrum is created based on the relative concentration of JC-1 bound within cells, which is dependent upon the mitochondrial membrane potential (ΔΨ). In low concentrations, JC-1 forms into monomers; however, in higher concentrations JC-1 aggregates into larger structures, enabling the emission spectra profile to be separated with flow cytometry. In healthy cells, the mitochondrial membrane has a polarized ΔΨ. JC-1 is taken up into the cell initially in a monomer form, from which it penetrates the mitochondrial membrane and accumulates forming larger complex aggregates. When the mitochondrial ΔΨ is depolarized, the JC-1 is unable to penetrate the mitochondrial membrane and it remains in its monomer form within the cytoplasm of the cell. Detection via flow cytometry separates JC-1 based on its structure utilizing 2 channels. The first channel, FL-1 (green) identifies both forms of JC-1 and the second channel, FL-2 (red) identifies only the aggregated JC-1 due to the formation of the aggregates causing a shift in the red emission spectrum. Separation of the channels is achieved through gating, where changes to the parameters between the populations of monomer and aggregate can be measured, to determine any changes in ΔΨ as shown in Figure 4.27.

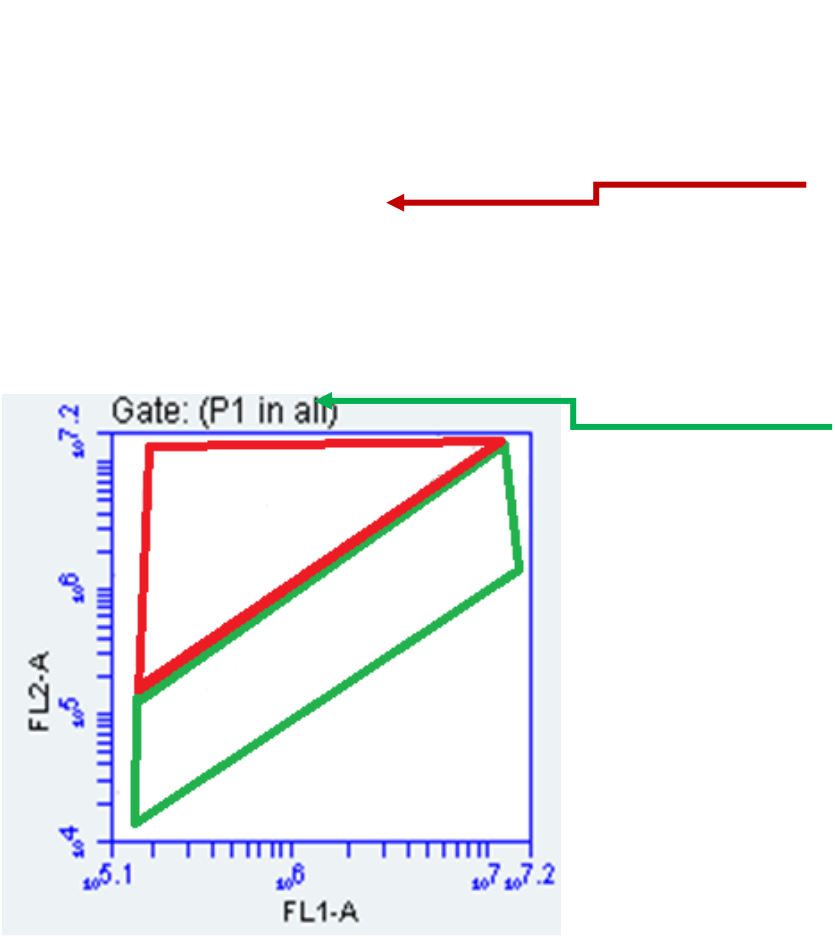

Figure 4.27 Flow cytometry gating in the separation of JC-1 fluorochrome. Gating to separate JC-1 populations of monomer and aggregates within the glioblastoma cultures. Red gating shows JC-1 aggregated within the mitochondrial matrix, where green gating shows JC-1 monomers unable to enter through the mitochondrial membrane. Cell populations in the red gate have a polarised mitochondrial membrane allowing JC-1 monomers to enter the mitochondria, thus increasing leading to the formation of aggregates. The populations in the green gate have de-polarised mitochondrial membrane which blocks Jc-1 monomers, the monomers remain in the cytoplasm of the cell without the formation of aggregates.

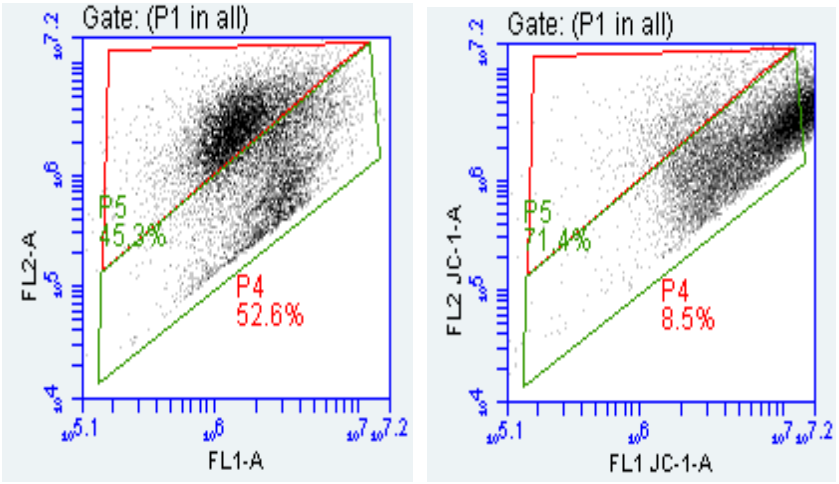

Figure 4.28 Depolarisation of the mitochondrial membrane by campthothecin. U251MG cells were treated with 100 µM camptothecin for 72 hours. FL1-A and FL2-A channels determine depolarisation values. Apoptosis induced by camptothecin leads to depolarisation of the ΔΨ, shown with a shift in the FL-1A channel. The gating protocol is from the BD Biosciences template and was adapted for glioblastoma cells. Red gating shows JC-1 aggregated within the mitochondria, where green gating shows JC-1 monomers unable to enter through the mitochondrial membrane.

Three glioblastoma cultures and the respective *HK*-KO (CRISPR transfected cultures) varients were assessed by flow cytometry for depolarisation of the mitochondrial membrane potential after treatment with 3-BPA for 72 hours at the determined ID_{50} concentrations. Positive depolarisation was determined via camptothecin treatment, where a shift in the population of cells from the red gate to green gate, also a higher reading in the FL-1 channel was seen. Examples of mitochondrial depolarisation after 72 hours of 100 µM camptothecin treatment are given in Figure 4.28.

A significant ($p<0.0001$) reduction in all JC-1 aggregate populations and an increase in monomer population was demonstrated for all parent (non-CRISPR transfected) cultures when treated with 3-BPA. An average of 44.5% change in depolarisation (JC-1 monomer form detected) in treated cultures compared to non-treated cells. A similar reduction in aggregate populations when treated with 3-BPA was not demonstrated in *HK2*-KO cultures, with an average change of 1.3% in depolarisation (JC-1 monomer form detected) in treated cultures compared to non-treated cells. This illustrates the significant effect of 3-BPA on depolarising the mitochondrial membrane when its *HK2* target is present, as demonstrated previously in the absence of *HK2* 3-BPA effectiveness is substantially reduced. The lowest monomer levels were seen in U251MG, with *HK2*-KO 15.7% and the lowest response of 0.4% change post treatment with 3-BPA. The highest values were seen in IN1979, with 82.7% and the highest response of 67% change post treatment with 3-BPA as shown in Table 4.19 and 4.20. Examples of results for the cultures are shown in Figure 4.29. The results indicate significant depolarisation of the mitochondrial membrane occurring after 72-hour 3-BPA treatment, the cytotoxic effect of 3-BPA has an impact on the membrane and functions of mitochondria.

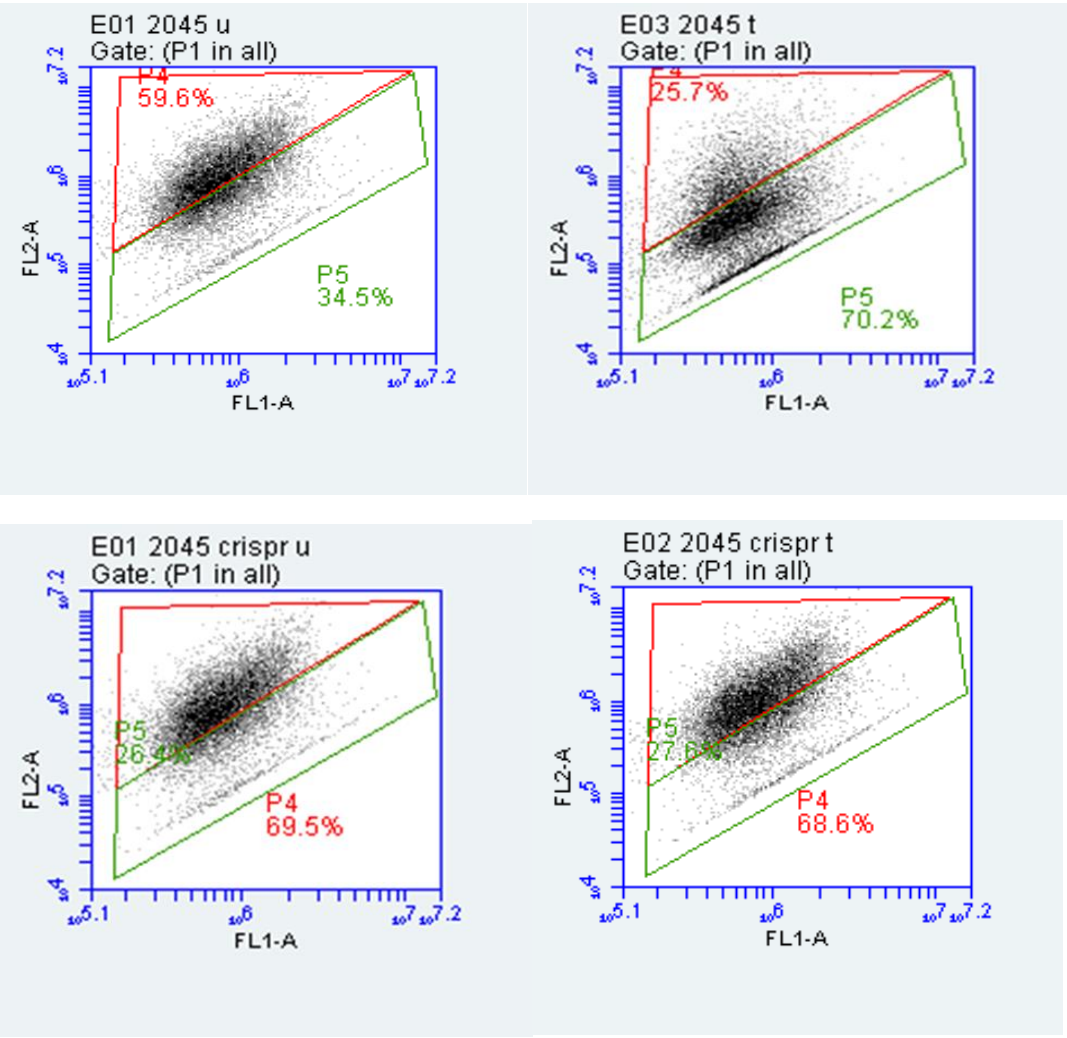

Figure 4.29 Measurement of mitochondrial membrane potential in *HK2*-KO and respective parent cultures with 3-BPA treatment. Untreated cultures are shown on the left (U), 3-BPA cultures treated for 72- hours on the right (T). 3-BPA treatment leads to depolarisation of the ΔΨ in parent cultures, shown with a shift in the FL-1A channel (increase in monomer % (green value)). No change in depolarization % was seen in *HK2*-KO cultures. Red gating shows JC-1 aggregated within the mitochondria, where green gating shows JC-1 monomers unable to enter through the mitochondrial membrane.

Table 4.19 Mitochondrial membrane potential depolarisation

	Untreated		3- BPA Treated	
Sample	Aggregate %	Monomer %	Aggregate %	Monomer %
U251MG*	40.5	53.2	13.5*	84 *
IN2045*	59.6	34.5	25.7*	70.2 *
IN1979*	81.3	15.7	14.9*	82.7 *
U251MG CRISPR	80.3	15.3	81.3	15.7
IN2045 CRISPR	69.5	26.4	68.6	27.6
IN1979 CRISPR	32	64.2	29.1	67.1

Table showing mitochondrial membrane assessment across all cultures. Aggregate % represents JC-1 crossing and accumulating within the mitochondrial membrane. Monomer % represent JC-1 accumulating in the cytoplasm of cells in a monomer form. Statistical significance denoted by *.

Table 4.20Mitochondrial membrane potential change with 3-BPA treatment

Sample	Untreated % of depolarisation	3-BPA treated % of depolarisation	% Change in depolarisation	p value
U251MG	53.2	84	30.8	<0.0001 *
IN2045	34.5	70.2	35.7	<0.0001 *
IN1979	15.7	82.7	67	<0.0001 *
U251MG CRISPR	15.3	15.7	0.4	0.0876
IN2045 CRISPR	26.4	27.6	1.2	0.0565
IN1979 CRISPR	64.2	67.1	2.2	0.1306

Table showing mitochondrial membrane assessment across all cultures. Change in depolarisation % represents the change in detected monomer values, where JC-1 accumulates in the cytoplasm of cells in a monomer form, after 3-BPA treatment. Statistical significance denoted by *.

4.7.3 Caspase

Caspase 3/7 analysis was carried out on three glioblastoma cultures and their respective *HK*-KO cultures to assess levels of caspase activity after treatment of 3-BPA for 72 hours at the determined ID_{50} concentrations. The level of caspase activity was measured along with a SRB, which gave a background measurement in which to normalise the caspase results. The positive control for apoptosis was generated using 100 µM camptothecin. The normalised caspase value (relative light units – RLU) showed a significant ($p<0.0001$) increase in caspase 3/7 readings across all parental glioblastoma cultures after 72- hour 3-BPA treatment. The average normalised caspase 3/7 value for 3-BPA parent cultures was 1379781.8 RLU, a

75.3% increase compared to the untreated cultures where the average value was 341158.2 RLU. No significant increase was determined in the caspase 3/7 values in any of *HK2*-KO cultures, with caspase 3/7 values for 3-BPA treated cultures 539210 RLU compared to 201615 RLU in the untreated *HK2*-KO cultures, as shown in Figure 4.30 and Table 4.21. Camptothecin treated cultures exhibited an effective induced level of caspase 3/7 across all parental and *HK2*-KO cultures after 72- hour treatment. The results show that 3-BPA affects the caspase 3/7 activity after 72-hour treatment in glioblastoma cultures, furthermore in the absence of the *HK2* target (*HK2*-KO cultures), 3-BPA is ineffective at influencing caspase 3/7 activity. The results indicate that one of the potential mechanisms of cell death, following 3-BPA treatment in glioblastoma cultures is dependant on the increase in caspase 3/7 activity.

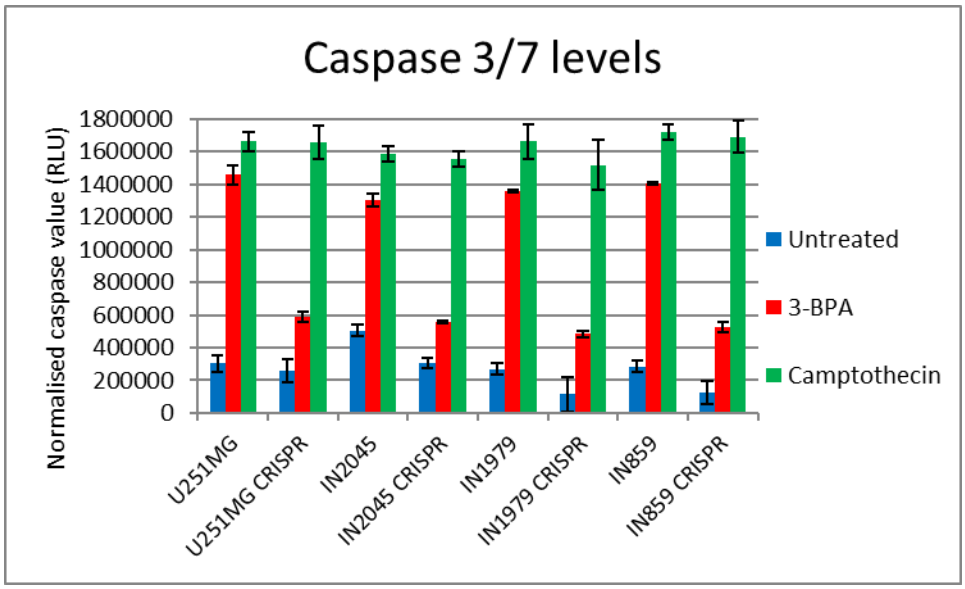

Figure 4.30 Measurement of Caspase 3/7 assay across all cultures after 3-BPA treatment. Results show the normalised level of activity of caspase 3/7 in *HK2*-KO and respective parental cultures after 72- hour 3-BPA treatment. A significant ($p<0.0001$) increase in caspase 3/7 is demonstrated across all parental cultures, no significant changes in caspase 3/7 levels were determined in *HK2*-KO cultures. Normalised caspase value measured in relative light units normalised by an SRB control. 100μM campthothecin was used to induce positive apoptosis.

Table 4.21Level of activity of caspase 3/7 in *HK2*-KO and parental cultures after 3-BPA treatment

Culture	Untreated (RLU)	3-BPA treated (RLU)	p- value
U251MG	304665	1456421	<0.0001 *
U251MG CRISPR	258567	587538	0.295
IN2045	505564	1300866	<0.0001 *
IN2045 CRISPR	306206	557646	0.638
IN1979	268937	1356421	<0.0001 *
IN1979 CRISPR	115260	485827	0.26
IN859	285467	1405421	<0.0001 *
IN859 CRISPR	126425	525827	0.374

Table showing the results of the normalised level of activity of caspase 3/7 in *HK2*-KO and respective parental cultures after 72- hour 3-BPA treatment. A significant ($p<0.0001$) increase in caspase 3/7 is demonstrated across all parental cultures, no significant changes in caspase 3/7 levels were determined in *HK2*-KO cultures. Normalised caspase value measured in relative light units normalised by an SRB control. Statistical significance denoted by *.

4.8. Recapitulating the ketogenic diet *in vitro* with 3-Hydroxybuterate

Substantial alterations in the response to inhibitors were demonstrated in glioblastoma cultures when *HK2* expression was knocked out by CRISPR. An increase in drug sensitivity to both metformin and TMZ was observed with the loss of *HK2*. The success of the CRISPR transfection knockout however cannot currently be reproduced *in vivo*. An alternative to *HK2* knockout is to restrict the level of glucose available to the glioblastoma cells, leading to the downregulation of the glucose pathway. One approach is to use a ketogenic diet (KD) to increase blood ketones to support the energy needs of normal tissues as an alternative substrate to glucose during prolonged starvation, (Woolf *et al.*, 2016). It is well documented that cancer cells rely increasingly on the glycolytic pathway as the predominant mechanism for energy production (Kazue *et al.*, 2011), and are unable to process ketone bodies. KD has also been shown to increase circulating levels of ketone bodies such as β-hydroxybutyrate and can impact metabolism leading to systemic metabolic changes. (Shukla, *et al.*, 2014). It has also been shown that the incorporation of a KD leads

to the reduction in tumour growth, along with the reduction in angiogenesis, inflammation, migration and invasion (Marsh *et al.*, 2008; Shelton *et al.*, 2010). A considerable setback of the ketogenic diet is patient accountability, and the difficulties in maintaining a strict diet; however, the development of a ketone compound would eliminate patient discrepancies.

This study investigated the ketone body 3-hydroxybuterate (3-HB) to determine the effects of ketone supplementation upon glioblastoma culture proliferation, compared to NHA in the absence or reduction of the availability of glucose. Four glioblastoma cultures IN2045, IN1979, IN859 and U251MG and an NHA control, were grown in the presence of 3-HB with either 6mM of glucose, 3mM of glucose or in the absence of glucose. All cells were seeded at 12000 cells in a T25 flask at day zero and counted in duplicates using a Countess Cell Counter as Stated in 2.1.5. Triplicate experiments were completed, with average data collected.

A reduction in proliferation was demonstrated in reduced glucose concentrations with the supplementation of 3-Hb compared to normal culture levels of 6mM of glucose (+ 3-HB). An average reduction of 53.8% across the 4 glioblastoma cultures was seen when grown in 3mM of glucose compared to cultures grown in normal glucose (6mM) + 3-HB. The range of reduction was 46.9% (IN2045) ($p=0.0001$), 54.2% (U251MG), 55.2% (IN1979) and 58.8% (IN859) ($p<0.0001$). Cell proliferation in the cultures was significantly ($p<0.0001$) diminished when glioblastoma cultures were grown in 0mM glucose (glucose free-Hams F10 media with no supplements), with the average reduction of 87.7%. The range of reduction was 71.5% (IN2045), 93.1% (U251MG), 93.4% (IN1979) and 92.9% (IN859) ($p<0.0001$). A similar trend was exhibited when 3-HB (and 0mM glucose) was supplemented as a replacement for glucose in cultures, where the average reduction in cell proliferation was significant ($p<0.0001$) at 90.2% compared to the respective cultures grown in 6mM glucose. The range of reduction was 74.6% (IN2045), 95.3% (U251MG), 95.5% (IN1979) and 95.6% (IN859) ($p<0.0001$), as seen in Figure 4.31 and Table 4.22. IN2045 however showed a reduced effect in both conditions, with >20% less change in proliferation compared to the other glioblastoma cultures. IN2045 in comparison is a lower *HK2* expressing culture and additionally has a

slower doubling time of 36 hours compared to U251MG and IN859 (24 hours) and IN1979 (34 hours), which may potentiate the altered effect of glucose reduction over the 8- day period. NHA showed a similar trend to the glioblastoma cultures, when glucose was reduced to 3mM the reduction in proliferation was 40%, furthermore, there was a significant loss ($p<0.0001$) in proliferation when grown in 0mM glucose media, where the reduction was 66.4%.

Importantly however, with the substitution of 3-HB added to the culture media (in the absence of glucose), NHA demonstrated an ability to proliferate under ketogenic conditions, where there was an 51.6% increased level of cell proliferation compared to that seen under 0mM glucose (glucose free-Hams F10 media with no supplements) conditions, contrary to the data generated from the glioblastoma cultures. NHA proliferation was reduced in cultures supplemented with just 3-HB compared to 6mM glucose + 3HB, where there was a 30.6% reduction ($p=0.0287$) in the level of proliferation, however compared to the glioblastoma cultures under 3-HB supplementation, NHA showed an increase of 59.8% in the level of proliferation, as seen in Figure 4.31 and Table 4.22. The data suggests that in the presence of reduced glucose, the glioblastoma cells lack the ability to metabolise the ketone body 3-HB, which was shown to support cell proliferation in NHA.

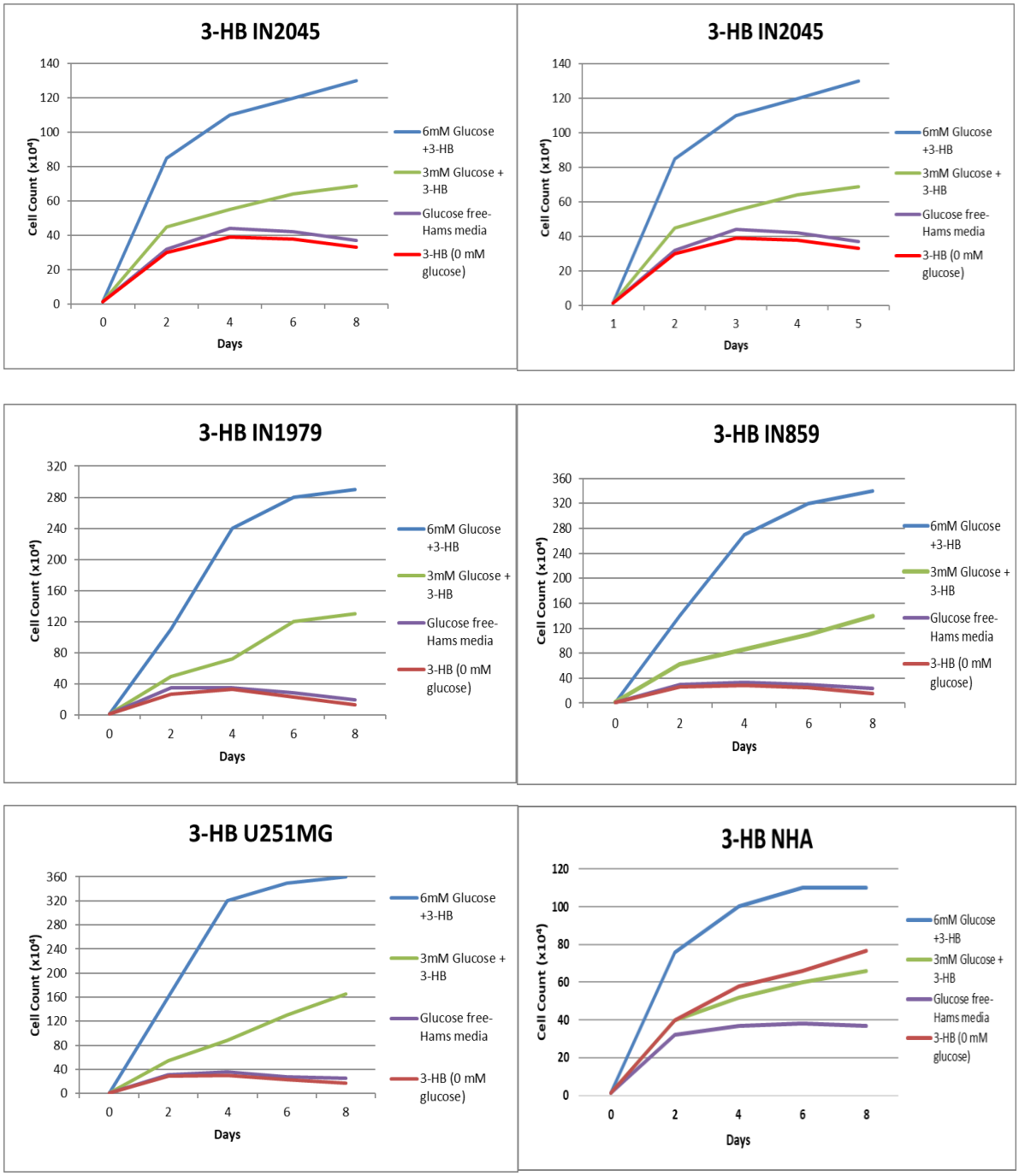

Figure 4.31 Cell proliferation in glioblastoma cultures and NHA, with varying levels of glucose and 3-HB. Cells were seeded at 12000 cells per flask and grown over 8 days, cells were counted in duplicates at each time point. Triplicate assays were conducted, and average values calculated. A significant ($p<0.0001$) reduction in glioblastoma proliferation was demonstrated with reduced levels of glucose and with the supplementation of 3-HB across all cultures. NHA cells showed the ability to proliferate when supplemented with 3-HB.

Table 4.22. Cell proliferation in glioblastoma cultures and NHA, with varying levels of glucose and 3-HB

IN2045	Cell count (Days)					% Change from 6mM +3-HB glucose
Day	0	2	4	6	8	
6mM Glucose +3-HB	$1.2x10^4$	$8.5x10^5$	$1.1 x10^6$	$1.2 x10^6$	$1.3 x10^6$	0
3mM Glucose +3-HB	$1.2x10^4$	$4.5 x10^5$	$5.5 x10^5$	$6.4 x10^5$	$6.9 x10^5$	46.9*
0mM Glucose	$1.2x10^4$	$3.2 x10^5$	$4.4 x10^5$	$4.2 x10^5$	$3.7 x10^5$	71.5*
3-HB	$1.2x10^4$	$3 x10^5$	$3.9 x10^5$	$3.8 x10^5$	$3.3 x10^5$	74.6*
IN1979	**Cell count (Days)**					**% Change from 6mM +3-HB glucose**
Day	0	2	4	6	8	
6mM Glucose +3-HB	$1.2x10^4$	$9 x10^5$	$2.4 x10^6$	$2.8 x10^6$	$2.9 x10^6$	0
3mM Glucose +3-HB	$1.2x10^4$	$4.9 x10^5$	$7.2 x10^5$	$1.2 x10^6$	$1.3 x10^6$	55.2*
0mM Glucose	$1.2x10^4$	$3.5 x10^5$	$3.5 x10^5$	$2.8 x10^5$	$1.9 x10^5$	93.4*
3-HB	$1.2x10^4$	$2.7 x10^5$	$3.3 x10^5$	$2.3 x10^5$	$1.3 x10^5$	95.5*
IN859	**Cell count (Days)**					**% Change from 6mM +3-HB glucose**
Day	0	2	4	6	8	
6mM Glucose +3-HB	$1.2x10^4$	$1.3 x10^6$	$2.7 x10^6$	$3.2 x10^6$	$3.4 x10^6$	0
3mM Glucose +3-HB	$1.2x10^4$	$6.2 x10^5$	8.60000	$1.1 x10^6$	$1.4 x10^6$	58.8*
0mM Glucose	$1.2x10^4$	$3 x10^5$	$3.3 x10^5$	$3 x10^5$	$2.4 x10^5$	92.9*
3-HB	$1.2x10^4$	$2.6 x10^5$	$2.9 x10^5$	$2.5 x10^5$	$1.5 x10^5$	95.6*
U251MG	**Cell count (Days)**					**% Change from 6mM +3-HB glucose**
Day	0	2	4	6	8	
6mM Glucose +3-HB	$1.2x10^4$	$1.6 x10^6$	$3.2 x10^6$	$3.5 x10^6$	$3.6 x10^6$	0
3mM Glucose +3-HB	$1.2x10^4$	$5.4 x10^5$	$8.8 x10^5$	$1.3 x10^6$	$1.6 x10^6$	54.2*
0mM Glucose	$1.2x10^4$	$3.1 x10^5$	$3.6 x10^5$	$2.8 x10^5$	$2.5 x10^5$	93.1*
3-HB	$1.2x10^4$	$2.9 x10^5$	$3 x10^5$	$2.3 x10^5$	$1.7 x10^5$	95.3*
NHA	**Cell count (Days)**					**% Change from 6mM +3-HB glucose**
Day	0	2	4	6	8	
6mM Glucose +3-HB	$1.2x10^4$	$7.6 x10^5$	$1 x10^6$	$1.1 x10^6$	$1.1 x10^6$	0
3mM Glucose +3-HB	$1.2x10^4$	$4. x10^5$	$5.2 x10^5$	$6 x10^5$	$6.6 x10^5$	40*
0mM Glucose	$1.2x10^4$	$3.2 x10^5$	$3.7 x10^5$	$3.8 x10^5$	$3.7 x10^5$	66.4*
3-HB	$1.2x10^4$	$4 x10^5$	$5.8 x10^5$	$6.6 x10^5$	$7.6 x10^5$	30.6

Tables showing cell counts for glioblastoma cultures and NHA across 8 days. A significant ($p<0.0001$) reduction in glioblastoma proliferation was demonstrated with reduced levels of glucose and with the supplementation of 3-HB across all cultures. A significant ($p<0.0001$) reduction in NHA proliferation was demonstrated in the absence of glucose. NHA cells showed the ability to proliferate when supplemented with 3-HB. Significance denoted with *.

4.9 Discussion

This chapter focussed on investigating the effect of *HK2* on proliferation and its potential as a therapeutic target. The efficacy of a range of potential *HK2* inhibitors for suppressing tumour growth was assessed, in both mono-treatments and in drug combination. Furthermore, their mechanisms of action were explored through use of flow cytometry and the mitochondrial membrane potential functional assay. The replacement of glucose with the ketone 3-HB was also explored as an alternative option for suppressing tumour growth. The findings of this study highlight the fundamental role of HK2 in promoting tumour growth in glioblastoma, where the impact of *HK2* downregulation via CRISPR mediated knockout revealed significant reduction ($p<0.007$) in cell growth in patient-derived glioblastoma cultures. The *HK2* inhibitors 3-BPA and LND along with metformin demonstrated anti-proliferative effects under both normoxic and hypoxic conditions, with significant reductions in cell growth. 3-BPA was shown to induce significant depolarisation of the mitochondrial membrane and initiate apoptosis across all glioblastoma cultures as shown with flow cytometry and caspase 3/7 pathway functional assays. The reduction in glucose was shown to suppress growth and, the glioblastoma cells demonstrated their ineffectiveness at metabolizing the ketone body 3-HB as a replacement, resulting in the inhibition of growth.

HK2 drives increased proliferation in glioblastoma

In this study *HK2* was knocked out using CRISPR in patient-derived cultures (IN1979, IN859, IN2045) and the established cell line U251MG. CRISPR-mediated *HK2* knockout led to a significant decrease ($p<0.007$) in cell growth of up to 44% after 7 days compared to parent cultures. The greatest reduction in proliferation was in cultures that had expressed the highest level of *HK2* overexpression. The impact of *HK2* downregulation upon the rate of proliferation in the cultures indicates its fundamental role in promoting tumour growth in glioblastoma, and its potential as a therapeutic target. Studies have shown increased levels of *HK2* to be associated with significant growth advantages in many tumours, which include medulloblastoma and breast cancers (Jiang *et al.*, 2012; Gershon *et al.*, 2013) and more recently, ovarian

cancer (Siu *et al*., 2019). It is documented that cancer cells require increased amounts of energy in order to maintain the augmented rates of proliferation and survival, where cells undergo a metabolic transformation relying increasingly on the glycolytic pathway as the predominant mechanism for energy production (vander Haiden *et al*., 2009; Kami *et al*, 2013). It has been proposed that the function of the metabolic switch is for the increased production of ATP, where glycolysis has been shown to drive ATP production at an amplified rate essential to support the increased energy demands in cancer cells (Cairns *et al*., 2011). *HK2* has a crucial catalytic role in the initiation of the glycolytic pathway and has been shown to be associated with an increased glucose flux as well as increasing tumour invasion, aggression and enhanced therapeutic resistance (Patra *et al*., 2013; Wolf *et al*., 2011 Galluzi *et al*, 2013; Lindgvist *et al*., 2018).

HK2 has been shown to bind to the voltage-dependent anion-selective channel (VDAC) releasing mitochondrial ATP to further fuel the glycolytic process (Palmieri *et al*., 2009). A recent study demonstrated the effect of *HK2* knockdown in a range of cell lines (including non-small-cell lung cancer (H460), glioblastoma cell line (U87) and liver cancer cell lines (Hep3B and HepG2) to result in the inhibition of cell proliferation, colony formation and xenograft tumor progression (Xu *et al*., 2018). The data presented in the current study indicates the potential therapeutic advantages of targeting *HK2* in glioblastoma, where *HK2* downregulation leads to the significant reduction in cell proliferation.

Increased sensitivity to TMZ in the absence of *HK2* in glioblastoma

The sensitivity to TMZ was significantly increased ($p<0.0001$) in *HK2* KO cultures, with average ID_{50} values decreased by 42.5% respectively compared to parent cultures. Additionally, a reduction in cell survival was also exhibited in the *HK2* KO cultures with TMZ, with an average reduction of 19.9% % respectively compared to parent cultures. The data reiterates the importance of *HK2* as a key mediator driving glycolysis and signifies the potential therapeutic advantages of targeting *HK2* in glioblastoma, where downregulation was shown to significantly increase the effectiveness of the therapeutic agent TMZ. The novel data presented in this study indicates the potential therapeutic advantages of targeting *HK2* in glioblastoma.

3-Bromopyruvic acid inhibits *HK2* in glioblastoma, initiating early apoptosis

All cultures treated with 3-BPA demonstrated an anti-proliferative response after treatment. Additionally, cultures expressing higher levels of *HK2* were more sensitive to 3-BPA and generally had significantly lower ID_{50} values ($p= 0.0192$), indicating the specificity of 3-BPA in targeting *HK2* causing dissociation from its mitochondrial bound complex. The substantial difference in the cytotoxic response of the glioblastoma cells to NHA demonstrates that 3-BPA mechanism of action relates specifically to cancer cells, via the targeting of mitochondrial bound *HK2*, as shown in Chapter 3 to be overexpressed in glioblastoma. Studies have also shown direct inhibition of mitochondrial *HK2* via covalent modification of its cysteine residues, resulting in its dissociation from the mitochondria (Ko *et al*., 2001; Chen *et al*., 2009). The dissociation of *HK2* induces the release of mitochondrial apoptosis-inducing factor (AIF) to the cytosol resulting in cell death. In another study 3-BPA was shown to inhibit the expression of *HK2* at mRNA and protein levels in both lung and liver cancers (Yadav *et al*., 2017).

The effects 3-BPA upon cell proliferation were also investigated under hypoxic conditions. Hypoxia is a distinguishing feature associated with tumour microenvironments; therefore, the effectiveness of a therapeutic molecule in generating an inhibitory response needs to be assessed under hypoxic conditions. It has been shown that hypoxia inducible factor 1 (HIF1) up-regulates many enzymes of the glycolytic pathway, including *HK2*, through binding to the hypoxia-responsive elements (HREs) in the *HK2* promoter (Mathupala *et al*., 2001). Under hypoxic conditions, ID_{50} values significantly increased ($p <0.0001$) in all culture samples, indicating an increased tolerance of 3-BPA. A similar trend was also exhibited in NHA. Increased resistance may be mediated through hypoxia induced proteomic and genomic changes. These changes often lead to angiogenesis activation and anaerobic metabolism to aid in survival, and lead to the release of proteins such as the transcription factor hypoxia-inducible factor 1 (HIF1), which regulates tumour cell adaption (Majmundar *et al*, 2010). HIF-1 increases tumour cell resistance to therapeutic agents and to hypoxic stress, leading to the generation of more

aggressive clones with greater resistance to therapeutic agents, eventually becoming the dominant cell type within the tumour (Sun *et al.*, 2011). HIF1 overexpression has been linked with the regulation of secondary mechanisms associated with survival adaptation in cancer cells, which are upregulated by the PI3K/Akt1/mTOR pathway (Wouters and Koritzinsky, 2008). HIF1 has also been shown to enhance cellular glycolytic potential by increasing the transcription of glucose transporters and glycolytic enzymes (Semenza, 2013). The effects of 3-BPA were shown to be reduced in cultures that had been CRISPR *HK2*-KO modified, where a significantly increased ($p<0.0001$) tolerance to 3-BPA was demonstrated after 72-hour treatment with average ID_{50} values 50% greater across *HK2*-KO cultures compared respectively to the parent culture. Cell survival was also shown to be significantly increased ($p=0.0024$) in all *HK2*-KO cultures compared to parent cultures after 3-BPA treatment. The elimination of the HK2 target reduces the effectiveness of 3-BPA, verifying the specificity of the inhibitor.

Apoptosis was induced by 3-BPA in all glioblastoma cultures, where significantly higher apoptosis ($p<0.0001$) was exhibited in cultures expressing higher levels of *HK2*. The average apoptotic value was 30% greater in these cultures compared to lower *HK2* overexpressing cultures. Furthermore, there was also a significant difference ($p= 0.0091$) between levels of apoptosis in high *HK2* expressing cultures treated under normoxic and hypoxic conditions. The data suggests that 3-BPA is less effective under hypoxic conditions, a reason for the reduced efficiency may be impacted by increased resistance through hypoxia induced proteomic and genomic changes, as previously stated above. HIF1 upregulation has also been shown to have inhibitory effects on a range of factors involved in apoptosis and the regulation of cell death mechanisms in glioblastoma (Yang *et al.*, 2012). The cultures that had the greatest change in apoptotic levels were those expressing higher *HK2* levels, the reduction in 3-BPA effectiveness at generating early apoptosis may be part due to increased resistance through hypoxic generated transcription factors. Additionally, these cultures have generally faster doubling times which would lead to more hypoxic stress-adapted cells, resulting in an increased resistance of 3-BPA during the 72-hour treatment. The same significant reduction of apoptosis is not seen in lower *HK2* expressing cultures, which may be due to there being a reduced *HK2* target for

3-BPA, thus the increased levels of hypoxia transcription factors have a lessened impact on its effectiveness. Additionally, the effects of 3-BPA were shown to be reduced in cultures that had been CRISPR *HK2*-KO modified, where a significant reduction ($p<0.0001$) in apoptosis was exhibited compared to the respective parent cultures after 3-BPA treatment. The data indicates that in the absence of *HK2*, 3-BPA has a minimal cytotoxic effect upon the cells, failing to induce early apoptosis.

Finally, a significant increase ($p<0.0001$) in the level of caspase was detected in all 3-BPA treated cultures, with an average increase of 75.3%, comparatively, no significant increase was determined in in any of the *HK2*-KO cultures. The data from this study shows that 3-BPA effects the caspase 3/7 activity in glioblastoma cultures, suggesting that one of the potential mechanisms of cell death following 3-BPA treatment in glioblastoma is dependent on the increase in caspase 3/7 activity. The data obtained from the functional assay reiterates the flow cytometry data, that in the absence of the *HK2* target, 3-BPA is ineffective at influencing apoptosis and caspase 3/7 activity. Caspase 3/7 are primary effectors at the end of the apoptotic caspase pathway, the combined experiments show strong evidence that the caspase dependent apoptotic pathway is induced as the main mechanism of cell death in glioblastoma from 3-BPA treatment. Additionally, significant depolarisation ($p<0.0001$) of the mitochondrial membrane was seen across all glioblastoma cultures after treatment with 3-BPA; with an average depolarisation change of 44.5%. Comparatively no reduction was demonstrated in *HK2*-KO cultures. It is well established that the apoptotic intrinsic pathway is regulated by mitochondria, through downstream caspase effectors, eventually activating caspase 3 and 7 which destroy the cell from within (Hunt, 2002; Boehning *et al.*, 2003). Mitochondrial activity is therefore fundamental for the activation of apoptotic factors, which itself is dependent upon the mitochondrial membrane potential ($\Delta\psi$). It has been shown that the combination of apoptogenic factors released by the mitochondria with the addition of the depolarisation of the transmembrane potential and the loss in oxidative phosphorylation are key factors in eliciting the intrinsic apoptotic pathway (Martínez-Reyes *et al.*, 2016). 3-BPAs cytotoxic effect causes apoptosis in glioblastoma cells, impacting on the membrane functions, leading to the depolarisation of the mitochondrial membrane. In the absence of HK2 3-BPA

effectiveness is substantially reduced. Gandham *et al*. (2015) showed that 3-BPA affects mitochondria through the targeting of HK2 bound complex which results in subsequent stimulation of AIF consequently leading to cell death. AIF initiates a caspase-independent pathway of apoptosis via DNA fragmentation and chromatin condensation. However, other studies have demonstrated 3-BPA effectiveness at generating apoptosis via a caspase mediated pathway, where the expression of caspase-3 increased in breast cancer cells (MDA-MB-231) following 3-BPA treatment (Chen *et al*., 2018). Inhibition of *HK2* by 3-BPA has been shown to decrease ATP and NADPH levels, thereby blocking glycolysis in tumour cells and halting growth (Chen *et al*., 2009; Galluzzi *et al*., 2012). 3-BPA has also been shown to induce apoptosis in breast cancer cells by downregulating induced myeloid leukaemia cell differentiation protein (Mcl-1) through PI3K/Akt signalling pathway and via the generation of reactive oxygen species leading to mitochondria-mediated apoptosis (Liu *et al*., 2014); as well as increasing mitochondrial membrane permeability through *HK2* inhibition, activating caspase 9 resulting in cellular apoptosis (Ferraro *et al*. 2008; Zuo *et al*., 2011). The data presented here signifies the potential of 3-BPA as a therapeutic for glioblastoma, where its effectiveness at inhibiting *HK2* and to generate apoptosis via caspase dependant (and independent) pathways has been shown. Moreover, 3-BPA demonstrates increased effectiveness in higher *HK2* expressing glioblastoma cultures, indicating its promising ability at treating a significant subset of glioblastoma patients.

LND also demonstrated an anti-proliferative response in all cultures, to a lesser degree. Cultures expressing higher levels of *HK2* were more sensitive to LND and generally had significantly lower ID_{50} values ($p= 0.0465$). The data indicates the specificity of lonidamine to inhibit aerobic glycolysis in cancer cells through the targeting of condensed mitochondrion (Price *et al*., 1996), consequently inhibiting the mitochondrially bound HK2 in tumour cells. The inhibition of HK2 results in the reduction of glycolysis and cellular ATP (Nath *et al*., 2015). A recent study demonstrated the ability of LND to inhibit the monocarboxylate transporter (MCT), preventing oxidation of the accumulated L-lactate through its conversion to

pyruvate, consequently, blocking entry into the mitochondria and the citric acid cycle (Nancolas *et al.*, 2016). The resultant effect would suggest the inability of the cell to compensate for the loss in glycolytic ATP additionally affected by HK2 inhibition. The substantial difference in the cytotoxic response of the glioblastoma cells to NHA demonstrates that the lonidamine mechanism of action relates specifically to cancer cells. Studies have shown LND to have low levels of toxicity to normal tissues (Prabhakara *et al.*, 2008), suggesting its mechanism of action has a high affinity for targeting cancer cells, through the selective inhibition of HK2 and other glycolytic components that are overexpressed in cancer cells, via targeting the mitochondrially bound *HK2*. The data presented here has shown the anti-proliferative effects of both 3-BPA and LND, highlighting the importance of 3-BPA inhibitory action upon glioblastoma, and its potential as a therapeutic agent in a subset of glioblastoma. 3-BPA hampers ATP generation through predominantly targeting *HK2*, along with other metabolic targets including lactate dehydrogenase (LDH) (Lis *et al.*, 2016), which are specifically upregulated in cancer cells. 3-BPA therefore offers a wide spectrum of glycolytic enzyme inhibitory potential, instigating complete breakdown of cancer cell metabolism whilst unaffecting healthy cell metabolism highlighting its chemotherapeutic potential.

Metformin induces anti-proliferative effects in glioblastoma

All glioblastoma cultures treated with metformin demonstrated an anti-proliferative response after treatment. No significant differences were determined between the response to metformin and the level of *HK2* expression. NHA had a high tolerance of metformin with the highest ID_{50} value compared to all the glioblastoma cultures. The substantial difference in the cytotoxic response of the glioblastoma cells to NHA demonstrates that mechanism of action of metformin relates exclusively to cancer cells, although not specifically through HK2 (Wahl and Venneti, 2018). Metformin is a biguanide drug with a primary function of preventing the production of glucose in the liver, resulting in the nutrient deprivation for cancer cells that rely exclusively on glucose metabolites for energy production and proliferation. The data here indicates metformin inhibits growth of glioblastoma. The importance of glucose deprivation via

metformin supplementation has been shown to have an inhibitory response and induce cell death, similar correlations have been demonstrated in breast cancer cell lines (Menendez *et al.*, 2012; Birsoy *et al.*, 2014). It has also been suggested that p53 status impacts metformin effectiveness, with increased sensitivity reported in P53 aberrant colon cancer cell lines compared to *P53* wild type cells (Buzzai *et al.*, 2007). The effects of metformin upon cell proliferation was also investigated under hypoxic conditions and ID_{50} values significantly increased ($p < 0.0125$) in all culture samples, indicating an increased tolerance of metformin treatment. A similar trend was also exhibited in NHA. It has been suggested that metformin activates AMPK resulting in the inhibition of the mTOR pathway (Pollak, 2012; Liu *et al.*, 2014; He and Wondisford, 2015). AMPK is a metabolic kinase important in regulating cellular metabolism and proliferation (Mihaylova and Shaw, 2011).

Additionally, metformin has also been shown to inhibit Akt (Mahvash *et al.*, 2010). Deregulation of both Akt expression and mTOR pathway is a frequent occurrence in cancer cells and upregulation is associated with increased cell proliferation and survival (Sharma *et al.*, 2015). In hypoxia HIF-1 is induced, which consequently induces upregulation of PDK1 in turn activating Akt as well as reducing oxidative phosphorylation and ROS via restricting pyruvate into the mitochondrial TCA cycle, thus promoting lactate production, further supplementing the up-regulation of glycolysis mediated by *HIF1* (Kim *et al.*, 2007; Lu *et al.*, 2008). Notably, HIF-1 upregulation of Akt counteracts the effectiveness of metformin inhibition, resulting in an increased tolerance. Similarly, *HIF1* upregulation has been shown to inhibit on a range of factors involved in apoptosis and stress responses and in the regulation of glioblastoma (Trachootham *et al.*, 2006; Yang *et al.*, 2012). The metabolic and genetic changes instigated through hypoxia increase the chemoresistance of the glioblastoma cultures, reducing the effectiveness of metformin. The effects of metformin were shown to be increased in cultures that had been CRISPR *HK2*-KO modified, where a significantly increased ($p<0.0001$) sensitivity to metformin was demonstrated after 72-hour treatment with average ID_{50} values decreased by 46.8% across *HK2*-KO cultures compared respectively to the parent culture. Cell survival was also shown to be significantly reduced ($p=0.0008$) in all *HK2*-KO cultures compared to parent cultures after metformin treatment.

Significant levels of apoptosis were not induced by metformin any of the glioblastoma indicating that metformin may act through another mechanism of cell death such as autophagy or necrosis. Metformin has been shown to induce autophagy flux through regulation of AMPK, triggered in response to cellular stress and increases in cellular metabolic demands (Zhang *et al.*, 2017), as shown in thyroid and endometrial cancer cells (Song *et al.*, 2016; Gu *et al.*, 2017). Autophagy activation has also been seen in glioblastoma cell lines (U251MG/ U87MG), where an increase level of autophagy was detected after metformin treatment (Sesen *et al.*, 2015). Additionally, metformin has been shown to induce autophagy in glioblastoma cells via the activation of AMPK and REDD1, downregulating the mTOR pathway (2014; Sesen *et al.*, 2015).

3-HB supplementation induces an anti-proliferative effect in glioblastoma

The reduction in glucose was shown to suppresses growth in all cultures. The glioblastoma cells demonstrated their ineffectiveness at metabolizing the ketone body 3-HB as a replacement, and cultures supplemented with 3-HB and no added glucose (Hams' free glucose media) showed significantly reduced ($p<0.0001$) cell proliferation (average growth decrease of 90.2%), compared to the respective cultures grown in normal glucose conditions. The data indicates the potential therapeutic advantages of reducing the level of glucose, though the means of a ketogenic diet or through therapeutic agents including 3-HB and metformin. 3-HB has been shown to have a higher calorific value compared to glucose as well as an efficient provision of energy in cells with functioning mitochondria (Veech *et al.*, 2004). The reduction in the availability of glucose impacts cancer growth, restricting the glucose metabolite energy source tumour cells necessitate, whilst concurrently lacking the ability to metabolise ketone bodies resulting in the inhibition of growth and tumorigenesis.

Studies have shown the effectiveness of 3-HB in reducing the proliferation of tumour cells in a range of cancers, including human glioblastoma cell lines (Woolf *et al.*, 2016). 3-HB treatment has also demonstrated the ability to increase the sensitivity of cancer cells to ionizing radiation, as well as the increased effectiveness of

chemotherapeutic agents when used in combination in glioblastoma cells, for the potentiation of lower doses (Scheck *et al.*, 2012; Rossi *et al.*, 2015; Silva-Nichols *et al.*, 2015). The switch to a ketogenic environment reduces the abundant availability of glucose. Cancer cells lack the ability to metabolise ketone bodies leading to a reduction in proliferation whilst unaffecting healthy cell growth with their ability to metabolise ketone bodies. The higher *HK2* expressing glioblastoma cultures (IN859, U251MG and IN1979) exhibited a lower tolerance to reduced levels of glucose compared to IN2045. These samples also have faster doubling times. In comparison IN2045 has a slower doubling time of 36 hours which may potentiate the altered effect of glucose reduction over the 8- day period. It has also been proposed that the effect of ketone bodies upon cancer growth was dependent on the tumor's energetic phenotype whereby cells with the predominant "glycolytic, Warburg-like phenotype" would be unable to metabolize 3-HB resulting in it accumulating intracellularly inhibiting tumor growth via signaling and epigenetic mechanisms; conversely tumours with "oxidative cells" would use 3-HB as an additional energy source resulting in an increased growth rate when this metabolite is available (Rodrigues *et al.*, 2017; Bartmann *et al.*, 2018). There are conflicting reports from studies, some demonstrate 3-HB to significantly reduce tumour growth in glioblastoma and pancreatic cancers (Shukla *et al.*, 2014; Martuscello *et al.*, 2016), whilst other studies state ketone bodies to be associated with cancer progression and metastasis, including epithelial and breast cancer (Bonuccelli *et al.*, 2010; Martinez-Outschoorn *et al.*, 2011).

The microenvironment created in tissue culture is often altered in comparison to the natural cellular environment which can generate genetic alterations, such an example is the concentration of glucose available to the cell. A healthy adult on average has circulating glucose levels around 5-6mmol/l, in comparison the glucose concentration in average tissue culture media ranges from 10-25 mmol/l. To address this discrepancy the use of an alternative culture media that has a similar glucose concentration can be used, for example Hams F-10 which has a 6mM concentration of glucose, comparable to the circulating blood glucose of the human body. The exaggerated abundance of glucose in the culture media can have detrimental and inaccurate effects on cellular responses to inhibitory molecules such as ketone

bodies, glucose pathway inhibitors and metformin, the latter of which has been shown to have reduced efficacy in ovarian and breast cancers (Litchfield, *et al.*, 2015).

The data obtained from this study would suggest that increased *HK2* expression in cells would indicate higher energetic phenotypes with increased doubling times, as potentially seen in IN859, U251MG and IN1979. Importantly, NHA demonstrated the ability to successfully proliferate, albeit at a slightly reduced level under ketogenic conditions. This is promising for the application of potential therapeutic approach, as a non-cancerous cell NHA, demonstrated the ability to metabolise ketone bodies. The data also showed that 3-HB supplementation and an increased level of ketones were non-toxic to healthy cells. This study indicates the potential therapeutic advantages of targeting both *HK2* and the glucose pathway, with both a reduction in cell proliferation and an increased chemosensitivity in a significant subset of glioblastoma.

Chapter 5

Expression arrays: Deregulated glucose metabolism in glioblastoma

5.1 Introduction

Qiagen RT expression profiler arrays (Qiagen, UK) were utilized to analyse the expression of 84 key genes involved in the regulation and enzymatic pathway of glucose metabolism in a panel of 6 glioblastoma biopsy tissues, 10 patient- derived cell cultures and the established cell line U251MG (as shown in Table 2.1) compared to normal brain tissue and NHA. The cumulative threshold (Ct) data obtained was normalised to 5 housekeeping genes (ACTB, B2M, GAPDH, HPRT1 and RPLP0). Alterations in the level of gene expression across the pathway were also determined in glioblastoma cell cultures grown under hypoxic conditions and post treatment conditions, including the addition of *HK2* inhibitors and CRISPR mediated *HK2* -KO. Un-abbreviated gene list is shown in full in the appendix.

5.1 Differential expression of glycolytic genes in glioblastoma tissue

Differential expression was investigated in 6 glioblastoma biopsy samples compared to 5 normal brain tissue samples. Upregulations of 50 of 84 genes in the glucose pathway was identified, as shown in Figure 5.1. The fold change increase in these 50 genes ranged from 2.06 (*AGL*) to 6.85 (*PCK2*). Additionally, downregulation was demonstrated in 6 genes, ranging from -2.54 (*SDHC)* to -3.65 (*UGP2*).

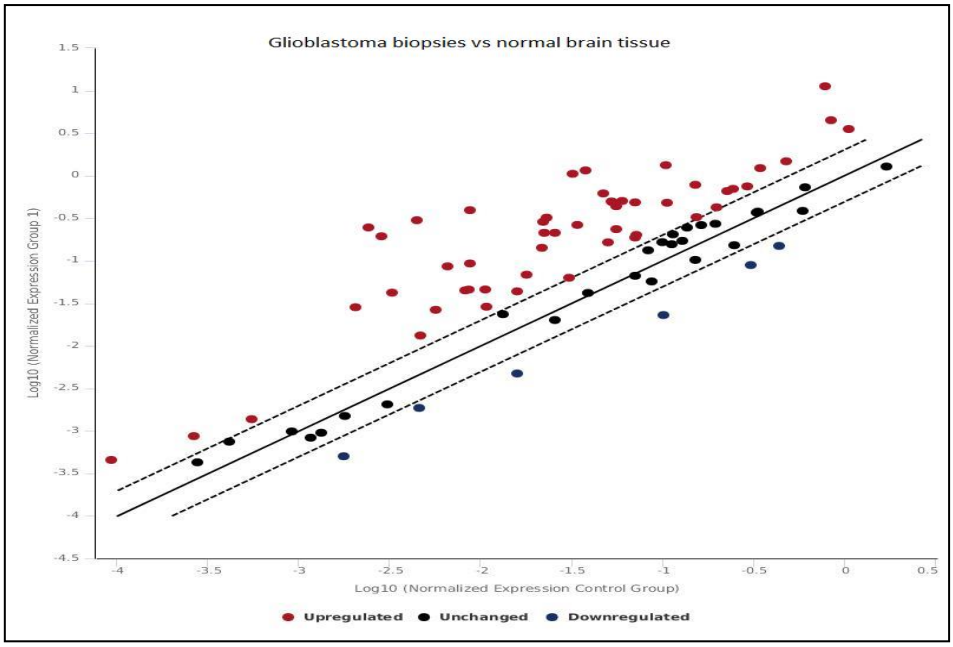

Figure 5.1 Scatter plot comparing the level of fold change across 84 genes in glioblastoma biopsies (n=6) compared to normal tissue (n=5). Each dot represents the expression of a gene. The y-axis represents fold-change expression of the glioblastoma sample, the x-axis represents expression of the normal tissue control. Genes (dots) further to the right show higher expression compared to normal tissue. Higher dots represented greater expression in the glioblastoma samples.

The level of significance for each gene fold change was calculated using a Student's t-test. Grouping the glioblastoma samples, a volcano plot approach was utilized to visually represent the significantly altered genes between samples, where representative samples were grouped to give a precise mean (Wentian *et al.*, 2014). The volcano plot shows significance versus fold-change on the y and x axes, respectively. The Y-axis represents the log10 p-value whilst the X-axis shows the log2 fold change level. The larger the difference in expression of a gene the more extreme it will lie on the X-axis. The more significant the difference, the smaller the p-value and thus the higher the -log10p-value value on the Y-axis. Genes with highly significant differences will lie higher, in the upper left and upper right parts of the volcano plot. The statistical calculations and volcano plots were completed using Qiagen PCR array data analysis web-based software (version of software).

Twenty-three genes showed highly significant differences in expression in the biopsies compared to normal tissue, comprising 19 of these genes were significantly overexpressed genes ranging from 2.99 (*ALDOA*) to 5.85 (*PRPS1L1*) ($p<0.005$) and 4 genes with downregulation ($p<0.005$) in the glioblastoma samples, as shown in

Table 5.1 and Figure 5.2. The variance in fold change of the genes were also examined between the individual biopsies to establish the degree of homogeneity between expression levels. A variation in the individual gene expression between the biopsies was shown, where 15 of the 23 significantly altered genes had a >2- fold variation between samples. Additionally, 8 of the genes demonstrated little variance (≤2-fold change), as shown in Figure 5.3 (Table A6 shown in the appendix). The data suggests that significant alteration in multiple genes is occurring in glioblastoma biopsies compared to normal tissue, however varied expression is demonstrated in 48% of the genes in the biopsy samples, indicative of the diverse heterogeneity of glioblastoma. The data indicates the occurrence of overexpression throughout the glucose pathway in glioblastoma tissue, with over 60% of the genes showing levels of overexpression ensuing within the tumour tissue. Furthermore, 19 of these genes (Table 5.1) demonstrated significant levels of upregulation across all 6 biopsy samples, indicating a substantially perturbed glucose pathway emerging in glioblastoma tissue.

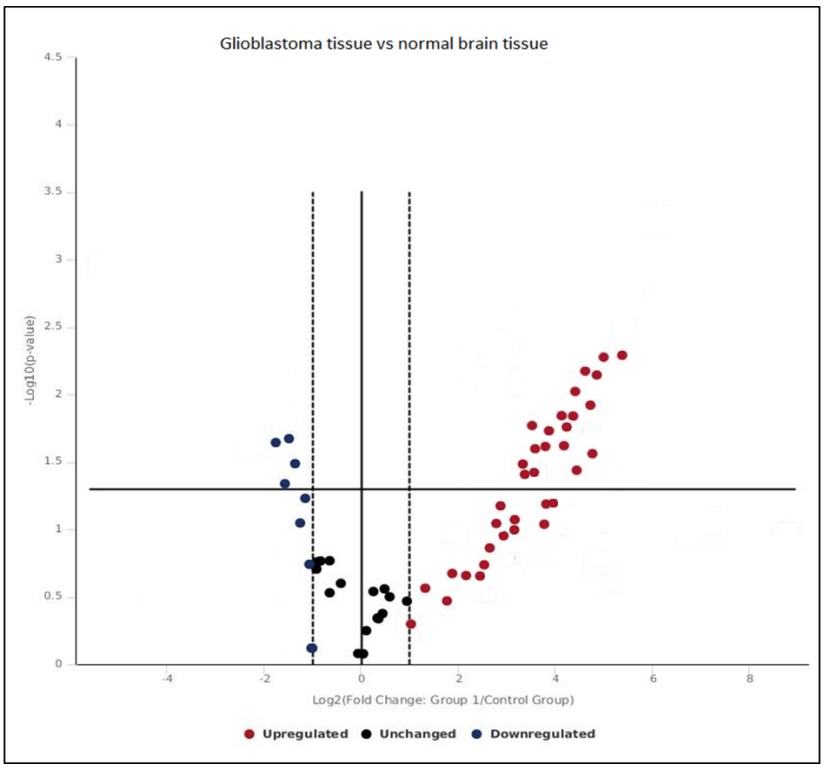

Figure 5.2 Volcano plot comparing the level of fold change across 84 genes in glioblastoma biopsies (n=6). Fold change compared to normal tissue. Represented genes above the threshold all show significant change ($p<0.05$). The volcano plot shows significance versus fold-change on the y and x axes, respectively. The Y-axis represents the log10 p-value whilst the X-axis shows the log2 fold change level.

Table 5.1 Expression fold change values of glycolytic genes in glioblastoma biopsies compared to normal brain

Gene	Log2 Fold Change	Gene	Log2 Fold Change
ALDOA	2.99	*PCK1*	3.74
ALDOB	3.33	*PCK2*	3.75
ENO1	5.07	*PGK1*	4.04
FBP2	4.04	*PGK2*	3.28
G6PC	3.78	*PKLR*	3.11
GCK	4.47	*PRPS1L1*	5.85
GYS1	5.43	*RBKS*	4.58
GYS2	4.65	*ACO2*	-1.88
HK2	5.58	*ENO2*	-2.3
HK3	3.5	*SUCLA2*	-1.73
MDH1	3.86	*UGP2*	-1.53
MDH2	4.85		

Table showing changes in fold change in glioblastoma biopsies (n=6) compared to normal tissue (n=5). All genes show significant change ($p<0.05$) as represented in the Volcano plot.

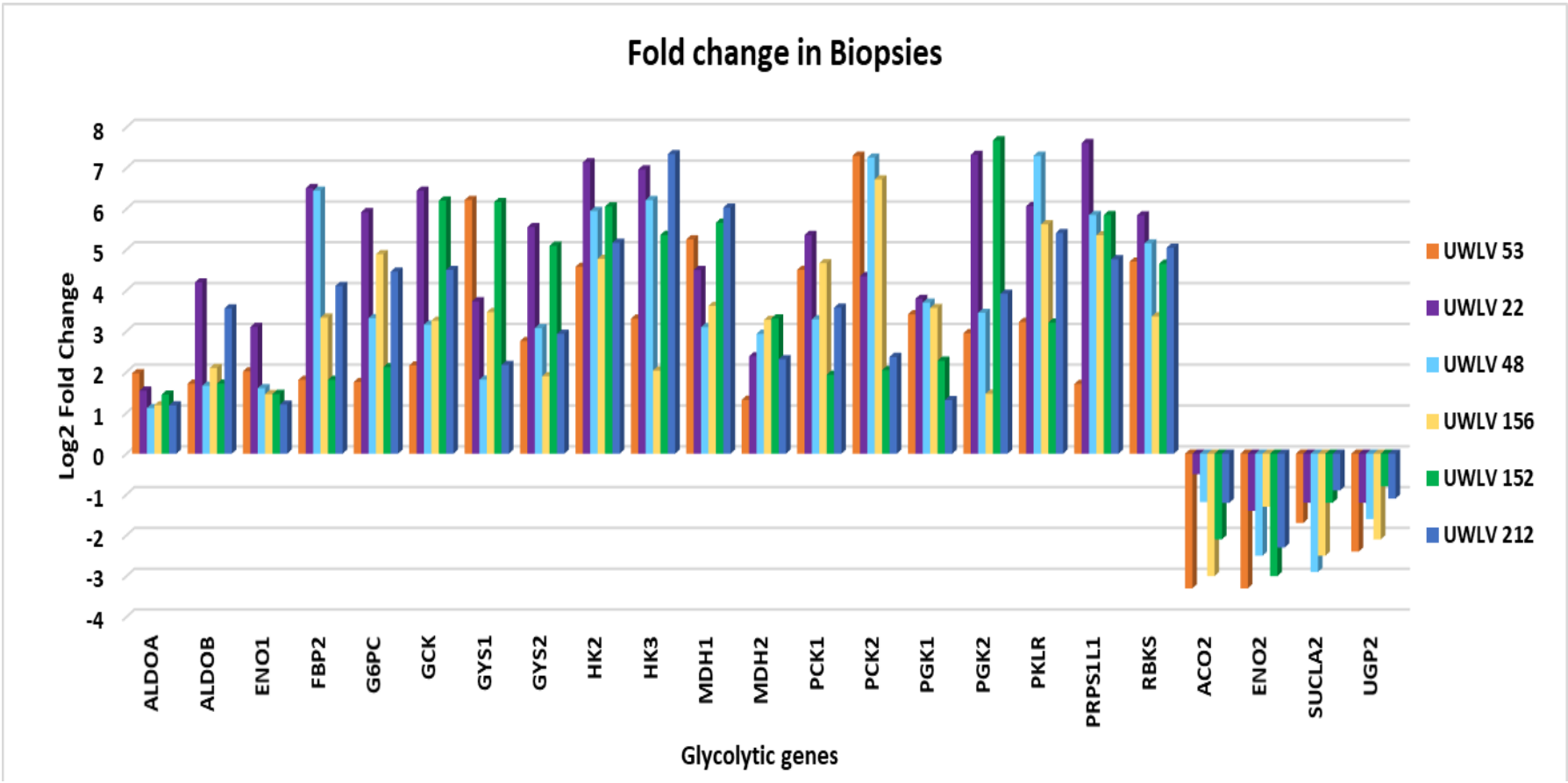

Figure 5.3 Bar chart comparing gene expression variation between the biopsy samples. The represented genes exhibit significantly altered levels of expression compared to normal tissue as shown in Figure 5.2 and Table 5.1. Expression data is shown for individual biopsies to compare levels of fold change.

5.2 Differential expression of glycolytic genes in glioblastoma culture

The glycolytic expression patterns of 10 glioblastoma cultures were investigated, including patient-derived cultures and the established cell line U251MG. The samples were compared to both normal brain tissue and NHA. Thirty-three genes showed significant alterations in the cultures compared to NHA, of which 31 were overexpressed ($p<0.005$) in the glioblastoma cultures and 2 genes were downregulated ($p<0.005$), as shown in Table 5.2 and Figure 5.4. The increased fold change expression across the glycolytic genes in the cultures ranged from 1.82 (*GSK3A*) to 6.21 (*ACLY*). The variance in fold change of the genes were also examined between the individual cultures to establish the degree of homogeneity of expression levels. Minor variation in the individual gene expression between the cultures was shown, where 82% of the significantly altered genes had ≤2- fold variation between the cultures, with only 6 genes demonstrating a variance ≥2-fold change, as shown in Figure 5.5 (Table shown in the appendix).

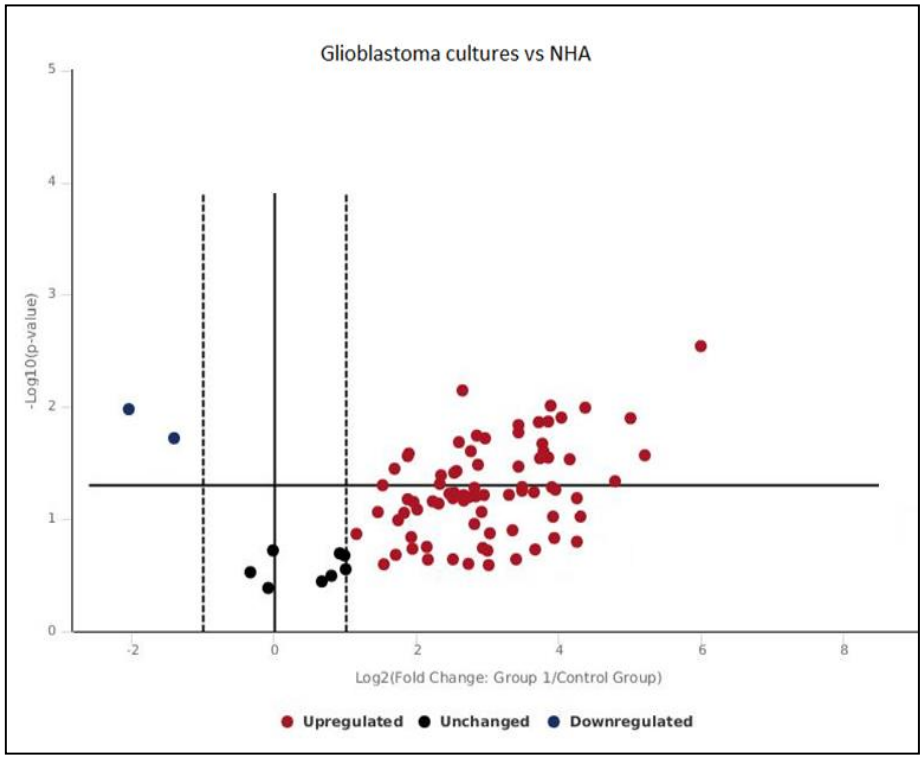

Figure 5.4 Volcano plot comparing the level of fold change in glioblastoma cultures compared to NHA in 84 genes in glioblastoma cultures (n=10). Fold change compared to NHA. Represented genes above the threshold all show significant change ($p<0.05$).

Table 5.2 Expression fold change values of glycolytic genes in glioblastoma cultures compared to NHA

Gene	Log_2 Fold Change
ACLY	6.21
ACO1	3.67
ACO2	3.18
CS	3.06
DLD	4.93
DLST	3.25
ENO3	4.42
FH	1.86
G6PD	3.18
GSK3A	1.82
H6PD	3.71
HK2	3.87
IDH2	3.24
IDH3G	2.79
MDH1	3.78
MDH2	3.29
OGDH	2.65
PC	4.42
PDHB	4.76
PDK2	4.4
PDP2	4.76
PFKL	5.06
PGAM2	3.61
PGM3	2.86
PHKG2	4.78
PKLR	2.56
PRPS1	3.99
PRPS1L1	2.74
RPE	3.24
SDHA	1.84
TKT	2.31

Gene	Fold Change
SUCLA2	-1.80
UGP2	-2.36

Table showing fold changes in glioblastoma cultures compared to NHA. All genes show significant change ($p<0.05$) as represented in the Volcano plot.

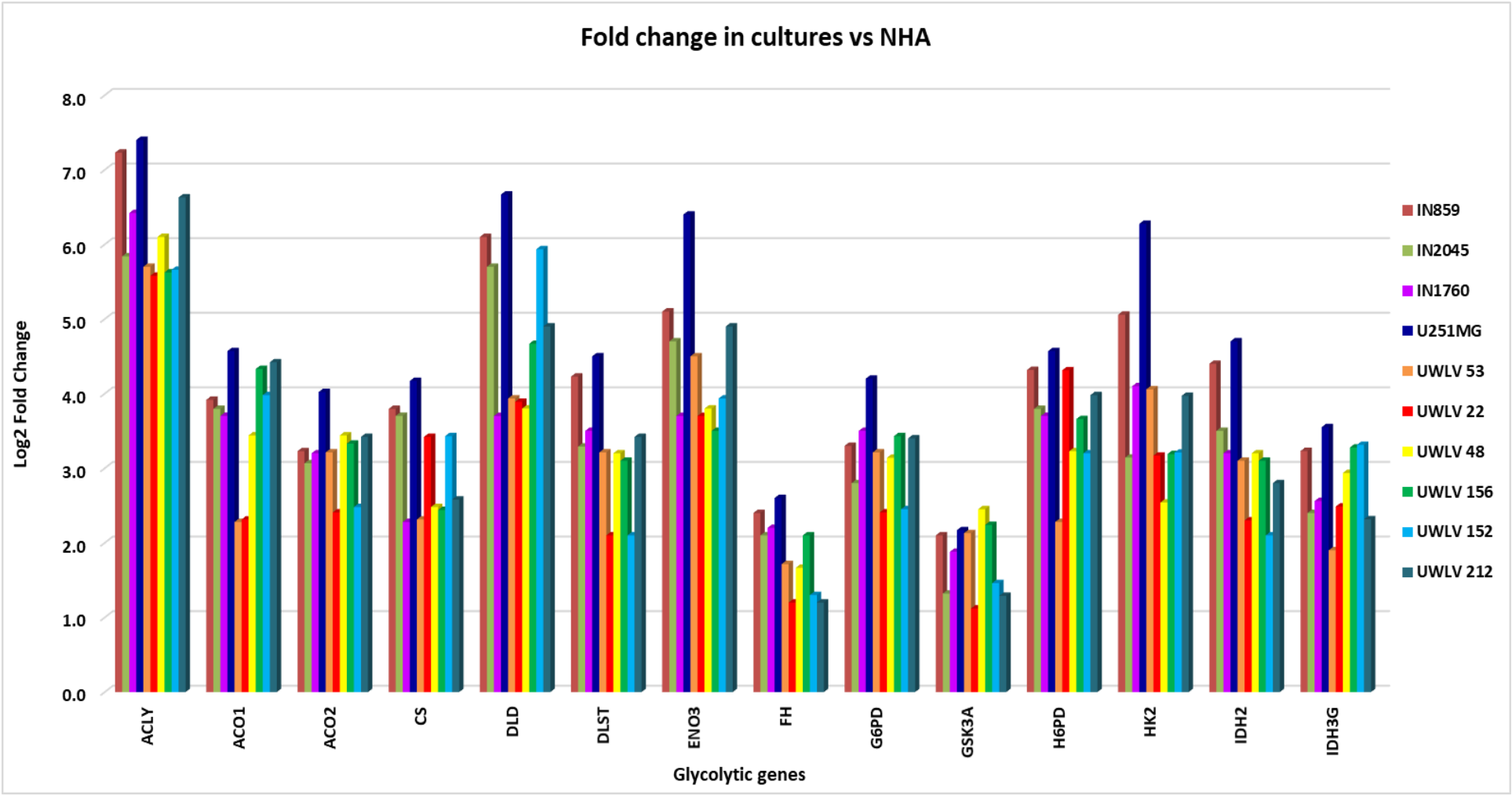

Figure 5.5a Bar chart comparing gene expression variation between the culture samples. The represented genes exhibit significantly altered levels of expression compared to NHA as shown in Figure 5.4 and Table 5.2. Expression data is shown for individual cultures to compare levels of fold change.

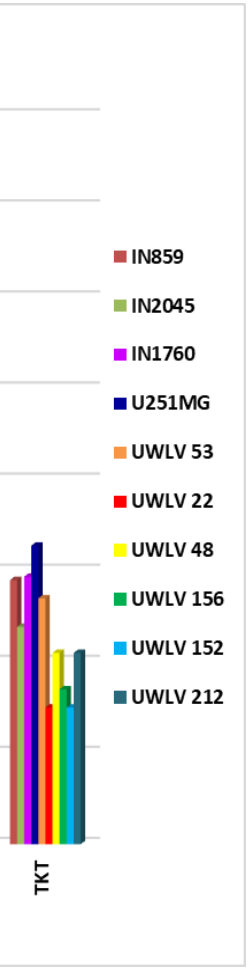

Figure 5.5b Bar chart comparing gene expression variation between the culture samples. The represented genes exhibit significantly altered levels of expression compared to NHA as shown in Figure 5.4 and Table 5.2. Expression data is shown for individual cultures to compare levels of fold change.

Comparison of glioblastoma cultures to normal brain tissue revealed a perturbed expression, the cultures were grouped in order to perform statistical calculations. Fifty-two genes in all culture samples demonstrated highly significant differences compared to normal tissue, where 50 of the genes exhibited significant overexpression ($p<0.005$) in the glioblastoma cultures. Additionally, 2 genes exhibited significant downregulation ($p<0.005$) in the glioblastoma samples, as shown in Table 5.3 and Figure 5.6. The increased fold change expression across the glycolytic genes in the cultures ranged from 2.26 (*PRPS1*) to 8.26 (*PCK2*). The variance in fold change of the genes were also examined between the individual cultures to establish the degree of homogeneity of expression levels. Minor variation in the individual gene expression between the cultures was shown, where 92% of the significantly altered genes had ≤2- fold variation between the cultures, with only 4 genes demonstrating a variance ≥2-fold change, as shown in Figure 5.7.

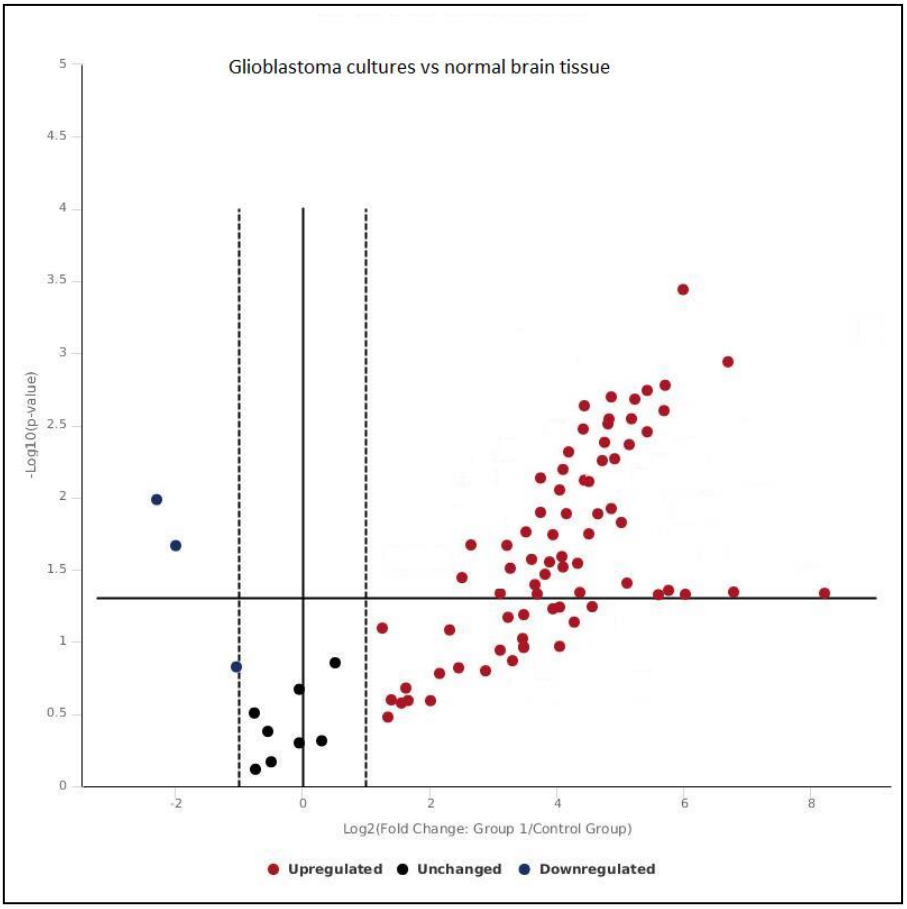

Figure 5.6 Volcano plot comparing the level of fold change across 84 genes in glioblastoma cultures (n=10). Fold change compared to normal tissue. Represented genes above the threshold all show significant change ($p<0.05$).

Table 5.3 Expression fold change values of glycolytic genes in glioblastoma cultures compared to normal brain

Gene	Log_2 Fold Change	Gene	Log_2 Fold Change
ACLY	6.18	*OGDH*	3.7
ACO1	5.29	*PC*	4.4
ACO2	3.99	*PCK2*	8.26
ALDOA	2.93	*PDHB*	3.37
BPGM	5.14	*PDK1*	2.59
CS	6.45	*PDK2*	2.8
DLD	4.88	*PDP2*	2.35
DLST	4.92	*PDPR*	5.45
ENO1	4.22	*PFKL*	2.36
ENO3	3.44	*PGAM2*	5.69
FH	4.15	*PGK1*	4.67
G6PC	2.98	*PGLS*	2.83
G6PC3	4.12	*PGM1*	3.89
G6PD	5.14	*PGM2*	3.71
GBE1	4.76	*PGM3*	2.14
GPI	4.27	*PHKB*	3
GSK3A	4.51	*PHKG2*	5.95
GSK3B	3.63	*PRPS1*	2.26
GYS1	5.46	*PRPS1L1*	3.21
H6PD	4.11	*PYGL*	3.59
HK2	6.67	*RPE*	3.05
IDH2	4.53	*RPIA*	4.73
IDH3G	2.45	*SDHA*	2.7
MDH1	2.68	*SUCLG2*	2.57
MDH2	3.57	*TKT*	3.22

Gene	Log_2 Fold Change
ALDOC	-2.81
PYGM	-2.67

Table showing fold changes in glioblastoma cultures biopsies compared to normal brain tissue. All genes show significant change ($p<0.05$) are represented in the Volcano plot.

Overexpression of multiple genes were demonstrated in both the glioblastoma biopsies and cultures compared to normal brain tissue. Notably the level of overexpression in both the biopsies and cultures were comparable in 10 of the genes, as shown in Table 5.4. Additionally, levels of overexpression were similar in the glioblastoma cultures when compared to both normal brain tissue and NHA in 30 genes as shown in Table 5.5.

Table 5.4 Expression fold change values of glycolytic genes in glioblastoma biopsies and cultures compared to normal brain

	Log2 Fold Change	
Gene	Biopsy	Culture
ALDOA	2.99	2.93
ENO1	5.07	4.22
G6PC	3.78	2.98
GYS1	5.43	5.46
HK2	5.58	6.67
MDH1	3.86	2.68
MDH2	4.85	3.57
*PCK2**	3.75	8.26
PGK1	4.04	4.67
PRPS1L1	5.85	3.21

Table showing fold change values in glioblastoma biopsies and patient derived cultures compared to normal brain tissue. All genes are significantly downregulated ($p<0.005$). * represents gene with fold change variation >2 between the biopsies and cultures.

Table 5.5 Expression fold change values of glycolytic genes in glioblastoma cultures compared to normal brain and NHA

Gene	Culture vs NHA	Culture vs normal	Gene	Culture vs NHA	Culture vs normal
ACLY	6.21	6.18	*MDH2*	3.29	3.57
ACO1	3.67	5.29	*OGDH*	2.65	3.7
ACO2	3.18	3.99	*PC*	4.42	4.4
*CS**	3.06	6.45	*PDHB*	4.76	3.37
DLD	4.93	4.88	*PDK2*	4.4	2.8
DLST	3.25	4.92	*PDP2**	4.76	2.35
ENO3	4.42	3.44	*PFKL**	5.06	2.36
*FH**	1.86	4.15	*PGAM2**	3.61	5.69
*G6PD**	3.18	5.14	*PGM3*	2.86	2.14
*GSK3A**	1.82	4.51	*PHKG2*	4.78	5.95
H6PD	3.71	4.11	*PRPS1*	3.99	2.26
*HK2**	3.87	6.67	*PRPS1L1*	2.74	3.21
IDH2	3.24	4.53	*RPE*	3.24	3.05
IDH3G	2.79	2.45	*SDHA*	1.84	2.7
MDH1	3.78	2.68	*TKT*	2.31	3.22

Table showing fold change values in patient derived cultures compared to normal brain tissue and NHA. All genes are significantly downregulated ($p<0.005$). * represents genes with fold change variation >2 between the cultures.

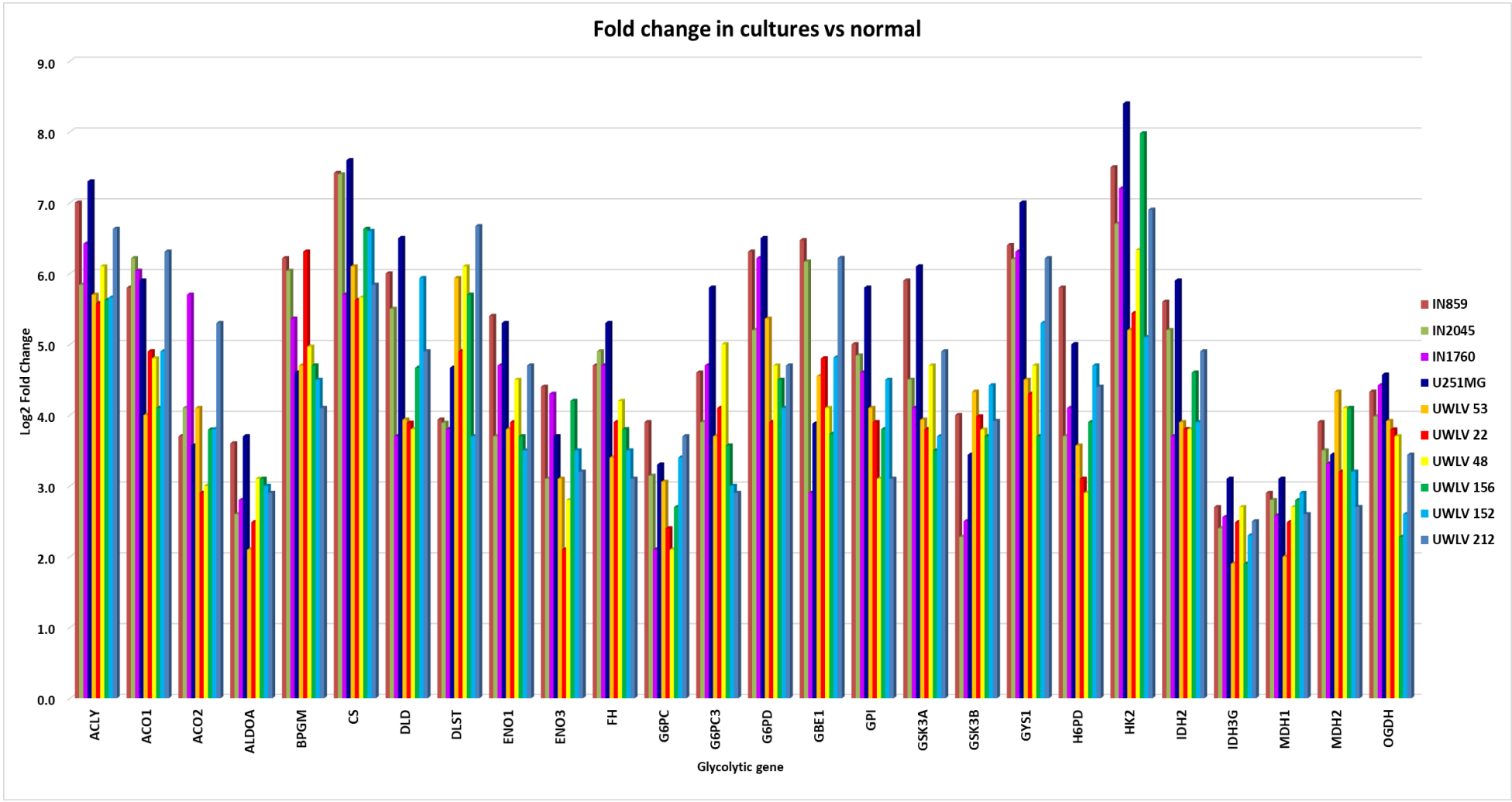

Figure 5.7a Bar chart comparing gene expression variation between the culture samples. The represented genes exhibit significantly altered levels of expression compared to normal brain as shown in Figure 5.6 and Table 5.3. Expression data is shown for individual cultures to compare levels of fold change.

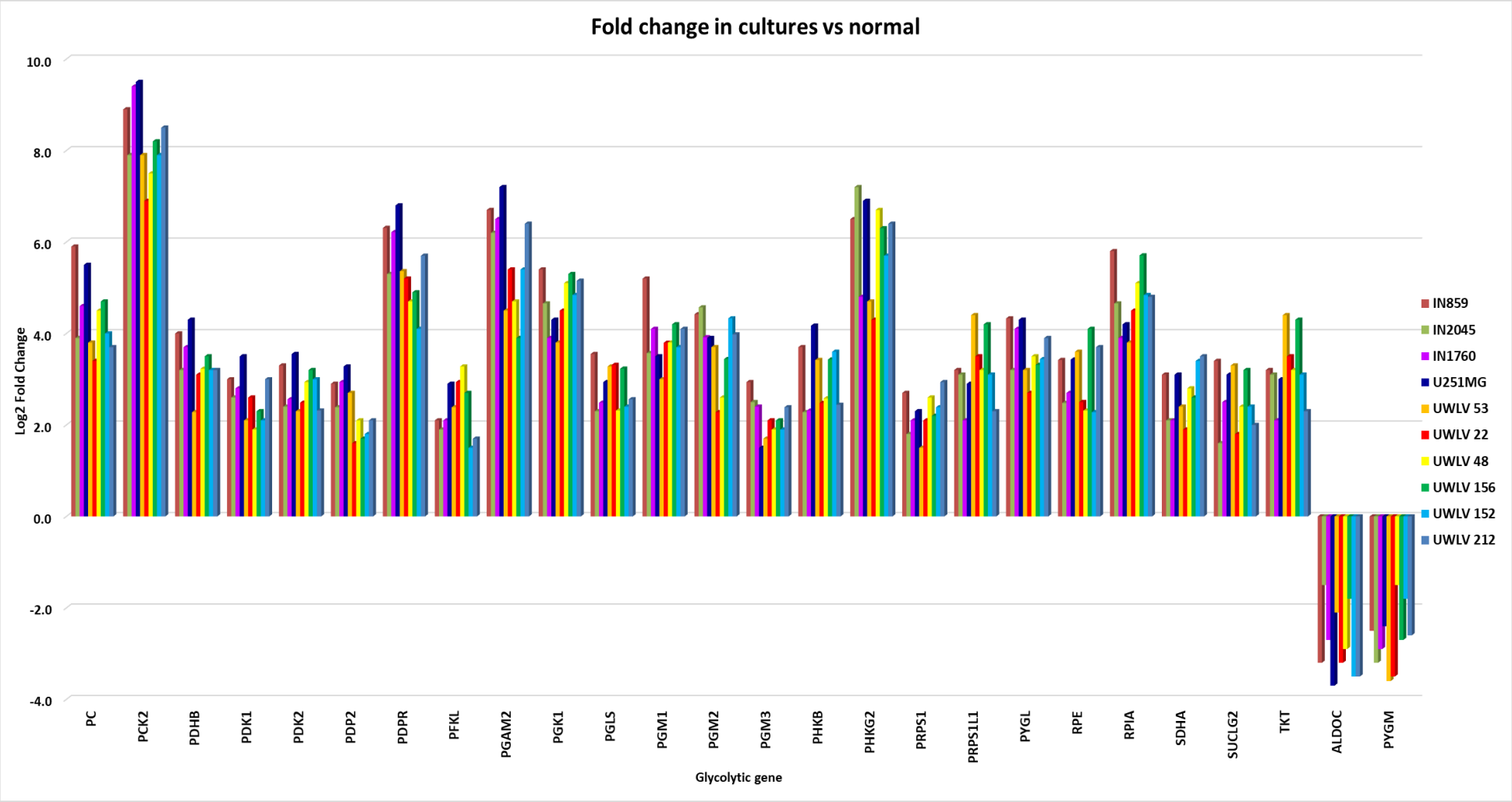

Figure 5.7b Bar chart comparing gene expression variation between the culture samples. The represented genes exhibit significantly altered levels of expression compared to normal brain as shown in Figure 5.6 and Table 5.3. Expression data is shown for individual cultures to compare levels of fold change.

5.3 Differential expression of glycolytic genes in paired glioblastoma biopsy tissue and derivative cell cultures

The glycolytic expression patterns of 6 glioblastoma tissue biopsies and their derivative paired cultures were investigated to determine whether differential expression is maintained in vitro and to confirm the validity of using patient-derived cultures as a model to investigate potential metabolic therapies. Significant overexpression ($p<0.005$) was exhibited on average in 14 of the 84 glucose pathway genes in all cultures compared to their respective glioblastoma tissue samples (n=6). No downregulation was demonstrated across any gene in the 6 paired samples, as shown in Table 5.6 and Figure 5.8. The increased fold change in expression across the glycolytic genes in the cultures ranged from 1.9 (*G6PC3*) to 4.03 (*PGM2*). Minute variation (<2-fold change) in the level of fold change was shown in 79% of the deregulated genes across all samples, indicating that the altered expression is present to a similar degree in all cultures as shown in Figure 5.9 (Table A7 shown in the appendix).

The expression profiler arrays determined overexpression in 17% glycolytic genes in the derivative cell cultures, with 14 of the 84 genes showing a significant increased level ($p<0.005$) of expression compared to their paired tissue samples. The data also shows the significant genetic similarity between the paired samples, with over 80% of the genes exhibiting comparable levels (<1-fold change) of expression across the glucose pathway, indicative of gene stability in the patient derived cultures, thus presenting as a useful tool and an accurate model for glioblastoma metabolism.

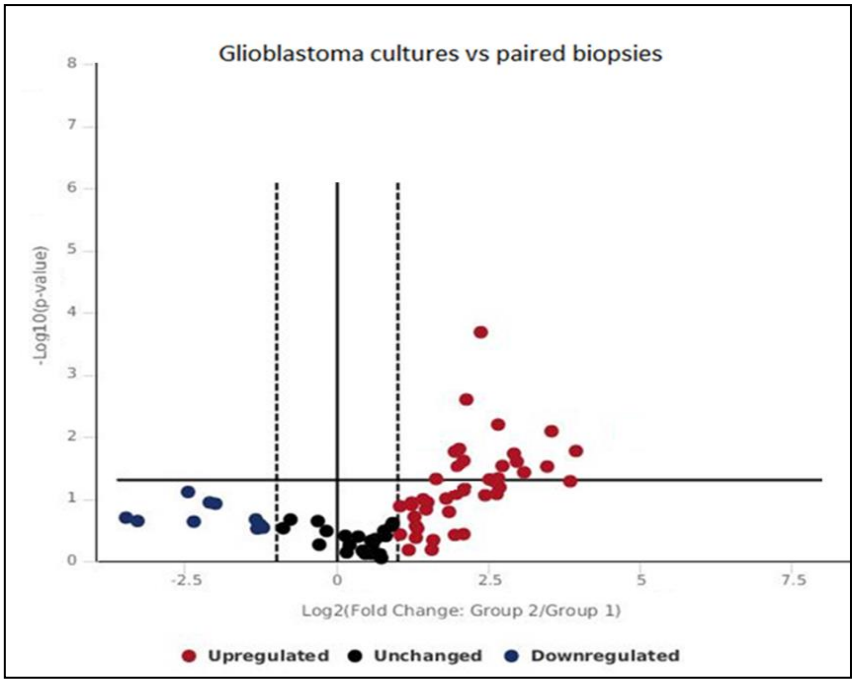

Figure 5.8 Volcano plot comparing the level of fold change across 84 genes in glioblastoma cultures. Fold change compared to the respective glioblastoma paired tissue in 6 samples. Represented genes above the threshold all show significant change ($p<0.05$).

Table 5.6 Expression fold change values of glycolytic genes in paired derivative cell cultures compared to glioblastoma biopsy tissue

Gene	Log_2 Fold Change
ACO1	2.42
ACO2	3.21
BPGM	3.86
DLAT	3.87
DLD	3.09
DLST	3.78
ENO1	2.62
G6PC3	1.9
G6PD	3.33
HK2	2.13
PDHA1	3.24
PDK2	2.26
PFKL	2.73
PGLS	3.45
PGM1	3.32
PGM2	4.03
PHKG2	3.42
PYGL	3.6
SDHB	2.89
TKT	3.54

Table showing changes in fold change in glioblastoma cultures compared to the respective glioblastoma paired tissue samples (n=6). Represented genes all show significant change ($p<0.05$) and represented in the Volcano plot, which graphs the log2 of the fold change in each gene's expression between the samples versus its p value from the t-test.

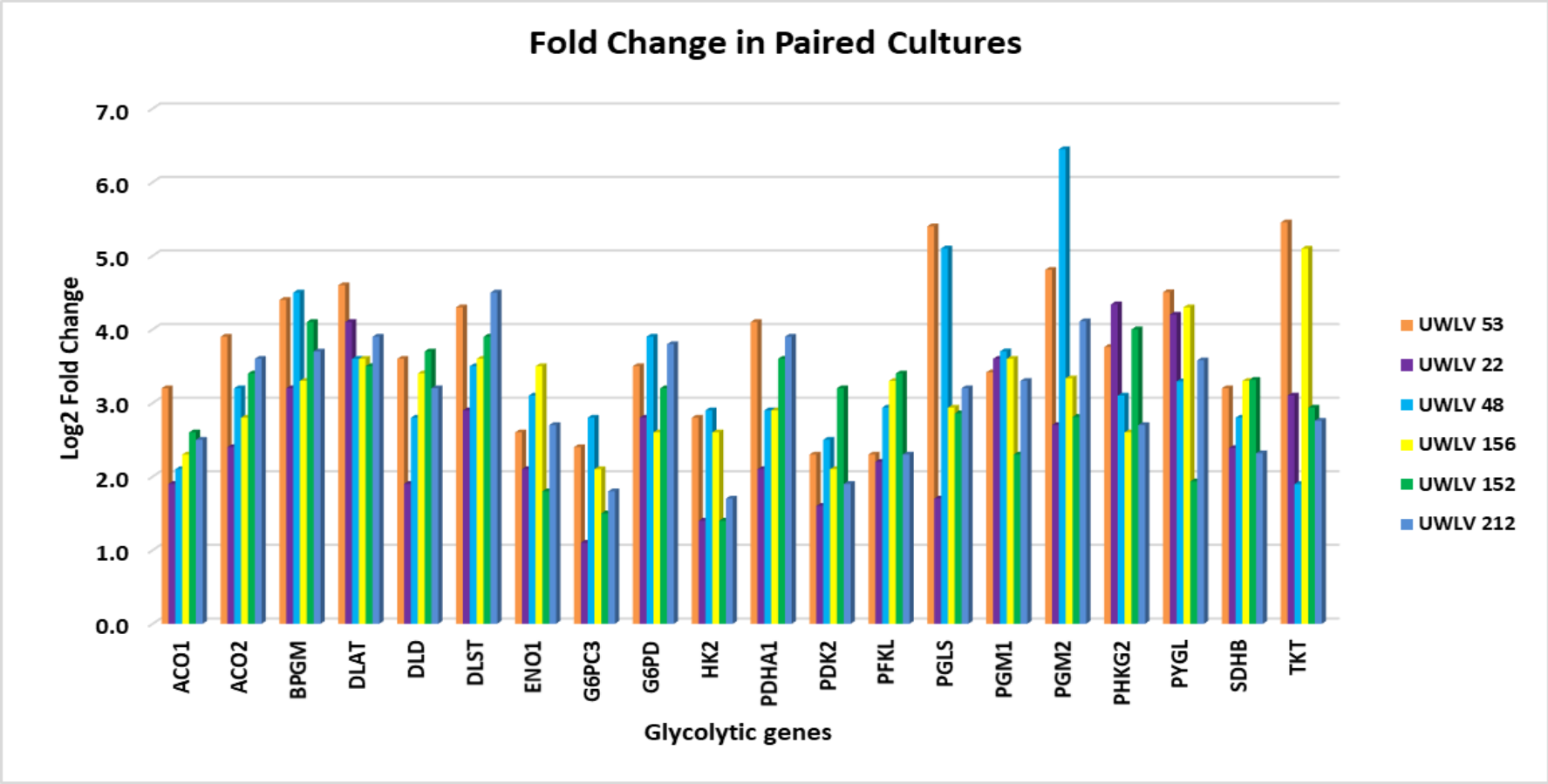

Figure 5.9 Bar chart comparing gene expression variation between the paired samples. The represented genes exhibit significantly altered levels of expression in culture compared to respective biopsy as shown in Figure 5.8 and Table 5.6. Expression data is shown for individual cultures to compare levels of fold change.

5.4 Differential expression of glycolytic genes in glioblastoma cultures under hypoxic conditions

The glycolytic expression patterns of 3 glioblastoma cultures, including 2 patient-derived cultures (IN859, IN2045) and the established cell line U251MG, were determined under hypoxic conditions compared to normoxia. Overexpression (≥2-fold change) was exhibited in 31 of the 84 glucose pathway genes in glioblastoma cultures under hypoxic conditions compared to normoxia, with additional downregulation (≤2-fold change) demonstrated in 19 of the genes as shown in Figure 5.10. The glioblastoma cultures were grouped to perform statistical calculations, where the hypoxic cultures were grouped and compared to the normoxic cultures. The data showed 13 genes with significant differences in cultures under hypoxic conditions compared to normoxia. Six of these genes were significantly overexpressed ($p<0.005$) in the hypoxic cultures, whilst a further 7 genes exhibited significant downregulation ($p<0.005$) in the hypoxic glioblastoma samples compared to the normoxic conditions, as shown in Table 5.7 and Figure 5.11. The increased fold change in expression across the glycolytic genes in the hypoxic cultures ranged from 5.03 (*PGK2*) to 6.31 (*PGK1*).

The data suggests that expression change alterations occur across a range of glycolytic pathway genes in glioblastoma when hypoxic stress is instigated. Greater than 59% of the genes in the glucose pathway demonstrate perturbed levels of expression under hypoxic conditions across all 3 glioblastoma cultures, furthermore, significant altered ($p<0.005$) mRNA levels were revealed in 15.5% of the glycolytic genes.

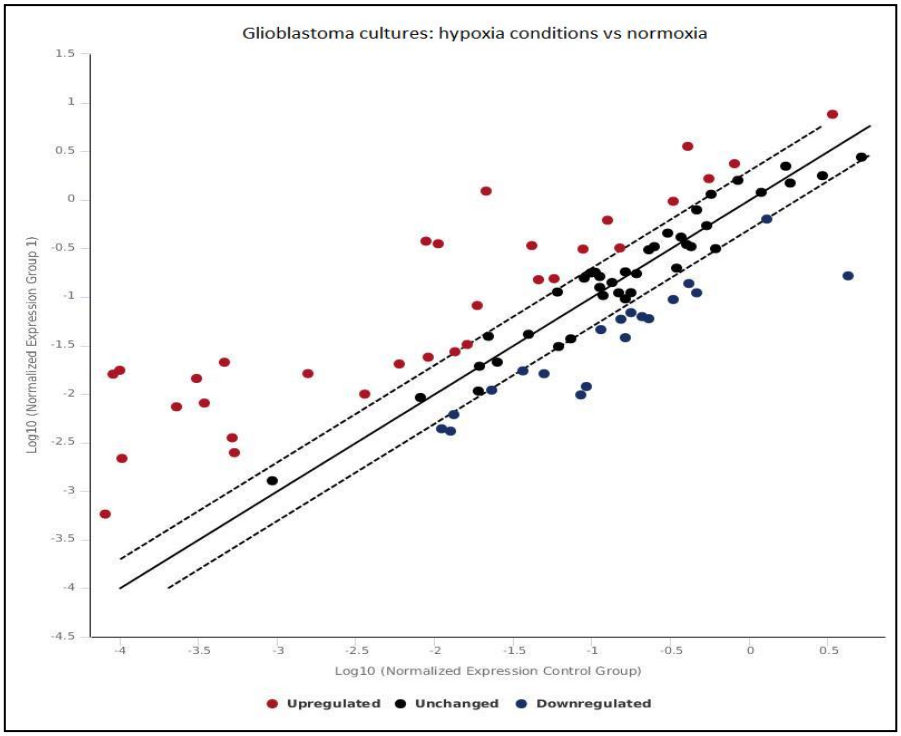

Figure 5.10 Scatter plot comparing the level of fold change across 84 genes in 3 glioblastoma cultures under hypoxic conditions compared to the respective normoxic cultures. Each dot represents the expression of a gene. The y-axis represents fold-change expression of the glioblastoma sample, the x-axis represents expression of the normal tissue control. Genes (dots) further to the right show higher expression compared to normal tissue. Higher dots represented greater expression in the glioblastoma samples.

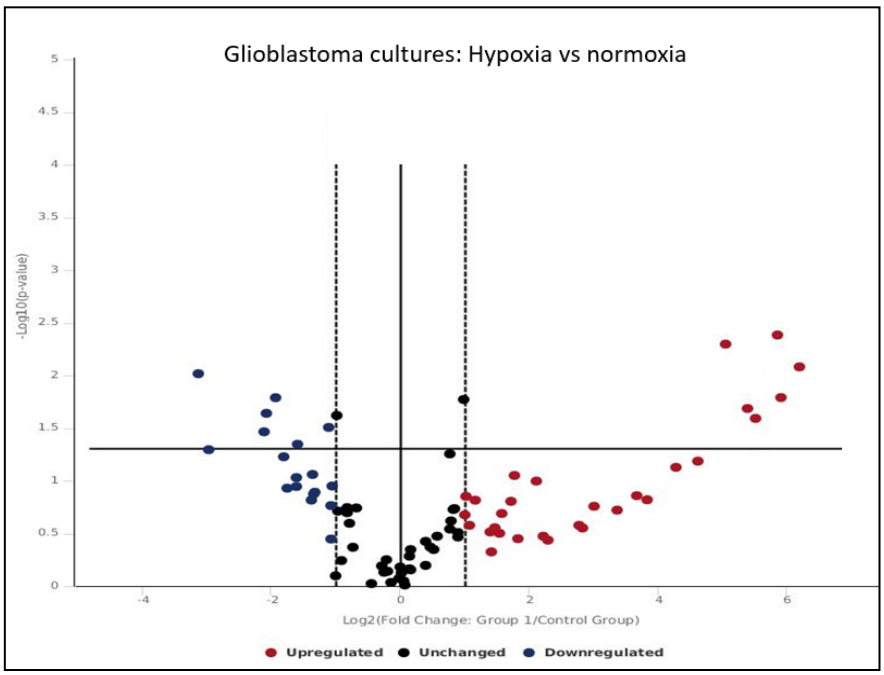

Figure 5.11 Volcano plot comparing the level of fold change across 84 genes in 3 glioblastoma cultures under hypoxia. Fold change across 84 genes in 3 glioblastoma cultures under hypoxia compared to the respective cultures under normoxic conditions in. Represented genes above the threshold all show significant change ($p<0.05$). The Volcano plot graphs the log2 of the fold change in each gene's expression between the samples versus its p value from the t-test.

Table 5.7 Expression fold change values of glycolytic genes in hypoxic cultures compared to the respective normoxic cultures

Gene	Log2 Fold Change	Gene	Log2 Fold Change
DLD	5.51	*ACLY*	-2.22
PGK1	6.31	*ACO2*	-2.73
PGM2	5.76	*DLST*	-3.52
PGK2	5.03	*GSK3A*	-1.02
SUCLG1	5.89	*H6PD*	-1.93
UGP2	5.3	*OGDH*	-2.62
		PFKL	-3.39

Table showing changes in expression levels of statistically significant genes (p=0.05) in 3 glioblastoma cultures under hypoxic conditions compared to normoxia.

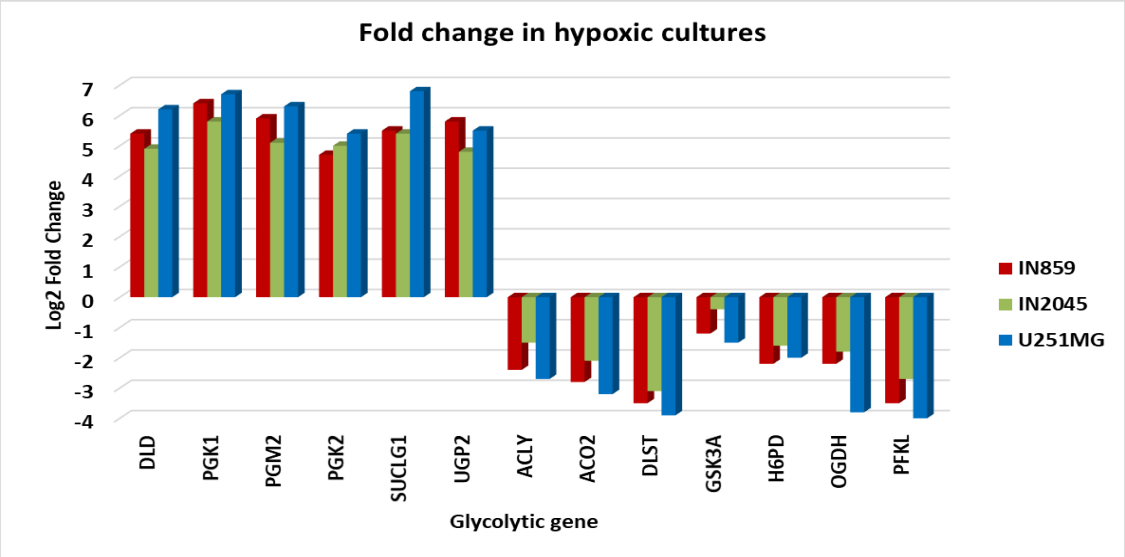

Figure 5.12 Bar chart showing gene expression variation between hypoxic cultures. The represented genes exhibit significantly altered levels of expression in culture compared to their respective cultures grown in normoxic conditions, as shown in Figure 5.11 and Table 5.6.

5.5 Differential expression of glycolytic genes after *HK2* induced CRISPR Knockout

The glycolytic expression patterns of 4 glioblastoma cultures, including 3 patient-derived cultures (IN2045, IN859, IN1979) and the established cell line U251MG, were determined in CRISPR HK2- KO cultures compared to the respective parent cultures and NHA. Overexpression (>2-fold variation) was exhibited in 15 of the 84 glucose pathway genes in *HK2* - KO cultures compared to NHA, with downregulation demonstrated in 31 of the genes. The glioblastoma cultures were grouped to perform statistical calculations, where the CRISPR HK2- KO cultures were grouped and compared to NHA. The data showed 24 genes with highly significant differences in the *HK2*-KO cultures compared to NHA. Two of these genes were significantly

overexpressed (p<0.005) in the *HK2*-KO cultures, whilst a further 22 genes exhibited significant downregulation (p<0.005) in the *HK2*-KO glioblastoma samples compared to NHA, as shown in Table 5.8 and Figure 5.13. The downregulation in fold change expression across the glycolytic genes in the *HK2*-KO cultures ranged from -1.27 (*GSK3A*) to -8.31 (*HK2*). The variance in fold change of the genes were also examined between the individual *HK2*-KO cultures to establish the degree of homogeneity in the levels of expression. An insignificant variation (<2-fold change) in the level of fold change was shown in 83% of the deregulated genes, indicating that the altered expression is present to a similar degree across all cultures. The *HK2*-KO cultures expression levels were also compared to the respective parent culture. Eighty- two of the 84 genes demonstrated altered expression values (>2-fold variation), 80 genes were shown to have down-regulated expression and 2 genes PYGM (4.21) and SDHC (2.41) exhibited overexpression across all *HK2*-KO cultures when compared to the parent cultures. 59 genes had significant downregulation (p<0.005) across all the *HK2*-KO cultures compared to the parent cultures as shown in Table 5.9 and Figure 5.14. The downregulation in fold change expression across the glycolytic genes in the *HK2*-KO cultures compared to the respective parent cultures ranged from -2.87 (*RPIA*) to -12.5 (*HK2*). Table 5.10 highlights the significant changes (p<0.05) in mRNA values for 11 glycolytic genes across all the patient derived glioblastoma cultures and the corresponding CRISPR *HK2*-KO modified cultures compared to normal tissue. Significant overexpression of the 11 glycolytic genes are identified in all parent cultures compared to normal brain tissue, however, significant downregulation of the 11 glycolytic genes was demonstrated in the *HK2*-KO downregulated cultures across all 4 culture samples. An insignificant variation (<2-fold change) in the level of fold change was shown in 93% of the deregulated genes, indicating that the altered expression is present to a similar degree across all cultures. CRISPR knockout of *HK2* promoted downregulation of gene expression across the glucose pathway with over 70% of genes significantly downregulated (p<0.005) downstream of *HK2,* compared to the corresponding parent cultures. Furthermore, CRISPR *HK2*-KO cultures demonstrated a similar expression pattern to NHA, comparatively to the respective parent cultures, with a greater number of genes (n=9) within the *HK2*-KO cultures exhibiting similar

levels of expression to NHA. The data indicates that with the HK2-KO a universal reduction in glycolytic gene expression occurs in the glioblastoma cultures, resulting in a similar expression pattern to the non-cancerous NHA culture.

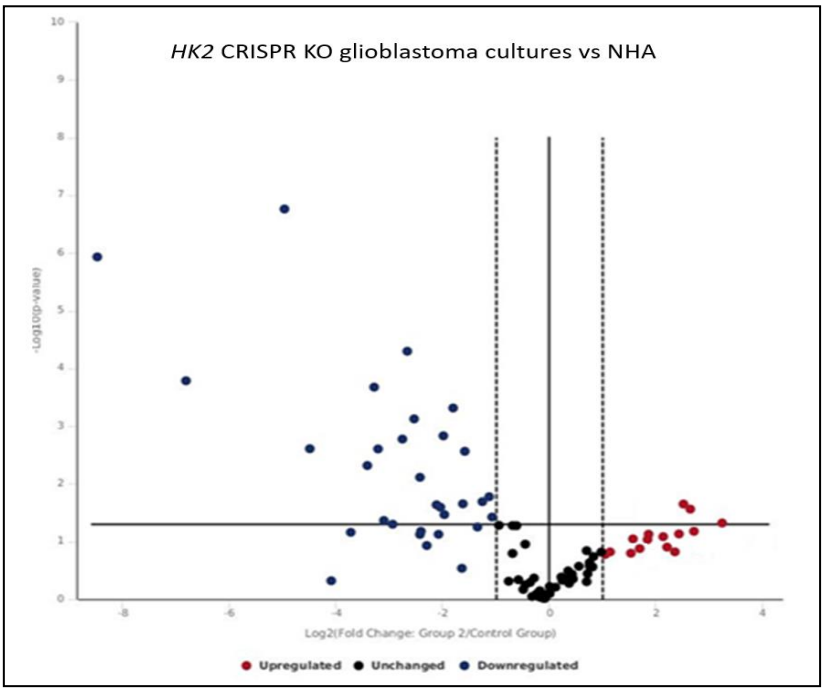

Figure 5.13 Volcano plot comparing the level of fold change across 84 genes in 4 CRISPR *HK2*- KO modified glioblastoma cultures. Fold change across 84 genes in 4 CRISPR *HK2*- KO modified glioblastoma cultures compared to NHA. Represented genes above the threshold all show significant expression change ($p<0.05$).

Table 5.8 Expression fold change values of glycolytic genes in *HK2*- KO cultures compared to NHA

Gene	Log2 Fold Change
PGM2	2.44
PGM3	2.6

Gene	Log2 Fold Change	Gene	Log2 Fold Change
ACO2	-1.3	*PC*	-6.5
ALDOC	-4.06	*PCK1*	-3.15
ENO2	-3.47	*PDK2*	-6.48
FBP1	-3.79	*PDK3*	-2.89
GSK3A	-1.27	*PDK4*	-5.9
HK2	-8.31	*PGAM2*	-4.8
HK3	-1.9	*PYGM*	-3.02
IDH3A	-2.22	*SDHA*	-2.88
IDH2	-2.34	*SDHC*	-3.59
MDH1	-4.2	*SUCLA2*	-2.91
MDH1B	-3.15	*UGP2*	-1.54

Table showing changes in fold change average in 4 CRISPR *HK2*-KO modified glioblastoma cultures compared to NHA. Represented genes all show significant change ($p<0.05$).

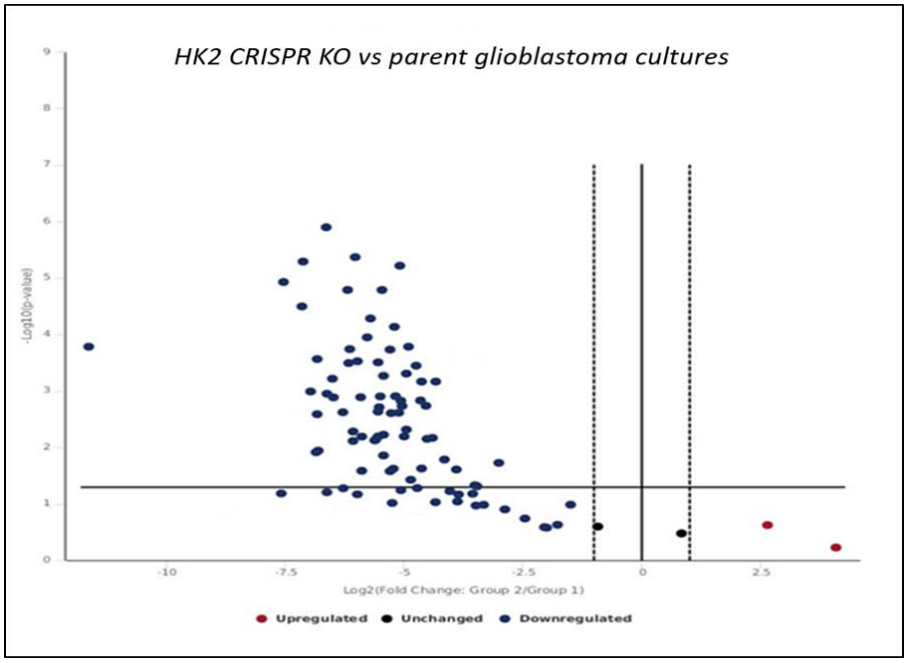

Figure 5.14 Volcano plot comparing the level of fold change across 84 genes in 4 CRISPR *HK2*- KO modified glioblastoma cultures. Fold change across 84 genes in 4 CRISPR *HK2*- KO modified glioblastoma cultures compared to the respective parent cultures. Represented genes above the threshold all show significant expression change ($p<0.05$).

Table 5.9 Expression fold change values of glycolytic genes in *HK2*- KO cultures and parent cultures compared to normal brain tissue

	Log_2 Fold Change	
Gene	**Parent**	**CRISPR**
ACO2	14.5	-4.52
ALDOA	54.13	-6.61
GSK3A	32.4	-3.84
HK2	820.97	-12.5
HK3	4.63	-6.75
IDH2	15.34	-6.65
IDH3A	20.47	-4.1
MDH1	11.83	-5.33
PC	8.65	-4.47
PDK2	19.58	-6.97
PGAM2	11.98	-4.86

Table showing changes in fold change values in patient derived glioblastoma cultures and corresponding CRISPR *HK2*-KO modified cultures compared to normal tissue. Represented genes all show significant change ($p<0.05$).

Table 5.10 Expression fold change values of glycolytic genes in *HK2*- KO cultures compared to the respective parent cultures

Gene	Log_2 Fold Change	Gene	Log_2 Fold Change
ACLY	-5.89	*IDH2*	-6.65
ACO2	-4.52	*IDH3A*	-4.1
AGL	-2.76	*MDH1*	-5.33
ALDOA	-6.61	*MDH2*	-5.01
ALDOB	-6.63	*OGDH*	-7.09
ALDOC	-4.28	*PC*	-4.47
BPGM	-4.18	*PCK1*	-5.36
CS	-4.67	*PCK2*	-5.3
DLAT	-3.46	*PDK1*	-4.59
DLST	-6.53	*PDK2*	-6.97
ENO2	-5.47	*PDK3*	-3.99
ENO3	-4.58	*PDP2*	-4.91
FBP1	-4.76	*PDPR*	-6.01
FH	-4.27	*PFKL*	-6.3
G6PC	-6.95	*PGAM2*	-4.86
G6PC3	-4.77	*PGK2*	-4.27
G6PD	-7.3	*PGLS*	-6.6
GALM	-5.69	*PGM2*	-6.61
GBE1	-6.19	*PGM3*	-5.7
GCK	-5.84	*PHKB*	-5.13
GPI	-5.52	*PHKG1*	-6.28
GSK3A	-3.84	*PKLR*	-4.6
GSK3A	-5.88	*PYGM*	-5.14
GSK3B	-4.73	*RBKS*	-4.77
GYS1	-5.3	*RPE*	-4.19
GYS2	-6.93	*RPIA*	-2.87
H6PD	-3.74	*SDHA*	-4.87
HK2	-12.5	*SDHD*	-5.82
HK3	-6.75	*SUCLA2*	-6.13

Table showing changes in fold change values in CRISPR *HK2*-KO modified glioblastoma cultures compared to corresponding patient derived cultures. Represented genes all show significant change ($p<0.05$).

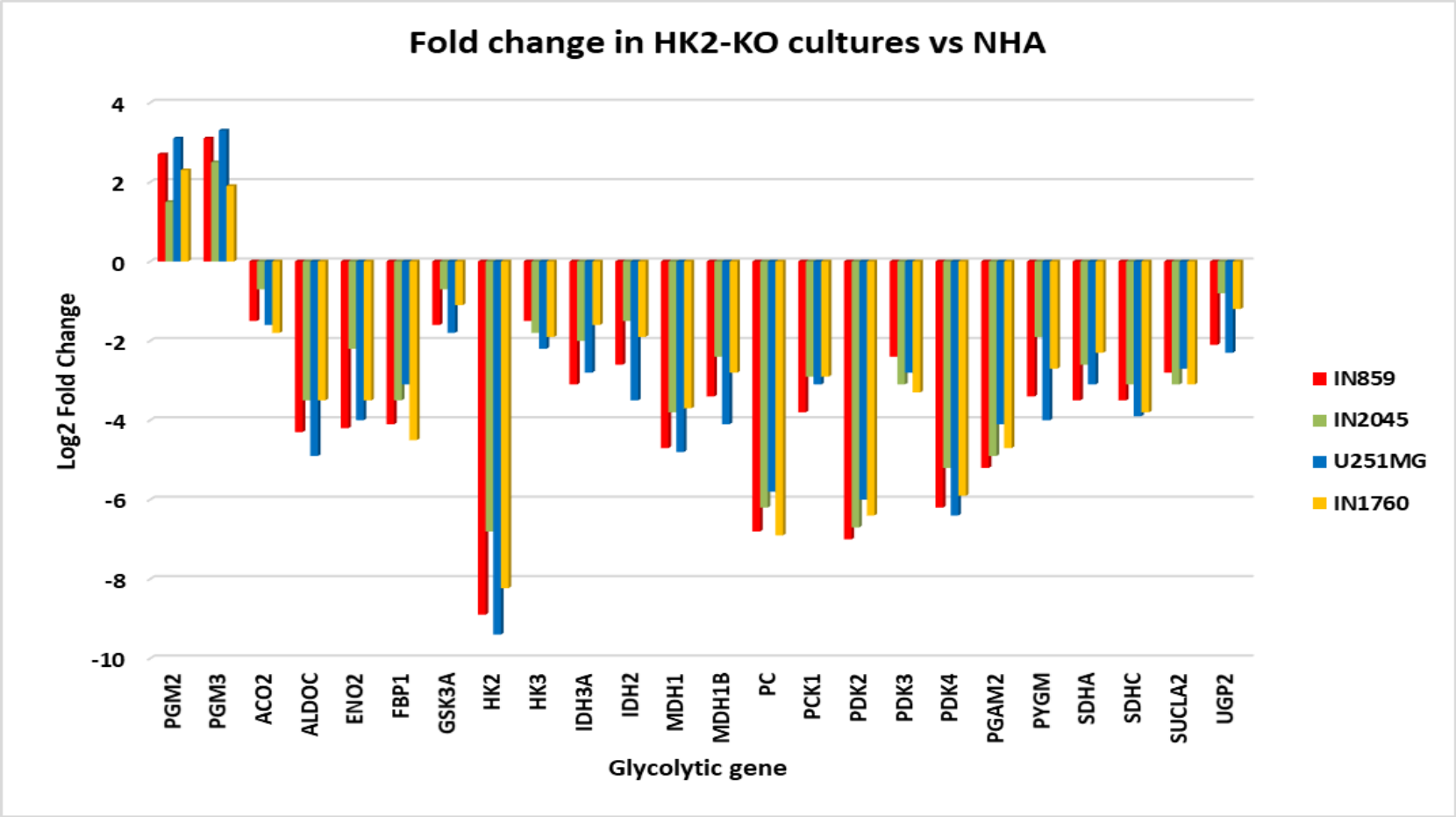

Figure 5.15 Bar chart comparing gene expression variation between *HK2*- KO modified glioblastoma cultures compared to NHA. The represented genes exhibit significantly altered levels of expression in the cultures compared to NHA as shown in Figure 5.13 and Table 5.8. Expression data is shown for individual cultures to compare levels of fold change.

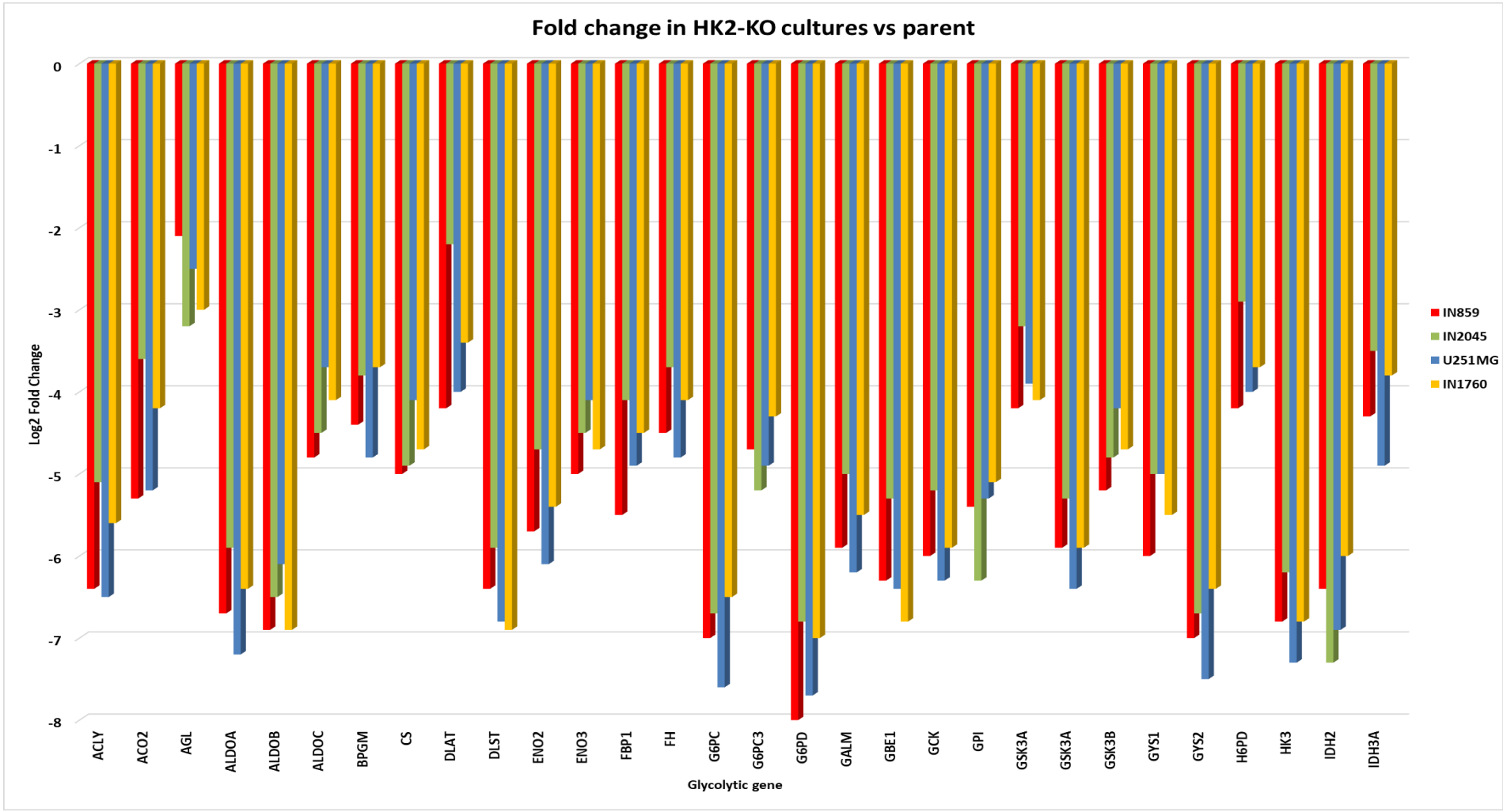

Figure 5.16a Bar chart comparing gene expression variation between *HK2*- KO modified glioblastoma cultures compared to the respective parent. The represented genes exhibit significantly altered levels of expression in the cultures compared to the parent culture as shown in Figure 5.14 and Table 5.9. Expression data is shown for individual cultures to compare levels of fold change.

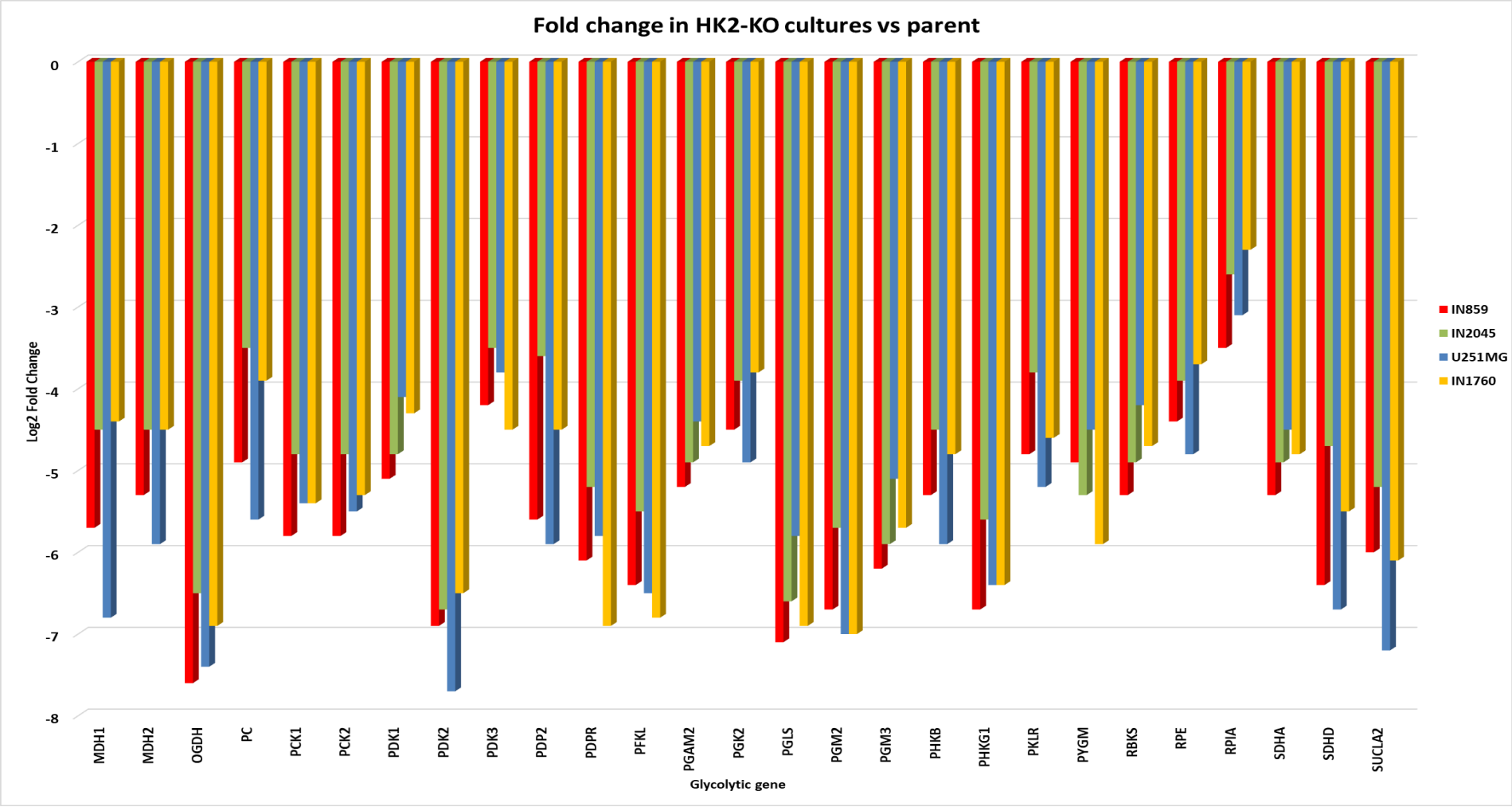

Figure 5.16b Bar chart comparing gene expression variation between *HK2*- KO modified glioblastoma cultures compared to the respective parent. The represented genes exhibit significantly altered levels of expression in the cultures compared to the parent culture as shown in Figure 5.14 and Table 5.9. Expression data is shown for individual cultures to compare levels of fold change.

5.6 Differential expression of glycolytic genes via multiple inhibitory methods

The glycolytic expression patterns of 3 glioblastoma cultures, including 2 patient-derived cultures and the cell line U251MG, was investigated after treatment with a specific inhibitor compared to the respective untreated cultures. The selected cultures represented both a high (IN859) and a low (IN2045) expressing *HK2* sample.

5.6.1 Differential expression of glycolytic genes after 3-HB supplementation

Three glioblastoma cultures were supplemented with the ketone body 3-HB at 500μM for 72 hours, as an alternative energy source in glucose deprived cultures, as described in Material and Methods and Chapter 4.6. The expression levels in the treated cultures were compared to the respective non-treated culture. Eighty- two of the 84 glycolytic genes displayed down-regulated expression (≤2-fold change) ranging from -1.96 to -9.8- fold change and 1 gene exhibited overexpression (2.5-fold change) across all 3-HB supplemented cultures when compared to the respective cultures grown in normal glucose (6mM) conditions. Sixty genes demonstrated significant downregulation ($p<0.005$) across all the 3-HB supplemented glioblastoma culture compared to the respective cultures grown in normal glucose conditions, as shown in Table 5.11 and Figure 5.17.

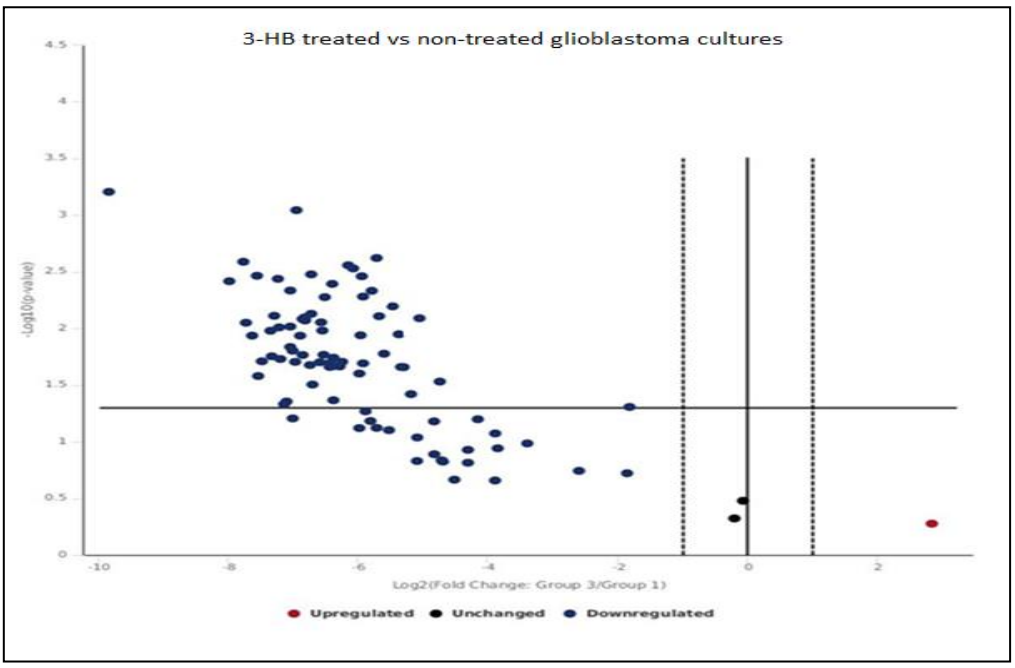

Figure 5.17 Volcano plot comparing the level of fold change in gene expression across 84 genes in 3 glioblastoma cultures supplemented with the ketone body 3-HB. Fold change in

gene expression compared to the respective cultures grown in normal glucose conditions. Represented genes above the threshold all show significant change ($p<0.05$)

Table 5.11 Expression fold change values of glycolytic genes in 3-HB supplemented cultures compared to the respective cultures grown in normal glucose conditions

Gene	Log_2 Fold Change	Gene	Log_2 Fold Change
ACLY	-5.12	*PCK2*	-5.85
ACO1	-7.75	*PDHA1*	-6.83
ACO2	-6.48	*PDHB*	-7.08
AGL	-6.96	*PDK1*	-7.87
ALDOA	-7.89	*PDK2*	-5.14
BPGM	-7.5	*PDK3*	-7.46
CS	-6.34	*PDP2*	-7.26
DLAT	-8.43	*PDPR*	-6.81
DLD	-5.88	*PFKL*	-7.59
DLST	-6.88	*PGAM2*	-6.21
ENO2	-7.02	*PGK1*	-6.3
FBP1	-6.41	*PGLS*	-7.87
FH	-6.76	*PGM1*	-6.38
G6PC3	-7.1	*PGM2*	-6.73
G6PD	-9.8	*PGM3*	-7.24
GBE1	-7.98	*PHKB*	-7.22
GPI	-6.98	*PHKG1*	-7.08
GSK3A	-5.96	*PHKG2*	-6.69
GSK3B	-6.35	*PKLR*	-6.1
GYS1	-7.78	*PRPS1*	-7.93
H6PD	-6.44	*PRPS1L1*	-5.65
HK2	-8.29	*PYGL*	-7.94
HK3	-6.41	*PYGM*	-6.4
IDH2	-6.11	*RBKS*	-7.62
IDH3A	-7.78	*RPE*	-7.85
IDH3B	-5.06	*RPIA*	-6.83
IDH3G	-6.41	*SDHA*	-6.28
MDH1	-5.32	*SDHD*	-6.3
MDH2	-5.98	*SUCLG2*	-6.84
OGDH	-6.19	*TPI1*	-7.52

Table showing changes in fold change values in 3- supplemented cultures compared to the respective cultures grown in normal glucose conditions. Represented genes all show significant change ($p<0.05$).

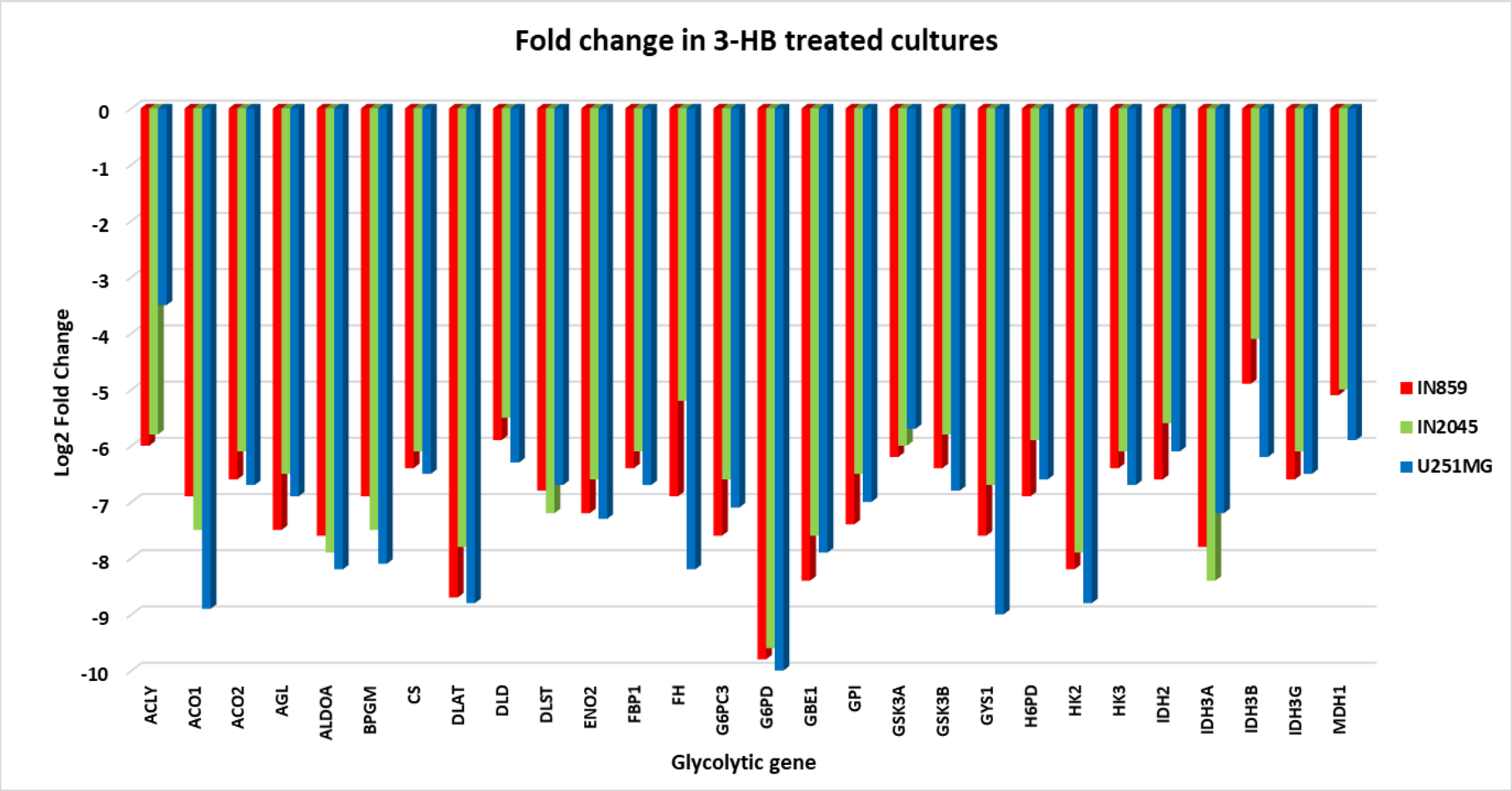

Figure 5.18a Bar chart comparing gene expression variation between 3-HB treated glioblastoma cultures compared to the respective parent. The represented genes exhibit significantly altered levels of expression in the cultures compared to the parent culture as shown in Figure 5.17 and Table 5.11. Expression data is shown for individual cultures to compare levels of fold change.

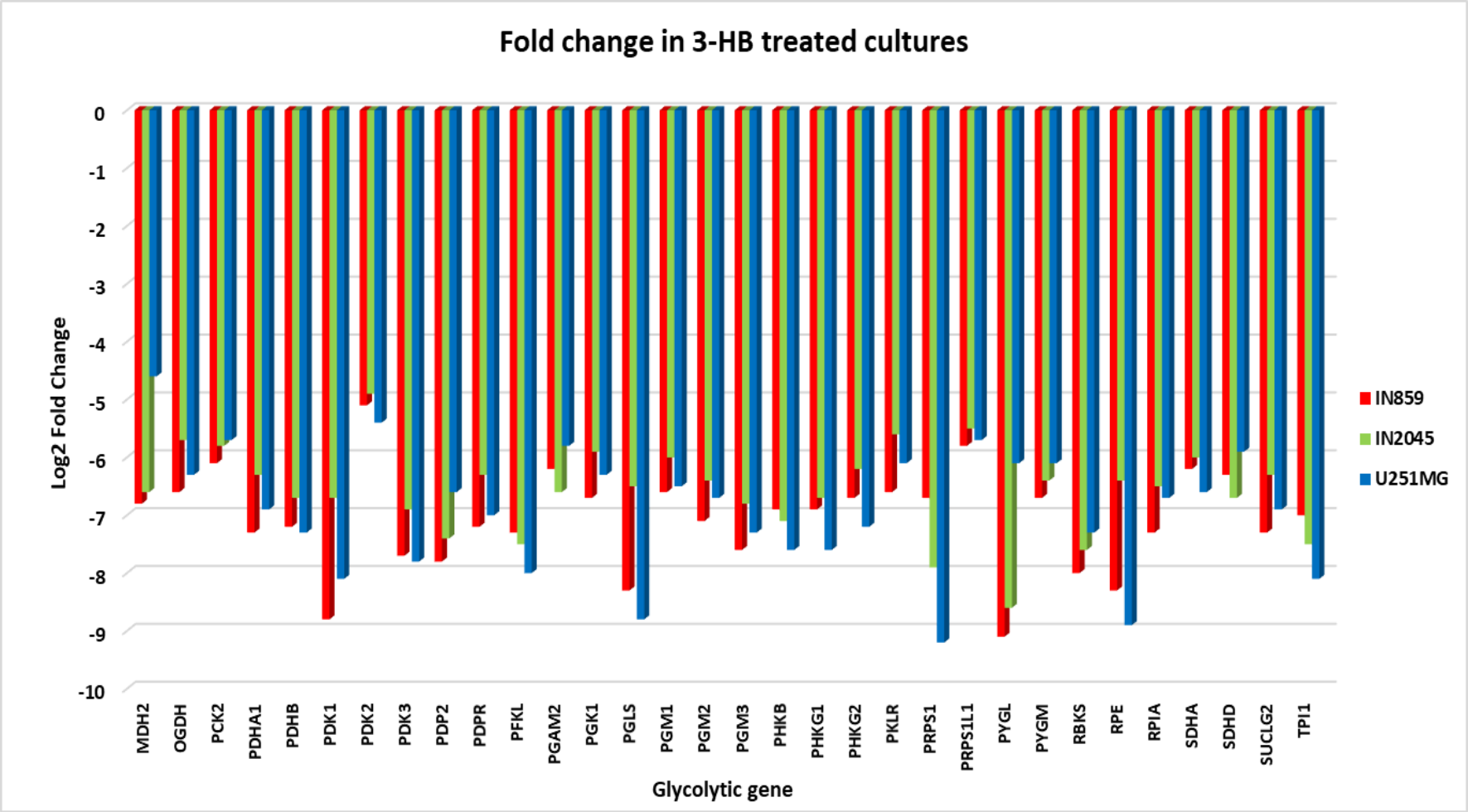

Figure 5.18b Bar chart comparing gene expression variation between 3-HB treated glioblastoma cultures compared to the respective parent. The represented genes exhibit significantly altered levels of expression in the cultures compared to the parent culture as shown in Figure 5.17 and Table 5.11. Expression data is shown for individual cultures to compare levels of fold change.

5.6.2 Differential expression of glycolytic genes after 72-hour 3-BPA treatment

Three glioblastoma cultures were treated with the *HK2* inhibitor 3-BPA at culture-specific ID_{50} values for 72 hours, as stated in 4.3.1. The expression levels were compared to the respective non-treated culture. 76 of the 84 genes demonstrated altered expression values, including 75 genes showing down-regulated expression (1.1 to 8.2- fold change) and 1 gene with overexpression (3.9- fold change) in all the 3-BPA treated cultures when compared to the respective non-treated cultures. 42 genes demonstrating significant downregulation ($p<0.005$) across all the 3-BPA treated glioblastoma samples compared to the respective non-treated cultures, as shown in Table 5.12 and Figure 5.19. The downregulation in fold change expression across the glycolytic genes in the 3-BPA treated cultures ranged from -4.66 (*FH*) to -8.35 (*PCK2*). An insignificant variation (<2-fold change) in the level of fold change was shown in 76% of the deregulated genes, indicating that the altered expression is present to a similar degree across all cultures.

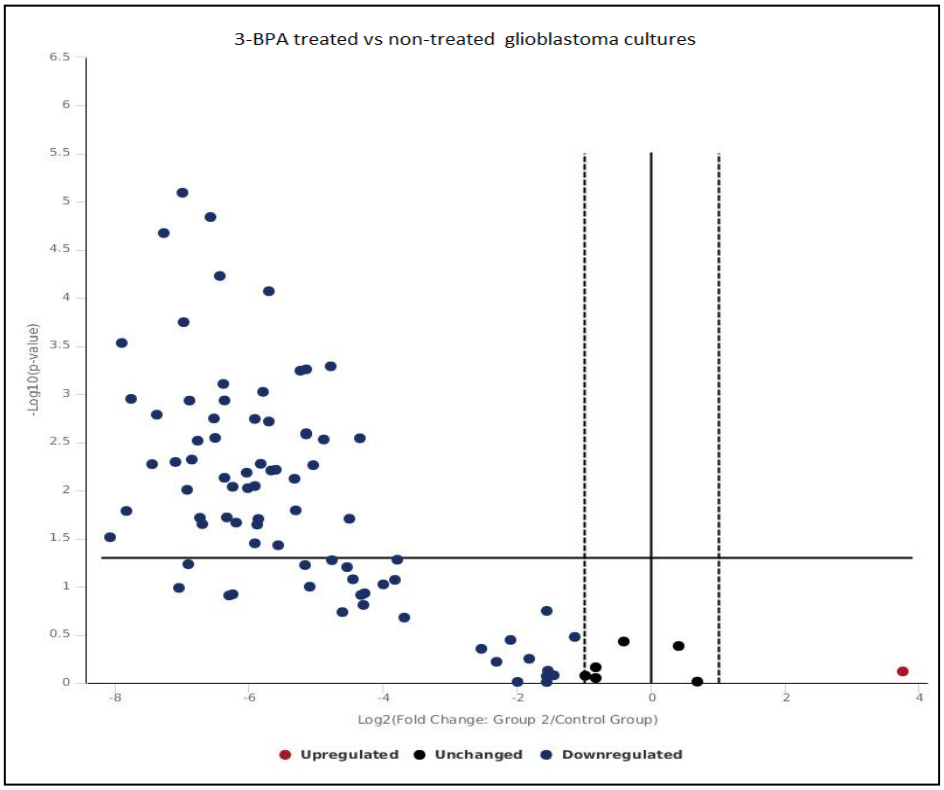

Figure 5.19 Volcano plot comparing the level of fold change across 84 genes in 3 glioblastoma cultures treated with *HK2* inhibitor 3-BPA. Fold change in gene expression at the relevant ID_{50} value, compared to the respective non-treated cultures. Represented genes above the threshold all show significant change ($p<0.05$).

Table 5.12 Expression fold change values of glycolytic genes in 3-BPA treated cultures compared to non-treated cultures

Gene	Log_2 Fold Change	Gene	Log_2 Fold Change
ACLY	-6.73	*MDH1*	-6.13
ACO1	-5.47	*MDH2*	-5.67
ACO2	-7.58	*OGDH*	-5.7
AGL	-5.6	*PC*	-7.51
ALDOA	-6.82	*PCK2*	-8.35
BPGM	-6.74	*PDHA1*	-5.26
CS	-5.76	*PDHB*	-5.08
DLAT	-6.02	*PDK2*	-6.05
DLST	-5.4	*PDP2*	-6.91
FH	-4.66	*PDPR*	-6.09
G6PD	-8.26	*PFKL*	-7.72
GPI	-5.63	*PGAM2*	-4.84
GSK3A	-7.71	*PGLS*	-8.08
GSK3B	-7.23	*PGM1*	-5.63
GYS1	-6.87	*PHKB*	-8.28
H6PD	-7.87	*PHKG2*	-5.78
HK2	-8.15	*PRPS1*	-6.36
IDH2	-7.69	*PYGL*	-5.59
IDH3A	-6.2	*RPIA*	-5.63
IDH3B	-7.84	*SDHA*	-6.68
IDH3G	-6.75	*TKT*	-7.75

Table showing changes in fold change values in 3-BPA treated and corresponding non-treated glioblastoma cultures. Represented genes all show significant change ($p<0.05$).

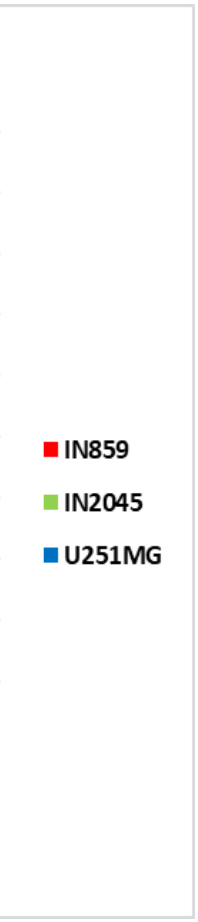

Figure 5.20a Bar chart comparing gene expression variation between 3-BPA treated glioblastoma cultures compared to the respective parent. The represented genes exhibit significantly altered levels of expression in the cultures compared to the parent culture as shown in Figure 5.19 and Table 5.12. Expression data is shown for individual cultures to compare levels of fold change.

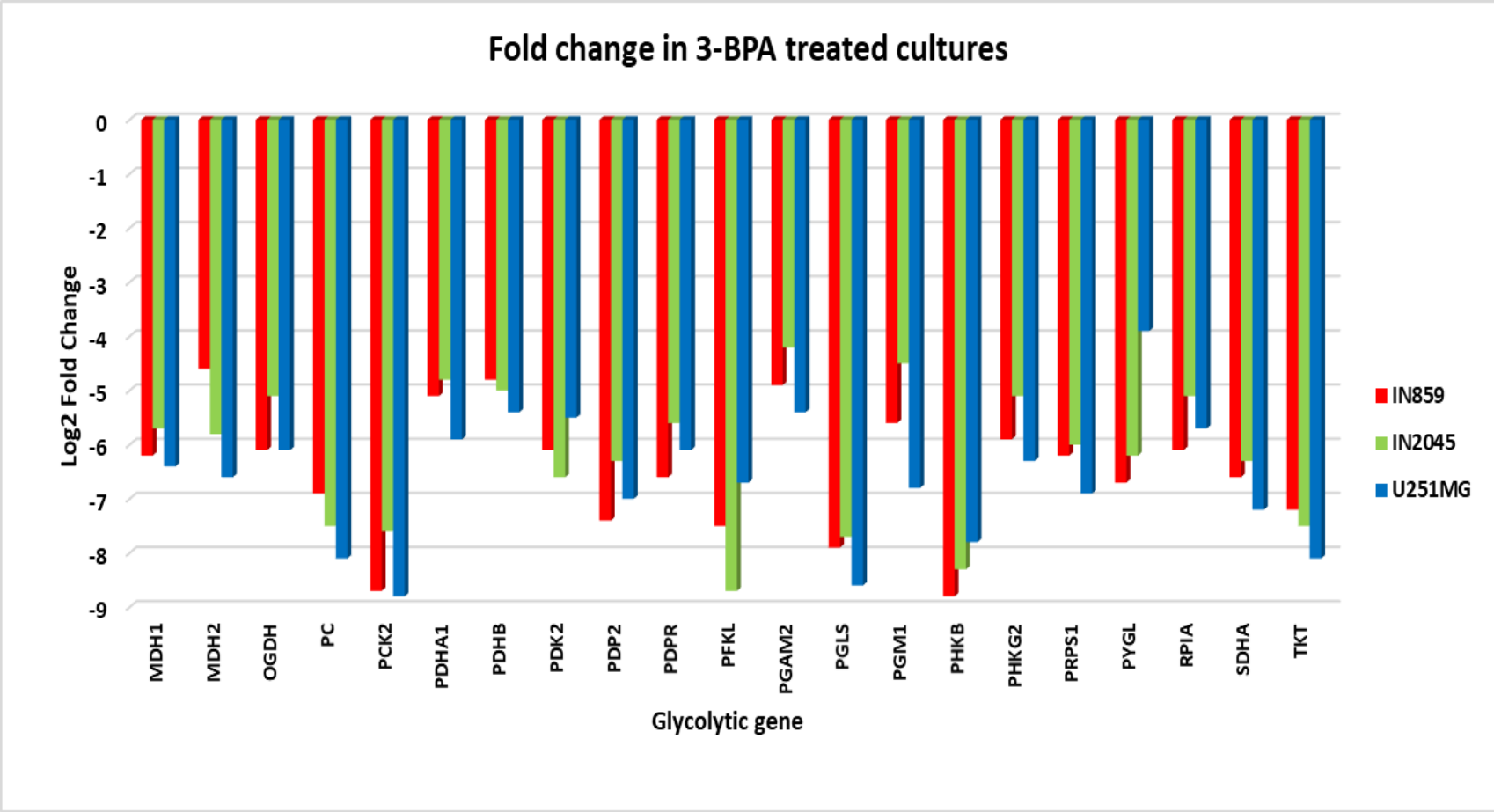

Figure 5.20b Bar chart comparing gene expression variation between 3-BPA treated glioblastoma cultures compared to the respective parent. The represented genes exhibit significantly altered levels of expression in the cultures compared to the parent culture as shown in Figure 5.19 and Table 5.12. Expression data is shown for individual cultures to compare levels of fold change

5.6.3 Differential expression of glycolytic genes after 72-hour metformin treatment

Three glioblastoma cultures were treated with metformin at culture specific ID_{50} values over 72 hours, as stated in 4.3.2. The expression levels were compared to the respective non-treated culture, and 71 of the 84 genes demonstrated altered expression values, including 74 genes showing down-regulated expression (2.02 to 7.98- fold change) and 1 gene exhibited overexpression (1.3- fold change) across all metformin treated cultures. 50 genes demonstrated significant downregulation ($p<0.005$) across all the metformin treated glioblastoma samples compared to the respective non-treated cultures, as shown in Table 5.13 and Figure 5.21. The downregulation in mRNA fold change expression across the glycolytic genes in the metformin treated cultures ranged from -3.33 (*RPE*) to -8.14 (*PFKL*). An insignificant variation (<2-fold change) in the level of fold change was shown in 84% of the deregulated genes, indicating that the altered expression is present to a similar degree across all cultures.

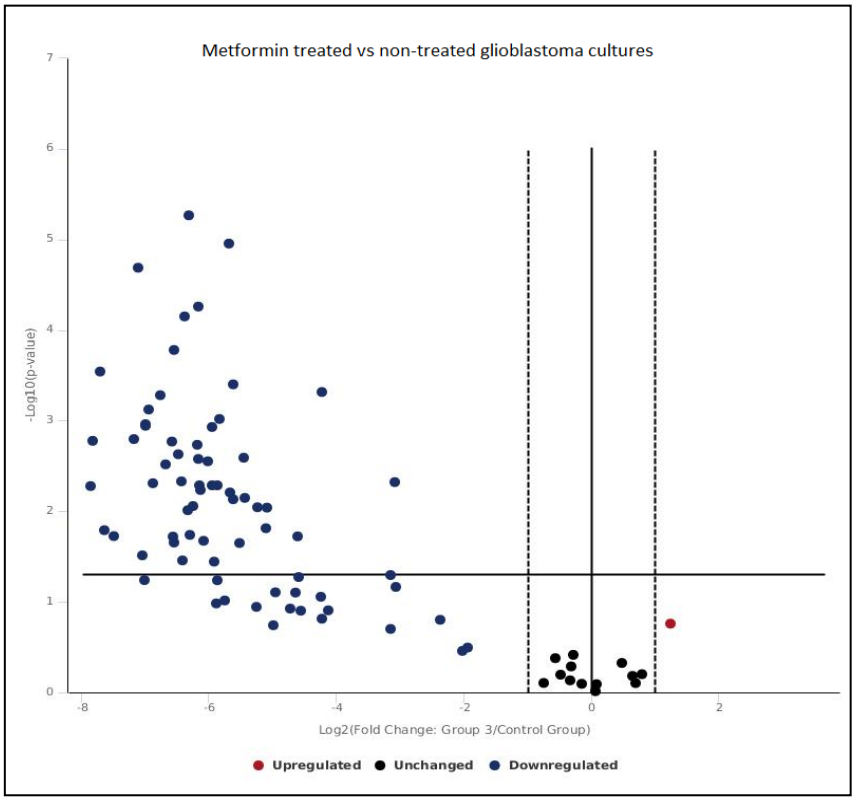

Figure 5.21 Volcano plot comparing the level of fold change across 84 genes in 3 glioblastoma cultures treated with metformin. Fold change in gene expression at the relevant ID_{50} value, compared to the respective non-treated cultures. Represented genes above the threshold all show significant change ($p<0.05$).

Table 5.13 Expression fold change values of glycolytic genes in metformin treated cultures compared to non-treated cultures

Gene	Log_2 Fold Change	Gene	Log_2 Fold Change
ACLY	-4.92	*MDH2*	-4.97
ACO1	-6.47	*OGDH*	-5.18
ACO2	-7.51	*PC*	-4.95
AGL	-5.22	*PCK2*	-5.49
ALDOA	-6.54	*PDHA1*	-6.25
BPGM	-7.16	*PDHB*	-6.23
CS	-6.42	*PDK1*	-5.3
DLAT	-5.91	*PDK2*	-6.28
DLD	-6.73	*PDP2*	-7.83
DLST	-8.11	*PDPR*	-6.34
ENO1	-7.94	*PFKL*	-8.14
ENO3	-6.51	*PGAM2*	-6.67
FH	-7.83	*PGK1*	-4.56
G6PD	-7.91	*PGLS*	-7.35
GBE1	-4.72	*PGM1*	-5.89
GPI	-7.93	*PGM2*	-5.67
GSK3A	-6.1	*PGM3*	-4.34
GSK3B	-6.62	*PHKB*	-6.97
GYS1	-4.94	*PHKG2*	-7.65
H6PD	-4.03	*PRPS1*	-7.51
HK2	-6.93	*PYGL*	-5.34
IDH2	-5.39	*RPE*	-3.33
IDH3A	-5.01	*RPIA*	-4.6
IDH3G	-7.05	*SDHA*	-7.69
MDH1	-5.09	*TKT*	-7.95

Table showing changes in fold change values in metformin treated and corresponding non-treated glioblastoma cultures. Represented genes all show significant change ($p<0.05$).

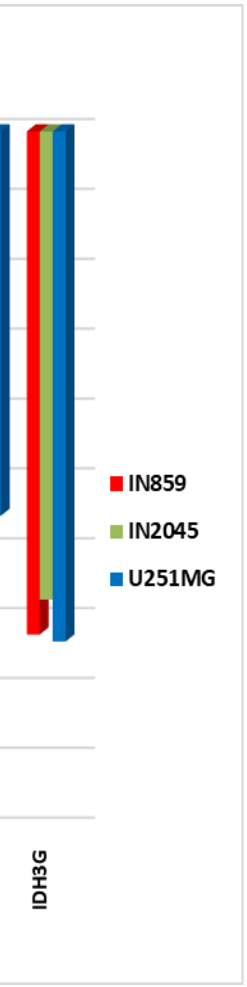

Figure 5.22a Bar chart comparing gene expression variation between metformin treated glioblastoma cultures compared to the respective parent. The represented genes exhibit significantly altered levels of expression in the cultures compared to the parent culture as shown in Figure 5.21 and Table 5.13. Expression data is shown for individual cultures to compare levels of fold change.

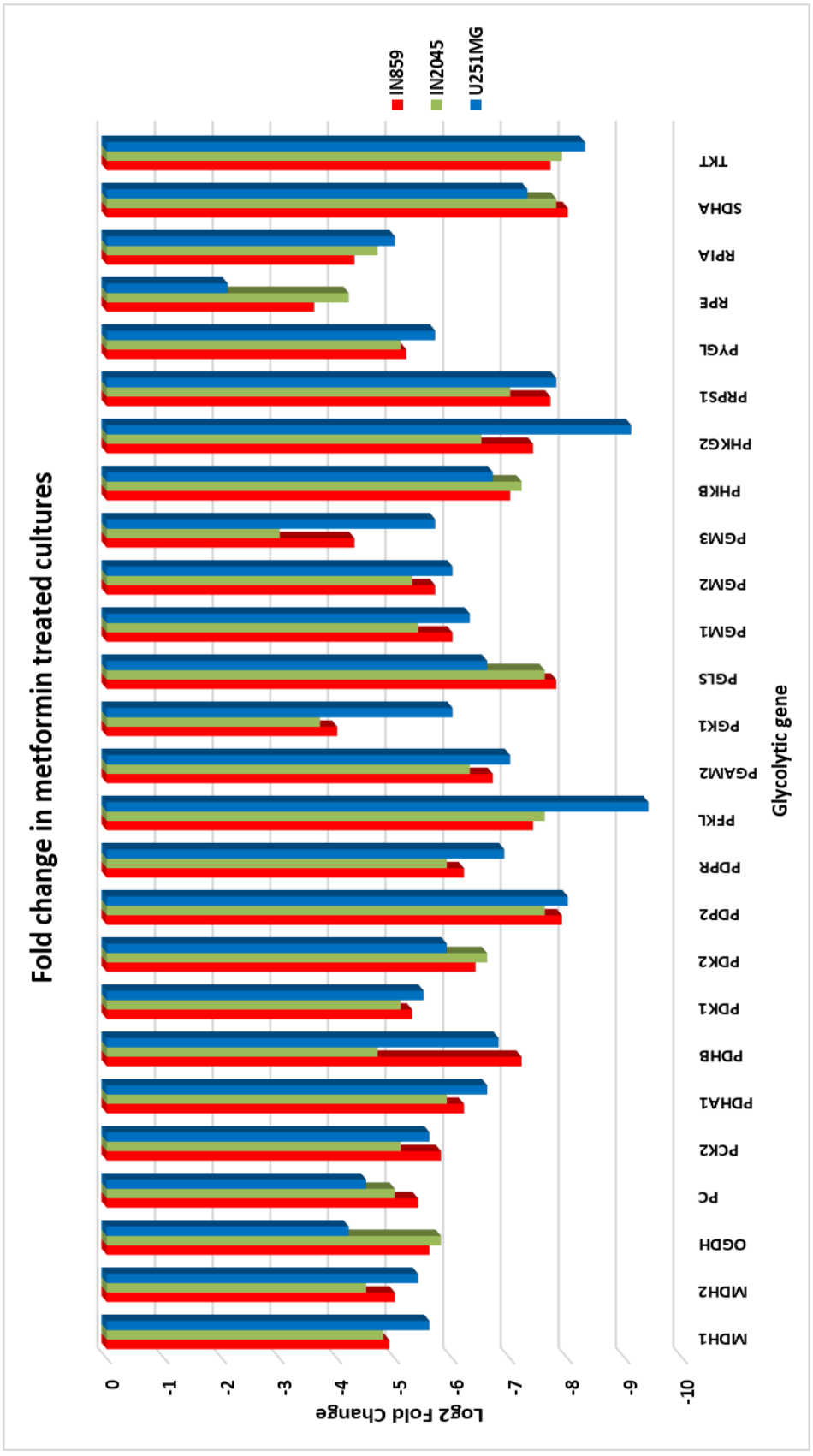

Figure 5.22b Bar chart comparing gene expression variation between metformin treated glioblastoma cultures compared to the respective parent. The represented genes exhibit significantly altered levels of expression in the cultures compared to the parent culture as shown in Figure 5.21 and Table 5.13. Expression data is shown for individual cultures to compare levels of fold change.

The data indicates differential expression between the cultures treated with the inhibitors compared to the non-treated cultures, across the genes in the glucose

pathway. The inhibitors metformin and 3-BPA, and the ketone body 3-HB were previously shown to have both a cytotoxic and anti-proliferative effect impacting glioblastoma cultures. The data presented here indicates that the inhibitors also have an impact upon the glucose pathway, with considerable downregulation of glycolytic genes across the entire pathway. Of the 84 genes tested in the arrays, 40 showed significant downregulation across all three of the inhibitors analysed, with altered mRNA levels shown compared to non-treated glioblastoma cultures, as shown in Table 5.14 and Figure 5.23. The data also corresponds closely to the CRISPR *HK2*-KO figures, where the knockout of *HK2* instigates downregulation of gene expression across the glucose pathway. In both the treated and CRISPR modified cultures the array data revealed extensive changes in gene expression across the glucose pathway compared to the respective non-treated cultures, either through the loss or inhibition of *HK2,* in the case of 3-BPA and the CRISPR modified cultures, or via the deficit of glucose in the case of metformin and 3-HB. Both these mechanisms of action result in a similar genetic pattern with widespread significant ($p<0.005$) downregulation of genes across the glucose pathway.

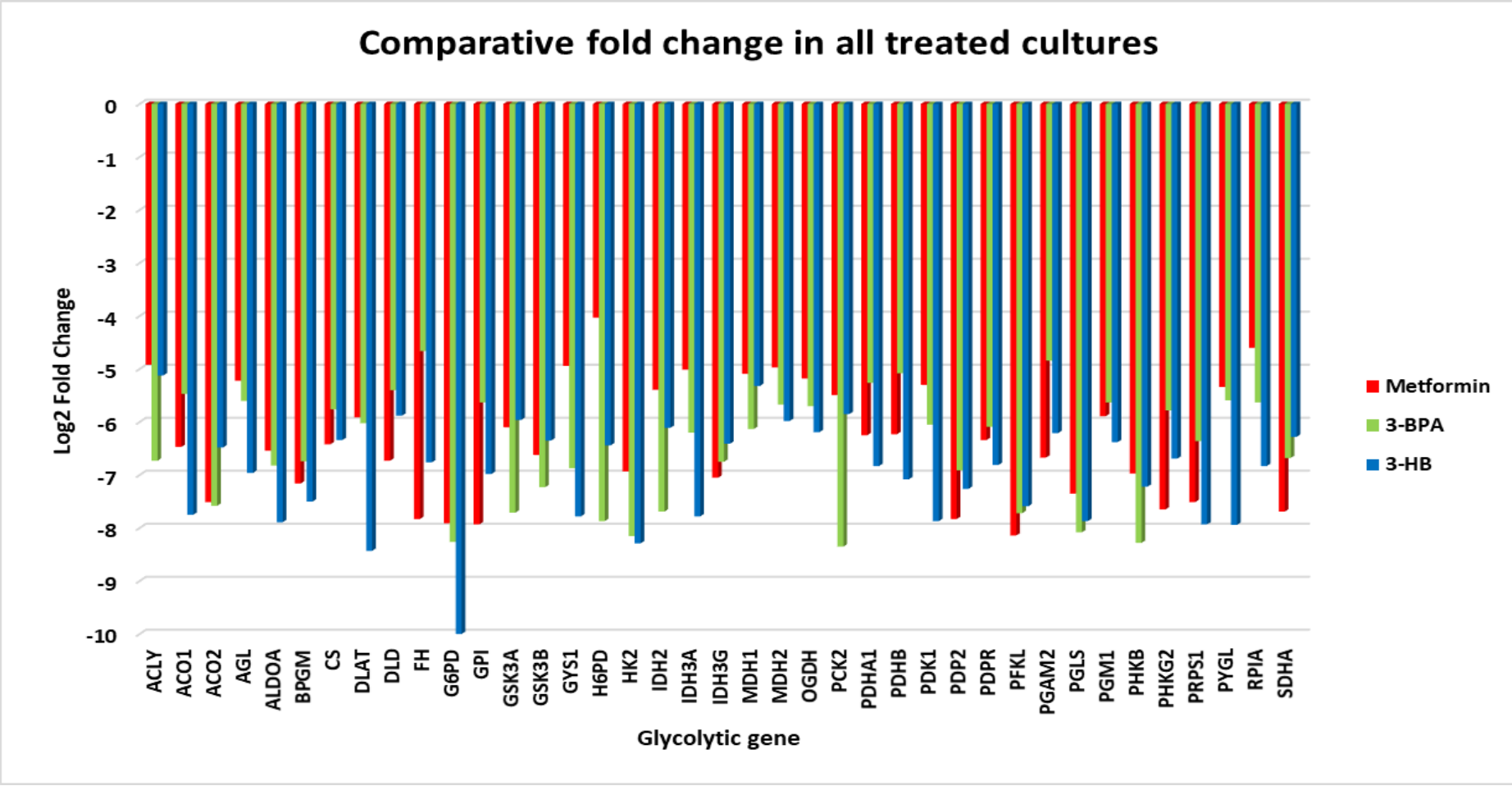

Figure 5.23 Bar chart comparing gene expression variation between the 3-HB, 3-BPA and metformin treated glioblastoma cultures. Cultures at the relevant ID_{50} value, compared to the respective non-treated cultures. Represented genes above the threshold all show significant change ($p<0.05$).

Table 5.14 Expression fold change values of glycolytic genes in treated cultures compared to non-treated cultures

	Log2 Fold Change			
Gene	*HK2*-KO	3-BPA	Metformin	3-HB
ACLY	-5.89	-6.73	-4.92	-5.12
*ACO2**	-4.52	-7.58	-7.51	-6.48
*AGL**	-2.76	-5.6	-5.22	-6.96
ALDOA	-6.61	-6.82	-6.54	-7.89
*BPGM**	-4.18	-6.74	-7.16	-7.5
CS	-4.67	-5.76	-6.42	-6.34
*DLAT**	-3.46	-6.02	-5.91	-8.43
*FH**	-4.27	-4.66	-7.83	-6.76
*G6PD**	-7.3	-8.26	-7.91	-10.08
GPI	-5.52	-5.63	-7.93	-6.98
GSK3A	-5.88	-7.71	-6.1	-5.96
*GSK3B**	-4.73	-7.23	-6.62	-6.35
*GYS1**	-5.3	-6.87	-4.94	-7.78
*H6PD**	-3.74	-7.87	-4.03	-6.44
*HK2**	-12.5	-8.15	-6.93	-8.29
IDH2	-6.65	-7.69	-5.39	-6.11
*IDH3A**	-4.1	-6.2	-5.01	-7.78
MDH1	-5.33	-6.13	-5.09	-5.32
MDH2	-5.01	-5.67	-4.97	-5.98
OGDH	-7.09	-5.7	-5.18	-6.19
*PCK2**	-5.3	-8.35	-5.49	-5.85
*PDK1**	-4.59	-6.05	-5.3	-7.87
*PDP2**	-4.91	-6.91	-7.83	-7.26
PDPR	-6.01	-6.09	-6.34	-6.81
PFKL	-6.3	-7.72	-8.14	-7.59
PGAM2	-4.86	-4.84	-6.67	-6.21
PGLS	-6.6	-8.08	-7.35	-7.87
PGM1	-6.61	-5.63	-5.89	-6.38
*PHKB**	-5.13	-8.28	-6.97	-7.22
*RPIA**	-2.87	-5.63	-4.6	-6.83
*SDHA**	-4.87	-6.68	-7.69	-6.28

Table showing fold change values in patient derived glioblastoma cultures treated with 3-BPA and metformin or modified with 3-HB supplementation or CRISPR *HK2*-KO, compared to corresponding non treated cultures. All genes are significantly downregulated in all 3 treatments ($p<0.005$). * represents genes with fold change variation >2 between the treatments.

Table 5.15 Expression fold change values of glycolytic genes in biopsy samples compared to treated/modified cultures

Gene	Biopsy	*HK2*-KO	3-BPA	Metformin	3-HB
ALDOA	2.99	-6.61	-6.82	-6.54	-7.89
ALDOB	3.33	-6.63	-	-	-
ENO1	5.07	-	-	-7.94	-
G6PC	3.78	-6.95	-	-	-
GCK	4.47	-5.84	-	-	-
GYS1	5.43	-5.3	-6.87	-4.94	-7.78
GYS2	4.65	-6.93	-	-	-
HK2	5.58	-12.5	-8.15	-6.93	-8.29
HK3	3.5	-6.75	-	-	-
MDH1	3.86	-5.33	-6.13	-5.09	-5.32
MDH2	4.85	-5.01	-5.67	-4.97	-5.98
PCK1	3.74	-5.36	-	-	-
PCK2	3.75	-5.3	-8.35	-5.49	-5.85
PGK1	4.04	-	-	-4.56	-6.3
PGK2	3.28	-4.27	-	-	-
PKLR	3.11	-4.6	-	-	-6.1
PRPS1L1	5.85	-	-	-	-5.65
RBKS	4.58	-4.77	-	-	-7.62
ACO2	-1.88	-4.52	-7.58	-7.51	-6.48
ENO2	-2.3	-5.47	-	-	-7.02
SUCLA2	-1.73	-6.13	-	-	-

Table showing fold change values in glioblastoma biopsies compared to patient derived glioblastoma cultures treated with 3-BPA and metformin or modified with 3-HB supplementation or CRISPR *HK2*-KO. Biopsy samples are compared to normal tissue and the cultures to their respective non-treated/parent cultures. All treated/modified cultures show a reversal of fold change across numerous upregulated genes in glioblastoma. All genes are significantly downregulated in all 3 treatments ($p<0.005$). – indicates no significant change.

5.7 Discussion

This chapter has focused on the investigation of the differential expression across 84 genes in the glucose pathway in glioblastoma biopsy (n=6) and patient- derived cultures (n=10) compared to normal brain tissue and NHA. Additionally, to determine the effects of *HK2* downregulation through loss or inhibition, and the deficit of glucose, upon the gene expression profile in patient- derived cultures.

Qiagen RT expression profiler arrays have previously been used to determine alterations in cell metabolism and reprogramming across a diverse range of disease types, including the metabolic reprogramming of macrophages and the altered expression in oral squamous cell carcinoma (Freemerman *et al.*, 2014; Pan *et al.*, 2017). The expression profiler arrays have also been utilized to determine genetic profiles and alterations for potential drivers of tumorigenesis, invasion and chemoresistance in a range of cancers, including human hepatocellular carcinomas (Govaere *et al.*, 2014) and the growth and migration of hypopharyngeal squamous cells (Kelly *et al.*, 2014).

The array data in this study revealed recurrent gene overexpression throughout the glucose pathway in both glioblastoma biopsies and patient -derived cell cultures compared to their normal counterparts. A variation in gene overexpression was observed amongst the biopsies throughout the pathway, suggesting that although the significant alteration across multiple genes is occurring, there is variation of expression in the biopsies, which may reflect the characteristic heterogeneity of glioblastoma (Howlader *et al.*, 2016). The study also showed that the differential expression is maintained in vitro, with similar expression patterns demonstrated between paired glioblastoma biopsy and culture samples.

Overexpression of the glycolytic pathway is prevalent in glioblastoma

Both glioblastoma biopsies (n=6) and patient-derived cell cultures (n=10) demonstrated gene overexpression, with over 60% of the genes showing upregulated levels within the tumour tissue and 88% in the cultures compared to normal brain tissue and NHA respectively. The biopsy samples were grouped for further analysis which revealed significant ($p<0.005$) upregulation in 22% of the glycolytic genes. Additionally, significant ($p<0.005$) upregulation was also seen in 37% of the glycolytic genes in the cultures. *HK2* overexpression was present across all glioblastoma samples, reiterating the qPCR data presented in Chapter 3. It is well documented that the high mutation rate in cancer cells leads to aberrant cellular metabolism, alterations of metabolic pathways significantly contribute in the development and growth of many tumours including gliomas (Kazue *et al.*, 2011; DeBerardinis and Tompson, 2012; Galluzi *et al*, 2013; Lindgvist *et al.*, 2018).

Glioblastoma cells rely increasingly on the glycolytic pathway as the predominant mechanism for energy production, the switch from oxidative phosphorylation to glycolysis, along with the associated accumulation of lactate by-products in the tumour microenvironment, characterises the best-known alteration in cancer cell metabolism (vander Haiden *et al*., 2009; Kami *et al*, 2013). It has been suggested that the metabolic switch functions to allow for increased production of cellular energy in the form of ATP, crucial for the production of precursors for macromolecule biosynthesis for the support of cell growth development, which is driven at an enhanced rate via glycolysis compared to oxidative phosphorylation (Cairns *et al*., 2011). The array data highlights an increased level of expression occurring throughout the glucose pathway in glioblastoma, potentially as a result of the higher demand for the generation of cellular energy.

Expression profile similarity between paired glioblastoma biopsies and cultures

The glycolytic gene expression profiles of paired glioblastoma biopsies and the respective patient-derived cell culture (n=6) were investigated to establish whether differential expression is maintained in vitro. The data showed genetic similarity between the glioblastoma biopsies and the paired culture samples, with over 80% of the glycolytic genes exhibiting comparable levels of mRNA expression across the pathway, only 14 of the 84 genes showing a significant ($p<0.005$) increase in levels of mRNA expression in culture compared to the paired tissue samples. Importantly of the 14 genes that show significantly altered levels of expression between the paired samples, 12 of which are not significantly up or downregulated ($p<0.005$) in glioblastoma biopsies compared to normal tissue. Only *ENO1* and *HK2* were both significantly upregulated ($p<0.005$) in biopsy samples compared to normal tissue, with additional alterations between paired samples.

The small amount of alterations in expression levels is suggestive of mRNA expression stability between the paired samples, presenting the patient-derived cultures as a useful tool for investigation and an accurate model for *in vitro* studies. Additionally, a comparability between the patient- derived cultures was shown, with minimal variance between individual glycolytic gene expression. The

microenvironment created in tissue culture is often altered to the natural cellular environment. Recent studies have highlighted the reliability of immortalised cell lines, where U251MG for example exhibits altered genotypic and phenotypical features compared to the progenitor sample, it has been documented that with increased passage U251MG loses its original glioblastoma signature, with the acquisition of additional genetic deletions (Torsvik *et al*., 2014). The use of patient-derived cultures set at short-term low passages reduces the probability of both genetic and phenotypic deviations from the original sample whilst providing a function cellular system (Roberts *et al*., 2017). The expression similarities between the paired biopsy – culture obtained by the novel data from this profiler array is fundamental for the development of accurate models, crucial for the advancement of effective treatments.

Hypoxia impacts the glycolytic pathway

Under hypoxic conditions, cultures demonstrated altered levels of gene expression across the glucose pathway, with up to 60% of the genes in the pathway showing differential levels of mRNA expression compared to the respective normoxia cultures. Furthermore, 6 of the 84 genes (*DLD, PGK1, PGM2, PGK2, SUCLG1, UGP2*) showed a significant increase ($p<0.005$) in the level of mRNA expression in hypoxic conditions compared to normoxia with a further 7 genes (*ACLY, ACO2, DLST, GSK3A, H6PD, OGDH, PFKL*) exhibiting significant downregulation under hypoxic stress across the 3 glioblastoma cultures. Interestingly, a study showed high *PGK1* expression to be associated with poor prognosis in breast cancer, where *PGK1* demonstrated a connection with HIF-1 which was shown to stimulate breast cancer progression and metastases (Fu *et al*., 2018). *PGK1* overexpression has been associated with gastric cancer and has been found to increase the invasiveness of gastric cancer cells (Zieker *et al*., 2010). In addition, *PGK1* phosphorylation was shown to correlate with macrophage-promoted tumour growth, with macrophage infiltration in glioblastoma, as well as an increased malignance and prognosis (Zhang *et al*., 2018). *PGK1* may therefore serve as a promising biomarker and target therapy for a range of cancers. Hypoxia is common characteristic of tumour microenvironments and it is well documented that hypoxic tumours are significantly more malignant, metastatic, and

chemo resistant with a poorer patient prognosis. (Vaupel, 2004). The proteomic and genomic alterations often lead to angiogenesis activation and anerobic metabolism to aid in survival. It has been suggested that hypoxia-inducible factor (*HIF-1*) induces multiple genes integral to angiogenesis, such as vascular endothelial growth factor (*VEGF*), which has a key involvement in metastatic spread (Masoumi *et al.*, 2011). The upregulation of key genes driving glycolysis via hypoxia may be beneficial for the tumour for both cell growth and survival, studies have shown that aerobic glycolysis generates less reactive oxygen species (ROS) allowing the cells to adapt to intermittently hypoxic conditions, which is a common occurrence in poorly vascularized tumours (Cairns *et al.*, 2011). The impact of hypoxia stress consequently effects metabolism, thus forcing genetic changes across the glucose pathway, as revealed in this data.

HK2 knockout leads to the downregulation of gene expression across the glucose pathway

HK2 knockout was shown to instigate the downregulation of gene expression across the glucose pathway in all cultures, with significant reduction ($p<0.005$) in expression in over 70% of the glycolytic genes, compared to the corresponding parent cultures. Furthermore, the *HK2*-KO cultures also exhibited similar levels of expression to NHA, with 60 of the 84 glycolytic genes demonstrating no significant fold change alterations. The data indicates a substantial divergence from the respective parent cultures, suggesting that the removal of *HK2* downstream pathway expression of multiple genes. *HK2* has been strongly implicated in aerobic glycolysis in cancer cells and has been shown to be abundantly overexpressed in a range of cancers, including glioblastoma as shown in Chapter 3 (Mathupala *et al.*, 2001; Wang *et al.*, 2014; Anderson *et al.*, 2016). A study showed that the upregulation of *HK2* in ovarian cancer cells led to increased stimulation of glycolysis, driving the glycolytic phenotype often associated in cancer cells (Mukherjee *et al.*, 2015). The data has also revealed that the downregulation of *HK2* results in the reduced expression of glycolytic genes downstream in the pathway, resulting in a similar genetic expression profile comparable to NHA. *HK2*-KO was shown to influence downregulation of multiple genes associated with glucose metabolism, including in glycolysis (*ALDOA, ENO2, GALM, PGAM2, PGK2, PGM2*), gluconeogenesis (*FBP1,*

G6PC, G6PC3, PC, PCK1, PCK2), and the TCA cycle (*ACLY, ACO2, CS, DLAT, DLST, FH, IDH2, MDH1, SDHA, SDHD, SUCLA2*). Importantly in the absence of *HK2*, the array data revealed the downregulation of regulatory genes (*PDK1, PDK2, PDK3, PDP2, PDPR*) associated with promoting glucose activity, and glycogen metabolism (*GSK3A, GSK3B, PHKB*). Interestingly, the pyruvate dehydrogenase kinase family (*PDK 1-4*) are gatekeeper enzymes that have been shown to implicated with altered glucose metabolism in tumours. *PDK1* has been shown to be overexpressed in range of cancers including breast and colorectal cancer cell lines (Lu *et al*., 2011; Pe *et al*., 2018). PDK1 overexpression has also been shown to shunt glucose metabolism towards glycolysis instead of oxidative phosphorylation, as well as being frequently associated with chemotherapy related drug resistance, invasion and metastasis (Cao *et al*., 2018). A study has shown PDK1 to upregulated in hypoxic cancer cells, interacting with *HIF1*, increasing hypoxic cell survival via the inhibition of apoptosis (Bonnet *et al*., 2007). The impact of *HK2*-KO consequently effects metabolism, forcing genetic changes across the glucose pathway, as revealed in this data

3-BPA and metformin treatments and the supplementation of 3-HB lead to downregulation of gene expression across the glucose pathway

The effects of two separate inhibitory molecules, 3-BPA and metformin and the supplementation of the ketone 3-HB as an alternative energy source, upon the glycolytic pathway were investigated via the profiler arrays, where the expression patterns of treated glioblastoma cultures were compared to the respective non-treated cultures. Similar expression profiles were demonstrated in cultures treated with both the *HK2* inhibitor 3-BPA and metformin at culture specific ID_{50} values over 72 hours. Both 3-BPA and metformin have previously been shown to have a cytotoxic inhibitory effect in glioblastoma cultures, as shown in Chapter 3. Studies have shown 3-BPA to be an efficient energy blocker through its inhibitory ability targeting *HK2*, making it a potential candidate as an antitumor drug (Cardaci *et al*., 2012; Azevedo-Silva *et al*., 2016; Lis *et al*., 2016). 3-BPA can inhibit the expression of *HK2* at both mRNA and protein levels in glioblastoma, as shown in chapter 2, and in a range of other cancers as detailed in studies (Attia *et al*., 2015; Yadav *et al*., 2017), with the advantage of a high affinity for targeting cancer cells. The disruption

of *HK2* via 3-BPA treatment results in the downregulation of gene expression across the entire glucose pathway as shown in the array data, notably 3-BPA had a similar impact on the pathway as compared to CRISPR *HK2*-KO, making 3-BPA an effective candidate as an antitumor drug in which to target the distinguished deregulated glycolytic activity in glioblastoma.

The array data also demonstrates that metformin causes a similar downregulation across genes in the glucose pathway. Metformin has been shown to posses' anti-tumour effects, clinical trials have demonstrated its promising additive effect in a range of cancers included (Lord *et al*., 2016; Dowling *et al*., 2018). The anti-tumour mechanism of metformin is not fully documented; data suggests metformin affects the activation of AMPK and has an inhibitory effect on the mTOR pathway (Pollak, 2012; He and Wondisford, 2015). The mTOR isoform, mTORC2 has been shown to regulate both cell survival and glucose metabolism, with its inhibition leading to the deregulation of both pathways (Mao *et al*., 2018). The array data here shows metformin treatment causes universal downregulation of genes in the glucose pathway, suggesting the reduction in glucose and or the inhibition of mTOR impacts glycolytic activity.

The ketone body 3-HB revealed comparable genetic expression values, the restriction of the level of glucose available to the glioblastoma cells, leads to the downregulation of the glucose pathway. Studies have shown the implementation of ketone bodies in culture, such as β-hydroxybutyrate, can impact cell metabolism, leading to systemic metabolic changes resulting in the depletion of an energy source for the glioblastoma cells, which are less effective at utilizing ketone bodies as an energy source (Shukla, *et al*., 2014; Martuscello *et al*., 2016). Additionally, 3-HB revealed comparable genetic expression values as seen in the *HK2*-KO cultures. Across both treated cultures over 70% of the genes showed similar significant downregulation ($p<0.005$) comprehensively across the glycolytic pathway. 3-BP, metformin and 3-HB (in the absence of glucose) were shown to influence downregulation of multiple genes associated with glucose metabolism, including those involved in glycolysis *(ALDOA, BPGM, GPI, PFKL, PGAM2, PGM1*), gluconeogenesis (*PCK2*), and the TCA cycle (*ACLY, ACO1, ACO2, CS, DLAT, DLD,*

FH, IDH2, MDH1, MDH2, SDHA). Importantly the array data revealed the downregulation of regulatory genes (*PDK1, PDP2, PDPR*) associated with promoting glucose and glycogen (*GSK3A, GSK3B, PHKB, PHKG*) metabolism, with the addition of the 3-BPA, metformin and 3-HB compounds. The importance of PDK1 driving tumorigenesis has already been highlighted, additionally *GSK3A* and *GSK3B* have been shown to have influential roles in many cancers, where overexpression has been established in colon, liver, ovarian, and pancreatic tumours (Mancinelli *et al*, 2017). Notably, downregulation of these genes has been shown to impact rates of proliferation as well as decreased angiogenesis in pancreatic and colorectal cancer growth (Shakoori *et al*., 2005; Ougolkov *et al*., 2005). A recent study by Wang *et al*. (2017) showed PHKB to be overexpressed at both an mRNA and protein level in colorectal tissues, moreover higher expression of the gene was shown to correlate with tumour, node and metastasis (TNM) and distal metastasis. Additionally, *PHKB* knockdown was shown to impact proliferation and induced cell cycle arrest (Wang *et al*., 2017). The array data obtained in this study highlights the impact of *HK2* upon downstream signalling in the glucose pathway, the data shows complex interactions where *HK2* upregulation in glioblastoma results in additional genetic aberrations, driving altered glucose metabolism, increased chemotherapy related drug resistance, invasion and metastasis. The array data highlights the importance and the prospective advantages of targeting both *HK2* and the abundant level of glucose in cancer cells to subsequently impact the genetic profile of the glycolytic pathway, leading to a potential metabolic reversal. Significant overexpression of genes throughout the glucose pathway were demonstrated in all glioblastoma samples, including both cultures and biopsy tissue. Furthermore, overexpression was augmented in cultures grown under hypoxic conditions, representational of the tumour microenvironment exhibited in glioblastoma. The removal of *HK2* via CRISPR mediated knockout, and through specific targeting by the inhibitor 3-BPA revealed extensive downregulation across genes in the glycolytic pathway. Additionally, the reduction in the supply of glucose through the addition of metformin and the supplementation of the ketone body 3-HB, similarly demonstrated extensive universal downregulation across the glycolytic genes. Significant downregulation was seen in 46% of the glycolytic genes across all inhibitory methods, furthermore, the

variation of expression in the significantly altered genes between cultures demonstrated minimal fold change disparity, indicating the inhibitory effects are present to a similar extent across all cultures.

HK2-KO switches overexpressed genes in glioblastoma biopsies

Importantly *HK2*-KO resulted in significant downregulation ($p<0.005$) of multiple genes (n=18) that were shown to be upregulated in glioblastoma biopsies (compared to normal tissue). 3-BPA and metformin also revealed significant reduction ($p<0.005$) in these genes (6 and 8 genes respectively) that were shown to be upregulated in glioblastoma biopsies. 3-HB supplementation in the absence of glucose also demonstrated significant downregulation in 10 of the upregulated genes demonstrated in the biopsies, as shown in Table 5.14. *ALDOA* was revealed to be downregulated by both the targeting of HK2 via 3-BPA and *HK2*-KO and by the restriction of glucose availability (metformin and of 3-HB). *ALDOA* has been associated with increased proliferation and metastasis of pancreatic cancer cells, as well as a prognostic marker for poor patient survival (Ji *et al*., 2016). A recent study has shown *ALDOA* overexpression to lead to increased migration and invasion of lung cancer cell lines and metastasis in vivo (Chang *et al*., 2019). *GYS1, MDH1* and *PCK2* were also shown to be overexpressed in the biopsy samples but downregulated in the absence of *HK2* and in reduced glucose. Both *MDH1* and *PCK2* has been shown to be elevated in prostate cancer (New *et al*., 2019), it has also been suggested that *PCK2* is responsible for the metabolic switch in prostate cancer as well as correlating with more aggressive tumours and lower survival rates (Zhao, *et al* 2017). In another study, GYS1 was shown to be upregulated in U87MG cell lines under hypoxia conditions (Zois and Harris, 2016). The data obtained in this study demonstrates the effectiveness at targeting HK2 as well as restricting glucose availability, whereby overexpressed genes present in glioblastoma, that are associated with increased proliferation and chemoresistance in multiple cancers were downregulated. This study demonstrates the predominant role of *HK2* within the glycolytic pathway, and its impact driving genetic alterations downstream, signifying

the importance in the development of inhibitors targeting *HK2* and mediating the levels of glucose within glioblastoma.

Chapter 6

Expression arrays: Altered mTOR signalling in glioblastoma

6.1 Introduction

mTOR is a serine/threonine protein kinase which integrates responses from many stimuli including nutrients, growth factors and cellular stresses in order to regulate cell growth, metabolism and survival (Saxton *et al.*, 2017). mTOR has two distinct protein complexes, mTORC1 and mTORC2. The first complex is rapamycin-sensitive and is responsible for the regulation of protein synthesis, cell cycle progression and proliferation (Liu *et al.*, 2013). mTORC2 is responsible for *Akt* activation, which is important for cell migration, proliferation and survival, as well as inhibiting apoptosis and autophagy. Although mTOR itself is not an oncogene, being part of the *PI3K/Akt* signalling pathway, it is an influential stimulator for cell proliferation and is frequently upregulated in cancer cells supporting tumour growth. mTORC1 has been shown to support rapid proliferation by activating transcription regulators including *HIF*1, which consequently drive and regulate the expression of genes involved in aerobic glycolysis (Liu *et al.*, 2013; Han *et al.*, 2015). Upregulation of mTORC2 also plays a role in cancer biology through the activation of PKC, SGK3 and FoxO1/3 transcription factors, which promotes proliferation and survival under oxygen deprivation (Chiarini *et al.*, 2015). Studies have shown the deregulation of multiple components of the mTOR pathway, such as *PI3K* amplification/mutation, the loss of *PTEN* function and the overexpression of *AKT* to be a common occurrence in many types of cancers (Pópulo, *et al.*, 2012). The expression profiler arrays include genes involved in both complexes, with additional upstream regulators of numerous mTOR responses and downstream genes that are regulated by cellular processes via the activation of mTOR complex. The profiler arrays were conducted using an optimized protocol from Qiagen, where extracted RNA was converted to cDNA as stated in 2.9 Materials and Methods. The Qiagen profiler arrays were used to identify and determine differences in mRNA expression across genes in the mTOR signalling

pathway occurring in glioblastoma cultures treated with metformin compared to the respective untreated cultures, previous studies have suggested that metformin affects the activation of AMPK and the inhibition of the mTOR pathway (He and Wondisford, 2015). Additionally, the profiler arrays were also used to determine any genetic alterations occurring in the mTOR pathway in the absence of *HK2,* utilizing *HK2*-KO modified CRISPR cultures. Un-abbreviated gene list is shown in full in the appendix.

6.2 Differential expression of glycolytic genes via multiple inhibitory methods

6.2.1. Differential expression of mTOR genes after *HK2* induced CRISPR Knockout

Dysregulated levels of expression were revealed across genes in the mTOR pathway in all 3 of the *HK2*-KO cultures compared to the respective parent cultures (cultures detailed in Table 2.1). Over 82% of the genes in the mTOR pathway exhibited altered levels in U251MG, with 67 presenting downregulated levels and 2 with upregulated expression. Furthermore, 54% of the genes demonstrated deregulated expression levels in the patient derived culture IN859 and 55% in IN2045, with over 40 genes showing downregulation, as shown in Figure 6.1. Grouping the glioblastoma cultures to perform statistical calculations, showed 46 genes demonstrating a significant ($p<0.005$) altered level of expression across all the *HK2*-KO cultures compared to the respective parent cultures. Forty-one of the genes exhibited significant ($p<0.005$) downregulated expression fold change in the *HK2*-KO cultures compared to the respective parent cultures. Furthermore, 5 genes showed significant ($p<0.005$) overexpression in the treated cultures, as shown in Table 6.1 and Figure 6.2. The downregulation in fold change expression across the genes in mTOR pathway in the *HK2*-KO cultures ranged from -1.01 (*RPTOR*) to -7.35 (PRKAG3). The variance in fold change of the genes were also examined between the individual cultures to establish the degree of homogeneity of expression levels. The variation of gene expression showed 89.1% of the significantly altered genes with less than 2- fold variation between the cultures, with only 5 genes demonstrating a variance greater than 2-fold change, as shown in Figure 6.3 (Table

shown in the appendix). The little variation in the level of fold change of the deregulated genes indicates that the altered expression is present to a similar degree across all *HK2*-KO cultures, suggesting the removal of *HK2* causes downregulation of mTOR signalling.

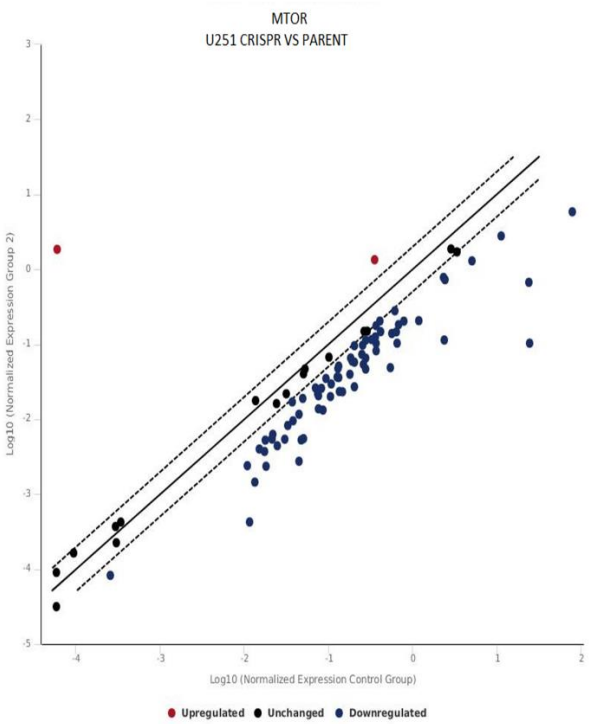

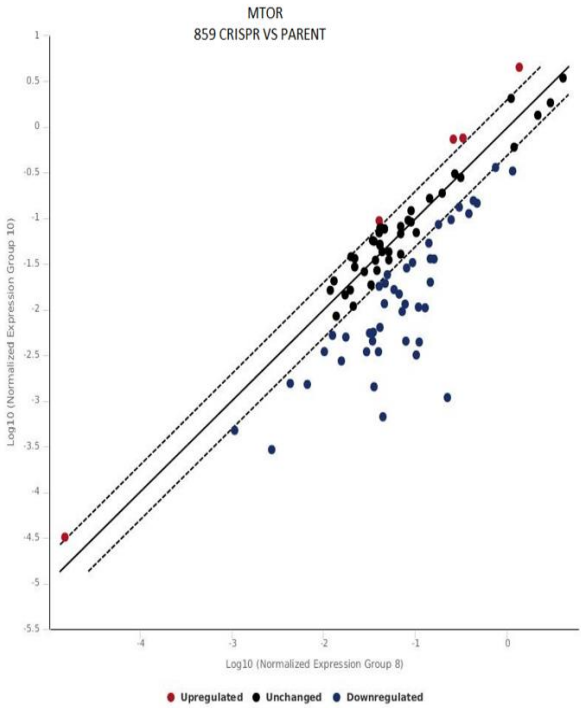

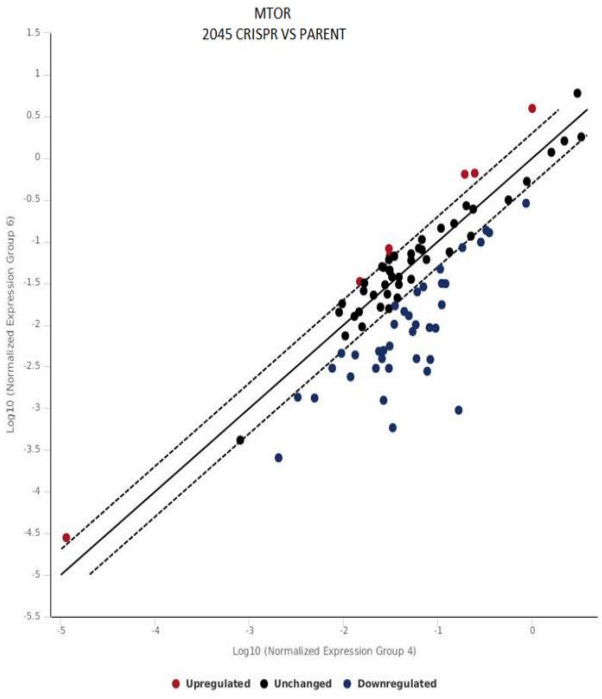

Figure 6.1 Scatter plot comparing the level of fold change across 84 genes in the mTOR pathway in 3 glioblastoma *HK2*-KO cultures compared to the respective parent cultures. Each dot represents the expression of a gene. The y-axis represents fold-change expression of the glioblastoma sample, the x-axis represents expression of the normal tissue control. Genes (dots) further to the right show higher expression compared to normal tissue. Higher dots represented greater expression in the glioblastoma samples.

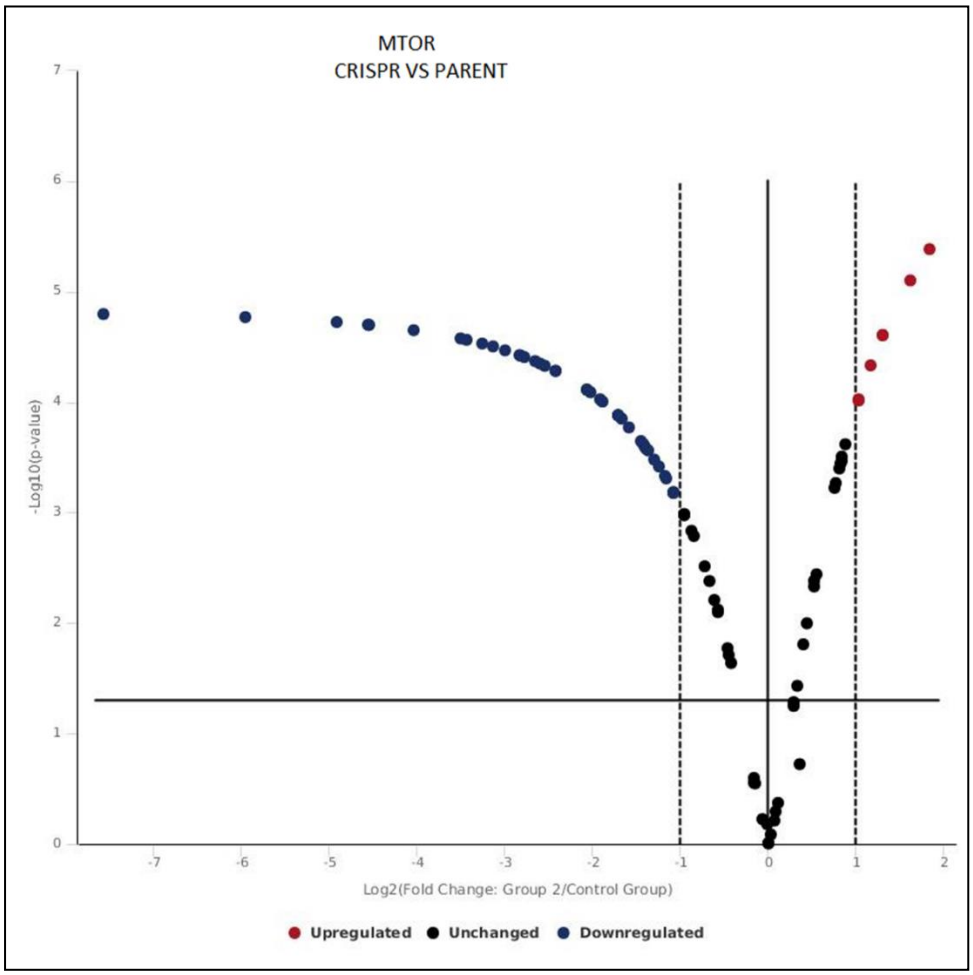

Figure 6.2 Volcano plot comparing the level of fold change across 84 genes associated in the mTOR pathway in 3 glioblastoma *HK2*-KO cultures. Fold change in gene expression compared to the respective parent cultures. Represented genes above the threshold all show significant change ($p<0.05$).

Table 6.1 Expression fold change values of mTOR genes in *HK2*-KO cultures compared to respective parent cultures

Gene	Log2 Fold Change	Gene	Log2 Fold Change
AKT1S1	-2.05	*PIK3CG*	-2.23
AKT2	-2.45	*PLD2*	-3.27
AKT3	-2.36	*PPP2R2B*	-1.78
CAB39	-2.1	*PPP2R4*	-4.17
CAB39L	-1.76	*PRKAG3*	-7.35
CDC42	-1.26	*PRKCB*	-2.6
CHUK	-3.17	*PRKCG*	-2.76
DDIT4	-2.72	*RHEB*	-6.34
DEPTOR	-1.68	*RPS6KA1*	-5.34
EIF4E	-2.53	*RPS6KA5*	-1.3
EIF4EBP1	-1.98	*RPS6KB2*	-1.93
EIF4EBP2	-2.67	*RPTOR*	-1.01
HRAS	-2.64	*SGK1*	-1.26
IGF1	-2.92	*STK11*	-5.24
IGFBP3	-1.57	*TELO2*	-3.1
IKBKB	-1.26	*TSC2*	-4.74
INS	-3.85	*ULK1*	-6.13
INSR	-2.32	*ULK2*	-3.27
IRS1	-3.08	*AKT1*	1.26
MAPK1	-3.18	*PRKAG2*	1.06
MLST8	-2.99	*PRKCA*	1.49
PIK3C3	-2.1	*RHOA*	1.88
PIK3CD	-1.33	*RPS6*	1.61

Table showing changes in fold change values in patient derived glioblastoma *HK2*-KO cultures compared to corresponding parent cultures. All genes are significantly downregulated ($p<0.05$).

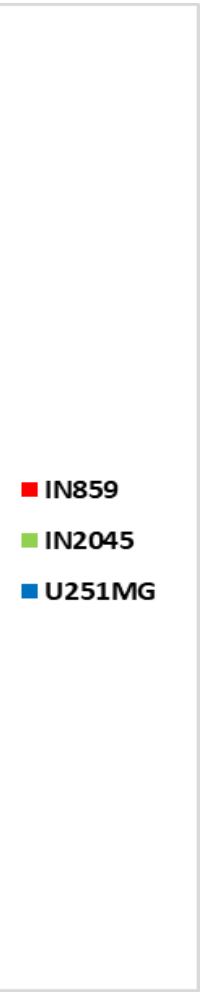

Figure 6.3 Bar chart comparing gene expression variation between *HK2*- KO modified glioblastoma cultures compared to parent cultures. The represented genes exhibit significantly altered levels of expression in the cultures compared as shown in Figure 6.2 and Table 6.1. Expression data is shown for individual cultures to compare levels of fold change variation.

6.2.2. Differential expression of mTOR genes after 72-hour metformin treatment

Three glioblastoma cultures were treated with metformin at culture specific ID_{50} values for 72 hours, as stated in 4.3.2. Dysregulated levels of expression were demonstrated throughout genes in the mTOR pathway in all 3 of the metformin treated glioblastoma cultures compared to the respective untreated culture. Over 66% of the genes in the mTOR pathway exhibited altered levels in U251MG, with 46 presenting downregulated levels and 10 with upregulated expression. Furthermore, 50% of the genes demonstrated deregulated expression levels in both patient derived cultures, IN859 and IN2045, with over 30 genes showing downregulation, as shown in Figure 6.4. Grouping the glioblastoma cultures to perform statistical calculations, showed 44 genes demonstrating significant ($p<0.005$) altered levels of expression across all the metformin treated glioblastoma samples compared to the respective non-treated cultures. 33 of the genes exhibited significant ($p<0.005$) downregulated expression fold change in metformin treated cultures compared to the respective non-treated cultures, furthermore, 11 genes showed significant ($p<0.005$) overexpression in the treated cultures, as shown in Table 6.2 and Figure 6.5. The downregulation in mRNA fold change expression across the gens in mTOR pathway in the metformin treated cultures ranged from -1.05 (*RPTOR*) to -5.69 (*INS*).

The variation of gene expression showed 84.8% of the significantly altered genes with less than 2- fold variation between the cultures, with 5 of the genes demonstrating a variance greater than 2-fold change, as shown in Figure 6.6 (Table shown in the appendix). The little variation in the level of fold change of the deregulated genes indicates that the altered expression is present to a similar degree across all cultures treated with metformin, suggesting metformin has an inhibitory impact on mTOR signalling.

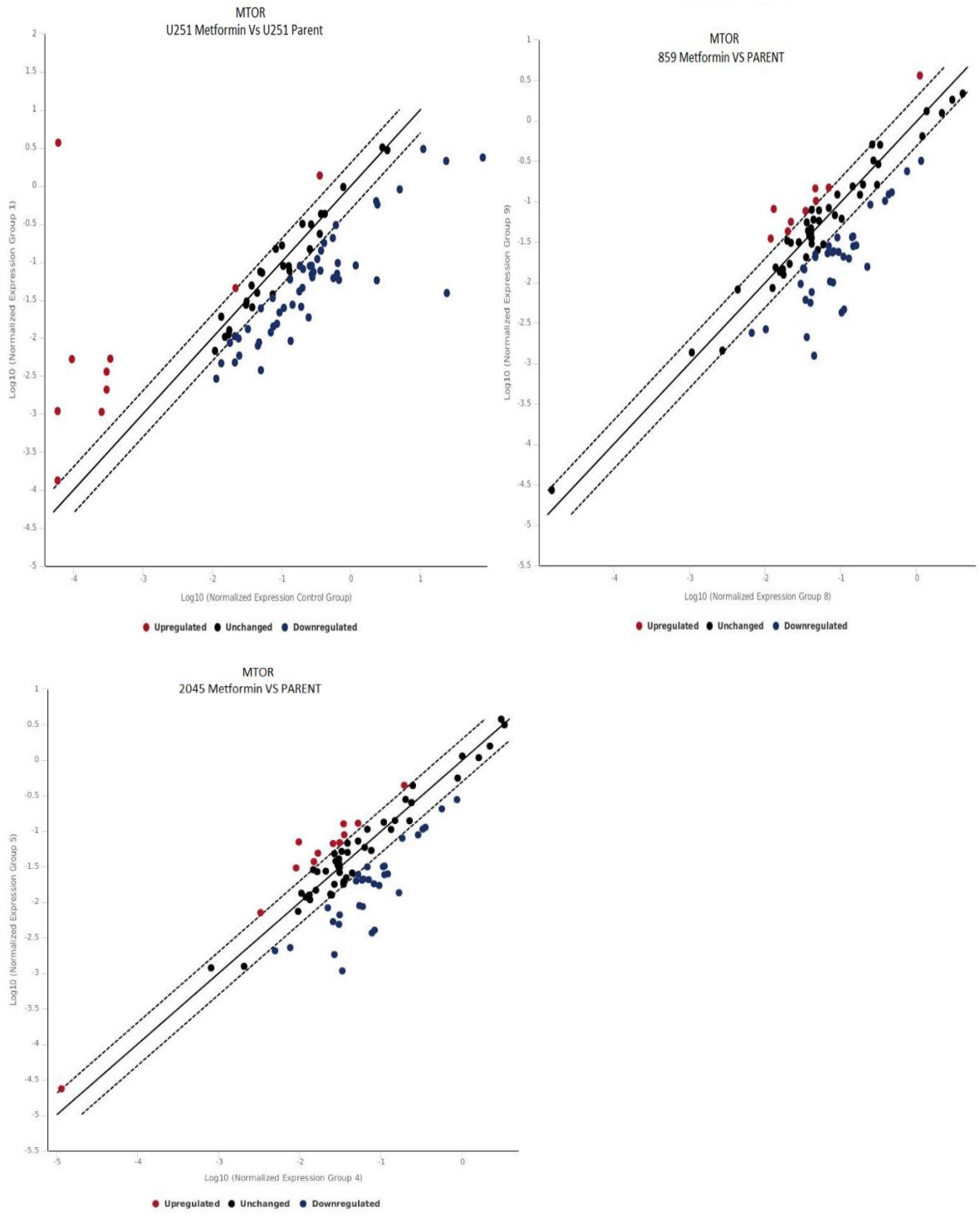

Figure 6.4 Scatter plot comparing the level of fold change across 84 genes in the mTOR pathway in 3 glioblastoma cultures treated with metformin compared to the respective non-treated cultures. Each dot represents the expression of a gene. The y-axis represents fold-change expression of the glioblastoma sample, the x-axis represents expression of the normal tissue control. Genes (dots) further to the right show higher expression compared to normal tissue. Higher dots represented greater expression in the glioblastoma samples.

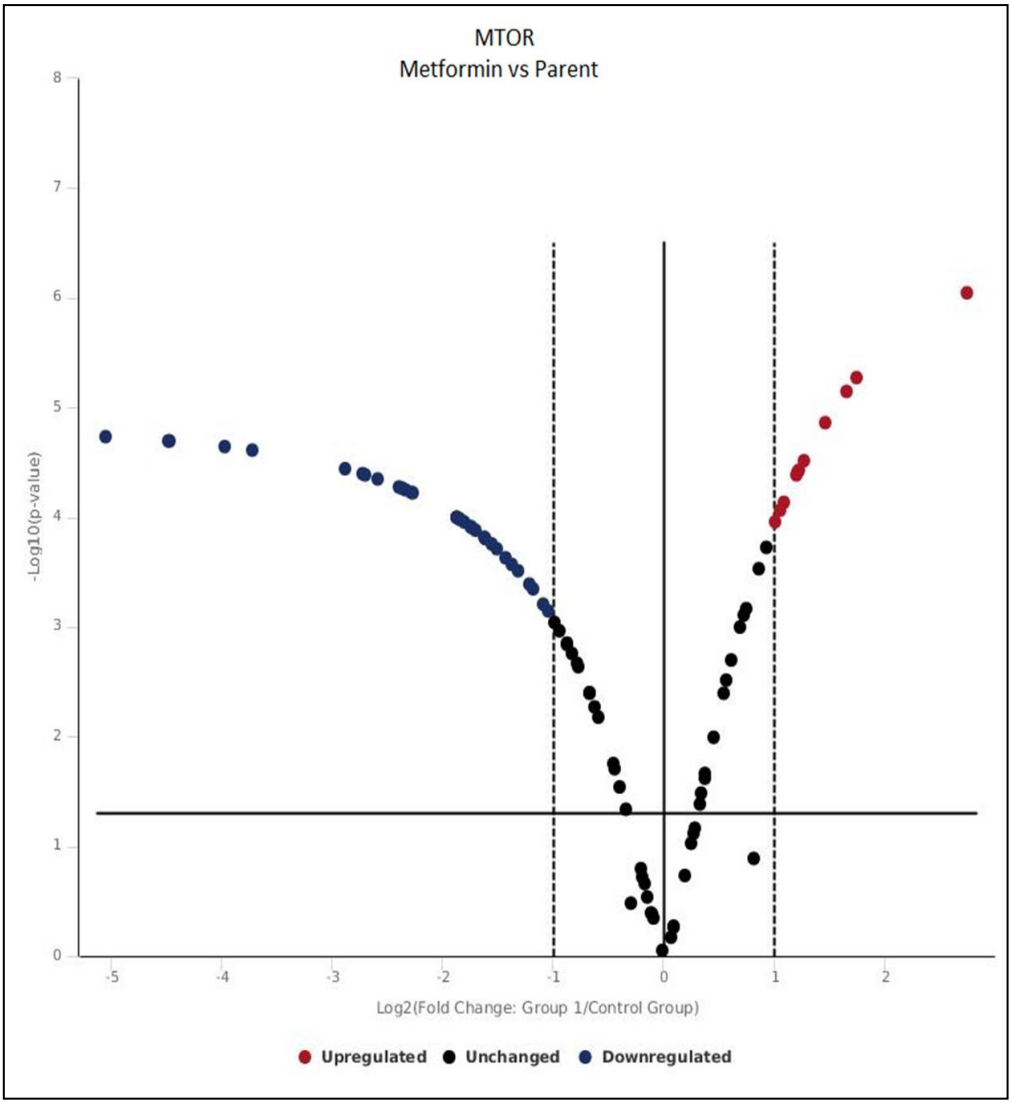

Figure 6.5 Volcano plot comparing the level of fold change across 84 genes associated in the mTOR pathway in 3 glioblastoma cultures treated with metformin. Fold change in gene expression at the relevant ID_{50} value, compared to the respective non-treated cultures. Represented genes above the threshold all show significant change ($p<0.05$).

Table 6.2 Expression fold change values of mTOR genes in metformin treated cultures compared to non-treated cultures

Gene	Log2 Fold Change	Gene	Log2 Fold Change
GSK3B	1.3	*HIF1A*	-1.94
PIK3CB	1.75	*HRAS*	-2.09
PRKAA2	1.15	*IGF1*	-1.85
PRKAG2	2.83	*IGFBP3*	-1.27
PRKCB	1.02	*INS*	-5.69
RHOA	1.13	*INSR*	-1.38
RPS6KB1	1.08	*IRS1*	-1.25
RRAGC	1.37	*MAPK1*	-2.5
RRAGD	1.74	*MAPK3*	-2.12
SGK1	1.33	*MLST8*	-4.48
TSC1	1.41	*MYO1C*	-2.28
AKT1S1	-1.58	*PPP2R4*	-2.19
AKT2	-2.61	*PRKAG3*	-2.22
AKT3	-1.49	*RHEB*	-2.83
CAB39L	-1.66	*RPS6KA5*	-2
CDC42	-1.37	*RPS6KB2*	-3.85
CHUK	-1.69	*RPTOR*	-1.05
DDIT4	-1.58	*STK11*	-4.31
EIF4E	-1.86	*TP53*	-2.33
EIF4EBP1	-2.34	*TSC2*	-2.3
EIF4EBP2	-1.66	*ULK1*	-2.63
FKBP8	-2.07	*ULK2*	-1.06

Table showing changes in fold change values in patient derived glioblastoma cultures treated with metformin compared to corresponding non treated cultures. All genes are significantly downregulated ($p<0.05$).

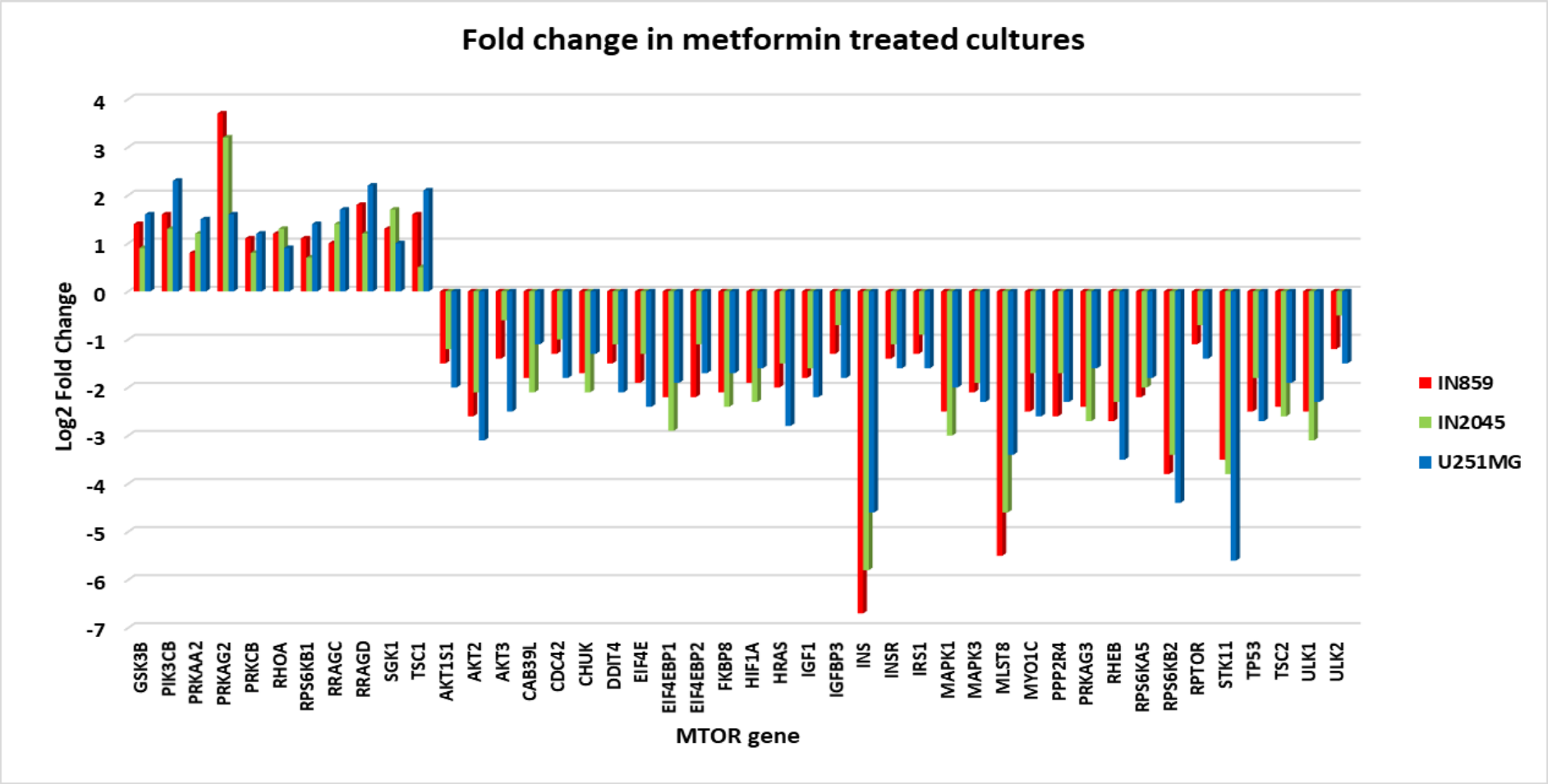

Figure 6.6 Bar chart comparing gene expression variation between metformin treated glioblastoma cultures compared to parent cultures. The represented genes exhibit significantly altered levels of expression in the cultures compared as shown in Figure 6.5 and Table 6.2. Expression data is shown for individual cultures to compare levels of fold change variation.

6.2.3. Differential expression of mTOR genes in *HK2* -KO cultures after 72-hour metformin treatment

The mTOR pathway expression patterns of 3 glioblastoma cultures with CRISPR mediated *HK2* knockout were compared to the respective parent cultures, all cultures were also treated with metformin at culture specific ID_{50} values over 72 hours. Metformin demonstrated an increased effectiveness in the absence of HK2 as detailed in Chapter 4.6, where *HK2* –KO cultures treated with metformin showed significantly increased sensitivity ($p<0.0001$). Taking this into account, expression profiler arrays were utilised to investigate the effect of metformin on the mTOR pathway in the *HK2-KO* cultures, to further evaluate metformin potential increased effectiveness as an mTOR pathway inhibitor. Deregulated levels of expression were revealed across genes in the mTOR pathway in all 3 of the metformin treated *HK2* knockout cultures compared to the respective parent cultures. Over 77% of the genes in the mTOR pathway exhibited altered levels in U251MG, with 57 presenting downregulated levels and 8 with upregulated expression. Additionally, 62% of the genes demonstrated deregulated expression levels in the patient derived culture IN859 and IN2045, with over 40 genes showing downregulation, as shown in Figure 6.7. The glioblastoma cultures were grouped to perform statistical calculations, which revealed 51 genes exhibiting a significant ($p<0.005$) altered level of expression across all the metformin treated *HK2*-KO cultures compared to the respective parent cultures. 43 of the genes exhibited significant ($p<0.005$) downregulated expression fold change in the cultures compared to the respective parent cultures, with a further 8 genes showing significant ($p<0.005$) overexpression in the treated cultures, as shown in Table 6.3 and Figure 6.8. The downregulation in mRNA fold change expression across the gens in mTOR pathway in the *HK2*-KO cultures ranged from -1.09 (*RPTOR*) to -6.99 (STK11). The variation of gene expression showed 92.2% of the significantly altered genes with less than 2- fold variation between the cultures, with 4 of the genes demonstrating a variance greater than 2-fold change, as shown in Figure 6.9 (Table shown in the appendix). The little variation in the level of fold change of the altered genes indicates that the expression fold change is present to a similar level across all *HK2*-KO cultures treated with metformin. The data shows a greater number of genes

were significantly altered in *HK2-KO* cells when treated with metformin, compared to the respective singular treatments, with extensive downregulation across the mTOR pathway.

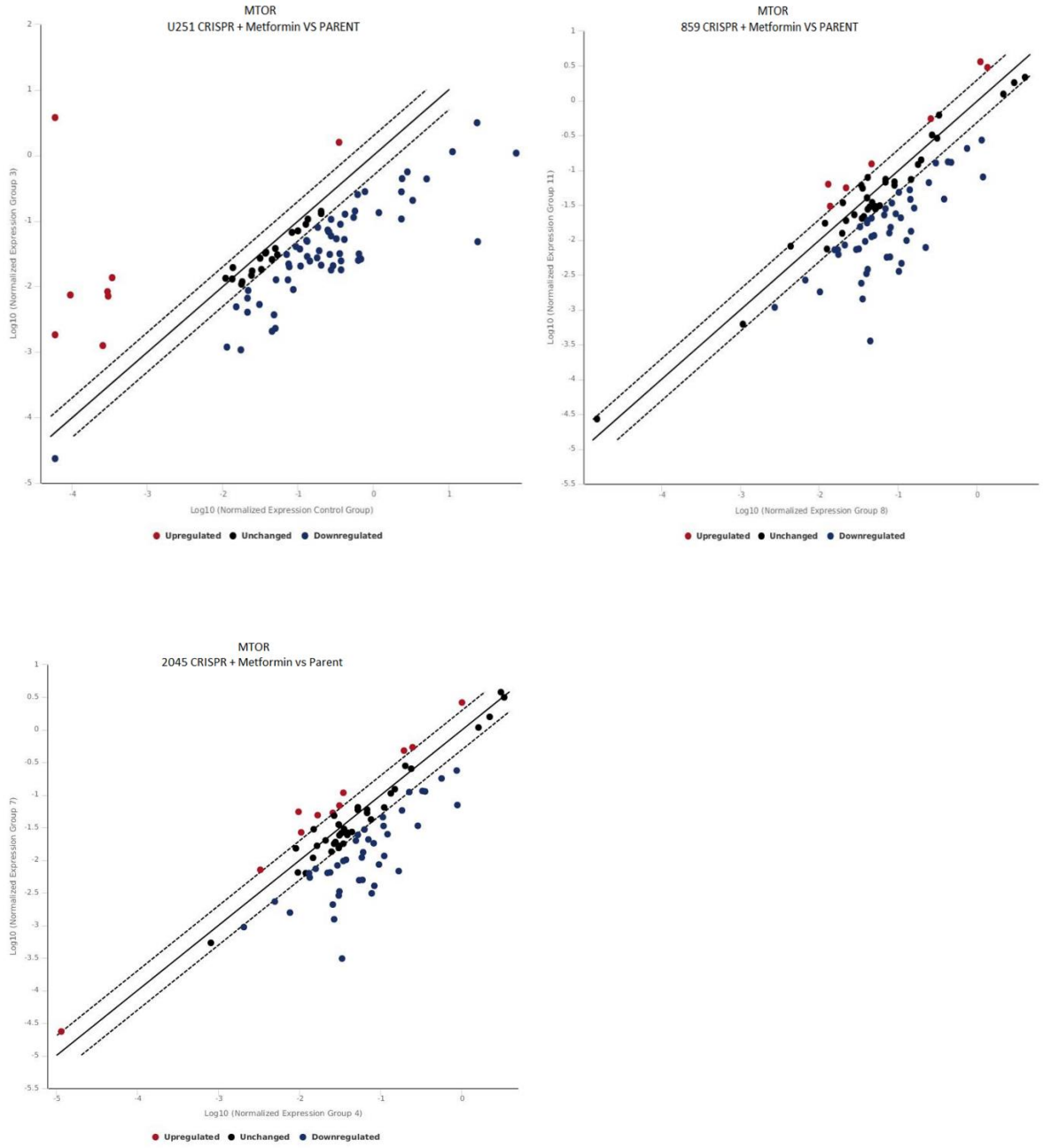

Figure 6.7 Scatter plot comparing the level of fold change across 84 genes in the mTOR pathway in 3 glioblastoma *HK2*-KO cultures treated with metformin compared to the respective parent non-treated cultures. Each dot represents the expression of a gene. The y-axis represents fold-change expression of the glioblastoma sample, the x-axis represents expression of the normal tissue control. Genes (dots) further to the right show higher expression compared to normal tissue. Higher dots represented greater expression in the glioblastoma samples.

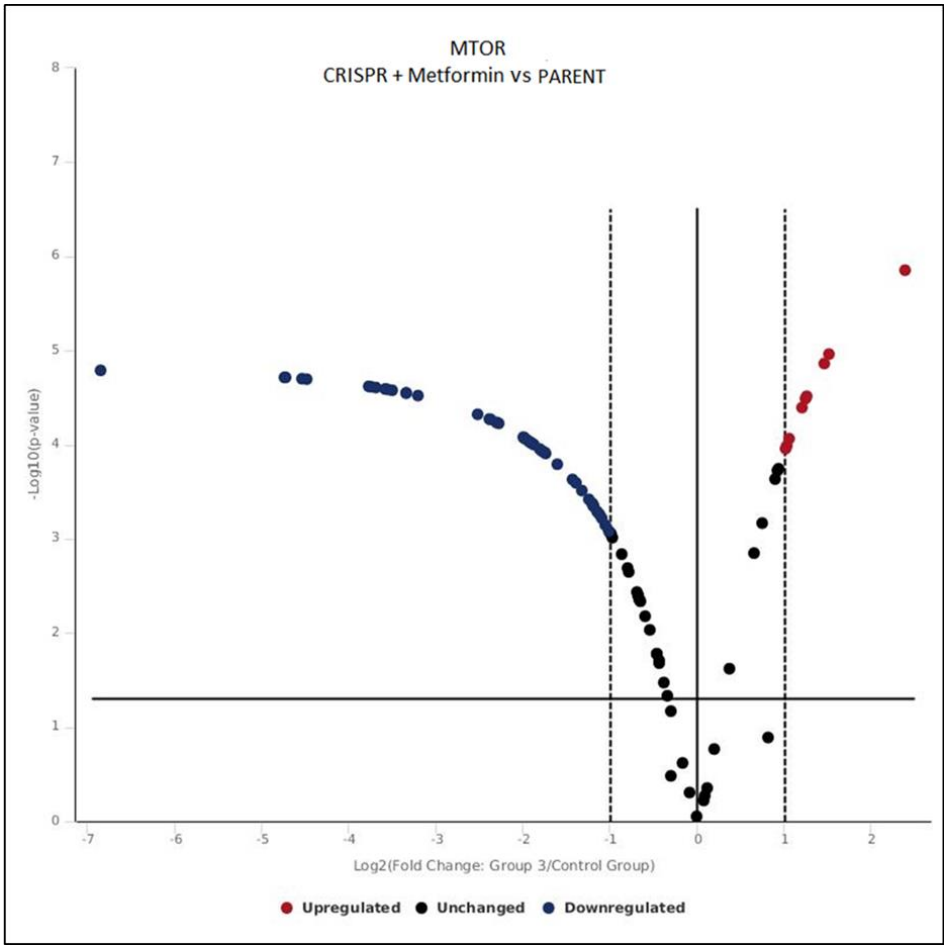

Figure 6.8 Volcano plot comparing the level of fold change across 84 genes associated in the mTOR pathway in 3 glioblastoma *HK2*-KO cultures treated with metformin. Fold change in gene expression at the relevant ID_{50} value, compared to the respective non-treated parent cultures. Represented genes above the threshold all show significant change ($p<0.05$).

Table 6.3 Expression fold change values of mTOR genes in metformin treated *HK2*-KO cultures compared to respective non-treated parent cultures

Gene	Log2 Fold Change	Gene	Log2 Fold Change
AKT1S1	-1.3	*PPP2CA*	-2.49
AKT2	-2.49	*PPP2R4*	-2.19
AKT3	-1.42	*PRKAA1*	-2.28
CAB39	-2.18	*PRKAB1*	-1
CDC42	-3.95	*PRKAG3*	-4.89
CHUK	-2.69	*PRKCG*	-2.36
DDIT4	-2.23	*RHEB*	-1.15
DDIT4L	-2.31	*RPS6KA1*	-2.01
DEPTOR	-3.83	*RPS6KA2*	-2.76
EIF4E	-3.86	*RPS6KA5*	-1.99
EIF4EBP1	-1.34	*RPS6KB2*	-4.79
EIF4EBP2	-2.66	*RPTOR*	-1.09
FKBP8	-2.07	*RRAGB*	-2.21
HIF1A	-3.38	*STK11*	-6.99
HRAS	-3.94	*TSC2*	-5.3
IGF1	-1.73	*ULK1*	-1.29
IGFBP3	-2.03	*ULK2*	-2.71
INS	-3.16	*VEGFA*	-3.68
INSR	-2.85	*PIK3CB*	1.75
IRS1	-2.35	*PRKCB*	1.02
MAPK1	-2.25	*PRKCE*	1.39
MLST8	-1.77	*RHOA*	1.31
MYO1C	-2.28	*RPS6*	1.4
PIK3C3	-2.14	*RPS6KB1*	1.08
PIK3CD	-3.95	*RRAGC*	1.88
PLD2	-2.62	*RRAGD*	2.47

Table showing changes in fold change values in patient derived glioblastoma *HK2*-KO cultures treated with metformin, compared to corresponding non-treated parent cultures. All genes are significantly downregulated ($p<0.05$).

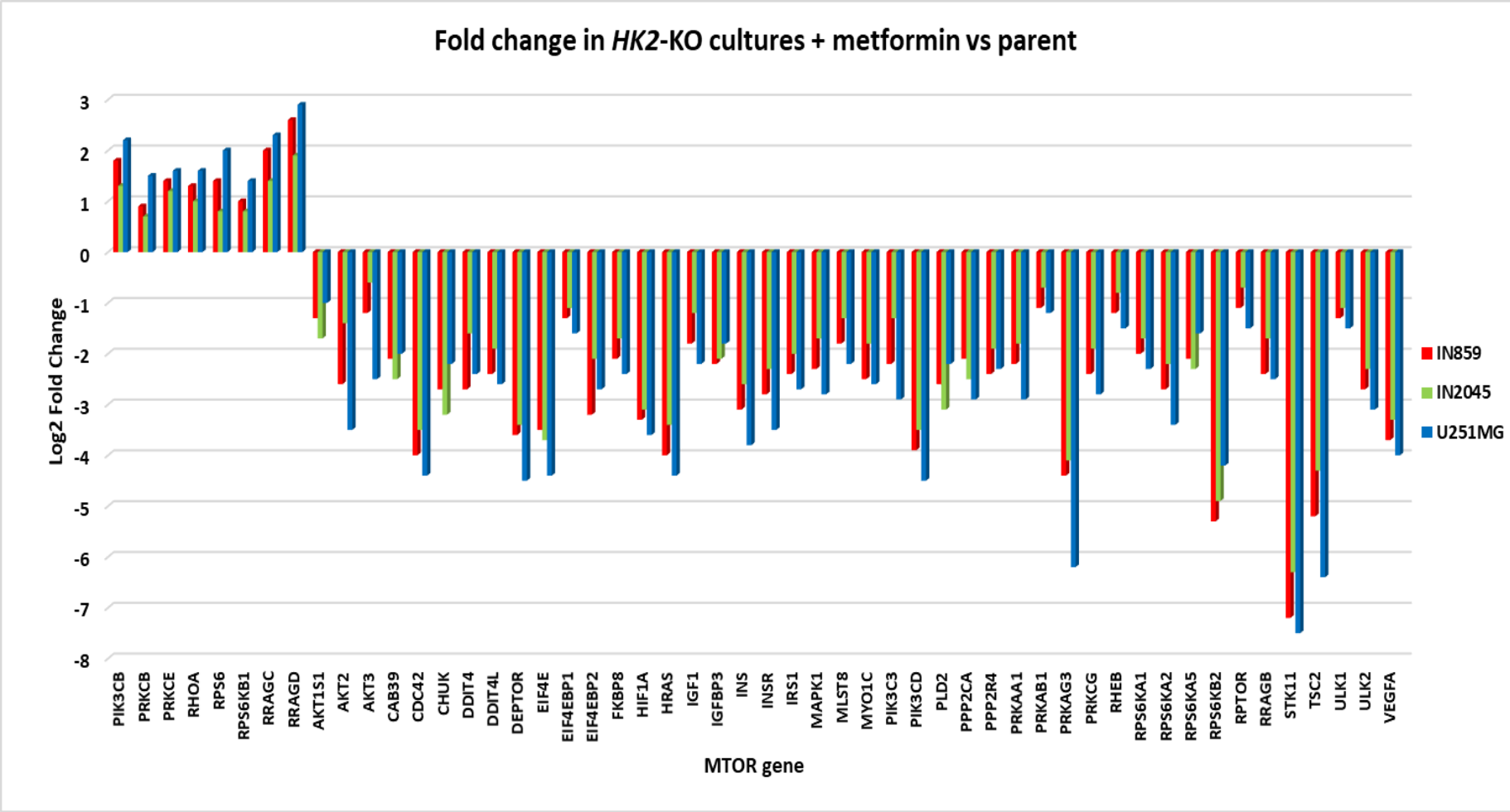

Figure 6.9 Bar chart comparing gene expression variation between *HK2*- KO modified glioblastoma cultures treated with metformin compared to parent cultures. The represented genes exhibit significantly altered levels of expression in the cultures compared as shown in Figure 6.8 and Table 6.3. Expression data is shown for individual cultures to compare levels of fold change variation.

Table 6.4 Expression fold change variation values of mTOR genes in all treated cultures compared to respective non-treated parent cultures

Log2 Fold Change			
Gene	Metformin	CRISPR	CRISPR + Metformin
RHOA	1.13	1.88	1.31
AKT1S1	-1.58	-2.05	-1.3
AKT2	-2.61	-2.45	-2.49
AKT3	-1.49	-2.36	-1.42
CDC42	-1.37	-1.26	-3.95
CHUK	-1.69	-3.17	-2.69
DDIT4	-1.58	-2.72	-2.23
EIF4E	-1.86	-2.53	-3.86
EIF4EBP1	-2.34	-1.98	-1.34
EIF4EBP2	-1.66	-2.67	-2.66
HRAS	-2.09	-2.64	-3.94
IGF1	-1.85	-2.92	-1.73
IGFBP3	-1.27	-1.57	-2.03
INS	-5.69	-3.85	-3.16
INSR	-1.38	-2.32	-2.85
IRS1	-1.25	-3.08	-2.35
MAPK1	-2.5	-3.18	-2.25
MLST8	-4.48	-2.99	-1.77
PPP2R4	-2.19	-4.17	-2.19
RHEB	-2.83	-6.34	-1.15
RPS6KA5	-2	-1.3	-1.99
RPS6KB2	-3.85	-1.93	-4.79
RPTOR	-1.05	-1.01	-1.09
STK11	-4.31	-5.24	-6.99
TSC2	-2.3	-4.74	-5.3
ULK1	-2.63	-6.13	-1.29
ULK2	-1.06	-3.27	-2.71

Table showing changes in expression values in all treated patient derived glioblastoma cultures, including *HK2*-KO, metformin and combination treatments, compared to corresponding non-treated parent cultures. All genes are significantly altered ($p<0.05$). Expression data is shown for individual treatments to compare levels of fold change.

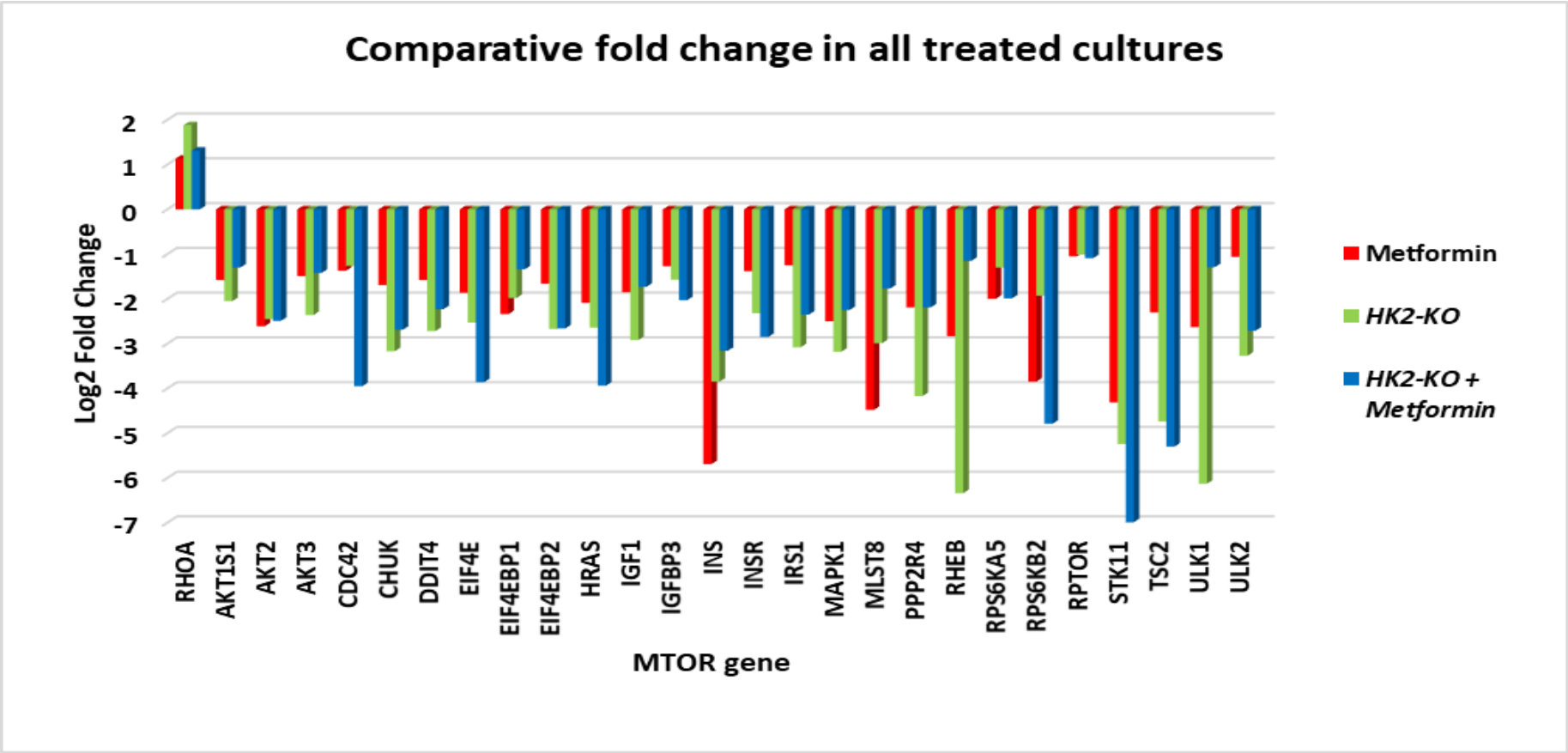

Figure 6.10 Bar chart comparing gene expression variation between all treated glioblastoma cultures compared to parent cultures. The represented genes exhibit significantly altered levels of expression across all treatments in all cultures, as shown in Table 6.4. Expression data is shown for individual treatments to compare levels of fold change variation.

6.3 Discussion

This chapter has focused on the investigation of the differential mRNA expression across 84 genes associated with the mTOR signalling pathway in patient- derived glioblastoma cultures (n=2) and U251MG, with the aim to determine the effects of metformin supplementation and/or the downregulation of *HK2* via CRISPR mediated knockout, upon the gene expression profile in the glioblastoma cultures. The array data in this study demonstrates differential expression across genes in the mTOR signalling pathway in both cultures where *HK2* had been downregulated via CRISPR mediated knockout and treated with metformin compared to the respective parent cultures. The data highlights the importance of *HK2* in mTOR signalling and the substantial inhibitory effect metformin has on the mTOR pathway. Previous studies have suggested metformin inhibits the mTOR pathway via the activation of *AMPK* (He, *et al*., 2015). Additionally, a greater number of genes were significantly altered in *HK2-KO* cells treated with metformin, with extensive downregulation across the mTOR pathway, indicating the combined inhibitory effect of both methods, impacting mTOR signalling.

HK2 knockout leads to significant downregulation across the mTOR pathway

HK2 knockout was associated with the downregulation of gene expression across the mTOR pathway in all 3 of the HK2 knockout cultures compared to the respective parent cultures. Furthermore, 55% of genes demonstrated significant substantially altered levels of expression across all the *HK2*-KO cultures compared to the respective parent cultures, with 48% of the genes presenting significant downregulation ($p<0.005$). The data suggests the importance of *HK2* role in the deregulation and frequently overexpressed mTOR signalling in glioblastoma. *HK2*-KO cultures revealed altered levels of expression in both mTOR upstream positive regulators *AKT2* (-2.45), *AKT3* (-2.36), *HR*AS (-2.64), *IGF1* (-2.92), *MAPK1* (-3.18 – fold change) and downstream positive regulators *EIF4E* (-2.53- fold change) *CDC42* (-1.26- fold change). Notably, both upstream and downstream negative regulators were upregulated in the HK2-KO cultures, including *PRKAG2* (1.06-fold change) and *PRKCA* (1.49- fold change) compared to the parent cultures, further suggesting HK2 as promoting mTOR activity. It has also been suggested that mTORC1 activity is

decreased by glucose deprivation, signifying the role of *HK2* as a mediator of mTOR signalling (Roberts, *et al.*, 2014). The array data confirmed this, *HK2*-KO cultures showed mTORC1 significant downregulation ($p<0.005$) of genes associated with mTORC1 signalling, *MLST8* (-2.99-fold change) and *RPTOR* (-1.01- fold change). The inhibition of mTORC1 activity results in driving autophagic processes associated with *AMPK* under glucose starvation. *HK2* has been shown to obstruct autophagy via the regulation of AMPK, impacting autophagic responses and subsequently increasing mTORC1 signalling, where *HK2* overexpression enhances the glucose dependent dephosphorylation of downstream targets of mTORC1. The knockdown of *HK2* was shown to inhibit this response (Soliman *et al.*, 2010). It has also been suggested that the depletion of *HK2* via siRNA knockdown, increases energetic stress, resulting in the activation of *AMPK*, and subsequently the inhibition mTORC1 activity (DeWaal *et al.*, 2018). Previous studies have also suggested that the activation of the *Akt*/mTORC1 pathway positively regulates *HK2* expression (Bhaskar *et al.*, 2009). The data suggests that *HK2* expression is stimulated by mTORC1 to metabolically support cellular growth and protection. Furthermore, *HK2* stimulates an inhibitory effect upon *AMPK*, resulting in the increased activity of mTORC1. In a glucose deprived environment, an increase in cellular stresses results in the activation of *AMPK* inducing autophagy; thus, providing an adaptive defence mechanism, preserving cellular integrity dependent on metabolic status (Roberts, *et al.*, 2015). The data here denotes that *HK2* overexpression also may perform a key function in the upregulation of the mTOR pathway driving cell cycle progression, growth and proliferation in glioblastoma.

Metformin treatment induces significant downregulation across the mTOR pathway

Metformin treatment was shown to induce the downregulation of gene expression across the mTOR pathway across all the cultures and 39% of genes exhibited significant ($p<0.005$) downregulated expression. Metformin have previously been shown to have a cytotoxic inhibitory effect in glioblastoma cultures, it has been suggested that metformin affects the activation of *AMPK* and has an inhibitory effect on the mTOR pathway (He *et al.*, 2015, Zakikhani, *et al.*, 2010, Fan, *et al.*, 2018).

The addition of metformin revealed altered levels of expression in genes associated with the mTOR complex mTORC1, where treated cultures showed significant downregulation ($p<0.005$) of *MLST8* (-4.48-fold change) and *RPTOR* (-1.05- fold change). Additionally, significant downregulation was shown in both mTOR upstream positive regulators *AKT*2 (-2.61), *AKT3* (-1.49), *HRAS* (-2.09), *IGF*1 (-1.85), *MAPK1* (-2.5), *MAPK3* (-2.12-fold change) and downstream positive regulators *HIF1A* (-1.94-fold change), *CDC42* (-1.37 fold change). Markedly, both upstream and downstream negative regulators were upregulated in the metformin treated cultures, including *PRKAA2* (1.15- fold change) *PRKAG2* (2.83-fold change) and *TSC1* (1.41- fold change) compared to the non-treated cultures. The array data indicates the potential mTOR inhibitory mechanism of metformin, resulting in the downregulation of upstream promotors and the upregulation of genes regulating mTOR activity. Studies have also stated that metformin inhibits respiratory complex I of the electron transport chain in mitochondria leading to the activation of *AMPK* and the inhibition of the mTOR pathway (Pollak, 2012; He and Wondisford, 2015). The data here shows the therapeutic potential of metformin treatment in glioblastoma, the investigation has shown metformin to have a substantial effect on mTOR signalling, causing significant reductions in gene expression across the inclusive pathway, highlighting its importance for targeting the frequently overexpressed mTOR signalling in glioblastoma (Han *et al.*, 2015).

Potential synergy between HK2-KO and metformin on mTOR activity.

The combination of metformin treatment in the *HK2*-KO cultures revealed comparable genetic profiles as seen with the monotherapies, occurring across the mTOR pathway in glioblastoma cultures. The array data shows a greater number of genes were significantly altered in the *HK2-KO* cells when treated with metformin, compared to the respective singular treatments, with extensive downregulation across the mTOR pathway. Both mTOR upstream positive regulators *AKT2* (-2.49), *AKT3* (-1.42), *HRAS* (-3.94), *IGF1* (-1.73), *MAPK1* (-2.25– fold change) and downstream positive regulators *EIF4E* (-3.86) *CDC42* (-3.95-fold change). The study demonstrates the potential advantages of both the downregulation of *HK2* alongside the addition of metformin to induce significant universal downregulation of genes in

the mTOR pathway, resulting in the reduction of the abundantly overexpressed mTOR signalling frequently occurring in glioblastoma. *HK2* has been shown to impact the mTOR pathway in cardiomyocytes (Roberts, *et al*., 2014), the knockdown of *HK2* may lead to the increase of energetic stress, activating *AMPK* resulting in the inhibition mTORC1 activity; additionally*, HK2* has been shown to enhance chemoresistance (Wolf *et al*., 2011), its downregulation may also potentially increase the effectiveness of metformin in regulating *AMPK* activation, thus increasing its' inhibitory effect in the mTOR pathway in glioblastoma. A study has also shown the synergistic effect of *HK2* knockdown with the supplementation of metformin on mTORC1 activity, where the combination was shown to inhibit mTORC1 (DeWaal *et al*., 2018). The study also determined that even in the absence of *AMPK*, the combinatory effect of metformin treatment in HK2 depleted hepatocellular carcinoma cells led to an increase in the expression of *REDD1*, a known inhibitor of mTORC1 (DeWaal *et al*., 2018), however the array data in this study determined that *REDD1 (DDIT4*) expression was reduced (-1.58- fold change) in cultures treated with metformin and in the absence of *HK2*. Both the addition of metformin and the knockdown of *HK2* demonstrated significant downregulation ($p<0.005$) of the mTORC1 associated genes *MLST8* (-1.77- fold change) and *RPTOR* (-1.09- fold change); as well as significant downregulation ($p<0.005$) of multiple genes associated with the mTOR signalling pathway, many of which have been strongly associated with cancer progression and development. Examples include the Serine/threonine kinase 11 (STK11), which has been strongly associated with Peutz-Jeghers syndrome, an autosomal disorder characterised by mucocutaneous melanin pigmentation, gastrointestinal polyposis, and an increased risk for the development of various neoplasms (Giardiello *et al*., 2000). STK11 has also been associated with somatic mutations in lung cancer, cervical, breast, intestinal, testicular, pancreatic and skin cancer (Lim *et al*., 2004; Sanchez-Cespedes, 2007; Jiang *et al*., 2018). HRAS is part of one of the most commonly deregulated pathways in human cancer and activating mutations in RAS genes occur in approximately 30% of all tumours (Ding *et al*, 2008). *HRAS* mutations are frequent in bladder and thyroid cancer (Sugita *et al*., 2018). Aberrant activation of Ras signalling is a frequent occurrence in glioblastoma, a study investigating the mutation analysis of *NRAS, HRAS* and *KRAS*

revealed somatic point mutations in 5% of the glioblastomas tested (Knobbe *et al*., 2004). Additionally, the development of specific and competitive inhibitors is challenging, because the RAS protein lacks a druggable binding pocket (Cox *et al*., 2014). This study also showed *MAPK1* to be downregulated when HK2 was knocked out, and with the supplementation of metformin. *PI3K/MAPK* pathways have been shown to be mutated in 90% of glioblastoma, and have been associated with many cancer hallmarks, including increased survival, proliferation, and migration (Hanahan and Weinberg, 2011). Studies have also shown the activation of *MAPK* signalling is often through *KRAS* mutations (McNeill *et al*.,2017). The downregulation of multiple genes that have been shown to instigate or propagate tumorigenesis in many cancers is an important finding, via the inhibition of *HK2* and through the inhibitory mechanisms of metformin. The array data has further confirmed the significance of *HK2* and its impact on the progression and development in glioblastoma, the downregulation of *HK2* shows the reversal of ubiquitous overexpression of mTOR genes, with substantial downregulation occurring across the pathway, compared to the parental cultures. Furthermore, the information presented here supplements the cytotoxic ability of metformin, which has previously been shown to impact the glucose pathway and cause anti-proliferative effects in glioblastoma cultures; the array data indicates metformin ability to target aberrant mTOR signalling in glioblastoma through potentially *AMPK* activation. Finally, the array data reveals a promising novel mechanism of targeting the dysregulated mTOR signalling in glioblastoma, with the combination of *HK2* KO and metformin increasing cellular stresses and leading to the potential activation of *AMPK* and/or the increased expression of *REDD1* resulting in the inhibitor of mTORC1; highlighting the potential application of a therapeutic treatment in a substantial subset of glioblastoma.

CHAPTER 7

Final discussion and conclusions

7.1 Discussion

Glioblastoma are the most common high-grade primary brain tumour in adults that represent up to 65% of brain tumours. Glioblastoma classification stringently follows WHO guidelines which were updated in 2016 to include molecular subtyping to characterise 2 sub-groups, based upon the isocitrate dehydrogenase (IDH) mutation status (Arevalo *et al.*, 2017). Prognosis is extremely poor with median survival of approximately 15 months (Bleeker *et al.*, 2012). The primary current treatment methods for glioblastoma is a multimode approach which involves surgical resection of the tumour tissue, radiation treatment followed by concomitant chemotherapy with TMZ, effective in a subset of patients based on MGMT methylation status (Stupp *et al.*, 2015). Furthermore, considerable side effects are regularly associated with treatment, impacting on the quality of life (Backes *et al.*, 2015; Oberoi *et al.*, 2015). Effective drug treatments are hindered predominantly by the complex genetic background of glioblastoma, with significant intra- and inter- tumour heterogeneity, encompassing a broad range of mutations, deletions and other molecular aberrations drastically limiting monotherapies (Backes *et al.*, 2015; Arevalo *et al.*, 2017). An alternative approach is the targeting of abnormal metabolic pathways that are universally dysregulated in glioblastoma. Treatments that modulate metabolism offer a potential therapeutic avenue in which to treat a higher percentage of patients, whilst sparing normal cells and reducing negative side effects (Wolf *et al.*, 2011). The development of therapeutic agents is crucial for improved patient stratification and for the advancement of glioblastoma treatment. This study has contributed to these areas with the identification of a promising molecular target. Analysis of glioblastoma biopsies in this study revealed the glycolytic enzyme *HK2* to be significantly upregulated, with overexpression as a common occurrence. *HK2* overexpression was detected in all 103 biopsy samples and in 15 patient- derived cultures. These findings were comparable to the reported frequencies in other cancers, including both lung and breast cancer (Wang *et al.*, 2014; Anderson *et al.*, 2016) and in glioblastoma cell lines (Wolf *et al.*, 2011). To further determine the

deregulated expression of *HK2*, the association between genetic and epigenetic mechanisms in glioblastoma was investigated. Pyrosequencing technology was used to conduct methylation changes across multiple CpG cites in the *HK2* promotor region in 103 biopsies and 15 patient- derived cultures and NHA. This study has identified genomic changes in glioblastoma distinct from normal brain tissue, with substantial epigenetic alterations present in glioblastoma. Hypomethylation was shown to be present in all the 103 biopsy samples compared to normal brain. Varied levels of reduction in promotor methylation was demonstrated across the multiple CpG sites (n=15) in the biopsies, with an average loss of 20% compared to normal brain tissue. Promotor hypomethylation was also established in the patient-derived samples with significantly reduced ($p<0.0001$) levels of methylation of 38.3% compared to normal tissue. These findings reflect previous studies, where global hypomethylation has been shown to be present in primary human glioblastomas (Cadieux *et al.*, 2006). This study established a strong correlation between the percentage of hypomethylation and the level of *HK2* expression in all glioblastoma samples. Hypomethylation of *HK2* was also shown to enhance levels of *HK2* expression, demonstrated across all 103 biopsies and the 15 patient- derived cultures. This study also revealed elevated *HK2* expression to be associated with outcome, where a significantly shorter ($P<0.0001$) OS was demonstrated in patient biopsy samples with higher *HK2* expression. The data obtained here compares to previous studies in which elevated *HK2* expression was significantly associated with shorter OS (Liu *et al.*, 2016; Wu *et al.*, 2017). The association between *HK2* expression and outcome offers an important insight to a potential prognostic marker and for further stratification of glioblastoma patients, independent of *MGMT* status, where patients differentiated by expression levels may potentially benefit from treatments that target *HK2*. Taking this into account, this study also evaluated the effects of *HK2* inhibition in glioblastoma, via *in vitro* studies using 15 patient- derived cultures. Array analysis of paired biopsy and culture samples revealed that the patient-derived glioblastoma cultures maintained a considerable proportion of gene expression present in the original tumour biopsies and may be used as an accurate pre-clinical model for glioblastoma molecular biology studies. Although there was a degree of differential expression in the cell cultures compared to the biopsies,

reflecting the influence of artificial culture conditions, the patient-derived cell cultures retained most of the characteristic signatures of glioblastoma making them appropriate *in vitro* models for the evaluation of targeted therapeutics. This study investigated *HK2* inhibition through CRISPR-mediated knockout, the removal of *HK2* demonstrated a significant decrease ($p<0.007$) in cell growth across all treated cultures compared to the respective parent cultures. Notably, cultures expressing increased levels of *HK2* were more greatly affected, with higher reductions in proliferation. An important finding of this study is the significantly increased ($p<0.0001$) sensitivity to TMZ in *HK2*-KO cultures, with substantial reduction in both the ID_{50} values and in cell survival (20% reduction) after treatment, compared to the parent cultures. Similarly, the efficacy of metformin was significantly increased ($p<0.0001$) in *HK2* depleted cultures, with average ID_{50} values decreased by 46.8% compared respectively to the parent culture. Expression profiler arrays were utilized to determine the wider effect of *HK2* knockout across the glycolytic pathway. *HK2* knockout was shown to result in the downregulation of 70% of the genes (59 of the 84), with significant reduction in expression across the glucose pathway in all cultures, compared to the corresponding parent cultures. This novel data suggests that targeting *HK2* results in the universal downregulation of genes in the glucose pathway, consequently affecting downstream pathway expression, highlighting the importance of *HK2* role in glycolysis, driving tumour growth and proliferation. The data here strongly supports the notion that *HK2* overexpression in cancer cells enhances resistance to therapies (Wolf *et al.*, 2011); as well as *HK2* influencing the magnitude of glucose within cells, driving an accelerated glucose flux in cells commonly associated with the Warburg effect (Patra *et al.*, 2013; Mukherjee *et al.*, 2015).

This study also validated a *HK2* specific inhibitor 3-BPA, as an effective anti-proliferative agent in all cultures under normoxic and hypoxic conditions. Moreover, 3-BPA demonstrated specificity in targeting *HK2*, where cultures expressing higher levels were more sensitive ($p= 0.0192$) to the inhibitor. An important finding was that 3-BPA anti-proliferative effects were specific to the glioblastoma cultures, whilst sparing healthy metabolising cells with a substantially lower inhibitory response in NHA. This study demonstrated that 3-BPA induces apoptosis in glioblastoma, where

significantly higher apoptosis ($p<0.0001$) was exhibited in cultures expressing higher levels of *HK2*. Additionally, a significant increase ($p<0.0001$) in the level of caspase 3/7 was detected in all 3-BPA treated cultures. Caspase 3/7 are primary effectors at the end of the apoptotic caspase pathway and the primary data strongly indicates that the caspase dependent apoptotic pathway is induced as the main mechanism of cell death in glioblastoma from 3-BPA treatment.

Importantly levels of apoptosis were reduced in the glioblastoma cultures under hypoxic conditions. The hypoxic data correlates to previous studies, where HIF1 upregulation was shown to have inhibitory effects on a range of factors involved in apoptosis and the regulation of cell death mechanisms in glioblastoma (Trachootham *et al.*, 2006; Yang *et al.*, 2012).

Expression profiler arrays were utilized to determine the wider effect of 3-BPA on the glycolytic pathway. Similarly to CRISPR-KO of *HK2*, 3-BPA supplementation was shown to result in the significant downregulation ($p<0.005$) of 50% of the genes (42 of the 84), with reduction in expression across the glucose pathway in all cultures, compared to the corresponding non-treated cultures. Notably this study demonstrated the synergy between TMZ and 3-BPA in a subset (33%) of glioblastoma cultures. This novel data shows 3-BPA as an efficient energy blocker through targeting *HK2*, making it a potential therapeutic candidate as an antitumor drug in a subset of glioblastoma. The significance of this data strengthens previous studies, which have shown 3-BPA to cause cytotoxic effects in human myeloid leukaemia (HL60) cells, hepatocellular carcinoma (HCC) cells and breast cancer cells (MCF-7) via the inhibition of ATP-producing glycolysis and mitochondrial respiration (Ko *et al.*, 2001; Calvino *et al.*, 2014; Lee *et al.*, 2017; Pulaski *et al.*, 2018).

The anti-diabetic drug metformin was also investigated in this study. The repurposing of existing licenced medication is advantageous in many aspects, reducing costs and time in the clinical trial process and offering a potential faster implementation of new therapeutic treatments for glioblastoma (Abbruzzese *et al.*, 2017). Metformin demonstrated an anti-proliferative effect in all cultures under normoxic and hypoxic conditions. Additionally, a substantial difference in the response of the glioblastoma cells compared to NHA, demonstrated that the

mechanism of action of metformin was exclusive to cancer cells, inhibiting glioblastoma proliferation through glucose deprivation, although not specifically through *HK2*. Similar correlations have been demonstrated in breast cancer cell lines (Menendez *et al.*, 2012; Birsoy *et al.*, 2014). Expression profiler arrays were also utilized to determine the wider effect of metformin on the glycolytic pathway. All cultures treated with metformin showed significant downregulation ($p<0.005$) in 59% of the genes (50 of the 84) with reduction in expression across the glucose pathway in all cultures, compared to the corresponding non-treated cultures. Importantly this study demonstrated the synergistic affiliation between TMZ and metformin in a subset (50%) of glioblastoma cultures, indicating the potential therapeutic advantages of combination treatments, prospectively allowing for smaller TMZ dosages with reduced side effects. This study also verified that metformin does not induce apoptosis in glioblastoma and may act through another mechanism of cell death such as autophagy. Studies have suggested that metformin activates AMPK resulting in the inhibition of the mTOR pathway, impeding cellular proliferation (Pollak, 2012; Liu *et al.*, 2014; He and Wondisford, 2015). Taking this into account, expression profiler arrays were used to investigate the effect of metformin on the mTOR pathway, where treatment was shown to induce the downregulation of gene expression across the signalling pathway in all the glioblastoma cultures, with 39% of the genes exhibiting significant reduced expression ($p<0.005$). The data indicates that metformin has an inhibitory effect on mTOR signalling in glioblastoma cultures, resulting in genetic alterations and downregulation across the entire pathway. Notably CRISPR-KO of *HK2* also generated similar results, with 48% of the genes presenting significant reduced expression ($p<0.005$), indicating universal mTOR pathway downregulation. Importantly the data shows a potential synergistic effect of *HK2*-KO and metformin on mTOR activity, with 61% of the mTOR genes exhibiting a significant altered level of expression ($p<0.005$). The data correlates to similar studies where *HK2* has been shown to impact the mTOR pathway (Roberts, *et al.*, 2014) and where siRNA knockdown of *HK2* was shown to inhibit mTORC1 (DeWaal *et al.*, 2018). The knockout of *HK2* may lead to the increase of energy stress, activating AMPK and resulting in the inhibition mTORC1 activity whilst simultaneously increasing the effectiveness of metformin at inhibiting the mTOR pathway in

glioblastoma. Finally, the glioblastoma cells were shown to be ineffective at metabolizing the ketone body 3-HB, however NHA demonstrated the ability to proliferate under ketogenic substrates. The data suggest the combination of a ketogenic diet with chemotherapy and/or radiotherapy may help improve tumour response and OS in glioblastoma patients.

7.2 Limitations

There are several limitations inherent to this study and its techniques used.

The use of patient-derived cultures was a strong feature of the study as it provided a more representative model of glioblastoma tumours. The panel of patient-derived cultures used would benefit from further characterisation both genetically and epigenetically, in order to distinguish differing genomic characteristics. This would also enable a more complete understanding of the variation in cellular response and identify potential treatment sub-groups. Due to the large variations in the culture doubling times it became a logistical problem to maintain many different patient-derived cultures, this resulted in smaller groups of cultures being utilised in some experiments, such as the CRISPR-*HK2* KO, combination treatments and some of the flow cytometry work. Functional studies and analysis of the cell death pathways were limited in the amount of techniques and instrumentation available. The use of a Seahorse machine would be beneficial, to investigate mitochondrial membrane functionality with *HK2* inhibition with various inhibitors. In addition, the study did not assess necrosis or autophagy as additional mechanisms of cell death with *HK2* inhibition. Finally, the pyrosequencing of the 103 biopsy samples was limited to a single set of primers covering CpGs 8,9,10 and 11. These primers were selected based on data interpretation from preliminary experimental runs of a subset of the biopsy samples. Ideally the methylation status of the 103 biopsies would have been investigated using all *HK2* primer sets, however cost and time constraints resulted in limitations. Access to the pyrosequencing machine at the University of Birmingham was through a collaboration, therefore access was not always viable.

7.3 Further study

This study has identified the important role that *HK2* enacts within the development of glioblastoma and determined the potential therapeutic advantages of targeting *HK2*. There are several directions in which this research could progress.

The *HK2* inhibitors had a strong cytotoxic and metabolic effect on the cells. The work carried out in this study investigated genetic and cellular changes such as cytotoxicity assays. Further investigations of the effect of the inhibitors on a proteomic level through ELISA and western blotting would be beneficial in determining functional effects of the inhibitors and their impact upon glycolytic associated proteins.

Cell culture modelling could be expanded with 3-D modelling and spheroid cultures offer a promising analytical tool, with more accurate representations of the authentic growing conditions and microenvironment of glioblastoma (Kaluzova *et al.*, 2015). The inhibition of *HK2* could be further studied in these models, whereby analysis of migration and invasion could be accurately gauged. The hypothesis is that with the downregulation of *HK2*, the glioblastoma cultures should demonstrate reduced invasive characteristics and display decreased migration. Additionally, following on from the 3D- modelling, xenograft mice models would be crucial for studying the effects of *HK2*-KO in terms of invasion, migration and chemoresistance in a system that better mimics the primary tumour as compared to cells grown *in vitro*, offering relevant predictive insights into clinical outcomes. The use of the patient-derived glioblastoma cultures as explants potentially would conserve original tumour characteristics such as heterogeneous histology, biomolecular signature, malignant genotype and phenotype, tumour architecture and tumour vasculature (Vandamme, 2014). The inhibitor 3-BPA showed promising results, demonstrating a high affinity and specificity for targeting *HK2*. The development of a better drug delivery system to administer 3-BPA will significantly increase its practical application in a range of cancers whilst simultaneously reducing any adverse effects. The development and use of a biodegradable polymer offer substantially increased uptake to the target region, whilst reducing systemic toxicity (Wicks *et al.*, 2015). Additionally, the application of nanotechnology offers many advantages such as increased BBB permeability for glioma tumours as well as lower effective dosages when in

combination with targeted liposomes such as folate or transferrin ligands (Gandham *et al.*, 2015; Zhang *et al.*, 2018; Fan *et al.*, 2019). The development of 3-BPA would potentially increase its potential as a therapeutic agent in future clinical oncology. This could be achieved through biochemical analysis, with analogue development in which 3-BPA could be modified, offering varied bioactive compounds for potential increased effectiveness, increased BBB permeability and targeting potential, whilst retaining chemical and biological similarity with the original model compound.

Appendix

Table A1. Methylation % for individual CpG sites in 103 biopsies

Biopsy	CpG 8 Methylation %	CpG 9 Methylation %	CpG 10 Methylation %	CpG 11 Methylation %
85	7.47	3.64	2.92	4.19
103	7	6.18	6.21	3.76
110	6.29	1.28	1.57	6.2
116	6.29	4.28	1.57	3.83
121	6.87	6.39	7.98	9.27
122	6.48	4.27	3.9	2.37
142	9.14	3.92	2.29	5.37
165	5.3	7.66	8.25	7.92
175	6.88	7.24	8.27	5.46
204	5.34	4.75	7.09	8.67
338	5.19	4.22	4.87	6.37
343	7.03	6.24	10.99	11.43
352	4.49	3.86	2.09	6.38
374	5.75	4.56	5.83	4.62
377	5.55	7.81	5.22	8.53
382	7.42	7.13	10.46	11.84
396	6.69	8.32	9.98	8.43
410	6.19	12.51	3.54	3.82
411	4.72	11.67	1.2	3.21
436	4.89	9.28	1.22	7.36
445	6.66	5.49	10.35	9.48
472	6.27	3.95	4.69	5.3
522	6.53	6.24	1.63	5.73
535	5.97	3.88	3.91	4.48
590	1.93	16.64	6.92	10.99
626	1.71	4.93	5.1	3.47
640	9.52	17.71	5.19	18.8
651	6.26	4.78	4.33	3.57
685	15.75	11.35	3.78	8.47
693	10.03	4.17	4.42	7.37
705	3.5	3.82	3.94	5.13
717	9.16	19.59	5.28	14.5
723	4.15	5.53	3.82	4.61
729	11.4	7.08	4.62	7.13
733	15.43	9.48	3.86	6.76

743	1.64	5.22	1.31	3.27
746	1.42	4.15	4.78	4.46
749	3.52	2.65	3.96	3.94
758	4.42	5.94	4.7	6.46
769	5.43	7.01	4.64	5.35
781	7.58	7.08	5.28	4.2
792	3.58	9.44	3.75	3.73
793	6.06	3.66	7.79	4.21
813	3.98	4.14	2.9	3.46
816	11.62	14.56	2.91	12.6
819	5.33	5.03	2.59	6.63
820	4.85	3.64	1.21	3.58
822	5.37	4.33	4.64	6.84
826	12.39	9.28	6.94	9.38
848	8.57	17.84	12.24	14.67
849	3.07	4.83	8.02	6.68
850	4.36	3.01	3.74	4.62
860	6.59	7.54	1.41	5.74
874	9.87	3.2	8.83	4.38
876	7.02	4.6	11.95	6.35
898	5.12	1.33	4	3.79
905	2.82	2.89	4.34	1.24
911	14.39	11.1	4	7.53
915	5.14	7.98	9.25	4.24
916	4.98	4.62	4.58	3.24
955	0	5.36	6.32	7.89
956	4.07	4.21	6.35	5.92
966	11.73	3.85	2.07	3.28
970	4.9	4.37	5.18	7.53
994	3.92	4.72	4.46	9.53
1000	5.93	4.56	2.16	2.56
1006	8.53	8.52	5.87	3.43
1014	6.25	4.53	4.09	4.25
1015	4.48	11.27	6.39	4.83
1016	7.66	4.56	4.97	3.56
1054	5.67	4.75	8.5	6.77
1062	11.15	6.91	3.44	5.35
1091	4.55	3.56	6.79	4.56
1098	12.64	12.97	2.67	9.69
1100	6.05	11.46	8.28	7.43
1101	4.1	13.63	10.43	2.9
1134	4.58	3.13	3.9	2.52
1176	7.29	5.9	4.35	4.08
1178	4.33	3.67	7.11	5.71
1342	6.76	7.32	2	3.22
1404	8.22	7	4.55	4.22
1414	4.93	3.78	6.13	9.82
1417	7.98	12.45	3.96	9.31
1428	9.48	5.12	6.82	5.31
1437	11.44	9.22	9.56	6.11
1446	3.19	9.12	10.32	7.49
1460	7.49	11.84	7.45	10.18
1547	7.43	4.89	7.22	5.87
1549	5.34	3.86	5.63	4.79
1565	6.76	7.33	8.35	7.35

1595	5.54	4.19	3.33	3.57
1606	12.32	9.93	12.57	11.34
1617	5.84	10.2	1.46	3.42
1643	10.23	9.35	7.56	7.23
1687	4.88	5.74	4.15	8.27
1728	3.97	3.13	2.86	12.2
1745	1.76	8.52	8.45	12.62
1793	7.58	7.4	1.9	9.13
1902	9.35	13.84	3.11	9.29
2229	5.3	7.66	8.25	3.86
2242	5.24	5.46	4.23	4.11
Normal	22.71	22.25	42.98	16.88
Normal	24.35	20.38	40.85	18.52
Normal	25.11	21.72	41.78	17.88
Normal	23.16	24.25	42.22	16.91
Normal	22.75	21.85	42.43	18.92
+ve control	95.76	96.18	94.74	94.43

Table showing *HK2* methylation % in biopsies and normal tissue in CpG 8- 10 via pyrosequencing. CpG 10 showed the highest level of deregulated methylation between normal tissue (average of 42.1%) and biopsies (average of 5.4%) and cultures (average of 3.8%).

Table A2. *HK2* fold change compared to *MGMT* status for 103 biopsies

Biopsy	*HK2* fold change	*MGMT* Status	Biopsy	*HK2* fold change	*MGMT* Status
103	41.05	Methylated	165	40.14	Methylated
110	186.30	Methylated	396	69.44	Methylated
116	6.69	Methylated	445	43.57	Methylated
122	263.74	Methylated	651	89.85	Methylated
377	120.25	Methylated	1000	149.84	Methylated
382	39.30	Methylated	1606	22.36	Methylated
522	30.76	Methylated	1643	98.55	Methylated
535	87.80	Methylated	343	20.06	Methylated
590	49.07	Methylated	1793	600.96	Unmethylated
626	195.30	Methylated	85	75.22	Unmethylated
640	51.06	Methylated	121	51.72	Unmethylated
685	446.04	Methylated	142	788.29	Unmethylated
693	819.78	Methylated	175	14.90	Unmethylated
705	121.62	Methylated	204	57.38	Unmethylated
717	65.26	Methylated	338	825.59	Unmethylated
723	77.04	Methylated	352	40.75	Unmethylated
729	132.68	Methylated	411	120.73	Unmethylated
733	276.44	Methylated	436	127.24	Unmethylated
743	285.95	Methylated	472	99.50	Unmethylated
746	867.62	Methylated	792	195.97	Unmethylated
749	216.62	Methylated	874	175.97	Unmethylated
758	409.23	Methylated	956	126.62	Unmethylated
769	172.12	Methylated	966	125.62	Unmethylated
781	320.24	Methylated	1006	298.95	Unmethylated
793	875.78	Methylated	1014	3.83	Unmethylated
813	216.62	Methylated	1015	288.42	Unmethylated
816	679.91	Methylated	1054	173.92	Unmethylated

819	288.42	Methylated	1062	136.68	Unmethylated
820	183.30	Methylated	1101	320.24	Unmethylated
822	763.67	Methylated	1178	346.44	Unmethylated
826	569.76	Methylated	1404	111.39	Unmethylated
848	122.12	Methylated	1414	140.13	Unmethylated
849	205.24	Methylated	1417	315.68	Unmethylated
850	475.90	Methylated	1428	7.43	Unmethylated
859	897.54	Methylated	1437	21.92	Unmethylated
860	26.13	Methylated	1446	153.26	Unmethylated
876	358.76	Methylated	1460	117.88	Unmethylated
898	669.94	Methylated	1549	142.08	Unmethylated
905	285.95	Methylated	1595	425.07	Unmethylated
911	172.12	Methylated	1687	149.52	Unmethylated
915	104.50	Methylated	1745	43.80	Unmethylated
916	883.25	Methylated	1902	31.10	Unmethylated
955	109.24	Methylated	374	136.68	Unmethylated
970	78.73	Methylated	410	140.13	Unmethylated
1016	159.04	Methylated	956	126.62	Unmethylated
1098	86.34	Methylated	994	221.23	Unmethylated
1100	43.78	Methylated	1091	115.79	Unmethylated
1134	23.62	Methylated	1565	269.10	Unmethylated
1176	149.45	Methylated	1617	178.40	Unmethylated
1342	148.30	Methylated	1728	764.99	Unmethylated
1547	106.31	Methylated	2242	189.65	Unmethylated
2229	18.39	Methylated			

Table showing *HK2* fold change compared to methylation status in 103 biopsies. No correlation between *HK2* expression and *MGMT* status was determined.

Table A3. *HK2* fold change compared to *MGMT* status for 13 cultures

Culture	HK2 fold change	*MGMT* Status
U251MG	1502.6	Methylated
IN 2045	219.8	Methylated
IN 1760	202.0	Methylated
IN 859	995.1	Methylated
IN 1528	386.0	Methylated
IN 1461	85.7	Unmethylated
IN 1472	403.4	Unmethylated
IN 1951	210.6	Unmethylated
NHA	30.4	Unmethylated
IN 1612	126.6	Unmethylated
IN 2093	132.8	Unmethylated
IN 1979	574.4	Unmethylated
IN 1265	97.4	Unmethylated

Table showing *HK2* fold change compared to methylation status in 13 cultures. No correlation between *HK2* expression and *MGMT* status was determined.

Table A4. Doubling time of culture panel

Culture	Doubling time (Hours)	Culture	Doubling time (Hours)

U251MG	24 (±1.56)	UWLV22	44 (±2.56)
U87MG	24 (±2.01)	IN1472	45 (±1.75)
IN859	24 (±2.22)	IN1682	50 (±1.42)
IN1612	28 (±1.5)	IN1265	50 (±2.8)
IN1528	32 (±1.26)	IN1951	55 (±2.08)
IN1979	34 (±2.51)	IN1461	60 (±1.82)
IN2045	36 (±1.64)	NHA	63 (±2.62)
IN1760	40 (±3.1)	IN2093	70 (±3.22)
UWLV22	35 (±2.13)	UWLV152	46 (±3.04)
UWLV48	45 (±2.55)	UWLV156	48 (±1.27)
UWLV53	33 (±1.32)	UWLV212	53 (±2.37)

Table showing doubling times for cultures used in this study.

Table A5. *MGMT* status of the glioblastoma culture panel

CULTURE	METHYLATION STATUS
U251MG	Methylated
IN 2045	Methylated
IN 1760	Methylated
IN 1461	Unmethylated
IN 1472	Unmethylated
IN 1951	Unmethylated
NHA	Unmethylated
IN 1612	Unmethylated
IN 859	Methylated
IN 1528	Methylated
IN 2093	Unmethylated
IN 1979	Unmethylated
IN 1265	Unmethylated

Table showing *MGMT* culture for cultures used in this study.

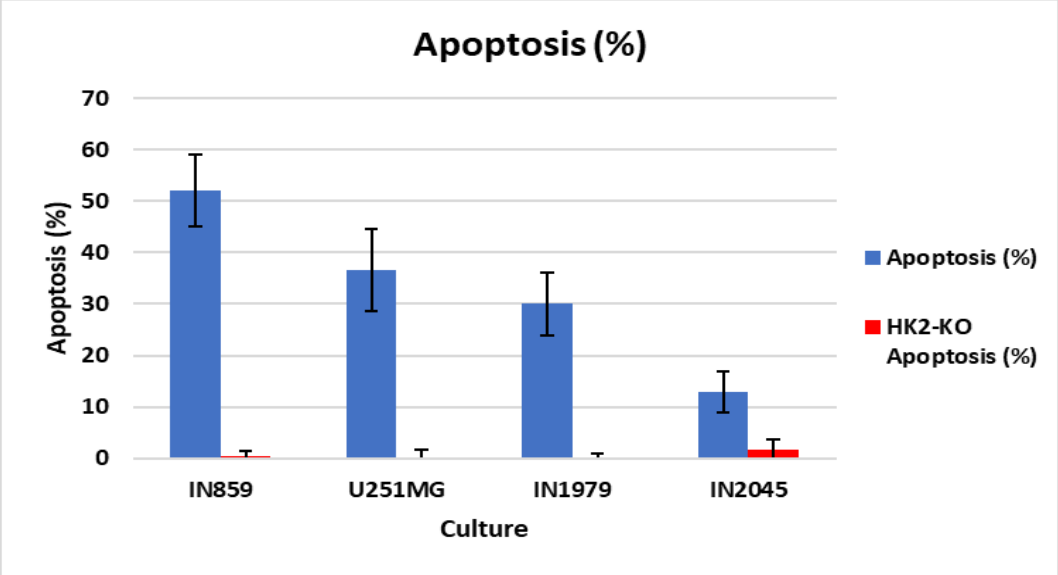

Figure A1 Showing induced apoptosis in *HK2*-KO cultures compared to parent cultures after 72-hour treatment with 3-BPA. The percentage of apoptosis was significantly ($p<0.0001$) reduced across all *HK2*-KO cultures compared to respective parent cultures. Cultures expressing higher levels of *HK2* showed a greater decreased level of apoptosis in *HK2*-KO cultures compared with parent cultures.

Table A5. Percentage of apoptosis in HK2-KO cultures compared to parent cultures

Cultures	Apoptosis (%)	*HK2*-KO Apoptosis (%)	% Change in Apoptosis
IN859	52	0.4	-99.2*
U251MG	36.7	0.2	-99.4*
IN2045	13	1.6	-87.6*
IN1979	30	0.1	-99.6*
Mean	38.2	0.58	-98.4*

Table showing percentage of apoptosis in *HK2*-KO cultures compared to parent cultures after 72-hour treatment with 3-BPA. Significantly ($p<0.0001$) reduced apoptosis was exhibited across all *HK2*-KO cultures compared to respective parent cultures. Cultures expressing higher levels of *HK2* showed a greater decreased level of apoptosis in *HK2*-KO cultures compared with parent cultures.

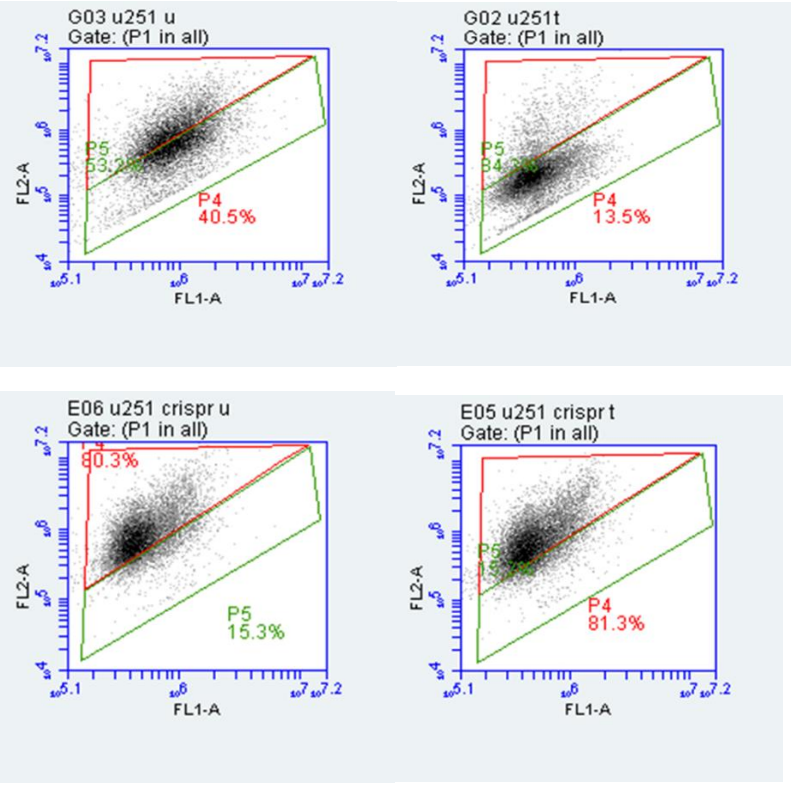

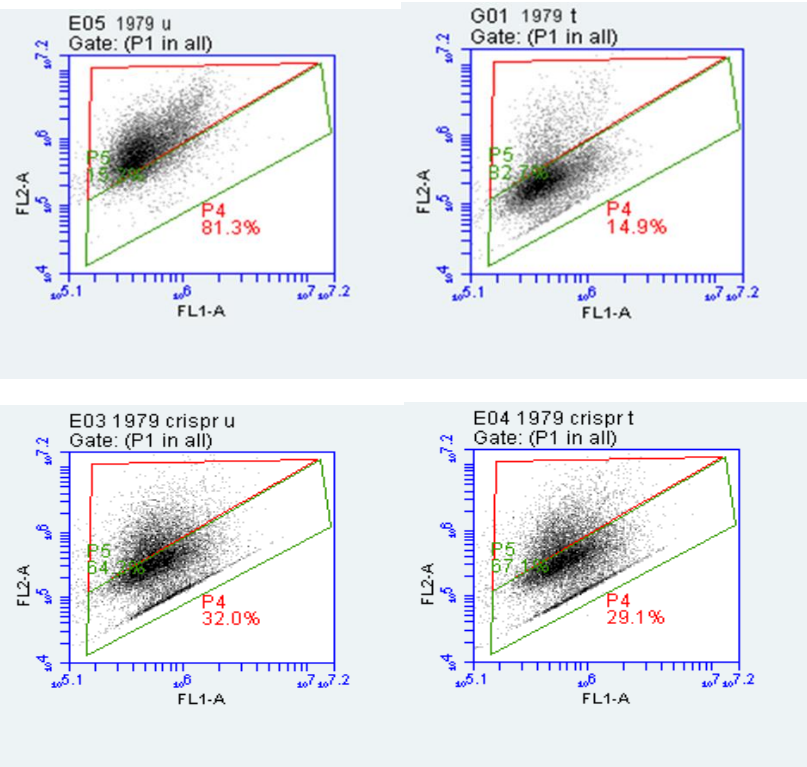

Figure A2 Showing the measurement of mitochondrial membrane potential in *HK2*-KO and respective parent cultures with 3-BPA treatment. Untreated cultures are shown on the left (U), 3-BPA cultures treated for 72- hours on the right (T). 3-BPA treatment leads to depolarisation of the ΔΨ in parent cultures, shown with a shift in the FL-1A channel (increase in monomer % (green value)). No change in depolarization % was seen in *HK2*-KO cultures. Red gating shows JC-1 aggregated within the mitochondria, where green gating shows JC-1 monomers unable to enter through the mitochondrial membrane.

Table A6. Glucose array showing gene expression in biopsies

Gene	UWLV 53	UWLV 22	UWLV 48	UWLV 156	UWLV 152	UWLV 212
ALDOA	2.0	1.5	1.1	1.2	1.4	1.2
ALDOB	1.7	4.2	1.7	2.1	1.7	3.6
ENO1	2.0	3.1	1.6	1.5	1.5	1.2
FBP2	1.8	6.5	6.4	3.3	1.8	4.1
G6PC	1.8	5.9	3.3	4.9	2.1	4.5
GCK	2.2	6.4	3.2	3.3	6.2	4.5
GYS1	6.2	3.7	1.8	3.5	6.2	2.2
GYS2	2.8	5.6	3.1	1.9	5.1	2.9
HK2	4.6	7.1	5.9	4.8	6.1	5.2
HK3	3.3	7.0	6.2	2.0	5.4	7.3
MDH1	5.3	4.5	3.1	3.6	5.7	6.0
MDH2	1.3	2.4	2.9	3.3	3.3	2.3
PCK1	4.5	5.4	3.3	4.7	1.9	3.6
PCK2	7.3	4.3	7.3	6.7	2.0	2.4
PGK1	3.4	3.8	3.7	3.6	2.3	1.3

PGK2	3.0	7.3	3.5	1.5	7.7	3.9
PKLR	3.2	6.1	7.3	5.6	3.2	5.4
PRPS1L1	1.7	7.6	5.8	5.4	5.8	4.8
RBKS	4.7	5.8	5.2	3.4	4.7	5.0
ACO2	-3.3	-0.5	-1.2	-3.0	-2.1	-1.2
ENO2	-3.3	-1.4	-2.5	-1.3	-3.0	-2.3
SUCLA2	-1.7	-1.2	-2.9	-2.5	-1.2	-0.9
UGP2	-2.4	-1.2	-1.6	-2.1	-0.8	-1.1

Table showing the variation in expression fold change in the biopy samples compared to normal tissue

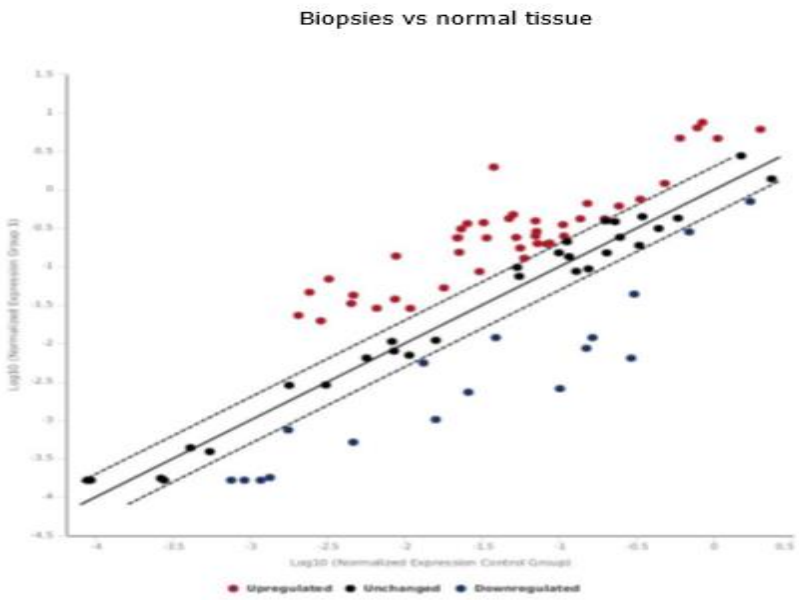

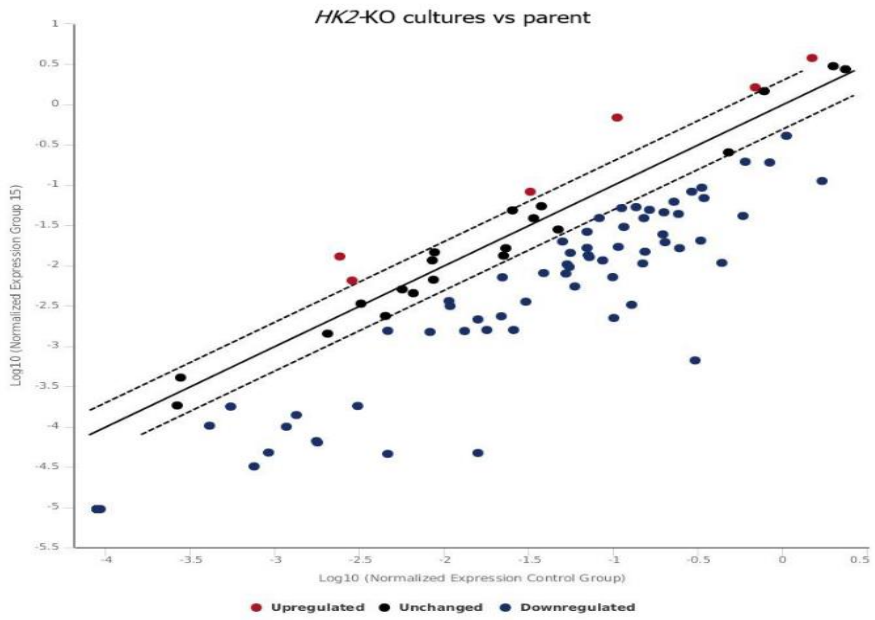

Figure A3. Glucose array scatter charts. Scatter charts showing gene fold change expression in biopsies compared to bomral tissue and in *HK2*-KO cultures compared to the respective parent culture.

Table A7. Glucose array showing gene expression in paired cultures

Gene	UWLV 53	UWLV 22	UWLV 48	UWLV 156	UWLV 152	UWLV 212
ACO1	3.2	1.9	2.1	2.3	2.6	2.5
ACO2	3.9	2.4	3.2	2.8	3.4	3.6
BPGM	4.4	3.2	4.5	3.3	4.1	3.7
DLAT	4.6	4.1	3.6	3.6	3.5	3.9
DLD	3.6	1.9	2.8	3.4	3.7	3.2
DLST	4.3	2.9	3.5	3.6	3.9	4.5
ENO1	2.6	2.1	3.1	3.5	1.8	2.7
G6PC3	2.4	1.1	2.8	2.1	1.5	1.8
G6PD	3.5	2.8	3.9	2.6	3.2	3.8
HK2	2.8	1.4	2.9	2.6	1.4	1.7
PDHA1	4.1	2.1	2.9	2.9	3.6	3.9
PDK2	2.3	1.6	2.5	2.1	3.2	1.9
PFKL	2.3	2.2	2.9	3.3	3.4	2.3
PGLS	5.4	1.7	5.1	2.9	2.9	3.2
PGM1	3.4	3.6	3.7	3.6	2.3	3.3
PGM2	4.8	2.7	6.4	3.3	2.8	4.1
PHKG2	3.8	4.3	3.1	2.6	4.0	2.7
PYGL	4.5	4.2	3.3	4.3	1.9	3.6
SDHB	3.2	2.4	2.8	3.3	3.3	2.3

TKT	5.5	3.1	1.9	5.1	2.9	2.8

Table showing the variation in expression fold change in the culture samples compared to biopsy

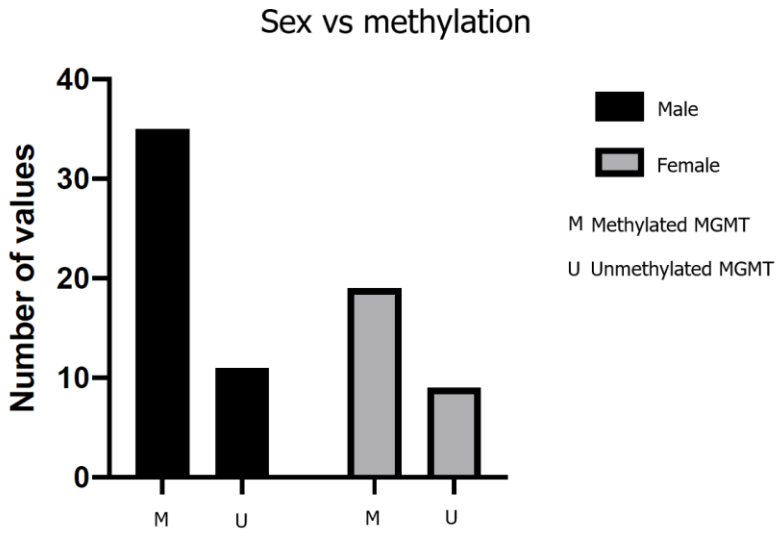

Figure A4. Sex vs *MGMT* methylation for patient OS. Females had higher rates of unmethylated *MGMT* promotors compared to male but was not significant (Chi-squared test p=0.44).

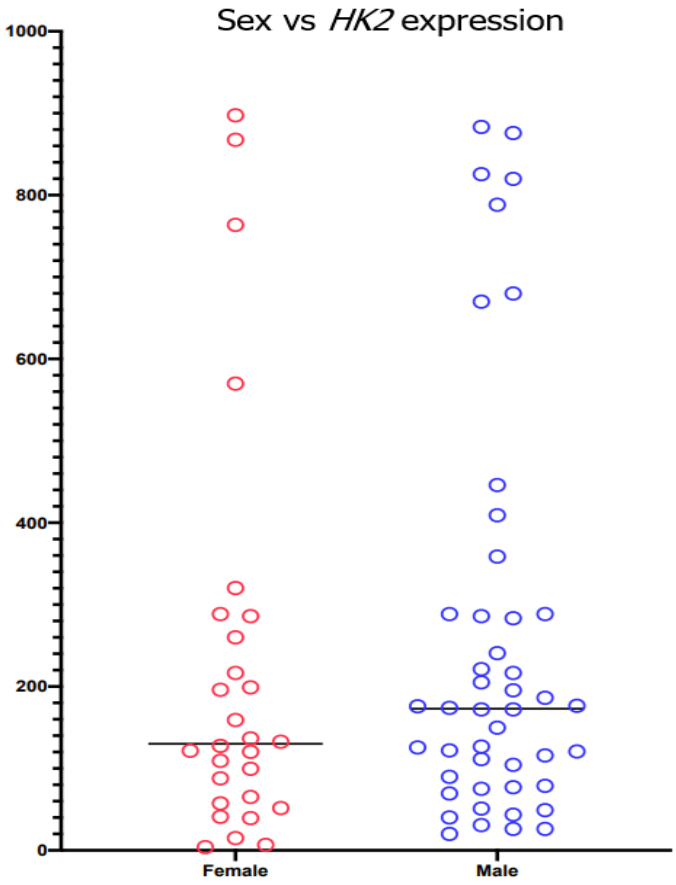

Figure A5. Sex vs *HK2* expression for patient OS. Males had elevated *HK2* over-expression compared to females (median 173 fold-change expression vs 130 fold-change expression), however, this was not significant (Mann-Whitney U test, p=0.47).

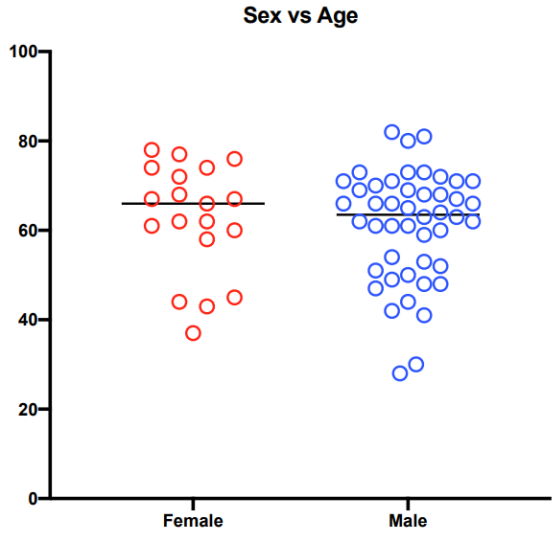

Figure A6. Sex vs age for patient OS. No imbalance of age between males and females. Females had identical median ages to men (64) and this was not significant (Mann Whitney U test p=0.75).

Table A8. Patient biopsy details

BTN W no.	Grade	IDH1	MGMT (Hospital diagnosis)	Gender	DOB	DODiag	DOD	Total Days	HK2 Fold Change	MGMT status (MS-PCR)
85	IV	not done	not done	M	18/04/1959	28/08/2007	16/01/2008	141	75.2	Unmethylated
103	IV	not done	not done	F	03/09/1930	29/10/2007	24/02/2008	118	41.1	Methylated
110	IV	not done	Allred 3+2	M	11/05/1948	12/11/2007	22/08/2008	284	186.3	Methylated
116	IV	not done	not done	F	21/10/1941	04/12/2007	17/05/2009	530	6.7	Methylated
121	IV	not done	not done	F	31/07/1946	19/03/2007	04/03/2008	351	51.7	Unmethylated
122	IV	not done	Allred 3+3	M	19/02/1955	21/12/2007	22/08/2010	975	26.1	Methylated
142	IV	not done	not done	M	08/06/1938	06/02/2008	31/03/2008	54	788.3	Unmethylated
165	IV	not done	not done	M	28/09/1935	02/04/2008	14/05/2008	42	40.1	Methylated
175	IV	not done	not done	F	22/04/1953	15/04/2008	28/07/2009	469	14.9	Unmethylated
204	IV	not done	not done	F	29/04/1954	10/06/2008	15/03/2009	278	57.4	Unmethylated
338	IV	not done	not done	M	29/12/1937	05/05/2009	08/06/2009	34	825.6	Unmethylated
343	IV	not done	not done	M	12/09/1939	12/11/2008	07/08/2009	268	20.1	Methylated
352	IV	not done	not done	M	26/05/1960	02/06/2009	14/06/2009	12	240.7	Unmethylated
374	IV	not done	Allred 5+3	F	20/11/1975	17/07/2009	20/03/2010	246	136.7	Unmethylated
377	IV	not done	not done	F	08/03/1965	22/07/2009	31/07/2010	374	120.3	Methylated
382	IV	not done	not done	F	07/01/1935	04/08/2009	11/09/2011	768	39.3	Methylated
396	IV	not done	Allred 4+2	M	08/12/1940	10/09/2009	17/09/2010	372	69.4	Methylated
410	IV	not done	not done	F	12/04/1931	15/10/2009	03/11/2009	19	260.1	Unmethylated
411	IV	not done	not done	M	27/09/1947	15/10/2009	13/03/2010	149	120.7	Unmethylated
436	IV	not done	Allred 4+3	F	07/07/1971	01/04/2009	29/03/2010	362	127.4	Unmethylated
445	IV	not done	not done	M	02/07/1980	26/11/2009	19/01/2010	54	669.9	Methylated
472	IV	not done	Allred 5+2	F	08/03/1965	22/07/2009	31/07/2010	198	99.5	Unmethylated
522	IV	not done	not done	M	22/06/1936	18/03/2010	05/05/2010	48	30.8	Methylated
535	IV	not done	not done	F	12/01/1948	17/05/2010	17/12/2010	214	87.8	Methylated
590	IV	not done	Allred 3+2	M	13/01/1960	15/07/2010	22/01/2012	556	49.1	Methylated
626	IV	not done	not done	M	22/05/1938	12/08/2010	11/06/2011	303	195.3	Methylated
640	IV	not done	not done	M	22/02/1957	20/08/2010	27/04/2011	250	51.1	Methylated
651	IV	not done	not done	M	29/03/1946	03/09/2010	18/08/2011	349	89.8	Methylated
685	IV	not done	not done	M	09/09/1943	21/10/2010	13/04/2011	174	446.0	Methylated
693	IV	not done	not done	M	14/04/1936	04/11/2010	07/11/2011	368	819.8	Methylated
705	IV	not done	Allred 2+2	F	10/05/1947	02/12/2010	02/05/2011	151	121.6	Methylated
717	IV	not done	not done	F	02/06/1944	04/01/2011	22/05/2011	138	65.3	Methylated

723	IV	not done	not done	M	04/03/1939	14/01/2011	17/09/2011	246	77.0	Methylated
729	IV	neg	not done	F	02/02/1936	03/02/2011	20/06/2011	137	132.7	Methylated
733	IV	not done	not done	M	16/02/1937	17/02/2011	21/06/2012	504	176.4	Methylated
743	IV	neg	not done	F	16/04/1952	24/03/2011	27/07/2012	491	286.0	Methylated
746	IV	not done	not done	F	12/10/1938	07/04/2011	23/03/2012	351	867.6	Methylated
749	IV	WT	methylated	F	26/03/1966	14/04/2008	01/02/2012	296	216.6	Methylated
758	IV	not done	Allred 2+2	M	18/07/1961	08/04/2011	28/02/2012	313	409.2	Methylated
769	IV	not done	not done	M	02/04/1941	20/05/2011	30/06/2012	420	172.1	Methylated
781	IV	neg	not done	F	23/04/1936	07/06/2011	01/09/2011	86	320.2	Methylated
792	IV	not done	Allred 2+2	F	12/10/1943	24/06/2011	27/02/2012	248	196.0	Unmethylated
793	IV	not done	not done	M	19/08/1930	24/06/2011	20/09/2011	88	875.8	Methylated
813	IV	not done	not done	M	03/01/1928	12/08/2011	19/05/2012	281	216.6	Methylated
816	IV	not done	not done	M	02/11/1957	18/08/2011	05/12/2011	109	679.9	Methylated
819	IV	not done	not done	F	24/10/1934	25/08/2011	11/03/2012	199	288.4	Methylated
820	IV	not done	Allred 2+3	M	28/02/1950	26/08/2011	02/10/2011	37	283.3	Methylated
822	IV	not done	not done	F	31/08/1949	01/09/2011	24/04/2012	236	763.7	Methylated
826	IV	not done	not done	F	12/11/1932	08/09/2011	29/01/2012	143	569.8	Methylated
848	IV	R132H	methylated	M	12/07/1961	11/04/2006	13/05/2012	206	122.1	Methylated
849	IV	not done	neg	M	31/01/1948	21/10/2011	25/03/2012	156	205.2	Methylated
859	IV	not done	not done	F	17/10/1950	11/11/2011	02/03/2012	112	897.5	Methylated
860	IV	not done	not done	M	19/07/1944	16/11/2011	13/01/2013	424	26.1	Methylated
874	IV	neg	Allred 3+3	M	18/03/1948	16/12/2011	14/07/2012	211	176.0	Unmethylated
876	IV	not done	Allred 2+1	M	12/06/1968	21/12/2011	22/03/2012	92	358.8	Methylated
898	IV	neg	Allred 3+2	M	12/12/1944	02/02/2012	22/06/2014	871	43.6	Methylated
905	IV	neg	Allred 3+2	M	15/04/1946	16/02/2012	12/04/2013	421	286.0	Methylated
911	IV	neg	Allred 3+2	M	07/05/1947	01/03/2012	06/07/2012	127	172.1	Methylated
915	IV	neg	Allred 4+3	M	28/07/1981	14/03/2012	02/10/2012	202	104.5	Methylated
916	IV	neg	not done	M	26/06/1930	15/03/2012	18/05/2012	64	883.3	Methylated
919	IV	neg	not done	F	13/04/1934	29/03/2012	19/05/2012	1374	126.6	Unmethylated
966	IV	not done	Allred 4+2	M	09/07/1957	12/07/2012	28/09/2014	808	125.6	Unmethylated
970	IV	not done	neg	M	19/07/1944	16/11/2011	13/01/2013	424	78.7	Methylated
1000	IV	neg	neg	M	22/10/1950	28/08/2012	22/07/2013	298	221.2	Methylated
1006	IV	neg	neg	F	23/08/1966	18/09/2012	22/03/2014	550	199.0	Unmethylated
1007	IV	neg	Allred 3+3	F	05/03/1944	05/10/2012	16/09/2013	346	159.0	Unmethylated
1008	IV	neg	10% Allred 3+2	M	12/03/1941	05/10/2012	08/01/2013	88	288.4	Unmethylated

1013	IV	neg	10% Allred 2+1	M	14/03/1948	11/10/2012	08/01/2013	298	149.8	Methylated
1015	IV	neg	10% Allred 3+2	M	12/03/1941	05/10/2012	08/01/2013	95	288.4	Unmethylated
1016	IV	neg	Allred 3+3	F	05/03/1944	05/10/2012	16/01/2013	146	109.2	Methylated
1054	IV	neg	not done	M	29/08/1970	20/12/2011	04/03/2013	210	173.9	Unmethylated
1091	IV	neg	not done	M	13/04/1947	07/02/2013	18/12/2013	319	115.8	Unmethylated
1404	IV	neg	mostly neg Allred 4+2	M	27/05/1965	17/07/2012	06/02/2014	569	111.4	Unmethylated
1428	IV	neg	<10%	M	24/04/1952	19/12/2013	28/07/2014	588	7.4	Unmethylated
1902	IV	neg	Allred 3+2	F	24/04/1961	29/07/2015	15/082016	364	31.1	Unmethylated
2229	IV	neg	Allred 3+3	M	23/07/1962	03/03/2016	08/062016	84	18.4	Methylated

Table showing biopsy details, including *MGMT* status, *HK2* expression, sex and OS. MS-PCR *MGMT* status was determined in the laboratory. MGMT hospital diagnosis was given upon receipt of sample collection.

Table A9. Array Gene List

Glycolytic genes	
ACLY ATP citrate lyase	PDHA1 Pyruvate dehydrogenase alpha 1
ACO1 Aconitase 1, soluble	PDHB Pyruvate dehydrogenase (lipoamide) beta3
ACO2 Aconitase 2, mitochondrial	PDK1 Pyruvate dehydrogenase kinase, isozyme 1
AGL Amylo-alpha-1, 6-glucosidase, 4-alpha-glucanotransferase	PDK2 Pyruvate dehydrogenase kinase, isozyme 2
ALDOA Aldolase A, fructose-bisphosphate	PDK3 Pyruvate dehydrogenase kinase, isozyme 3
ALDOB Aldolase B, fructose-bisphosphate	PDK4 Pyruvate dehydrogenase kinase, isozyme 4
ALDOC Aldolase C, fructose-bisphosphate	PDP2 Pyruvate dehyrogenase phosphatase catalytic subunit 2
BPGM 2,3-bisphosphoglycerate mutase	PDPR Pyruvate dehydrogenase phosphatase regulatory subunit
CS Citrate synthase	PFKL Phosphofructokinase, liver
DLAT Dihydrolipoamide S-acetyltransferase	PGAM2 Phosphoglycerate mutase 2 (muscle)
DLD Dihydrolipoamide dehydrogenase	PGK1 Phosphoglycerate kinase 1
DLST Dihydrolipoamide S-succinyltransferase (E2 component of 2-oxo-glutarate complex)	PGK2 Phosphoglycerate kinase 2
ENO1 Enolase 1, (alpha)	PGLS 6-phosphogluconolactonase
ENO2 Enolase 2 (gamma, neuronal)	PGM1 Phosphoglucomutase 1
ENO3 Enolase 3 (beta, muscle)	PGM2 Phosphoglucomutase 2
FBP1 Fructose-1,6-bisphosphatase 1	PGM3 Phosphoglucomutase 3
FBP2 Fructose-1,6-bisphosphatase 2	PHKA1 Phosphorylase kinase, alpha 1 (muscle)
FH Fumarate hydratase	PHKB Phosphorylase kinase, beta
G6PC Glucose-6-phosphatase, catalytic subunit	PHKG1 Phosphorylase kinase, gamma 1 (muscle)
G6PC3 Glucose 6 phosphatase, catalytic, 3	PHKG2 Phosphorylase kinase, gamma 2 (testis)

G6PD Glucose-6-phosphate dehydrogenase	PKLR Pyruvate kinase, liver and RBC
GALM Galactose mutarotase (aldose 1-epimerase)	PRPS1 Phosphoribosyl pyrophosphate synthetase 1
GBE1 Glucan (1,4-alpha-), branching enzyme 1	PRPS1L1 Phosphoribosyl pyrophosphate synthetase 1-like 1
GCK Glucokinase (hexokinase 4)	PRPS2 Phosphoribosyl pyrophosphate synthetase 2
GPI Glucose-6-phosphate isomerase	PYGL Phosphorylase, glycogen, liver
GSK3A Glycogen synthase kinase 3 alpha	PYGM Phosphorylase, glycogen, muscle
GSK3B Glycogen synthase kinase 3 beta	RBKS Ribokinase
GYS1 Glycogen synthase 1 (muscle)	RPE Ribulose-5-phosphate-3-epimerase
GYS2 Glycogen synthase 2 (liver)	RPIA Ribose 5-phosphate isomerase A
H6PD Hexose-6-phosphate dehydrogenase (glucose 1-dehydrogenase)	SDHA Succinate dehydrogenase complex, subunit A, flavoprotein (Fp)
HK2 Hexokinase 2	SDHB Succinate dehydrogenase complex, subunit B, iron sulfur (Ip)
HK3 Hexokinase 3 (white cell)	SDHC Succinate dehydrogenase complex, subunit C, integral membrane protein, 15kDa
IDH1 Isocitrate dehydrogenase 1 (NADP+), soluble	SDHD Succinate dehydrogenase complex, subunit D, integral membrane protein
IDH2 Isocitrate dehydrogenase 2 (NADP+), mitochondrial	SUCLA2 Succinate-CoA ligase, ADP-forming, beta subunit
IDH3A Isocitrate dehydrogenase 3 (NAD+) alpha	SUCLG1 Succinate-CoA ligase, alpha subunit
IDH3B Isocitrate dehydrogenase 3 (NAD+) beta	SUCLG2 Succinate-CoA ligase, GDP-forming, beta subunit
IDH3G Isocitrate dehydrogenase 3 (NAD+) gamma	TALDO1 Transaldolase 1
MDH1 Malate dehydrogenase 1, NAD (soluble)	TKT Transketolase
MDH1B Malate dehydrogenase 1B, NAD (soluble)	TPI1 Triosephosphate isomerase 1
MDH2 Malate dehydrogenase 2, NAD (mitochondrial)	UGP2 UDP-glucose pyrophosphorylase 2
OGDH Oxoglutarate (alpha-ketoglutarate) dehydrogenase (lipoamide)	ACTB Actin, beta
PC Pyruvate carboxylase	B2M Beta-2-microglobulin
PCK1 Phosphoenolpyruvate carboxykinase 1 (soluble)	GAPDH Glyceraldehyde-3-phosphate dehydrogenase
PCK2 Phosphoenolpyruvate carboxykinase 2 (mitochondrial)	HPRT1 Hypoxanthine phosphoribosyltransferase 1

mTOR genes	
AKT1 V-akt murine thymoma viral oncogene homolog 1	PLD1 Phospholipase D1, phosphatidylcholine-specific
AKT1 substrate 1 (proline-rich)	PLD2 Phospholipase D2
AKT2 V-akt murine thymoma viral oncogene homolog 2	PPP2CA Protein phosphatase 2, catalytic subunit, alpha isozyme
AKT3 V-akt murine thymoma viral oncogene homolog 3 (protein kinase B, gamma)	PPP2R2B Protein phosphatase 2, regulatory subunit B, beta
CAB39 Calcium binding protein 39	PPP2R4 Protein phosphatase 2A activator,

	regulatory subunit 4
CAB39L Calcium binding protein 39-like	PRKAA1 Protein kinase, AMP-activated, alpha 1 catalytic subunit
CDC42 Cell division cycle 42 (GTP binding protein, 25kDa)	PRKAA2 Protein kinase, AMP-activated, alpha 2 catalytic subunit
CHUK Conserved helix-loop-helix ubiquitous kinase	PRKAB1 Protein kinase, AMP-activated, beta 1 non-catalytic subunit
DDIT4 DNA-damage-inducible transcript 4	PRKAB2 Protein kinase, AMP-activated, beta 2 non-catalytic subunit
DDIT4L DNA-damage-inducible transcript 4-like	PRKAG1 Protein kinase, AMP-activated, gamma 1 non-catalytic subunit
DEPTOR DEP domain containing MTOR-interacting protein	PRKAG2 Protein kinase, AMP-activated, gamma 2 non-catalytic subunit
EIF4B Eukaryotic translation initiation factor 4B	PRKAG3 Protein kinase, AMP-activated, gamma 3 non-catalytic subunit
EIF4E Eukaryotic translation initiation factor 4E	PRKCA Protein kinase C, alpha
EIF4EBP1 Eukaryotic translation initiation factor 4E binding protein 1	PRKCB Protein kinase C, beta
EIF4EBP2 Eukaryotic translation initiation factor 4E binding protein 2	PRKCE Protein kinase C, epsilon
FKBP1A FK506 binding protein 1A, 12kDa	PRKCG Protein kinase C, gamma
FKBP8 FK506 binding protein 8, 38kDa	PTEN Phosphatase and tensin homolog
GSK3B Glycogen synthase kinase 3 beta	RHEB Ras homolog enriched in brain
HIF1A Hypoxia inducible factor 1, alpha subunit	RHOA Ras homolog gene family, member A
HRAS V-Ha-ras Harvey rat sarcoma viral oncogene homolog	RICTOR RPTOR independent companion of MTOR, complex 2
HSPA4 Heat shock 70kDa protein 4	RPS6 Ribosomal protein S6
IGF1 Insulin-like growth factor 1 (somatomedin C)	RPS6KA1 Ribosomal protein S6 kinase, 90kDa, polypeptide 1
IGFBP3 Insulin-like growth factor binding protein 3	RPS6KA2 Ribosomal protein S6 kinase, 90kDa, polypeptide 2
6 IKBKB Inhibitor of kappa light polypeptide gene enhancer in B-cells, kinase beta	RPS6KA5 Ribosomal protein S6 kinase, 90kDa, polypeptide 5
ILK Integrin-linked kinase	RPS6KB1 Ribosomal protein S6 kinase, 70kDa, polypeptide 1
INS Insulin	RPS6KB2 Ribosomal protein S6 kinase, 70kDa, polypeptide 2
INSR Insulin receptor	RPTOR Regulatory associated protein of MTOR, complex 1
IRS1 Insulin receptor substrate 1	RRAGA Ras-related GTP binding A
MAPK1 Mitogen-activated protein kinase 1	RRAGB Ras-related GTP binding B
MAPK3 Mitogen-activated protein kinase 3	RRAGC Ras-related GTP binding C
MAPKAP1 Mitogen-activated protein kinase associated protein 1	RRAGD Ras-related GTP binding D
MLST8 MTOR associated protein, LST8 homolog (S. cerevisiae)	SGK1 Serum/glucocorticoid regulated kinase 1
MTOR Mechanistic target of rapamycin (serine/threonine kinase)	STK11 Serine/threonine kinase 11

MYO1C Myosin IC	STRADB STE20-related kinase adaptor beta
PDPK1 3-phosphoinositide dependent protein kinase-1	TELO2 TEL2, telomere maintenance 2, homolog (S. cerevisiae)
PIK3C3 Phosphoinositide-3-kinase, class 3	TP53 Tumor protein p53
PIK3CA Phosphoinositide-3-kinase, catalytic, alpha polypeptide	TSC1 Tuberous sclerosis 1
PIK3CB Phosphoinositide-3-kinase, catalytic, beta polypeptide	TSC2 Tuberous sclerosis 2
PIK3CD Phosphoinositide-3-kinase, catalytic, delta polypeptide	ULK1 Unc-51-like kinase 1 (C. elegans)
PIK3CG Phosphoinositide-3-kinase, catalytic, gamma polypeptide	ULK2 Unc-51-like kinase 2 (C. elegans)

References

Abbruzzese, C., Matteoni, S., Signore, M., Cardone, L., Nath, K., Glickson, J.D. and Paggi, M.G. (2017) Drug repurposing for the treatment of glioblastoma multiforme. *Journal of Experimental & Clinical Cancer Research* , 36(1), pp. 169 .

Abella, J. and Park, M. (2009) Breakdown of endocytosis in the oncogenic activation of receptor tyrosine kinases. AJP: *Endocrinology and Metabolism*, 296(5), pp. E973-E984 .

Adeberg, S., Bernhardt, D., Harrabi, S.B., Nicolay, N., Rieber, J., Koenig, L., Repka, M., Mohr, A., Abdollahi, A. and Weber, K. (2017) Metformin Enhanced in vitro Radiosensitivity Associates with G2/M Cell Cycle Arrest and Elevated pAMPK Levels in Glioblastoma. *Radiology and Oncology* , 51(4) .

Akins, N. S., Nielson, T. C., & Le, H. V. (2018). Inhibition of Glycolysis and Glutaminolysis: An Emerging Drug Discovery Approach to Combat Cancer. *Current topics in medicinal chemistry.* 18(6), 494–504. doi:10.2174/1568026618666180523111351 .

Aldea, M.D., Petrushev, B., Soritau, O., Tomuleasa, C.I., Berindan-Neagoe, I., Filip, A.G., Chereches, G., Cenariu, M., Craciun, L. and Tatomir, C. (2014) Metformin plus sorafenib highly impacts temozolomide-resistant glioblastoma stem-like cells .

Alifieris, C. and Trafalis, D.T. (2015) Glioblastoma multiforme: Pathogenesis and treatment. *Pharmacology & therapeutics* , 152pp. 63-82 .

Alphandéry E. (2018). Glioblastoma Treatments: An Account of Recent Industrial Developments. *Frontiers in pharmacology*, 9, 879. doi:10.3389/fphar.2018.00879 .

An, Z., Aksoy, O., Zheng, T., Fan, Q. W., & Weiss, W. A. (2018). Epidermal growth factor receptor and EGFRvIII in glioblastoma: signaling pathways and targeted therapies. *Oncogene*, 37(12), 1561–1575. doi:10.1038/s41388-017-0045-7 .

Anderson M, Marayati R, Moffitt R, Yeh JJ. (2016) Hexokinase 2 promotes tumor growth and metastasis by regulating lactate production in pancreatic cancer. *Oncotarget.* 2016;8:56081–94 .

Andrzejewski S, Klimcakova E, Johnson RM, Tabaries S, Annis MG, McGuirk S, Northey JJ, Chenard V, Sriram U, Papadopoli DJ, *et al*. (2017). PGC-1α promotes breast cancer metastasis and confers bioenergetic flexibility against metabolic drugs. *Cell Metab* 26: 778–787 e77 5.

Arevalo, O., Valenzuela, R., Esquenazi, Y., Rao, M., Tran, B., Zhu, J., Bhattacharjee, M., Doyle, N. and Riascos, R. (2017) The 2016 World Health Organization Classification of Tumors of the Central Nervous System: A Practical Approach for Gliomas, Part 2. Isocitrate Dehydrogenase Status—Imaging Correlation. *Neurographics* , 7(5), pp. 344-349 .

Arkin, M.R., Tang, Y. and Wells, J.A. (2014) Small-molecule inhibitors of protein-protein interactions: progressing toward the reality. *Chemistry & biology* , 21(9), pp. 1102-1114 .

Armulik, A., Genové, G., Mäe, M., Nisancioglu, M.H., Wallgard, E., Niaudet, C., He, L., Norlin, J., Lindblom, P. and Strittmatter, K. (2010) Pericytes regulate the blood–brain barrier. *Nature* , 468(7323), pp. 557 .

Ashkenazi, A. (2015) Targeting the extrinsic apoptotic pathway in cancer: lessons learned and future directions. *The Journal of clinical investigation* , 125(2), pp. 487-489 .

Attia, Y.M.; El-Abhar, H.S.; Al Marzabani, M.M.; Shouman, S.A. (2015) Targeting glycolysis by 3-bromopyruvate improves tamoxifen cytotoxicity of breast cancer cell lines. *BMC Cancer* 2015, 15, 838.

Azevedo-Silva, J.; Queiros, O.; Baltazar, F.; Uaszewski, S.; Goffeau, A.; Ko, Y.H.; Pedersen, P.L.; Preto, A.; Casal, M. The anticancer agent 3-bromopyruvate: A simple but powerful molecule taken from the lab to the bedside. *J. Bioenerg.* Biomembr. 2016, 48, 349–362 .

Backes, C., Harz, C., Fischer, U., Schmitt, J., Ludwig, N., Petersen, B. S., … Meese, E. (2015). New insights into the genetics of glioblastoma multiforme by familial exome sequencing. *Oncotarget*, 6(8), 5918–5931. doi:10.18632/oncotarget.2950 .

Bara, J.J., Richards, R.G., Alini, M. and Stoddart, M.J. (2014) Concise review: Bone marrow-derived mesenchymal stem cells change phenotype following in vitro culture: implications for basic research and the clinic. *Stem cells* , 32(7), pp. 1713-1723 .

Barrow, J., Adamowicz-Brice, M., Cartmill, M., MacArthur, D., Lowe, J., Robson, K., Brundler, M., Walker, D., Coyle, B. and Grundy, R. (2010) Homozygous loss of ADAM3A revealed by genome-wide analysis of pediatric high-grade glioma and diffuse intrinsic pontine gliomas. *Neuro-Oncology*, 13(2), pp. 212-222 .

Bartmann C, Janaki Raman SR, Flöter J, Schulze A, Bahlke K, Willingstorfer J, Strunz M, Wöckel A, Klement RJ, Kapp M, Djuzenova CS, Otto C, Kämmerer U. (2018). Beta-hydroxybutyrate (3-OHB) can influence the energetic phenotype of breast cancer cells, but does not impact their proliferation and the response to chemotherapy or radiation. *Cancer Metab*. 2018 Jun 11;6:8. doi: 10.1186/s40170-018-0180-9. PMID: 29942509; PMCID: PMC5996481 .

Bashtrykov, P., Ragozin, S. and Jeltsch, A. (2012) Mechanistic details of the DNA recognition by the Dnmt1 DNA methyltransferase. *FEBS Letters*, 586(13), pp. 1821-1823 .

Basu, S., & Murphy, M. E. (2016). Genetic Modifiers of the p53 Pathway. *Cold Spring Harbor perspectives in medicine*, 6(4), a026302. doi:10.1101/cshperspect.a026302 .

Basu, S., Gnanapradeepan, K., Barnoud, T., Kung, C. P., Tavecchio, M., Scott, J., … Murphy, M. E. (2018). Mutant p53 controls tumor metabolism and metastasis by regulating PGC-1α. *Genes & development*, 32(3-4), 230–243. doi:10.1101/gad.309062.117 .

Bayat Mokhtari, R., Homayouni, T. S., Baluch, N., Morgatskaya, E., Kumar, S., Das, B., & Yeger, H. (2017). Combination therapy in combating cancer. *Oncotarge*t, 8(23), 38022–38043. doi:10.18632/oncotarget.16723 .

Baylin, S. and Jones, P. (2011) A decade of exploring the cancer epigenome — biological and translational implications. *Nature Reviews Cancer*, 11(10), pp. 726-734 .

Bell, E.H., Zhang, P., Fisher, B.J., Macdonald, D.R., McElroy, J.P., Lesser, G.J., Fleming, J., Chakraborty, A.R., Liu, Z. and Becker, A.P. (2018) Association of *MGMT* Promoter Methylation Status With Survival Outcomes in Patients With High-Risk Glioma Treated With Radiotherapy and Temozolomide: An Analysis From the NRG Oncology/RTOG 0424 Trial. *JAMA oncology* .

Ben-Horin, H, Tassini, M, Vivi, A, Navon, G and Kaplan, O. (1995) Mechanism of action of the antineoplastic drug lonidamine: 31P and 13C nuclear magnetic resonance studies. *Cancer Res*.55(13):2814-21 .

Benitez, J.A., Ma, J., D'Antonio, M., Boyer, A., Camargo, M.F., Zanca, C., Kelly, S., Khodadadi-Jamayran, A., Jameson, N.M. and Andersen, M. (2017) PTEN regulates glioblastoma oncogenesis through chromatin-associated complexes of DAXX and histone H3. 3. *Nature communications* , 8pp. 15223 .

Bernstein, B., Meissner, A. and Lander, E. (2007) The Mammalian Epigenome. *Cell,* 128(4), pp. 669-681 .

Bertoli, C. and de Bruin, Robertus Antonius Maria (2014) Cell Division: Turning cell cycle entry on its head*. Elife* , 3pp. e03475 .

Bhaskar, P. T., Nogueira, V., Patra, K. C., Jeon, S. M., Park, Y., Robey, R. B., & Hay, N. (2009). mTORC1 hyperactivity inhibits serum deprivation-induced apoptosis via increased hexokinase II and GLUT1 expression, sustained Mcl-1 expression, and glycogen synthase kinase 3beta inhibition. *Molecular and cellular biology*, 29(18), 5136–5147. doi:10.1128/MCB.01946-08 .

Birsoy, K., Possemato, R., Lorbeer, F.K., Bayraktar, E.C., Thiru, P., Yucel, B., Wang, T., Chen, W.W., Clish, C.B. and Sabatini, D.M. (2014) Metabolic determinants of cancer cell sensitivity to glucose limitation and biguanides. *Nature* , 508(7494), pp. 108 .

Bleeker, F. E., Atai, N. A., Lamba, S., Jonker, A., Rijkeboer, D., Bosch, K. S., … Van Noorden, C. J. (2010). The prognostic IDH1(R132) mutation is associated with reduced NADP+-dependent IDH activity in glioblastoma. *Acta neuropathologica*, 119(4), 487–494. doi:10.1007/s00401-010-0645-6 .

Boehning D, Patterson RL, Sedaghat L, Glebova NO, Kurosaki T, Snyder SH (2003) "Cytochrome c binds to inositol (1,4,5) trisphosphate receptors, amplifying calcium-dependent apoptosis". *Nature Cell Biology*. 5 (12): 1051–61 .

Bonnet S, Archer SL, Allalunis-Turner J, Haromy A, Beaulieu C, Thompson R, Lee CT, Lopaschuk GD, Puttagunta L, Bonnet S, Harry G, Hashimoto K, Porter CJ, Andrade MA, Thebaud B, Michelakis ED (2007) A mitochondria-K+ channel axis is suppressed in cancer and its normalization promotes apoptosis and inhibits cancer growth. *Cancer Cell*. 2007 Jan;11(1):37-51 .

Bonuccelli G, Tsirigos A, Whitaker-Menezes D, Pavlides S, Pestell RG, Chiavarina B, *et al*. Ketones and lactate 'fuel' tumor growth and metastasis: evidence that epithelial cancer cells use oxidative mitochondrial metabolism. *Cell Cycle*. 2010;9(17):3506–3514. doi: 10.4161/cc.9.17.12731 .

Bonuccelli G, Tsirigos A, Whitaker-Menezes D, Pavlides S, Pestell RG, Chiavarina B, Frank PG, Flomenberg N, Howell A, Martinez-Outschoorn UE, Sotgia F, Lisanti MP. (2010) Ketones and lactate "fuel" tumor growth and metastasis: Evidence that epithelial cancer cells use oxidative mitochondrial metabolism. *Cell Cycle*. 2010 Sep 1;9(17):3506-14. doi: 10.4161/cc.9.17.12731. Epub 2010 Sep 21. PMID: 20818174; PMCID: PMC3047616 .

Brennan, C.W., Verhaak, R.G., McKenna, A., Campos, B., Noushmehr, H., Salama, S.R., Zheng, S., Chakravarty, D., Sanborn, J.Z., Berman, S.H. and Beroukhim, R., (2013) The somatic genomic landscape of glioblastoma. *Cell,*155(2), pp.462-477 .

Brennan, C.W., Verhaak, R.G., McKenna, A., Campos, B., Noushmehr, H., Salama, S.R., Zheng, S., Chakravarty, D., Sanborn, J.Z., Berman, S.H. and Beroukhim, R., (2013) The somatic genomic landscape of glioblastoma. *Cell*,155(2), pp.462-477 .

Brenneman, B.R., Floyd, D.H., Harris, T. and Purow, B. (2016) Assessing and augmenting the immune response to glioblastoma using repurposed pharmaceuticals.

Bricker DK, Taylor EB, Schell JC, Orsak T, Boutron A, Chen YC, Cox JE, Cardon CM, Van Vranken JG, Dephoure N, Redin C, Boudina S, Gygi SP, Brivet M, Thummel CS, Rutter J; "A mitochondrial pyruvate carrier required for pyruvate uptake in yeast, Drosophila, and humans."; *Science*, 2012 .

Brocato, J., Chervona, Y., & Costa, M. (2014). Molecular responses to hypoxia-inducible factor 1α and beyond. *Molecular pharmacology*, 85(5), 651–657. doi:10.1124/mol.113.089623 .

Brodbelt A, Greenberg D, Winters T, Williams M, Vernon S, Collins VP; (UK) National Cancer Information Network Brain Tumour Group. (2015). Glioblastoma in England: 2007-2011. *Eur J Cancer*. 2015 Mar;51(4):533-42. doi: 10.1016/j.ejca.2014.12.014. Epub 2015 Feb 3 .

Buckanovich, R.J., Brown, J., Shank, J., Griffith, K.A., Reynolds, R.K., Johnston, C., McLean, K., Uppal, S., Liu, J.R. and Cabrera, L. (2017) A phase II clinical trial of metformin as a cancer stem cell targeting agent in stage IIc/III/IV ovarian, fallopian tube, and primary peritoneal cancer .

Budihardjo, I., Oliver, H., Lutter, M., Luo, X. and Wang, X. (1999) Biochemical pathways of caspase activation during apoptosis. *Annual Review of Cell and Developmental Biology* , 15(1), pp. 269-290 .

Butkytė, S., Čiupas, L., Jakubauskienė, E., Vilys, L., Mocevicius, P., Kanopka, A. and Vilkaitis, G. (2016) Splicing-dependent expression of microRNAs of mirtron origin in human digestive and excretory system cancer cells. *Clinical epigenetics* , 8(1), pp. 33 .

Buzzai, M., Jones, R.G., Amaravadi, R.K., Lum, J.J., DeBerardinis, R.J., Zhao, F., Viollet, B. and Thompson, C.B. (2007) Systemic treatment with the antidiabetic drug metformin selectively impairs p53-deficient tumor cell growth. *Cancer research* , 67(14), pp. 6745-6752 .

Cadieux B, Ching TT, VandenBerg SR, Costello JF. (2006) Genome-wide hypomethylation in human glioblastomas associated with specific copy number alteration, methylenetetrahydrofolate reductase allele status, and increased proliferation. *Cancer Res*. 2006 Sep 1;66(17):8469-76 .

Cadieux, B., Ching, T., VandenBerg, S. and Costello, J. (2006) Genome-wide Hypomethylation in Human Glioblastomas Associated with Specific Copy Number Alteration, Methylenetetrahydrofolate Reductase Allele Status, and Increased Proliferation. *Cancer Research*, 66(17), pp. 8469-8476 .

Cairns RA, Harris I, McCracken S, Mak TW. (2011). Cold Spring Harb Symp Quant Biol. 2011;76:299-311. doi: 10.1101/sqb.2011.76.012856. Epub 2011 Dec 12 .

Calvino, E.; Estan, M.C.; Sanchez-Martin, C.; Brea, R.; de Blas, E.; Boyano-Adanez, M.D.; Rial, E.; Aller, P. (2014) Regulation of death induction and chemosensitizing action of 3-bromopyruvate in myeloid leukemia cells: Energy depletion, oxidative stress, and protein kinase activity modulation. *J. Pharmacol*. Exp. Ther. 2014, 348,324–335 .

Cancer Cell. 2013 Oct 14;24(4):403-4. doi: 10.1016/j.ccr.2013.09.017 .

Cantor, J. and Sabatini, D. (2012) *Cancer Cell Metabolism*: One Hallmark, Many Faces. Cancer Discovery, 2(10), pp. 881-898 .

Cao, W., Wei, W., Zhan, Z., Xie, D., Xie, Y., & Xiao, Q. (2018). Regulation of drug resistance and metastasis of gastric cancer cells via the microRNA647-ANK2 axis. *International journal of molecular medicine*, 41(4), 1958–1966. doi:10.3892/ijmm.2018.3381 .

Cao, X.H.; Bloomston, M.; Zhang, T.; Frankel, W.L.; Jia, G.; Wang, B.; Hall, N.C.; Koch, R.M.; Cheng, H.; Knopp, M.V.; *et al*. (2008) Synergistic antipancreatic tumor effect by simultaneously targeting hypoxic cancer cells with HSP90 inhibitor and glycolysis inhibitor. *Clin. Cancer Res*. 2008, 14, 1831–1839 .

Cardaci, S.; Desideri, E.; Ciriolo, M.R. (2012) Targeting aerobic glycolysis: 3-bromopyruvate as a promising anticancer drug*. J. Bioenerg. Biomembr*. 2012, 44, 17–29 .

Chae, Y.K., Arya, A., Malecek, M.K., Shin, D.S., Carneiro, B., Chandra, S., Kaplan, J., Kalyan, A., Altman, J.K., Platanias, L. and Giles, F. (2016) Repurposing metformin for cancer treatment: current clinical studies. *Oncotarget* , 7(26), pp. 40767-40780 .

Chae, Y.K., Arya, A., Malecek, M.K., Shin, D.S., Carneiro, B., Chandra, S., Kaplan, J., Kalyan, A., Altman, J.K., Platanias, L. and Giles, F. (2016) Repurposing metformin for cancer treatment: current clinical studies. *Oncotarget* , 7(26), pp. 40767-40780 .

Chang Yu, Chiou J, Yi-Fang Yang, Chia-Yi Su, Yuan-Feng Lin, Chia-Ning Yang, Pei-Jung Lu, Ming-Shyan Huang, Chih-Jen Yang and Michael Hsiao. (2019). Therapeutic Targeting of Aldolase A Interactions Inhibits Lung Cancer Metastasis and Prolongs Survival. *Cancer Res* July 29 2019 DOI: 10.1158/0008-5472.CAN-18-4080 .

Chaudhry, A., Benson, L., Varshaver, M., Farber, O., Weinberg, U., Kirson, E. and Palti, Y. (2015) NovoTTF™-100A System (Tumor Treating Fields) transducer array layout planning for glioblastoma: a NovoTAL™ system user study. *World journal of surgical oncology* , 13(1), pp. 316 .

Chen Y, Wei L, Zhang X, Liu X, Chen Y, Zhang S, Zhou L, Li Q, Pan Q, Zhao S, Liu H. (2018) 3-Bromopyruvate sensitizes human breast cancer cells to TRAIL-induced apoptosis via the phosphorylated AMPK-mediated upregulation of DR5. *Oncol Rep.* 2018 Nov;40(5):2435-2444. doi: 10.3892/or.2018.6644. Epub 2018 Aug 14. PubMed PMID: 30132536; PubMed Central PMCID: PMC6151892 .

Chen, P., Wang, A.Y. and DePinho, R.A. (2018) Lysyl oxidase secreted by PTEN-deficient glioblastoma cells recruits macrophages and promotes malignant growth .

Chen, W., Ostrowski, R. P., Obenaus, A., & Zhang, J. H. (2009). Prodeath or prosurvival: two facets of hypoxia inducible factor-1 in perinatal brain injury. *Experimental neurology,* 216(1), 7–15. doi:10.1016/j.expneurol.2008.10.016 .

Chen, Z.; Zhang, H.; Lu,W.; Huang, P. (2009) Role of mitochondria-associated hexokinase II in cancer cell death induced by 3-bromopyruvate. *BBA-Bioenergetics* 2009, 1787, 553–560 .

Chiarini F, Evangelisti C, McCubrey JA, Martelli AM. (2015) Current treatment strategies for inhibiting mTOR in cancer. *Trends in Pharmacological Sciences*. 2015;36(2):124-135. doi:10.1016/j.tips.2014.11.004 .

Chiasserini D., Davidescu M., Orvietani P.L., Susta F., Macchioni L., Petricciuolo M., Castigli E., Roberti R., Binaglia L., Corazzi L. (2017) 3-Bromopyruvate treatment induces alterations of metabolic and stress-related pathways in glioblastoma cells. *J. Proteom*. 2017;152:329–338. doi: 10.1016/j.jprot.2016.11.013 .

Chiasserini, D.; Davidescu, M.; Orvietani, P.L.; Susta, F.; Macchioni, L.; Petricciuolo, M.; Castigli, E.;

Chong D, Ma L, Liu F, Zhang Z, Zhao S, Huo Q, Zhang P, Zheng H, Liu H. (2017) Synergistic antitumor effect of 3-bromopyruvate and 5-fluorouracil against human colorectal cancer through cell cycle arrest and induction of apoptosis. 2017 Sep;28(8):831-840. doi: 10.1097/CAD.0000000000000517 .

Christofk, H.R., Vander Heiden, M.G., Harris, M.H., Ramanathan, A., Gerszten, R.E., Wei, R., Fleming, M.D., Schreiber, S.L. and Cantley, L.C. (2008) The M2 splice isoform of pyruvate kinase is important for cancer metabolism and tumour growth. *Nature* , 452(7184), pp. 230 .

Christopher, A.F., Kaur, R.P., Kaur, G., Kaur, A., Gupta, V. and Bansal, P. (2016) MicroRNA therapeutics: Discovering novel targets and developing specific therapy. *Perspectives in clinical research* , 7(2), pp. 68-74 .

Cox AD, Fesik SW, Kimmelman AC, Luo J, Der CJ. (2014) Drugging the undruggable RAS: Mission possible? *Nat Rev Drug Discov*. 2014 Nov;13(11):828-51. doi: 10.1038/nrd4389. Epub 2014 Oct 17 .

Crispo, F., Condelli, V., Lepore, S., Notarangelo, T., Sgambato, A., Esposito, F., … Landriscina, M. (2019). Metabolic Dysregulations and Epigenetics: A Bidirectional Interplay that Drives Tumor Progression. *Cells*, 8(8), 798. doi:10.3390/cells8080798 .

Crosby M. E. (2007). Cell Cycle: Principles of Control. *The Yale Journal of Biology and Medicine*, 80(3), 141–142 .

David J. Roberts, Valerie P. Tan-Sah, Jeffery M. Smith and Shigeki Miyamoto (2013). Akt Phosphorylates HK-II at Thr-473 and Increases Mitochondrial HK-II Association to Protect Cardiomyocytes August 16, 2013, *The Journal of Biological Chemistry* 288, 23798-23806 .

De Carvalho, D., You, J. and Jones, P. (2010) DNA methylation and cellular reprogramming. *Trends in Cell Biology,* 20(10), pp. 609-617 .

de Groot, J.F., Fuller, G., Kumar, A.J., Piao, Y., Eterovic, K., Ji, Y. and Conrad, C.A. (2010) Tumor invasion after treatment of glioblastoma with bevacizumab: radiographic and pathologic correlation in humans and mice. *Neuro-oncology* , 12(3), pp. 233-242 .

de Souza CF, Sabedot TS, Malta TM, Stetson L, Morozova O, Sokolov A, Laird PW, Wiznerowicz M, Iavarone A, Snyder J, deCarvalho A, Sanborn Z, McDonald KL, Friedman WA, Tirapelli D, Poisson L, Mikkelsen T, Carlotti CG Jr, Kalkanis S, Zenklusen J, Salama SR, Barnholtz-Sloan JS, Noushmehr H. (2018) A Distinct DNA Methylation Shift in a Subset of Glioma CpG Island Methylator Phenotypes during Tumor Recurrence. *Cell Rep*. 2018 Apr 10;23(2):637-651. doi: 10.1016/j.celrep.2018.03.107.

DeBerardinis RJ, Chandel NS. (2016). Fundamentals of cancer metabolism. *Sci Adv*. 2016 May 27;2(5): e1600200. doi: 10.1126/sciadv.1600200. PMID: 27386546; PMCID: PMC4928883 .

DeBerardinis, R. and Thompson, C. (2012) Cellular Metabolism and Disease: What Do Metabolic Outliers Teach Us?. *Cell*, 148(6), pp. 1132-1144 .

Deeken JF, Löscher W. (2007). The blood-brain barrier and cancer: transporters, treatment, and Trojan horses. *Clin Cancer Res*. 2007 Mar 15;13(6):1663-74 .

Delgado-Lopez, P. and Corrales-Garcia, E. (2016) Survival in glioblastoma: a review on the impact of treatment modalities. *Clinical and Translational Oncology*, 18(11), pp. 1062-1071 .

DeWaal D, Nogueira V, Terry AR, Patra KC, Jeon SM, Guzman G, Au J, Long CP, Antoniewicz MR, Hay N. (2018). Hexokinase-2 depletion inhibits glycolysis and

induces oxidative phosphorylation in hepatocellular carcinoma and sensitizes to metformin. *Nat Commun*. 2018 Jun 26;9(1):2539. doi: 10.1038/s41467-018-04182-z .

Di Martino A, Kucharczyk P, Capakova Z, Humpolicek P, Sedlarik V (2017) Enhancement of temozolomide stability by loading in chitosan-carboxylated polylactide-based nanoparticles. *J Nanopart Res*. 2017;19(2):71. doi: 10.1007/s11051-017-3756-3. Epub 2017 Feb 16 .

Dibble CC, Manning BD. (2013). Signal integration by mTORC1 coordinates nutrient input with biosynthetic output. *Nat Cell Biol*. 2013 Jun;15(6):555-64. doi: 10.1038/ncb2763 .

Ding L, Getz G, Wheeler DA, Mardis ER, McLellan MD, Cibulskis K, Sougnez C, Greulich H, Muzny DM, Morgan MB, Fulton L, Fulton RS, Zhang Q, Wendl MC, Lawrence MS, Larson DE, Chen K, Dooling DJ, Sabo A, Hawes AC, Shen H, Jhangiani SN, Lewis LR, Hall O, Zhu Y, Mathew T, Ren Y, Yao J, Scherer SE, Clerc K, Metcalf GA, Ng B, Milosavljevic A, Gonzalez-Garay ML, Osborne JR, Meyer R, Shi X, Tang Y, Koboldt DC, Lin L, Abbott R, Miner TL, Pohl C, Fewell G, Haipek C, Schmidt H, Dunford-Shore BH, Kraja A, Crosby SD, Sawyer CS, Vickery T, Sander S, Robinson J, Winckler W, Baldwin J, Chirieac LR, Dutt A, Fennell T, Hanna M, Johnson BE, Onofrio RC, Thomas RK, Tonon G, Weir BA, Zhao X, Ziaugra L, Zody MC, Giordano T, Orringer MB, Roth JA, Spitz MR, Wistuba II, Ozenberger B, Good PJ, Chang AC, Beer DG, Watson MA, Ladanyi M, Broderick S, Yoshizawa A, Travis WD, Pao W, Province MA, Weinstock GM, Varmus HE, Gabriel SB, Lander ES, Gibbs RA, Meyerson M, Wilson RK. (2008) Somatic mutations affect key pathways in lung adenocarcinoma. *Nature*. 2008 Oct 23;455(7216):1069-75. doi: 10.1038/nature07423 .

Dong, G., Mao, Q., Xia, W., Xu, Y., Wang, J., Xu, L., & Jiang, F. (2016). PKM2 and cancer: The function of PKM2 beyond glycolysis. *Oncology letters*, 11(3), 1980–1986. doi:10.3892/ol.2016.4168 .

Dowling, R.J., Parulekar, W.R., Gelmon, K.A., Shepherd, L.E., Virk, S., Ennis, M., Mao, F., Ligibel, J.A., Hershman, D.L. and Rastogi, P. (2018) CA15-3/MUC1 in CCTG

MA-32 (NCT01101438): A phase III RCT of the effect of metformin vs.placebo on invasive disease free and overall survival in early stage breast cancer (BC).

Eckel-Passow, J.E., Lachance, D.H., Molinaro, A.M., Walsh, K.M., Decker, P.A., Sicotte, H., Pekmezci, M., Rice, T., Kosel, M.L. and Smirnov, I.V. (2015) Glioma groups based on 1p/19q, IDH, and TERT promoter mutations in tumors. *New England Journal of Medicine ,* 372(26), pp. 2499-2508 .

Ehrlich M. (2009). DNA hypomethylation in cancer cells. *Epigenomics.* 2009 Dec;1(2):239-59. doi: 10.2217/epi.09.33. PMID: 20495664; PMCID: PMC2873040 .

Ehrlich, M. (2009) DNA hypomethylation in cancer cells. *Epigenomics*, 1(2), pp. 239-259 .

El Sayed S.M., Baghdadi H., Zolaly M., Almaramhy H.H., Ayat M., Donki J.G. (2017) The promising anticancer drug 3-bromopyruvate is metabolized through glutathione conjugation which affects chemoresistance and clinical practice: An evidence-based view. *Med.* Hypotheses. 2017;100:67–77. doi: 10.1016/j.mehy.2017.01.014 .

El Sayed, S.M.; Mohamed, W.G.; Seddik, M.A.H.; Ahmed, A.S.A.; Mahmoudi, A.G.; Amer, W.H.; Nabo, M.M.H.; Hamed, A.R.; Ahmed, N.S.; Abd-Allah, A.A.R. Safety and outcome of treatment of metastatic melanoma using 3-bromopyruvate: A concise literature review and case study. *Chin. J. Cancer* 2014, 33, 356–364 .

Elmore, S. (2007) Apoptosis: a review of programmed cell death. *Toxicologic pathology* , 35(4), pp. 495-516 .

Elstrom RL1, Bauer DE, Buzzai M, Karnauskas R, Harris MH, Plas DR, Zhuang H, Cinalli RM, Alavi A, Rudin CM, Thompson CB. 2004. Akt stimulates aerobic glycolysis in cancer cells. *Cancer Res.* 2004 Jun 1;64(11):3892-9 .

England, B., Huang, T. and Karsy, M. (2013) Current understanding of the role and targeting of tumor suppressor p53 in glioblastoma multiforme. *Tumor Biology* , 34(4), pp. 2063-2074 .

Esteller, M. (2002) CpG island hypermethylation and tumor suppressor genes: a booming present, a brighter future. *Oncogene*, 21(35), pp. 5427-5440 .

Esteller, M., Toyota, M., Sanchez-Cespedes, M., Capella, G., Peinado, M.A., Watkins, D.N., Issa, J.P.J., Sidransky, D., Baylin, S.B. and Herman, J.G. (2000) Inactivation of the DNA repair gene O6-methylguanine-DNA methyltransferase by promoter hypermethylation is associated with G to A mutations in K-ras in colorectal tumorigenesis. *Cancer research*, 60(9), pp.2368-2371 .

Evan, G.I. and Vousden, K.H. (2001) Proliferation, cell cycle and apoptosis in cancer. *Nature*, 411(6835), pp. 342-348 .

Evans, J.M., Donnelly, L.A., Emslie-Smith, A.M., Alessi, D.R. and Morris, A.D. (2005) Metformin and reduced risk of cancer in diabetic patients. *BMJ (Clinical research ed.)*, 330(7503), pp. 1304-1305 .

Fabian, M.R. and Sonenberg, N. (2012) The mechanics of miRNA-mediated gene silencing: a look under the hood of miRISC. *Nature Structural and Molecular Biology* , 19(6), pp. 586 .

Fan T, Sun G, Sun X, Zhao L, Zhong R, Peng Y. Tumor Energy Metabolism and Potential of 3-Bromopyruvate as an Inhibitor of Aerobic Glycolysis: Implications in Tumor Treatment. *Cancers (Basel).* 2019;11(3):317. Published 2019 Mar 6. doi:10.3390/cancers11030317

Fan, T., Sun, G., Sun, X., Zhao, L., Zhong, R., & Peng, Y. (2019). Tumor Energy Metabolism and Potential of 3-Bromopyruvate as an Inhibitor of Aerobic Glycolysis: Implications in Tumor Treatment. *Cancers*, 11(3), 317. doi:10.3390/cancers11030317.

Ferraro, E., Pulicati, A., Cencioni, M. T., Cozzolino, M., Navoni, F., di Martino, S., … Cecconi, F. (2008). Apoptosome-deficient cells lose cytochrome c through proteasomal degradation but survive by autophagy-dependent glycolysis. *Molecular biology of the cell,* 19(8), 3576–3588. doi:10.1091/mbc.E07-09-0858 .

Feustel, S.M., Meissner, M. and Liesenfeld, O. (2012) Toxoplasma gondii and the blood-brain barrier. *Virulence* , 3(2), pp. 182-192 .

Filho, Rachid A. El-Aouar *et al*. (2017) Heterogeneous Family of Cyclomodulins: Smart Weapons That Allow Bacteria to Hijack the Eukaryotic Cell Cycle and Promote Infections. *Front. Cell. Infect. Microbiol*. 2017 .

Fisher, P., Tihan, T., Goldthwaite, P., Wharam, M., Carson, B., Weingart, J., Repka, M., Cohen, K. and Burger, P. (2008) Outcome analysis of childhood low-grade astrocytomas. Pediatr. *Blood Cancer*, 51(2), pp. 245-250 .

Floridi A, Paggi MG, D'Atri S, De Martino C, Marcante ML, Silvestrini B, Caputo A. (1981) Effect of lonidamine on the energy metabolism of Ehrlich ascites tumor cells. *Cancer Res.* 1981 Nov; 41(11 Pt 1):4661-6 .

Frezza, C., Zheng, L., Folger, O., Rajagopalan, K.N., MacKenzie, E.D., Jerby, L., Micaroni, M., Chaneton, B., Adam, J. and Hedley, A. (2011) Haem oxygenase is synthetically lethal with the tumour suppressor fumarate hydratase. *Nature* , 477(7363), pp. 225 .

Fruman, D. A., Chiu, H., Hopkins, B. D., Bagrodia, S., Cantley, L. C., & Abraham, R. T. (2017). The PI3K Pathway in Human Disease. *Cell,* 170(4), 605–635. doi:10.1016/j.cell.2017.07.029 .

Fu D, He C, Wei J, Zhang Z, Luo Y, Tan H, Ren C. (2018). PGK1 is a Potential Survival Biomarker and Invasion Promoter by Regulating the HIF-1α–Mediated Epithelial-Mesenchymal Transition Process in Breast Cancer. *Cell Physiol Biochem* 2018;51:2434-2444. doi: 10.1159/000495900 .

Fujimoto, A., Totoki, Y., Abe, T., Boroevich, K., Hosoda, F., Nguyen, H., Aoki, M., Hosono, N., Kubo, M., Miya, F., Arai, Y., Takahashi, H., Shirakihara, T., Nagasaki, M., Shibuya, T., Nakano, K., Watanabe-Makino, K., Tanaka, H., Nakamura, H., Kusuda, J., Ojima, H., *et al*., and Nakagawa, H. (2012) Whole-genome sequencing of liver cancers identifies etiological influences on mutation patterns and recurrent mutations in chromatin regulators. *Nature Genetics*, 44(7), pp. 760-764 .

Fulda, S. and Debatin, K. (2006) Extrinsic versus intrinsic apoptosis pathways in anticancer chemotherapy. *Oncogene* , 25(34), pp. 4798-4811 .

Fuse, M., Kojima, S., Enokida, H., Chiyomaru, T., Yoshino, H., Nohata, N., Kinoshita, T., Sakamoto, S., Naya, Y. and Nakagawa, M. (2012) Tumor suppressive microRNAs (miR-222 and miR-31) regulate molecular pathways based on microRNA expression signature in prostate cancer. *Journal of human genetics* , 57(11), pp. 691-699 .

Galluzzi L, Vitale I, Abrams JM, Alnemri ES, Baehrecke EH, Blagosklonny MV, Dawson TM, Dawson VL, El-Deiry WS, Fulda S, Gottlieb E, Green DR, Hengartner MO, Kepp O, Knight RA, Kumar S, Lipton SA, Lu X, Madeo F, Malorni W, Mehlen P, Nuñez G, Peter ME, Piacentini M, Rubinsztein DC, Shi Y, Simon HU, Vandenabeele P, White E, Yuan J, Zhivotovsky B, Melino G, Kroemer G. (2012) *Cell Death Differ*. 2012 Jan;19(1):107-20. doi: 10.1038/cdd.2011.96. Epub 2011 Jul 15 .

Gandham, S. K., Talekar, M., Singh, A., & Amiji, M. M. (2015). Inhibition of hexokinase-2 with targeted liposomal 3-bromopyruvate in an ovarian tumor spheroid model of aerobic glycolysis. *International journal of nanomedicine*, 10, 4405–4423. doi:10.2147/IJN.S82818 .

Gandham, S.K.; Talekar, M.; Singh, A.; Amiji, M.M. Inhibition of hexokinase-2 with targeted liposomal 3-bromopyruvate in an ovarian tumor spheroid model of aerobic glycolysis. Int. J. *Nanomed.* 2015, 10,4405–4423 .

Gao, Y., Xu, D., Yu, G., & Liang, J. (2015). Overexpression of metabolic markers HK1 and PKM2 contributes to lymphatic metastasis and adverse prognosis in Chinese gastric cancer. *International journal of clinical and experimental pathology*, 8(8), 9264–9271 .

Gatenby, R.A. and Gillies, R.J. (2004) Why do cancers have high aerobic glycolysis? *Nature Reviews Cancer* , 4(11), pp. 891 .

Gershon TR, Crowther AJ, Tikunov A, Garcia I, Annis R, Yuan H, Miller CR, Macdonald J, Olson J, Deshmukh M. (2013) Hexokinase-2-mediated aerobic glycolysis is integral to cerebellar neurogenesis and pathogenesis of medulloblastoma. *Cancer Metab*. 2013 Jan 23;1(1):2. doi: 10.1186/2049-3002-1-2. PubMed PMID: 24280485; PubMed Central PMCID: PMC3782751 .

Geschwind, J.F. H.; Ko, Y.H.; Torbenson, M.S.; Magee, C.; Pedersen, P.L. (2002) Novel therapy for liver cancer: Direct intraarterial injection of a potent inhibitor of ATP production. *Cancer Res*. 2002, 62, 3909–3913.

Giardiello FM, Brensinger JD, Tersmette AC, Goodman SN, Petersen GM, Booker SV, Cruz-Correa M, Offerhaus JA. (2000) Very high risk of cancer in familial Peutz-Jeghers syndrome. *Gastroenterology*. 2000 Dec;119(6):1447-53 .

Gilbert, M.R., Dignam, J.J., Armstrong, T.S., Wefel, J.S., Blumenthal, D.T., Vogelbaum, M.A., Colman, H., Chakravarti, A., Pugh, S. and Won, M. (2014) A randomized trial of bevacizumab for newly diagnosed glioblastoma. *New England Journal of Medicine ,* 370(8), pp. 699-708 .

Glick, M.; Biddle, P.; Jantzi, J.; Weaver, S.; Schirch, D. (2014) The antitumor agent 3-bromopyruvate has a short half-life at physiological conditions. *Biochem. Biophys. Res. Commun*. 2014, 452, 170–173 .

Goldberg AD1, Allis CD, Bernstein E. (2007) Epigenetics: a landscape takes shape. *Cell.* 2007 Feb 23;128(4):635-8 .

Goldberg, R.M., Sargent, D.J., Morton, R.F., Fuchs, C.S., Ramanathan, R.K., Williamson, S.K., Findlay, B.P., Pitot, H.C. and Alberts, S.R. (2004) A randomized controlled trial of fluorouracil plus leucovorin, irinotecan, and oxaliplatin combinations in patients with previously untreated metastatic colorectal cancer. Journal of Clinical *Oncology* , 22(1), pp. 23-30 .

Goodwin, M.L., Gladden, L.B., Nijsten, M.W. and Jones, K.B. (2015) Lactate and cancer: revisiting the Warburg effect in an era of lactate shuttling. *Frontiers in nutrition ,* 1pp. 27 .

Gottlob K, Majewski N, Kennedy S, Kandel E, Robey RB, Hay N. (2001) Inhibition of early apoptotic events by Akt/PKB is dependent on the first commited step of glycolysis and mitochondrial hexokinase. *Genes Dev* 2001; 15 (11): 1406–18 .

Govaere O, Komuta M, Berkers J, Spee B, Janssen C, de Luca F, Katoonizadeh A, Wouters J, van Kempen LC, Durnez A, Verslype C, De Kock J, Rogiers V, van Grunsven LA, Topal B, Pirenne J, Vankelecom H, Nevens F, van den Oord J, Pinzani

M, Roskams T. (2014) Keratin 19: a key role player in the invasion of human hepatocellular carcinomas. Gut. 2014 Apr;63(4):674-85. doi: 10.1136/gutjnl-2012-304351. *Epub* 2013 Aug 19 .

Grasso, C., Wu, Y., Robinson, D., Cao, X., Dhanasekaran, S., Khan, A., Quist, M., Jing, X., Lonigro, R., Brenner, J., Asangani, I., Ateeq, B., Chun, S., Siddiqui, J., Sam, L., Anstett, M., Mehra, R., Prensner, J., Palanisamy, N., Ryslik, G., Vandin, F., Raphael, B., Kunju, L., Rhodes, D., Pienta, K., Chinnaiyan, A. and Tomlins, S. (2012) The mutational landscape of lethal castration-resistant prostate cancer. *Nature*, 487(7406), pp. 239-243 .

Greer, S. N., Metcalf, J. L., Wang, Y., & Ohh, M. (2012). The updated biology of hypoxia-inducible factor. *The EMBO journal*, 31(11), 2448–2460. doi:10.1038/emboj.2012.125 .

Gregersen LH, Jacobsen A, Frankel LB, Wen J, Krogh A, Lund AH. 2012. MicroRNA-143 down-regulates Hexokinase 2 in colon cancer cells. *BMC Cancer*. 2012 Jun 12;12:232. doi: 10.1186/1471-2407-12-232 .

Gu, C., Cheng, J., Zhang, B., Yang, S., Xie, F., Sun, J., Huang, L., Yu, J. and Li, M. (2017) Protopanaxadiol and metformin synergistically inhibit estrogen-mediated proliferation and anti-autophagy effects in endometrial cancer cells. *American journal of translational research* , 9(9), pp. 4071 .

Guay, C., Joly, Ã., Pepin, Ã., Barbeau, A., Hentsch, L., Pineda, M., Madiraju, S., Brunengraber, H. and Prentki, M. (2013) A Role for Cytosolic Isocitrate Dehydrogenase as a Negative Regulator of Glucose Signaling for Insulin Secretion in Pancreatic ÃŸ-Cells. PLoS ONE, 8(10), p. e77097 .

Gui, Y., Guo, G., Huang, Y., Hu, X., Tang, A., Gao, S., Wu, R., Chen, C., Li, X., Zhou, L., He, M., Li, Z., Sun, X., Jia, W., Chen, J., Yang, S., Zhou, F., Zhao, X., Wan, S., Ye, R., Liang, C., *et al.*, and Cai, Z. (2011) Frequent mutations of chromatin remodeling genes in transitional cell carcinoma of the bladder. Nature Genetics, 43(9), pp. 875-878 .

Hackenberg, M., Barturen, G., Carpena, P., Luque-Escamilla, P., Previti, C. and Oliver, J. (2010) Prediction of CpG-island function: CpG clustering vs. sliding-window methods. BMC Genomics, 11(1), p. 327 .

Halestrap AP. (2013) Monocarboxylic acid transport. Compr Physiol. 2013 Oct; 3(4):1611-43 .

Halestrap, A.P.; Wilson, M.C. The monocarboxylate transporter family-Role and regulation. IUBMB Life 2012, 64, 109–119 .

Hanahan D, Weinberg RA. (2011) Hallmarks of cancer: the next generation Cell. 2011 Mar 4;144(5):646-74. doi: 10.1016/j.cell.2011.02.013 .

Hanif, F., Muzaffar, K., Perveen, K., Malhi, S. M., & Simjee, S. (2017). Glioblastoma Multiforme: A Review of its Epidemiology and Pathogenesis through Clinical Presentation and Treatment*. Asian Pacific journal of cancer prevention : APJCP*, 18(1), 3–9. doi:10.22034/APJCP.2017.18.1.3 .

Hata, A. and Lieberman, J. (2015) Dysregulation of microRNA biogenesis and gene silencing in cancer. *Science signaling* , 8(368), pp. re3 .

Hatziapostolou M, Polytarchou C, Iliopoulos D. (2013). miRNAs link metabolic reprogramming to oncogenesis. *Trends Endocrinol Metab*. 2013 Jul;24(7):361-73. doi: 10.1016/j.tem.2013.03.002 .

Hay, N. and Sonenberg, N. (2004) Upstream and downstream of mTOR. *Genes & development* , 18(16), pp. 1926-1945 .

Heckman-Stoddard, B.M., DeCensi, A., Sahasrabuddhe, V.V. and Ford, L.G. (2017) Repurposing metformin for the prevention of cancer and cancer recurrence. *Diabetologia* , 60(9), pp. 1639-1647 .

Hedenfalk, I., Duggan, D., Chen, Y., Radmacher, M., Bittner, M., Simon, R., Meltzer, P., Gusterson, B., Esteller, M., Raffeld, M. and Yakhini, Z. (2001) *Gene-expression profiles in hereditary .*

Hegi, M.E., Diserens, A., Gorlia, T., Hamou, M., de Tribolet, N., Weller, M., Kros, J.M., Hainfellner, J.A., Mason, W. and Mariani, L. (2005) *MGMT* gene silencing and

benefit from temozolomide in glioblastoma. *New England Journal of Medicine* , 352(10), pp. 997-1003 .

Heras-Sandoval, D., Pérez-Rojas, J.M., Hernández-Damián, J. and Pedraza-Chaverri, J. (2014) The role of PI3K/AKT/mTOR pathway in the modulation of autophagy and the clearance of protein aggregates in neurodegeneration. *Cellular signalling* , 26(12), pp. 2694-2701 .

Herman, J. and Baylin, S. (2003) Gene Silencing in Cancer in Association with Promoter Hypermethylation. *New England Journal of Medicine*, 349(21), pp. 2042-2054 .

Herman, J., Latif, F., Weng, Y., Lerman, M., Zbar, B., Liu, S., Samid, D., Duan, D., Gnarra, J. and Linehan, W. (1994) Silencing of the VHL tumor-suppressor gene by DNA methylation in renal carcinoma. *Proceedings of the National Academy of Sciences,* 91(21), pp. 9700-9704 .

Hervouet, E., Vallette, F. and Cartron, P. (2009) Dnmt3/transcription factor interactions as crucial players in targeted DNA methylation. *Epigenetics,* 4(7), pp. 487-499 .

Hesketh, P.J. (2008) Chemotherapy-induced nausea and vomiting. *New England Journal of Medicine ,* 358(23), pp. 2482-2494 .

Holdhoff, M., Ye, X., Supko, J. G., Nabors, L. B., Desai, A. S., Walbert, T., … Schiff, D. (2017). Timed sequential therapy of the selective T-type calcium channel blocker mibefradil and temozolomide in patients with recurrent high-grade gliomas. *Neuro-oncology,* 19(6), 845–852. doi:10.1093/neuonc/nox020 .

Hong, C., Piazza, M., Ho, W. and Zhuang, Z. (2015) Bi-02disruption Of Perivascular Astrocytic Foot Processes Characterizes Mri Enhancement In Pediatric Brain Tumors. *Neuro-oncology* , 17(Suppl 3), pp. iii2 .

Horbinski C. (2013). What do we know about IDH1/2 mutations so far, and how do we use it?. *Acta neuropathologica*, 125(5), 621–636. doi:10.1007/s00401-013-1106-9 .

Howlader, N., Noone, A., Krapcho, M., Garshell, J., Neyman, N., Altekruse, S., Kosary, C., Yu, M., Ruhl, J. and Tatalovich, Z. (2016) SEER Cancer Statistics Review, 1975–2012, *National Cancer Institute*; 2015 .

Hsu, M. C., & Hung, W. C. (2018). Pyruvate kinase M2 fuels multiple aspects of cancer cells: from cellular metabolism, transcriptional regulation to extracellular signaling. *Molecular cancer*, 17(1), 35. doi:10.1186/s12943-018-0791-3 .

Hui Liu, Hongwei Yang, Xin Wang, Yanyang Tu (2018). The contribution of hexokinase 2 in glioma. Volume: 4 Issue :2 Page: 54-58 .

Hunt, T. (2002) Molecular biology of the cell: A problems approach. *Garland Science*.

Icard, P.; Zhang, X.D.; Lemoisson, E.; Louis, M.H.; Allouche, S.; Lincet, H.; Poulain, L. (2012) Experimental results using 3-bromopyruvate in mesothelioma: In vitro and in vivo studies. *J. Bioenerg. Biomembr*. 2012, 44, 81–90 .

Ihrlund, L. S., Hernlund, E., Khan, O., & Shoshan, M. C. (2008). 3-Bromopyruvate as inhibitor of tumour cell energy metabolism and chemopotentiator of platinum drugs. *Molecular oncology*, 2(1), 94–101. doi:10.1016/j.molonc.2008.01.003 .

Ihrlund, L.S.; Hernlund, E.; Khan, O.; Shoshan, M.C. 3-Bromopyruvate as inhibitor of tumour cell energy metabolism and chemopotentiator of platinum drugs. *Mol. Oncol*. 2008, 2, 94–101 .

Inoki, K., Zhu, T. and Guan, K. (2003) TSC2 mediates cellular energy response to control cell growth and survival. *Cell* , 115(5), pp. 577-590 .

Ito, S., D`Alessio, A., Taranova, O., Hong, K., Sowers, L. and Zhang, Y. (2010) Role of Tet proteins in 5mC to 5hmC conversion, ES-cell self-renewal and inner cell mass specification. *Nature*, 466(7310), pp. 1129-1133 .

Jeon, S., Chandel, N.S. and Hay, N. (2012) AMPK regulates NADPH homeostasis to promote tumour cell survival during energy stress. *Nature* , 485(7400), pp. 661 .

Ji S, Zhang B, Liu J, Qin Y, Liang C, Shi S, Jin K, Liang D, Xu W, Xu H, Wang W, Wu C, Liu L, Liu C, Xu J, Ni Q, Yu X. (2016). ALDOA functions as an oncogene in the

highly metastatic pancreatic cancer. *Cancer Lett*. 2016 Apr 28;374(1):127-135. doi: 10.1016/j.canlet.2016.01.054. *Epub* 2016 Feb 12 .

Jiang B. (2017). Aerobic glycolysis and high level of lactate in cancer metabolism and microenvironment. *Genes Dis*. 2017 Feb 14;4(1):25-27. doi: 10.1016/j.gendis.2017.02.003. PMID: 30258905; PMCID: PMC6136593 .

Jiang S, Zhang LF, Zhang HW, Hu S, Lu MH, Liang S, Li B, Li Y, Li D, Wang ED, Liu MF. (2012) A novel miR-155/miR-143 cascade controls glycolysis by regulating hexokinase 2 in breast cancer cells. *EMBO J.* 2012 Apr 18;31(8):1985-98. doi: 10.1038/emboj.2012.45. *Epub* 2012 Feb 21. PubMed PMID: 22354042; PubMed Central PMCID: PMC3343331 .

Jiang YL, Zhao ZY, Li BR, Yang F, Li J, Jin XW, Wang H, Yu ED, Sun SH, Ning SB. (2018) The altered activity of P53 signaling pathway by STK11 gene mutations and its cancer phenotype in Peutz-Jeghers syndrome. *BMC Med Genet*. 2018 Aug 9;19(1):141. doi: 10.1186/s12881-018-0626-5 .

Jin, D. H., Kim, Y., Lee, B. B., Han, J., Kim, H. K., Shim, Y. M., & Kim, D. H. (2017). Metformin induces cell cycle arrest at the G1 phase through E2F8 suppression in lung cancer cells. *Oncotarget*, 8(60), 101509–101519. doi:10.18632/oncotarget.21552 .

Jones PA, Baylin SB. The epigenomics of cancer. Cell. 2007 Feb 23;128(4):683-92. doi: 10.1016*/j.cell*.2007.01.029. PubMed PMID: 17320506; PubMed Central PMCID: PMC3894624 .

Jones, P. (2002) DNA methylation and cancer. Oncogene, 21(35), pp. 5358-5360 .

Jones, P.A. and Baylin, S.B. (2007) The epigenomics of cancer. *Cell*, 128(4), pp.683-692 .

Jordan, K., Kasper, C. and Schmoll, H. (2005) Chemotherapy-induced nausea and vomiting: current and new standards in the antiemetic prophylaxis and treatment. *European journal of cancer* , 41(2), pp. 199-205

Jurkowska, R., Jurkowski, T. and Jeltsch, A. (2010) Structure and Function of Mammalian DNA Methyltransferases. *ChemBioChem*, 12(2), pp. 206-222 .

Kaluzova, M., Bouras, A., Machaidze, R. and Hadjipanayis, C.G. (2015) Targeted therapy of glioblastoma stem-like cells and tumor non-stem cells using cetuximab-conjugated iron-oxide nanoparticles. *Oncotarget* , 6(11), pp. 8788-8806 .

Kaminska, B., Czapski, B., Guzik, R., Król, S. K., & Gielniewski, B. (2019). Consequences of IDH1/2 Mutations in Gliomas and an Assessment of Inhibitors Targeting Mutated IDH Proteins. *Molecules* (Basel, Switzerland), 24(5), 968. doi:10.3390/molecules24050968 .

Kandoth, C., McLellan, M.D., Vandin, F., Ye, K., Niu, B., Lu, C., Xie, M., Zhang, Q., McMichael, J.F. and Wyczalkowski, M.A. (2013) Mutational landscape and significance across 12 major cancer types. *Nature* , 502(7471), pp. 333 .

Kelly, E. A., Samuels, T. L., & Johnston, N. (2014). Chronic pepsin exposure promotes anchorage-independent growth and migration of a hypopharyngeal squamous cell line. Otolaryngology--head and neck surgery : *official journal of American Academy of Otolaryngology-Head and Neck Surgery,* 150(4), 618–624. doi:10.1177/0194599813517862 .

Kim, D. J., Vo, M. T., Choi, S. H., Lee, J. H., Jeong, S. Y., Hong, C. H., … Park, J. W. (2019). Tristetraprolin-mediated hexokinase 2 expression regulation contributes to glycolysis in cancer cells. *Molecular biology of the cell*, 30(5), 542–553. doi:10.1091/mbc.E18-09-0606 .

Kim, R., Coates, J., Bowles, T., McNerney, G., Sutcliffe, J., Jung, J., Gandour-Edwards, R., Chuang, F., Bold, R. and Kung, H. (2009) Arginine Deiminase as a Novel Therapy for Prostate Cancer Induces Autophagy and Caspase-Independent Apoptosis. *Cancer Research,* 69(2), pp. 700-708 .

Kim, Y.C. and Guan, K. (2015) mTOR: a pharmacologic target for autophagy regulation. *The Journal of clinical investigation* , 125(1), pp. 25-32 .

Kim,W.; Yoon, J.H.; Jeong, J.M.; Cheon, G.J.; Lee, T.S.; Yang, J.I.; Park, S.C.; Lee, H.S. (2007) Apoptosis-inducing antitumor efficacy of hexokinase II inhibitor in hepatocellular carcinoma. *Mol. Cancer Ther*. 2007, 6, 2554–2562.

Kischkel, FC; Hellbardt, S; Behrmann, I; Germer, M; Pawlita, M; Krammer, PH; Peter, ME (1995) "Cytotoxicity-dependent APO-1 (Fas/CD95)-associated proteins form a death-inducing signaling complex (DISC) with the receptor". *The EMBO Journal.* 14 (22): 5579–88. PMC 394672. PMID 8521815 .

Kitambi, S.S., Toledo, E.M., Usoskin, D., Wee, S., Harisankar, A., Svensson, R., Sigmundsson, K., Kalderen, C., Niklasson, M., Kundu, S., Aranda, S., Westermark, B., Uhrbom, L., Andang, M., Damberg, P., Nelander, S., Arenas, E., Artursson, P., Walfridsson, J., Forsberg Nilsson, K., Hammarstrom, L.G.J. and Ernfors, P. (2014) RETRACTED: Vulnerability of glioblastoma cells to catastrophic vacuolization and death induced by a small molecule. *Cell* , 157(2), pp. 313-328 .

Knobbe CB, Reifenberger J, Reifenberger G. (2004) Mutation analysis of the Ras pathway genes NRAS, HRAS, KRAS and BRAF in glioblastomas. *Acta Neuropathol*. 2004 Dec;108(6):467-70. Epub 2004 Oct 28 .

Ko, Y.H.; Pedersen, P.L.; Geschwind, J.F. (2001) Glucose catabolism in the rabbit VX2 tumor model for liver cancer: Characterization and targeting hexokinase. *Cancer Lett*. 2001, 173, 83–91 .

Ko, Y.H.; Smith, B.L.; Wang, Y.C.; Pomper, M.G.; Rini, D.A.; Torbenson, M.S.; Hullihen, J.; Pedersen, P.L. Advanced cancers: Eradication in all cases using 3-bromopyruvate therapy to deplete ATP. *Biochem. Biophys. Res. Commun.* 2004, 324, 269–275.

Ko, Y.H.; Verhoeven, H.A.; Lee, M.J.; Corbin, D.J.; Vogl, T.J.; Pedersen, P.L. A translational study "case report"on the small molecule "energy blocker" 3-bromopyruvate (3BP) as a potent anticancer agent: From bench side to bedside. *J. Bioenerg. Biomembr*. 2012, 44, 163–170 .

Kobayashi, S. (2015) Choose delicately and reuse adequately: the newly revealed process of autophagy. *Biological and Pharmaceutical Bulletin* , 38(8), pp. 1098-1103 .

Koizume, S., & Miyagi, Y. (2015). Diverse Mechanisms of Sp1-Dependent Transcriptional Regulation Potentially Involved in the Adaptive Response of Cancer

Cells to Oxygen-Deficient Conditions. *Cancers,* 8(1), 2. doi:10.3390/cancers8010002 .

Kordes, S., Pollak, M.N., Zwinderman, A.H., Mathôt, R.A., Weterman, M.J., Beeker, A., Punt, C.J., Richel, D.J. and Wilmink, J.W. (2015) Metformin in patients with advanced pancreatic cancer: a double-blind, randomised, placebo-controlled phase 2 trial. The *Lancet Oncology* , 16(7), pp. 839-847 .

Korshunov, A., Schrimpf, D., Ryzhova, M., Sturm, D., Chavez, L., Hovestadt, V., Sharma, T., Habel, A., Burford, A. and Jones, C. (2017) H3-/IDH-wild type pediatric glioblastoma is comprised of molecularly and prognostically distinctsubtypes with associated oncogenic drivers. *Acta Neuropathologica ,* 134(3), pp. 507-516 .

Krause, D.S. and Van Etten, R.A. (2005) Tyrosine kinases as targets for cancer therapy. *New England Journal of Medicine,* 353(2), pp.172-187 .

Łabuzek K, Suchy D, Gabryel B, Bielecka A, Liber S, Okopień B. (2010) Quantification of metformin by the HPLC method in brain regions, cerebrospinal fluid and plasma of rats treated with lipopolysaccharide. *Pharmacol Rep*. 2010 Sep-Oct;62(5):956-65 .

Ladomersky, E., Scholtens, D. M., Kocherginsky, M., Hibler, E. A., Bartom, E. T., Otto-Meyer, S., … Wainwright, D. A. (2019). The Coincidence Between Increasing Age, Immunosuppression, and the Incidence of Patients With Glioblastoma. *Frontiers in pharmacology,* 10, 200. doi:10.3389/fphar.2019.00200 .

Litchfield, L. M., Mukherjee, A., Eckert, M. A., Johnson, A., Mills, K. A., Pan, S., Shridhar, V., Lengyel, E., & Romero, I. L. (2015). Hyperglycemia-induced metabolic compensation inhibits metformin sensitivity in ovarian cancer. *Oncotarget*, 6(27), 23548–23560. https://doi.org/10.18632/oncotarget.4556 .

Lee CY. Strategies of temozolomide in future glioblastoma treatment. *Onco Targets Ther.* 2017 Jan 9;10:265-270. doi: 10.2147/OTT.S120662. PubMed PMID: 28123308; PubMed Central PMCID: PMC5234558 .

Lee HG, Kim H, Son T, Jeong Y, Kim SU, Dong SM, Park YN, Lee JD, Lee JM, Park JH. (2016) Regulation of HK2 expression through alterations in CpG methylation of the HK2 promoter during progression of hepatocellular carcinoma. *Oncotarget.* 2016

Jul 5;7(27):41798-41810. doi: 10.18632/oncotarget.9723. PubMed PMID: 27260001; PubMed Central PMCID: PMC5173097 .

Lee JY, Lee I, Chang WJ, Ahn SM, Lim SH, Kim HS, Yoo KH, Jung KS, Song HN, Cho JH, Kim SY, Kim KM, Lee S, Kim ST, Park SH, Lee J, Park JO, Park YS, Lim HY, Kang WK. (2016) MCT4 as a potential therapeutic target for metastatic gastric cancer with peritoneal carcinomatosis. *Oncotarget.* 7(28):43492-43503. doi: 10.18632/oncotarget.9523. Epub 2016 May 20. PubMed PMID: 27224918; PubMed Central PMCID: PMC5190039 .

Lee, J.E., Lim, J.H., Hong, Y.K. and Yang, S.H. (2018) High-Dose Metformin Plus Temozolomide Shows Increased Anti-tumor Effects in Glioblastoma In vitro and In vivo Compared with Monotherapy. *Cancer research and treatment : official journal of Korean Cancer Association*

Lee, M.; Jo, A.; Lee, S.; Bin Kim, J.; Chang, Y.; Nam, J.Y.; Cho, H.; Cho, Y.Y.; Cho, E.J.; Lee, J.H.; *et al*. (2017) 3-Bromopyruvate and buthionine sulfoximine effectively kill anoikis-resistant hepatocellular carcinoma cells. PLoS ONE 2017, 12, e0174271.

Lewandowicz, G., Harding, B., Harkness, W., Hayward, R., Thomas, D. and Darling, J. (2000) Chemosensitivity in childhood brain tumours in vitro: evidence of differential sensitivity to lomustine (CCNU) and vincristine. European journal of cancer , 36(15), pp. 1955-1964 .

Li P, Wu M. (2017) Epigenetic Mechanisms of Glioblastoma. In: De Vleeschouwer S, editor. Glioblastoma [Internet]. Brisbane (AU): Codon Publications; 2017 Sep 27. Chapter 3. Available from: https://www.ncbi.nlm.nih.gov/books/NBK469995/ doi: 10.15586/codon.glioblastoma.2017.ch3 .

Li P, Wu M. Epigenetic Mechanisms of Glioblastoma. (2017). Glioblastoma Brisbane (AU): Codon Publications; 2017 Sep 27. Chapter 3. Available from: https://www.ncbi.nlm.nih.gov/books/NBK469995/ doi: 10.15586/codon.glioblastoma.2017.ch3 .

Licchesi, J.D. and Herman, J.G. (2009) Methylation-specific PCR. DNA Methylation: Methods and Protocols pp. 305-323 .

Lim W, Olschwang S, Keller JJ, Westerman AM, Menko FH, Boardman LA, Scott RJ, Trimbath J, Giardiello FM, Gruber SB, Gille JJ, Offerhaus GJ, de Rooij FW, Wilson JH, Spigelman AD, Phillips RK, Houlston RS. (2004). Relative frequency and morphology of cancers in STK11 mutation carriers*. Gastroenterology*. 2004 Jun;126(7):1788-94 .

Lin H, *et al*. (2016) Discovery of a novel 2,6-disubstituted glucosamine series of potent and selective hexokinase 2 inhibitors. *ACS Med Chem Lett*. 2016;7:217–22 .

Lin, S. and Gregory, R.I. (2015) MicroRNA biogenesis pathways in cancer. *Nature* reviews cancer , 15(6), pp. 321-333 .

Ling, H., Vincent, K., Pichler, M., Fodde, R., Berindan-Neagoe, I., Slack, F. and Calin, G. (2015) Junk DNA and the long non-coding RNA twist in cancer genetics. *Oncogene,* 34(39), pp. 5003-5011 .

Lipton, J.O. and Sahin, M. (2014) The neurology of mTOR. *Neuron* , 84(2), pp. 275-291 .

Lis P, Dyląg M, Niedźwiecka K, Ko YH, Pedersen PL, Goffeau A, Ułaszewski S. (2016) The HK2 Dependent "Warburg Effect" and Mitochondrial Oxidative Phosphorylation in Cancer: Targets for Effective Therapy with 3-Bromopyruvate. *Molecules*. 2016 Dec 15;21(12):1730. doi: 10.3390/molecules21121730. PubMed PMID: 27983708; PubMed Central PMCID: PMC6273842 .

Litchfield LM, Mukherjee A, Eckert MA, Johnson A, Mills K, Pan S, Shridhar V, Lengyel E, Romero IL. (2015) Hyperglycemia-induced metabolic compensation inhibits metformin sensitivity in ovarian cancer. *Oncotarget.* 2015 Sep 15;6(27):23548-60 .

Liu J., Guo S., Li Q., Yang L., Xia Z., Zhang L., Huang Z., and Zhang N. (2013). Phosphoglycerate dehydrogenase induces glioma cells proliferation and invasion by stabilizing forkhead box M1. *J. Neurooncol*. 111:245–255. 10.1007/s11060-012-1018.

Liu XH1, Zheng XF, Wang YL. (2009). Inhibitive effect of 3-bromopyruvic acid on human breast cancer MCF-7 cells involves cell cycle arrest and apoptotic induction. *Chin Med J (Engl).* 2009 Jul 20;122(14):1681-5 .

Liu Z *et al*. Potent Half-Sandwich Iridium(III) Anticancer Complexes Containing C(?)N-Chelated and Pyridine Ligands. *Organometallics* 33:5324-5333 (2014). Read more (PubMed: 25328266) .

Liu Z, Zhang YY, Zhang QW, Zhao SR, Wu CZ, Cheng X, Jiang CC, Jiang ZW, Liu H. (2014). 3-Bromopyruvate induces apoptosis in breast cancer cells by downregulating Mcl-1 through the PI3K/Akt signaling pathway. *Anticancer Drugs*. 2014 Apr;25(4):447-55. doi: 10.1097/CAD.0000000000000081 .

Locasale J.W., Grassian A.R., Melman T., Lyssiotis C.A., Mattaini K.R., Bass A.J., Heffron G., Metallo C.M., Muranen T., Sharfi H., *et al*. (2011). Phosphoglycerate dehydrogenase diverts glycolytic flux and contributes to oncogenesis. *Nat. Genet*. 43:869–874. 10.1038/ng.890 .

Lord, S., Liu, D., Haider, S., Gaude, E., Teoh, E., Neel, P., Zhang, Q., Gleeson, F., Wakelam, M. and Frezza, C. (2016) Abstract LB-200: Integrating dynamic 18F-FDG PET-CT, tumor metabolomics and functional genomics to understand metformin's pharmacodynamic effects in breast cancer: results of a phase 0 clinical trial .

Luissint, A., Artus, C., Glacial, F., Ganeshamoorthy, K. and Couraud, P. (2012) Tight junctions at the blood brain barrier: physiological architecture and disease-associated dysregulation. *Fluids and Barriers of the CNS* , 9(1), pp. 23 .

Maachani, U.B., Tandle, A., Shankavaram, U., Kramp, T. and Camphausen, K. (2016) Modulation of miR-21 signaling by MPS1 in human glioblastoma. *Oncotarget* , 7(33), pp. 52912-52927 .

Maeting, Ines; Schmidt, Georg; Sahm, Hermann; Stahmann, K.-Peter (2000). "Role of a peroxisomal NADP-specific isocitrate dehydrogenase in the metabolism of the riboflavin overproducer Ashbya gossypii". *Journal of Molecular Catalysis B: Enzymatic*. 10: 335–343. doi:10.1016/S1381-1177(00)00135-1 .

Maier, H. Britton,P. (2012). Involvement of Autophagy in Coronavirus Replication. *Viruses.* 4. 3440-51. 10.3390/v4123440 .

Majewski N., Nogueira V., Bhaskar P., Coy P.E., Skeen J.E., Gottlob K., Chandel N.S., Thompson C.B., Robey R.B., Hay N. (2004) Hexokinase-mitochondria interaction

mediated by Akt is required to inhibit apoptosis in the presence or absence of Bax and Bak. *Mol. Cell*. 2004; 16: 819-830 .

Majmundar, A. J., Wong, W. J., & Simon, M. C. (2010). Hypoxia-inducible factors and the response to hypoxic stress. *Molecular cell*, 40(2), 294–309. doi:10.1016/j.molcel.2010.09.022 .

Malta TM, de Souza CF, Sabedot TS, Silva TC, Mosella MS, Kalkanis SN, Snyder J, Castro AVB, Noushmehr H. (2018) Glioma CpG island methylator phenotype (G-CIMP): biological and clinical implications*. Neuro Oncol.* 2018 Apr 9;20(5):608-620. doi: 10.1093/neuonc/nox183. PubMed PMID: 29036500; PubMed Central PMCID: PMC5892155 .

Mancinelli R, Carpino G, Petrungaro S, Mammola CL, Tomaipitinca L, Filippini A, Facchiano A, Ziparo E, Giampietri C. (2017). Multifaceted Roles of GSK-3 in Cancer and Autophagy-Related Diseases. *Oxid Med Cell Longev*. 2017; 2017:4629495. doi: 10.1155/2017/4629495. Epub 2017 Dec 12. PMID: 29379583; PMCID: PMC5742885 .

Mao Z, Zhang W. (2018) Role of mTOR in Glucose and Lipid Metabolism*. Int J Mol Sci.* 2018 Jul 13;19(7):2043. doi: 10.3390/ijms19072043. PubMed PMID: 30011848; PubMed Central PMCID: PMC6073766 .

Marbaniang, C., & Kma, L. (2018). Dysregulation of Glucose Metabolism by Oncogenes and Tumor Suppressors in Cancer Cells. *Asian Pacific journal of cancer prevention : APJCP,* 19(9), 2377–2390. doi:10.22034/APJCP.2018.19.9.2377 .

Marie, S. K., & Shinjo, S. M. (2011). Metabolism and brain cancer. *Clinics* (Sao Paulo, Brazil), 66 Suppl 1(Suppl 1), 33–43. doi:10.1590/s1807-59322011001300005 .

Marsh J., Mukherjee P., Seyfried T. N. (2008). Drug/diet synergy for managing malignant astrocytoma in mice: 2-deoxy-D-glucose and the restricted ketogenic diet. *Nutr. Metab.* (Lond) 5:33. 10.1186/1743-7075-5-33 .

Martinez-Outschoorn UE, Lin Z, Whitaker-Menezes D, Howell A, Sotqia F, Lisanti MP. (2012) Ketone body utilization drives tumor growth and metastasis. *Cell Cycle*. 2012;11(21):3964–3971. doi: 10.4161/cc.22137 .

Martinez-Outschoorn UE, Prisco M, Ertel A, Tsirigos A, Lin Z, Pavlides S, Wang C, Flomenberg N, Knudsen ES, Howell A, Pestell RG, Sotgia F, Lisanti MP. (2011) Ketones and lactate increase cancer cell "stemness," driving recurrence, metastasis and poor clinical outcome in breast cancer: achieving personalized medicine via Metabolo-*Genomics. Cell Cycle*. 2011 Apr 15;10(8):1271-86. doi: 10.4161/cc.10.8.15330. PMID: 21512313; PMCID: PMC3117136 .

Martínez-Reyes, I., Diebold, L.P., Kong, H., Schieber, M., Huang, H., Hensley, C.T., Mehta, M.M., Wang, T., Santos, J.H. and Woychik, R. (2016) TCA cycle and mitochondrial membrane potential are necessary for diverse biological functions. *Molecular cell ,* 61(2), pp. 199-209 .

Martuscello RT, Vedam-Mai V, McCarthy DJ, Schmoll ME, Jundi MA, Louviere CD, Griffith BG, Skinner CL, Suslov O, Deleyrolle LP, Reynolds BA. (2016). A Supplemented High-Fat Low-Carbohydrate Diet for the Treatment of Glioblastoma. *Clin Cancer Res*. 2016 May 15;22(10):2482-95. doi: 10.1158/1078-0432.CCR-15-0916. Epub 2015 Dec 2 .

Maruthur, N.M., Tseng, E., Hutfless, S., Wilson, L.M., Suarez-Cuervo, C., Berger, Z., Chu, Y., Iyoha, E., Segal, J.B. and Bolen, S. (2016) Diabetes Medications as Monotherapy or Metformin-Based Combination Therapy for Type 2 DiabetesA Systematic Review and Meta-analysisDiabetes Medications as Monotherapy or Metformin-Based Combination Therapy. *Annals of Internal Medicine* , 164(11), pp. 740-751 .

Masoumi Moghaddam, S., Amini, A., Morris, D. L., & Pourgholami, M. H. (2012). Significance of vascular endothelial growth factor in growth and peritoneal dissemination of ovarian cancer. *Cancer metastasis reviews*, 31(1-2), 143–162. doi:10.1007/s10555-011-9337-5 .

Massey, T. and Robertson, N. (2018) Repurposing drugs to treat neurological diseases. *Journal of neurology* pp. 1-3 .

Mathupala S, Rempel A, Pedersen P. (2001) Glucose catabolism in cancer cells: identification and characterization of a marked activation response of the type II

hexokinase gene to hypoxic conditions*. J. Biol. Chem*. 276:43407–43412. doi:10.1074/jbc.M108181200 .

Matsuzaki, T., Tungalagsuvd, A., Iwasa, T., Munkhzaya, M., Yano, K., Mayila, Y., … Irahara, M. (2017). Clinical outcome of various metformin treatments for women with polycystic ovary syndrome. *Reproductive medicine and biology*, 16(2), 179–187. doi:10.1002/rmb2.12026 .

Mattaini KR, Sullivan MR, Vander Heiden MG. (2016). The importance of serine metabolism in cancer. *J Cell Biol*. 2016 Aug 1;214(3):249-57. doi: 10.1083/jcb.201604085. Epub 2016 Jul 25. PMID: 27458133; PMCID: PMC4970329 .

Mayumi T, Makoto S, Hideyuki S. Pyruvate kinase M2: multiple faces for conferring benefits on cancer cells. (2012) Published in Clinical cancer research : *an official journal of the American Association for Cancer Research*. 2012 DOI:10.1158/1078-0432.CCR-12-0859 .

McCommis, K. S., & Baines, C. P. (2012) The role of VDAC in cell death: friend or foe?. *Biochimica et biophysica* acta, 1818(6), 1444–1450. doi:10.1016/j.bbamem.2011.10.025 .

McGranahan, N. and Swanton, C. (2015) Biological and Therapeutic Impact of Intratumor Heterogeneity in Cancer Evolution. *Cancer Cell*, 27(1), pp. 15-26 .

McGuire, S. (2016) World Cancer Report 2014. Geneva, Switzerland: World Health Organization, *International Agency for Research on Cancer, WHO Press, 2015. Advances in nutrition* (Bethesda, Md.) , 7(2), pp. 418-419 .

McNeill RS, Canoutas DA, Stuhlmiller TJ, Dhruv HD, Irvin DM, Bash RE, Angus SP, Herring LE, Simon JM, Skinner KR, Limas JC, Chen X, Schmid RS, Siegel MB, Van Swearingen AED, Hadler MJ, Sulman EP, Sarkaria JN, Anders CK, Graves LM, Berens ME, Johnson GL, Miller CR. (2017) Combination therapy with potent PI3K and MAPK inhibitors overcomes adaptive kinome resistance to single agents in preclinical models of glioblastoma. *Neuro Oncol*. 2017 Oct 19;19(11):1469-1480. doi: 10.1093/neuonc/nox044 .

Melstrom, K. and Sentovich, S.M. (2017) Colon and Rectal Surgical Emergencies. in Surgical Emergencies in the Cancer Patient. *Springer*, pp.177-187.

Menendez MT, Teygong C, Wade K, Florimond C, Blader IJ. (2015). siRNA Screening Identifies the Host Hexokinase 2 (HK2) Gene as an Important Hypoxia-Inducible Transcription Factor 1 (HIF-1) Target Gene in Toxoplasma gondii-Infected Cells. *MBio.* 2015 Jun 23;6(3): e00462. doi: 10.1128/mBio.00462-15 .

Menendez, J.A., Oliveras-Ferraros, C., Cufí, S., Corominas-Faja, B., Joven, J., Martin-Castillo, B. and Vazquez-Martin, A. (2012) Metformin is synthetically lethal with glucose withdrawal in cancer cells. *Cell cycle* , 11(15), pp. 2782-2792 .

Merchant, M.S., Geller, J.I., Baird, K., Chou, A.J., Galli, S., Charles, A., Amaoko, M., Rhee, E.H., Price, A., Wexler, L.H., Meyers, P.A., Widemann, B.C. Tsokos, M. and Mackall, C.L. (2012) Phase I trial and pharmacokinetic study of lexatumumab in pediatric patients with solid tumors. *Journal of clinical oncology: official journal of the American Society of Clinical Oncology ,* 30(33), pp. 4141-4147 .

Messaoudi, K., Clavreul, A. and Lagarce, F. (2015) Toward an effective strategy in glioblastoma treatment. Part I: resistance mechanisms and strategies to overcome resistance of glioblastoma to temozolomide. *Drug discovery today* .

Meyer, M., Reimand, J., Lan, X., Head, R., Zhu, X., Kushida, M., Bayani, J., Pressey, J.C., Lionel, A.C., Clarke, I.D., Cusimano, M., Squire, J.A., Scherer, S.W., Bernstein, M., Woodin, M.A., Bader, G.D. and Dirks, P.B. (2015) Single cell-derived clonal analysis of human glioblastoma links functional and genomic heterogeneity. *Proceedings of the National Academy of Sciences of the United States of America* , 112(3), pp. 851-856 .

Michlewski, G., & Cáceres, J. F. (2019). Post-transcriptional control of miRNA biogenesis. *RNA* (New York, N.Y.), 25(1), 1–16. doi:10.1261/rna.068692.118

Mihaylova, M.M. and Shaw, R.J. (2011) The AMPK signalling pathway coordinates cell growth, autophagy and metabolism. *Nature cell biology* , 13(9), pp. 1016 .

Miranda-Gonçalves, V., Lameirinhas, A., Henrique, R., & Jerónimo, C. (2018). Metabolism and Epigenetic Interplay in Cancer: Regulation and Putative Therapeutic Targets. *Frontiers in genetics,* 9, 427. doi:10.3389/fgene.2018.00427 .

Miroshnikova, Y.A., Mouw, J.K., Barnes, J.M., Pickup, M.W., Lakins, J.N., Kim, Y., Lobo, K., Persson, A.I., Reis, G.F. and McKnight, T.R. (2016) Tissue mechanics promote IDH1-dependent HIF1α–tenascin C feedback to regulate glioblastoma aggression. *Nature cell biology* , 18(12), pp. 1336 .

Molenaar, R.J., Verbaan, D., Lamba, S., Zanon, C., Jeuken, J.W., Boots-Sprenger, S.H., Wesseling, P., Hulsebos, T.J., Troost, D. and Van Tilborg, A.A. (2014) The combination of IDH1 mutations and *MGMT* methylation status predicts survival in glioblastoma better than either IDH1 or *MGMT* alone. *Neuro-oncology* , 16(9), pp. 1263-1273 .

Monga, V., Jones, K. and Chang, S. (2017) CLINICAL RELEVANCE OF MOLECULAR MARKERS IN GLIOMAS. *Revista Médica Clínica Las Condes* , 28(3), pp. 343-351 .

Moriwaki, K., & Chan, F. K. (2013). RIP3: a molecular switch for necrosis and inflammation. *Genes & development*, 27(15), 1640–1649. doi:10.1101/gad.223321.113 .

Mukherjee A, Ma Y, Yuan F, Gong Y, Fang Z, Mohamed EM, Berrios E, Shao H, Fang X. (2015). Lysophosphatidic Acid Up-Regulates Hexokinase II and Glycolysis to Promote Proliferation of Ovarian Cancer Cells*. Neoplasia.* 2015 Sep;17(9):723-734. doi: 10.1016/j.neo.2015.09.003 .

Munoz, J.L., Rodriguez-Cruz, V., Greco, S.J., Nagula, V., Scotto, K.W. and Rameshwar, P. (2014) Temozolomide induces the production of epidermal growth factor to regulate MDR1 expression in glioblastoma cells. *Molecular cancer therapeutics ,* 13(10), pp. 2399-2411 .

Nagarajan, R. P., Zhang, B., Bell, R. J., Johnson, B. E., Olshen, A. B., Sundaram, V., Costello, J. F. (2014). Recurrent epimutations activate gene body promoters in primary glioblastoma. *Genome research*, 24(5), 761–774. doi:10.1101/gr.164707.113.

Nair, V., Sreevalsan, S., Basha, R., Abdelrahim, M., Abudayyeh, A., Rodrigues Hoffman, A. and Safe, S. (2014) Mechanism of metformin-dependent inhibition of mammalian target of rapamycin (mTOR) and Ras activity in pancreatic cancer: role of specificity protein (Sp) transcription factors. *The Journal of biological chemistry* , 289(40), pp. 27692-27701 .

Nakamura, S. and Yoshimori, T. (2017) New insights into autophagosome-lysosome fusion. *Journal of cell science* , 130(7), pp. 1209-1216 .

Nancolas B, Guo L, Zhou R, Nath K, Nelson DS, Leeper DB, Blair IA, Glickson JD, Halestrap AP. (2016) The anti-tumour agent lonidamine is a potent inhibitor of the mitochondrial pyruvate carrier and plasma membrane monocarboxylate transporters. *Biochem J.* 2016 Apr 1;473(7):929-36. doi: 10.1042/BJ20151120. Epub 2016 Feb 1. PubMed PMID: 26831515; PubMed Central PMCID: PMC4814305 .

Nancolas, B., Guo, L., Zhou, R., Nath, K., Nelson, D. S., Leeper, D. B., … Halestrap, A. P. (2016). The anti-tumour agent lonidamine is a potent inhibitor of the mitochondrial pyruvate carrier and plasma membrane monocarboxylate transporters. *The Biochemical journal*, 473(7), 929–936. doi:10.1042/BJ20151120 .

Nath K, Nelson DS, Heitjan DF, Leeper DB, Zhou R, Glickson JD. (2015) Lonidamine induces intracellular tumor acidification and ATP depletion in breast, prostate and ovarian cancer xenografts and potentiates response to doxorubicin. *NMR Biomed*. 2015 Mar; 28(3):281-9 .

Neary CL, Pastorino JG. (2013) Akt inhibition promotes hexokinase 2 redistribution and glucose uptake in cancer cells. *J Cell Physiol* 2013; 228 (9): 1943–8 .

Neri, F., Krepelova, A., Incarnato, D., Maldotti, M., Parlato, C., Galvagni, F., Matarese, F., Stunnenberg, H. and Oliviero, S. (2013) Dnmt3L Antagonizes DNA Methylation at Bivalent Promoters and Favors DNA Methylation at Gene Bodies in ESCs. *Cell*, 155(1), pp. 121-134 .

Nestor, C.E., Ottaviano, R., Reinhardt, D., Cruickshanks, H.A., Mjoseng, H.K., McPherson, R.C., Lentini, A., Thomson, J.P., Dunican, D.S. and Pennings, S. (2015)

Rapid reprogramming of epigenetic and transcriptional profiles in mammalian culture systems. *Genome biology* , 16(1), pp. 11 .

New M, Van Acker T, Sakamaki JI, Jiang M, Saunders RE, Long J, Wang VM, Behrens A, Cerveira J, Sudhakar P, Korcsmaros T, Jefferies HBJ, Ryan KM, Howell M, Tooze SA. (2019). MDH1 and MPP7 Regulate Autophagy in Pancreatic Ductal Adenocarcinoma. *Cancer Res*. 2019 Apr 15;79(8):1884-1898. doi: 10.1158/0008-5472.CAN-18-2553. Epub 2019 Feb 14 .

Newman JC, Verdin E. (2014) Beta-hydroxybutyrate: much more than a metabolite. *Diabetes Res Clin Pract*. 2014;106:173–181. doi: 10.1016/j.diabres.2014.08.009 .

Nguyen, T. A., Menendez, D., Resnick, M. A., & Anderson, C. W. (2014). Mutant TP53 posttranslational modifications: challenges and opportunities. *Human mutation*, 35(6), 738–755. doi:10.1002/humu.22506 .

Noch, E., & Khalili, K. (2009). Molecular mechanisms of necrosis in glioblastoma: the role of glutamate excitotoxicity. *Cancer biology & therapy*, 8(19), 1791–1797. doi:10.4161/cbt.8.19.9762 .

Oberoi, R.K., Parrish, K.E., Sio, T.T., Mittapalli, R.K., Elmquist, W.F. and Sarkaria, J.N. (2015) Strategies to improve delivery of anticancer drugs across the blood–brain barrier to treat glioblastoma. *Neuro-oncology* , 18(1), pp. 27-36 .

Ohgaki, H. and Kleihues, P. (2007) Genetic pathways to primary and secondary glioblastoma. *The American journal of pathology* , 170(5), pp. 1445-1453 .

Okatsu K, Iemura S, Koyano F, Go E, Kimura M, Natsume T, Tanaka K, Matsuda N (Nov 2012) Mitochondrial hexokinase HKI is a novel substrate of the Parkin ubiquitin ligase*. Biochemical and Biophysical Research Communications*. 428 (1): 197–202. doi:10.1016/j.bbrc.2012.10.041. PMID 23068103 .

Oliver JA, Ortiz R, Melguizo C, Alvarez PJ, Gómez-Millán J, Prados J. (2014). Prognostic impact of *MGMT* promoter methylation and *MGMT* and CD133 expression in colorectal adenocarcinoma. *BMC Cance*r. 2014 Jul 11;14:511. doi: 10.1186/1471-2407-14-511 .

Ougolkov, M. Fernandez-Zapico, D. Savoy, R. Urrutia A, and Billadeau, D. (2005). Glycogen synthase kinase-3β participates in nuclear factor κB-mediated gene transcription and cell survival in pancreatic cancer cells, *Cancer Research*, vol. 65, no. 6, pp. 2076–2081, 2005 .

Ozdemir-Kaynak, E., Qutub, A. A., & Yesil-Celiktas, O. (2018). Advances in Glioblastoma Multiforme Treatment: New Models for Nanoparticle Therapy. *Frontiers in physiology*, 9, 170. doi:10.3389/fphys.2018.00170 .

Palmieri D, Fitzgerald D, Shreeve SM, Hua E, Bronder JL, Weil RJ, Davis S, Stark AM, Merino MJ, Kurek R, Mehdorn HM, Davis G, Steinberg SM, Meltzer PS, Aldape K, Steeg PS (2009). Analyses of resected human brain metastases of breast cancer reveal the association between up-regulation of hexokinase 2 and poor prognosis. *Molecular Cancer Research.* 7 (9): 1438–45. doi:10.1158/1541-7786.MCR-09-0234. PMC 2746883 .

Pammolli F, Magazzini L, Riccaboni M. (2011) Nat Rev Drug Discov. 2011 Jun;10(6):428-38. doi: 10.1038/nrd3405. The productivity crisis in pharmaceutical R&D .

Pan L, Yang H, Tang W, Xu C, Chen S, Meng Z, Li K, Chen H. (2017) Pathway-focused PCR array profiling of CAL-27 cell with over-expressed ZNF750. *Oncotarget*. 2017 Dec 9;9(1):566-575. doi: 10.18632/oncotarget.23075. PMID: 29416636; PMCID: PMC5787490 .

Papagiannakopoulos, T., Shapiro, A. and Kosik, K.S. (2008) MicroRNA-21 targets a network of key tumor-suppressive pathways in glioblastoma cells. *Cancer research* , 68(19), pp. 8164-8172 .

Park, K., Wan-Teck Lim, D., Okamoto, I., & Yang, J. C. (2019). First-line afatinib for the treatment of EGFR mutation-positive non-small-cell lung cancer in the 'real-world' clinical setting. *Therapeutic advances in medical oncology*, 11, 1758835919836374. doi:10.1177/1758835919836374 .

Parsa, A.T., Waldron, J.S., Panner, A., Crane, C.A., Parney, I.F., Barry, J.J., Cachola, K.E., Murray, J.C., Tihan, T. and Jensen, M.C. (2007) Loss of tumor suppressor PTEN

function increases B7-H1 expression and immunoresistance in glioma. *Nature medicine ,* 13(1), pp. 84 .

Parzych, K.R. and Klionsky, D.J. (2014) An overview of autophagy: morphology, mechanism, and regulation. *Antioxidants & redox signaling* , 20(3), pp. 460-473 .

Pastor, W., Aravind, L. and Rao, A. (2013) TETonic shift: biological roles of TET proteins in DNA demethylation and transcription. *Nature Reviews Molecular Cell Biology,* 14(6), pp. 341-356 .

Patra KC, Hay N. (2014). The pentose phosphate pathway and cancer. *Trends Biochem Sci.* 2014 Aug;39(8):347-54. doi: 10.1016/j.tibs.2014.06.005. Epub 2014 Jul 15. Review.PMID: 2503750 .

Patra KC, Wang Q, Bhaskar PT, *et al*. (2013) Hexokinase 2 is required for tumor initiation and maintenance and its systemic deletion is therapeutic in mouse models of cancer. Cancer Cell. 2013 Sep 9;24(3):399]. *Cancer Cell*. 2013;24(2):213–228. doi:10.1016/j.ccr.2013.06.014 .

Perry A, Wesseling P. (2016). Histologic classification of gliomas. *Handb Clin Neurol*. 2016;134:71-95. doi: 10.1016/B978-0-12-802997-8.00005-0 .

Peschiaroli A, Giacobbe A, Formosa A, Markert EK, Bongiorno-Borbone L, Levine AJ, Candi E, D'Alessandro A, Zolla L, Finazzi Agrò A, Melino G. (2013) miR-143 regulates hexokinase 2 expression in cancer cells. *Oncogene.* 2013 Feb 7;32(6):797-802. doi: 10.1038/onc.2012.100 .

Pfeifer GP. Defining Driver DNA Methylation Changes in Human Cancer. *Int J Mol Sci.* 2018 Apr 12;19(4):1166. doi: 10.3390/ijms19041166. PMID: 29649096; PMCID: PMC5979276.

Phan, L.M., Yeung, S.C.J. and Lee, M.H. (2014) Cancer metabolic reprogramming: importance, main features, and potentials for precise targeted anti-cancer therapies. *Cancer biology & medicine,* 11(1), pp.1-19 .

Philips, A., Henshaw, D.L., Lamburn, G. and O'Carroll, M.J. (2018) Brain tumours: rise in Glioblastoma Multiforme incidence in England 1995–2015 suggests an adverse environmental or lifestyle factor*. Journal of environmental and public health* , 2018 .

Piantadosi, S. (2017) Clinical trials: a methodologic perspective. John Wiley & Sons.

Pirola, C.J., Fernandez Gianotti, T., Castano, G.O., Mallardi, P., San Martino, J., Mora Gonzalez Lopez Ledesma, M., Flichman, D., Mirshahi, F., Sanyal, A.J. and Sookoian, S. (2015) Circulating microRNA signature in non-alcoholic fatty liver disease: from serum non-coding RNAs to liver histology and disease pathogenesis. *Gut* , 64(5), pp. 800-812 .

Pollack, I., Hamilton, R., James, C., Finkelstein, S., Burnham, J., Yates, A., Holmes, E., Zhou, T. and Finlay, J. (2006) Rarity of PTEN deletions and EGFR amplification in malignant gliomas of childhood: results from the Children's Cancer Group 945 cohort. Journal of Neurosurgery*: Pediatrics*, 105(5), pp. 418-424 .

Pollak, M.N. (2012) Investigating metformin for cancer prevention and treatment: the end of the beginning. *Cancer discovery* , 2(9), pp. 778-790 .

Ponten, J. and MACINTYRE, E.H. (1968) Long term culture of normal and neoplastic human glia. Acta Pathologica Microbiologica Scandinavica , 74(4), pp. 465-486 .

Ponten, J. and Westermark, B. (1978) Properties of human malignant glioma cells in vitro. *Medical biology* , 56(4), pp. 184-193 .

Pópulo H, Lopes JM, Soares P. (2012) The mTOR signalling pathway in human cancer, *Int J Mol Sci*. 2012;13(2):1886-918. doi: 10.3390/ijms13021886. Epub 2012 Feb 10. Review. PMID: 22408430 .

Possemato R., Marks K.M., Shaul Y.D., Pacold M.E., Kim D., Birsoy K., Sethumadhavan S., Woo H.K., Jang H.G., Jha A.K., *et al*. (2011). Functional genomics reveal that the serine synthesis pathway is essential in breast cancer*. Nature.* 476:346–350. 10.1038/nature10350 .

Poteet, E., Choudhury, G.R., Winters, A., Li, W., Ryou, M.G., Liu, R., Tang, L., Ghorpade, A., Wen, Y., Yuan, F., Keir, S.T., Yan, H., Bigner, D.D., Simpkins, J.W. and Yang, S.H. (2013) Reversing the Warburg effect as a treatment for glioblastoma. *The Journal of biological chemistry* , 288(13), pp. 9153-9164 .

Potter, N., Phipps, K., Harkness, W., Hayward, R., Thompson, D., Jacques, T., Harding, B., Thomas, D., Rees, J., Darling, J. and Warr, T. (2009) Astrocytoma

derived short-term cell cultures retain molecular signatures characteristic of the tumour in situ. *Experimental Cell Research*, 315(16), pp. 2835-2846 .

Prabhakara S, Kalia VK Indian J (2008) Optimizing radiotherapy of brain tumours by a combination of temozolomide & lonidamine*. Med Res*. 2008 Aug; 128(2):140-8 .

Price GS, Page RL, Riviere JE, Cline JM, Thrall DE. (1996) Pharmacokinetics and toxicity of oral and intravenous lonidamine in dogs. *Cancer Chemother Pharmacol*. 1996;38:129–135 .

Prins, R.M., Soto, H., Konkankit, V., Odesa, S.K., Eskin, A., Yong, W.H., Nelson, S.F. and Liau, L.M. (2011) Gene expression profile correlates with T-cell infiltration and relative survival in glioblastoma patients vaccinated with dendritic cell immunotherapy. Clinical cancer research : *an official journal of the American Association for Cancer Research ,* 17(6), pp. 1603-1615 .

Puente, X., Pinyol, M., Quesada, V., Conde, L., Ordóñez, G., Villamor, N., Escaramis, G., Jares, P., Beà, S., González-Díaz, M., Bassaganyas, L., Baumann, T., Juan, M., López- Alava, E., Miguel, J., Royo, R., Gelpí, J., Torrents, D., Orozco, M., Pisano, D., Valencia, A., Guigó, Stratton, M., Campbell, P., Gut, I., López-Guillermo, A., Estivill, X., Montserrat, E., López-Otín, C. and Campo, E. (2011) Whole-genome sequencing identifies recurrent mutations in chronic lymphocytic leukaemia. *Nature*, 475(7354), pp. 101-105 .

Pulaski, Lukasz & Jatczak-Pawlik, Izabela & Sobalska, Marta & Strapagiel, Dominik & Bartosz, Grzegorz & Sadowska-Bartosz, Izabela. (2018). 3-Bromopyruvate induces expression of antioxidant genes. *Free Radical Research*. 53. 1-251. 10.1080/10715762.2018.1541176 .

Qian S, Xinxin C, Jianhui M, Haiyong P, Fang W, Xiaojun Z, Yanan W, Yanling J, Hongwang Y, Rongrong C, Long C, Yu Z, June G, Hiroaki O, Tong C, Ming-Rong W, Youyong L, Han Y, Kwiatkowski D, Hongbing Z. (2011). Mammalian target of rapamycin up-regulation of pyruvate kinase isoenzyme type M2 is critical for aerobic glycolysis and tumor growth. *Proceedings of the National Academy of Sciences Mar* 2011, 108 (10) 4129-4134; DOI:10.1073/pnas.1014769108 .

Qin J, Wen B, Liang Y, Yu W, Li H (2019) Histone Modifications and their Role in Colorectal Cancer (Review). *Pathol Oncol Res*. 2019 May 4. doi: 10.1007/s12253-019-00663-8. [Epub ahead of print] .

Radke, J., Koch, A., Pritsch, F., Schumann, E., Misch, M., Hempt, C., Lenz, K., Löbel, F., Paschereit, F., Heppner, F.L., Vajkoczy, P., Koll, R., & Onken, J. (2019). Predictive *MGMT* status in a homogeneous cohort of IDH wildtype glioblastoma patients. Acta *Neuropathologica Communications .*

Ramirez, Y.P., Weatherbee, J.L., Wheelhouse, R.T. and Ross, A.H. (2013) Glioblastoma multiforme therapy and mechanisms of resistance. *Pharmaceuticals* , 6(12), pp. 1475-1506 .

Reardon D. A., Freeman G., Wu C., Chiocca E. A., Wucherpfennig K. W., Wen P. Y., *et al*. (2014). Immunotherapy advances for glioblastoma. *Neuro Oncol*. 16, 1441–1458. 10.1093/neuonc/nou212 .

Reardon DA, Groves MD, Wen PY, Nabors L, Mikkelsen T, Rosenfeld S, *et al*. (2013). A phase I/II trial of pazopanib in combination with lapatinib in adult patients with relapsed malignant glioma. *Clinical cancer research : an official journal of the American Association for Cancer Research*. 2013;19:900–908 .

Reardon, D.A., Freeman, G., Wu, C., Chiocca, E.A., Wucherpfennig, K.W., Wen, P.Y., Fritsch, E.F., Curry, W.T., Sampson, J.H. and Dranoff, G. (2014) Immunotherapy advances for glioblastoma. *Neuro-oncology* , 16(11), pp. 1441-1458 .

Roberts, D. J., & Miyamoto, S. (2015) Hexokinase II integrates energy metabolism and cellular protection: Akting on mitochondria and TORCing to autophagy. *Cell death* and differentiation, 22(2), 248–257. doi:10.1038/cdd.2014.173 .

Roberts, S. and Speirs, V. (2017) Advances in the development of improved animal-free models for use in breast cancer biomedical research. *Biophysical reviews* , 9(4), pp. 321-327 .

Robey R., Hay N. (2006) Mitochondrial hexokinases, novel mediators of the antiapoptotic effects of growth factors and Akt. *Oncogene*. 2006; 25: 4683-4696 .

Robey RB, Hay N. Is Akt the "Warburg kinase"-Akt-energy metabolism interactions and oncogenesis. *Semin Cancer Biol*. 2009 Feb;19(1):25-31. doi: 10.1016/j.semcancer.2008.11.010. Epub 2008 Dec 14. PubMed PMID: 19130886; PubMed Central PMCID: PMC2814453 .

Rock, K., McArdle, O., Forde, P., Dunne, M., Fitzpatrick, D., O'Neill, B., & Faul, C. (2012). A clinical review of treatment outcomes in glioblastoma multiforme--the validation in a non-trial population of the results of a randomised Phase III clinical trial: has a more radical approach improved survival?. *The British journal of radiology*, 85(1017), e729–e733. doi:10.1259/bjr/83796755 .

Rodrigues LM, Uribe-Lewis S, Madhu B, Honess DJ, Stubbs M, Griffiths JR. (2017) The action of β-hydroxybutyrate on the growth, metabolism and global histone H3 acetylation of spontaneous mouse mammary tumours: evidence of a β-hydroxybutyrate paradox. *Cancer Metab*. 2017 Feb 28;5:4. doi: 10.1186/s40170-017-0166-z. PubMed PMID: 28261475; PubMed Central PMCID: PMC5331634 .

Rossi A. P., Woolf E. C., Brooks K. S., Fairres M. J., Scheck A. C. (2015). Abstract 3346: the ketone body β-hydroxybutyrate increases radiosensitivity in glioma cell lines in vitro. *Cancer Res*. 75:3346 10.1158/1538-7445.am2015-3346 .

Rusten, T., Haglund, K. and Stenmark, H. (2007) Aberrant Receptor Signaling and Trafficking as Mechanisms in Oncogenesis. *Crit Rev Oncog*, 13(1), pp. 39-74 .

Saber MM, Al-Mahallawi AM, Nassar NN, Stork B, Shouman SA. (2018) Targeting colorectal cancer cell metabolism through development of cisplatin and metformin nano-cubosomes. *BMC Cancer*. 2018 Aug 15;18(1):822. doi: 10.1186/s12885-018-4727-5. PMID: 30111296; PMCID: PMC6094476 .

Sanchez-Cespedes M. (2007) A role for LKB1 gene in human cancer beyond the Peutz-Jeghers syndrome. *Oncogene*. 26 (57): 7825–32. doi:10.1038/sj.onc.1210594. PMID 17599048 .

Sankar, A., Sythana, S., Jhansi, A., Shanmugasundharam, P. and Aumithra, M. (2013) Development and validation for simultaneous estimation of sitagliptin and

metformin in pharmaceutical dosage form using RP-HPLC method. *International Journal of Pharma Tech Research* , 5(4), pp. 1736-1744 .

Sansom, C. (2009) Temozolomide--Birth of a blockbuster-The history of anti-cancer drug temozolomide can be traced back over 30 years--And it all started with some novel nitrogen chemistry. *Chemistry World* , 6(7), pp. 48 .

Santa-Maria, I., Alaniz, M.E., Renwick, N., Cela, C., Fulga, T.A., Van Vactor, D., Tuschl, T., Clark, L.N., Shelanski, M.L., McCabe, B.D. and Crary, J.F. (2015) Dysregulation of microRNA-219 promotes neurodegeneration through post-transcriptional regulation of tau. *The Journal of clinical investigation* , 125(2), pp. 681-686 .

Saxton, R.A. and Sabatini, D.M. (2017) mTOR signaling in growth, metabolism, and disease. *Cell* , 168(6), pp. 960-976 .

Scheck A. C., Abdelwahab M. G., Fenton K., Stafford P. (2012). The ketogenic diet for the treatment of glioma: insights from genetic profiling. *Epilepsy Res*. 100, 327–337. 10.1016/j.eplepsyres.2011.09.022 .

Schimazu T, Hirschey MD, Newman J, He W, Shirakawa K, Le Moan N, *et al*. (2013) Suppression of oxidative stress by β-hydroxybutyrate, an endogenous histone deacetylase inhibitor. *Science*. 2013;339(6116):211–214. doi: 10.1126/science.1227166 .

Schleich, Kolja & Lavrik, Inna. (2013) Mathematical modeling of apoptosis. Cell communication and signaling : CCS. 11. 44. 10.1186/1478-811X-11-44 .

Schuhmacher, A., Gassmann, O., & Hinder, M. (2016). Changing R&D models in research-based pharmaceutical companies. *Journal of translational medicine*, 14(1), 105. doi:10.1186/s12967-016-0838-4 .

Schultz, S., Pinsky, G.S., Wu, N.C., Chamberlain, M.C., Rodrigo, A.S. and Martin, S.E. (2005) Fine needle aspiration diagnosis of extracranial glioblastoma multiforme: Case report and review of the literature. *CytoJournal* , 2pp. 19-6413-2-19 .

Semenza GL. (2013) HIF-1 mediates metabolic responses to intratumoral hypoxia and oncogenic mutations. *J Clin Invest*. 2013 Sep;123(9):3664-71. doi: 10.1172/JCI67230. Epub 2013 Sep 3 .

Sesen, J., Dahan, P., Scotland, S.J., Saland, E., Dang, V., Lemarié, A., Tyler, B.M., Brem, H., Toulas, C. and Moyal, E.C. (2015) Metformin inhibits growth of human glioblastoma cells and enhances therapeutic response. *PloS one* , 10(4), pp. e0123721.

Shakoori, A. Ougolkov, Z. W. Yu (2005). Deregulated GSK3β activity in colorectal cancer: its association with tumor cell survival and proliferation, *Biochemical and Biophysical Research Communications*, vol. 334, no. 4, pp. 1365–1373, 2005 .

Sharma, N., Nanta, R., Sharma, J., Gunewardena, S., Singh, K.P., Shankar, S. and Srivastava, R.K. (2015) PI3K/AKT/mTOR and sonic hedgehog pathways cooperate together to inhibit human pancreatic cancer stem cell characteristics and tumor growth*. Oncotarget* , 6(31), pp. 32039-32060 .

Sharma, S., Kelly, T. and Jones, P. (2009) Epigenetics in cancer. *Carcinogenesis*, 31(1), pp. 27-36 .

Shelton L. M., Huysentruyt L. C., Mukherjee P., Seyfried T. N. (2010). Calorie restriction as an anti-invasive therapy for malignant brain cancer in the VM mouse. *ASN Neuro* 2:e00038. 10.1042/AN20100002 .

Sherr CJ, McCormick F. (2002). The RB and p53 pathways in cancer. *Cancer Cell*. 2002 Aug;2(2):103-12 .

Sheu-Gruttadauria, J. and MacRae, I.J. (2018) Phase Transitions in the Assembly and Function of Human miRISC. *Cell* , 173(4), pp. 946-957. e16 .

Shin YJ, Sa JK, Lee Y, Kim D, Chang N, Cho HJ, Son M, Oh MYT, Shin K, Lee JK, Park J, Jo YK, Kim M, Paddison PJ, Tergaonkar V, Lee J, Nam DH. (2019). PIP4K2A as a negative regulator of PI3K in PTEN-deficient glioblastoma. *J Exp Med*. 2019 May 6;216(5):1120-1134. doi: 10.1084/jem.20172170. Epub 2019 Mar 21 .

Shukla SK, Gebregiworgis T, Purohit V, Chaika NV, Gunda V, Radhakrishnan P, Mehla K, Pipinos II, Powers R, Yu F, Singh PK. (2014). Metabolic reprogramming induced

by ketone bodies diminishes pancreatic cancer cachexia. *Cancer Metab*. 2014 Sep 1;2:18. doi: 10.1186/2049-3002-2-18. Erratum in: *Cancer Metab*. 2014;2:22. PMID: 25228990; PMCID: PMC4165433 .

Siegel, R.L., Miller, K.D. and Jemal, A. (2016) Cancer statistics, 2016. CA*: a cancer journal for clinicians,* 66(1), pp. 7-30 .

Silva-Nichols H. B., Woolf E. C., Deleyrolle L. P., Reynolds B. A., Scheck A. C. (2015). The ketone body β-hydroxybutyrate radiosensitizes glioblastoma multiforme stem cells. *Neuro Oncol*. 17:v35 10.1093/neuonc/nov204.77 .

Siu MKY, Jiang YX, Wang JJ, Leung THY, Han CY, Tsang BK, Cheung ANY, Ngan HYS, Chan KKL. (2019) Hexokinase 2 Regulates Ovarian Cancer Cell Migration, Invasion and Stemness via FAK/ERK1/2/MMP9/NANOG/SOX9 *Signaling Cascades. Cancers* (Basel). 2019 Jun 12;11(6):813. doi: 10.3390/cancers11060813. PubMed PMID: 31212816; PubMed Central PMCID: PMC6627345 .

Skinner R., Trujillo A., Ma X., Beierle E. A. (2009). Ketone bodies inhibit the viability of human neuroblastoma cells. *J. Pediatr. Surg*. 44, 212–216. 10.1016/j.jpedsurg.2008.10.042 .

Soliman GA, Acosta-Jaquez HA, Dunlop EA, Ekim B, Maj NE, Tee AR, Fingar DC. (2010) mTOR Ser-2481 autophosphorylation monitors mTORC-specific catalytic activity and clarifies rapamycin mechanism of action. *J Biol Chem*. 2010 Mar 12;285(11):7866-79. doi: 10.1074/jbc.M109.096222. Epub 2009 Dec 18 .

Song JJ, Lee YJ (May 2008). "Differential cleavage of Mst1 by caspase-7/-3 is responsible for TRAIL-induced activation of the MAPK superfamily". *Cellular Signalling*. 20 (5): 892–906. doi:10.1016/j.cellsig.2008.01.001. PMC 2483832 .

Song L, Guo Y, Xu B. (2017). Expressions of Ras Homolog Gene Family, Member A (RhoA) and Cyclooxygenase-2 (COX-2) Proteins in Early Gastric Cancer and Their Role in the Development of Gastric Cancer. *Med Sci Monit*. 2017 Jun 18;23:2979-2984. doi: 10.12659/msm.902367. PMID: 28624843; PMCID: PMC5484605 .

Sottoriva, A., Spiteri, I., Piccirillo, S., Touloumis, A., Collins, V., Marioni, J., Curtis, C., Watts, C. and Tavare, S. (2013) Intratumor heterogeneity in human glioblastoma

reflects cancer evolutionary dynamics. *Proceedings of the National Academy of Sciences,* 110(10), pp. 4009-4014 .

Spoerri, L., Oo, Z.Y., Larsen, J.E., Haass, N.K., Gabrielli, B. and Pavey, S. (2015) Cell cycle checkpoint and dna damage response defects as anticancer targets: from molecular mechanisms to therapeutic opportunities. in Stress Response Pathways in *Cancer. Springer,* pp.29-49 .

Stephens, K. E., Miaskowski, C. A., Levine, J. D., Pullinger, C. R., & Aouizerat, B. E. (2013). Epigenetic regulation and measurement of epigenetic changes. *Biological research for nursing*, 15(4), 373–381. doi:10.1177/1099800412444785 .

stress-related pathways in glioblastoma cells. J. Proteom. 2017, 152, 329–338 .

Stupp, R., Taillibert, S., Kanner, A.A., Kesari, S., Steinberg, D.M., Toms, S.A., Taylor, L.P., Lieberman, F., Silvani, A. and Fink, K.L. (2015) Maintenance therapy with tumor-treating fields plus temozolomide vs temozolomide alone for glioblastoma: a randomized clinical trial. *Jama* , 314(23), pp. 2535-2543 .

Sturm, D., Witt, H., Hovestadt, V., Khuong-Quang, D., Jones, D., Konermann, C., Pfaff, E., Tönjes, M., Sill, M., Bender, S., Kool, M., Zapatka, M., Becker, N., Zucknick, M., Hielscher, T., Liu, X., Fontebasso, A., Ryzhova, M., Albrecht, S., Jacob, K., Wolter, M., Ebinger, M., Schuhmann, M., van Meter, T., Frühwald, M., Hauch, H., Pekrun, A., Radlwimmer, B., Niehues, T., von Komorowski, G., Dürken, M., Kulozik, A., Madden, J., Donson, A., *et al.*, and Pfister, S. (2012) Hotspot Mutations in H3F3A and IDH1 Define Distinct Epigenetic and Biological Subgroups of Glioblastoma. *Cancer Cell,* 22(4), pp. 425-437 .

Sugita S, Enokida 1, Yoshino H, Miyamoto K, Yonemori 1, Sakaguchi T, Osako Y, Nakagawa M. (2018) HRAS as a potential therapeutic target of salirasib RAS inhibitor in bladder cancer. *Int J Oncol*. 2018 Aug;53(2):725-736. doi: 10.3892/ijo.2018.4435. Epub 2018 Jun 11 .

Sun, R.C. and Denko, N.C. (2014) Hypoxic regulation of glutamine metabolism through HIF1 and SIAH2 supports lipid synthesis that is necessary for tumor growth. *Cell metabolism* , 19(2), pp. 285-292 .

Sun, Y., Liu, Z., Zou, X., Lan, Y., Sun, X., Wang, X., Liu, H. (2015). Mechanisms underlying 3-bromopyruvate-induced cell death in colon cancer. *Journal of bioenergetics and biomembranes*, 47(4), 319–329. doi:10.1007/s10863-015-9612-1 .

Sun, Y., Tao, C., Huang, X., He, H., Shi, H., Zhang, Q. and Wu, H. (2016) Metformin induces apoptosis of human hepatocellular carcinoma HepG2 cells by activating an AMPK/p53/miR-23a/FOXA1 pathway. *OncoTargets* and therapy , 9pp. 2845-2853 .

Takai, D. and Jones, P. (2002) Comprehensive analysis of CpG islands in human chromosomes 21 and 22. *Proceedings of the National Academy of Sciences*, 99(6), pp. 3740-3745 .

Takata, F., Dohgu, S., Matsumoto, J., Machida, T., Kaneshima, S., Matsuo, M., Sakaguchi, S., Takeshige, Y., Yamauchi, A. and Kataoka, Y. (2013) Metformin induces up-regulation of blood–brain barrier functions by activating AMP-activated protein kinase in rat brain microvascular endothelial cells. *Biochemical and biophysical research communications* , 433(4), pp. 586-590 .

Thakkar, J. P., Dolecek, T. A., Horbinski, C., Ostrom, Q. T., Lightner, D. D., Barnholtz-Sloan, J. S., & Villano, J. L. (2014). Epidemiologic and molecular prognostic review of glioblastoma. Cancer epidemiology, biomarkers & prevention : a publication of the *American Association for Cancer Research*, cosponsored by the American Society of Preventive Oncology, 23(10), 1985–1996. doi:10.1158/1055-9965.EPI-14-0275 .

Tieu, M. T., Lovblom, L. E., McNamara, M. G., Mason, W., Laperriere, N., Millar, B. A., … Chung, C. (2015). Impact of glycemia on survival of glioblastoma patients treated with radiation and temozolomide. *Journal of neuro-oncology*, 124(1), 119–126. doi:10.1007/s11060-015-1815-0 .

Timp, W. and Feinberg, A. (2013) Cancer as a dysregulated epigenome allowing cellular growth advantage at the expense of the host. *Nature Reviews Cancer*, 13(7), pp. 497-510 .

Tomczak, K., Czerwinska, P. and Wiznerowicz, M. (2015) The Cancer Genome Atlas (TCGA): an immeasurable source of knowledge. *Contemporary oncology* (Poznan, Poland) , 19(1A), pp. A68-77 .

Torre, L.A., Bray, F., Siegel, R.L., Ferlay, J., Lortet-Tieulent, J. and Jemal, A. (2015) Global cancer statistics, 2012. *CA: a cancer journal for clinicians* , 65(2), pp. 87-108 .

Torsvik, A., Stieber, D., Enger, P.Ø., Golebiewska, A., Molven, A., Svendsen, A., Westermark, B., Niclou, S.P., Olsen, T.K. and Chekenya Enger, M. (2014) U-251 revisited: genetic drift and phenotypic consequences of long-term cultures of glioblastoma cells. *Cancer medicine* , 3(4), pp. 812-824 .

Unoki, M., Nishidate, T. and Nakamura, Y. (2004) ICBP90, an E2F-1 target, recruits HDAC1 and binds to methyl-CpG through its SRA domain. *Oncogene,* 23(46), pp. 7601-7610 .

Vale, C. L., Burdett, S., Fisher, D. J., Navani, N., Parmar, M. K., Copas, A. J., & Tierney, J. F. (2015). Should Tyrosine Kinase Inhibitors Be Considered for Advanced Non-Small-Cell Lung Cancer Patients With Wild Type EGFR? Two Systematic Reviews and Meta-Analyses of Randomized Trials. *Clinical lung cancer*, 16(3), 173–182.e4. doi:10.1016/j.cllc.2014.11.007 .

van den Bent MJ, Smits, Kros JM, Chang SM. (2017). Diffuse Infiltrating Oligodendroglioma and Astrocytoma*. J Clin Oncol*. 2017 Jul 20;35(21):2394-2401. doi: 10.1200/JCO.2017.72.6737. Epub 2017 Jun 22 .

van Tellingen O, Yetkin-Arik B, de Gooijer MC. (2015). Overcoming the blood-brain tumor barrier for effective glioblastoma treatment. Drug Resistance Updates : Reviews and *Commentaries in Antimicrobial and Anticancer Chemotherapy*. 2015 Mar;19:1-12. DOI: 10.1016/j.drup.2015.02.002

Vandamme TF. (2014). Use of rodents as models of human diseases. *J Pharm Bioallied Sci.* 2014 Jan;6(1):2-9. doi: 10.4103/0975-7406.124301. PMID: 24459397; PMCID: PMC3895289 .

Vander Heiden, M.G., Cantley, L.C. and Thompson, C.B. (2009) Understanding the Warburg effect: the metabolic requirements of cell proliferation. *Science* (New York, N.Y.), 324(5930), pp. 1029-1033.

Varela, I., Tarpey, P., Raine, K., Huang, D., Ong, C., Stephens, P., Davies, H., Jones, D., Lin, M., Teague, J., Bignell, G., Butler, A., Cho, J., Dalgliesh, G., Galappaththige, D., Greenman, W., Subimerb, C., Dykema, K., Furge, K., Campbell, P., Teh, B., Stratton, M. and Futreal, P. (2011) Exome sequencing identifies frequent mutation of the SWI/SNF complex gene PBRM1 in renal carcinoma. *Nature*, 469(7331), pp. 539-542.

Vartanian A, Agnihotri S, Wilson MR, Burrell KE, Tonge PD, Alamsahebpour A, Jalali S, Taccone M, Mansouri S, Golbourn B, Aldape KD, Zadeh G. (2016) Targeting hexokinase 2 enhances response to radio-chemotherapy in glioblastoma. *Oncotarget.* 2016 Oct 25;7(43):69518-69535. doi: 10.18632/oncotarget.11680.

Veech RL. (2004) The therapeutic implications of ketone bodies: the effects of ketone bodies in pathological conditions: ketosis, ketogenic diet, redox states, insulin resistance, and mitochondrial metabolism. *Prostaglandins Leukot Essent Fatty Acids*. 2004;70(3):309–319. doi: 10.1016/j.plefa.2003.09.007.

Verhaak, R.G., Hoadley, K.A., Purdom, E., Wang, V., Qi, Y., Wilkerson, M.D., Miller, C.R., Ding, L., Golub, T. and Mesirov, J.P. (2010) Integrated genomic analysis identifies clinically relevant subtypes of glioblastoma characterized by abnormalities in PDGFRA, IDH1, EGFR, and NF1. *Cancer cell* , 17(1), pp. 98-110 .

Vermeulen, K., Van Bockstaele, D.R. and Berneman, Z.N. (2003) The cell cycle: a review of regulation, deregulation and therapeutic targets in cancer. *Cell proliferation*, 36(3), pp. 131-149 .

Vichai, V., Kirtikara, K. (2006). Sulforhodamine B colorimetric assay for cytotoxicity screening. *Nat Protoc* 1, 1112–1116 (2006). https://doi.org/10.1038/nprot.2006.179

Vidal E, Sayols S, Moran S, Guillaumet-Adkins A, Schroeder MP, Royo R, Orozco M, Gut M, Gut I, Lopez-Bigas N, Heyn H, Esteller M. (2017) A DNA methylation map of human cancer at single base-pair resolution. *Oncogene.* 2017 Oct 5;36(40):5648-

5657. doi: 10.1038/onc.2017.176. Epub 2017 Jun 5. PubMed PMID: 28581523; PubMed Central PMCID: PMC5633654 .

Vidali S, Aminzadeh S, Lambert B, Rutherford T, Sperl W, Kofler B, Feichtinger RG. (2015) Mitochondria: the ketogenic diet—a metabolism-based therapy. *Int J Biochem Cell Biol.* 2015;63:55–59. doi: 10.1016/j.biocel.2015.01.022 .

von Karstedt, S., Montinaro, A. and Walczak, H. (2017) Exploring the TRAILs less travelled: TRAIL in cancer biology and therapy. *Nature Reviews Cancer* , 17(6), pp. 352-366 .

von Pawel, J., Harvey, J.H., Spigel, D.R., Dediu, M., Reck, M., Cebotaru, C.L., Humphreys, R.C., Gribbin, M.J., Fox, N.L. and Camidge, D.R. (2014) Phase II Trial of Mapatumumab, a Fully Human Agonist Monoclonal Antibody to TumorNecrosis Factor-Related Apoptosis-Inducing Ligand Receptor 1 (TRAIL-R1), in Combination With Paclitaxel and Carboplatin in Patients With Advanced Non–Small-Cell Lung Cancer. *Clinical lung cancer* , 15(3), pp. 188-196. e2 .

Wahl, D.R. and Venneti, S. (2018) Cancer Metabolism. *Imaging and Metabolism. Springer,* pp.129-154.

Wang L., Hua Xiong., Fengxia Wu., Haojie Huang., Junxuan Lu., Yibin Deng. (2014) Hexokinase 2-mediated Warburg effect is required for PTEN- and p53-deficiency-driven prostate cancer growth. *Cell Rep.* 2014;8:1461–74 .

Wang, G., Shen, W., Liu, C. *et al*. (2017). Phosphorylase kinase β affects colorectal cancer cell growth and represents a novel prognostic biomarker. *J Cancer Res Clin Oncol* (143: 971. https://doi.org/10.1007/s00432-017-2362-1 .

Wang, M., Zhang, C., Song, Y., Wang, Z., Wang, Y., Luo, F., … Xu, Y. (2017). Mechanism of immune evasion in breast cancer. *OncoTargets* and therapy, 10, 1561–1573. doi:10.2147/OTT.S126424 .

Watkins, S., Robel, S., Kimbrough, I.F., Robert, S.M., Ellis-Davies, G. and Sontheimer, H. (2014) Disruption of astrocyte–vascular coupling and the blood–brain barrier by invading glioma cells. *Nature communications* , 5pp. 4196 .

Weller, M., Stupp, R., Reifenberger, G., Brandes, A., van den Bent, M., Wick, W. and Hegi, M. (2009) *MGMT* promoter methylation in malignant gliomas: ready for personalized medicine?. *Nature Reviews Neurology*, 6(1), pp. 39-51.

Wenger A, Ferreyra Vega S, Kling T, Bontell TO, Jakola AS, Carén H. (2019). Intratumor DNA methylation heterogeneity in glioblastoma: implications for DNA methylation-based classification*. Neuro Oncol*. 2019 May 6;21(5):616-627. doi: 10.1093/neuonc/noz011 .

Westermark, B., Ponten, J. and Hugosson, R. (1973) Determinants for the establishment of permanent tissue culture lines from human gliomas. *Acta Pathologica Microbiologica Scandinavica Section a Pathology* , 81(6), pp. 791-805 .

Wicks, R. T., Azadi, J., Mangraviti, A., Zhang, I., Hwang, L., Joshi, A., … Tyler, B. M. (2015). Local delivery of cancer-cell glycolytic inhibitors in high-grade glioma. *Neuro-oncology,* 17(1), 70–80. doi:10.1093/neuonc/nou143 .

Wicks, R.T.; Azadi, J.; Mangraviti, A.; Zhang, I.; Hwang, L.; Joshi, A.; Bow, H.; Hutt-Cabezas, M.; Martin, K.L.; Rudek, M.A.; *et al*. Local delivery of cancer-cell glycolytic inhibitors in high-grade glioma. *Neuro-Oncology* 2015, 17, 70–80 .

William, D., Mokri, P., Lamp, N., Linnebacher, M., Classen, C. F., Erbersdobler, A., & Schneider, B. (2017). Amplification of the EGFR gene can be maintained and modulated by variation of EGF concentrations in in vitro models of glioblastoma multiforme. *PloS one*, 12(9), e0185208. doi:10.1371/journal.pone.0185208 .

Wilson J.E. (2003) Isozymes of mammalian hexokinase: structure, subcellular localization and metabolic function. *J. Exp. Biol*. 2003; 206: 2049-2057 .

Wolf, A., Agnihotri, S., & Guha, A. (2010). Targeting metabolic remodeling in glioblastoma multiforme. *Oncotarget,* 1(7), 552–562. doi:10.18632/oncotarget.190 .

Wolf, A., Agnihotri, S., Micallef, J., Mukherjee, J., Sabha, N., Cairns, R., … Guha, A. (2011). Hexokinase 2 is a key mediator of aerobic glycolysis and promotes tumor growth in human glioblastoma multiforme. *The Journal of experimental medicine,* 208(2), 313–326. doi:10.1084/jem.20101470 .

Wolff EM, Byun HM, Han HF, Sharma S, Nichols PW, Siegmund KD, *et al*. (April 2010). Hypomethylation of a LINE-1 promoter activates an alternate transcript of the MET oncogene in bladders with cancer. *PLoS Genetics*. 6 (4): e1000917. doi:10.1371/journal.pgen.1000917. PMC 2858672. PMID 20421991.

Wong, A., Ye, M., Levy, A., Rothstein, J., Bergles, D. and Searson, P.C. (2013) The blood-brain barrier: an engineering perspective. *Frontiers in neuroengineering* ,6pp.7.

Woolf EC, Syed N, Scheck AC. (2016) Tumor Metabolism, the Ketogenic Diet and β-Hydroxybutyrate: Novel Approaches to Adjuvant Brain Tumor Therapy. *Front Mol Neurosci.* 2016 Nov 16;9:122. doi: 10.3389/fnmol.2016.00122. PubMed PMID: 27899882; PubMed Central PMCID: PMC5110522 .

Wouters BG, Koritzinsky M. (2008) Hypoxia signalling through mTOR and the unfolded protein response in cancer. *Nat Rev Cancer.* 2008 Nov;8(11):851-64. doi: 10.1038/nrc2501. Epub 2008 Oct 10 .

Wu, J., Hu, L., Wu, F., Zou, L., & He, T. (2017). Poor prognosis of hexokinase 2 overexpression in solid tumors of digestive system: a meta-analysis. *Oncotarget,* 8(19), 32332–32344. doi:10.18632/oncotarget.15974 .

Xiao, H.J., Li, S.S., Zhang, D.P., Liu, T.J., Yu, M.Wang, F. (2013). Separate and concurrent use of 2-deoxy-D-glucoseand 3-bromopyruvate in pancreatic cancer cells. *Oncol. Rep*. 2013, 29, 329–334 .

Xu S, Catapang A, Doh HM, Bayley NA, Lee JT, Braas D, Graeber TG, Herschman HR. 2018 Hexokinase 2 is targetable for HK1 negative, HK2 positive tumors from a wide variety of tissues of origin*. J Nucl Med*. 2018 Jun 7. pii: jnumed.118.212365. doi: 10.2967/jnumed.118.212365 .

Xu S., Catapang A, Braas D, Stiles L, Doh H, Lee JT, Graeber TG, Damoiseaux R, Shirihai O and Herschman H (2018). *Cancer & Metabolism* 20186:7 https://doi.org/10.1186/s40170-018-0181-8 .

Xu, H., Zong, H., Ma, C., Ming, X., Shang, M., Li, K., He, X., Du, H. and Cao, L. (2017) Epidermal growth factor receptor in glioblastoma. *Oncology letters* , 14(1), pp. 512-516 .

Xu, R.H.; Pelicano, H.; Zhou, Y.; Carew, J.S.; Feng, L.; Bhalla, K.N.; Keating, M.J.; Huang, P. (2005) Inhibition of glycolysis in cancer cells: A novel strategy to overcome drug resistance associated with mitochondrial respiratory defect and hypoxia. *Cancer Res.* 2005, 65, 613–621

Yadav, S.; Pandey, S.K.; Kumar, A.; Kujur, P.K.; Singh, R.P.; Singh, S.M. (2017) Antitumor and chemosensitizing action of 3-bromopyruvate: Implication of deregulated metabolism. *Chem.-Biol. Interact*. 2017, 270, 73–89 .

Yamazaki, Y. and Kanekiyo, T. (2017) Blood-brain barrier dysfunction and the pathogenesis of Alzheimer's disease. *International journal of molecular sciences* , 18(9), pp. 1965 .

Yan, H., Parsons, D. W., Jin, G., McLendon, R., Rasheed, B. A., Yuan, W., … Bigner, D. D. (2009). IDH1 and IDH2 mutations in gliomas. *The New England journal of medicine,* 360(8), 765–773. doi:10.1056/NEJMoa0808710 .

Yan, Y., Xu, Z., Dai, S., Qian, L., Sun, L., & Gong, Z. (2016). Targeting autophagy to sensitive glioma to temozolomide treatment. *Journal of experimental & clinical cancer research* : CR, 35, 23. doi:10.1186/s13046-016-0303-5

Yang, H., Fang, F., Chang, R. and Yang, L. (2013) MicroRNA-140-5p suppresses tumor growth and metastasis by targeting transforming growth factor β receptor 1 and fibroblast growth factor 9 in hepatocellular carcinoma. *Hepatology* , 58(1), pp. 205-217 .

Yang, L., Lin, C., Wang, L., Guo, H. and Wang, X. (2012) Hypoxia and hypoxia-inducible factors in glioblastoma multiforme progression and therapeutic implications. *Experimental cell research* , 318(19), pp. 2417-2426 .

Yao Q, Cai G, Yu Q, Shen J, Gu Z, Chen J, Shi W, Shi J. 2018. IDH1 mutation diminishes aggressive phenotype in glioma stem cells. *Int J Oncol*. 2018 Jan;52(1):270-278. doi: 10.3892/ijo.2017.4186 .

YaoD, Ren J, Shi J, Feng L, Wang K, Zeng T, Jin Y, Gao L. (2016). R132H mutation in IDH1 gene reduces proliferation, cell survival and invasion of human glioma by downregulating Wnt/β-catenin signaling*. Int J Biochem Cell Biol*. 2016 Apr;73:72-81. doi: 10.1016/j.biocel.2016.02.007. Epub 2016 Feb 6 .

Ye, J., Mancuso, A., Tong, X., Ward, P.S., Fan, J., Rabinowitz, J.D. and Thompson, C.B. (2012) Pyruvate kinase M2 promotes de novo serine synthesis to sustain mTORC1 activity and cell proliferation. *Proceedings of the National Academy of Sciences of the United States of America* , 109(18), pp. 6904-6909 .

Yee, D., Paoloni, M., van't Veer, L., Sanil, A., Yau, C., Forero, A., Chien, A., Wallace, A., Moulder, S. and Albain, K. (2017) Abstract P6-11-04: The evaluation of ganitumab/metformin plus standard neoadjuvant therapy in high-risk breast cancer: Results from the I-SPY 2 trial

Yost, S., Pastorino, S., Rozenzhak, S., Smith, E., Chao, Y., Jiang, P., Kesari, S., Frazer, K. and Harismendy, O. (2013) High-Resolution Mutational Profiling Suggests the Genetic Validity of Glioblastoma Patient-Derived Pre-Clinical Models. *PLoS ONE*, 8(2), p. e56185.

You, J. and Jones, P. (2012) Cancer Genetics and Epigenetics: Two Sides of the Same Coin?. *Cancer Cell,* 22(1), pp. 9-20 .

Yuan TL, Cantley LC. (2008). PI3K pathway alterations in cancer: variations on a theme*. Oncogene*. 2008 Sep 18;27(41):5497-510. doi: 10.1038/onc.2008.245 .

Zaal, E. A., & Berkers, C. R. (2018). The Influence of Metabolism on Drug Response in Cancer. *Frontiers in oncology*, 8, 500. doi:10.3389/fonc.2018.00500 .

Zadeh G, Bhat KP, Aldape K. (2013). EGFR and EGFRvIII in glioblastoma: partners in crime.

Zahonero C, Aguilera P, Ramirez-Castillejo C, Pajares M, Bolos MV, Cantero D, *et al*. (2015). Preclinical Test of Dacomitinib, an Irreversible EGFR Inhibitor, Confirms Its Effectiveness for Glioblastoma. *Molecular cancer therapeutics*. 2015;14:1548–1558 .

Zakikhani, M., Blouin, M., Piura, E. and Pollak, M.N. (2010) Metformin and rapamycin have distinct effects on the AKT pathway and proliferation in breast cancer cells. *Breast cancer research and treatment* , 123(1), pp. 271-279 .

Zarghooni, M., Bartels, U., Lee, E., Buczkowicz, P., Morrison, A., Huang, A., Bouffet, E. and Hawkins, C. (2010) Whole-Genome Profiling of Pediatric Diffuse Intrinsic Pontine Gliomas Highlights Platelet-Derived Growth Factor Receptor and Poly (ADP-ribose) Polymerase As Potential Therapeutic Targets. *Journal of Clinical Oncology,* 28(8), pp. 1337-1344 .

Zhang Y, Yu G, Chu H, Wang X, Xiong L, Cai, Liu R, Gao H, Tao B, Li W, Li G, Liang J, Yang W. (2018) Macrophage-Associated PGK1 Phosphorylation Promotes Aerobic Glycolysis and Tumorigenesis. *Mol Cell*. 2018 Jul 19;71(2):201-215.e7. doi: 10.1016/j.molcel.2018.06.023 .

Zhang, B., Zhou, Y., Lin, N., Lowdon, R. F., Hong, C., Nagarajan, R. P., … Wang, T. (2013). Functional DNA methylation differences between tissues, cell types, and across individuals discovered using the M&M algorithm. *Genome research*, 23(9), 1522–1540. doi:10.1101/gr.156539.113 .

Zhang, C., Zhang, J., Zhang, A., Shi, Z., Han, L., Jia, Z., Yang, W., Wang, G., Jiang, T. and You, Y. (2010) MiR-221 and miR-222 target PUMA to induce cell survival in glioblastoma. *Molecular cancer* , 9(1), pp. 229 .

Zhang, D., Xuan, J., Zheng, B., Zhou, Y., Lin, Y., Wu, Y., Zhou, Y., Huang, Y., Wang, Q. and Shen, L. (2017) Metformin improves functional recovery after spinal cord injury via autophagy flux stimulation*. Molecular neurobiology* , 54(5), pp. 3327-3341 .

Zhang, Q., Pan, J., Lubet, R. A., Komas, S. M., Kalyanaraman, B., Wang, Y., & You, M. (2015). Enhanced antitumor activity of 3-bromopyruvate in combination with rapamycin in vivo and in vitro. *Cancer prevention research* (Philadelphia, Pa.), 8(4), 318–326. doi:10.1158/1940-6207.CAPR-14-0142 .

Zhang, Q.; Pan, J.; North, P.E.; Yang, S.; Lubet, R.A.; Wang, Y.; You, M. (2012) Aerosolized 3-bromopyruvate inhibits lung tumorigenesis without causing liver toxicity. *Cancer Prev. Res*. 2012, 5, 717–725 .

Zhang, Y. and Yang, J. (2013) Altered energy metabolism in cancer. *Cancer Biology & Therapy*, 14(2), pp. 81-89 .

Zhang, Y.; Wei, J.; Xu, J.; Leong, W.S.; Liu, G.; Ji, T.; Cheng, Z.; Wang, J.; Lang, J.; Zhao, Y.; *et al*. Suppression of tumor energy supply by liposomal nanoparticle-mediated inhibition of aerobic glycolysis. *ACS Appl. Mater. Int.* 2018, 10, 2347–2353 .

Zhang, Z., Deng, X., Liu, Y., Liu,Y., Sun, L., Chen, F. (2019). PKM2, function and expression and regulation. *Cell & Biosciencevolume* 9, Article number: 52. 2019 .

Zhao J, Li J, Fan TWM, Hou SX. (2017). Glycolytic reprogramming through PCK2 regulates tumor initiation of prostate cancer cells. *Oncotarget.* 2017 Jun 28;8(48):83602-83618. doi: 10.18632/oncotarget.18787. PMID: 29137367; PMCID: PMC5663539 .

Zhao, Y., Liu, H., Riker, A.I., Fodstad, O., Ledoux, S.P., Wilson, G.L. and Tan, M. (2011) Emerging metabolic targets in cancer therapy. *Frontiers in bioscience (Landmark edition)* , 16pp. 1844-1860 .

Zheng, H., Ying, H., Yan, H., Kimmelman, A.C., Hiller, D.J., Chen, A., Perry, S.R., Tonon, G., Chu, G.C. and Ding, Z. (2008) p53 and Pten control neural and glioma stem/progenitor cell renewal and differentiation*. Nature* , 455(7216), pp. 1129 .

Zhuo B, Li Y, Li Z, Qin H, Sun Q, Zhang F, Shen Y, Shi Y, Wang R. (2015) PI3K/Akt signaling mediated hexokinase-2 expression inhibits cell apoptosis and promotes tumor growth in pediatric osteosarcoma. *Biochem Biophys Res Commun* 2015; 464 (2): 401–6. 2018; Volume: 4, Issue: 2, Page: 54-58

Zieker D, Königsrainer I, Tritschler I, Löffler M, Beckert S, Traub F, Nieselt K, Bühler S, Weller M, Gaedcke J, Taichman RS, Northoff H, Brücher BL, Königsrainer A. (2010). Phosphoglycerate kinase 1 a promoting enzyme for peritoneal dissemination

in gastric cancer. *International Journal of Cancer*. 2010 126 (6): 1513–20. doi:10.1002/ijc.24835.

Zimmermann, M., Arachchige-Don, A. S., Donaldson, M. S., Dallapiazza, R. F., Cowan, C. E., & Horne, M. C. (2012). Elevated cyclin G2 expression intersects with DNA damage checkpoint signaling and is required for a potent G2/M checkpoint arrest response to doxorubicin. *The Journal of biological chemistry*, 287(27), 22838–22853. doi:10.1074/jbc.M112.376855 .

Zois CE, Harris AL. (2016). Glycogen metabolism has a key role in the cancer microenvironment and provides new targets for cancer therapy. *J Mol Med* (Berl). 2016 Feb;94(2):137-54. doi: 10.1007/s00109-015-1377-9. Epub 2016 Feb 17. PMID: 26882899; PMCID: PMC4762924 .

Zuo X, Djordjevic JT, Bijosono Oei J, Desmarini D, Schibeci SD, Jolliffe KA, Sorrell TC. (2011) Miltefosine induces apoptosis-like cell death in yeast via Cox9p in cytochrome c oxidase. *Mol Pharmacol*. 2011 Sep;80(3):476-85. doi: 10.1124/mol.111.072322. Epub 2011 May 24 .